KFA

KERNFORSCHUNGSANLAGE JÜLICH GmbH

Institut für Kernphysik

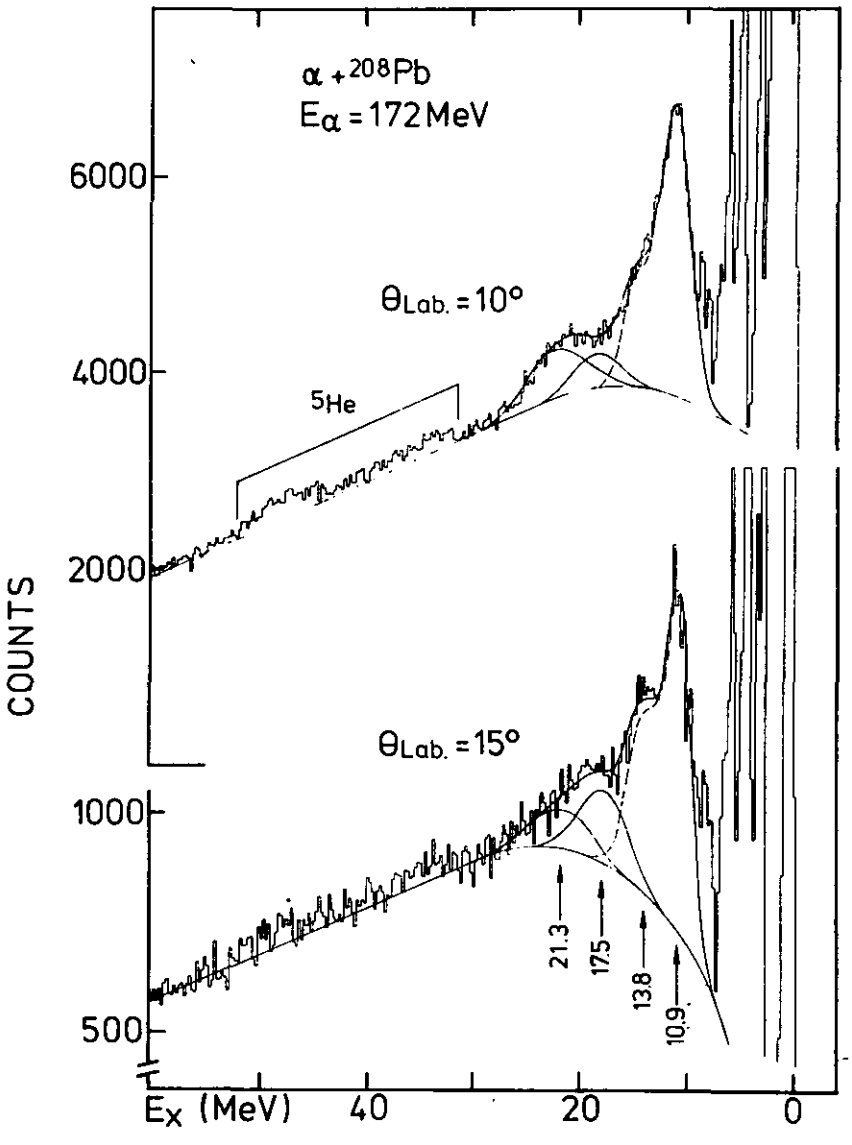

Jül - Spez - 99
Februar 1981
ISSN 0170 - 8937

Annual Report 1980

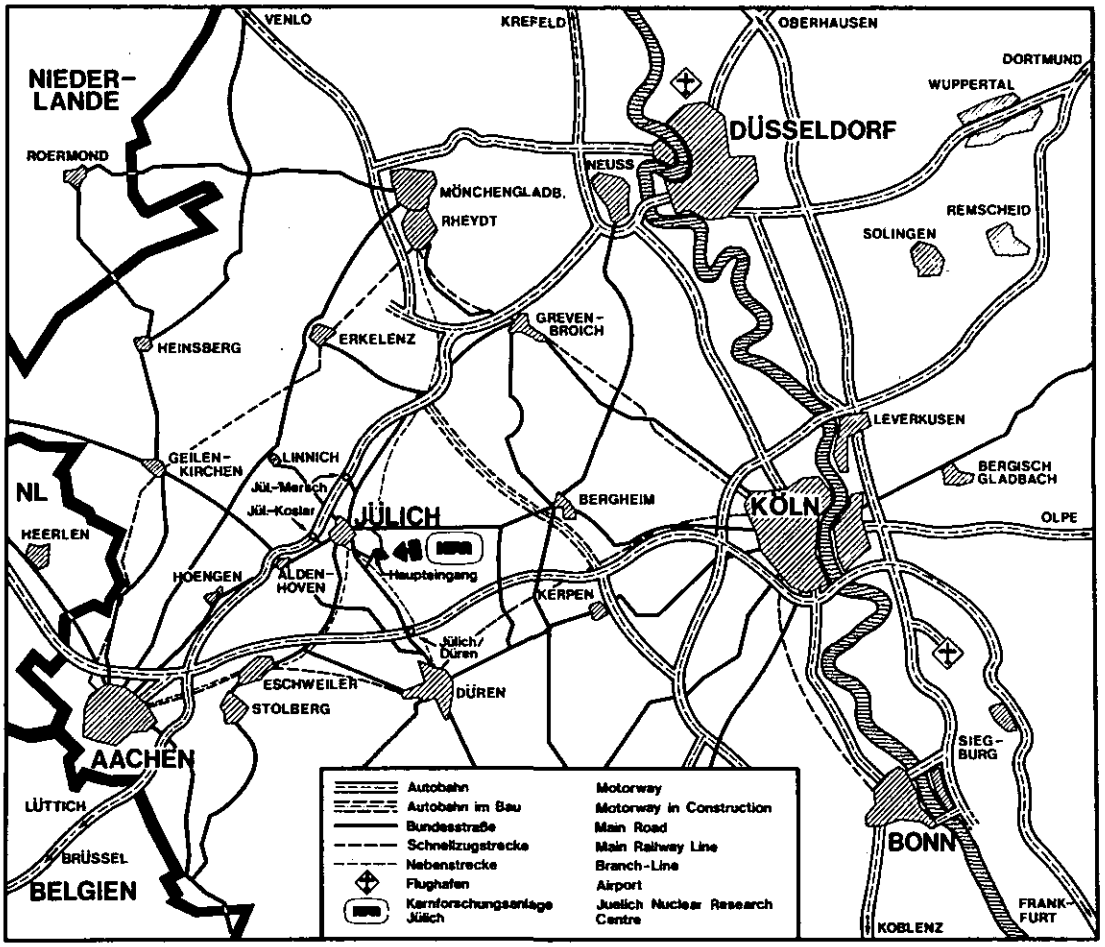

Als Manuskript gedruckt

Spezielle Berichte der Kernforschungsanlage Jülich – Nr. 99
Institut für Kernphysik Jül - Spez - 99

Zu beziehen durch: ZENTRALBIBLIOTHEK der Kernforschungsanlage Jülich GmbH
Postfach 1913 · D-5170 Jülich (Bundesrepublik Deutschland)
Telefon: (0 24 61) 610 · Telex: 8 335 56 kfa d

Annual Report 1980

Front cover: Spectra of 172 MeV α scattering from ^{208}Pb. The background lines and fits to the new giant resonances are indicated as well as the separate peaks for resonances at 17.5 and 21.3 MeV and the sum of giant quadrupole resonance and giant monopole resonance (dashed lines).

PREFACE

The present annual report of the Institute of Nuclear Physics (IKP) at the Kernforschungsanlage Jülich (KFA) covers the period from January to December 1980. It contains short descriptions of recent and current research work that has been carried out by the members of our institute or by guest groups frequently in close cooperation with scientists of the IKP.

Most of the experimental studies make use of the variable energy beams of protons, deuterons, ^{3}He- or alpha particles accelerated in our cyclotron JULIC. Neutron rich nuclei are investigated with the use of our large fission product separator JOSEF at the research reactor DIDO of the KFA. Also neutron capture studies are performed at this reactor. Again several of our staff members have carried out experiments in other laboratories in national and international cooperation with scientists at the ILL, CERN, and other institutions. Cooperation and international exchange is also characteristic for the scientific program of the members of the Institute for Theoretical Nuclear Physics of our IKP Department.

Studies of giant resonance phenomena have been continued and new structures were observed at excitation energies of 17.5 and 21.3 MeV in ^{208}Pb through scattering of 172 MeV α-particles. Our large magnetic spectrograph "Big Karl" has served for an increasing number of high-resolution experiments. The study of 1^{+} states in ^{208}Pb is in progress and so is the spectroscopy of the ^{209}Bi(d,^{3}He)^{208}Pb reactor for a group at the MPI Heidelberg. Part of the work on high-spin states aimed at the investigation of isomers in the odd-odd lanthanums and of the backbending in ^{182}Os and the role of the $i_{13/2}$ neutron. In ^{149}Gd a $\nu f_{7/2}^{3} \times 3^{-} \times 3^{-}$ two-phonon octupole multiplet has been observed. The one-particle spectrum has been identified in $^{147}_{65}Tb_{82}$. The g-factor of the first excited 2^{+} state of ^{100}Zr has been measured in the context of a systematic investigation of the transitional nuclei with A ≈ 100. The electronic K X ray isotope shifts of the stable lead isotopes have been studied in co-operation with the ISOLDE group and theorists from the IKP and ORNL. The study of the structure of the doubly closed ^{132}Sn has been continued in a CERN-ISOLDE cooperation. Also here the experimental work was accompanied by detailed calculations made by our theorists. In addition to the investigation of the nuclear structures, mainly of collective states, the theory group has dealt with precritical phenomena and the generalized spin- and isospin-

dependent interaction. Furthermore, $^{16}O + ^{16}O$ fusion has been studied at astrophysically interesting temperatures by ATDHF in order to gain insight into quantum corrections and collective masses. Also direct fragmentation was studied in peripheral collisions at higher bombarding energies. Investigations of an energy independent but non-local optical potential have been initiated.

In our detector laboratory a significant improvement has been achieved of the quality of ion-implanted n^+ contacts on HPGe. A multi-detector telescope has been fabricated and tested at Orsay. Improvements have been made also for the production of spacially sensitive detectors.

As in the last years the cyclotron was used to a significant fraction of the 6282 h beamtime by external groups (20 %) and in addition by other groups (8 %) of the KFA. Various components of the machine were improved. The project for axial injection of heavy ions from a Mafios source was started. Our curved crystal spectrometer has been installed for on beam measurements and it was used already for a high resolution study of ^{146}Eu.

The solar energy group has essentially completed the development of a procedure for the short term test of the thermal performance of a flat plate collector. Long term testing is on its way. These activities are within the frame of the IEA program "collector test" coordinated by the Operating Agent who is a member of our institute. Efficiency testing of a commercial warm water system is going on, while other systems are being set up for testing. The group is engaged in several bilateral cooperations, especially with Brazil, Egypt and Indonesia.

Most of the work of the experimentalists has been supported by our technical staff through engaged and very cooperative work which I want to gratefully acknowledge.

Otto Schult

INSTITUTE FOR NUCLEAR PHYSICS

Managing director:	Prof. Dr. O. Schult
Experimental Nuclear Physics I, director:	Prof. Dr. C. Mayer-Böricke
Experimental Nuclear Physics II, director:	Prof. Dr. O. Schult
Theoretical Physics, acting director:	Prof. Dr. J. Speth

Kernforschungsanlage Jülich GmbH
Postfach 1913, 5170 Jülich, W.-Germany

CONTENTS

I. EXPERIMENTAL NUCLEAR PHYSICS

1. NUCLEAR REACTIONS AND SCATTERING PROCESSES

1.1. Elastic Deuteron Scattering

J. Bojowald, M. Rogge and P. Turek

The data of elastically scattered deuterons were reanalysed employing an additional volume absorption term in the imaginary part of the optical potential. In our previous analyses[1] using a surface absorption term only the radius parameter r_w was decreasing with increasing incident deuteron energy. This result is an indication that deuterons with higher incident energy penetrate deeper into the nucleus and volume absorption will become more and more important similar to the results of proton scattering[2,3]. Already in recent global fit analyses[4] of deuteron scattering data a volume absorption potential term was used. Additionally vector analysing power data measured at 52 MeV[5] were included in our fit procedure.

Analyses calculated with a volume absorption term only resulted in worse fits to our 58.7 MeV and 85 MeV data as compared to the fit quality in the case of surface absorption only. Therefore the final fit procedure was done with a combination of volume and surface absorption terms in the imaginary potential. During the course of the analyses the geometry of both potentials could be set equal. The reproduction of the experimental data was in general not essentially improved e.g. with different radius parameters for the two absorption terms. The start parameters of the spin orbit potential were "folding model" parameters as in ref. 1.

The best fit potential parameters for the target nuclei ^{27}Al, ^{89}Y, ^{120}Sn and ^{208}Pb at 58.7 and 85 MeV are listed in table 1. A smooth behaviour of the parameters for different target masses and deuteron energies can be seen. By using a combination of volume and surface absorption terms the radius parameter r_w of the imaginary potential and the depth V_{so} of the spin-probit potential are roughly independent from mass and energy and therefore they were fixed at constant values. For good fits to the vector analysing power data, the radius and diffuseness parameters r_{so} and a_{so} should be equal but in light nuclei they are somewhat smaller than in heavier target nuclei. The constant value of V_{so} and the resulting mass dependence of r_{so} are in good agreement with folding model analyses[6] based on the results of proton scattering[3,7]. The potential depth W_{vol} reflects no systematic dependence from the target mass; the energy dependence is much weaker as compared with the result in ref. 4. In contrast to ref. 4 a mass dependence but no energy dependence is necessary for a_o.

E_d (MeV)	Nucl.	V (MeV)	a_o (fm)	W_{vol} (MeV)	W_{surf} (MeV)	a_w (fm)	V_{so} (MeV)	r_{so} (fm)	χ^2/N	$J_W/_{2A}$ (MeV·fm^3)
58.7	^{27}Al	72.5	0.73	2.3	9.0	0.82	6.0	0.90	1.15	354.2
	^{89}Y	80.6	0.79	2.3	10.5	0.86	6.0	0.95	1.45	338.9
	^{120}Sn	82.9	0.82	2.3	11.8	0.87	6.0	0.95	0.81	341.2
	^{208}Pb	86.1	0.83	2.3	12.2	0.90	6.0	0.95	0.85	337.5
85	^{27}Al	68.3	0.77	4.8	7.6	0.82	6.0	0.90	0.98	344.8
	^{89}Y	75.1	0.80	4.8	9.0	0.86	6.0	0.95	1.26	317.2
	^{120}Sn	76.3	0.82	4.8	9.9	0.87	6.0	0.95	0.47	314.0
	^{208}Pb	80.4	0.84	4.8	10.2	0.90	6.0	0.95	0.88	316.1

r_c = 1.30 fm; r_o = 1.18 fm; r_w = 1.27 fm; $a_{so} = r_{so}$

Table 1: Optical model parameters for elastic deuteron scattering (best fit parameters with average values for W_{vol} and V_{so}).

The derived formulas describe the mass and energy dependence of the different optical model parameters in the energy range between E_d = 50 and 90 MeV:

$$V = 82.2 - 0.22\,E_d + 1.23\,Z/A^{1/3} \quad \text{(MeV)}$$
$$W_{vol} = 0.86 \cdot \sqrt{E_d - 52} \quad \text{(MeV) for } E_d \geq 52 \text{ MeV}$$
$$W_{surf} = 7.6 + 1.08\,A^{1/3} - 0.7\,W_{vol} \quad \text{(MeV)}$$
$$a_o = 0.67 + 0.028\,A^{1/3} \quad \text{(fm)}$$
$$a_w = 0.73 + 0.028\,A^{1/3} \quad \text{(fm)}\ .$$

The analyses of the data measured at 52 MeV[5] resulted in very small values for W_{vol}. Therefore W_{vol} was fixed at zero for $E_d \leq 52$ MeV.

In order to get a good reproduction of the experimental data in some cases the best fit parameters are somewhat different from the values resulting from the formulas. This is an indication for special features of the target nuclei[8]. For this reason it is important to use best fit optical model parameters also to calculate the cross sections of inelastic scattering and nuclear reactions[9].

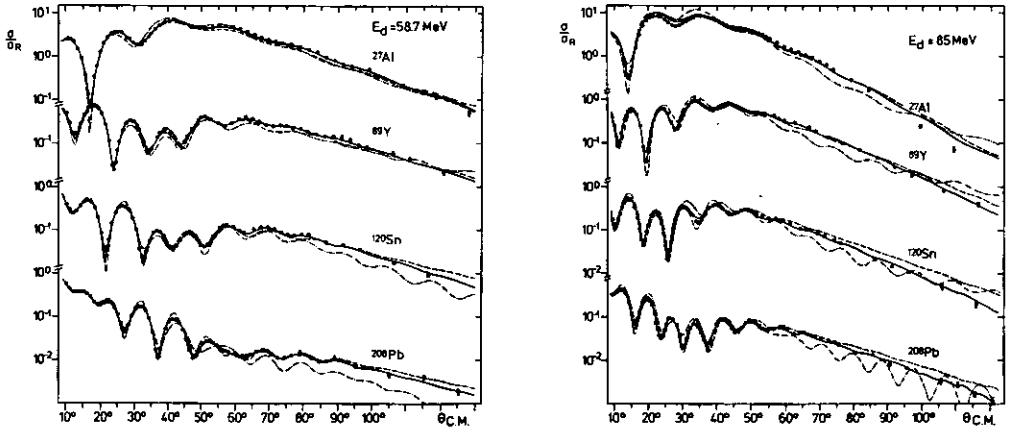

Figure 1: Experimental angular distributions of elastic deuteron scattering and their comparison to the results of optical model calculations. For details see in the text.

Fig. 1 shows the data measured at 58.7 and 85 MeV in comparison with the optical model curves calculated with the parameters of table 1 (solid curves), with the potential F from ref. 4 (dashed curves) and with the "average parameter set" of ref. 5 (dashed-dotted curves). The fits with the parameter sets of ref. 4 and ref. 5 show partly strong deviations in some angular regions.

Fig. 2 shows some of the angular distributions of ref. 5 and theoretical curves calculated with the potential parameters of ref. 5 (dashed-dotted curves) and with our parameters listed in table 2 (solid and dashed curves). Using the parameters of table 2 the fits to the vector analysing power data are not as well as in ref. 5 but the elastic cross sections are reproduced much better.

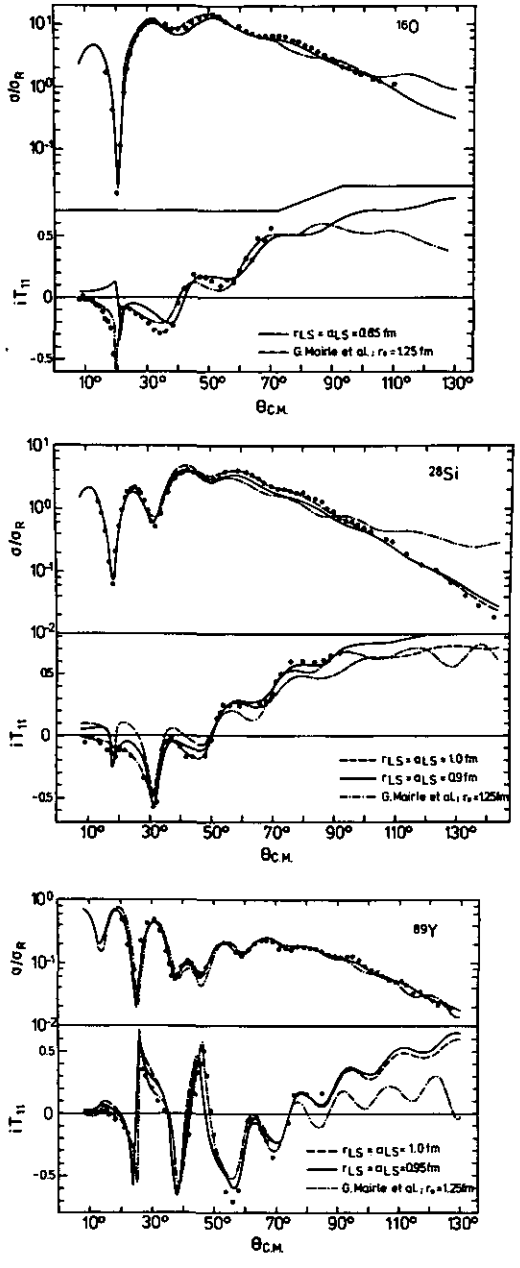

Figure 2: Differential cross sections and vector analysing power data of ref. 5 and their comparison to results of optical model calculations.

Nucl.	V (MeV)	a_w (fm)	W_{surf} (MeV)	a_w (fm)	V_{so} (MeV)	r_{so} (fm)	χ^2/N	$J_R/2A$ (MeV·fm^3)
^{12}C	75.4	0.74	9.5	0.80	6.0	0.85	6.7	451.6
^{16}O	75.5	0.73	10.4	0.81	6.0	0.85	16.8	414.4
^{28}Si	75.3	0.77	10.8	0.82	6.0	0.90	6.3	377.3
^{58}Ni	78.8	0.77	12.0	0.83	6.0	0.95	14.4	347.2
^{89}Y	82.1	0.80	12.4	0.86	6.0	0.95	11.7	346.8
^{197}Au	87.2	0.82	13.9	0.87	6.0	0.95	11.1	342.3

$r_c = 1.30$ fm; $r_o = 1.18$ fm; $r_w = 1.27$ fm; $a_{so} = r_{so}$; $W_{vol} = 0$

Table 2: Optical model parameters at 52 MeV. The parameters are the result of fitting differential cross sections and analysing power data of ref. 5 simultaneously.

As can be seen from the figure it is difficult to get very good fits for both, the differential cross sections and the vector analysing power data simultaneously. But it seems that our optical potential parameter set with the "folding model" spin-orbit term is a good compromise for an acceptable reproduction of both, the differential cross sections and the vector analysing power data.

References

1) Annual Report 1979, KFA-IKP, Jül-Spez-72, p. 1
2) F.D. Becchetti and G.W. Greenless, Phys. Rev. 182 *(1969) 1190*
3) W.T.H. van Oers et al., Phys. Rev. C3 (1971) 1550 and Phys. Rev. C10 (1974) 307
4) W.W. Daehnick et al., Phys. Rev. C21 (1980) 2253
5) G. Mairle et al., Nucl. Phys. A339 (1980) 61
6) P.W. Keaton and D.D. Armstrong, Phys. Rev. C8 (1973) 1692
7) F.A. Brieva and J.R. Rook, Nucl. Phys. A297 (1978) 206
8) R.P. Goddard and W. Haeberle, Nucl. Phys. A316 (1979) 116
9) A. Budzanowski et al., Z. Physik A293 (1979) 293

1.2. Scattering of 130 MeV helions on ^{58}Ni

A. Djaloeis, C. Alderliesten, J. Bojowald, W. Oelert and P. Turek*

This work reports on a measurement and a theoretical analysis of the elastic and inelastic scattering of helions from ^{58}Ni at E_τ = 130 MeV; as for the inelastic transitions, only those to the (1.45 MeV, 2^+) and to the giant resonance (GR) region ($E_x \approx 16.3$ MeV) are considered.

The experimental details have been described elsewhere[1]. The results are shown in fig. 1.

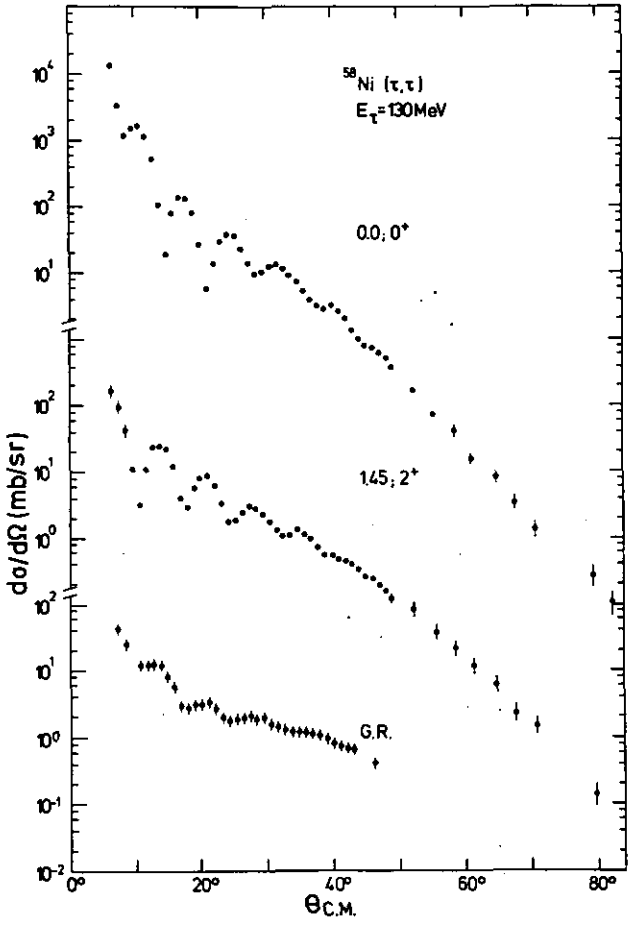

Figure 1: Experimental angular distributions for the scattering of 130 MeV helions on ^{58}Ni.

The elastic scattering angular distribution was analyzed in terms of the optical model using the computer programme OPTY[2]. The analytical form of the optical potential is given in ref. [3]. The spin orbit potential was neglegted for reasons reported previously[3]. The calculations for the inelastic transitions were performed using the programme DWUCK70[4]. The inelastic form factors were taken to be the first derivative of the optical model potential, i.e. complex coupling.

Theoretical fits to the angular distributions for the transition to the two lowest ^{58}Ni states are shown in fig. 2. The resulting optical potential parameters from the best-fit to the elastic scattering angular distribution are listed in table 1. The shallow helion optical potential with either a volume (set TVSH) or a surface (set TSSH) absorption gives a satisfactory description of the data but with preference to the volume absorption which is reflected in the lower χ^2-value for the elastic scattering. This result supports the preference for the volume absorption reported earlier[5] in a model independent analysis of other helion elastic scattering data at E_τ = 130 MeV. The extracted values of the deformation parameters and other related quantities for the (1.45 MeV,

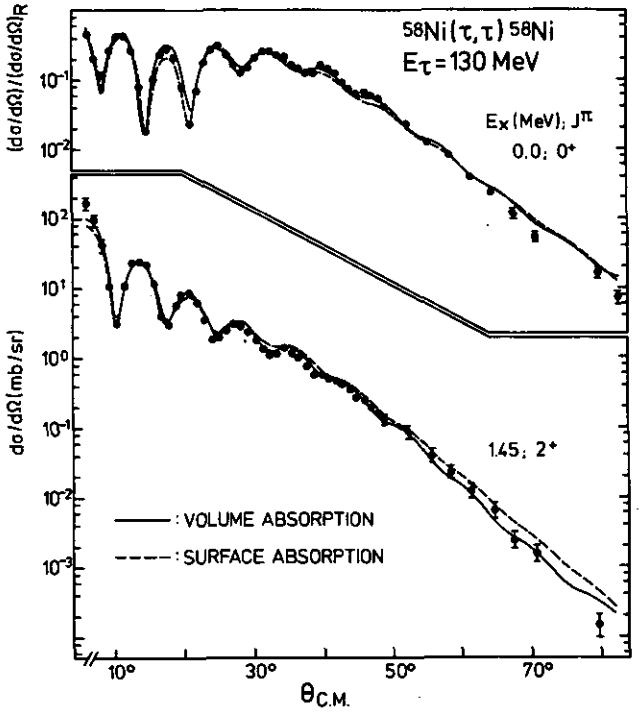

Figure 2: Experimental angular distribution for the helion elastic scattering relative to that of the Rutherford scattering and its comparison to the prediction of the best-fit optical potentials (top). DWBA predicted angular distribution for the transition to the (1.45 MeV, 2^+) state and comparison to the experimental data (bottom).

Set	$U^{a)}$ (MeV)	r_U (fm)	a_U (fm)	$W_V{}^{a)}$ (MeV)	$W_S{}^{b)}$ (MeV)	r_W (fm)	a_W (fm)	χ^2/N	$J_R{}^{c)}$ (MeV·fm^3)	$J_I{}^{c)}$ (MeV·fm^3)
TVSH	106.7	1.172	0.873	20.6	-	1.546	0.659	3.3	327	119
TSSH	95.5	1.223	0.779	-	19.0	1.185	0.834	4.5	309	107

a) Woods-Saxon shape

b) Woods-Saxon derivative shape

c) Volume integral of potential (R = real, I = imaginary part) per particle pair

Table 1: Helion optical model parameters extracted in the present work.

E_x (MeV)	L-transfer	β_L	$\beta_L R_U$ (fm)	EWSR-fraction (%)	Potential Set
1.45	2	0.16±0.01	0.73±0.03	5.0±0.5	DVSH
	2	0.17±0.01	0.81±0.04	6.0±0.6	DSSH
16.3 (GR)	2	0.14±0.02	0.66±0.09	46±14	DVSH
	2	0.13	0.57	35	"
	4	0.09	0.41	5	"
	2	0.16±0.02	0.76±0.09	63±20	DSSH
	2	0.13	0.64	43	"
	4	0.10	0.47	7	"

Table 2: Deformation parameters, deformation lengths and isoscalar EWSR fraction extracted in the present work.

2^+) state are listed in table 2. These values are in reasonable agreement with those reported previously[6].

For the GR case comparison between theory and experiment for TVSH and TSSH sets in shown in fig. 3.

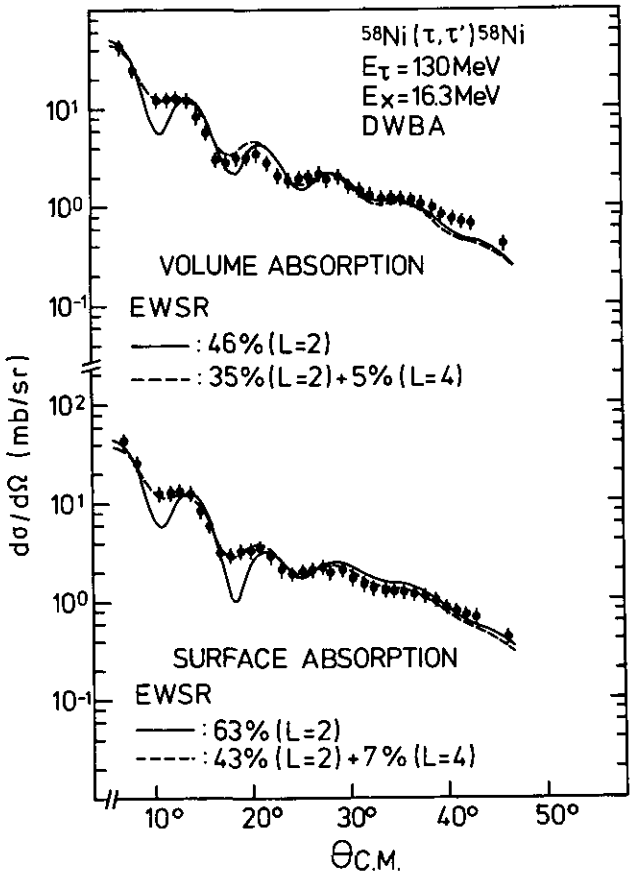

Figure 3: Experimental angular distribution for the inelastic scattering to the GR state and comparison with the DWBA prediction using shallow helion optical potentials (see text).

For both types of absorption considered, the theoretical curves (solid lines) exhibit more pronounced oscillations than the data. Furthermore, the positions of maxima of the theoretical cross sections are shifted towards larger angles relative to those of the experiment. The dashed curves show the effects of including a small (∼6 % of EWSR) L=4 admixture to the L=2 curve. The fit quality is significantly improved because the theoretical maxima are shifted towards smaller angles and at the same time the amplitude of the oscillation pattern is reduced.

The deformation parameters, deformation lengths and the isoscalar EWSR strengths extracted in this work for the GR region are listed in table 2. Assuming an L=2 transfer (pure GQR) the isoscalar L=2 strength was found to be about 55 %, in good agreement with the values determined previously[7]. Inclusion of ∼ 6 % L=4 contribution reduces the L=2 strength to about 40 %.

References

1) A. Djaloeis, C. Alderliesten, J. Bojowald, C. Mayer-Böricke, W. Oelert and P. Turek, Nucl. Phys. A342 (1980) 252

2) H. Dabrowski, R. Planeta and A. Djaloeis, KFA-report, Jül-1637, KFA-IKP Jülich, W. Germany

3) A. Djaloeis, J.-P. Didelez, A. Galonsky and W. Oelert, Nucl. Phys. A306 (1978) 221

4) P.D. Kunz, Programme DWUCK70, University of Colorado, USA

5) A. Djaloeis and S. Gopal, Nucl. Phys., in press

6) D.H. Youngblood, J.M. Moss, C.M. Rozsa, J.D. Bronson, A.D. Bacher and D.R. Brown, Phys. Rkv. C13 (1976) 994, and references therein

7) F.E. Bertrand, Ann. Rev. Nucl. Sci. 36 (1976) 457, and references therein

*Fysisch Laboratorium, Rijksuniversiteit, Utrecht, The Netherlands

1.3. The Charged Particle Decay of the Isoscalar Giant Quadrupole Resonance in ^{15}N and ^{18}O

Ph. Gerhardt, P. Grabmayr*, K.T. Knöpfle*, Liu Kan Pao**, G. Mairle*, C. Mayer-Böricke, W. Nitsche*, W. Oelert, H. Riedesel*, M. Rogge, K. Schindler*, H.R. Schmidt*, A. Stuirbrink*, C. Sükösd, P. Turek, G.J. Wagner**

The decay of the isoscalar giant resonance states of light nuclei proceeds via a dominant direct decay-process in contrast to the decay of heavier nuclei[1,2,3]. To get more structure information of the giant resonance region in light nuclei we have performed coincidence experiments of the type (α,α'c) whereby c is the coincident charged decay particle (p,t and α). The experiments were performed with the 155 MeV α-beam of the Jülich isochronous cyclotron JULIC at the target nuclei ^{15}N and ^{18}O [4]. Two α'-telescopes were combined with 8 decay-telescopes, four covering the range around recoil and four covering the range around antirecoil direction. The two α'-telescopes were mounted in the maximum of a L=2 angular distribution ($\theta_{Lab}=13^0$) symetrical to the incoming beam. The energy resolution in the α'-spectrum was about 360 keV. To measure the L=1 and L=3 contributions in the decay yield of ^{18}O the α'-telescopes were set up at 18^0 and 22^0 respectively in two additional runs.

Figures 1 and 2 show the measured single α'-spectra for ^{15}N and ^{18}O (upper part) and the corresponding spectra coincident with protons, α's and tritons.

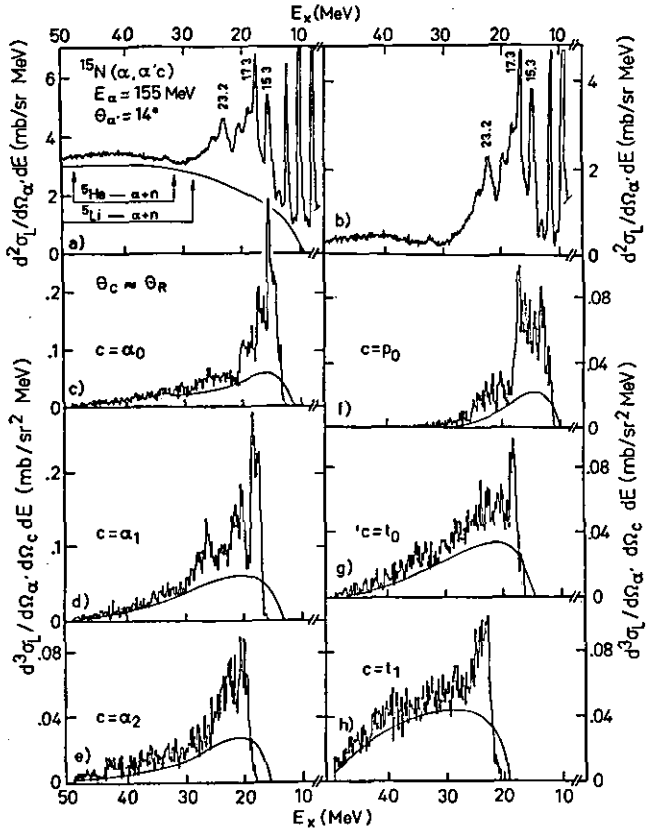

Figure 1: a) α single spectrum of the $^{15}N(\alpha,\alpha')$ reaction; b) the spectrum after subtracting the background, indicated by the solid curve in a); c) ...h) the corresponding coincidence spectra measured in recoil direction of the excited ^{15}N nucleus. The coincidence particle is marked by c. The solid lines show the assumed quasi-free contributions.

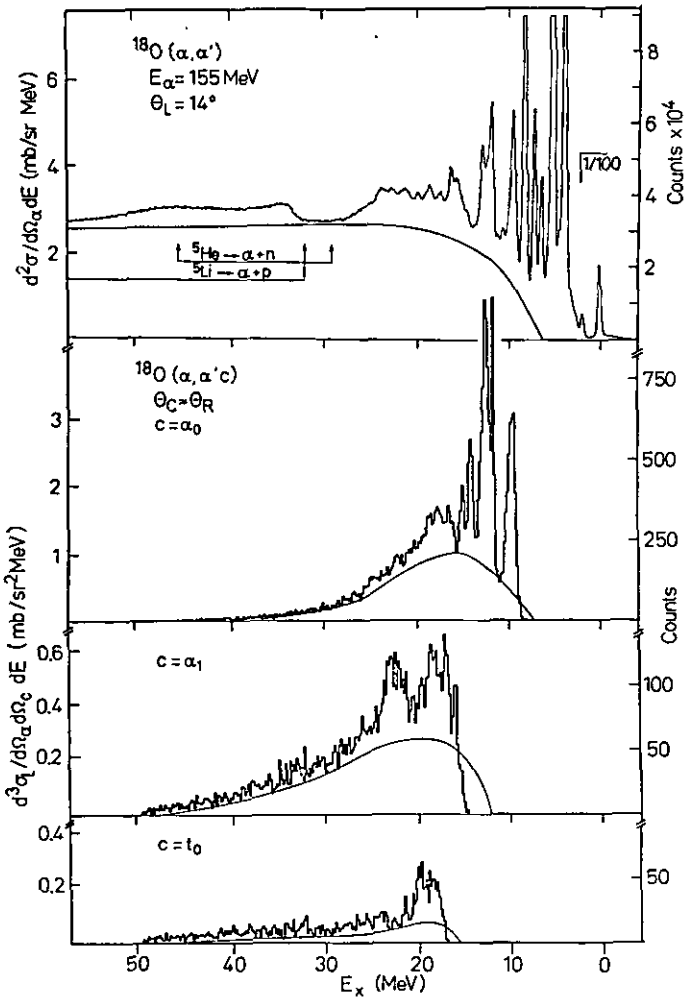

Figure 2: α-single spectrum of the $^{18}O(\alpha,\alpha')$ reaction (upper part). Corresponding coincidence spectra measured in recoil direction of the excited ^{18}O nucleus (lower part). The coincidence particle is marked by c. The solid lines show the assumed quasi-free contributions.

After subtracting a yield of apparently quasi-free scattering processes (solid lines in the coincidence spectra) we observe in both nuclei a dominant decay via the α channels. This is very similar to the result in ^{16}O [1], however in ^{16}O the strength in the α_1 channel is much larger than in the α_0 channel. In ^{15}N and ^{18}O the experimental yield in the α_0 channel exceeds the predicted yield in Hauser-Feshback calculations done with the code CASCADE[5]. This discrepancy is an indication for a direct process in this reaction. An additional hint to a direct decay process is the recoil-antirecoil asymetry in the angular correlation functions. An example for this asymetry is demonstrated in the case of ^{20}Ne in contribution (1.4.) of this annual report. For ^{15}N and ^{18}O the shapes of the angular correlation functions are very similar to those of ^{20}Ne. One can explain the asymetry by coherent mixing of different L values or contributions from quasi-free scattering in PWBA calculations. Here a L=3 admixture was necessary to fit the experimental data.

For the first time a triton yield was observed in the decay of giant resonances in light nuclei (Γ_t/Γ=10 %). ^{15}N is the only light nucleus (A<28) which shows comparable strength in the α- and p_0-channels. A more comprehensive analysis of the data is in progress.

References

1) K.T. Knöpfle, G.J. Wagner, P. Paul, H. Breuer, C. Mayer-Böricke, M. Rogge and P. Turek, Phys. Lett. 74B (1978) 191

2) H. Riedesel, K.T. Knöpfle, K. Schindler, G.J. Wagner, C. Mayer-Böricke, W. Oelert, M. Rogge and P. Turek, Contributed Paper to the Workshop on Nuclear Physics with Real and Virtual Photons, Bologna, 1980

3) G.J. Wagner, in Giant Multipole Resonances, ed. F.E. Bertrand (1980) 251

4) Jahresbericht MPI Heidelberg (1980) Art. 9.2.1.

5) F. Pühlhofer, Nucl. Phys. A217 (1977) 267

* MPI für Kernphysik, Heidelberg

** Inst. of Nucl. Research, Academia Sinica, Shanghai (VR China)

1.4. Charged Particle Decay of Excited States in ^{20}Ne and ^{22}Ne

C. Sükösd, K.T. Knöpfle**, C. Mayer-Böricke, H. Riedesel**, M. Rogge, K. Schindler**, P. Turek and G.J. Wagner***

The study and analysis of the charged particle decay of the excited states of ^{20}Ne and ^{22}Ne were continued. The ^{20}Ne(α,α'c) and ^{22}Ne(α,α'c) (c = charged particle) measurements were performed with the 155 MeV α-beam of the isochronous cyclotron JULIC. In the experiments two α'-telescopes situated at 13.5° symmetrically to the beam axis and eight decay telescopes were used. The gas-target window consisted of 2.4 μ thin Havar-foil, thinner than in the previous experiments[1] to decrease the effective detection threshold for the charged decay particles. For the coincidences the combination of the two α'-telescopes with the eight non-symmetrically positioned decay telescopes yielded 16 points for the angular correlation function. Also the energy resolution of the inelastically scattered α'-particles was improved to 400 keV.

On the kinematic map for the α-decay (fig. 1) the α_0 line can well be separated from the other reaction loci.

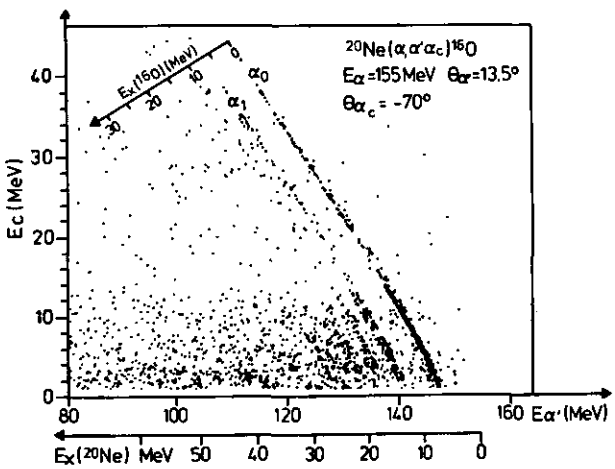

Figure 1: Map of the events in the plane of energy of scattered particles ($E_{\alpha'}$) and energy of decay-α's (E_C) for ^{20}Ne.

Although on the projection onto the ^{16}O axis (fig. 1) in some cases even the ($\alpha_1\alpha_2$) group could have been separated from the ($\alpha_3\alpha_4$) group, in the analysis these were treated together and in the followings they will be denoted as α_1 decay.

Comparison of the decay of ^{20}Ne and ^{22}Ne

Fig. 2 shows a comparison between the charged particle decays of the two Ne isotopes. In the upper part of the figure the spectra of the inelastically scattered α'-particles are shown. The giant resonance region is magnified as indicated. The two, well structured parts of the splitted GQR are clearly seen between 12 and 30 MeV in the excitation energy scale. The solid lines represent the assumed nonresonant physical continuum.

The lower part of the figure shows the summed spectra sorted according to the different charged particle decay channels. The summation includes all the measured 16

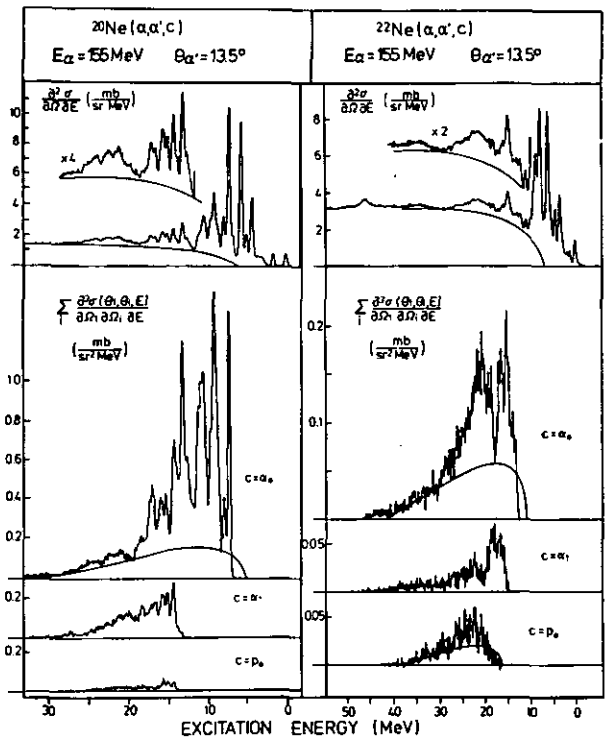

Figure 2: Comparison of energy-spectra of ^{20}Ne and ^{22}Ne measured in coincidence with decay-particles. In the upper part the corresponding singles-spectra are shown.

angle-points. The solid lines show the assumed quasi-free contributions calculated using PWIA approximation.

For both nuclei a dominance of the α_0 decay is evident. However, there are big differences in the absolute magnitudes of the corresponding cross-sections. This can be understood in terms of threshold effects, especially as a consequence of the neutron-alpha competition in the decay. Apart from structure effects this is mainly governed by the difference of the neutron and α-particle emission shreshholds: B_n and B_α. B_n-B_α is 12.135 MeV for the ^{20}Ne and it is only 0.7 MeV for the ^{22}Ne. The Coulomb-barrier practically doesn't influence the competition in the case of ^{20}Ne but it may reduce the alpha emission probability

in the favour of the neutron emission in the case of ^{22}Ne.

The p_0 decay channel of ^{20}Ne

In the yield for the p_0 decay (fig. 2) a quasi-free scattering (QFS) contribution is possible. Only in the lower energy part of the giant resonance, around 16 MeV excitation energy emerges a small resonant part, indicated by the structure in this bump; but in the anti-recoil direction it cannot be seen any more because the particles were stopped in the gas-target window due to their lower laboratory energy in this direction. Because of the poor statistics the only possible statement is that the main features of the spectrum can be well described by a QFS model, and all other reaction types - although present - play only a minor role.

The α_0 decay-channel of ^{20}Ne

Much more interesting is the α_0 decay channel (fig. 2). The spectrum is rich in structures. Angular correlation functions were extracted for 12 excited states (fig. 3). The most striking characteristics of them is the increasing forward-backward asymmetry and the decreasing half-width of the angular correlation functions with increasing excitation energy.

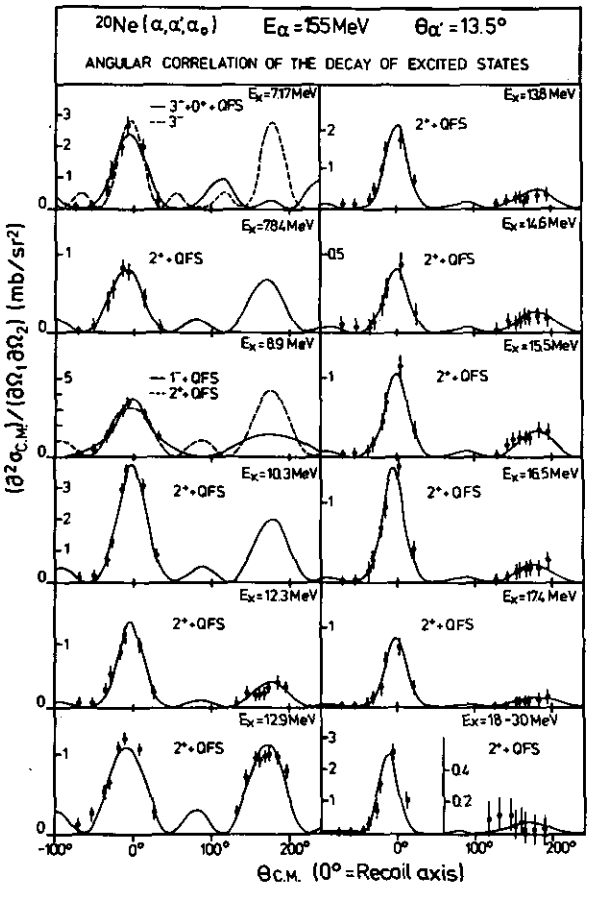

Figure 3: Angular correlation functions for some excited 2^+-states in ^{20}Ne which decay to the ground state in ^{16}O. The curves are fits with coherent amplitudes for L=2 excitation and quasifree scattering according to eq. 1.

At 12.9 MeV excitation energy there is a state that was thought to have monopole character on the basis of our previous measurements[1,2]. Now, due to the more extended angular range it turned out that it has a quite pure L=2 angular correlation function with a half-width of about 50^0 and with practically no asymmetry.

It was shown[2,3], that for explaining asymmetries in the angular correlation functions mixed multipolarities of different odd-even parities are needed. Generally some contributions of 3^- or 1^- to the dominant 2^+ multipolarity were used[4]. In our case it turned out however, that for explaining the observed asymmetry and the small half-width at least 5^- contributions would be needed. Instead of mixing two pure multipolarities, our idea was to explain it in terms of coherent interference between the dominant L=2 excitation and the quasi-free scattering present everywhere in the studied excitation energy range. This latter has no fix multipolarity but it is delocalised in the angular momentum space. This delocalisation was determined by developing the angular dependent part of the quasi-free scattering amplitude in spherical functions. Then the measured angular correlation points were fitted using the function:

$$W_{exp}(\theta) = S \cdot (\sin\delta \cdot \sqrt{\frac{5}{4\pi}} \cdot P_2(\cos\theta) + \cos\delta \cdot \Psi_{QFS}(\theta))^2 \qquad \text{eq.1}$$

Here the δ is the mixing angle for the two interfering reactions and S is related to the angular integral of the angular correlation functions. Fig. 3 shows the fits to the experimental points (solid lines).

Also in the α_1 decay channel we observed a quasi-free scattering contribution. Because the α_1,α_2 and α_3,α_4 decays could not be separated in the experiment the theoretical treatment of these angular correlation functions is hardly possible and so only very few physical informations can be extracted.

The detailed analysis of the data for $^{20,22}Ne$ will be presented elsewhere[5].

References

1) C. Sükösd et al., Annual Report IKP, KFA Jülich, Jül-Spez-72, p. 4
2) K.T. Knöpfle, Lecture Notes in Physics 108, 317
3) K.T. Knöpfle, Habilitationsarbeit (1980) 50 (unpublished)
4) K.T. Knöpfle et al., Phys. Lett. 74B (1978) 191
H. Riedesel et al., Phys. Rev. Lett. 41 (1978) 377
5) C. Sükösd, K.T. Knöpfle, C. Mayer-Böricke, H. Riedesel, M. Rogge, K. Schindler, P. Turek and G.J. Wagner, to be published.

* IKP der KFA, now at Eötvös University, Budapest

** MPI für Kernphysik, Heidelberg

1.5. Splitting of the Giant Monopole Resonance in Actinide Nuclei

H.P. Morsch, M. Rogge, P. Turek, C. Mayer-Böricke

Recent studies of the giant monopole resonance in heavy nuclei[1] have been continued by investigating α scattering from ^{232}Th and ^{238}U. To disentangle giant monopole (GMR) and giant quadrupole (GQR) resonances[2] measurements have been performed at 100 and 172 MeV. Because contaminations of H, C and O could not be avoided in the targets for most of the angles measured contaminant spectra have been taken which have been substracted from the Th and U spectra. These are given in fig. 1. No contamination was

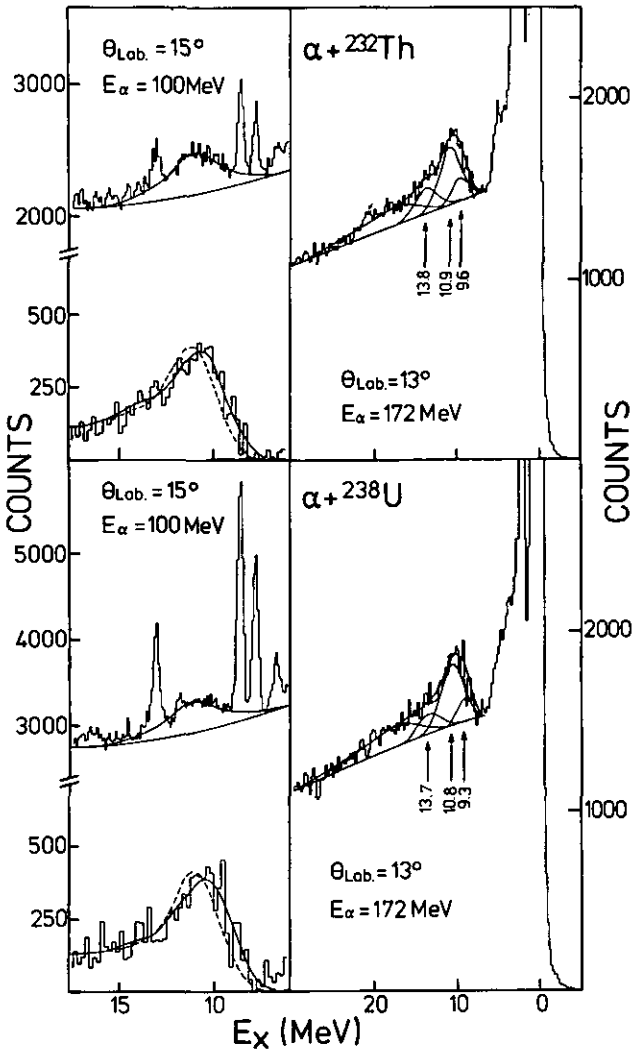

Figure 1: Spectra of 100 and 172 MeV α scattering from ^{232}Th and ^{238}U. Background and fits to the giant resonances are indicated. Left bottom parts: giant resonance peak (from the right hand spectra) after background subtraction.

substracted in the 100 MeV spectra displayed. At the lower incident energy a quite symmetric giant resonance bump is observed (see also ref. 3) which is mainly due to L=2 excitation. In contract, an asymmetric form of the giant resonance peak is found at 172 MeV. Further, the maximum of the resonance peak is about 600 keV lower in excitation energy than the giant resonance peak in the 100 MeV spectra. This is clearly seen on the left hand side of fig.1. Such effects have not been observed for the other nuclei studied previously[1]. As a consequence of this fact in a first fit of the giant resonance peaks no good description of the 172 MeV data is obtained (dashed lines in fig. 1). In this analysis four Gaussian peaks (as in ref. 4) are assumed for GQR, GMR and the new giant resonances found recently[4]. Only if we assume a splitting of the monopole resonance into two peaks, one below and one above the GQR, a good fit to the data (solid fit lines in fig. 1) is obtained. Energies and widths (except for the bump at $E_x \sim 20$ MeV) are given in table 1. Fig. 2 shows the differential cross sections in comparison with microscopic DWBA calculations.

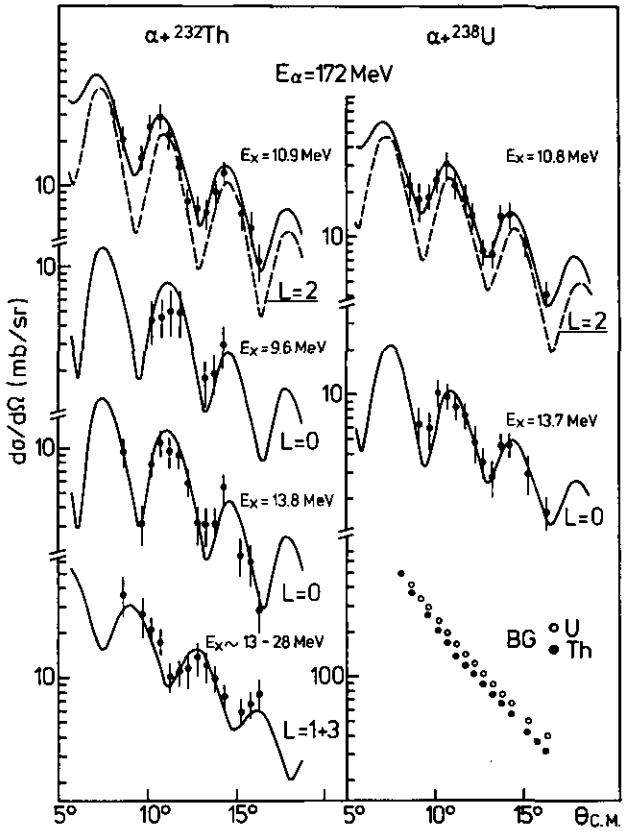

Figure 2: Differential cross sections and DWBA calculations. The angular dependence of the background in the region of the GQR is shown in the right bottom part.

The angular distributions for the GQR show more pronounced structure than found for ^{208}Pb [5]. They are well described by a mixture of L=2 and 4 excitation with strengths given in table 1. Although the width of the GQR is larger

	E_x (MeV)	Γ (MeV)	L	S(% EWSR)
^{232}Th	9.6±0.3	2.3±0.3	0	28
	10.9±0.3	3.0±0.4	2,4	62,10
	13.8±0.4	3.0±0.5	0	66
^{238}U	9.3±0.3	2.0±0.3	0	30
	10.8±0.3	3.0±0.4	2,4	66,10
	13.7±0.4	3.0±0.5	0	65

Table 1: Resonance parameters and sum rule strengths for L=0, 2, 4 excitations. The L=0 strengths are obtained using a transition density similar to ρ_{TR3} in ref. 5.

than in the case of ^{208}Pb no L=6 (or L=3) component was needed to fit the data. This may indicate that due to deformation effects in the present cases the higher multipole strength is strongly spread in energy and therefore contributes mainly to the substracted background.

The angular distributions of the other resonances in table 1 are consistent with the assumption of L=0 excitations. The additional component with E_x<10 MeV has the same features as the high energy monopole resonance: its strength is very small in the 100 MeV fits but contributes significantly to the 172 MeV data. The sum rule strengths for both L=0 excitations (table 1) exhaust about the same monopole strength as found for ^{208}Pb. These facts indicate a splitting of the monopole excitation in Th and U. Such features of the GMR in deformed nuclei have been predicted by microscopic calculations[6,7]. They can be understood as mixing of GQR and GMR.

References

1) H.P. Morsch, M. Rogge, P. Turek, C. Sükösd, C. Mayer-Böricke, Annual Report 1979, KFA-IKP Jülich, Jül-Spez-72 (1980), p. 8

2) H.P. Morsch, M. Rogge, P. Turek, C. Sükösd, C. Mayer-Böricke, Phys. Rev. C20, 1600 (1979)

3) M. Harakeh, H.P. Morsch, K.v.d.Weg, A.v.d.Woude and F.E. Bertrand, Phys. Rev. C21, 768 (1980)

4) H.P. Morsch, M. Rogge, P. Turek and C. Mayer-Böricke, Phys. Rev. Lett. 45, 337 (1980)

5) H.P. Morsch, C. Sükösd, M. Rogge, P. Turek, H. Machner and C. Mayer-Böricke, Phys. Rev. C22, 489 (1980)

6) D. Zawischa, J. Speth and D. Pal, Nucl. Phys. A311, 445 (1978)

7) Y. Abgrall, B. Morand, E. Caurier, and B. Grammaticos, Proc. International Conference on Nuclear Physics, Berkeley, 1980, p. 174

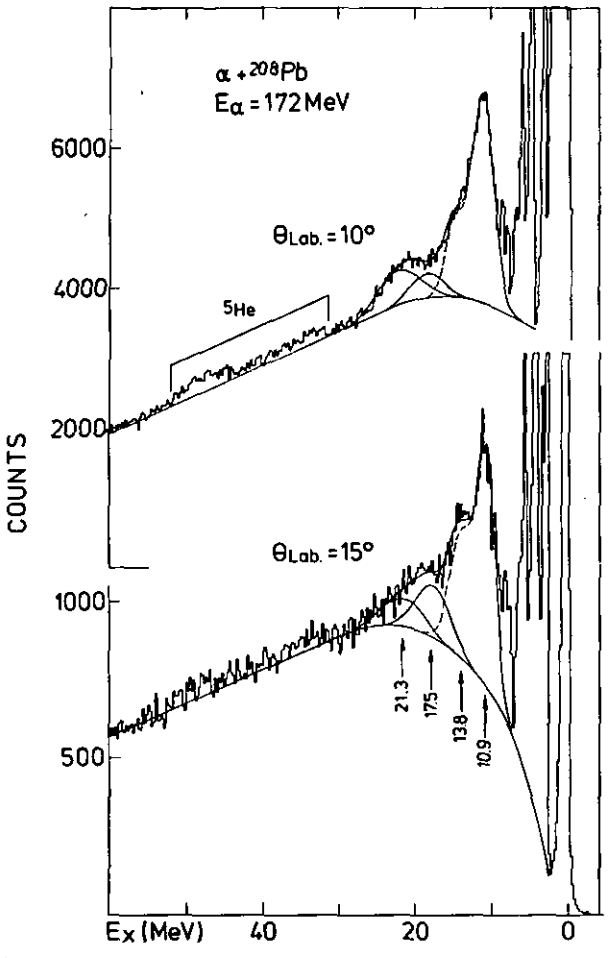

Figure 1: Spectra of 172 MeV α scattering from ^{208}Pb. The background lines and fits to the giant resonances are indicated. The dashed lines represent the sum of GMR and GQR.

1.6. Evidence for New Giant Resonances in Heavy Nuclei

H.P. Morsch, M. Rogge, P. Turek, C. Mayer-Böricke

Within a systematic study of giant resonances in heavy nuclei[1] the region above the giant monopole resonance (GMR) has been investigated. The ^{208}Pb spectra in fig. 1 indicate broad structures extending from the GMR up to about 28 MeV of excitation. This region was analysed in our spectra by assuming a background as indicated in fig. 1. As clearly seen in the figure a different shape of the high energy bump is observed at different scattering angles, this indicates the excitation of more then one resonance. A consistent fit to the data is obtained by assuming two resonances at E_x = 17.5 ± 0.8 MeV and E_x = 21.3 ± 0.8 MeV. Differential cross sections are given in fig. 2. They show quite pronounced structure which indicate excitations of rather pure multipolarity. The lines in fig. 2 represent results of microscopic DWBA calculations which are discussed in more detail in refs. 2,3. The data for the 17.5 MeV resonance are well described assuming L=3 excitation with a strength of 60 % of the EWSR strength. This is in good agreement with (e,e') results[4]. The excitation of the 21.3 MeV resonance was interpreted assuming an isoscalar giant dipole resonance. This is considered as a compressional mode of excitation (squeezing mode) which is related to the nuclear breathing mode (GMR). Assuming a transition density as discussed in ref. 3 the cross sections in fig. 2 correspond to 90 % of the EWSR for isoscalar dipole excitation. It should be noted that a collective isoscalar 1^- excitation was predicted by ref. 5 close to the excitation energy of the high lying resonance at 21.3 MeV.

Fig. 2 shows also the cross sections for the resonance at E_x = 13.8 MeV analysed with the new background form in fig. 1. As compared to the analysis in ref. 6 the cross section is increased and shows a less pronounced diffraction pattern. These differences can be explained assuming a small contribution of higher multipolarity (L=4, 3.5 % EWSR; L=6, 6 % EWSR).

Clear evidence for the existence of the high lying giant resonances is obtained also for other heavy nuclei. The spectra from ^{232}Th and ^{238}U (shown in sect. 1.5.) indicate these high lying excitations. Similar to the case of Pb the spectra taken at different angles show that the high lying bump consists of more then one resonance. The angular distribution (see fig. 2 in sect. 1.5.) is consistent with a sum of L=3 and 1 excitation exhausting about 45 and 90 % of the corresponding EWSR strength.

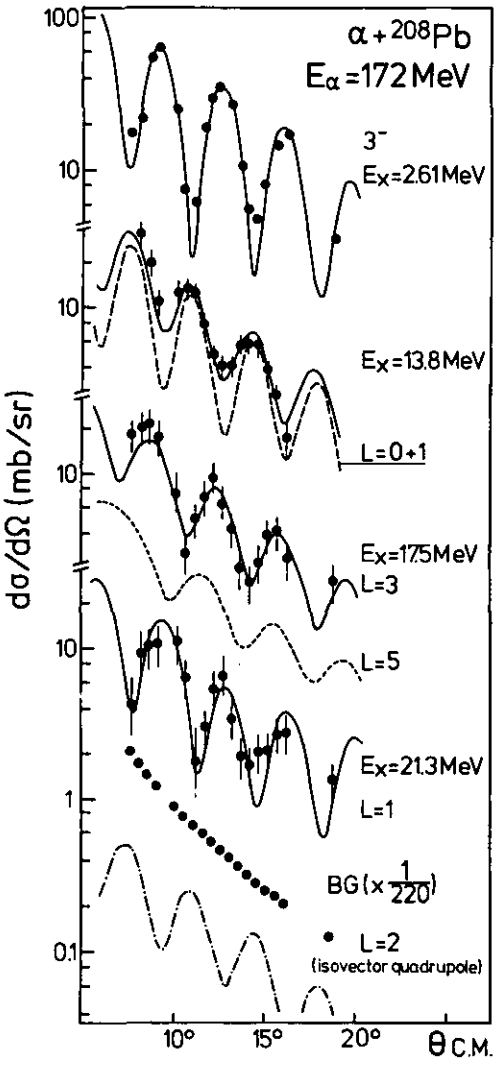

Figure 2: Differential cross sections for excitation of the 3^- state at 2.61 MeV, the GMR and the new high lying giant resonances in comparison with DWBA calculations. Also the angular dependence of the background under the new resonances is given. The dot-dashed line indicates the estimated cross section (ref. 2) for excitation of the isovector giant quadrupole resonance ($E_x \sim 23$ MeV).

References

1) H.P. Morsch, M. Rogge, P. Turek, C. Sükösd, C. Mayer-Böricke, Annual Report 1979, KFA-IKP Jülich, Jül-Spez-72 (1980), p. 8

2) H.P. Morsch, M. Rogge, P. Turek, C. Mayer-Böricke, Phys. Rev. Lett. 45, 337 (1980)

3) H.P. Morsch, P. Decowski, Phys. Lett. 95B, 160 (1980)

4) M. Nagao and Y. Torizuka, Phys. Rev. Lett. 30, 1068 (1973)

5) J. Wambach, V. Klemt, and J. Speth, Phys. Lett. 77B, 245 (1978)

6) H.P. Morsch, C. Sükösd, M. Rogge, P. Turek, C. Mayer-Böricke, Phys. Rev. C22, 489 (1980)

1.7. Small Angle Measurements of α Scattering from ^{208}Pb

H.P. Morsch, S.A. Martin, G.P.A. Berg, J. Meissburger, M. Rogge, P. Turek, C. Sükösd, J. Reich

To study giant resonances at low momentum transfer we started small angle scattering experiments using the magnetic spectrograph Big Karl. The 172 MeV α beam was used for these experiments. This yields strong excitation[1] of giant resonances. The beam analysing system was run in the achromatic mode, midplane and exit slits of the monochromator were used to clean up the beam. In first test runs we were able to measure to forward angles as low as 1.4^0. Below 2^0 the background was increasing, so more efforts have to be made to obtain good results in this extreme small angle region. A spectrum of the giant quadrupole region taken at 3.4^0 is shown in fig. 1. The arrows indicate the position of giant quadrupole (E_x = 10.9 MeV) and monopole excitation (E_x = 13.8 MeV). Also the structure at 9.3 MeV.[2] is quite strongly excited. Apart from a study of these excitations in the small angle region the new giant resonances[3] (L=3 and 1) are of particular interest. They should exhibit large differences in the angular region below 3^0.

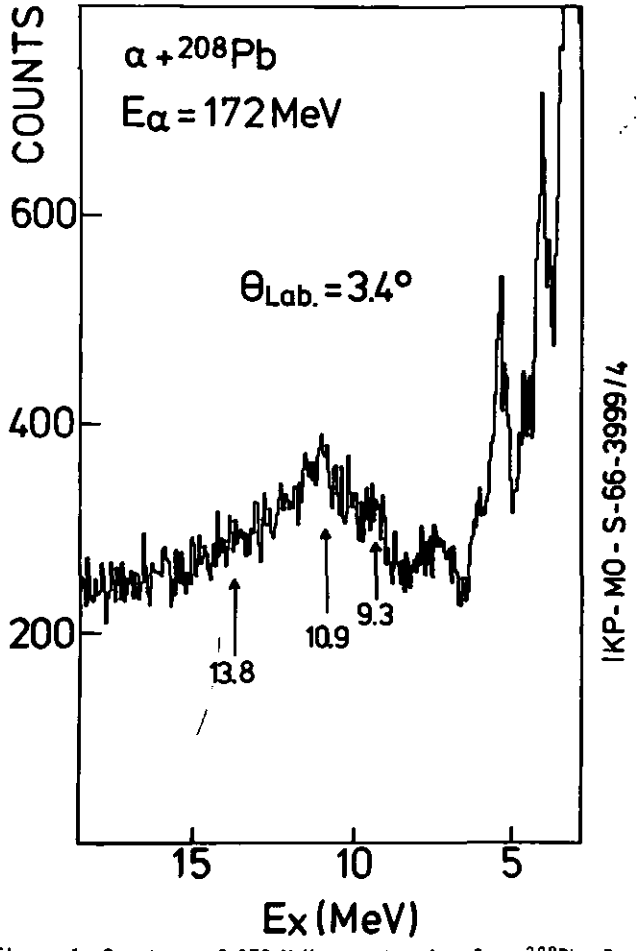

Figure 1: Spectrum of 172 MeV α scattering from ^{208}Pb. Positions of giant quadrupole, giant monopole resonances and the structure at 9.3 MeV are indicated.

References

1) H.P. Morsch, M. Rogge, P. Turek, C. Sükösd and C. Mayer-Böricke, Phys. Rev. C20, 1600 (1979)

2) H.P. Morsch, P. Decowski and W. Benenson, Phys. Rev. Lett, 263 (1976) and Nucl. Phys. A297, 317 (1978)

3) H.P. Morsch, M. Rogge, P. Turek, C. Mayer-Böricke, Phys. Rev. Lett. 45, 337 (1980)

1.8. Coulomb Excitation of the Giant Dipole Resonance in Hadron Scattering

P. Decowski and H.P. Morsch

Recently strong efforts have been made to study the excitation of giant resonances in hadron scattering at small momentum transfer. This allows to distinguish between giant monopole and quadrupole excitation. In heavy nuclei the excitation energy of the giant monopole resonance coincides with that of the isovector giant dipole resonance (GDR). This raises the question to which extend the GDR is excited in hadron scattering. The nuclear excitation of the GDR is usually quite weak[1], however, in small angle experiments Coulomb excitation could be of large importance. This is supported by recent estimates[2] which suggest that Coulomb excitation of the GDR may be the dominant contribution to small angle spectra in the giant resonance region for different scattering systems.

There are problems in calculating Coulomb excitation of dipole type in the standard DWBA codes. The form factor falls off quite slowly to large distances. This requires a computation up to large radii. Further the cut-off (even at large radii) gives rise to convergence problems in the calculation of differential cross sections. Typical examples for differential cross sections calculated by the DWBA program DWUCK are shown in fig. 1 by dashed (dot-dashed) lines using 130 (100) and 90 (70) partial waves for α and ^{3}He scattering, respectively.

In order to take into account the integration of the Coulomb excitation up to infinity and to avoid cut off problems we made calculations using analytic forms of the Coulomb integrals[3]. In practice this was done by calculating DWBA scattering amplitudes up to a cut-off radius of 25 fm. Coulomb correction terms were added which approximate the integral from the cut-off radius up to infinity. The results given by the solid lines in fig. 1 yield smooth angular distributions. The absolute cross sections are fixed by the energy weighted sum rule. The forward angle cross sections for ^{3}He and α scattering with energies of about 100 MeV are of the order of 1 mb/sr. This is much lower than the experimental cross sections[4] indicating that at these energies the giant monopole resonance is excited dominantly. Cross sections for α scattering at different incident energies are given in fig. 2. The small angle cross sections increase rapidly with incident energy. This may indicate that Coulomb excitation of the GDR may be the dominant process at high incident energies.

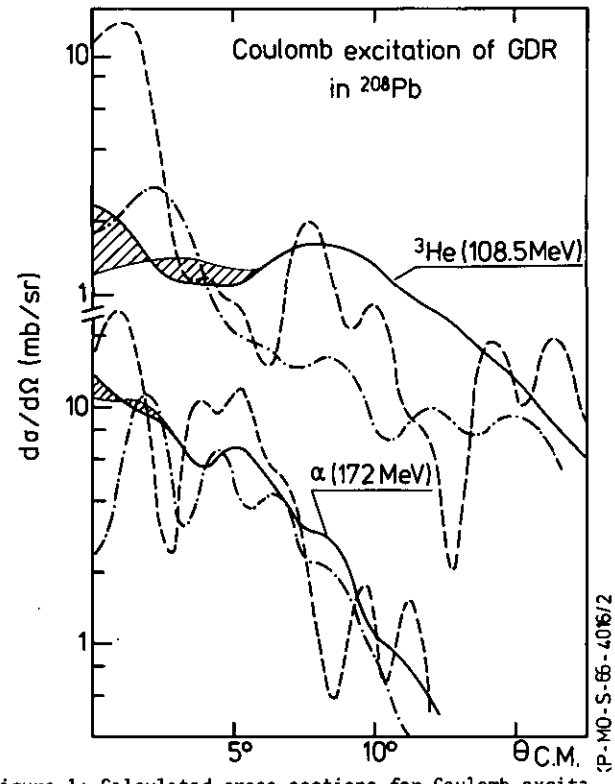

Figure 1: Calculated cross sections for Coulomb excitation of the GDR in ^{3}He and α scattering from Pb. The shaded areas show the change of cross section by using different numbers of partial waves as in the case of broken lines.

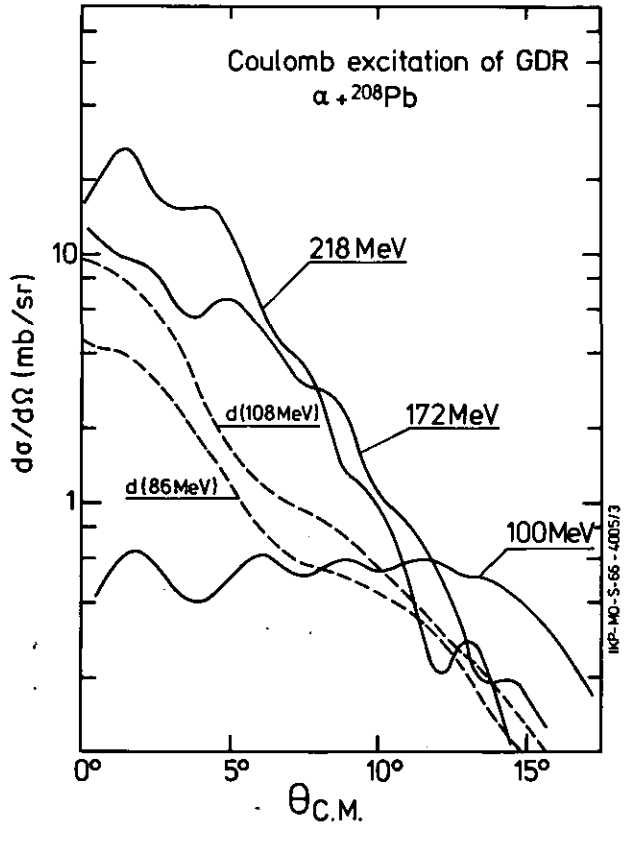

Figure 2: Differential cross sections for Coulomb excitation of the GDR in α and d scattering from Pb.

References

1) H.P. Morsch and P. Decowski, Phys. Lett. 95B (1980) 160
2) C. Djalali et al., Z. Phys. A298 (1980) 79
3) H. Lenske, Ph.D.Theses, Jül-Spez-47, 1979
M. Abramowitz and A. Segun, "Handbook of Mathematical Functions", Dover Publications, N.Y., 1968
4) D.H. Youngblood et al., Phys. Rev. Lett. 39 (1977) 1188
M. Buenerd et al., Phys. Lett. 84B (1979) 305

1.9. Giant Resonances Observed in α Induced Fission of ^{238}U

H.P. Morsch, M. Rogge, C. Stüböd, H. Machner, P. David, J. Debrus*, H. Janßen* and J. Schulze**

In recent scattering experiments at different laboratories the decay of the giant quadrupole resonance (GQR) into the fission channel was investigated[1-4]. Although the interpretation of the data is controversial, no significance of fission decay of the GQR is observed in the coincidence spectra. To investigate the fission decay of giant resonances in actinide nuclei α induced fission was measured at an incident energy of 172 MeV. At this energy giant resonances are stronger excited than at lower incident energies, so more definite results on the fission decay of giant resonances are expected. Inelastic α particles were detected at an angle of 13^0. Coincident with these inelastic events fission products were measured at angles of -75^0 (recoil axis for $E_x \sim 11$ MeV), -100^0, -120^0, -140^0, -165^0 in plane and 90^0 out of plane. A strong peak at about B_f is observed at angles close to the recoil axis which is due to threshold effects, further smaller peaks above B_{nf} and B_{2nf} which are due to second and third chance fission (see fig. 1). In addition to these sharp

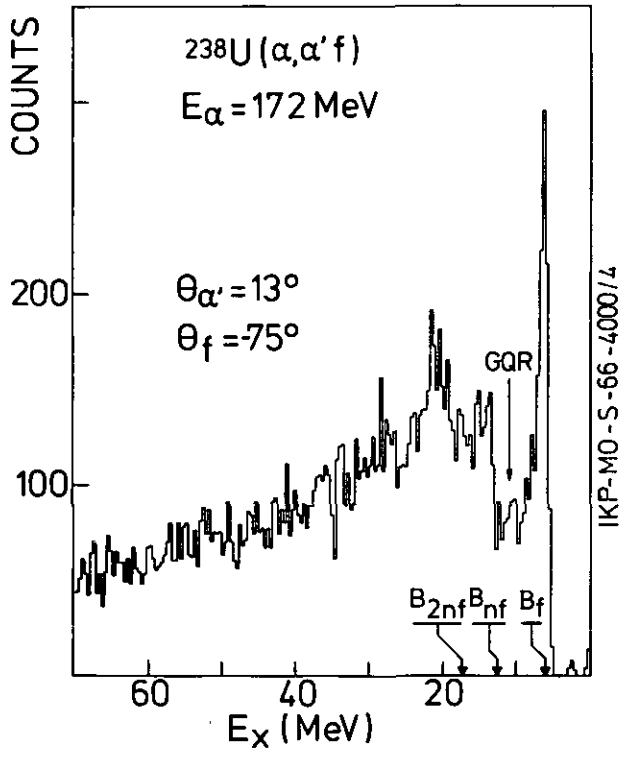

Figure 1: Spectrum of 172 MeV α scattering in coincidence with fission decay in recoil axis (for E_x = 11 MeV).

structures a broad bump is observed which extends from B_{nf} up to about 28 MeV of excitation. This coincides with the high energy bump in the singles spectra (see fig. 1 in sect. 1.5.) which is due to excitation of new giant resonances[5]. In contrast to these excitations which are seen quite strongly in the fission decay there is only weak evidence for the fission decay of the GQR (E_x = 10.8 MeV). This may indicate that the GQR has quite different decay properties than the new giant resonances[5].

References

1) J. v. d. Plicht, M.N. Harakeh, A. v. d. Woude, P. David and J. Debrus, Phys. Rev. Lett. 42, 1121 (1979)

2) A.C. Shotter, C.K. Gelbke, T.C. Awes, B.B. Back, J. Mahoney, T.J.M. Symons, and P.K. Scott, Phys. Rev. Lett. 43, 569 (1979)

3) E.E. Gross, J.R. Beene, C.E. Bemis, F.E. Bertrand and W.P. Jones, Proc. Int. Conf. Nuclear Physics, Berkeley, 1980, p. 208

4) D.H. Dowell, L.S. Cardman, P. Axel, G. Bolme and S.E. Williamsson, Proc. Int. Conf. Nuclear Physics, Berkeley, 1980, p. 221

5) H.P. Morsch, M. Rogge, P. Turek, C. Mayer-Böricke, Phys. Rev. Lett. 45, 337 (1980)

*Institut für Strahlen- u. Kernphysik, Univ. Bonn

1.10. Isoscalar Transition Rates in $^{14,15}N$ and $^{17,18}O$

Ph. Gerhardt, P. Grabmayr*, K.T. Knöpfle*, Liu Ken Pao**, G. Mairle*, C. Mayer-Böricke, W. Nitsche*, W. Oelert, H. Riedesel*, M. Rogge, K. Schindler*, H.R. Schmidt*, A. Stuirbrink*, C. Sükösd, G.J. Wagner**

Collective excitations of the target nuclei $^{14,15}N$ and $^{17,18}O$ were studied at the Jülich cyclotron by inelastic scattering of 155 MeV alpha particles[1,2]. Isoscalar transition rates were extracted by comparing the experimental angular distributions to DWBA calculations using collective form factors. The relevant optical potential parameters were obtained by analyzing the elastically scattered alpha particles. The ratio of the matrix element for protons and neutrons could be determined by comparison to electro-magnetic transition rates for deep lying states. For quadrupole transitions the values of this ratio exceed the (in a collective model[3]) theoretically expected values N/Z in all nuclei with neutron excess. In the excitation energy range of the giant resonance dominant E2 strength was found in all nuclei, see Fig. 1. Between 30 and 60 % of the energy-weighted isoscalar sum-rule strength was found. The shape of the energy spectra changes with reaction angle in the region of the giant resonance, suggesting contributions from different multipolarities. In fact, for some resolved fine structure peaks E3-strength could be observed as can be seen in the figure.

References

1) Annual Report MPI Heidelberg (1976) 91
2) See also H.R. Schmidt, Staatsexamensarbeit, Heidelberg (1980)
3) A.M. Bernstein, V.R. Brown and V.A. Madsen, Phys. Lett. 71B (1977) 48

* MPI Heidelberg

** Institute of Nuclear Research, Academia Sinica, Shanghai (VR China)

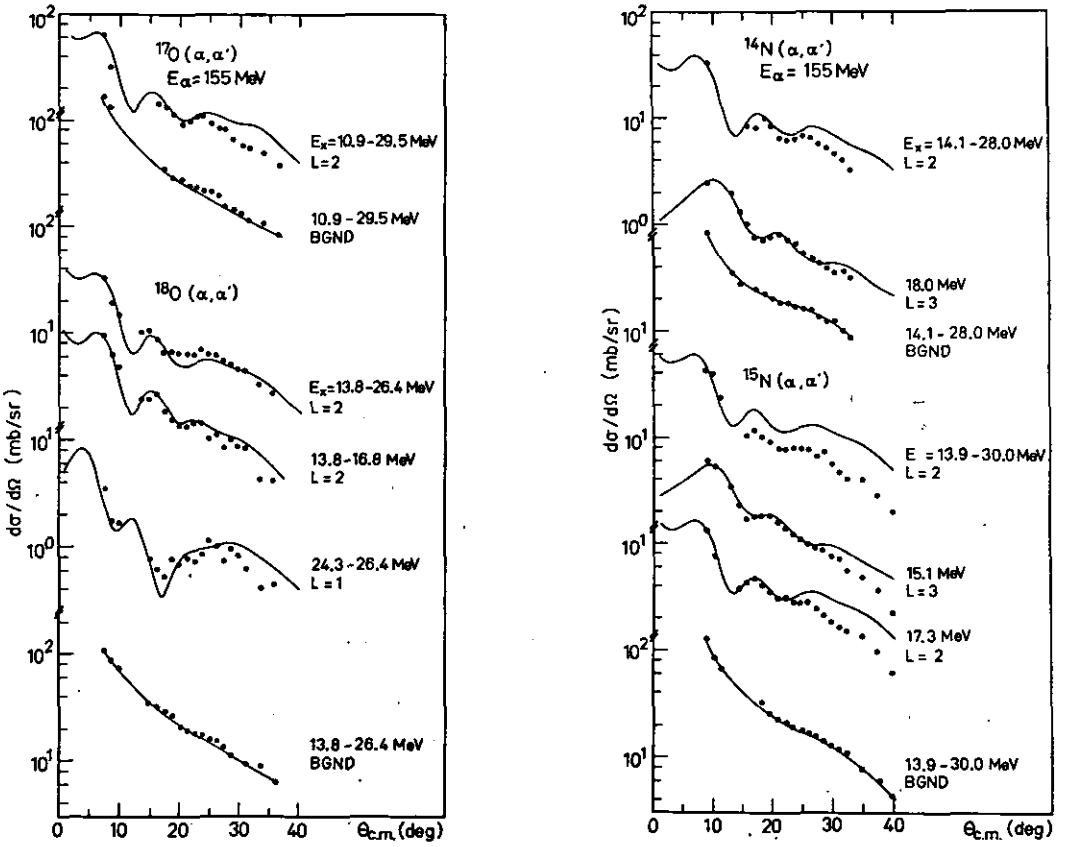

Figure 1: Experimental and DWBA-theoretical angular distributions for alpha inelastic scattering to final states and to excitation energy regions in the range of the giant resonance.

1.11. Continuous Spectra of Protons and Deuterons from the α+α Interaction at E_{inc} = 110 - 172 MeV

G. Paić, B. Antolković*, A. Djaloeis, J. Bojowald and C. Mayer-Böricke*

Analysis of the continuous spectra of protons and deuterons from the α+α interaction at E_{inc} = 110 - 172 MeV has been completed. The experimental spectra have been compared with the predictions of the Fermi statistical partition model[1]. At each angle the absolute and relative magnitudes of contributing n-body final state components have been extracted. The theoretical curves obtained are shown together with the experimental spectra in Figs. 1 and 2.

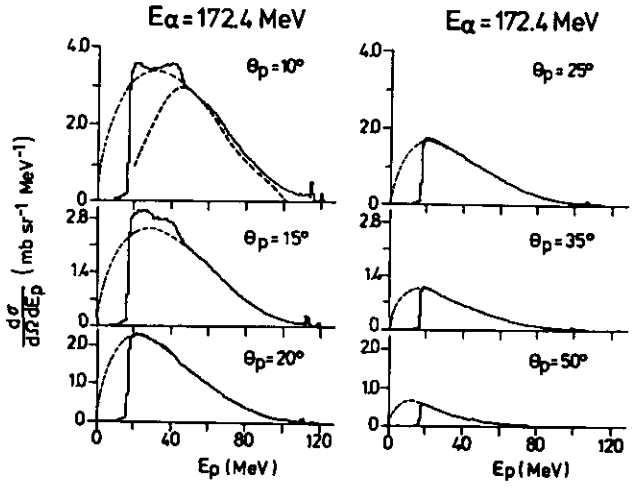

Figure 1: Inclusive proton spectra from α+α interactions measured at different angles at E_α = 172.4 MeV. The thin dashed curves represent the fits obtained applying the Fermi statistical partition model. The thick dashed curve represents the prediction of the Serber mechanism for a three-body final state. The structures at low energies at 10° and 15° are due to the sequential processes involving the formation and decay of ^{5}Li.

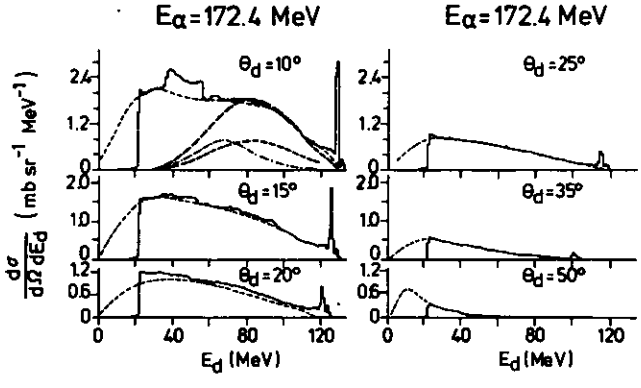

Figure 2: Inclusive deuteron spectra from α+α interactions measured at different angles at E_α = 172.4 MeV. The thin dashed curves represent the fits obtained applying the Fermi statistical partition model. The thick dashed curve represents the prediction of the Serber mechanism for a three-particle final state (that curve is represented with two different normalizations); the dot-dashed curve represents the same prediction when a four-body final state is assumed. The structures at low energies at 10°, 15° and 20° are due to the sequential processes involving the formation and decay of ^{6}Li.

To test for the possible contribution of a quasifree breakup to the continuum, some theoretical spectra have been calculated in the framework of the Serber[2] mechanism. The spectra are shown for θ = 10° at E_α = 172.4 MeV (Figs. 1 and 2) where the contribution of such a mechanism is expected to be the largest[3].

In the case of the deuteron spectrum, the theoretical energy distributions were calculated assuming, both three and four particles in the final state. The curves obtained are shown in Figs. 1 and 2.

From the comparison of the continuum part of the proton and deuteron experimental spectra with the predictions of the applied model it is visible that the Fermi statistical partition model gives a very satisfactory agreement to the overall shape of the spectra. However, at forward angles the p and d spectra exhibit an enhancement above the theoretical prediction of the Fermi partition model at $50 \leq E_p \leq 80$ MeV and at $60 \leq E_d \leq 80$ MeV, respectively. As shown by the theoretical curves calculated using the Serber mechanism one cannot rule out a small contribution from this mechanism.

The experimental angular distributions for different breakup modes are given in Figs. 3 and 4. The differential cross sections indicate that, according to the Fermi partition model, the process is not purely isotropic in the center of mass system. The theoretical cross sections calculated from the Fermi partition model (assuming isotropy in the c.m. system) are shown for two modes of decay in Fig. 4. It is visible that the fits of the model for the angular distributions are much less satisfactory than in the case of the spectral shapes. The agreement in the shape of the spectra can be understood under the assumption that anisotropy in the center of mass does not affect the spectral shape too much. It is also necessary to say that isotropy is not a requirement of Fermi's model, as it was pointed out by Hagedorn[4]. The isotopry was introduced only to make the calculations possible at this stage.

The agreement between the data and the Fermi statistical partition model indicates that:

(i) the emitted particle forming the continuous spectra mainly stem from processes involving very low partial waves, and furthermore,

(ii) the colliding system at these low partial waves appears to form a fused system allowing total energy sharing among all participating particles, followed by an explosion in the available phase space.

For reactions among light nuclei, this mechanism which has already been extensively used in high energy physics[4], therefore constitutes an important supplement to the peripheral phenomena involved in two-body or quasi two-body processes[5-8] which usually include only higher partial waves of the relative motion of the particles in the incident channel.

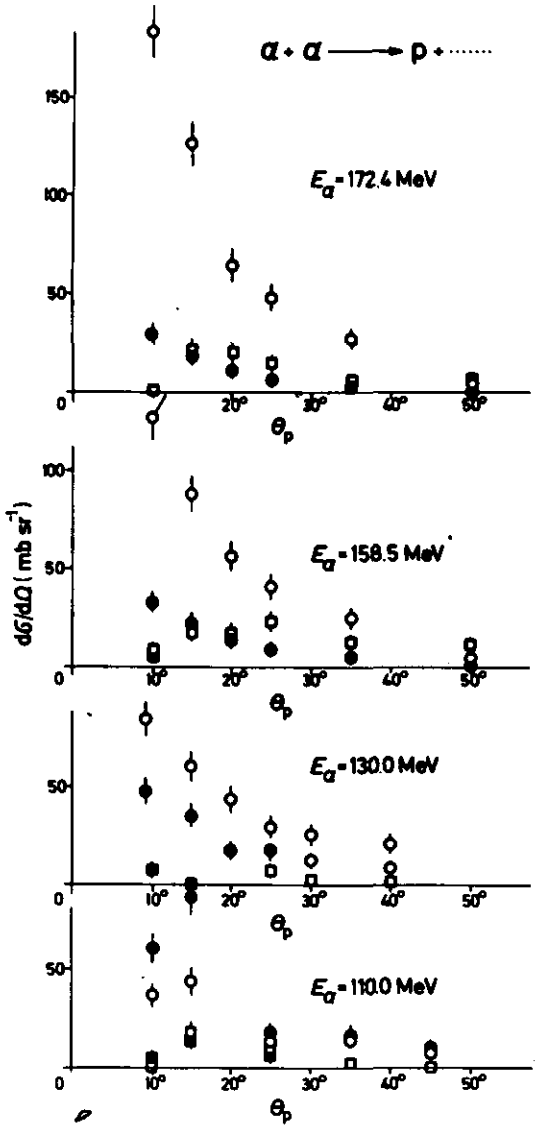

Figure 3: Experimental angular distributions for different breakup modes at different energies extracted by applying the Fermi statistical partition theory to the proton inclusive spectra. The dots denote the ptα mode, the circles the pdnα, the solid squares the pn $^6Li_{2.18}$ mode, the open squares the more complicated breakup modes (more than four fragments in the final state).

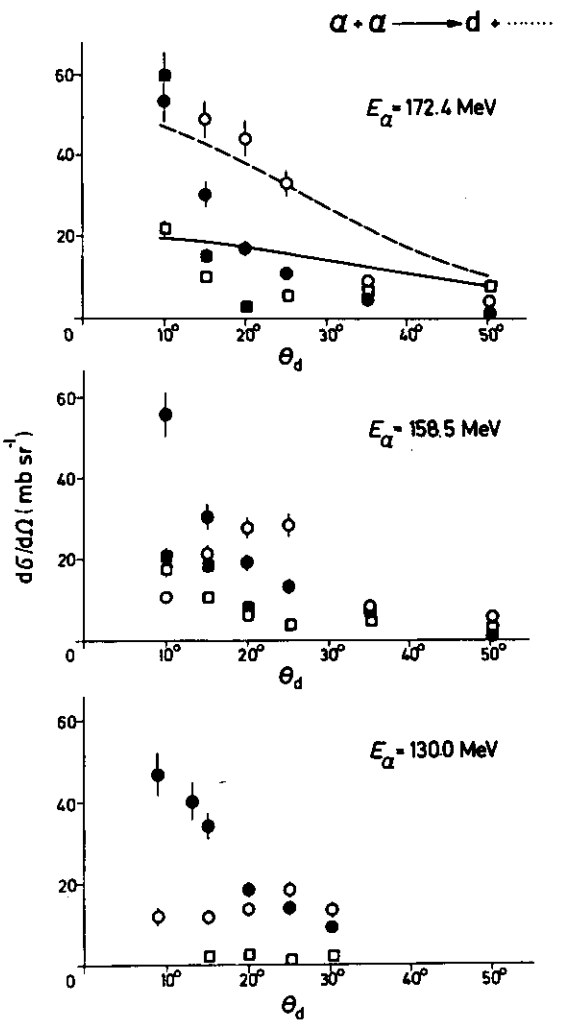

Figure 4: Same as Fig. 3 but for the deuteron spectra. The dots denote the ddα mode, the circles the dpnα mode, the solid squares the dt^{3}He mode and the open squares the more complicated breakups. The full and dashed lines show the expected distribution from the Fermi statistical partition model for the ddα and dpnα breakup modes, respectively.

References

1) E. Fermi, Progr. Theor. Phys. 5 (1950) 570

2) R. Serber, Phys. Rev. 72 (1947) 1008

3) J.R. Wu, C.C. Chang, H.D. Holmgren, and R.W. Koontz, Phys. Rev. 20C (1979) 1284

4) R. Hagedorn, Il Nuovo Cimento, Vol. XV, No. 3, (1960) 434

5) T. Sawada, G. Paić, M.B. Epstein and J.G. Rogers, Nucl. Phys. A141 (1970) 169

6) G. Paić, J.C. Young and D.J. Margaziotis, Phys. Lett. 32B (1970) 437

7) C. Alderliesten, A. Djaloeis, J. Bojowald, C. Mayer-Böricke, G. Paić and T. Sawada, Phys. Rev. C18, (1978) 2001

8) A. Djaloeis, J. Bojowald, C. Alderliesten, C. Mayer-Böricke, G. Paić and Z. Bajzer, Nucl. Phys. A273 (1976) 29

*Institute Rudjer Bošković, Zagreb, Yugoslavia

1.12. Investigation of the Reaction $^{13}C(p,\alpha)^{10}B$ for Proton Energies from 22.5 to 45 MeV

S.E. Abdel Kariem, F. Weng*, G. Staudt**

Recent studies[1] of few nucleon transfer reactions on light nuclei have been continued by investigating the reaction $^{13}C(p,\alpha)^{10}B$ up to an excitation energy of about 6 MeV. The experiments were performed with the proton beam of the isochronous cyclotron JULIC. Both solid state and gas targets (methane) enriched with ^{13}C were used. The outgoing α-particles were detected through a ΔE-E counter telescope.

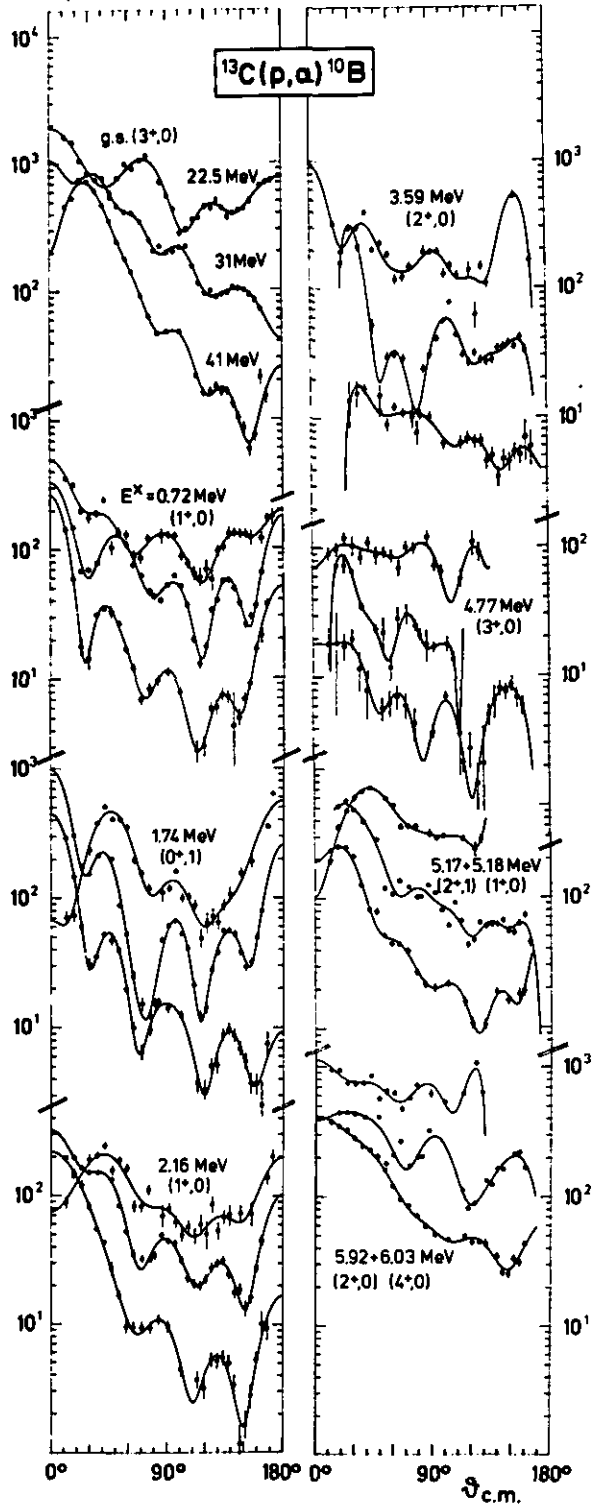

Fig. 1: Differential cross sections for $^{13}C(p,\alpha)^{10}B$ at E_p = 22.5, 31 and 41 leading to final states in ^{10}B up to E^X = 6.03 MeV. The solid lines represent Legendre polynomial fits.

In figure 1 differential cross sections for ten transitions populating states in ^{10}B up to E^X = 6.03 MeV are given for three incident energies (E_p = 22.5, 31 and 41 MeV), but the transitions to E^X = 5.17 and 5.18 MeV, and to E^X = 5.92 and 6.03 MeV, respectively, are not resolved.

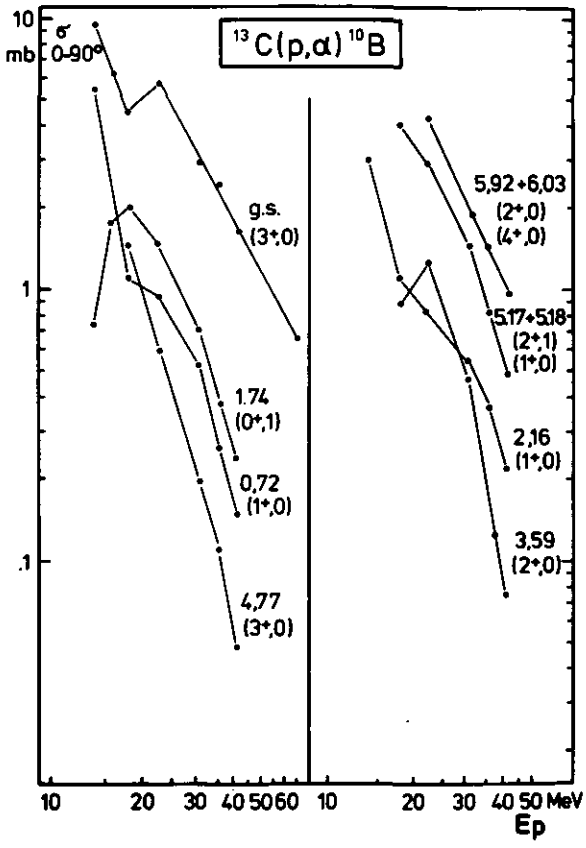

Fig. 2: Energy dependence of angle integrated cross sections σ_{0-90} for the (p,α) transitions on ^{13}C given in figure 1.

In figure 2 the integrated cross sections σ_{0-90} are shown together with data of lower energies[2]. The value for the ground state transition at E_p = 65 MeV is taken from literature[3]. From the shape of the angular distributions as well as from the energy dependence of the integrated cross sections one can conclude, that at incident energies of about 25 MeV the direct reaction mechanism starts to predominate. This conclusion agrees with results of previous investigations[4].

Parentage amplitudes for three nucleon transfer reactions on 1p shell nuclei are calculated by Kurath and Millener[5], using SU3 formalism. With these predictions the relative magnitudes of the integrated cross sections σ_{0-90} at E_p = 41 MeV are well accounted for (fig. 3). This result shows, that first a three nucleon pickup on light nuclei passes through a triton cluster in a relative 0s-state mainly[6], and that secondly the influence of the kinematic effects on the transition strength is of minor importance, because the comparison between spectroscopic and experimental data does not contain any correction from DWBA calculations.

Investigations on other nuclei of the 1p- and sd-shell led to similar results[1].

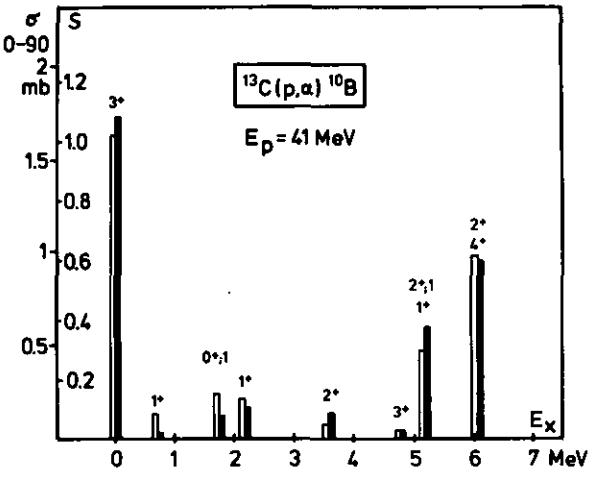

Fig. 3: Spectroscopic strengths (black bars) in comparison with experimental cross sections (opten bars) of $^{13}C(p,\alpha)^{10}B$ at E_p = 41 MeV.

References

1) F. Weng, T. Rohwer, G. Staudt, Annual Report 1979, Institut für Kernphysik of KFA Jülich, Jül-Spez-72, p. 12

2) K. Scholl, Diplomarbeit Tübingen, 1976

3) T. Kammuri, H. Shimaoka, P.D. Kunz, S. Kato, K. Okada, M. Kondo, K. Hosono, T. Saito, N. Matsuoka, S. Nagamachi, T. Noro, K. Ogino and Y. Kadota, Phys. Lett. 90B (1980) 197

4) F. Hoyler, T. Rohwer, H. Sauer, G. Staudt, Annual Report 1978, Institut für Kernphysik of KFA Jülich, Jül-Spez-36, p. 14

5) D. Kurath and D.J. Millener, Nucl. Phys. A238 (1975) 269

6) J.W. Smits, Dissertation (Rijksuniversiteit te Groningen) 1977

*Physikalisches Institut der Universität Tübingen

1.13. Investigation of the $^{54,56,58}Fe(d,^3He)^{53,55,57}Mn$ Reactions at 80 MeV

N.G. Puttaswamy, W. Oelert, A. Djaloeis, C. Mayer-Böricke and P. Turek

Improved shell-model calculations are now being made[1] for nuclei around doubly-magic ^{56}Ni. In order to determine the spectroscopic factors (S-factors) for such nuclei, we have studied the $(d,^3He)$ reaction on the even iron isotopes at E_d=80 MeV. The $^{54}Fe(d,^3He)$ reaction has been studied previously at 51.7 MeV[2] and 34.4 MeV[3] but the S-factors were extracted using zero-range, local DWBA. The $^{56,58}Fe(d,^3He)$ reactions have been studied for the first time.

An energy resolution of about 70 keV has been obtained using counter telescopes. The ^3He spectrum from the $^{54}Fe(d,^3He)$ reaction at $\theta_{lab} = 9.9^o$ is shown in fig. 1. Energy levels up to an excitation energy (E_x) of 4 MeV are known from previous studies[4]; in the present experiment, we see significant cross section for states with $4<E_x<7$ MeV. Experimental angular distributions in the range $6^o<\theta_{lab}<35^o$ are compared with predictions from DWBA calculations which include finite-range and non-local effects. The energies and S-factors for the strongest $f_{7/2}$, $s_{1/2}$ and $d_{3/2}$ hole states in Mn-nuclei are given in table 1. The predictions of shell-model calculations[1] using the modified Kuo-Brown interaction are also shown in the table. A detailed comparison between experimental and theoretical S-factors is now being made.

	^{53}Mn					^{55}Mn			^{57}Mn		
		C^2S					C^2S			C^2S	
J^π	E_x	Expt	Expt[a]	Expt[b]	Theory[c]	E_x	Expt	Theory[c]	E_x	Expt	Theory[c]
$7/2^-$	0.0	3.07	4.38	4.93	2.67	0.13	2.52	3.14	0.084	2.49	2.13
$1/2^+$	2.73	1.09	0.68	1.60	-	2.43	0.82	-	1.76	0.59	-
$3/2^+$	3.03	1.36	1.97	3.49	-	2.73	1.52	-	1.96	1.38	-

a) Ref. 2 (E_d = 51.7 MeV)
b) Ref. 3 (E_d = 34.4 MeV)
c) Ref. 1

Table 1: Excitation energy (E_x) and spectroscopic-factors (C^2S) for the strongest $f_{7/2}$, $s_{1/2}$ and $d_{3/2}$ hole-states in Mn-nuclei.

References

1) P.W.M. Glaudemans in Structure of Medium-heavy Nuclei 1979, ed. 'Demokritos' Tandem Accelerator Group (The Institute of Physics, Bristol and London, 1980) p. 11, and private communication

2) G. Mairle et al., Nucl. Phys. A134 (1969) 180

3) E. Newman and J.C. Hiebert, Nucl. Phys. A110 (1968) 366

4) R.L. Auble, Nuclear Data Sheets 21 (1977) 323

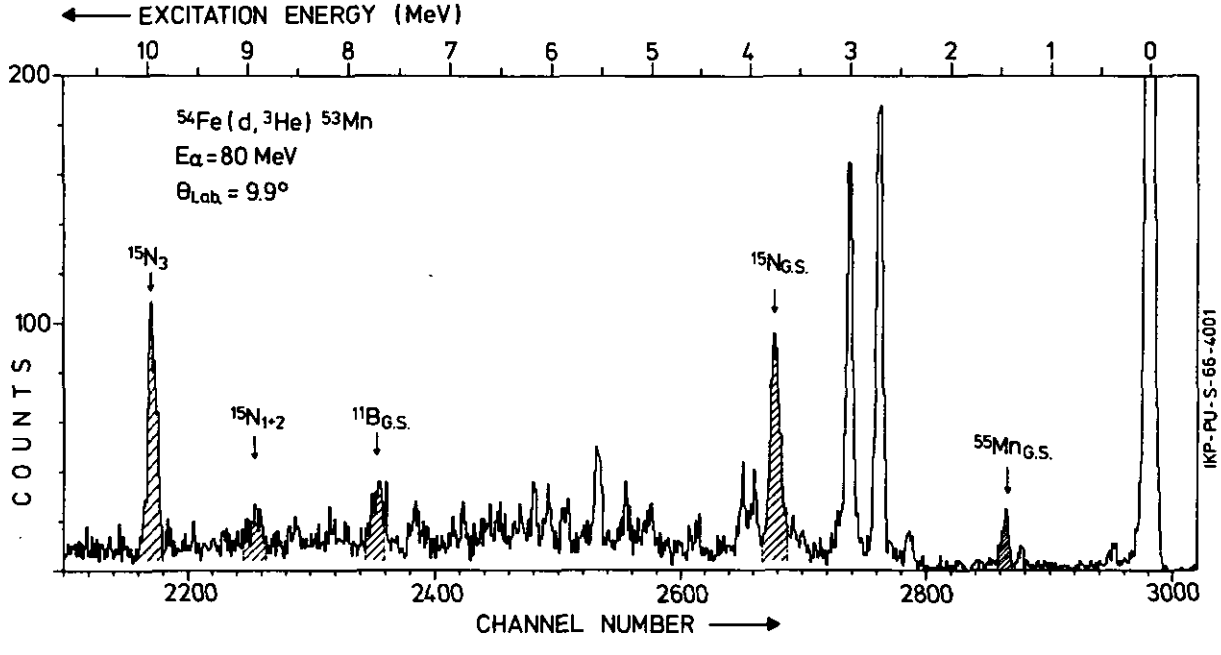

Figure 1: Spectrum of ^3He particles from the $^{54}Fe(d,^3He)^{53}Mn$ reaction at θ_{lab}=9.9° and E_d=80 MeV.

1.14. Helion Induced Reactions on some s-d Shell Nuclei

A. Djaloeis, S. Gopal, J. Bojowald, C. Mayer-Böricke, W. Oelert, N.G. Puttaswamy and P. Turek

Triton spectra from helion (τ) induced reactions on ^{27}Al at E_τ=130 MeV are found to exhibit an additional little bump at $10 \lesssim E_x \lesssim 22$ MeV in the residual ^{27}Si nucleus[1]. In view of this, further experiments have been performed on ^{24,25,26}Mg and ^{28}Si targets. Experimental method and arrangement were similar to those used previously[1]. The d-, t-, τ- and α-spectra were accumulated simultaneously.

Examples of d- and t-spectra and τ- and α-spectra are shown in figs. 1 and 2, respectively. It is interesting

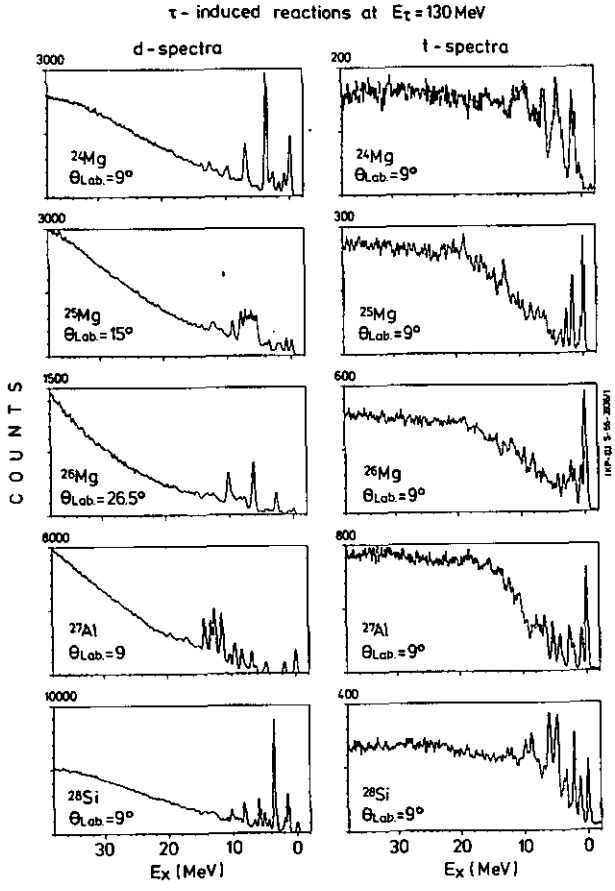

Figure 1

to note that in the t-spectra from ^{25}Mg and ^{26}Mg target nuclei, the bump also appears as in case of ^{27}Al in the $10 \lesssim E_x \lesssim 22$ MeV region, whereas it practically disappears in the ^{24}Mg and ^{28}Si cases. Since the observed feature is probably due to nuclear structure effects, it would be worthwhile to study the excitation energy region of interest in terms of some microscopic models.

Data reduction for transitions to low-lying levels has been partially completed and is still in progress. Fig. 3 shows detailed d-spectra for ^{27}Al and ^{28}Si targets in the low excitation energy region. The overall energy resolution is about 500 keV. Peak identification follows from the energy calibration and the Endt and van der Leun compilation[2]. For unknown peaks their centroid positions are estimated to be correct to within 100 keV. Figs. 4 and 5 show angular distributions for transitions to the levels (peaks) indicated in fig. 3. Analysis in terms of the DWBA theory is in progress.

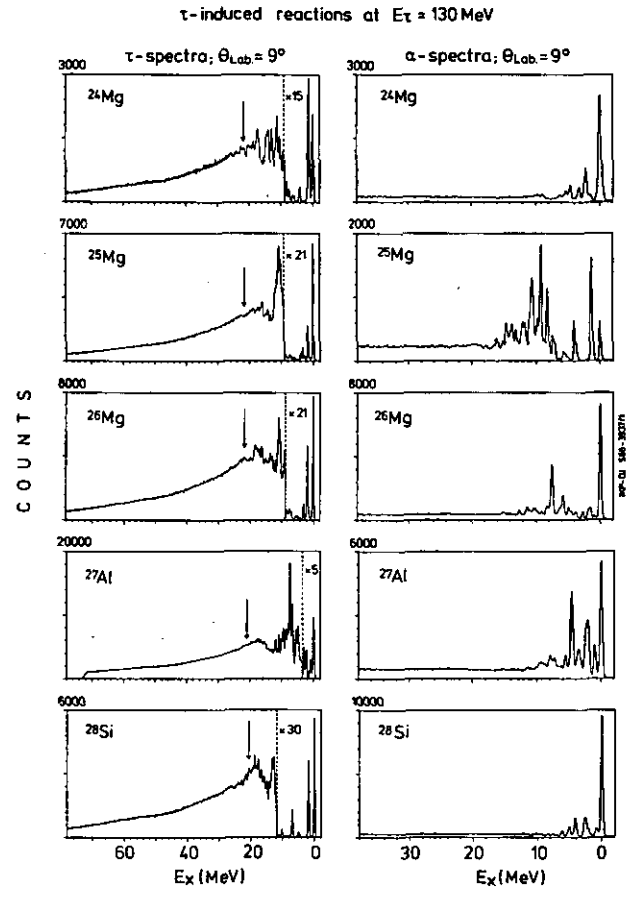

Figure 2

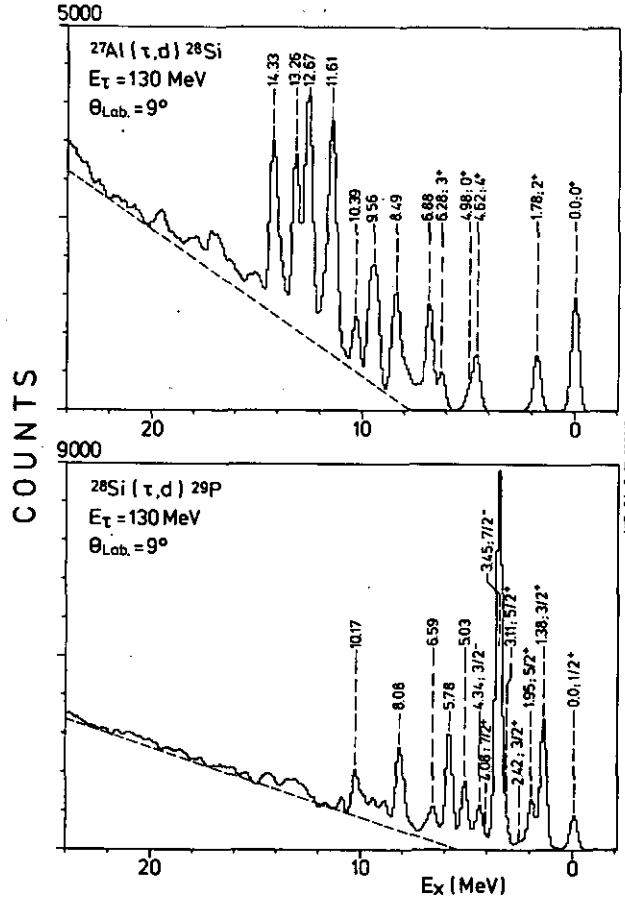

Figure 3

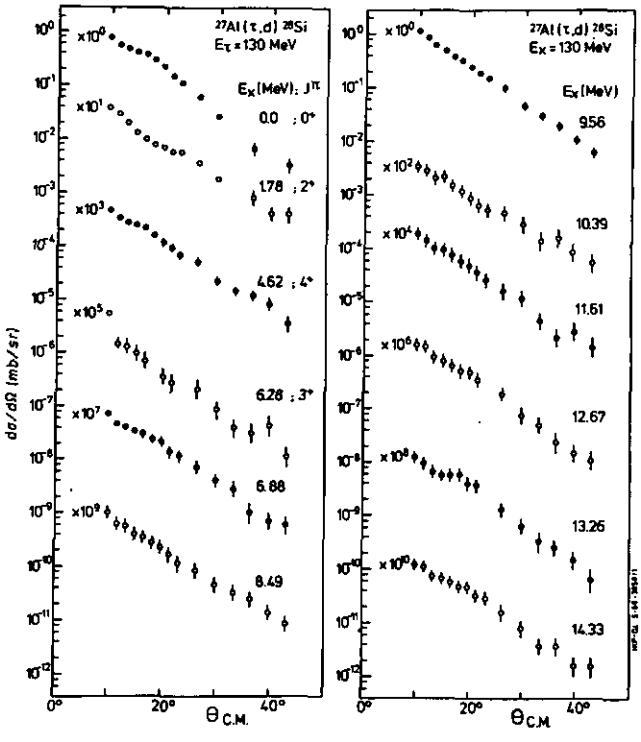

Figure 4

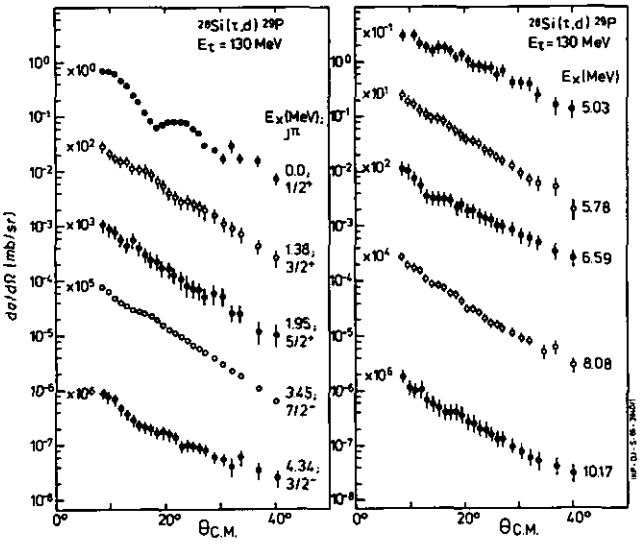

Figure 5

References

1) S. Gopal et al., KFA-IKP Annual Report 1979, Jül-Spez-72 (1980) p. 17 and submitted to Phys. Rev. C

2) P. Endt and C. van der Leun, Nucl. Phys. A310 (1978) 1

1.15. Measurement and DWBA Interpretation of the $^{58}Ni(\tau,d)^{59}Cu$ Reaction at a High Incident Energy

A. Djaloeis, C. Alderliesten, J. Bojowald, C. Mayer-Böricke, W. Oelert and P. Turek*

This work reports on a measurement and a DWBA analysis of the $^{58}Ni(\tau,d)^{59}Cu$ reaction at E_τ = 130 MeV. Angular distributions of four strong transitions leading to the (0.0 MeV, $3/2^-$), (0.91 MeV, $5/2^-$), (3.04 MeV, $9/2^+$) and 4.11 MeV states in ^{59}Cu, respectively, have been obtained. All of them, except the one to the proton-unbound 4.11 MeV state, have been theoretically analyzed in the frame-work of the zero-range DWBA theory using the DWUCK[2] programme. Experimental details and methods of extracting the experimental cross sections have been described elsewhere[1]. The resulting angular distributions are given in fig. 1.

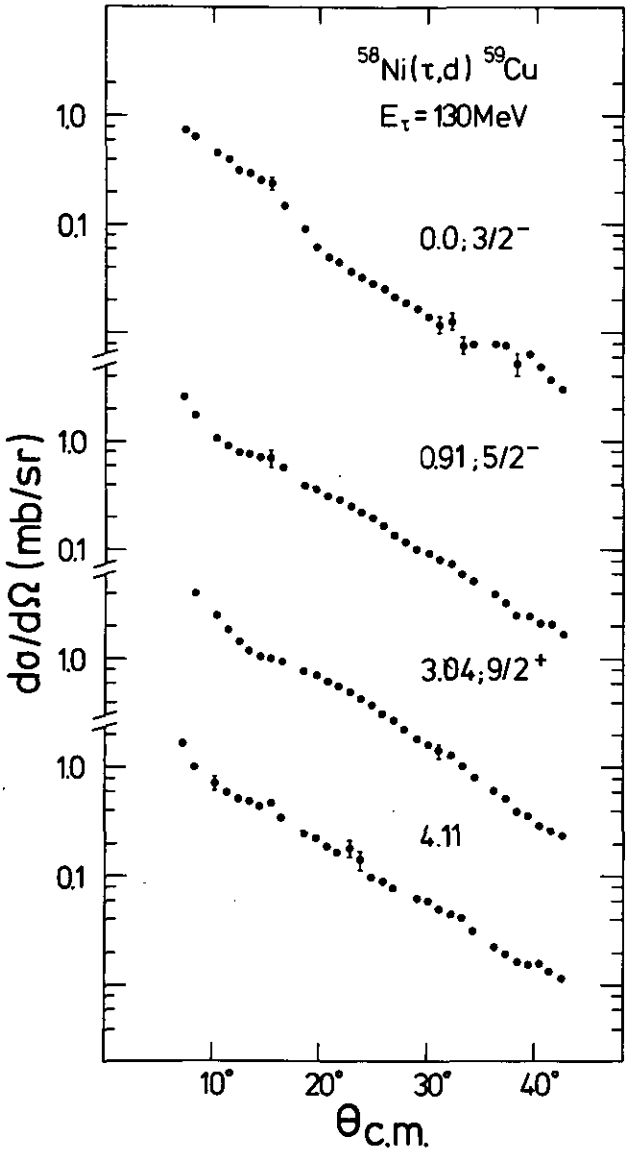

Figure 1: Experimental angular distributions of the $^{58}Ni(\tau,d)^{59}Cu$ reaction at E_τ = 130 MeV.

A list of the optical model and DWBA parameters used in the present work is given in table 1.

Fig. 2 shows the comparison between the experimental data and the theoretical predictions based on the published surface type helion optical potentials and the published[3,4] deuteron optical potentials BSSD and FSSD (table 1). Cross sections predicted by the shallow potentials (SS and VS) are in general almost an order of magnitude higher than those by the deep ones. In addition,

Set	$V^{a)}$ (MeV)	r_V (fm)	a_V (fm)	$W_S^{b)}$ (MeV)	$W_V^{a)}$ (MeV)	r_W (fm)	a_W (fm)	Ref.
τ:DSSH	100.0	1.211	0.805	20.2	-	1.180	0.817	1)
DVSH	105.7	1.180	0.880	-	19.9	1.574	0.651	1)
DSDH	158.3	1.218	0.667	25.4	-	0.916	1.044	1)
DVDH	156.3	1.224	0.658	-	30.1	1.236	1.080	1)
TSDH	145.7	1.369	0.408	34.0	-	1.077	0.879	Present
TVDH	161.7	1.315	0.464	-	38.6	1.443	0.766	"
d:BSSD	69.9	1.250	0.730	14.8	-	1.151	0.915	3
FSSD	65.6	1.250	0.695	13.3	-	1.047	0.985	4

In all sets r_c = 1.3 fm

Proton bound-state parameters[5]: λ = 25 (Thomas spin-orbit form); r_o = 1.20 fm; a = 0.65 fm; r_c = 1.25 fm; V_p^x ∿ 70 MeV (adjusted to give the correct proton binding energy for the final state involved)

† the analytical form of the potential shapes is that used in ref.1)

a) Woods-Saxon

b) Woods-Saxon derivative

Table 1: Optical model† and DWBA parameters.

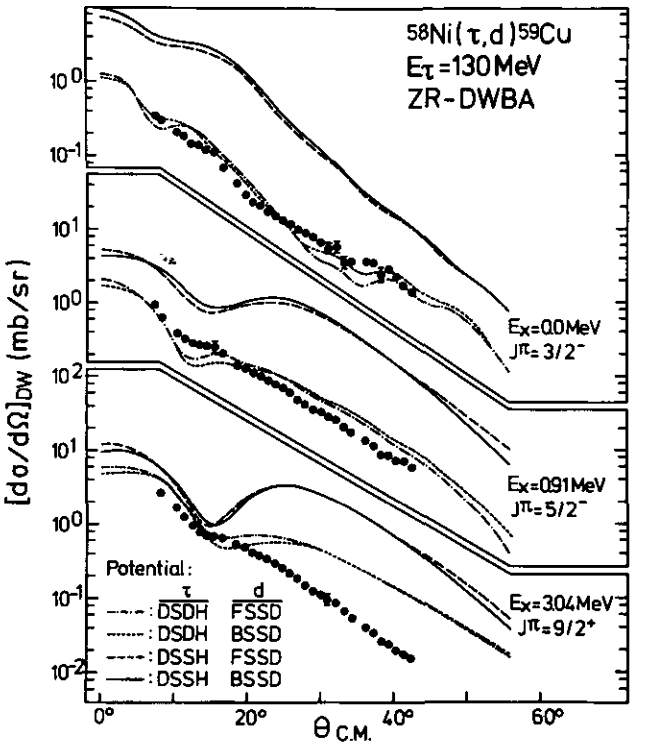

Figure 2: DWBA predicted angular distributions of the $^{58}Ni(\tau,d)^{58}Cu$ reaction for the transitions leading to the (0.0 MeV, $3/2^-$), (0.91 MeV, $5/2^-$) and (3.04 MeV, $9/2^+$) states in ^{59}Cu as predicted by various combinations of helion and deuteron optical potentials (published surface type τ-potentials in combination with published d-potentials; see table 1).

the shallow potentials fail to reproduce the shape of the experimental (E_x = 0.91 MeV, $5/2^-$) and (E_x = 3.04 MeV, $9/2^+$) angular distributions. Except for dips at $\theta_{c.m.} \sim 8^0$, the deep potentials give a reasonable description of the ground-state transition. For $\theta_{c.m.} \lesssim 20^0$, similar conclusions can be drawn for the other two transitions. At larger angles the deep potentials predict cross sections which are consistently larger than the experimental values. In general, replacing BSSD with FSSD does not give significant effects.

The angular distributions of the (τ,d) reaction predicted using the helion potential sets TSDH and TVDH are shown in fig. 3. For each transition, the value of the spectroscopic factor $C^2S_{\ell j}$ has been extracted by matching the theoretical curve to the experimental angular distribution. The error involved in this procedure is about 30 %.

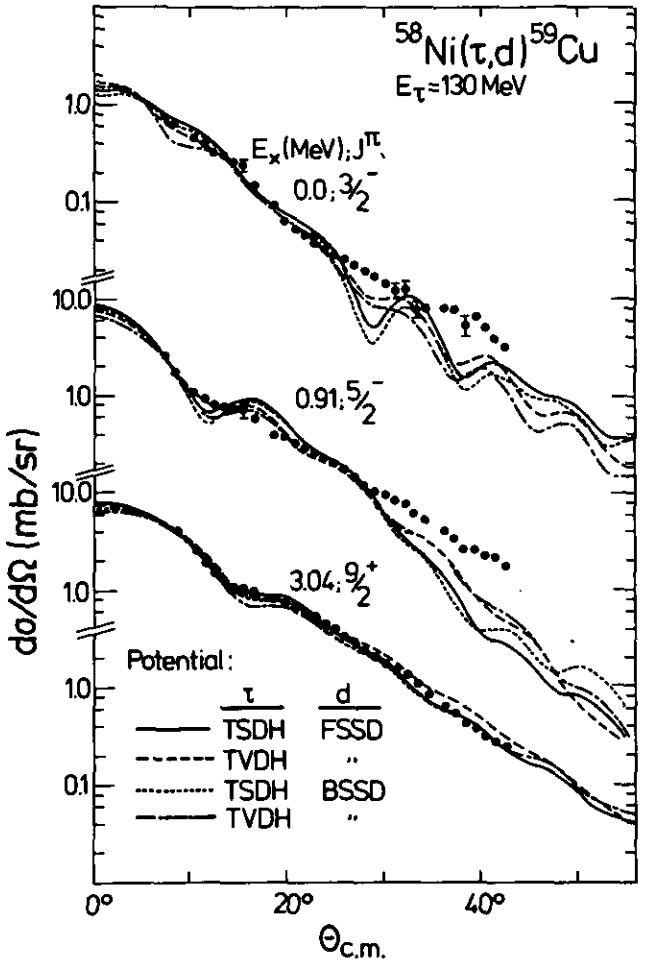

Figure 3: DWBA predicted angular distributions of the ^{58}Ni(τ,d)^{59}Cu reaction for the transitions leading to the (0.0 MeV, $3/2^-$), (0.91 MeV, $5/2^-$) and (3.04 MeV, $9/2^+$) final states in ^{59}Cu. The calculations were performed using the helion optical potentials obtained in this work, combined with the BSSD deuteron potential (see table 1).

The extracted values of $C^2S_{\ell j}$ are 1.0±0.3, 4.1±1.2 and 2.7±0.9 for the (0.0 MeV, $3/2^-$), the (E_x = 0.91 MeV, $5/2^-$) and the (E_x = 3.04 MeV, $9/2^+$) states, respectively. Considering the errors involved and the scatter of the corresponding values available in the literature[5], the present results can be regarded as reasonable. The DWBA analysis of the present data of the ^{58}Ni(τ,d)^{59}Cu reaction at E_τ = 130 MeV indicates that satisfactory fits could only be achieved when the optical potential in the entrance channel is represented by a deep helion potential ($V_\tau \approx$ 150 MeV). This result seems to be at variance with that found in the previous[1] analysis of the ^{58}Ni(τ,α) reaction at the same incident energy where a shallow τ optical model potential is needed to describe the data. It is worth pointing out that a similar discrepancy also exists in the τ optical model potentials needed to describe the ^{51}V(d,τ)^{50}Ti (ref. 6) and the ^{58}Ni(τ,α)^{57}Ni (ref. 7) reactions at relatively high incident energies. Furthermore, the use of a deep τ optical model to describe the present data is consistent with results of similar analyses of the ^{58}Ni(τ,d)^{59}Cu reaction at E_τ = 90 MeV (ref. 8) and ^{12}C(τ,d)^{13}N reaction at E_τ = 80 MeV (ref. 9). In fact, the authors of ref. 9) investigated this problem in detail and argued that the finite range effects could not account for the qualitative discrepancy between shallow and deep τ potentials. The need for a shallow τ potential to describe the 130 MeV ^{58}Ni(τ,α) data[1] and a deep one for the present case might be related to the oversimplification of the actual reaction mechanism by the DWBA theory.

In spite of the seeming discrepancy in the absolute depth of the real part of the helion optical potential involved in the analysis of the ^{58}Ni(τ,d)^{59}Cu and ^{58}Ni(τ,α)^{57}Ni reactions, it is worth noting that a good DWBA description of the experimental data seems to require the relation $V_{(a+x)} \sim V_x^b + V_a$ to be satisfied. Here V_x^b represents the bound-state potential depth of the transferred particle x. In the present case, since $V_x^b \sim$ 70 MeV, fixing $V_d \sim$ 70 MeV leads to $V_\tau \sim$ 140 MeV, a value close to the observed results. It is worth mentioning that the potential depth relation is also satisfied by the d and τ optical model potentials used in the analysis[5] of the ^{58}Ni(τ,d)^{59}Cu reaction at 35 and 39 MeV. However, the relation does not seem to be able to give information on the absolute depths of the optical potentials involved. A similar conclusion based on theoretical arguments was given by Stock et al.[10].

References

1) A. Djaloeis et al., Nucl. Phys. A142 (1980) 252
2) P.D. Kunz, Computer code DWUCK70, University of Colorado, Boulder (Colorado), USA
3) J. Bojowald et al., Annual Report 1979, Jül-Spez-72, KFA-IKP Jülich, W. Germany, p. 1
4) G. Duhamel et al., Nucl. Phys. A174 (1971) 485
5) P.K. Bindal, D.H. Youngblood and R.L. Kozub, Phys. Rev. C14 (1976) 521, and references therein
6) J.N. Craig, N.S. Wall and R.H. Bassel, Phys. Rev. Lett. 36 (1976) 656
7) N.S. Cahnt et al., Cyclotron Laboratory Progress Report, University of Maryland, 1977, p. 72
8) N. Matsuoka et al., Annual Report of the Resear Center for Nuclear Physics, Osaka University, Osaka, Japan, 1977, p. 136
9) J.P. Didelez et al., Phys. Rev. C13 (1976) 1388
10) R. Stock et al., Nucl. Phys. A104 (1967) 136

*Fysisch Laboratorium, Rijksuniversiteit, Utrecht, The Netherlands

1.16. Angular and Target Mass Dependence of the "Broad Structure" in Triton Spectra from (τ,t) Reactions at E_τ = 130 MeV

S. Gopal, A. Djaloeis, J. Bojowald, O. Bousshid, C. Mayer-Böricke, W. Oelert, N.G. Puttaswamy and P. Turek

Observation of a broad structure ("bump") in t-spectra from (τ,t) reactions at 68 and 90 MeV (ref. 1) and 130 MeV (ref. 2) has been reported. Here we present the results of further experimental works at E_τ = 130 MeV which have been performed with the following objectives:

(i) to study the A-dependence of the t-bump cross section; for this purpose ^{27}Al, ^{59}Co, ^{93}Nb and ^{197}Au were used as targets, and

(ii) to extract angular distributions of the bump cross section; for this purpose triton spectra have been measured from 7.5° to 24° (lab.) in 1.5° steps.

The experimental details have been given elsewhere[2].

Fig. 1 shows some of the measured triton spectra for ^{27}Al, ^{59}Co, ^{93}Nb and ^{197}Au targets. The spectra at very forward angles (θ_L=9°, 10.5°) exhibit a pronounced and asymmetric broad structure ("bump"). It can be seen that the t-bump cross section falls rapidly with angle and that the bump, except perhaps for ^{27}Al, practically disappears at θ_L=24°. It is interesting to note, that for ^{27}Al case, an additional small bump (shown by an arrow) located at $E_x \approx 18$ MeV of the residual ^{27}Si nucleus is observed.

Fig. 2 shows the angle-average values of centroid energy E_c and FWHM Γ as a function of A. These values are found to be independent of A. The target-average of these values are $\overline{E_c}$=87±2 MeV and $\overline{\Gamma}$=48±2 MeV, close to $2/3E_\tau$ and $1/3E_\tau$, respectively. This feature is similar to that observed previously[1,2]. The Γ value is almost twice as large as Nomura's estimate[3] $\Gamma = \sqrt{E_\tau \cdot B_d(\tau)}$, $B_d(\tau)$ being the deuteron binding energy in the projectile.

Fig. 3 shows the A-dependence of the t-bump cross section for θ_L=9°, 12°, 15° and 18°. The bump cross section tends to favour the $A^{1/2}$ dependence at forward angles (θ_L=9°, 12°, 15°); however, considering the error bars, the $A^{1/3}$ dependence cannot be ruled out. At θ_L=18°, the $A^{1/3}$ dependence is more favourable.

Fig. 4 shows angular distributions of the t-bump cross section (in lab. system). For all measured targets the cross section tends to decrease exponentially with angle, possibly with a weak oscillation pattern superimposed.

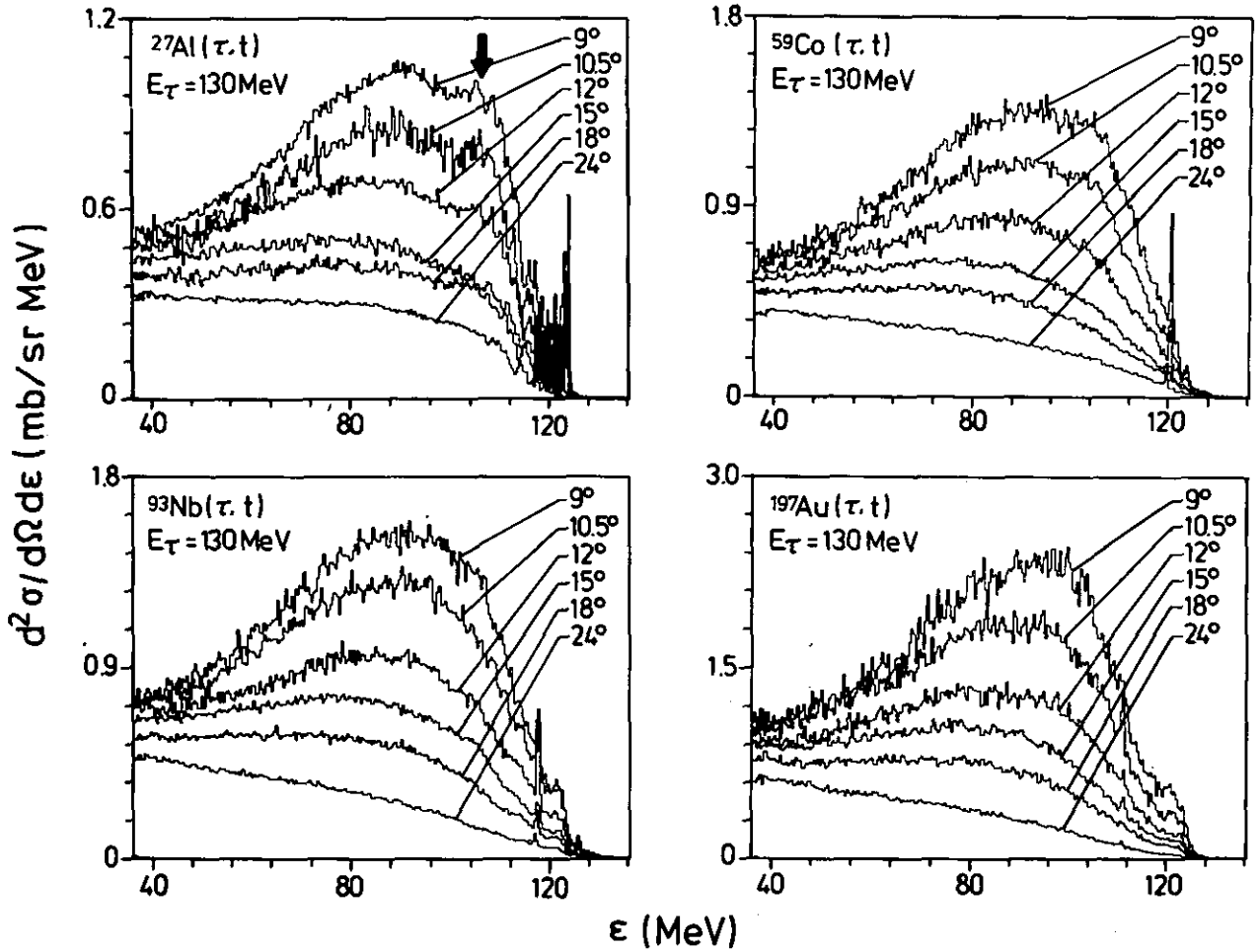

Figure 1: Measured t-spectra from (τ,t) reactions on ^{27}Al, ^{59}Co, ^{93}Nb and ^{197}Au targets at E_τ = 130 MeV.

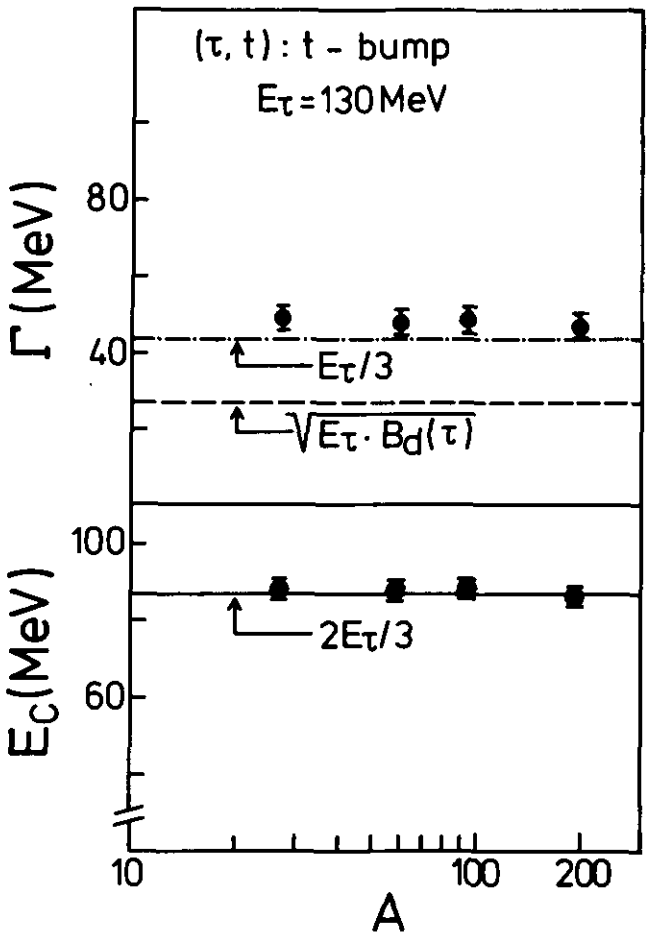

Figure 2: Target mass (A) dependence of the extracted centroid energy E_c and width Γ of the t-bump. Dashed curve represents the Nomura's empirical relation (see text).

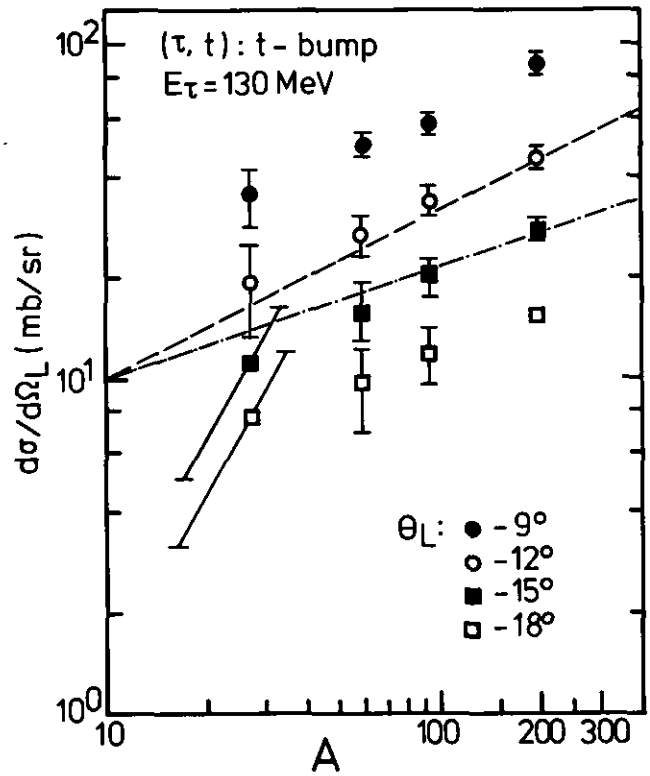

Figure 3: A-dependence of the t-bump cross sections for $\theta_L = 9^o$, 12^o, 15^o and 18^o. The slopes representing $A^{1/2}$ and $A^{1/3}$ dependences are denoted by the dashed and dot-dashed curves, respectively.

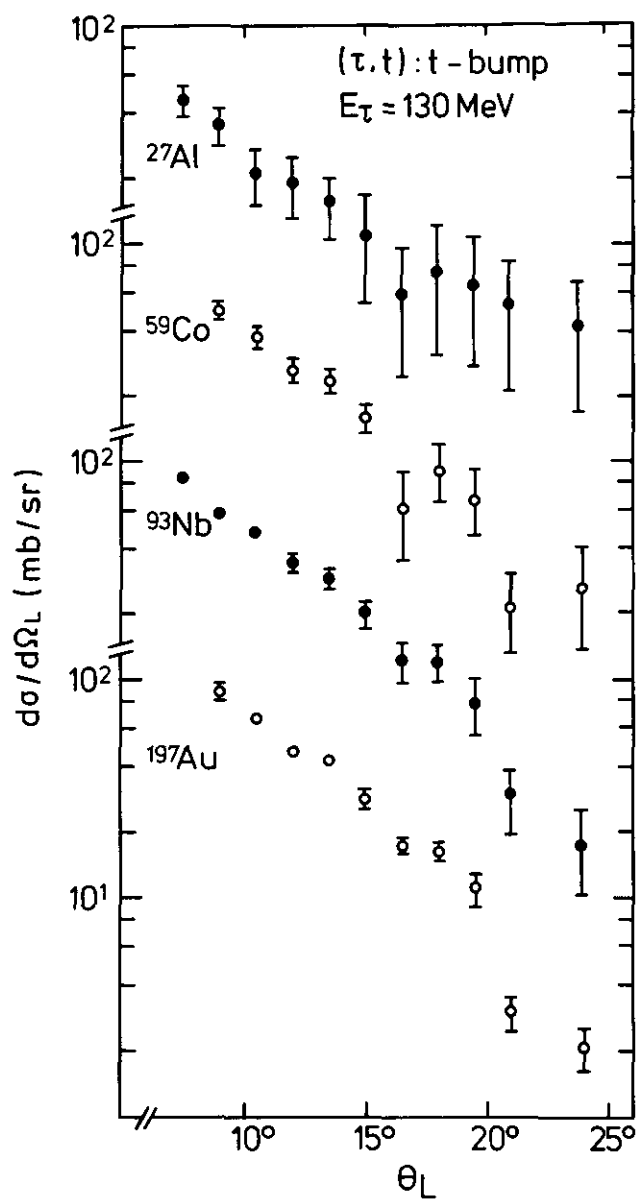

Figure 4: Experimental angular distributions of the t-bump cross sections for ^{27}Al, ^{59}Co, ^{93}Nb and ^{197}Au targets at E_τ = 130 MeV.

References

1) O. Bousshid, H. Machner, C. Alderliesten, U. Bechstedt, A. Djaloeis, P. Jahn and C. Mayer-Böricke, KFA-IKP Annual Report 1979, Jül-Spez-72, Jülich, West Germany, p. 16 and Phys. Rev. Lett. 45 (1980) 980

2) S. Gopal, A. Djaloeis, O. Bousshid, J. Bojowald, C. Mayer-Böricke, W. Oelert, N.G. Puttaswamy and P. Turek, KFA-IKP Annual Report 1979, Jül-Spez-72, Jülich, West Germany, p. 17 and Proc. Int. Conf on Nuclear Physics, Berkeley, USA, 1980, p. 253

3) M. Nomura, Proc. Int. Symp. on Nuclear Direct Reaction Mechanism, 1978, Fukuoka, Japan, p. 709

1.17. Study of the Reaction Mechanism of the Alpha-Transfer on sd-Shell Nuclei

W. Oelert, A. Djaloeis and P. Turek

The effort of extracting quantitative information on spectroscopic strength distributions of four-nucleon correlations in nuclei has been mutually stimulated by recent theoretical development and experimental progress. For nuclei of the sd-shell theoretical calculations of alpha-spectroscopic factors have been performed[1] with the method described by Bennett[2] from complete $d_{5/2}$-$s_{1/2}$-$d_{3/2}$ shell-model wave functions generated by the Chung-Wildenthal empirical particle-hole interactions. During the last year we continued the systematic investigation of the alpha transfer reaction study both theoretically and experimentally.

Details of the $^{24}Mg(d,^6Li)^{20}Ne$ and of the $^{26}Mg(d,^6Li)^{22}Ne$ reaction study, analyzed in the framework of the finite range distorted wave Born approximation has been given elsewhere[3]. As a result it could be concluded: Rather good agreement is observed between sd-shell model predictions and present experimental values of relative spectroscopic factors. The average experimental values for excited states are somewhat larger than the theoretical ones, relative to the ground-state transition. This result might be due to a physically larger reduced matrix element of the individual four-nucleon creation operator leading from nucleus A to excited states of nucleus A-4, than predicted by the shell-model calculations[1].

It should be mentioned, however, that the assumed direct one-step reaction process might not meet always the actual physical conditions. This hypothesis is supported by the experimental results for the low lying 4^+ states. In ^{22}Ne the experimental angular distribution of the first 4^+ state cannot be fitted by DWBA calculations; the extracted "spectroscopic factor" is a factor of 10 larger than the predicted one. In ^{20}Ne the experimental angular distribution of the first 4^+ state is poorly fitted by DWBA calculations; the extracted spectroscopic factor is about a factor of 2 larger than the predicted one. Finally, the experimental angular distribution of the second 4^+ state in ^{22}Ne is well fitted by DWBA calculations - the extracted spectroscopic factor is only 10-30 % larger than the predicted relative value.

This result suggests the probable importance of two step processes like a reaction mechanism described in the coupled reaction channel framework. In order to investigate the significance of this hypothesis computer codes written by W. Chung have been used to calculate spectroscopic factors for the transitions from excited target states J_i^π to states in the final nucleus. A selection of relative spectroscopic factors (normalized to the respective ground state transition) for final 4^+ states in ^{20}Ne and ^{22}Ne excited from the initial target state J_i^π (ground state and first excited 2^+ state) by an angular momentum transfer L_{tr} is given in the table. The relative spectroscopic factor for the excitation of the 4_1^+ states in ^{22}Ne from the target ground state (the direct one step process) is relatively small (0.02), whereas the one for the 4_2^+ state in ^{22}Ne is relatively large (0.69). On the other side both states are characterized by the same spectroscopic factor for the transition from the 2^+ target state (two step process) via a $\ell = 2$ transfer (0.14). The probable influence on the shape and on the magnitude of the one step direct angular distribution can be estimated best by the spectroscopic factor for the two step process relative to the direct one step process, given in the table. It is seen,

J_i^π	L_{tr}	^{20}Ne 4_1^+ 4.13(MeV)	^{22}Ne 4_1^+ 3.42 (MeV)	^{22}Ne 4_2^+ 5.40 (MeV)
0^+	4	.41	.02	.69
2^+	2,4,6	.76, .14, ≤01	.14, .00, .08	.14, .05, .03
Relative $\frac{2^+ \to 4_n^+}{0^+ \to 4_n^+}$		1.85, .34, ≤02	7.0, 0, 4.0	.22, .07, .04

Table caption: Relative spectroscopic factors for the excitation of final 4^+ states in ^{20}Ne and ^{22}Ne needed for two step reaction mechanism considerations, see text for discussion.

that theoretically the 4_1^+ state is by a factor of 7 stronger populated from the 2^+ target state via a $\ell = 2$ transfer than by the one step process, whereas for the 4_2^+ state in ^{22}Ne the one step mechanism is dominant.

Tentatively the above outlined experimental results for the 4^+ states in ^{20}Ne and ^{22}Ne seem to be intelligible by the calculations of the spectroscopic factors within the consideration of two step reaction mechanism processes. In fact, coupled reaction channel (CRC) calculations do agree reasonably well with the magnitude of the experimental cross sections (within a factor of two). It cannot be expected to get an exact agreement, since too many parameters of the calculations remain unresolved as e.g. optical potentials for CRC, the optimum choice of at least the main transition paths, the kind of two step process as e.g. $(d,d')(d',^6Li)$, $(d,^6Li)(^6Li,^6Li')$, $(d,\alpha)(\alpha,^6Li)$, $(d,^4H)(^4H,^6Li)$, etc.. Further investigations are in progres.

References

1) W. Chung et al., Phys. Lett. 79B (1978) 381 and to be published
2) C.L. Bennett, Nucl. Phys. A284 (1977) 301
3) W. Oelert et al., Phys. Rev. C22 (1980) 408

1.18. The $^{22}Ne(d,^{6}Li)^{18}O$ Reaction

M.G. Betigeri, T.H. Fortune, C. Mayer-Böricke, W. Oelert, B. Rubio, and P. Turek*

The alpha transfer reaction from ^{22}Ne to ^{18}O is of special interest, because of the extra two neutrons above the "alpha like" nucleus ^{20}Ne. It is expected that the ground state spectroscopic factor is smaller than the one for the $^{20}Ne \rightarrow ^{16}O$ or the one for the $^{24}Mg \rightarrow ^{20}Ne$ transition. The presently extracted value of the relative spectroscopic factor is in fact only a quarter of the one for the $^{20}Ne \rightarrow ^{16}O$ transition. It is however by a factor of two too small in comparison to shell model calculations[1]. It remains an open question whether this disagreement is due to i) an influence of the lower lying p-shell (4p 2h or 6p 4h contributions), ii) the correct choice of the optical potentials (see the influence of the ^{6}Li real potential depth in Fig. 1), iii) the inadequate use of the one step direct reaction process, or iiii) less alpha clustering in the ^{22}Ne ground state than predicted by the shell model.

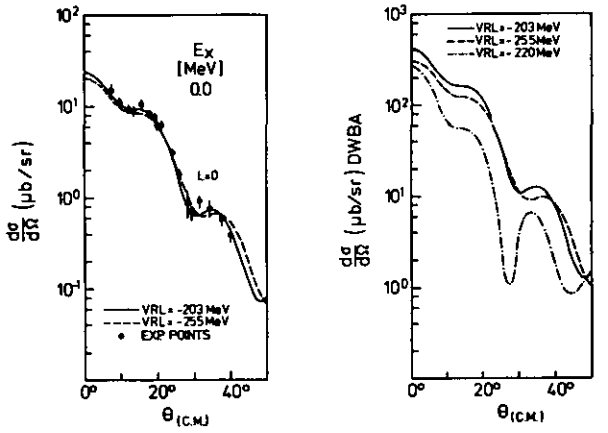

Figure 1: Angular distribution of the ground state transition $^{22}Ne \rightarrow ^{18}O$ compared to DWBA calculations with different potential depths for the real ^{6}Li optical potential.

The relative spectroscopic factor of the first excited 2^+ state at 1.98 MeV is only half the value as expected by the shell model[1]. Contributions from the p-shell (dotted and dashed dotted curves in Fig. 2) could account for this deviation, however, as can be seen in Fig. 2, the decrease of the experimental cross section with increasing angle is not reproduced by any of the np-mh DWBA calculations for the four low angle data points ($<15^0$ c.m.).

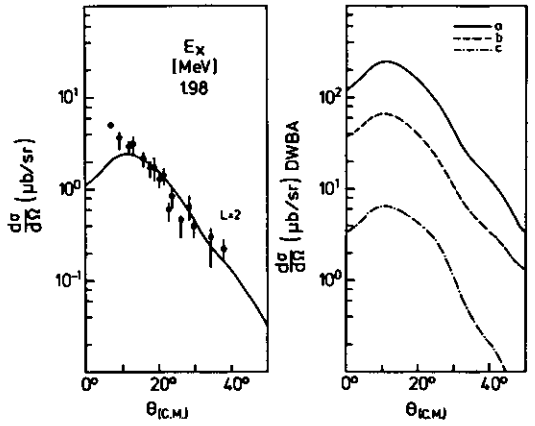

Figure 2: Angular distribution of the transition to the 2^+ state in ^{18}O. DWBA calculations are included for calculations assuming all four transfered particles being from the sd-shell (solid line); two particles from the sd, two from the p-shell (dashed line); and all four particles being from the p-shell (dashed dotted line).

A further summary of the $^{22}Ne(d,^{6}Li)^{18}O$ reaction study results in: i) spectroscopic strength, which is predicted[1] to be strong has been found and agreement is obtained within a factor of two between theoretical and experimental values, ii) spectroscopic strength which is predicted to be relatively week (less than 5 % of the ground state transition strength) is not expected to be observable and has not been observed; iii) furhter spectroscopic strength has been observed which is most likely due to excitation of p-shell components in the final state and which is therefore not predicted in the sd shell model framework.

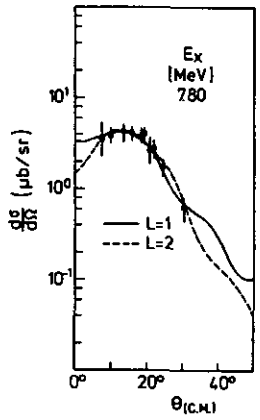

Figure 3: Angular distribution of the transition to the 7.80 MeV state in ^{18}O. Both L=1 and L=2 DWBA transfer calculations would agree to the experimental angular distribution shape.

A level at 7.8 MeV excitation energy (angular distribution see Fig. 3) which was suggested[2] to be a 2^+ state, to carry a strong 6 particle configuration and to be the band head of a rotational band is observed. A spin parity assignment of 2^+ would agree with the present data, however a 6p configuration seems to be very unlikely.

The analysis of the data and its interpretation is in progress.

References

1) W. Chung et al., Phys. Lett. 79B, 381 (1978) and to be published

2) J.B.A. England et al., Lecture Notes in Physics 92, 470 (1978); Edited by B.A. Robson, Springer-Verlag

*University of Philadelphia, USA

1.19. The Reactions $^{50,52}Cr(d,^{6}Li)^{46,48}Ti$ at E_d=65 MeV

M.G. Betigeri, W. Chung, A. Djaloeis, C. Mayer-Böricke, W. Oelert, and P. Turek

The $^{50,52}Cr(d,^{6}Li)^{46,48}Ti$ reactions have been studied at E_d = 65 MeV bombarding energy. Angular distributions of the outgoing ^{6}Li particles were measured for final states in $^{46,48}Ti$ nuclei from 15° to 50° (Lab). Typical energy spectra are shown in Fig. 1 and Fig. 2. In both cases a

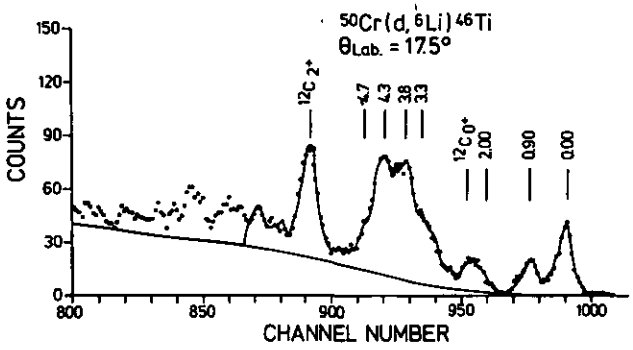

Figure 1: ^{6}Li spectrum of the $^{50}Cr(d,^{6}Li)^{46}Ti$ reaction.

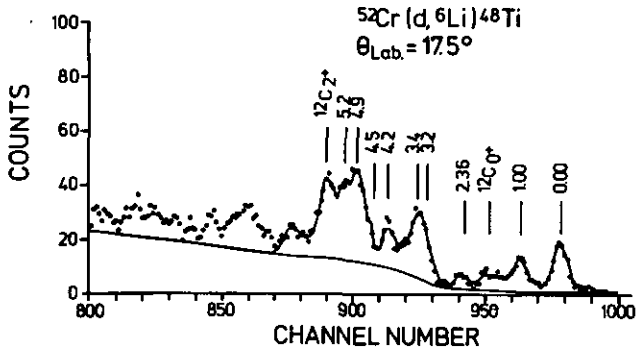

Figure 2: ^{6}Li spectrum of the $^{52}Cr(d,^{6}Li)^{48}Ti$ reaction.

rather strong yield is observed at excitation energies between 3 and 5 MeV. It has been tried to fit the shape of the spectra by a superposition of a few peak shapes using the computer code Autofit[1] (solid line in Figs.1 and 2). Although the region is characterized by high level density, in all the measured spectra it was possible to identify peaks (for each reaction) with excitation energy constant to within 150 keV, half the experimental full width half maximum. Typical angular distributions for E_x > 3 MeV for the case of the $^{52}Cr(d,^{6}Li)^{48}Ti$ reaction are shown in Fig. 3. A spin assignment of J ≥ 4 seems rather likely for the majority of the observed strength. A closer look with better energy resolution is needed for excitation energies above 3 MeV to investigate the possible selective excitation of cluster states.

For the low lying states relative spectroscopic factors obtained from the alpha pick up $(d,^{6}Li)$ and the two neutron transfer (p,t)[2] reactions leading to the same final nucleus are compared in Fig. 4

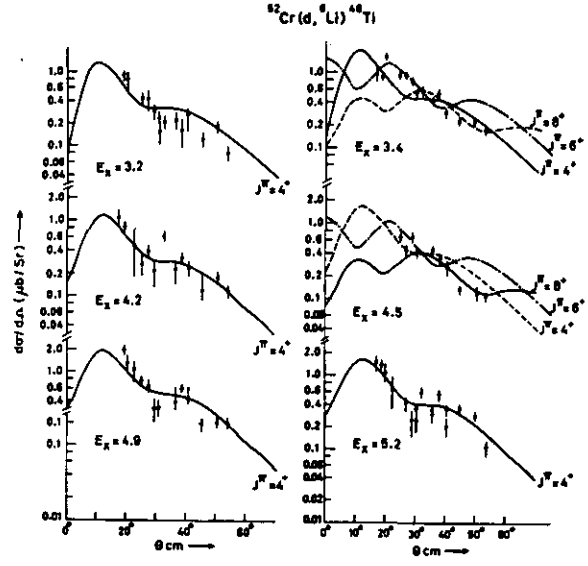

Figure 3: Angular distributions of ^{6}Li particles in transitions of peaks observed in the $^{52}Cr(d,^{6}Li)^{48}Ti$ reaction at excitation energies larger than 3 MeV.

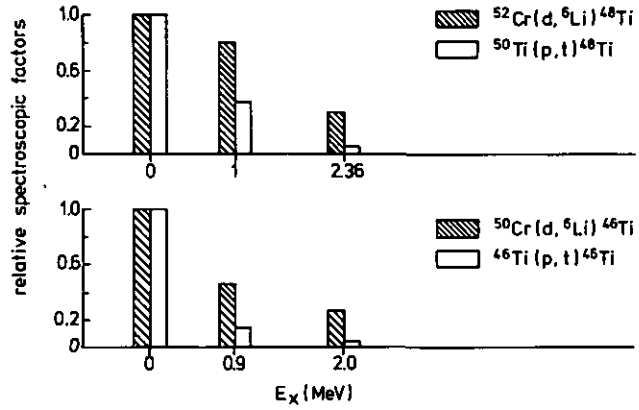

Figure 4: Relative spectroscopic factors for final states in ^{46}Ti and ^{48}Ti.

The relative alpha pick up spectroscopic factor to the 2^+ state at 1.0 MeV in ^{48}Ti (0.82) is seen to be higher than that one to the 0.9 MeV state in ^{46}Ti (0.46). A similar trend is also to be noted in the two neutron transfer reactions, the corresponding relative spectroscopic factors being 0.36 and 0.14, respectively. This result qualitatively indicates that the same pair of neutrons is involved in both the two particle and the four particle transfer reactions.

References

1) Code Autofit, Oak Ridge National Laboratory, unpublished

2) J. Rapaport, et al., Nucl. Phys. A208 (1973) 371; M.W. Baer, et al., Ann. Phys. (New York) 76 (1973) 437

1.20. Emission of Complex Particles in Ni(α,x) and ^{197}Au(α,x) Reactions at E_α = 172.5 MeV*

*G. Gaul**, R. Glasow**, H. Löhner***, B. Ludewigt**, R. Santo**

In continuation of our previous work we have investigated the Au(α,x) reaction at E_α = 172.5 MeV using the achromatic α-beam. Spectra of reaction products up to ^{11}B have been measured with telescopes consisting of surface barrier ΔE-detectors and Ge(Li)- and NaJ-counters as E-detectors. Data are now available at 6 angles between $16^0 \leq \theta_L \leq 72^0$. Figures 1a, b shows energy spectra from ^{58}Ni(α,x) as compared with Au(α,x) at $\theta = 55^0$. While the shapes of the corresponding spectra are very similar, the absolute magnitudes differ significantly. As a systematic trend in the data we observe an increase in the cross section when the N/Z ratio of the corresponding isotope approaches the N/Z ratio of the target nucleus. The effect is particularly striking in the case of the Be isotopes.

For the analysis of the complex particle spectra we have used the coalescence model, where the p-spectra were directly taken from experiment. For low energies, however, the spectra contain appreciable compound evaporation contributions, which had to be subtracted in order to calculate the complex particle spectra. A large error has therefore to be associated with the calculation of spectra below 15 MeV/nucleon. The solid lines in figure 2 represent standard coalescence calculation[1,2], whereas the dotted lines are the results of modified calculations including Coulomb corrections[3]. The extracted p_0 values are collected in table 1. While the overall agreement with the data

	d	t	^{3}He
p_0 MeV/c	211	247	245

Table 1: Momentum radii p_0 as extracted from coalescence model calculations (see fig. 2).

is fair, there are systematic differences in the cross section magnitudes with increasing angle. This indicates that in comparison with detailed and accurate data the coalescence model may be a too crude model for the description of complex particles.

In particular, it has to be investigated wether the particles are emitted from a hot equilibrated source or a more direct reaction mechanism dominates. To answer this question we have started coincidence measurements, where the correlations of emitted particles were measured within and out of the reaction plane. Four counter telescopes were used, three of which were mounted in the reaction plane. The analysis of this part of the data is still in progress.

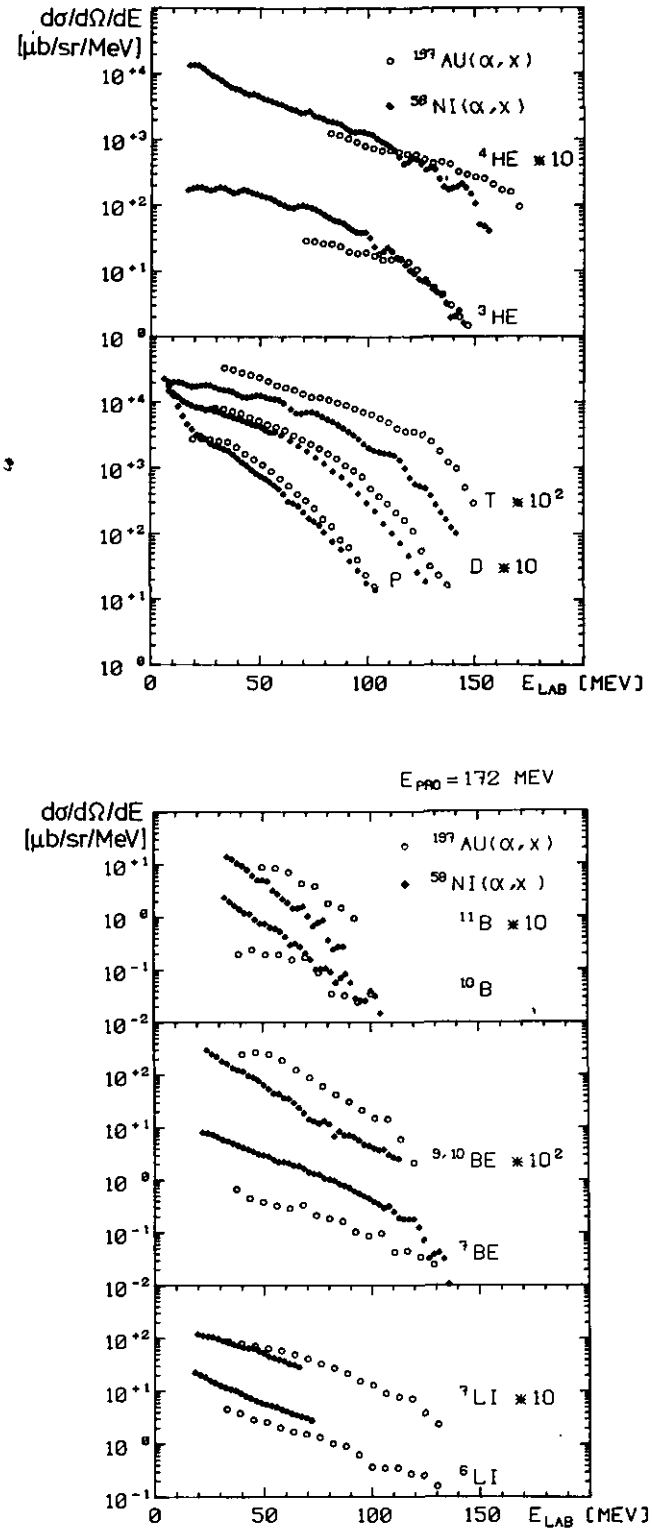

Fig. 1a, b: Experimental energy spectra from ^{58}Ni(α,x) and ^{197}Au(α,x) reactions at $\theta_{LAB} = 55^0$.

*Reported by Bundesminister für Forschung und Technologie, Bonn.

References

1) H.H. Gutbrod, et al., Phys. Rev. Lett. 37 (1976) 667
2) H. Löhner, et al., Z.f.Phys., A292 (1979) 35
3) T.C. Awes, et al., Phys. Rev. Lett. 45 (1980) 513

* Institut für Kernphysik, Universität Münster

**Now at Lawrence Berkeley Laboratory

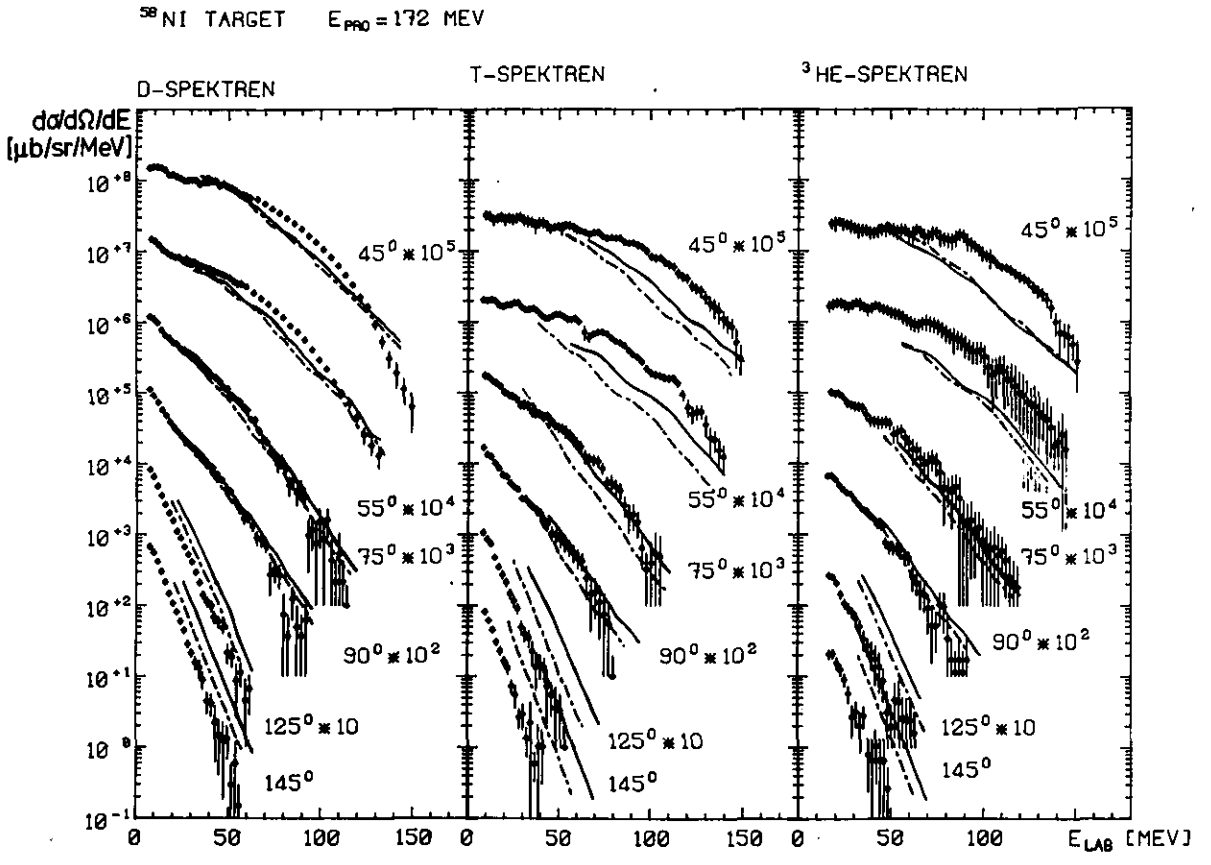

Fig. 2: Experimental d,t, ^{3}He energy spectra from ^{58}Ni(α,x)-reactions together with coalescence calculations (see text).

1.21. Study of the Pre-Compound Reaction Mechanism using (α,α'c) Reactions

U. Bechstedt, H. Machner, A. Budzanowski, P. Jahn and C. Mayer-Böricke*

The investigation of the decay of continuum states via particle emission started last year[1] was continued. To complete the measurements of angular correlations we performed another experiment again measuring the ^{58}Ni(α,α'c) reaction (c = charged particle A≤4) at an incident energy of E_{α} = 140 MeV.

The principal set up at the scattering chamber was the same as in the previous experiment[1]. The α' telescope was fixed at an angle of -30° (negative angles are at right hand side of the beam looking into beam direction). Two telescopes for the detection of decay particles were mounted looking face to face under 180°. The α' telescope consisted of a 1 mm thick Si surface barrier detector as ΔE counter and a Ge(Li) crystal cooled by liquid nitrogen as E detector. The decay telescopes consisted each of three Si surface barrier detectors with thicknesses of 50 µm, 400 µm and 2000 µm for the backward telescope and of 50 µm, 400 µm and a stack of two 2000 µm detectors as third counter for the forward one. In using thinner ΔE detectors in comparison to the previous run[1] we could extend the energy range of all three telescopes to lower energies.

Data were accumulated in eight parameter list mode. Parameters recorded were: 1. the energy measured with the α' telescope, 2. particle identification signal from the α' telescope, 3. time between α' event and decay particle from either of the two decay telescopes, 4. energy deposited in the first counter from either of the two decay telescopes, 5. and 6. like 4. but for the second and the third counter, respectively, 7. total energy deposited in either of the two decay telescopes, 8. a bit pattern setting bits in the data acqisition computer depending on which decay counters give signals. This bit pattern allows for the separation of the different coincidences during data reduction. Particle identification for the decay telescopes is done off line according to the energy range relationship. This allows us to neglect on veto counters for the decay telescopes because during data reduction we can leave out the backbending tail in the particle spectrum originating from particles not stopped in the telescope.

Data reduction is in progress.

Reference

1) U. Bechstedt, et al., Annual Report 1979, IKP, KFA Jülich, Jül-Spez-72, März 1980, p. 30

*permanent address: Institute of Nuclear Physics, Krakow, Poland

1.22. Analysis of Composite Particle Emission from $^{65}Zn^*$ in the Framework of ECM

H. Machner

It has recently been shown that complex particle emission from proton induced reactions could be treated in the exciton model assuming the coalescence of excited nucleons to clusters (exciton coalescence model, ECM)[1]. This model takes only participant-participant interactions into account in contrast to participant-spectator interactions as in the model of ref. 2. The energy distributions of the participating nucleons are, however, not very different of those of the spectator nucleons at excitation energies under discussion here. Therefore the results are expected to be very similar. A further test of ECM would be to compare its predictions with data from complex particle induced reactions.

For this purpose we have chosen the data of a Ghoshal type experiment[3,4]. The composite system $^{65}Zn^*$ at 37.4 MeV excitation energy has been produced via three different projectile-target combinations: ^{63}Cu + 24.7 MeV d, ^{62}Ni + 24.3 MeV ^3He and ^{61}Ni + 35.5 MeV α. Light charged particles up to α's have been measured.

The only model dependent parameters which differ for the different reactions are the initial exciton number n_0 and for composite particle emission a scaling factor γ for the cross section[1]. It is always assumed that the first projectile-target interaction leads to a 1p+1h excitation in the target nucleus. The projectile nucleons are added as additional excited particles. The complex particle emission is possible if there are as many excited nucleons as in the complex ejectile particle plus one additional nucleon which carries the recoil momentum. Thus for α-emission n_0 is

for d-induced reactions: 5p+3h
for ^3He-induced reactions: 5p+2h
for α-induced reactions: 5p+1h

The different choice of n_0 strongly influences the shapes of angle integrated spectra as can be seen from fig. 1. The compound cross section has been calculated by the evaporation approximation. More details of the calculations may be found in ref. 5.

The scaling factor γ is related to a coalescence sphere in momentum space by the relation[1]

$$\gamma_{x+y} = \left|\frac{4}{3}\pi(P_0/mc)^3\right|^{x+y-1}$$

for an ejectile particle with x protons and y neutrons. The coalescence radius is denoted by P_0 and m and c being nucleon mass and velocity of light, respectively. From these P_0 values reduced values have been obtained following ref. 6. Assuming phase space relation between momentum and local space radii R have been obtained. They are compiled in table I. In the last column the radii R_x of the ejectile particles are given. It turns out that there is a correlation between R and R_x. In addition P_0 is largest in the cases where projectile and ejectile particle are identical. This behaviour suggests that a part of the projectile particles survive the interactions with the target nucleus.

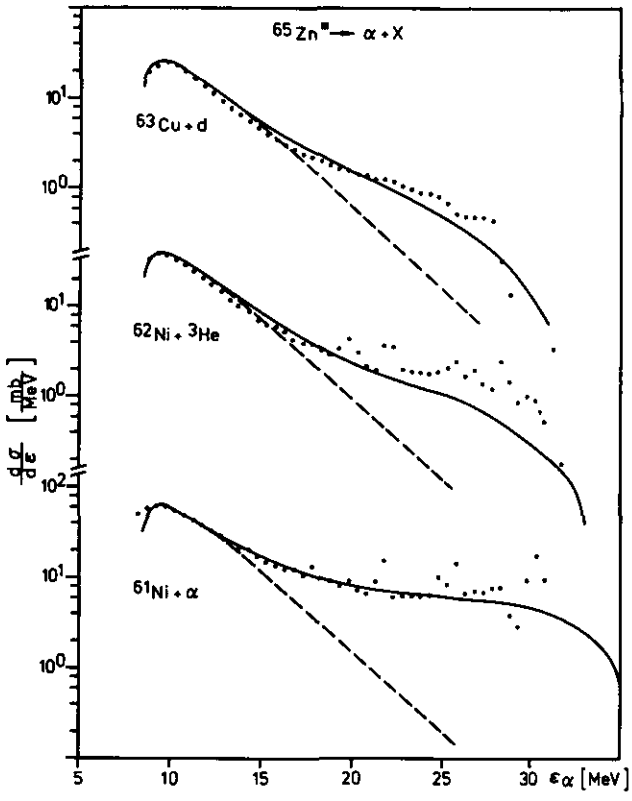

Figure 1: Alpha decay of $^{65}Zn^*$ with E^*=37.4 MeV. The data[4] are represented by dots while the evaporative contribution is dashed line drawn. The sum of evaporation plus preequilibrium contribution is solid line drawn. Different entrance channels are indicated next to the appropriate curves.

entrance channel	exit channel	$P_0/\frac{MeV}{c}$	R/fm	R_x/fm
d		251	3.46	3.24-
^3He	d	247	3.51	4.31
α		207	4.15	
d	t	288	2.28	
^3He	t	261	2.52	1.82
α	t	242	2.71	
^3He	^3He	365	1.80	1.97
d		327	1.70	
^3He	α	315	1.77	1.63
α		360	1.55	

Table 1: Radii of coalescence spheres in momentum space P_0 and of emitting volume R; in the last column the ejectile radii R_x from ref. 7 are given.

Thus the coalescence model, previously applied to high energy data and modified to fit in the frame of the exciton model can well describe the influence of different entrance channels to different exit channels. Data analysis suggests that complex particles do survive in part interactions with nucleons in nuclear matter. The emitting volume for the excited nucleus has approximately the same size as the emitted complex particle, except for t-emission[5].

References

1) H. Machner, Phys. Lett. 86B (1979) 129
2) F. Hachenberg, H.C. Chiang and J. Hüfner, Phys. Lett. 92B (1980) 183
3) S.N. Ghoshal, Phys. Rev. 80 (1950) 929
4) J. Bisplinghoff et al., Nucl. Phys. A269 (1976) 147
5) H. Machner, Phys. Rev. C21 (1980) 2695
6) A. Mekjian, Phys. Rev. C17 (1978) 1051
7) P. Marmier, E. Sheldon, Physics of Nuclei and Particles, Academic Press 1970

1.23. Proton Induced Reactions on Ba

K. Prescher and G. Brinkmann**

In a study of p-induced reactions on Ba having in mind cosmochemical applications[1] we investigated the energy region from 12 to 45 MeV using the stacked-foil technique.

The experimental excitation functions for Ba were compared with calculations based on the hybrid model of Blann[2]. The generally good agreement between theory and experiment is shown as an example in fig. 1. Some discrepancies, however, here still remain with concern to the energy shift (≈ 4 MeV in fig. 1) between theory and experiment. One of the reasons may be the application of a rather crude mass formula. More precise calculations are being performed on the basis of actual nuclide masses. The discrepancy in the excitation function of the (p,2pxn)-reactions (for example fig. 2) surely is due to the preequilibrium emission of

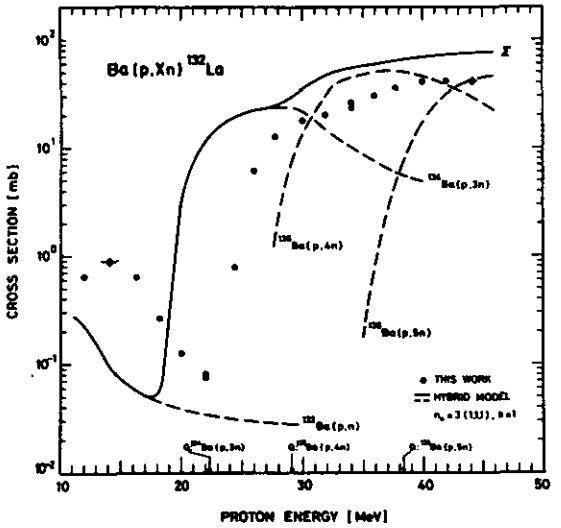

Fig. 1: Comparison of the experimental excitation function for the reaction Ba(p,xn)^{132}La with hybrid model calculations.

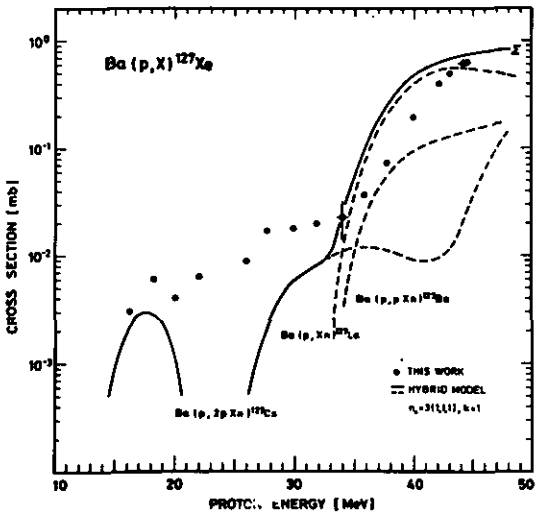

Fig. 2: Comparison of the experimental excitation function for the reaction Ba(p,X)^{127}Xe with hybrid model calculations.

α-particles which was not considered in the present form of the program OVERLAID ALICE[2].

In order to derive depth dependent solar cosmic ray production rates, the energy range has to be extended to higher energies. These experiments are under study and point out that a redetermination of earlier data[3] is urgently needed.

References

1) K. Prescher, G. Brinkmann, W. Herr (1980) NEANDC(E) - 212 U Vol.V INDC (Ger)-22 /L + special.
2) M. Blann, UR-NSRL-181 (1978)
3) W.A. Kaiser, Phil.Trans.R.Soc.Lond.A.285 (1977) 337.

*Institute of Nuclear Chemistry, University of Cologne.

1.24. Integral Excitation Funtions for α-Induced Reactions on Iron and Nickel

R. Michel, G. Brinkmann* and W. Herr**

In the course of a systematic study of α-induced reactions with target elements $22 \leq Z \leq 28$[1,2] we have measured 38 excitation functions for the production of radionuclides $42 \leq A \leq 65$ from natural iron and nickel for $16 \leq E_\alpha \leq 173$ MeV[3]. Such cross sections are useful for calculating the contribution of solar α-particles to the production of cosmogenic nuclides in extraterrestrial matter. In spite of the fact that the p/α ratio in the cosmic radiation is ≈ 10, α-induced reactions may become the dominant production modes for particular nuclides, as e.g. for ^{57}Co, ^{58}Co and ^{59}Ni.

Because there is still a considerable lack of experimental excitation functions for cosmogenically relevant reactions, also the capability of nuclear reaction theories to predict unknown excitation functions is of actual interest. Therefore, we have compared our experimental data with "a priori" calculations applying the hybrid model of Blann[4] using the code OVERLAID ALICE[5]. While for the p-induced reactions in the energy region up to 45 MeV the hybrid model is very successful in predicting unknown excitation functions[e.g.6], for α-induced reactions this is only true with severe restrictions. So the (α,p2n)-, (α,2pn)-, (α,2p3n)-, (α,2p4n)-, (α,3pn)- and (α,4p3n)-reactions are not adequately described by this theory because of the contribution of incomplete α-break-up and/or other direct reactions. As an example, in fig. 1 the excitation function for the production of ^{57}Ni from Ni is presented which is dominated by the ^{58}Ni(α,2p3n)-reaction. The discrepancies between 30 and 60 MeV can be attributed to the neglect of preequilibrium emission of α-particles. However, above 80 MeV the deviation between theory and experiment rather should be due to a direct knock-out of a single neutron by the impinging α-particle. On the other hand, for (α,xn)-reactions and for those reactions leading to products far away from the target nuclides, the "a priori" calculations agree quite well with the experimental data, as it is shown in fig. 2.

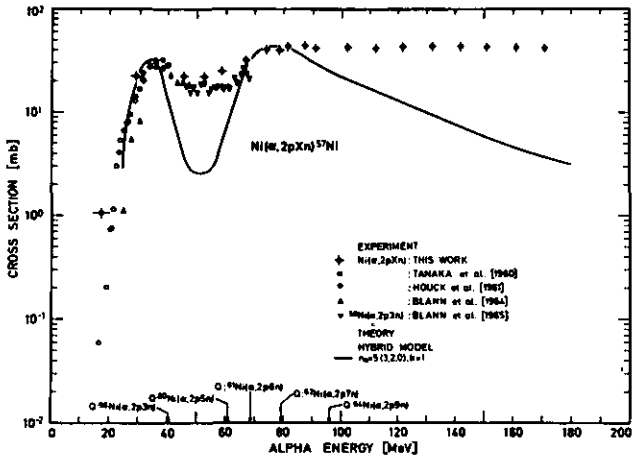

Fig. 1: Experimental cross sections and hybrid model calculations for the production of ^{57}Ni from Ni. For a detailed discussion and for references of the work of other authors see[2].

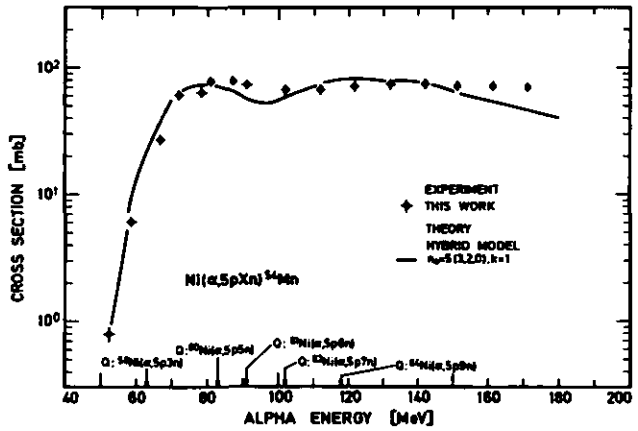

Fig. 2: Experimental excitation function and hybrid model calculation for the production of ^{54}Mn from Ni.

References

1) R. Michel and G. Brinkmann, Nucl.Phys. A338 (1980) 167
2) G. Brinkmann, Thesis, University of Cologne (1980)
3) G. Brinkmann and R. Michel, to be published
4) M. Blann, Phys.Rev.Letters 27 (1971) 337
5) M. Blann, (1978) UR-NSRL-181
6) R. Michel and G. Brinkmann, J.Radioanal.Chem. 59 (1980) 467

*Institute of Nuclear Chemistry, University of Cologne

1.25. On the Production of Heavy Neutron-Rich Nuclei by Fast-Neutron Induced Reactions

H.J. Probst and P. Jahn

Neutron-rich nuclei outside the region of fission products can be produced by fast-neutron induced reactions. In order to explore this possibility, a small test experiment has been performed. Its aim was to produce and detect ^{188}W ($T_{1/2}$ = 69 d) and ^{194}Os ($T_{1/2}$ = 6 a). These isotopes can be reached via the (n,n2p) and (n,nα) reactions on Os and Pt, respectively.

The target arrangement consisted of lucite parts containing an Os and a Pt target of 20 mm diameter and 2 mm thickness. Os powder and Pt foils of natural isotopic composition were used. The arrangement contained also Al foils for monitoring the neutron flux and for checking the beam alignment. It was placed into the beam axis just behind an ordinary Faraday cup. For the irradiation a 80 MeV deuteron beam of 1 μA was stopped in the graphite plate of the cup during a period of 24 hours.

After a cooling time of four months the γ-ray spectrum of the target arrangement was measured with a Ge(Li) spectrometer. During a measuring time of 10^5 seconds 37500 counts were accumulated in the 155 keV line in the decay of ^{188}Re ($T_{1/2}$ = 20 h); the statistical error amounts to ≈ 15 % due to the large background. The decay of ^{194}Os will be measured later.

It should be mentioned that the method can of course be substantially improved not only by dismounting the target and using a better source geometry but also by performing chemical separations. These procedures, however, are much more difficult to apply in the case of short-living nuclei.

1.26. (d,t...)-Excitation Functions for Al, V, Nb and Au[+)]

M. Merkel, H. Münzel**

Stacks of Al, V, Nb and Au foils have been irradiated with deuterons up to 90 MeV. Above 50 MeV the experiments were performed at BK1 of the JULIC-Cyclotron. The targets were thick enough to stop all tritons formed by nuclear reactions. With the method described in [1] the tritium activities were measured. From these thick-target yields excitation functions for the formation of tritons have been calculated. They are given in fig. 1 together with curves calculated using the code PREEQ[2]. The dashed lines give the results obtained with the formation probability for complex particles $\gamma_\beta = 0.1$ and $\gamma_\beta = 0.01$. It should be mentioned that the calculations take only the first emitted particles into account. Therefore at higher energies, where usually more than one particle will be emitted, these calculations underestimate the particle emission. Therefore calculations with the program AMALTHEE[3] which considers two particles in the outgoing channel are in progress.

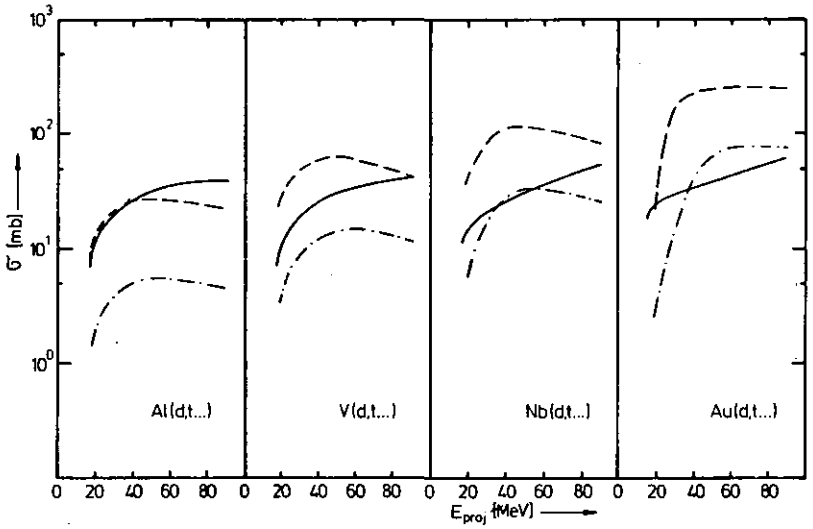

Fig.1 Excitation functions for (d,t...)-reactions
—— experimental values
– – Theory (γ_β=0.1)
–·– Theory (γ_β=0.01)

Target	Incident proj. energy [MeV]	Thick-target yield[++]
Al	12.0	2.05 E-6
	18.0	2.03 E-5
	24.0	7.27 E-5
	38.0	2.91 E-4
	50.8	7.53 E-4
	70.0	1.77 E-3
	89.8	3.35 E-3
V	12.0	2.05 E-6
	18.0	1.51 E-5
	24.0	5.19 E-5
	38.0	1.99 E-4
	50.5	4.61 E-4
	70.0	1.23 E-3
	89.8	2.30 E-3
Nb	12.0	2.37 E-6
	18.0	1.85 E-5
	24.0	5.14 E-5
	38.0	1.60 E-4
	50.8	3.42 E-4
	70.0	7.26 E-4
	89.8	1.42 E-3
Au	12.0	6.80 E-7
	18.0	1.97 E-5
	24.0	5.08 E-5
	38.0	1.46 E-4
	50.8	2.69 E-4
	70.0	5.98 E-4
	89.8	1.12 E-3

[++]The yields are given as the number of tritons per incident projectile

Table 1: Thick-target yields for (d,t...) reactions

[+)]This work was supported by the Bundesministerium für Forschung und Technologie, Federal Republic of Germany

References

1) M. Merkel, H. Münzel, Nucl. Phys. A333 (1980) 173
2) E. Běták, Computer Physics Communications 9 (1975) 92
3) O. Bersillon, L. Fangere, NEANDC (E) 184 "L" (1977)

*Fachbereich 8 für Anorganische Chemie und Kernchemie
Technische Hochschule Darmstadt

1.27. Non-Equilibrium Particle Emission in 75 MeV α-Particle Bombardment of ^{209}Bi

J.P. Didelez, R.M. Lieder, B. Bochev, T. Kutsarova, T. Morek, M. Müller-Veggian and C. Mayer-Böricke*

As an extension of our previous study of non-equilibrium processes for the reaction ^{209}Bi(α,ch.p.xnγ) at 45 MeV incident energy[1,2], measurements of energy spectra and angular distributions of p, d and t have been carried out at E_α = 75 MeV. The particle-γ coincidence technique has been used in order to obtain spectra of charged particles for individual reaction channels. The coincidences were measured by placing the particle detector telescope at angles of 45°, 90° and 135°. Some results concerning proton emission at E_α = 75 MeV have already been published[2].

In fig. 1 yield curves corresponding to the proton spectra at 45° for various (α,pxn) channels are shown. As in

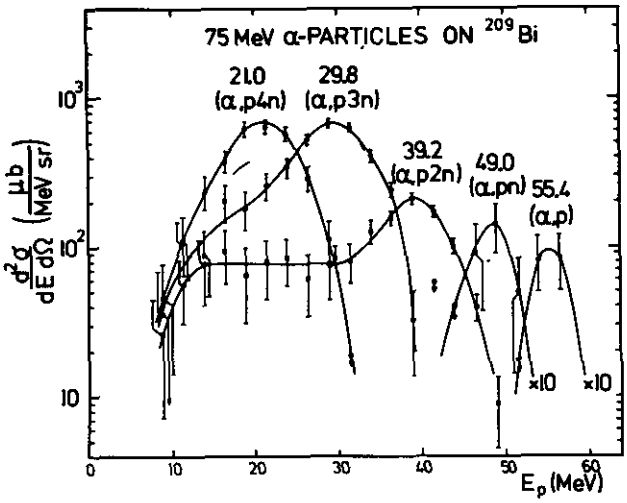

Figure 1: Yield curves for the (α,pxn) reaction at E_α = 75 MeV and a telescope angle of 45°. They are obtained by setting gates on 2.5 MeV portions of the proton spectrum and integrating γ-lines corresponding to the ground state transitions of the final Po nuclei. The curves are eye-guiding lines.

the case of the 45 MeV experiment, pronounced peaks can be seen in the proton spectrum of each channel. A new feature observed in the 75 MeV experiment is the existence of low energy tails. In fig. 1 tails are seen for the (α,p2n) and (α,p3n) channels. Similar results are obtained for the (α,dn), (α,d2n), (α,tn) and (α,t2n) channels. For the (α,pn) channel no tail has been observed probably due to the small yield of this channel. For the (α,p), (α,d) and (α,t) channels no tails are expected since high energy γ-rays have a very small transition probability as compared to n-emission probability. However, due to statistical uncertainties this statement could not be proved experimentally. The tails observed in the other channels extend to energies as small as the detection thresholds for p, d and t. The yields of the tails are by a factor of ≈3, ≈7, ≈7 and ≈7 smaller than those of the maxima of the peaks for (α,p2n), (α,dn), (α,tn) and (α,t2n) channels, respectively.

The angular distributions of protons are shown in fig. 2 for pxn channels with x = 2, 3, 4. For the (α,p2n) and (α,p3n) reactions angular distributions for the peak as

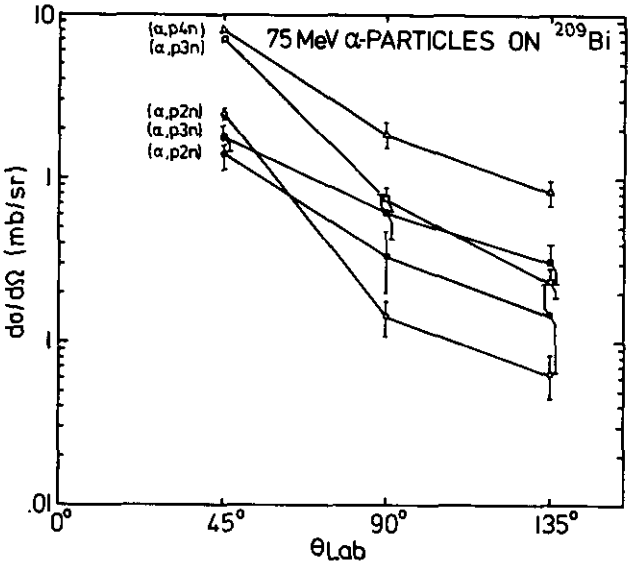

Figure 2: Energy-integrated angular distributions of protons for the ^{209}Bi(α,pxn) reactions at E_α = 75 MeV. Open and full symbols are for the protons from the peak and tail regions, respectively. The curves are eye-guiding lines.

well as tail regions are given. The anisotropies of the angular distributions are larger for the peak regions than for the tails.

The energies of the particles and their angular distributions are characteristic of a nonequilibrium process. The existence of peaks in the proton spectra and their energies can be understood within the framework of the yrast picture[2,3]. The protons associated with the peaks carry away almost all available excitation energy. They are emitted from the highly-excited final nucleus as the first particles and the neutrons are evaporated subsequently[2,3].

For the tail regions most probably one neutron is emitted with a large energy. In this case the neutron and one proton are emitted in the non-equilibrium phase and the remaining neutrons are evaporated. Such an interpretation of the p spectra is supported by the angular distribution results. The anisotropies of the angular distributions are larger for the peak regions than for the tails since in the former case the protons are emitted as first particle whereas in the latter case the protons are emitted from a system which is already cooled down somewhat by the emission of the fast neutron.

References

1) B. Bochev, R.M. Lieder, J.P. Didelez, T. Kutsarova, H. Beuscher, D. Haenni, H. Machner, T. Morek, M. Müller-Veggian, A. Neskakis, and C. Mayer-Böricke, Annual Report 1979, Jülich, Jül-Spez-72 (1980) p. 33

2) R.M. Lieder, B. Bochev, T. Kutsarova, H. Beuscher, D.R. Haenni, T. Morek, M. Müller-Veggian, A. Neskakis, C. Mayer-Böricke, and J.P. Didelez, Contribution to the Nobel Symposium on Nuclei at very high spin Sven Gösta Nilsson in Memoriam, 23-27 June, 1980, Örenäs Castle, Sweden

3) R.M. Lieder, B. Bochev, T. Kutsarova, J.P. Didelez, and C. Mayer-Böricke, separate contribution to this report

*Institut de Physique Nucléaire, F-91406 Orsay, France

1.28. Study of Continuous Particle Spectra from 200 MeV Proton Bombardment

J.P. Didelez, N. Frascaria*, E. Gerlic*, E. Hourani*, H. Morlet*, H. Machner, D. Protić, G. Riepe, C. Sükösd*

The investigation of continuous particle spectra has been pursued. At high energies the emission of more than one particle in the pre-equilibrium phase is possible[1]. To avoid uncertainties as e.g. projectile fragmentation for this investigation, high energy protons have been chosen as the projectile particles.

The experiments were carried out with the 200 MeV proton beam of the Orsay synchrocyclotron. Energy spectra of charged particles (p,d,t) were measured using a HPGe multi-detector telescope[2] consisting of 7 detectors with a total thickness of 80 mm. To reduce the effects from slit scattering a HPGe active collimator[3] was mounted at the first place of the stack. The central circular area with 6 mm diameter was connected in coincidence with subsequent detectors, thus defining the solid angle. In similar experiments at lower bombarding energies an active collimator was found to be necessary for small angle measurements[4,5]. For those experiments the active collimators had been made from scintillation material.

Data taking was accomplished using the system CALI[6] connected to a Hewlett-Packard on-line computer. The signals from detectors $E_1 \ldots E_7$ were recorded on magnetic tape. In addition, the analog sum of the preamplifier outputs was fed to another linear chain and as well recorded, thus escaping the difficulties resulting from ADC-thresholds.

Spectra from the bombardment of ^{27}Al and ^{197}Au in the angular range from 14^0 to 150^0 (laboratory system) were taken. As an example the spectrum from $^{27}Al(p,p'x)$ at $\theta_{Lab}=14^0$ is shown in fig. 1. The position of the GQR is indicated. The broad structure around $\epsilon_p=160$ MeV stems from quasi-free scattering (QFS)[7]. Data analysis is in progress.

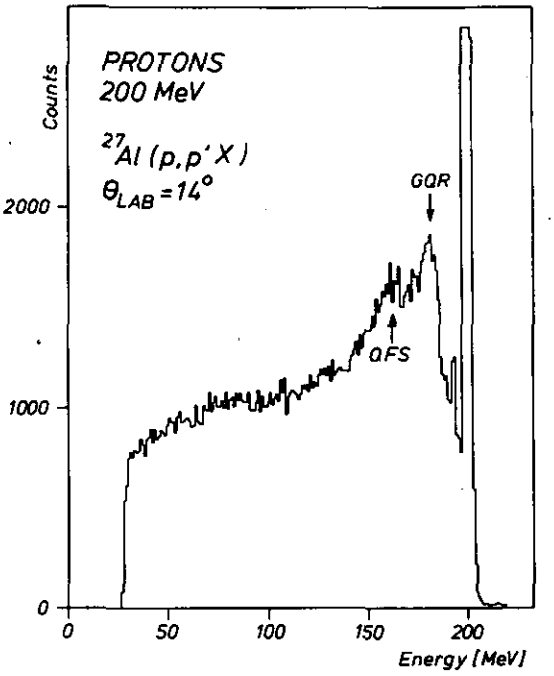

Figure 1: Spectrum of protons from the bombardment of ^{27}Al with 200 MeV protons. Data are averaged over 1 MeV bins. The structure at $\epsilon_p \approx 180$ MeV (corresponding to $E_x=20$ MeV) is from the excitation of the giant quadruple resonance (GQR) while the bump around $\epsilon_p \approx 160$ MeV is from quasi-free scattering (QFS).

References

1) H. Machner in Proceedings of the International Workshop on Gross Properties of Nuclei and Nuclear Excitations, Hirschegg, 1980, 142

2) G. Riepe et al., Nuclear Instr. Meth. 117 (1980) 361

3) see contribution from detector laboratory in this report

4) F.E. Bertrand et al., Nucl. Instr. Meth. 101 (1972) 475

5) A.A. Cowley et al., Phys. Rev. C22 (1980) 2633

6) J. Pouthas, Nucl. Instr. Meth. 135 (1976) 187

7) P.G. Roos and N.S. Wall, Phys. Rev. 140 (1965) 1237, ibid 150 (1966) 811

*Institut de Physique Nucléaire, Orsay, Frankreich

1.29. Elastic and Inelastic Proton Scattering on ^{106}Pd and ^{108}Pd at E_p = 43.8 MeV

G.P.A. Berg, E. Fretwurst, R. Kolalis**, G. Lindström*, S.A. Martin, J. Meißburger, W. Oelert, K.F. von Reden*, V. Riech*, P. Vlachodimitropoulos**

High precision proton scattering experiments on the even isotopes of Palladium were started, in order to compare these results with a microscopic description of the optical model[1]. For this purpose it is of major importance, to include the inelastic channels to the strongly excited first one quadrupole phonon (around 0.5 MeV) and octupole state (around 2 MeV) as well as to the weakly excited and narrowly spaced two quadrupole phonon triplet states (around 1 MeV). An extremely good energy resolution (better than 10 keV) and high accuracy for the absolute cross sections (better than 5%) are essential for this experiment. Preliminary results for ^{106}Pd(p,p') at 45 MeV were obtained with the magnetic spectrograph BIG KARL and proved that the necessary energy resolution could be achieved[2].

The main purpose of the investigations carried out in the last year was the determination of reliable absolute cross sections in a usual detector experiment performed in the large scattering chamber of the JULIC-cyclotron laboratory. These results shall serve as normalization standards for further BIG KARL-experiments.

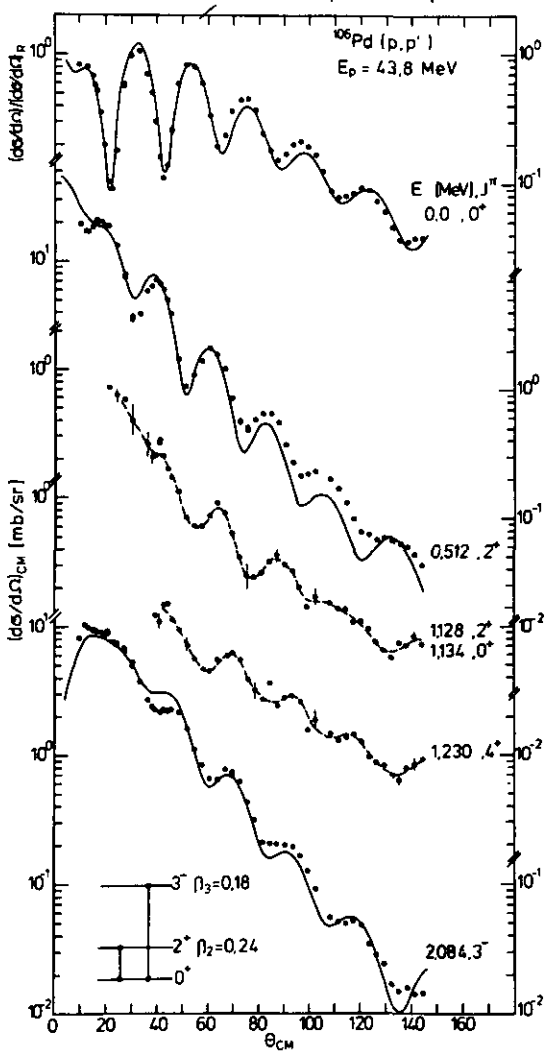

Fig. 1: ^{106}Pd(p,p-) angular distributions
The solid lines represent preliminary CC-calculations corresponding to the indicated coupling scheme. The dashed lines drawn through the triplet state angular distributions are intended to guide the eye.

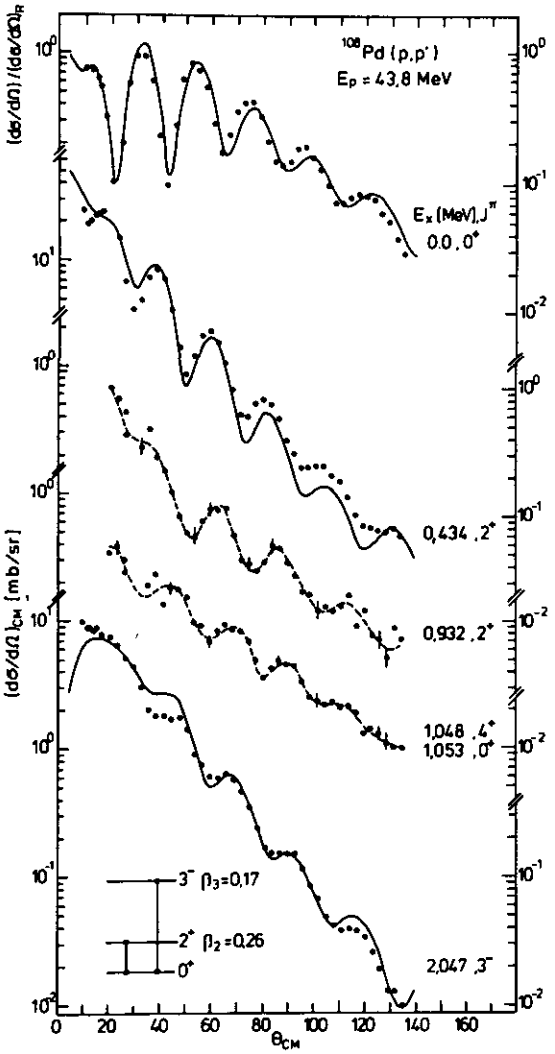

Fig. 2: ^{108}Pd(p,p') angular distributions
(For explanation see figure 1)

The thicknesses of the self-supporting metallic Palladium targets were determined to an accuracy of about 2% using a combination of weighing, alpha-particle energy loss and Rutherford scattering for thin targets as well as comparative proton scattering at higher energies for thick targets. Ge(Li)-detectors of the side entry type from the detector group of the IKP[3] were used troughout the experiment.

Fig. 1 and 2 show the measured differential cross sections for the transitions to the ground state and the excited states under investigation (see above). It should be mentioned that in the cases of ^{106}Pd and ^{108}Pd the not resolved levels in the triplet have a spacing of 5 keV. In the other Pd-isotopes presently under investigation the minimum level spacing is 10 keV. In addition the cross section accuracy for these triplet states has to be improved appreciably in order to analyze the data with respect to the anharmonicity effects which are responsible for their energy splitting.

First results of coupled channels calculations using the code ECIS[4] are included in the figures. In the present state of a 7-parameter optical model search with start parameters from KOIKE et al.[5] the couplings with the two phonon states were not included. The same potentials are used for both ^{106}Pd and ^{108}Pd. However these preliminary calculations show already a good overall fit to the absolute cross sections of the ground state and the one phonon states. Further improvements are presently in progress.

In conclusion we like to mention, that the experiments which will be carried out using the high energy resolution performance of BIG KARL are accompanied by detector experiments at lower energies (25 and 15 MeV) in Hamburg[6].

References

1) H.V. von Geramb, Microscopic optical potentials, Lect. Notes Phys. 89, Springer, 1979
H.V. von Geramb, G. Pálla in Synopsis 1978/79 der Theoretischen Kernphysik, I. Institut für Experimentalphysik, Universität Hamburg

2) G.P.A. Berg et al., KFA Jülich, Inst. f. Kernphysik, Annual Report 1979, p. 40

3) D. Protić, G. Riepe, Detector Laboratory, KFA Jülich, Institut für Kernphysik

4) J. Raynal, C.E.N. Saclay

5) M. Koike et al., Nucl. Phys. A248 (1975), 237

6) G. Lindström et al., Frühjahrstagung der DPG, München 1980
G. Lindström et al., Int. Symposium on High Precision Nuclear Physics, Bad Honnef 1980

* I. Institut für Experimentalphysik, Universität Hamburg

**Institute of Physics, University of Leningrad

1.30. Search for Spin-Flip excitations in ^{208}Pb

G.P.A. Berg, P. Decowski, I. Katayama, S.A. Martin, J. Meißburger, P. Morsch, M. Rogge, B. Styczen, P. Turek

Collective spin-flip excitations are expected in ^{208}Pb at excitation energies E_x > 5 MeV[1]. Such excitations have been found in proton[2] and electron[3] scattering. The study of these excitations is motivated by possibility to obtain information of the spin-dependent nucleon-nucleon forces. In the investigated energy region the level spacing is smaller than 10 keV. Therefore high resolution measurements are necessary.

In order to identify spin-flip excitations p-, d-, and α-particle inelastic scattering on ^{208}Pb have been measured. Incident particles energies were 45 MeV for p and d, and 90 MeV for α. The resolution was 8-11 keV except for the α inelastic scattering, where the resolution was 35 keV due to not optimized magnet system. Thicknesses of the targets were typically 200 ÷ 300 μg/cm^2.

Isovector and isoscalar components are excited in p inelastic scattering. Comparison of p and d scattering allows to sort out isoscalar excitations. Because in α scattering isoscalar (ΔT=0) non-spin-flip (Δs=0) components are excited the comparison of d and α scattering will help to sort out isoscalar non-spin-flip excitations.

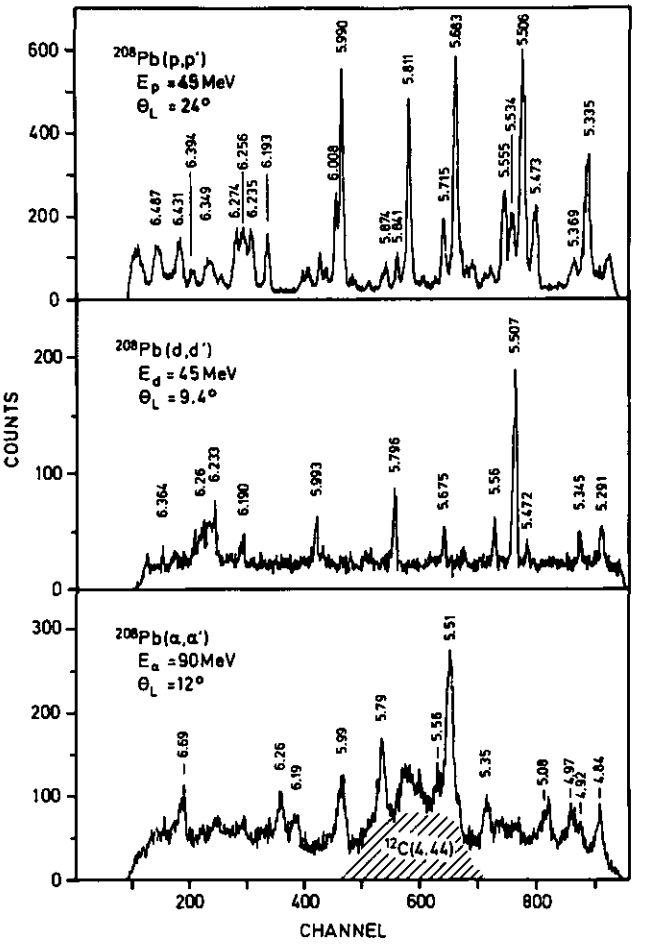

Fig. 1: Spectra of inelastic p-, d-, and α-scattering on ^{208}Pb

On fig. 1 sample spectra of p,d, and α particle inelastic scattering on ^{208}Pb are shown in the excitation energy region E_x = 5 - 6.5 MeV. The strongly excited peaks are seen in all three spectra except the E_x = 5.335, 5.534 and 6.008 MeV states which may have dominant isovector components. Comparisons of calculations and experimental cross section angular destribution will decide about spin-flip or non-spin-flip character of these excitations. For the search of weak spin-flip excitations it is necessary to measure high resolution α- and d-scattering spectra without background which come from slit-scattered particles.

References

1) P. Ring and J. Speth, Nucl. Phys. A235 (1974) 315

2) H.P. Morsch, P. Decowski, and W. Benenson, Nucl. Phys. A297 (1978) 317

3) R. Frey, A. Friebel, W. Mettner, D. Meuer, A. Richter, E. Spamer and O. Titze, Phys. Lett. 77B (1978) 367

1.31. High Resolution Spectroscopy of $^{102}Ru(d,p)^{109}Ru$ and $^{104}Ru(p,d)^{103}Ru$ Reactions

G.P.A. Berg, M. Demarteau, A. Hardt, W. Hürlimann, M. Köhler, S.A. Martin, J. Meißburger, W. Oelert, I. Oelrich[+], J. Scheerer[+], H. Seyfarth, B. Styczen

The high resolution magnetic spectrometer BIG KARL was used to investigate the low lying states of ^{103}Ru by $^{102}Ru(d,p)$ stripping and $^{104}Ru(p,d)$ pick-up reactions at incident energies of E_d = 45 MeV and E_p = 29 MeV. The resolution of $\Delta E/E$ (1.7 - 2.5)·10^{-4} was sufficient to separate all strongly excited states up to $E_x \approx 900$ keV excitations energy. For these levels cross section angular distributions have been measured in the range of $\Theta_{lab} = 4^0 - 43^0$. A DWBA analysis has been employed in order to verify a number of tentative spin and parity assignments, to resolve existing ambignities and to obtain spectroscopic factors. In total a number of ∿ 20 excited states in ^{103}Ru could be identified and excitation energies with an error of about ± 2 keV have been determined. The angular distributions of the $l_n = 2$ transitions are shown in Fig. 1 and Fig. 2 for $^{102}Ru(d,p)^{103}Ru$ and $^{104}Ru(p,d)^{103}Ru$ respectively. The sums of the deduced spectroscopic factors ΣC^2S giving the neutron distributions of the populated shell orbits are shown in Table I.

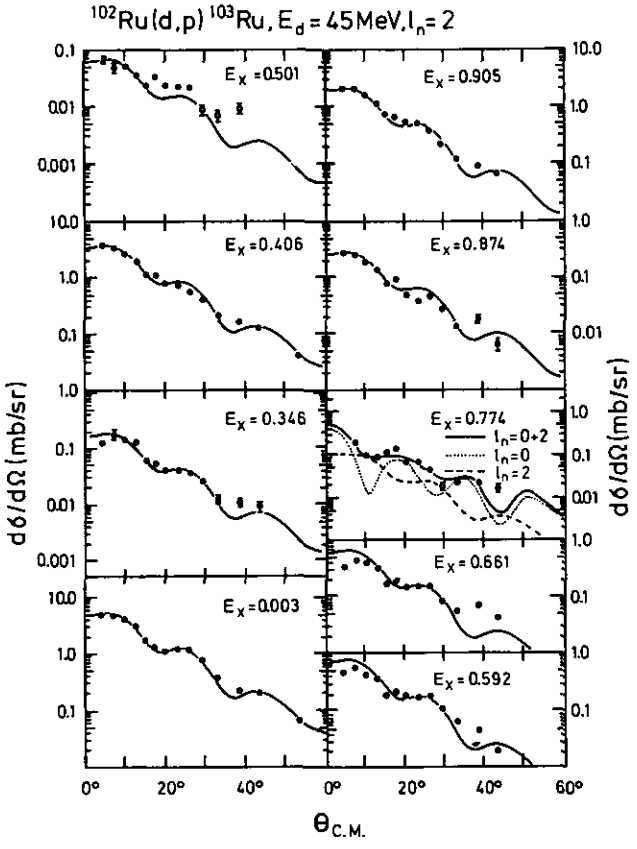

Figure 1: Measured cross section angular distributions of the $^{102}Ru(d,p)^{103}Ru$ reaction for all transitions identified as l_n = 2. Solid lines represent DWBA calculations.

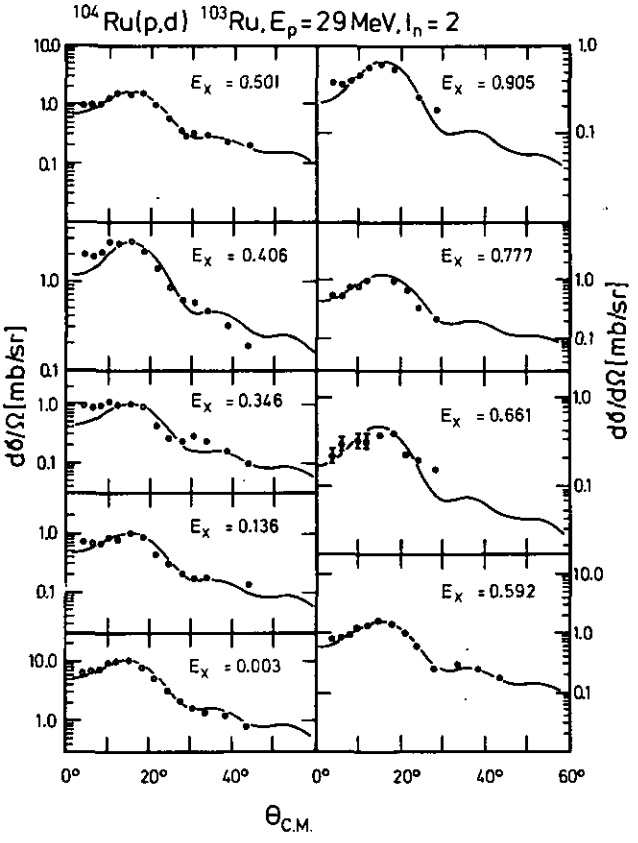

Figure 2: Measured angular distributions and DWBA results for l_n = 2 transitions of the $^{104}Ru(p,d)^{103}Ru$ reaction.

		^{102}Ru ΣC^2S from (d,p)		^{104}Ru $\Sigma(2j_n+1)C^2S$		
l	shell orbit	this work	Fortune[b]	(p,d)-this work	(d,t)-Diehl[c]	(d,p)-Fortune[b]
0	3s1/2	1.45 (0.55)[a]	1.18 (0.82)[a]	0.51	0.70	1.22 (0.78)[a]
2	2d5/2,2d3/2	4.97 (5.03)	4.60 (5.40)	2.81	3.63	4.80 (5.20)
3	2f7/2	0.89	1.50	0.69	-	-
4	1g7/2	1.94	3.35	1.30	2.83	1.86
5	1h11/2	2.35	3.25	1.55	1.92	3.36

Table I: Sum of deduced spectroscopic factors of $^{102}Ru(d,p)^{103}Ru$ and $^{104}Ru(p,d)^{103}Ru$ reactions and comparison of values from literature.

a) Neutron numbers for (d,p) reactions calculated from shell model limits are given in paranthesis
b) H.T. Fortune, G.C. Morrison, J.A. Nolen, Phys. Rev. C3 (1971) 337
c) R.C. Diehl, B.L. Cohen, R.A. Mayer, L.H. Goldman, Phys. Rev. C1 (1970) 2086

[+]Technische Universität München

1.32. High Resolution Study of ^{23}Na and ^{24}Mg States Excited via (p,α) Reactions

F. Hoyler, G. Staudt*, G.P.A. Berg, W. Hürlimann, I. Katayama, S.A. Martin, J. Meißburger, B. Styczen*

The spectroscopic factors for the transfer of a three-nucleon cluster calculated by Chung and Wildenthal[1] for nuclei of the sd-shell using SU3 formalism can be tested by investigations of transition strengths in (p,α) reactions at high incident energies. To gain information from the excitation of high lying states, an energy resolution of at least 50 keV is required.

A first experiment was run in the achromatic mode of the isochronous cyclotron JULIC with beam currents of 800 nA and a solid angle of 8 10^{-4} sterad, approximately, because small cross-sections were expected. Figure 1 shows spectra

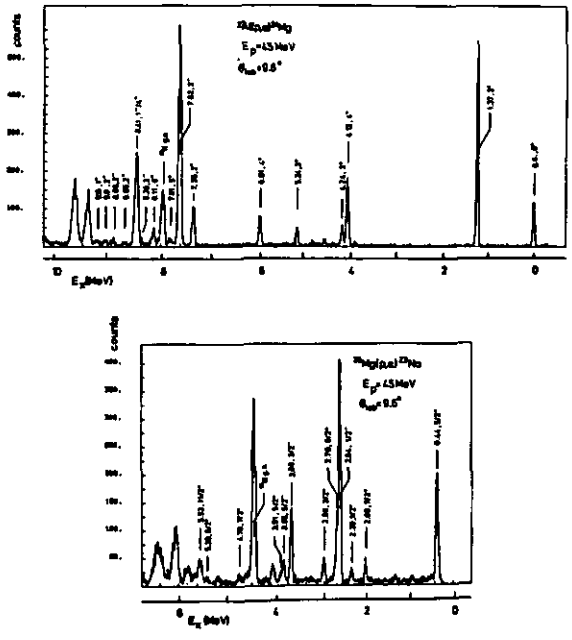

Fig. 1: Spectra of α-particles from ^{26}Mg(p,α)^{23}Na and ^{27}Al(p,α)^{24}Mg at 9.6° measured at E_ϕ = 45 MeV.

of the reactions mentioned below at E_p = 45 MeV. The spectrum of the reaction ^{27}Al(p,α)^{24}Mg was taken in two steps using different parameters for the magnetic spectrometer. In the spectrum of the reaction ^{26}Mg(p,α)^{23}Na the transition to the ground state has been missed. From the spectra one obtains an energy resolution $\frac{\delta E}{E}$ = 1 °/oo.

For both reactions we give in figure 2 the differential cross sections at θ_{LAB} = 9.6° (open bars) together with the predictions of the shell model calculations of Chung and Wildenthal (black bars). In line with previous results[2], we find a rather good agreement between the experimental and the calculated data, even neglecting any corrections from kinematical effects.

In a recent experiment angular distributions in the range of θ_{lab} = 5° - 27° have been measured for excitation energies E_x = 2.0 - 5.5 MeV and E_x = 5.6 - 9.2 MeV in a different magnet setting with a resolution of ΔE ≈ 35 keV.

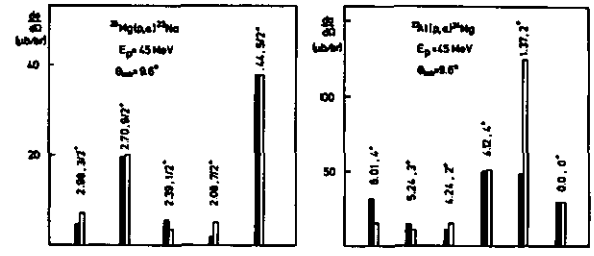

Fig. 2: Comparison of measured differential cross sections at 9.6° (open bars) with spectroscopic strength, calculated by Chung and Wildenthal (black bars).

References

1) W. Chung and B.H. Wildenthal (private communication)

2) F. Hoyler, T. Rohwer, G. Staudt, Annual Report 1979, Institut für Kernphysik of KFA Jülich, JÜl-Spez-72, p. 14

*Physikalisches Institut der Universität Tübingen

1.33. Excitation of proton particle-hole states in ^{208}Pb by ^{209}Bi(d,^{3}He)^{208}Pb reactions

G.P.A. Berg, W. Hürlimann, I. Katayama, G. Mairle, S.A. Martin, J. Meißburger, U. Schmidt-Rohr*, B. Styczen, G.J. Wagner**

In the doubly-closed ^{208}Pb nucleus single particle hole states corresponding to the $3s_{1/2}$, $2d_{3/2}$, $1h_{11/2}$ and higher shells can be excited easily using the proton pick-up reaction (d,^{3}He) as shown in Fig. 1a. By coupling of the $1h_{9/2}$ proton to these hole states there will be multiplets in ^{209}Bi. The residual interaction can be determined from this level splitting.

Previous experiments of ^{209}Bi(d,^{3}He)^{208}Pb by the Heidelberg group did not resolve the multiplet states completely because of the resolution of 100 keV limited by the detector telescopes (see Fig. 1b). In Fig. 1c a spectrum of this reaction is shown recently measured in Osaka with the high resolution spectrometer RAIDEN. The resolution of 20 keV resolves clearly the group of five states between E_x = 3.71 - 4.38 MeV excitation energy. Using the magnetic spectrometer BIG KARL we obtained a resolution of 12 keV for ^{209}Bi targets with 350 μg/cm^2 thickness resolving the doublets at E_x = 4.26 and 4.38 MeV (see Fig. 1d). For these states cross section angular distributions will be measured for the determination of the transfered orbital angular momenta.

*Max-Planck-Institut für Kernphysik, Heidelberg

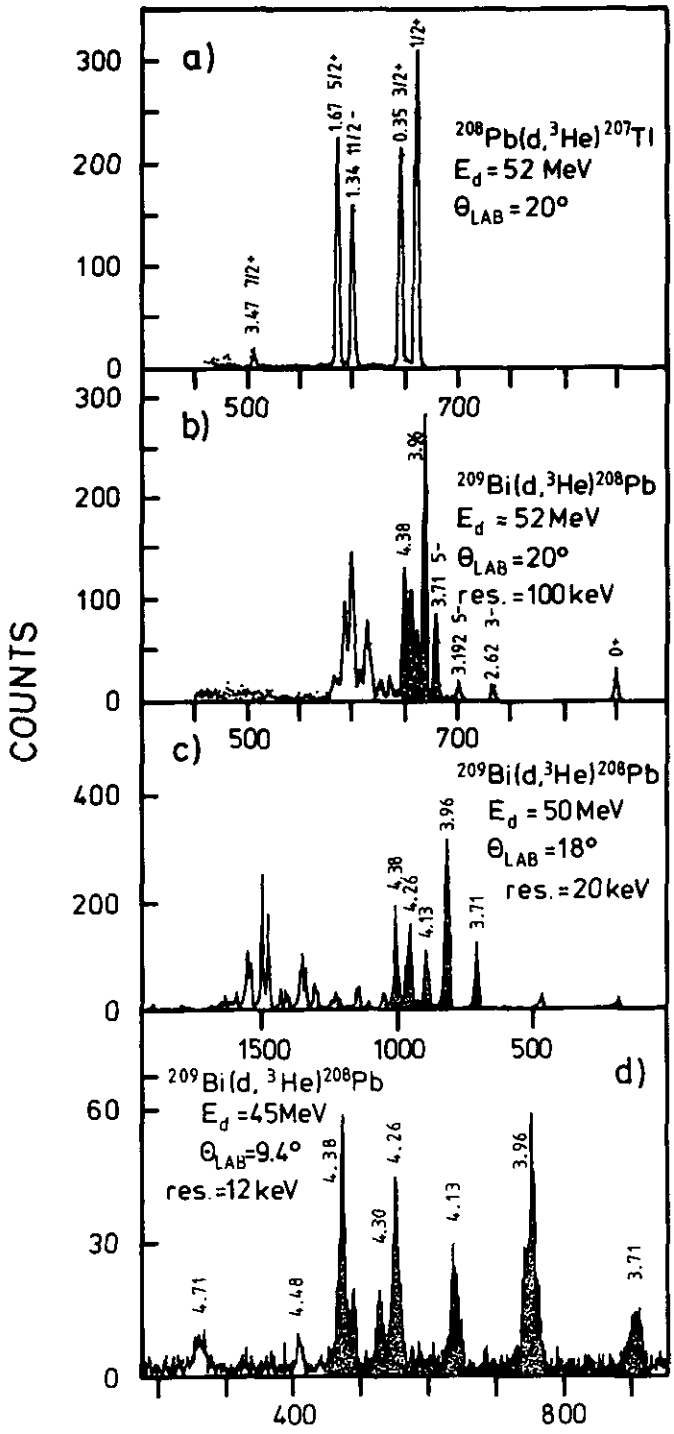

Fig. 1: a,b.: Spectra of the Heidelberg group measured with detector telescopes of the ^{208}Pb(d,^{3}He)^{207}Tl and ^{209}Bi(d,^{3}He). Both spectra are measured with the same experimental arrangement, therefore energies can be compared directly. c: This spectra was measured at Osaka using the QDMDQ spectrograph RAIDEN. d: BIG KARL Spectrum

1.34. Investigation of (d,^{6}Li) Reactions on f-p-Shell Target Nuclei

G.P.A. Berg, W. Hürlimann, S. Martin, J. Meißburger, W. Oelert, B. Styczen

Investigations of four-nucleon transfer reactions are motivated by the possibility to obtain information on four-nucleon correlations and spectroscopic factors for the transfer of α-clusters. While cross sections of (d,^{6}Li) reactions are found to be 10-100 μb/sr for s-d-shell target nuclei, they decrease to typically 1 μb/sr for f-p-shell nuclei.

We started the investigation of (d,^{6}Li) reactions on even mass Zn isotops using the high resolution magnetic spectrometer BIG KARL with a large solid angle (up to 10 msr). In Fig. 1 spectra of the ^{66,68}Zn (d,^{6}Li)^{62,64}Ni

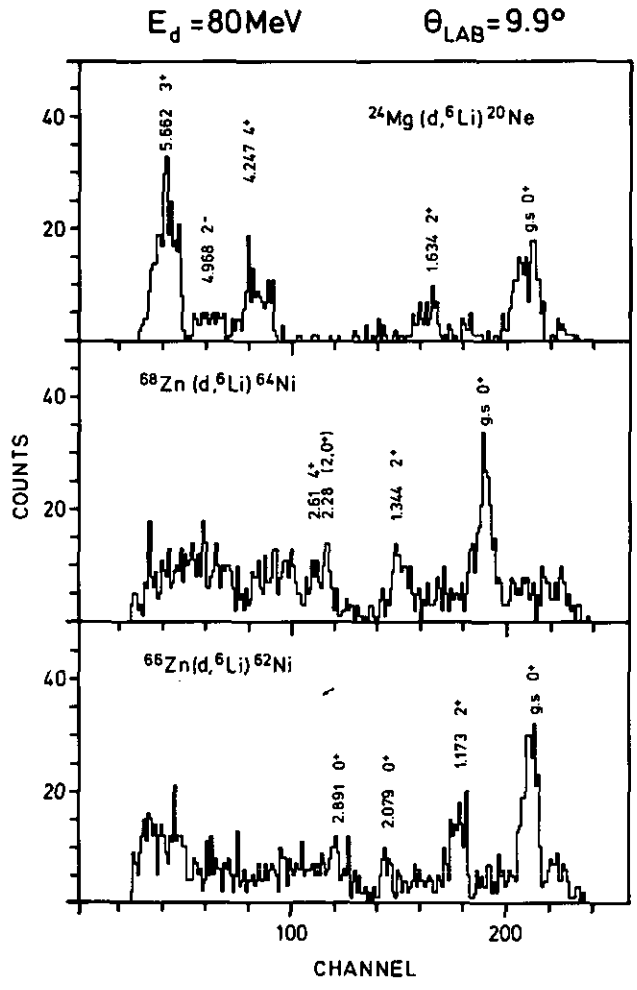

Figure 1: Spectra of the (d,^{6}Li) reactions. See Text for details.

reactions are shown at E_d = 80 MeV incident energy and θ_{lab} = 9.9° scattering angle. The solid angle was 3.2 msr. The resolution of ΔE = 250 keV is mainly due to target thickness effects, ^{66}Zn was 0.84 mg/cm^2 and ^{68}Zn was 1.06 mg/cm^2 thick.

For comparison a ^{24}Mg-spectra (target thickness 1.05 mg/cm^2) is shown in Fig. 1 with the same corrections for the magnet system adjusted for the kinematics of Zn-targets. Therefore the resolution (ΔE ≈ 350 keV) of the ^{24}Mg spec-

trum is slightly worse. The background in the Zn-spectra is due to the insufficient particle identification in the present ΔE-detector. Our new ionisation chamber with a better ΔE resolution will be soon in operation and will be used in the following measurements of the (d,^{6}Li) experiment.

1.35. $(0^+ \rightarrow 4_1^+)$-Hexadecapole Transition in $^{204}Pb(\alpha,\alpha')^{204}Pb$

G.P.A. Berg, H.J. Gils[+], S.A. Martin, J. Meißburger, H. Rebel[+], W. Stach[++], B. Styczen, R. de Swiniarski[+++], S. Zagromski[+]

There is considerable evidence for collective hexadecapole motion in spherical and quasi-spherical nuclei. Inelastic alpha particle scattering[1] in the 100 MeV region showed a high sensitivity to magnitude and phase of the L = 4 transition amplitudes and revealed a correlation between a strong lowering of the energy level ratio $E4_1^+/E2_1^+$ and an enhancement of the $4_1^+ \rightarrow 0^+$ hexadecapole transition. It is desirable to compare electromagnetic transition rates with the isoscalar rates induced by alpha particle scattering as there might be interesting differences, in particular for nuclei with large neutron excess. Furthermore, as the analysis of the scattering cross sections is necessarily based on a specific reaction model, a comparison may shed some light to the model dependence of the extracted isoscalar transition rates.

The specific case of the $0^+ \rightarrow 4_1^+$ transition in ^{204}Pb provides a favourable situation since Signorini and Morinaga[2] suceeded in measuring the $4_1^+ \rightarrow 0^+$ γ-transition in presence of the dominating $4_1^+ \rightarrow 2^+ \rightarrow 0^+$ cascading transitions. We have started measurements of inelastic alpha particle scattering from ^{204}Pb in order to provide precise differential cross sections for a detailed theoretical analysis.

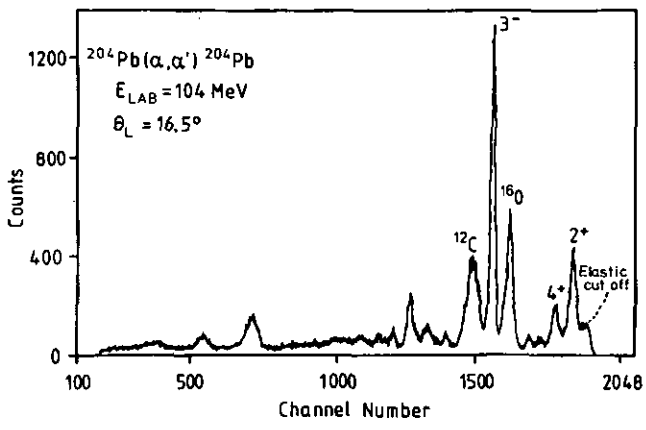

Fig. 1: Spectrum of alpha particles inelastically scattered from a ^{204}Pb target (with ^{12}C and ^{16}O impurities).

In order to measure the 4_1^+-peak relatively weak compared to the elastic scattering intensity we used the magnetic spectrometer BIG KARL. Fig. 1 displays a spectrum of inelastically scattered α-particles from a ^{204}Pb target (2.04 mg/cm^2 thick) where the peak of interest is clearly identified. The intensity of the peak is strongly varying with the scattering angle. Up to now spectra for seven angles between θ_L = 9° and 18.5° have been taken for E_{Lab} = 104 MeV. Further runs are in preparation.

References

1) H. Faust, A. Hanser, H. Klewe-Nebenius, H. Rebel, J. Buschmann, and H.J. Gils, J. Phys. 6, Nucl. Phys. 4 (1978) 247

2) C. Signorini and H. Morinaga, Phys. L 40B (1972) 549

+ Teilinstitut Kernphysik des Instituts für Angewandte Kernphysik der KfK, Karlsruhe

++ Tandemlaboratorium Universität Erlangen

+++ Institut des Sciences Nucléaires, Université de Grenoble

1.36. A Multi-Purpose Coincidence Measuring Equipment

M. Rogge, C. Sükösd, J. Bojowald

The various requirements of logic conditions and counting rates made it desirable to assemble a coincidence equipment to meet a wide range of demands. It should be compatible with the normal analog electronics on one side and with the ND6600 analyser on the other. For this reason the analyser was completed by an additional bit pattern input and a possibility to accept "zero" in the ADCs.

As an example a simplified diagram for a Giant Resonance decay experiment in 8 parameter list-mode is given in fig. 1. The experimental setup is scetched on the left with two arrays of detectors, consisting of two α'-telescopes and four decay-telescopes.

In the ND6600 the following parameters are stored on Mag. tape in case there is a coincidence between the α'- and decay-telescopes resulting in an event-pulse.

1) E_D: The energy of the scattered α'-particle. This is the normalized sum of pulses from the detectors of one telescope. The energy pulses of the two α'-telescopes are mixed in order to be fed to the same ADC. Pile-up rejection is used in both telescopes (not shown in diagram). Cross pile-up is avoided by logic conditions. 2) PI_D: Particle identifier signal generated by conventional analog electronics. Pulses of both α'-telescopes are mixed.

3) Time: Time difference of pulses of one α'-telescope and one of the decay detectors. Precoincidence and TPHC-time are normally adjusted to 500 nsec range. On the decay branch the "or"-blocks are disabled by veto 50 nsec after a decay-pulse for 500 nsec - and 500 nsec after an event-pulse for 6 sec. 4) 5) 6): Adjusted and mixed energy pulses of all 1^{st}, all 2^{nd}, and all 3^{rd} detectors of the decay telescopes ("column energy"). 7): Adjusted, added, and mixed energy pulses of all decay telescopes ("row energy"). 8): Bit pattern indicating which of the α'-telescopes and which of the decay detectors were involved in the coincidence.

By the bit pattern and the partly redundant information in ADCs 4 to 7 a particle identification is possible during the off-line evaluation of the data. The information is only stored on MT if a event-pulse occures. (If there is no pulse in some of the ADCs at that instant "zero" is stored.)

Care was taken to avoid pile-up in the analog branches and deadtime caused by updating properties of fast and slow digital branches as well as multiple firing of the CFDs at low thresholds. Pulses were added before the MA to reduce the costs but LGs were introduced where it seemed necessary for energy resolution.

To test stability, resolution and working conditions a test pulser (triggered by a monitor counter) can be fed sequentially to the preamplifiers of all telescope combinations. This provides a possibility to measure the percentage of wrong bit combinations and to correct for deadtime and instabilities after the experiment.

For control purposes during a run 4 time spectra, 6 energy spectra, one bit spectrum, and 3 Pulser spectra with different conditions are stored in the ND. Possibilities to store 4 singles spectra at least with reduced intensity are prepared.

Within the concept it is possible to expand the system to more counters on both coincidence branches. Additional conditions as anticoincidences, vetos, etc. are easily introducable. Some limitations araise from the maximal number of eight 8K-Listmode parameters (of which now one or two can be used for the bit pattern) and from the restricted memory of the ND6600.

The experiments described in sections 1.4 and 1.9. are partially or totally done with variations of this arrangement.

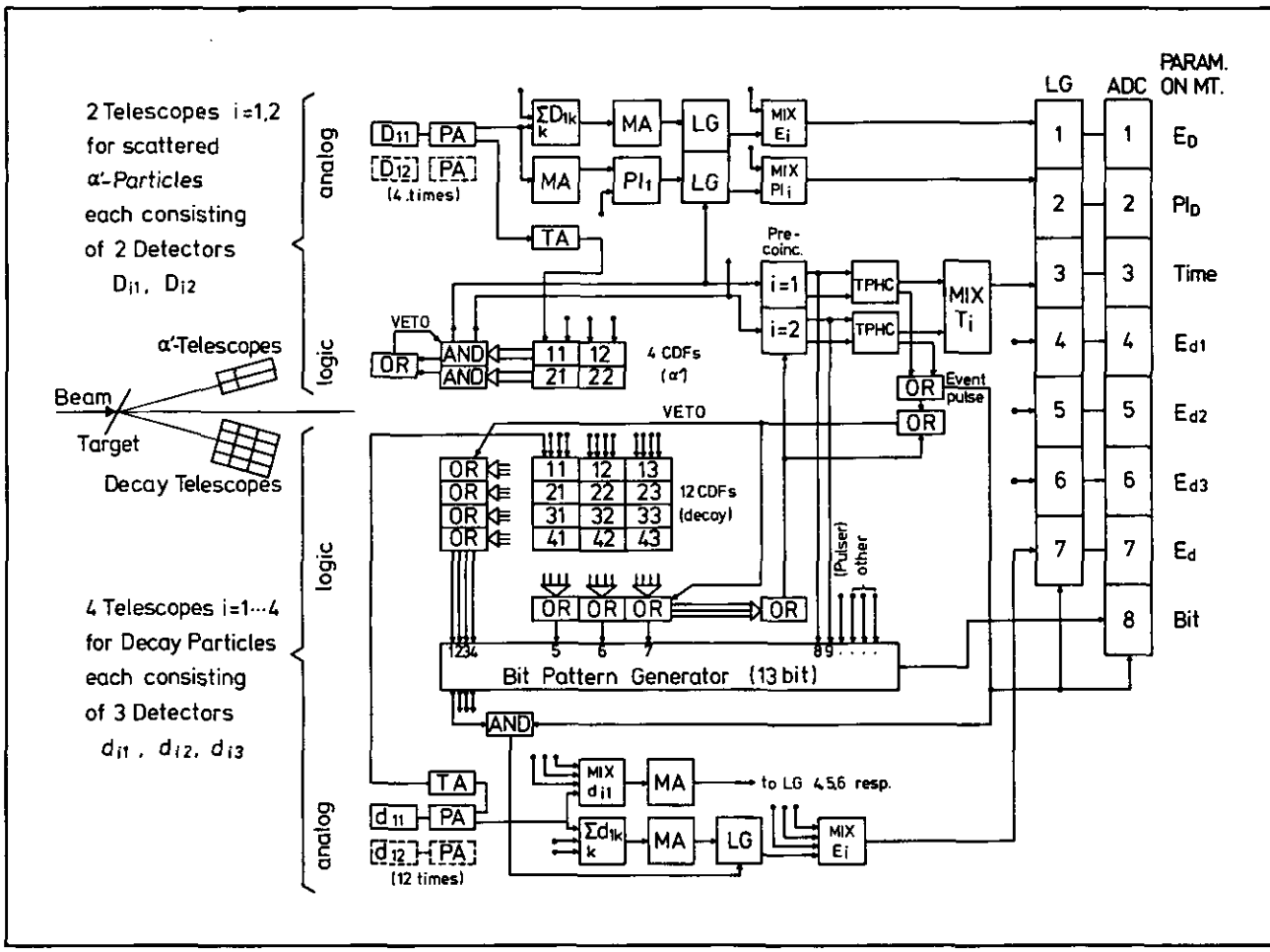

Figure 1: Simplified diagram of the electronics for a coincidence measurement. D_{ik}, d_{ik} =Si or Ge(Li) Detectors or the corresponding energy-pulses; PI = Particle Identifier; PA = Preamplifier; TA = Timing Amplifier; MA = Main Amplifier; LG = Linear Gate; TPHC = Time to Pulse high Converter; CFD = Constant Fraction or other Timing Discriminator; ↔ to resp. from corresponding device.

1.37. Investigation of the reaction $^{14}N(p,^3He)^{12}C$ at 41 MeV

V. Rapp, G. Staudt**

Continuing our previous measurements of $(p,^3He)$ reactions[1] we have analysed the $^{14}N(p,^3He)^{12}C$ reaction at E_p = 41 MeV. Details of the experimental set up are given in ref. 1. Recent measurements have been taken in list-mode form, and a suitable set of programmes will help with the off-line reduction of the data[2].

Apart from the direct pick-up mechanism there are knock-out and heavy particle ones, as well. A comparison of $\delta_{0^0-90^0}$ for transitions leading to positiv and negativ parity states in ^{12}C exhibits a relatively low intensity for the knock-out process. If one limits the cross sections to the first 90^0 or 120^0, the heavy particle contribution will be reduced considerably.

Using unpolarised projectiles and target nuclei the differential cross section can be expressed as being[3]

$$\frac{d\delta}{d\Omega} = \left(\sum_{\Delta j m\, m3_{He} m_p} \left| \sum_{\Delta l \Delta s} A_{\Delta l \Delta s \Delta j}\, \beta^{\Delta l m\, m3_{He}\, m_p}_{\Delta s \Delta j} \right| \right.$$

$A_{\Delta l \Delta s \Delta j}$ and $\beta^{\Delta l m\, m3_{He}\, m_p}_{\Delta s \Delta j}$ are the spectroscopic amplitude[4] and the reduced transition amplitude, respectively. The deuteron can be transfered in its ground state (s=1; t=0;) and in its first excited state (s=0; t=1;), thus one gets two possible coupling modes of l and s for most j's, which obliges a coherent addition of their transition amplitudes. The first T=1 state in ^{12}C is at E_x = 15,11 MeV[5].

For our DWBA-calculations we used the proton potential from literature which was obtained closest to our energy range of investigations[6]. For the bound state radius and diffuseness we had average starting parameters and for the exit channel we used the ^3He potential family obtained by Trost et al.[7] and varied depth and diffuseness of the real part to find the best fit of the ground state transition of the strongest coupling mode of l and s[4]. The final parameters can be seen in table 1.

A proton potential smoothly varying with mass number and energy will have some attractivity. Thus a new potential for A > 12 in the entrance channel[8] and the same fitting procedure as before has been applied and the parameters obtained, are shown in table 2. With these two sets of parameters the differential cross sections for the transitions leading to positive parity states in ^{12}C have been calculated with the code DWUCK following the sum rule given above. The angular distributions with DWBA curves can be seen in figure 1. Potential 1 fits the angular distributions better, But if one compares the integrated cross sections with experiment (figure 2), then the more general potential (table 2) exhibits an improvement on the comparison of $\delta_{0^0-90^0}$ with spectroscopic factors only[1], whereas the particular proton potential (table 1) just runs the other way.

TABLE 1

	V_r	R_r	A_r	V_i	R_i	A_i	
$^{14}N-p$	38·52	1·13	0·77	6·95	1·33	0·43	VOL.
				1·75	1·33	0·43	SUR.
	8·77	1·07	0·63				L-S.
$^{12}C-d$		0·99	0·52				VOL.
$^{12}C-^3He$	114·73	1·15	0·69				VOL.
				15·1	1·25	0·8	SUR.

TABLE 2

	V_r	R_r	A_r	V_i	R_i	A_i	
$^{14}N-p$	40·69	1·21	0·56	2·94	1·4	0·75	VOL.
				4·43	1·4	0·75	SUR.
	13·3	1·21	0·56				L-S.
$^{12}C-d$		0·98	0·47				VOL.
$^{12}C-^3He$	120·75	1·15	0·66				VOL.
				15·1	1·25	0·8	SUR.
	1·7	1·14	0·69				L-S.

Table 1 and 2: Optical potential parameters for DWBA calculations

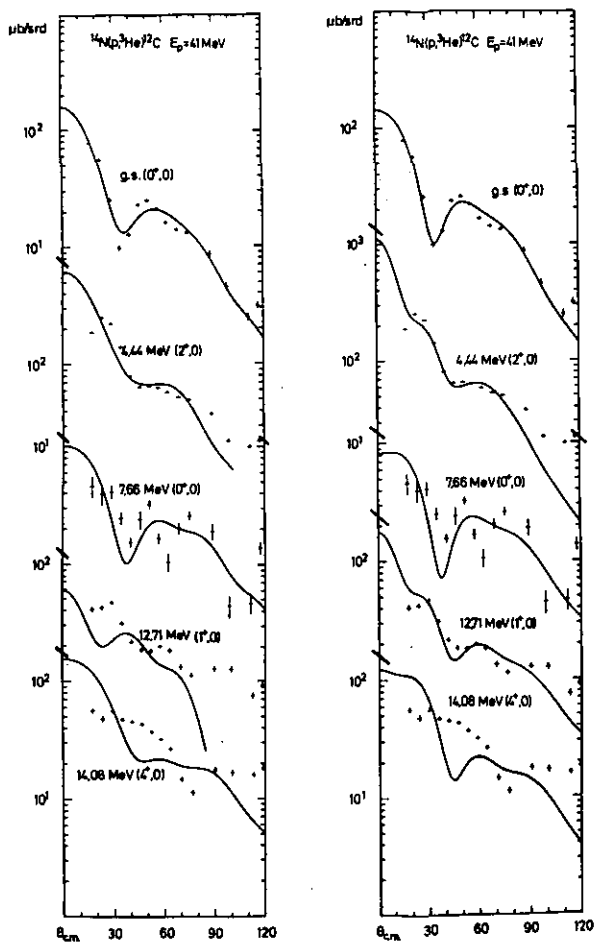

Fig. 1: Angular distributions and DWBA calculations using potential 1 (left) and potential 2 (right)

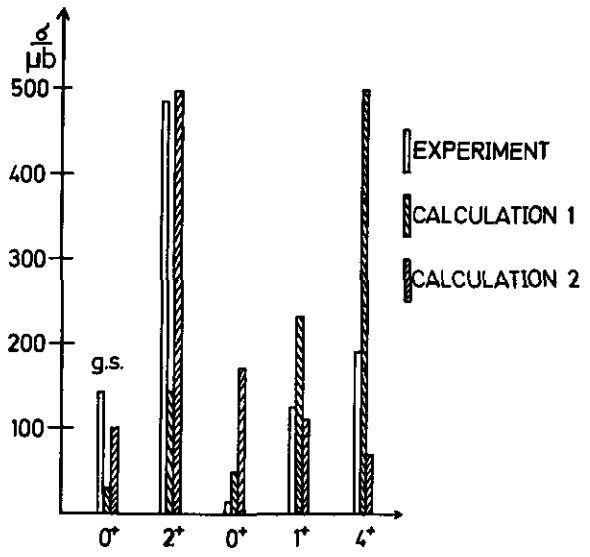

Fig. 2: Comparison between $\delta_{exp,0^0-90^0}$ and δ_{th} using potential 1 (calculation 1) and potential 2 (calculation 2).

Looking at the two 0^+ states which have almost identical spectroscopic factors an obvious rise in the theoretical cross section with increasing excitation energy of the residual nucleus hints at an improved orbital momentum matching. The larger radial parameter of the entrance potential 2 leads to a greater damping of the wave function and increases the normalisation constant C, almost by a factor of 5. Different contributions from partial waves in the entrance channel have probably caused the relative changes in the integrated cross sections.

It turns out that kinematic effects do play their part in the transition strength of (p,^{3}He) reactions, contrary to (p,α) ones[9], since their Q-values are highly negative.

References

1) V. Rapp, F. Weng, G. Staudt, Jülich Annual Report 1979, p. 11
2) V. Rapp, to be published
3) G.R. Satchler, Nucl. Phys. 55, (1964) 1
4) S. Cohen and D. Kurath, Nucl. Phys. A141 (1970) 145
5) F. Ajzenberg-Selove, Nucl. Phys. A248 (1975) 1
6) A.A. Rush et al., Nucl. Phys. A166 (1971) 378
7) H.J. Trost et al., Nucl. Phys. A337 (1980) 377
8) H. Leeb and G. Eder, Lecture Note in Physics 89, P. 181
9) F. Hoyler, T. Rohwer, G. Staudt, Jülich Annual Report 1979, p. 14

*Physikalisches Institut der Universität Tübingen

2. NUCLEAR SPECTROSCOPY

2.1. Dynamic K X-Ray Energy Shifts

G.L. Borchert, P.G. Hansen[+], B. Jonson[++], H.L. Ravn[++], O.W. B. Schult

The energies of K X-rays are significantly influenced by the atomic nucleus and affected by changes of the outer electron structure of the atom. The most well known of these effects are the isotope shifts and chemical shifts[1,2]. We have carried out various K X-ray shift measurements at CERN with a specially built DuMond spectrometer where use was made of sources which were produced with ISOLDE or at the CENG or ILL reactors at Grenoble. After the K X-ray shift measurement of the $K\alpha_1$, α_2 and β_1 lines of $^{131,132}Xe$ which led to the detection of the hyperfine shift[3], the shake-off effect[4] was investigated through a comparison of K X-ray energies from sources excited through photo ionization (PI) and electron capture (EC). In addition the atomic structure effect was discovered[5] and explained well in a ^{165}Er (EC) and ^{165}Ho (PI) experiment.

We have extended these studies and found very good agreement also for the ^{159}Dy (EC) and ^{159}Tb (PI) pair[6], where as in the case of Er/Ho the occupation numbers are different for 4f electrons. In the frame of a comprehensive investigation of the effects of various outer electron orbitals also the shifts have been measured between the K X-rays following photo ionization of ^{181}Ta and those following electron capture decay of ^{181}W which should have the additional electron the 5 d shell. While the accuracy of the data obtained by Wang et al.[7] does not allow the discrimination between a 1 s electron shift and an effect of 4 f electrons, our much more accurate data which include the shift of the $K\beta_{2,4}$ doublet and of the KO line and which are depicted in Fig. 1 clearly rule out a 1 s shift as the single cause. Even a 1 s shift together with the effect of 4 f electrons is inconsistent with the measured shift pattern, which cannot be explained by the 5 d electron either. In view of this large discrepancy we have begun a systematic measurement of the K X-ray shifts of various pairs of PI and EC sources of elements where the 5 d shell is gradually filled. The results which we have obtained so far are shown in Fig. 2 where the differences between the measured and calculated[15] shifts are plotted versus the occupation numbers n(PI)/n(EC) of the electrons in the 5 d orbits. It is interesting to see how the discrepancy for the Kα and Kβ lines is descreasing and even reverses sign as the 5 d shell is being filled. The effect of the KO line may be constant or slightly decreasing, but it remains rather large. The reason for this strange behaviour of the elements in the transition region is not understood so far. We suspect that it is not an atomic but rather a solid state effect.

+ Institute of Physics, Aarhus University, Aarhus, Denmark

++ CERN, Geneva, Switzerland

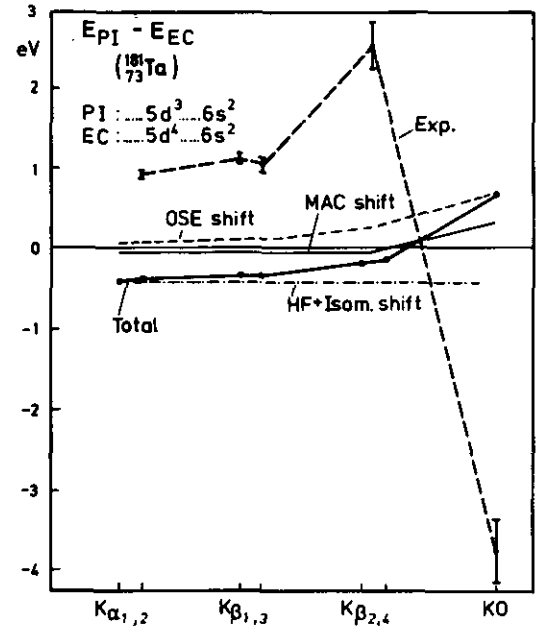

Fig. 1: K X-ray shifts of ^{181}Ta. Besides the experimental points (Exp.), calculated contributions are plotted as arising from shake off (OSE) and the hyperfine shift (HF). Also the isomer shift (Isom.) has been taken into account because of the 35 % EC population of the 63 keV level in ^{181}Ta.

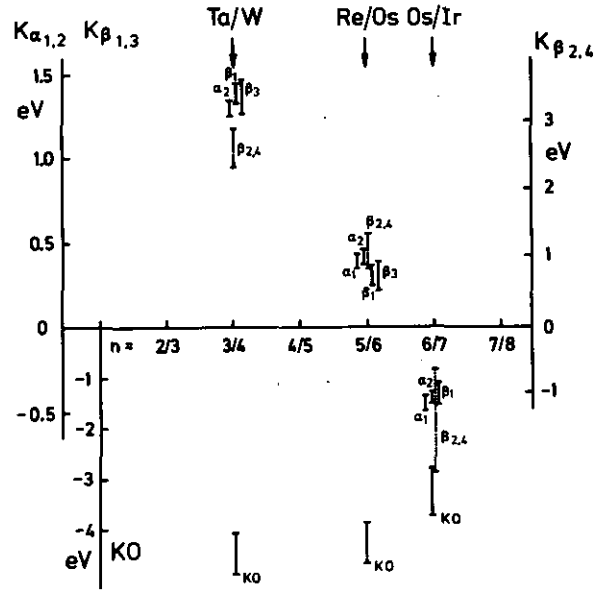

Fig. 2: Differences between the measured and expected K X-ray line shifts, plotted versus n, the number of electrons in the d5/2 orbits with e.g. 3/4 at the Ta/W pair indicating 3 for Ta and 4 for W.

References

1) F. Boehm in: Atomic Inner Shell Processes, Academic Press, New York, 1975, p. 412
2) O.I. Sumbaev, E.V. Petrovich, V.S. Sykor, A.S. Rylinikov, and A.I. Grushko, Sov. J. Nucl. Phys. 5 (1967) 387
3) G.L. Borchert, P.G. Hansen, B. Jonson, H.L. Ravn, O.W.B. Schult, and P. Tidemand-Petersson, and the Isolde Collaboration, Phys. Lett. 63A (1977) 15
4) G.L. Borchert, P.G. Hansen, B. Jonson, I. Lindgren, H.L. Ravn, O.W.B. Schult and P. Tidemand-Petersson, and the Isolde Collaboration, Phys. Lett. 65 A (1978) 297
5) G.L. Borchert, P.G. Hansen, B. Jonson, I. Lindgren, H.L. Ravn, O.W.B. Schult and P. Tidemand-Petersson, and the Isolde Collaboration, Phys. Lett. 66A (1978) 374
6) G.L. Borchert, P.G. Hansen, B. Jonson, H.L. Ravn, O.W.B. Schult, Proc. XVIII Int.Winter Meeting on Nucl. Phys. Bormio (1980) 579
7) K.-C. Wang, A.A. Hahn, F. Boehm and P. Vogel, Phys. Rev. A18 (1978) 2580

2.2 Isotope Shifts of K X-Rays of Lead

G.L. Borchert, P.G. Hansen[+], J.B. Mc Grory[++], B. Jonson[*], H.L. Ravn[*], O.W.B. Schult and J. Speth

During the past years progress in nuclear theory has allowed more detailed predictions of ground-state properties of heavier nuclei in particular in the lead region[1]. In the vicinity of a doubly magic nucleus it is interesting to learn how e.g. the mean square charge radius $\langle r^2 \rangle$ of the nucleus varies as nucleons are added to or removed from the core. This effect can be studied through isotope shift measurements, and the K X-ray shifts, albeit very small, are simply related[2] to the changes $\delta \langle r^2 \rangle$ of the mean square charge radius.

Measurements of isotope shifts of K X-rays in the lead region have been performed by Boehm and co-workers[3,4] with the use of a Cauchois spectrometer. In view of the high accuracy which we have achieved in other K X-ray shift measurements[5] we felt it worth while to also use our CERN DuMond spectrometer for a new measurement of K X-ray shifts of the lead isotopes 204, 206, 207 and 208.

In contrast to the previous work, where a ^{169}Yb source of $\sim$ 200 Ci and samples of 1 - 2 grams were used to obtain peak count rates of $\sim$ 300/sec, we have installed a $\sim$50 Ci ^{169}Yb source for the fluorescence excitation of metallic lead samples of only $\sim$ 11 mg (4 mm x 2 mm x 0.12 mm) and also obtained peak count rates of $\sim$ 350/sec. Because of the high resolution of the crystal spectrometer and due to the small source thickness (0.12 mm) the actual line widths that we have obtained in the second order of reflection, where our measurements were performed, were only 1.1 times the natural line widths. As we have only used metallic samples fabricated in the same way, chemical shifts are negligible.

We have measured the isotope shifts of the $K\alpha_1$ lines of all possible combinations of the four sources with each once in the upper and once in the lower source position in order to eliminate the vertical aberration error.

The positions of the K X-ray reflections were obtained through a direct fit, through the application of the center of gravity method, and through a difference method. For this preliminary analysis, the maximum error resulting from the application of these three methods was taken. A more refined fit is planned in the near future. Out of these data the isotope shifts (preliminary results) listed in Table I have been obtained through a "level fit" where all possible combinations have been used and where corrections have been made for the isotopic compositions of the samples. The previous results[4] are included in column 5 for comparison.

The Coulomb shifts $\delta E_{Coulomb}$ are given[2] by

$$\delta E_{Coulomb} = 1880 \frac{meV}{fm^2} \cdot \delta \langle r^2 \rangle \{1 - 1.12 \cdot 10^{-3} \frac{\delta \langle r^4 \rangle}{\delta \langle r^2 \rangle} + \ldots\}$$

for Z=82. Neglecting higher order terms we therefore obtain the $\delta \langle r^2 \rangle$ values given in column 2 of Table II. In column 4 are listed the data according to Ref. 4. In column 3 are listed our theoretical values. For the ^{208,207}Pb pair there is good agreement between the experimental numbers and they essentially agree with the theoretical shift which - as is shown in Table 2 of Ref. 1 - is due to the effect of the $p_{1/2}$ neutron hole ($Z\delta r^2$ = 5.018 fm^2) on the monopole mode of the Z=82 proton core for which r^2(proton, Woods Saxon) = 36,074 fm^2. From these numbers one could deduce an effective neutron charge of 0.14. For the ^{208,206}Pb pair the two experimental shifts differ by more than what one would expect. Both numbers agree with the theoretical shift which is less than twice the ^{208,207}Pb shift. That the use of a state-independent effective neutron charge is not a good approximation becomes obvious from the wave function[1] of the ^{206}Pb ground state, where also the $f_{5/2}$, $p_{3/2}$, $f_{7/2}$, $h_{9/2}$ and $i_{13/2}$ two neutron holes contribute with smaller effective neutron charges. In fact the theoretical ^{208,206}Pb shift is only 1.88 times the ^{208,207}Pb shift. Our experimental ratio is 1.63 $\pm$ 0.27, that of Ref. 4 is 1.34 $\pm$ 0.28.

For the ^{208,204}Pb pair the consistent experimental results are in excellent agreement with the calculated isotope shift.

Isotope 1	Isotope 2	$E\alpha_1(1) - E\alpha_1(2)$ (meV)	Coulomb Shift (meV) this work	Coulomb Shift (meV) Ref. 4
204	208	420 $\pm$ 21	422 $\pm$ 21	
204	207	276 $\pm$ 21	278 $\pm$ 21	
204	206	183 $\pm$ 25	185 $\pm$ 25	200 $\pm$ 38
206	208	237 $\pm$ 21	238 $\pm$ 21	186 $\pm$ 18
206	207	93 $\pm$ 23	93 $\pm$ 23	50 $\pm$ 20
207	208	144 $\pm$ 21	144 $\pm$ 21	136 $\pm$ 25

Table I: $K\alpha_1$-Isotope shifts (preliminary results)

	$\delta \langle r^2 \rangle_{exp}$ (fm^2) this work	$\delta \langle r^2 \rangle_{theor}$ (fm^2)	$\delta \langle r^2 \rangle_{exp}$ (fm^2) Ref. 4
$\langle r^2 \rangle$208 - $\langle r^2 \rangle$207	0.077 $\pm$ 0.011	0.061	0.072 $\pm$ 0.013
$\langle r^2 \rangle$208 - $\langle r^2 \rangle$206	0.126 $\pm$ 0.011	0.116	0.099 $\pm$ 0.010
$\langle r^2 \rangle$208 - $\langle r^2 \rangle$204	0.224 $\pm$ 0.011	0.226	0.205 $\pm$ 0.022

Table II: Isotope shifts of the mean square charge radii

References

1) J. Speth, L. Zamick and P. Ring, Nucl. Phys. A232 (1974) 1
2) E.C. Seltzer, Phys. Rev. 188 (1969) 1916
3) R.B. Chesler and F. Boehm, Phys. Rev. 166 (1968) 1206
4) P.L. Lee and F. Boehm, Phys. Rev. C8 (1973) 819
5) G.L. Borchert, P.G. Hansen, B. Jonson, H.L. Ravn and O.W.B. Schult, Proc. Int. Conf. on X-ray Processes and Inner Shell Ionization, Stirling, 25-29. August 1980

+) Institute of Physics, University of Aarhus, Aarhus, Denmark
++) Oak Ridge National Laboratory, Oak Ridge, Tennessee, USA
*) CERN-ISOLDE, Geneva, Switzerland

2.3. Isomeric State in ^{134}La

T. Morek, B. Bochev, T. Kutsarova, R.M. Lieder, M. Müller-Veggian

^{134}La levels were populated with the ^{136}Ba(p,3n) reaction using 30 MeV protons. Excitation functions and four parameter (E_γ, E_γ, $t_{\gamma\gamma}$, $t_{\gamma RF}$) γ-γ coincidences were measured. The results give evidence for an isomeric state in ^{134}La with a half life of 29±5 µs. The decay scheme of this isomer in ^{134}La is shown in Fig. 1. The γ transi-

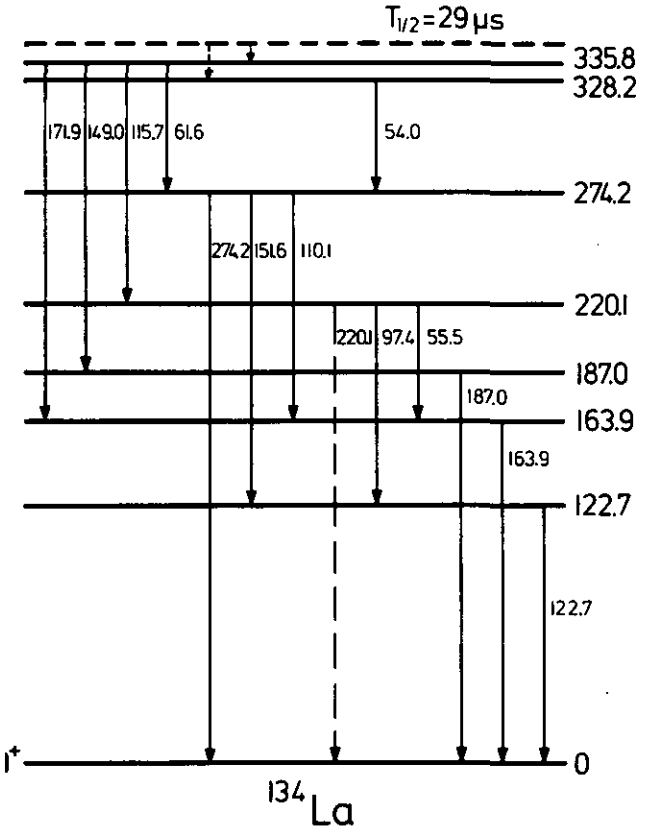

Figure 1: Decay scheme of the isomer in ^{134}La.

tions of 97.4, 110.1, 115.7, 122.7, 151.6, 163.9 and 274.2 keV clearly show this half life. The other transitions were placed in the decay scheme of the isomer on the basis of γ-γ coincidence measurement and the energy balance. All of these transitions have in addition a long-living component with a half life in the microsecond range, but contaminations do not allow to determine the exact value of the half-life.

A spin and parity of 1^+ has been assigned to the ground state of ^{134}La [1]. The isomeric state in ^{134}La may be of $\pi g_{7/2}\ \nu h_{11/2}^{-1}$ or $\pi d_{5/2}\ \nu h_{11/2}^{-1}$ configuration as discussed in more detail in the ^{136}La contribution to the present annual report.

Reference

1) R.C. Greenwood et al., Nucl. Phys. A270 (1976) 29

2.4. Isomeric States in ^{136}La

T. Morek, B. Bochev, T. Kutsarova, R.M. Lieder, M. Müller-Veggian

We have started a study of the odd-odd nucleus ^{136}La with the (p,3n) reaction using protons from the cyclotron at Jülich. Standard in-beam γ-spectroscopy methods were used including four parameter (E_γ, E_γ, $t_{\gamma\gamma}$, $t_{\gamma RF}$) γ-γ coincidences, two parameter E_γ-$t_{\gamma RF}$ coincidences, γ-ray angular distributions and multispectrum scaling.

As result of our studies a partial level scheme of ^{136}La is shown in Fig. 1. We have identified two isomeric states

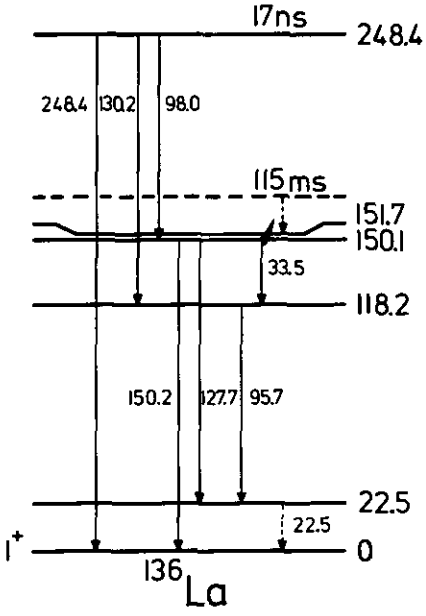

Figure 1: Partial level scheme of ^{136}La.

in ^{136}La. One of them having a half life of $T_{1/2}$=115±5 ms was previously reported[1]. Our results confirm that a 95.7 keV transition occurs in the decay of this isomer but we do not find a transition of 66.8 keV as reported in ref. 1. The analysis of the X-ray peaks in the γ spectra which were registered a few milliseconds after the beam pulse shows that the K_α component of the La X rays has a too large intensity in comparison with that of the K_β line. This suggests that a 33.5 keV transition occurs in the isomeric decay. Extracting the conversion coefficient of this transition from the intensity balance in the delayed spectra it was found that the multipolarity of this transition is rather small and cannot explain the long half life of the isomer. This fact suggests that an additional isomeric transition of low energy might exist which has not been observed.

The second isomeric state has a half life of $T_{1/2}$=17 ± 4ns. We have found six γ transitions of the energies 95.7, 98.0, 127.7, 130.2, 150.2, 248.4 keV with this half-life. The energy balance suggests that the 248.5 keV transition deexcites the isomeric state to the ground state and that a γ transition of 22.5 keV should exist which has not been observed in the experiments.

In atomic beam experiments[2] the ^{136}La ground state has been determined to have a spin I=1 and it can be interpreted as the 1^+ member of the $\pi d_{5/2}\ \nu d_{3/2}$ multiplet. A two-particle interpretation can be also used to explain the structure of the isomeric states in ^{136}La as it was done in the other N=79 nucleus ^{138}Pr. The configurations of the long-living isomer in ^{136}La and the isomer in ^{134}La (cf. contribution to the present annual report) may contain an $h_{11/2}$ neutron hole since low-lying isomers of $\nu h_{11/2}^{-1}$ configuration are known to exist in the isotones ^{135,137}Ce. The proton may be of $d_{5/2}$ or $g_{7/2}$ configuration since the ground states and first excited states, respectively, in ^{133,135}La are of this configuration. The long-living isomer in ^{136}La and the isomer in ^{134}La may, therefore, have a $\pi g_{7/2}\ \nu h_{11/2}^{-1}$ or a $\pi d_{5/2}\ \nu h_{11/2}^{-1}$ configuration. At present not enough experimental information is available to assign a configuration to the 17 ns isomer in ^{136}La.

References

1) L.K. Peter, Nuclear Data Sheets, 26)1979) 473

2) S. Ingelman, C. Ekstrom, M. Olsmats, B. Wannberg, *Physica Scripta 7 (1973) 24*

2.5. New Side Bands in ^{134}Ce

M. Müller-Veggian, H. Beuscher, D.R. Haenni, R.M. Lieder, A. Neskakis

After the discovery of a 10^+ isomer in ^{134}Ce [1] with a $(\nu h_{11/2})^{-2}$ configuration, similar to that of the 10^+ isomers in the heavier isotopes ^{136}Ce, ^{138}Ce [2], it seemed interesting to study the structure of this nucleus in more detail.

The final compound nucleus ^{134}Ce following the $^{134}Ba(\alpha,4n)$ reaction at 60 MeV was investigated by in-beam γ and e^- spectroscopy.

The nucleus ^{134}Ce exibits a very complex level structure. New side bands were observed in addition to the ground state cascade[3], which shows backbending at the critical angular momentum I_c=10, similarly to $^{128,130,132}Ce$ [3,4].

The most intense band is a well-developed negative-parity-band which feeds into the 4^+ by a 1125.6 keV transition. Similarly to the negative-parity-band observed in the isotope ^{136}Ce a sequence of odd states with $(5^-, 7^-, 9^-)$ and even $(6^-, 8^-)$ spin were found. Levels with spin and parity 5^-, 7^- were observed in the nucleus ^{138}Nd [5]. Negative parity bands were also found in the neighbouring $^{132,134}Ba$ [6,7]. The 5^- and 7^- states are present in $^{134,136,138}Ce$. The excitation energy of the 5^- in $^{134,136,138}Ce$ is slightly changing with neutron number suggesting that the probable configuration of the 5^- state in ^{134}Ce is $(\nu h_{11/2}^{-1} \otimes \nu s_{1/2}^{-1})_{5^-}$ or $(\nu h_{11/2}^{-1} \otimes \nu d_{3/2}^{-1})_{5^-}$ similarly to the heavier isotopes.

Another band was observed in ^{134}Ce. This new band is populated weakly by the 10^+ isomer. The spin sequence found is 0^+, 2^+, (3^+), 4^+, 6^+, 8^+. This band structure has an intermediate character between the pure vibrational and rotational bands. Such quasi-gamma bands are common in soft and transitional nuclei. Quasi-gamma-bands were found to exist in $^{132,134,136,138}Ce$, $^{136,138,140}Nd$, ^{132}Ba [8].

The location of the 3^+ state in ^{134}Ce seems to be reasonable comparing the excitation energies of the 3^+ state in ^{136}Ce and in the isotones ^{136}Nd, ^{138}Nd [8]. This state together with some low spin states has been also weakly seen in the decay of ^{134}Pr and ^{134m}Pr [8], but no spin assignment has been given.

Other new states and a new cascade were found, which are very weakly populated.

Furthermore on the top of the 10^+ isomer a cascade of γ-rays was established in a study of delayed coincidence. This cascade seems to have a rotational character. The energies and multipolarities of the γ-rays are similar to those of the transitions in the $h_{11/2}$ neutron band in ^{135}Ce [8]. The cascades observed on the top of the 10^+ isomer in ^{136}Ce and ^{138}Nd are very similar to the ground state cascade of ^{137}Ce, ^{139}Nd respectively[2,5]. This fact support the interpretation that the 10^+ isomer in ^{134}Ce has also a $(\nu h_{11/2})^{-2}$ configuration.

Recent g-factor measurements for the 10^+ isomer in ^{134}Ce [9] confirm that the 10^+ isomer is a neutron state of a $(\nu h_{11/2})^{-2}$ configuration. It is very interesting to look at the B(E2) values of the $10^+ \to 8^+$ states in the nuclei $^{130,132,134,136}Ce$. The B(E2) values of the $10^+ \to 8^+$ transitions become more hindered with respect to the single particle unit with increasing neutron number and follow the same behaviour of the B(E2) values of the $4^+ \to 2^+$ transitions [3,10]. In the nucleus ^{134}Ce two 10^+ states exist. The B(E2) value of the collective 10^+ is almost a factor 3 enhanced with respect to the single particle unit. The 10^+ isomeric state decays by the 397.5 keV to the 8^+ collective state and also by a 191.5 keV to another 8^+. It is very interesting to see that the B(E2) value connected with the 397.5 keV transition is hindered with respect to the single particle unit by a factor $\sim$300 whereas the B(E2) value connected with the 191.5 keV is hindered by a factor $\sim$8, which is very similar to the retardation found for the $10^+ \to 8^+$ transition in ^{136}Ce (R≡6) [11]. The different hindrance factor of the $10^+ \to 8^+$ transitions in ^{134}Ce can be understood taking into account the different nature of the 8^+ states.

Considering the experimental results that the neighbouring odd $h_{11/2}$ proton nuclei La don't show backbending it was concluded, using blocking arguments, that the backbending in the Ce region is due to the $h_{11/2}$ protons[12]. The existence of new side bands suggest that the $h_{11/2}$ neutrons may play a role in the backbending in this mass region.

References

1) M. Müller-Veggian, H. Beuscher, D.R. Haenni, R.M. Lieder, C. Mayer-Böricke, Annual Report 1977, KFA, IKP p. 30

2) M. Müller-Veggian, Y. Gono, R.M. Lieder, A. Neskakis, C. Mayer-Böricke, Nucl. Phys. A304 (1978) 1

3) W. Dehnhardt, S.D. Mills, U. Neumann, D. Pelte, G. Poggi, B. Povh and P. Taras, Nucl. Phys. A225 (1974) 1

4) J. Gizon, A. Gizon, R.M. Diamond and F.S. Stephens, Nucl. Phys. A290 (1977) 272

5) M. Müller-Veggian, H. Beuscher, D.R. Haenni, R.M. Lieder and A. Neskakis, Nucl. Phys. A344 (1980) 89

6) J. Gizon, A. Gizon, D.J. Hoken, Nucl. Phys. A252 (1975) 509

7) T. Morek, H. Beuscher, B. Bochev, D.R. Haenni, R.M. Lieder, T. Kutsarova, M. Müller-Veggian, A. Neskakis, to be published in Zeit. f. Physik

8) Table of Isotopes, seventh edition, 1978, edited by C.M. Lederer, V.S. Shirley

9) M.B. Goldberg, C. Broude, A. Zemel, J. Gerber, G.J. Kumbartzki, K.-H. Speidel, Proc. Int. Conf. on Nucl. Behaviour of High angular momentum (Strasbourg, April 1980) p. 49

10) D. Husar, S.J. Mills, H. Gräf, U. Neumann, D. Pelte, G. Seiler-Clark, Nucl. Phys. A292 (1977) 267

11) M. Müller-Veggian, H. Beuscher, R.M. Lieder, Y. Gono, D.R. Haenni, A. Neskakis, C. Mayer-Böricke, Z. für Physik A290 (1979) 43

12) D. Ward, H. Bertschat, P.A. Butler, P. Colombani, R.M. Diamond, F.S. Stephens, Phys. Lett. 56B (1975) 139

2.6. Electromagnetic Decay of the 0_2^+ State in $^{146}_{82}Gd_{64}$ +)

R. Julin+, J. Kantele+, M. Luontama+, A. Passoja+, P. Kleinheinz, J. Blomqvist++

In (α,xn) experiments the ^{146}Gd yrast levels have been well investigated, but little is known about low spin states above the yrast line. Some time ago an (α,2n) measurement at the reaction threshold[1] revealed the lowest 2^+ state at 1972 keV, and an early (α,2ne⁻) experiment[2] proposed the first excited 0_2^+ state of ^{146}Gd at 2179 keV. The 0^+ states in the doubly closed shell nucleus ^{146}Gd are of particular interest and we have now carried out ^{144}Sm(^{3}He,n) in-beam γ-ray and conversion-electron studies at the cyclotron at Jyväskylä to detect these states and investigate their properties.

In the present measurements we have confirmed the existence of the 0_2^+ state in ^{146}Gd and determined its energy more accurately as 2165.0(4) keV through observation of the E0($0_2^+ \rightarrow 0_1^+$) transition following the ^{144}Sm(^{3}He,n) reaction with ^{3}He beams between 14 and 27 MeV. Conversion electrons were detected with a Si(Li)+ magnetic lens spectrometer[3], and Ge(Li) detectors were used for γ-ray measurements. Self supporting 88.6 and 96.5 % enriched ^{144}Sm metal targets were employed.

In the conversion electron spectrum a prominent high-energy K line was observed at 2114.8(4) keV. The K to L energy difference was measured as 41.9(5) keV which conclusively shows that the conversion takes place in Gadolinium. No corresponding γ-line was observed; comparison with the 1579.3 keV $3_1^- \rightarrow 0_1^+$ E3 transition in ^{146}Gd gave the conversion coefficient ratio $\alpha_K(2165.0)/\alpha_K(1579.3) > 100$ which establishes E0 multipolarity for the 2165.0 keV transition.

The Gd mass number assignment for the 2165.0 keV E0 transition is based on the following observations:

(i) Measurements with targets of different enrichment in ^{144}Sm gave the same intensity ratio I(2165)/I(1579) ≈ 3, thus the target mass number must be 144.

(ii) The excitation function follows the Coulomb barrier at lower energies, being similar to what one would expect for the (^{3}He,n) reaction. ^{144}Gd cannot be the final nucleus since it is excluded by the Q-value.

(iii) The final nuclei ^{145}Gd and ^{147}Gd must be excluded since they have far to many open competing γ-decay channels to allow an intense E0 transition of 2 MeV, Besides, ^{147}Gd would involve ^{3}He radiative capture.

Consequently, the isotope assignment is firmly ^{146}Gd, in which the E0 transition obviously is associated with the decay of the 0_2^+ state at 2165.0 keV (fig. 1).

In the γ-ray measurements a search was made for the competing 193.7 keV E2($0_2^+ \rightarrow 2_1^+$) transition (cf. fig. 1), but no such transition was found. From a comparison of γ-ray and electron spectra, a limit of $I_K(2165.0)I_\gamma(193.7) > 4$ is obtained equivalent to the ratio E0/E2 > 85/15. The intensity of the E3($0_2^+ \rightarrow 3_1^+$) transition is certainly negligible.

The half life of the 2165 keV 0^+ level is too short to be determined from the slope of the time curve measured

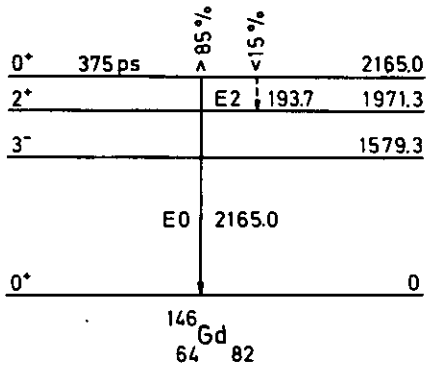

Fig. 1: Decay of the 0_2^+ state in ^{146}Gd

relative to the cyclotron beam pulses. It was determined by a centroid shift method specifically developed[4] for application with the Si(Li)+ lens electron spectrometer. The electronic prompt walk was extracted from the time centroids of background electrons with energies above and below the 2165 keV line accepted in the fixed momentum window of the magnetic lens. A thick target was used in this measurement to increase counting statistics. The results, shown in fig. 2., give the half life of the 2165.0 keV level as $T_{1/2} = 375 \pm 40$ ps. Since there is no reason to believe that a competing $0_2^+ \rightarrow 2_1^+$ transition would be much enhanced we ignore it (1 W.U. would correspond to a γ-branch of < 1 %). From the measured half life, together with the theoretical branching ratios π/K = 0.158, K/L = 7.5, L/M ≈ 3, and the electronic factor $\Omega_K = 1.136 \times 10^{-11}$ s^{-1} the reduced E0 transition rate becomes

$$\rho^2(E0,2165.0 \rightarrow 0) = 0.0122(13)$$

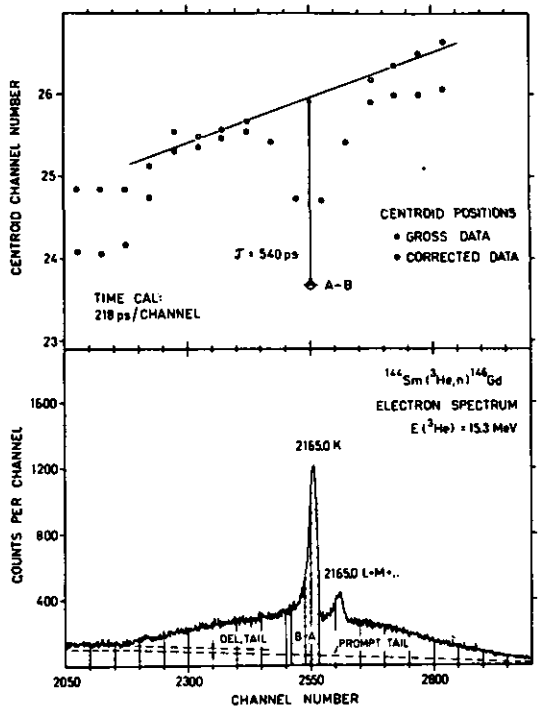

Fig. 2: Conversion electron spectrum (lower part) from the ^{144}Sm(^{3}He,n) reaction at 15.3 MeV. The upper figure shows time centroid positions corresponding to the energy slices indicated below.

corresponding to 0.70(8) ρ^2_{SP} with the effective single particle unit as defined in ref. (5).

In ^{146}Gd one expects the first excited 0^+ state to be the two-proton excitation, but its excitation energy, as high as 2.165 MeV, indicates that the 0^+_2 state must be strongly mixed with the ground state. In the case of maximum mixing of the ground- and two-proton states, the E0 transition rate should be one single particle unit, provided that the proton E0 effective charge is e.

Experimental data on effective monopole charges are still scarce; the E0 effective charge is therefore empirically not well determined but should be around e for protons. A weak state dependence of the effective neutron monopole charge has been found[6] in ^{206}Pb and is supported by theoretical calculations[7]. From a more detailed analysis of the ^{146}Gd 0^+ levels it is concluded that such a state dependence for the effective proton monopole charge must be < 0.05 e.

Of great interest would be the identification of the next higher lying 0^+ states. These are expected to be the two-neutron excitation, clearly higher than the two proton 0^+ state, and the two-phonon octupole 0^+ state expected at 3.2 MeV. Our attempts to observe the E0 decay of these states by internal pair formation have so far remained unsuccessful.

References

1) M. Ogawa, R. Broda, K. Zell, P.J. Daly, P. Kleinheinz, Phys. Rev. Lett. 41 (1978) 289

2) B. Spoelstra, Nucl. Phys. A174 (1971) 63

3) M. Luontama, J. Kantele, R. Julin, A. Passoja, T. Poikolainen, M. Pylvänäinen, N. I. & M. 159 (1973) 339

4) R. Julin, J. Kantele, M. Luontama, A. Passoja, to be published

5) A. Bohr and B.R. Mottelson, Nuclear Structure, Vol. 2, (Benjamin, New York, 1975) p. 553

5) J.W. Tape, E.G. Adelberger, D. Burch and L. Zamik, Phys. Rev. Lett. 29 (1972) 878; R. Julin et al. Phys. Lett. 65B (1976) 337

7) J. Speth, L. Zamik, P. Ring, Nucl. Phys. A232 (1974) 1

+) Condensed version of Phys. Lett. 94B (1970) 123

\+ University of Jyväskylä, Finland

++ AFI Stockholm, Sweden

2.7. Proton Single Particle States Above Z=64 from $^{147}_{65}Tb_{82}$

Y. Nagai, J. Styczen, M. Piiparinen, P. Kleinheinz, D. Bazzacco, P. v. Brentano*, J. Blomqvist+*

The ^{147}Tb nucleus has one proton outside the ^{146}Gd closed core and thus is the principal source of information on the single particle energies of the $s_{1/2}$, $d_{3/2}$, and $h_{11/2}$ shell model states which occur above Z=64. Two β-decaying isomers are known[1,2] in ^{147}Tb, and recently the high spin excitations built on the 1.9 min $\pi h_{11/2}$ single particle state were investigated[3] in an (α,8n) experiment. There are however no data on the $s_{1/2}$ and $d_{3/2}$ single proton states, and their energies so far could only be estimated by extrapolation[4,5] from the lower Z N=82 isotones.

The 1.6 h ^{147}Tb ground state spin parity has since long been firmly adopted as $5/2^+$, only recently[2] as $(5/2^+)$, and is attributed to the $d_{5/2}$ shell model orbit. However, the $\pi h_{11/2}$ nature of 1.9 min ^{147}Tb makes a $d_{5/2}$ assignment for the 1.6 h level highly questionable. The $\pi h_{11/2} \rightleftarrows d_{5/2}$ E3 transition[5] in ^{145}Eu has 4 W.u., and comparable E3 enhancements have been measured in several odd proton nuclei[6,1] in this region. On the other hand a decay branch connecting the two ^{147}Tb isomers has not been observed, its partial half life therefore must be >> 1.9 min. Since an E3 transition of one Weißkopf unit and E_γ > 3 keV has $T_{1/2}$ < 6 sec, a $d_{5/2}$ assignment for 1.6 h Tb appears very unlikely. From the energy systematics in Z<65 N=82 isotones one knows that the $s_{1/2}$, $d_{3/2}$, and $h_{11/2}$ single proton states lie close together, and they should therefore lie at low excitation in ^{147}Tb. Since pairing is important at Z=64 also the $\pi d^{-1}_{5/2}\, j_o^2$ and $\pi g^{-1}_{7/2}\, j_o^2$ two-particle one-hole levels are expected at low energy, analogous to ^{145}Eu where e.g. the $\pi h_{11/2}\, j_o^{-2}$ one-particle two-hole state[1] lies at 716 keV.

In order to locate the positive parity single particle states we have investigated the ^{147}Tb nucleus through the ^{144}Sm(^{6}Li,3n) reaction using in-beam γ- and electron spectroscopy. A coincidence measurement at 29 MeV bombarding energy (fig. 1) reveals a cascade of three γ-rays with 253, 101, and 365 keV which from excitation function studies and coincidences with X-rays is attributed to ^{147}Tb. We have also observed this cascade in β-decay of ^{147}Dy produced through the (α,9n) reaction at 120 to 140 MeV beam energy. Gamma rays of 253 and 101 keV also occur[9] in ^{149}Tb, but this nucleus is not populated in the (^{6}Li,3n) in-beam experiments.

Conversion electron measurements with a mini-orange establish M1 multipolarity for the 253 and 365 keV transitions, and a γ-ray singles timing measurement with a pulsed beam gave $T_{1/2}$ < 1.3 ns for the 253 and 365 keV lines and < 2 ns for the 101 keV line.

The measured transition intensities together with the intensities observed in the coincidence experiment (fig. 1) establish the transition sequence as shown in

the level scheme of fig. 2. Intensity balance together with the $T_{1/2}$ limit requires magnetic dipole character also for the 101 keV γ ray. The observed cascade therefore establishes four levels of the same parity.

Since as discussed above one expects in ^{147}Tb below 1 MeV only the 1/2, 3/2, 5/2, and 7/2 states of positive parity, the experimental results require that they form a monotonic spin sequence. As a 7/2 ground state would connect with the 11/2 isomer through an M2 transition of $T_{1/2} \leq 10$ ms the only possible spin sequence is 1/2 (grd. st.), 3/2 (253 keV), 5/2 (354 keV), and 7/2 (719 keV) as shown in fig. 2.

So far the position of the $h_{11/2}$ state relative to the positive parity levels is not known, but its 1.9 *min* half life excludes that it lies above the 354 keV $5/2^+$ state. The energy systematics of odd Tb isotopes independently suggests a rather low excitation. In $^{151}_{86}$Tb the $h_{11/2}$ level is found[7] at 100 keV, and for $^{149}_{84}$Tb the α-decay data[1] suggest ∿ 40 keV excitation for the $h_{11/2}$ state. From a pairing analysis of the measured level energies one would expect the $h_{11/2}$ level in ^{147}Tb to lie slightly below the $s_{1/2}$ state.

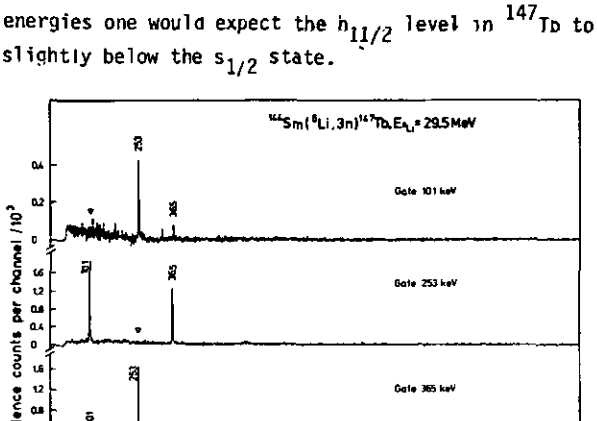

Fig. 1: Coincidence spectra for transitions in ^{147}Tb measured in the (^{6}Li,3n) reaction

For the Z=64 single particle energy gap our analysis gives a value of about 2.5 MeV, in agreement with our earlier[5] approximate estimate and as expected slightly higher than the 1829 keV $d_{5/2}$ to $h_{11/2}$ energy difference measured[9] in ^{133}Sb.

In conclusion the present study suggests an $s_{1/2}$ assignment for the 1.6 h ^{149}Tb activity, in contrast to the previously adopted $d_{5/2}$ assignment. The results also locate the three other positive parity single proton states and show that the $h_{11/2}$ level must lie below the $d_{5/2}$ state at 353 keV. The pronounced discontinuity in the experimental quasiparticle energies when going from ^{145}Eu to ^{147}Tb provides strong support for a large energy gap in the single particle spectrum at Z=64.

* University of Cologne
+ AFI Stockholm, Sweden

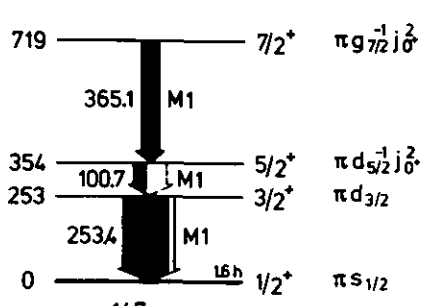

Fig. 2: Level scheme of ^{147}Tb established from the present experiments

References

1) Table of Isotopes, 7th edition, Eds. C.M. Lederer and V.S. Shirley (Wiley, 1978)

2) B. Harmatz, W.B. Ewbank, Nucl. Data Sheets 25, 113 (1978)

3) R. Broda, M. Behar, P. Kleinheinz, P.J. Daly, and J. Blomqvist, Z. Physik A293, 135 (1979)

4) B.H. Wildenthal, E. Newman, and R.L. Auble, Phys. Rev. C3, 1199 (1971)

5) P. Kleinheinz, R. Broda, P.J. Daly, S. Lunardi, M. Ogawa, and J. Blomqvist, Z. Physik A290, 279 (1979)

6) W.D. Fromm, L. Funke, and K.A. Schilling, Phys. Scr. 12, 91 (1975)

7) P. Kemnitz, L. Funke, F. Stary, E. Will, G. Winter, S. Elfström, S.A. Hjorth, A. Johnson, and Th. Lindblad, Nucl. Phys. A311, 11 (1978)

8) R.R. Chasman, Phys. Rev. C21, 456 (1980)

9) K. Sistemich, W.-D. Lauppe, T.A. Khan, H. Lawin, H.A. Selic, J.P. Bocquet, E. Monnand, and F. Schussler, Z. Physik A285, 305 (1978)

2.8. Twoparticle-Phonon Exchange Coupling in Dysprosium Nuclei

P.J. Daly[+], P. Kleinheinz, R. Broda, S. Lunardi, H. Backe[++], J. Blomqvist[+++]

In earlier studies[1,2] we have identified isomeric states involving two $h_{11/2}$ valence protons in the N = 82 and N = 83 nuclei ^{148}Dy and ^{149}Dy. A final analysis[3] of the in-beam data showed that in both cases these yrast isomers are dominantly fed through E1 transitions of about 1 MeV. The next higher yrast transition in ^{149}Dy is of M1 character, whereas only $\lambda = 1$ is known for the corresponding yrast transition in ^{149}Dy (cf. fig. 1).

At I = 10 the ^{148}Dy valence spin is exhausted, and higher yrast states must involve breaking of the ^{146}Gd core. Since the 3^- octupole state is the lowest core excitation, one would expect the yrast line to continue by excitations of the type $10^+ \times 3^-$, and we interprete the 3980 keV 11^- level as the lowest lying member of an octupole multiplet built on the $(\pi h^2_{11/2})10^+$ state. Since the $(\pi h_{11/2} d^{-1}_{5/2})3^-$ configuration provides the dominant amplitude of the 3^- core excitation, one expects that the energies of the $h_{11/2}$ particle plus octupole multiplet members will be strongly affected by the Pauli principle.

The figure 2 shows the particle-phonon exchange diagram appropriate to the ^{148}Dy case. The corresponding diagram[4] for the Z = 65 nucleus ^{147}Tb, which has one $h_{11/2}$ proton in its ground state, is included for comparison. The equations giving the energy shifts δE for the individual particle plus octupole multiplet members are also given, where W denotes a Racah coefficient and X is a 9j symbol. The crucial point here is that the energy factor containing the interaction matrix element is the same as in the ^{149}Tb case, and this makes it possible to use that empirical energy factor from one particle-phonon coupling to describe the exchange interaction of two particles with the phonon. The measured[3] 772 keV $15/2^+$ to $17/2^+$ energy splitting in ^{147}Tb gives for that factor a value of $\langle|H|\rangle^2/\Delta E$ = 856 keV which we have used to calculate the expected energy shifts for the four highest spin members of the $\pi h^2_{11/2} \times 3^-$ octupole multiplet in ^{148}Dy as shown to the right. (The $\pi h^2_{11/2}$ couplings I' = 10 and I' = 8 both contribute to the 11^- and 10^- states, and the theoretical energies shown are the lower energy solutions from diagonalizing the interaction in this two dimensional basis). The good agreement gives strong support for the identification of the observed 3.980 MeV 11^- and 4.476 MeV 12^- states in ^{148}Dy with the calculated $\pi h^2_{11/2} \times 3^-$ multiplet members.

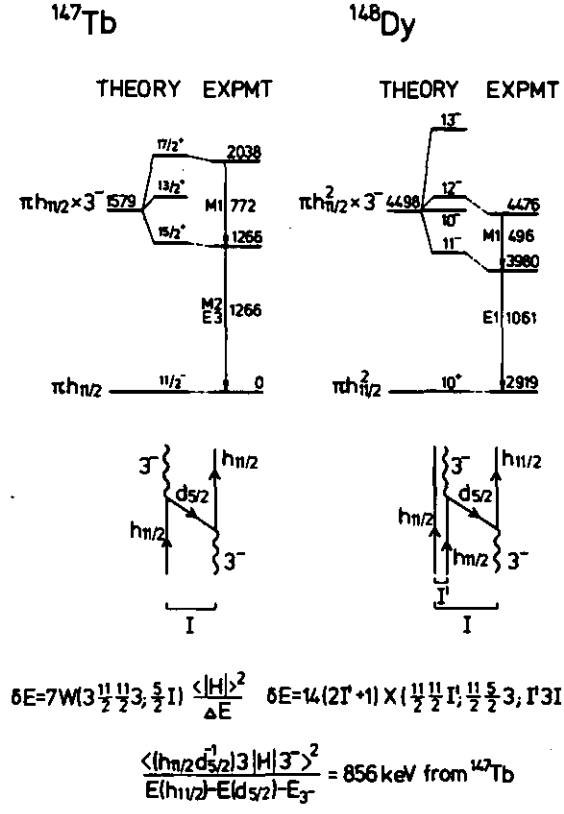

Fig. 2: One-particle-phonon and two-particle-phonon exchange coupling involving the 1579 keV octupole excitation in the ^{146}Gd core. Experimental and calculated $\pi h_{11/2} \times 3^-$ and $\pi h^2_{11/2} \times 3^-$ multiplet members in ^{147}Tb and ^{148}Dy are shown.

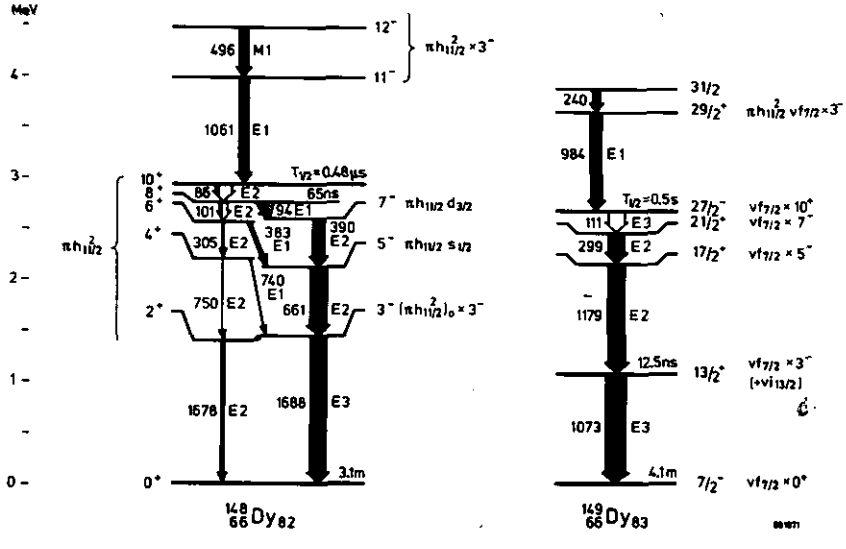

Fig. 1: Yrast states in ^{148}Dy and ^{149}DY. Intensities from (α,xn) experiments; multipolarities from conversion electron data.

The fact that the excitation energy of the 3 octupole state is higher in ^{148}Dy than in ^{146}Gd can also be understood as a Pauli interference effect. In this case, the geometrical blocking coefficient $14(2I' + 1)X$ for $I' = 0$ equals 2/12 assuming that two of the twelve $h_{11/2}$ protons are present in the ^{148}Dy 0^+ ground state. With the same empirical matrix element, the calculated energy shift is $\Delta E = +143$ keV, which is close to the experimental number of E_3-(^{148}Dy) - E_3-(^{146}Gd) = 109 keV. This slightly smaller increase of the 3^- energy in ^{148}Dy is not unexpected since the proton pair in the ^{148}Dy ground state also partially occupies the $s_{1/2}$ and $d_{3/2}$ orbitals.

As far as we know, this type of particle phonon exchange coupling involving two particles has not been observed before; it is encouraging that the empirical coupling strength derived from the one-particle case describes the more complex situation so well.

It is noteworthy that octupole excitations with $\Delta I = 1$ systematically occur above 3 MeV in the Dy isotopes where the two $h_{11/2}$ valence protons are aligened. The 3.65 MeV $29/2^+$ state of ^{149}Dy (fig. 1) has a predominant $(\pi h^2_{11/2}\ \nu f_{7/2} \times 3^-)29/2^+$ configuration, analogous to the 11^- level of ^{148}Dy. In the heavier isotones the situation becomes more complex, but there are several candidates for such $\Delta I = 1$ octupole excitations. In $^{150}Dy_{84}$ a 742 keV E1 transition deexcites[5] the 5813 keV 19^- octupole state to the $(\pi h^2_{11/2}\ \nu f_{7/2} h_{9/2})18^+$ level, and in ^{151}Dy the $(\pi h^2_{11/2}\ \nu h_{9/2} f^2_{7/2})41/2^-$ state is fed[6] by an 839 keV E1 from the $(41/2^- \times 3^-)43/2^+$ yrast state at 5743 keV. In all cases these octupole excitations are built on yrast states in which all available $\pi h_{11/2}$, $\nu f_{7/2}$ and $\nu h_{9/2}$ valence spins are fully aligned. The fact that octupole core excitation competes successfully with lifting of a neutron into the $i_{13/2}$ orbital reemphasizes the rather high single particle energy of that orbital noted in earlier[7] spectroscopy studies.

References

1) P.J. Daly, P. Kleinheinz, R. Broda, A.M. Stefanini, S. Lunardi, H. Backe, L. Richter, R. Willwater, F. Weik, Z. Physik A288 (1978) 103

2) A.M. Stefanini, P.J. Daly, P. Kleinheinz, M.R. Maier, R. Wagner, Nucl. Phys. A258 (1976) 34 and Phys. Lett. 62B (1976) 405

3) P.J. Daly, P. Kleinheinz, R. Broda, S. Lunardi, H. Backe, J. Blomqvist, Z. Physik A298 (1980) 173

4) R. Broda, M. Behar, P. Kleinheinz, P.J. Daly, J. Blomqvist, Z. Physik A293 (1979) 135

5) S. Lunardi, M. Ogawa, H. Backe, M. Piiparinen, Y. Nagai, P. Kleinheinz, Proc. ASHPIN, Argonne (1979), ANL/PHY-79-4, p. 403

6) M. Piiparinen, S. Lunardi, P. Kleinheinz, H. Backe, J. Blomqvist, Z. Physik A290 (1979) 337. (Recent conversion electron measurements at Jülich confirm the 839 keV E1 multipolarity suggested by T.L. Khoo in Proc. ASHPIN, Argonne (1979), ANL/PHY-79-4, p. 95)

7) S. Lunardi, M. Ogawa, M.R. Maier, P. Kleinheinz, Proc. ASHPIN, Argonne (1979), ANL/PHY-79-4, p. 393

+ Visitor from Chemistry Dept. Purdue University, Lafayette In, USA

++ TH Darmstadt

+++ AFI Stockholm, Sweden

2.9. An (α,4n) Study of $^{152}_{86}Dy_{66}$

J. Styczen, Y. Nagai, M. Piiparinen, A. Ercan, P. Kleinheinz

The ^{152}Dy nucleus has attracted great interest since some time ago[1,2] its yrast levels have been measured up to 13 MeV, and several ns-isomers above 5 MeV which decay through E2 transitions with $\gtrsim$ 1 W.u. have been located. For detailed comparison with theoretical calculations these results were of limited value since the ^{152}Dy yrast levels below 5 MeV were not thoroughly investigated and therefore could not provide a clearcut spin parity assignment for the $T_{1/2}$ = 60 ns isomer at 6 MeV. We have therefore reinvestigated this nucleus using the (α,4n) reaction which is superior to HI induced reactions for determination of level assignments below 5 MeV. In these studies we have discovered the 53.3 keV E2 isomeric transition depopulating the 60 ns isomer which we have reported[3-6] a year ago. Even with this result the isomeric spin and parity were still uncertain since the multipolarity of the crucial lower lying 604 keV transitions was unclear[1,7,8]. We have in the meantime carried out additional γγ coincidence, angular distribution, γ-ray timing and conversion electron measurements which provide a certain 17^+ assignment[6] for the 60 ns isomer. This result would determine the yrast level spin parities up to 36^- if one uses the earlier versions[1,2] of the ^{152}Dy level scheme resulting from the (HI,xn) studies. However in the latest version[9] a number of previously firmly established yrast transition multipolarities have been withdrawn and therefore the parities of the high lying yrast states are again unknown.

Due to the appreciable sidefeeding of the levels below 5 MeV in our (α,4n) measurements all the low lying γ-rays had pronounced angular distributions which generally confirm the previous[7,8,1] spin assignments, provided firm spin values for previously not assigned levels as well as for a number of ^{152}Dy levels which were not observed before. The results of the conversion electron measurements, which were performed with an ironfree orange spectrometer, are summarized in fig. 2. Of particular interest is the α_K-value for the 604 keV transition which definitely settles M1 multipolarity for that transition and the 17^+ assignment for the 60 ns isomer.

Another interesting result of our measurements is the observation[6] of the 3.9(4) ns half life for the 3160 keV 11^- level (fig. 3), which decays through a 2.5 times enhanced E2 transition. This 11^- level is the lowest yrast isomer in ^{152}Dy and has been overlooked in the previous investigations.

As we have mentioned the parities of the ^{152}Dy yrast levels above 5 MeV are still undetermined which limits crucial comparison with theoretical results. There exist already a number of theoretical studies[10-19] of ^{152}Dy, but none of these predict 17^+ for the 5 MeV 60 ns isomer.

Of particular note is probably a calculation[10] from 1977, which included pairing and predicted four oblate yrast traps with the same spins as the four ns-isomers observed in experiment.

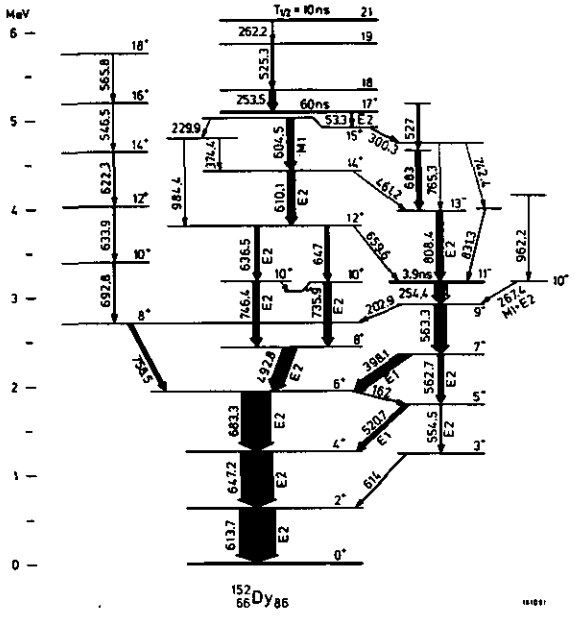

Fig. 1: Level scheme of ^{152}Dy as observed in the present (α,4n) experiments.

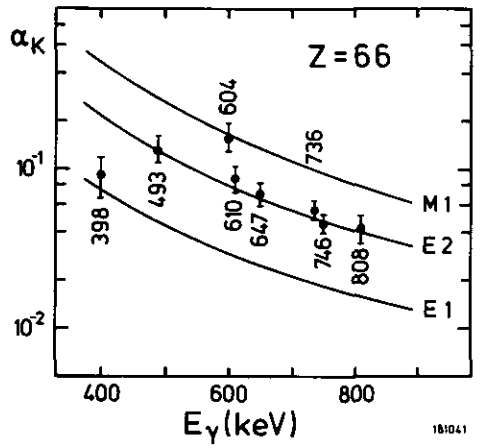

Fig. 2: Conversion coefficients for transitions in ^{152}Dy

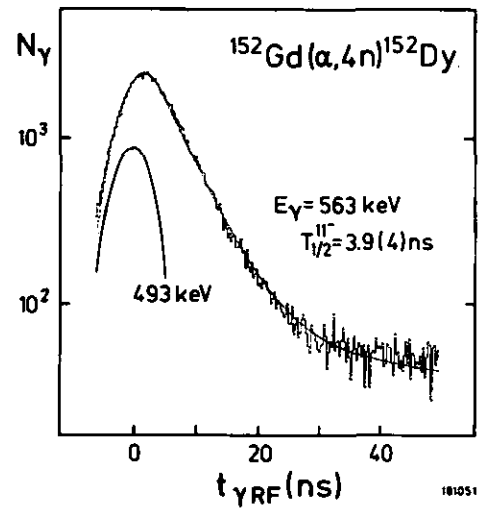

Fig. 3: Half life of the $I^\pi = 11^-$ state at 3160 keV in ^{152}Dy

References

1) T.L. Khoo, R.K. Smither, B. Haas, O. Häusser, H.R. Andrews, D. Horn, B. Ward, Phys. Rev. Lett. 41 (1978) 1027

2) B. Haas, H.R. Andrews, O. Häusser, D. Horn, J.R. Sherpey-Schafer, P. Taras, W. Trautman, D. Ward, T.L. Khoo, R.K. Smither, Phys. Lett. 84B (1979) 178

3) Y. Nagai, J. Styczen, M. Piiparinen, P. Kleinheinz, Inst. f. Kernphysik, KFA Jülich, Annual Report 1979, p. 59

4) Y. Nagai, J. Styczen, M. Piiparinen, P. Kleinheinz, Z. Phys. A296 (1980) 91

5) Y. Nagai, J. Styczen, M. Piiparinen, P. Kleinheinz, Proc. Int. Conf. on Nuclear Behaviour at High Angular Momentum, Strasbourg, p. 71 (1980)

6) Y. Nagai, J. Styczen, M. Piiparinen, P. Kleinheinz, Proc. Int. Conf. on Nuclear Physics, Berkeley, p. 304, (1980)

7) J.F.W. Jansen, M.S.A. de Voigt, Z. Sujkowski, D. Chmielewska, Nucl. Phys. A321 (1979) 365

8) J.C. Merdinger, F.A. Beck, T. Byrski, C. Gehringer, J.P. Vivien, E. Bozek, J. Styczen, Phys. Rev. Lett. 42 (1979) 23

9) B. Haas, D. Ward, H.R. Andrews, O. Häusser, A.J. Ferguson, J.F. Sharpey-Schafer, T.K. Alexander, W. Trautmann, D. Horn, P. Taras, P. Skensved, T.L. Khoo, R.K. Smither, I. Ahmad, C.N. Davids, W. Kutschera, S. Levenson, C.L. Dors, preprint (Nov. 1980), submitted to Nucl. Phys.

10) C.G. Andersson. J. Krumlinde, Nucl. Phys. A291 (1977)21

11) C.G. Andersson, G. Hellström, G. Leander, I. Ragnarsson, S. Aberg, K. Krumlinde, S.G. Nilsson, Z. Szymanski, Nucl. Phys. A309 (1978' 141

12) M. Cerkaski, J. Dudek, P. Rozmej, Z. Szymanski, S.G. Nilsson, Nucl. Phys. A315 (1979) 269

13) C.G. Andersson, S.E. Larsson, G. Leander, P. Möller, S.G. Nilsson, I. Ragnarsson, S. Aberg, R. Bengtsson, J. Dudek, B. Nerb-Pomorska, K. Pomorski, Z. Szymanski, Nucl. Phys. A268 (1976) 205

14) G. Leander, C.G. Andersson, S.G. Nilsson, I. Ragnarsson, S. Aberg, J. Almberger, T. Dossing, K. Neergard, Proc. Symp. on High Spin Phenomena in Nuclei, Argonne 1979, ANL/PHY-79-4, p. 197

15) M. Ploszajczak, A. Faessler, Proc. Symp. on High Spin Phenomena in Nuclei, Argonne 1979, ANL/PHY-79-4, p. 551
A. Faessler, M. Ploszajczak, Z. Phys. A295 (1980) 87

16) K. Neergard, T. Dossing, K. Matsuyanagi, Proc. Symp. on High Spin Phenomena in Nuclei, Argonne 1979, ANL/PHY-79-4, p. 565

17) R.R. Chasman, Phys. Lett. B (in press)

18) T. Dossing, K. Neergard, H. Sagawa, Invited talk in Int. Conf. on Nuclear Behaviour at High Angular Momentum, Strasbourg (1980)

19) T. Dossing, K. Neergard, H. Sagawa, lecture given in 1980 Nobel Symp. in Örenäs, Physica Scripta (in press)

2.10. Study of Band Crossings in ^{182}Os

R.M. Lieder, J. Borggren, J. Pedersen* and G. Sletten**

The study[1,2] of side bands in ^{182}Os has been continued by γ-γ coincidence measurements involving a low-energy photon detector as well as measurements of conversion electrons with a mini-orange spectrometer. These experiments were carried out at the Tandem Van de Graaff accelerator of the Niels Bohr Institute using the (^{18}O,4n) and (^{16}O,4n) reactions, respectively. The beam energies were 80 MeV. The conversion-electron studies allowed to determine the parities of all seven side bands previously established in ^{182}Os. The level scheme of ^{182}Os is shown in fig. 1. Band # 1 is a strongly-coupled band. The angular-distribution measurements yielded that the dipole-quadrupole mixing parameters δ of the cascade transitions in this band have small positive values. This has also been observed[3] for the two strongly-coupled bands of $5/2^+[402]$ and $9/2^-[514]$ configuration, respectively, in the odd-proton nucleus ^{181}Re. Considering furthermore the negative parity of band # 1 in ^{182}Os it may be concluded that it has a $5/2^+[402] \otimes 9/2^-[514]$ configuration. The bands # 2 and 3 show a strong Coriolis mixing and the dipole-quadrupole mixing parameters of the cascade transitions have negative values. These features are similar to those of the mixed $i_{13/2}$ neutron band in ^{181}Os [ref. 3] which is dominated by the $9/2^+[624]$ configuration. This suggests that bands # 2 and 3 consist of a quasi-neutron of $9/2^+[624]$ configuration and one of opposite parity which has most probably the $7/2^-[514]$ configuration. For the remaining bands no assignments can be made at present. The fact that the transitions deexciting the band # 7 into band # 6 have dipole-quadrupole mixing parameters of positive sign may indicate that also these bands have two-quasiproton configurations. It is an interesting result that two-quasineutron and two-quasiproton bands lie close to the yrast line in ^{182}Os.

The aligned angular momenta of all bands in ^{182}Os are plotted in fig. 2 against the rotational frequency. The sudden increase of the aligned angular momentum at a certain frequency as observed in some of the bands is caused by the backbending effect. The characteristic frequencies are $\hbar\omega = 0.26$ MeV for the yrast band and $\hbar\omega = 0.29$ MeV for three of the side bands. Both backbending frequencies can be understood in the framework of the cranking model[4] by the rotation alignment of $i_{13/2}$ neutrons.

References

1) R.M. Lieder et al., Annual Report 1979, Institut für Kernphysik der KFA Jülich, Jül-Spez-72 (1980) 48

2) R.M. Lieder, Nucl. Phys. A347 (1980) 69

3) A. Neskakis et al., Nucl. Phys. A261 (1976) 189

4) S. Frauendorf et al., Contrib.: Informal Meeting about Future Aspects of UNISOR, Nashville, 1979

*Niels Bohr Institute, Copenhagen

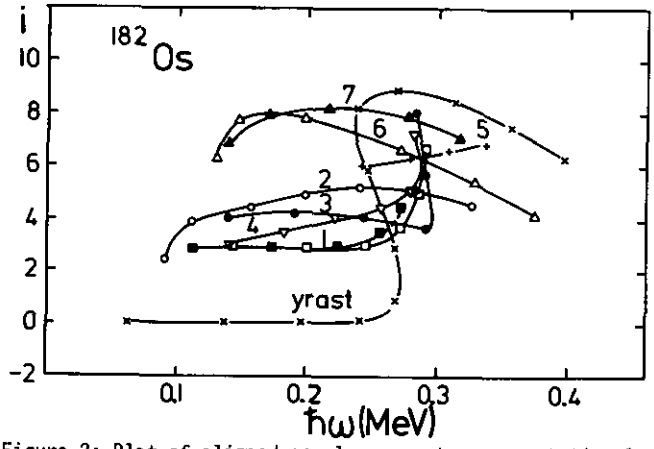

Figure 2: Plot of aligned angular momentum vs. rotational frequency for bands in ^{182}Os.

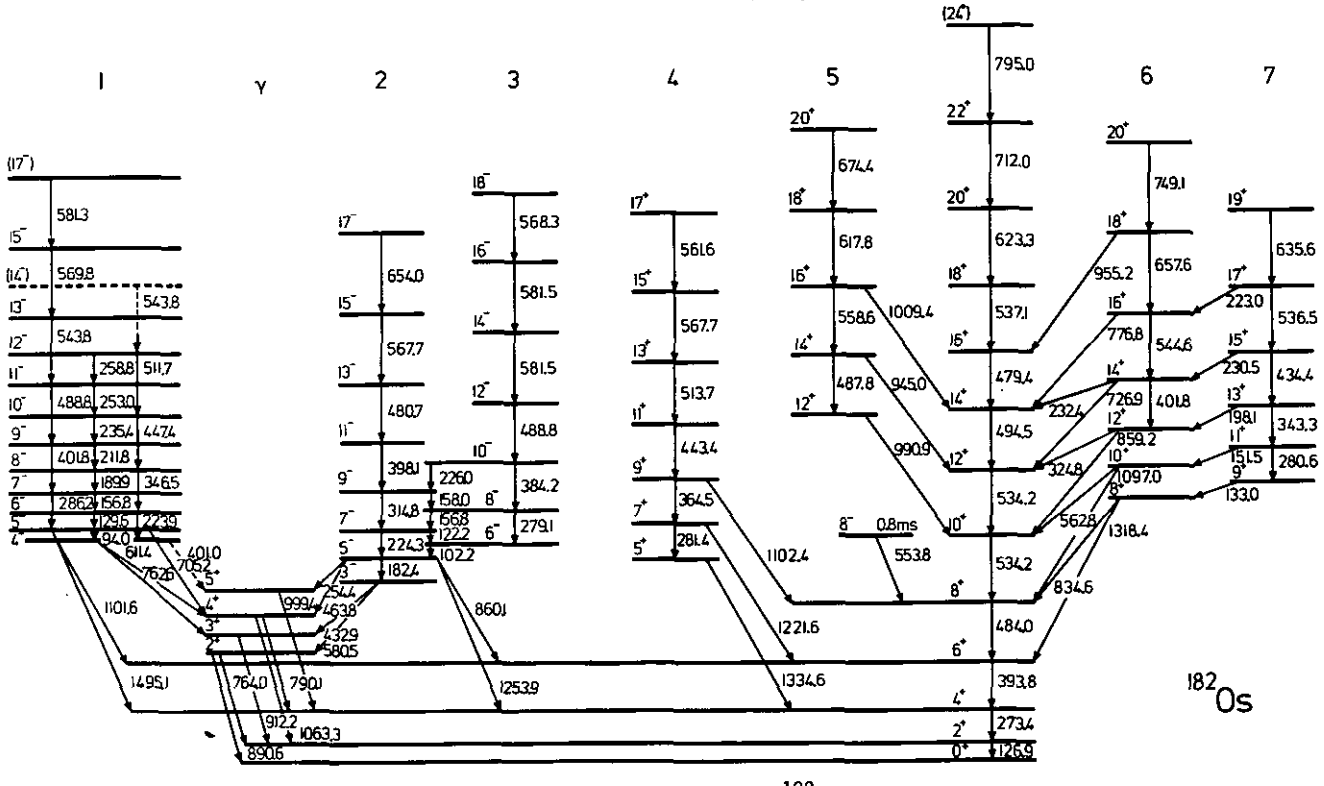

Figure 1: Level scheme of ^{182}Os.

2.11. Interpretation of Proton Spectra from Non-Equilibrium Reactions in the Framework of the Yrast Picture

R.M. Lieder, B. Bochev, T. Kutsarova, J.P. Didelez and C. Mayer-Böricke*

The study of proton emission for (α,pxn) reactions by particle-γ coincidence techniques provided an important new information about the non-equilibrium deexcitation process[1,2,3]. In the spectra of protons emitted in 45 MeV and 75 MeV α-particle bombardment of ^{209}Bi pronounced peaks have been observed for different (α,pxn) reaction channels. The energies of the proton peaks are independent of the angle of the particle detector and decrease with the increasing number of emitted neutrons. At a beam energy of 75 MeV the proton spectra have additional low-energy tails for the (α,p2n) and (α,p3n) channels.

The observation of pronounced proton peaks for individual (α,pxn) channels and their energies can be explained within the socalled yrast picture which is schematically shown in fig. 1 [2].

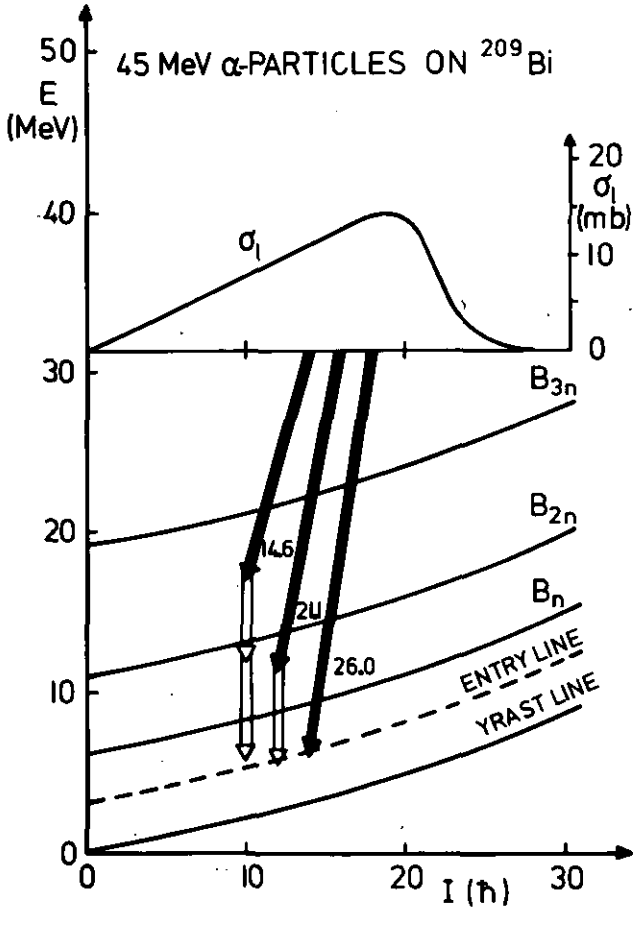

Figure 1: Schematic diagram depicting the decay of the excited nucleus for different reaction channels at 45 MeV.

This yrast picture is based on the assumption that target and projectile fuse. In fig. 1 the decay of the fused system to the final nuclei is depicted for the ^{209}Bi(α,pxn) reaction at E_α = 45 MeV in a plane of the excitation energy and the angular momentum. The spin distribution σ_ℓ as obtained by an optical model calculation[4] is inserted at the excitation energy of the fused system reduced by the binding energy of the proton. Furthermore an averaged yrast line for the final Po nuclei is shown. The lines above which the emission of x neutrons becomes possible are indicated by the corresponding binding energies B_{xn}. The location of the entry line at ≈ 0.5 B_n above the yrast line is taken from compound-nucleus reaction studies[5]. The emitted protons are indicated in fig. 1 by filled arrows, the length of which are approximately given by the energies and angular momenta carried away by the protons. The emitted neutrons are indicated by open vertical arrows the length of which correspond to their binding energies. The observation of separated proton peaks for different (α,pxn) channels can be understood as follows. When the proton populates a state located between the yrast line and the line denoted B_n no further neutron can be emitted so that an (α,p) reaction takes place. If the proton populates a state lying between the lines B_n and B_{2n} sufficient binding energy is available to emit a neutron. Therefore, the (α,p) reaction becomes very unlikely and the (α,pn) channel opens. In the case that the proton excites a state located between the lines B_{2n} and B_{3n} two neutrons can be emitted and the (α,p2n) channel becomes most probable. The widths of the proton peaks corresponds approximately to the widths of the regions in fig. 1 populated by the protons of different reaction channels.

The observation that the energy of the proton peak is independent of the angle is expected in the framework of the yrast picture described above. Furthermore it is expected that an increase of the beam energy is accompanied by a corresponding shift of the proton peak of the (α,p) channel. This expectation is experimentally verified since for an increase of the beam energy by 30 MeV to 75 MeV the proton peak shifts by 28.5±1.6 MeV.

From the yrast picture some important characteristics of the deexcitation process in non-equilibrium reactions can be deduced. For the (α,p) channel the energy of the entry point has been directly determined from the excitation energy and the energy of the proton peak. Taking into consideration the energy of the yrast line at the estimated angular momentum of the entry point the entry line was determined to lie ≈ 0.5 B_n above the yrast line for both the 45 MeV and 75 MeV experiments. It can be concluded that the entry line has the same location for non-equilibrium and compound-nucleus reactions and that this location is independent of the excitation energy. For the channels with x≥1 average neutron energies can now be determined. The neutrons connected with the protons from the peak regions carry away on average only small kinetic energies, namely ≈ 0.5 MeV and ≈ 2 MeV for 45 MeV and 75 MeV bombarding energies, respectively. These neutrons are considered to be evaporated. For the tail regions in the proton spectra as observed for 75 MeV in (α,p2n) and (α,p3n) p-spectra the emission of non-equilibrium neutrons becomes possible.

References

1) B. Bochev, R.M. Lieder, J.P. Didelez, T. Kutsarova, H. Beuscher, D. Haenni, H. Machner, T. Morek, M. Müller-Veggian, A. Neskakis, and C. Mayer-Böricke, Annual Report 1979, Jülich, Jül-Spez-72 (1980) p.33

2) R.M. Lieder, B. Bochev, T. Kutsarova, H. Beuscher, D.R. Haenni, T. Morek, M. Müller-Veggian, A. Neskakis, C. Mayer-Böricke, and J.P. Didelez, Contribution to the Nobel Symposium on Nuclei at very high spin Sven Gösta Nilsson in Memoriam, 23-27 June, 1980, Örenäs Castle, Sweden

3) J.P. Didelez, R.M. Lieder, B. Bochev, T. Kutsarova, T. Morek, M. Müller-Veggian and C. Mayer-Böricke, separate contribution to this report

4) J.P. Didelez, R.M. Lieder, H. Beuscher, D. Haenni, H. Machner, M. Müller-Veggian, and C. Mayer-Böricke, Nucl. Phys. A341 (1980) 421

5) J.J. Simpson, P.O. Tjøm, I. Espe, G.B. Hagemann, B. Herskind, B.B. Back, and F. Folkman, Nucl. Phys. A325 (1979) 216

*Institut de Physique Nucléaire, F-91406 Orsay, France

2.12. Study of the Mechanism of the (α,dxn) and (α,txn) Reactions at E_α = 45 MeV

T. Kutsarova, B. Bochev, J.P. Didelez, R.M. Lieder, T. Morek, M. Müller-Veggian and C. Mayer-Böricke*

In order to investigate the non-equilibrium reaction mechanism energy spectra and angular distributions of protons, deuterons and tritons have been measured for individual channels of the ^{209}Bi(α,ch.p.xn) reaction at 45 MeV incident energy by means of (ch.p.,γ) coincidences. Some results of this study have already been published[1-3]. The main results are that pronounced peaks exist for individual reaction channels in the spectra of charged particles and that the angular distributions of the emitted particles are strongly forward peaked. For each proton channel the peak has almost Gaussian shape and its mean energy and width is independent of the angle of emission. This observation suggests that the protons are emitted from a fused system[2,4]. For the (α,dn) and (α,t) channels the particle spectra show structures which change with the angle of observation.

The triton spectra obtained at 45°, 90° and 135° with respect to the beam direction in coincidence with all detected γ rays are shown in fig. 1. All spectra show a

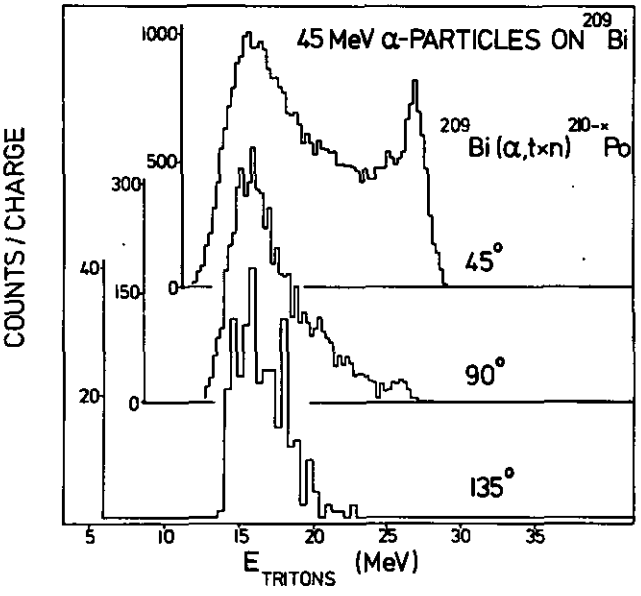

Figure 1: Spectra of tritons in coincidence with all detected γ rays for the ^{209}Bi(α,txn) reaction at 45 MeV.

broad distribution peaking at ≈16 MeV. However, in the 45° spectrum additionally a pronounced peak appears at ≈ 26 MeV. To obtain t spectra for individual reaction channels gates have been set on characteristic γ transitions in the residual nuclei. The resulting spectra are shown in fig. 2. The (α,tn) channel shows a peak at ≈ 16 MeV whereas two peaks can be distinguished in the (α,t) channel at ≈21 and ≈26 MeV, respectively. The angular distribution of the 26 MeV peak is much more strongly forward peaked than that of the 21 MeV peak. A similar effect may exist for the (α,dxn) reaction. In fig. 3 the d spectra of the (α,dn) channel are shown for 45° and 90° with respect to the beam direction. In the 45° spectrum the deuteron peak extends to higher energies than in the 90° spectrum. The 45° spectrum may con-

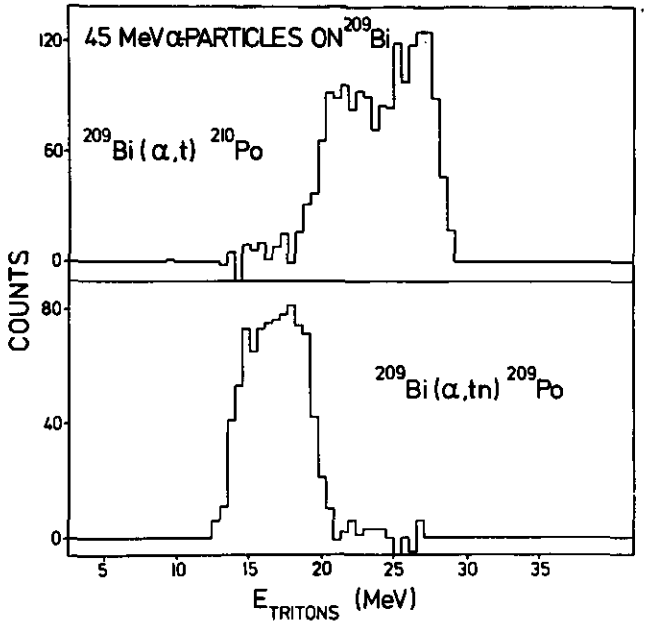

Figure 2: Spectra of tritons at 45° in coincidence with γ transitions of the residual nuclei for (α,txn) reaction channels.

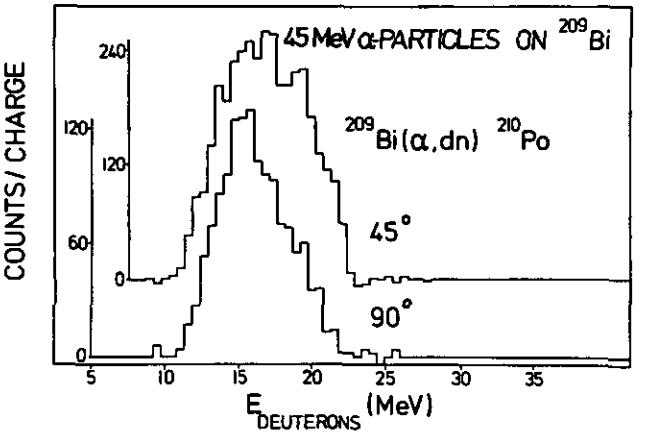

Figure 3: Spectra of deuterons for the (α,dn) channel in coincidence with γ transitions of the residual nucleus ^{210}Po.

sist therefore of two unresolved peaks. The high-energy component of ≈ 18 MeV has an angular distribution which is much more forward peaked than that of the low-energy component of ≈ 15 MeV.

The energies of the peaks observed in the individual (α,dxn) and (α,txn) channels are given in table 1. The

Channel	$E^{c.m.}_{part}$
(α,d)	22.9±1.0
(α,dn)	17.6±1.5 15.5±1.0[a]
(α,t)	26.2±1.5 21.0±1.5[a]
(α,tn)	15.8±1.0

a) The energy is taken from the 90° experiment.

Table 1: The c.m. energies for particle peaks of the ^{209}Bi(α,dxn) and ^{209}Bi(α,txn) reaction channels at 45 MeV bombarding energy.

peaks at 22.9, 15.5, 21.0 and 15.8 MeV of the (α,d), (α,dn), (α,t) and (α,tn) channels, respectively, are considered to result from non-equilibrium emission after fusion of the α particle with the target nucleus[2]. The peaks at 17.6 MeV and 26.2 MeV of the (α,dn) and (α,t) channels, respectively, are probably due to an incomplete fusion reaction, since the energies of these peaks are only a few MeV less than the energies corresponding to the beam velocity. The strong forward peaking of the angular distributions supports this interpretation.

References

1) B. Bochev, R.M. Lieder, J.P. Didelez, T. Kutsarova, H. Beuscher, D. Haenni, H. Machner, T. Morek, M. Müller-Veggian, A. Neskakis, and C. Mayer-Böricke, Annual Report 1979, Jülich, Jül-Spez-72 (1980) p. 33

2) R.M. Lieder, B. Bochev, T. Kutsarova, H. Beuscher, D.R. Haenni, T. Morek, M. Müller-Veggian, A. Neskakis, C. Mayer-Böricke, and J.P. Didelez, Contribution to the Nobel Symposium on Nuclei at very high spin Sven Gösta Nilsson in Memorium 23-27 June, 1980, Örenäs Castle, Sweden

3) B. Bochev, R.M. Lieder, J.P. Didelez, T. Kutsarova, H. Beuscher, D.R. Haenni, T. Morek, M. Müller-Veggian, A. Neskakis, and C. Mayer-Böricke, Proc. of the Int. Conf. on Nuclear Physics, Berkeley, California, USA, 24.-30. Aug. 1980, p. 452

4) R.M. Lieder, B. Bochev, T. Kutsarova, J.P. Didelez and C. Mayer-Böricke, separate contribution to this report

*Institut de Physique Nucléaire, F-91406 Orsay, France

2.13. Energy Spectrum of Delayed Neutrons from ^{85}As

M. Shaanan

During the second half of this year the activity on the measurement of delayed neutrons by the time of flight method was resumed. Our efforts were concentrated on the measurement of the spectrum of neutrons from ^{85}As. The reason for this choice is twofold. First, for this nucleus there was a lack of high-energy neutrons (En > 1.5 MeV)[1,2,3] unexplained by either of the theoretical approaches used to describe the processus of neutron emission. Also, a certain number of neutron energies whose existence was predicted[2] were not seen in the previously measured spectra with the ^{3}He-spectrometer.

The apparatus was the same as the one used before[4] except that the flight path was 60 cm, and the energy window was set at 2 MeV electrons which corresponds to ∼5 MeV protons. The resolving power of the spectrometer at this setting is shown in fig. 1. Three different measurements were performed and the spectra were summed up, taking in consideration the different calibration of the system for each measurement. This time spectrum is shown in fig. 2.

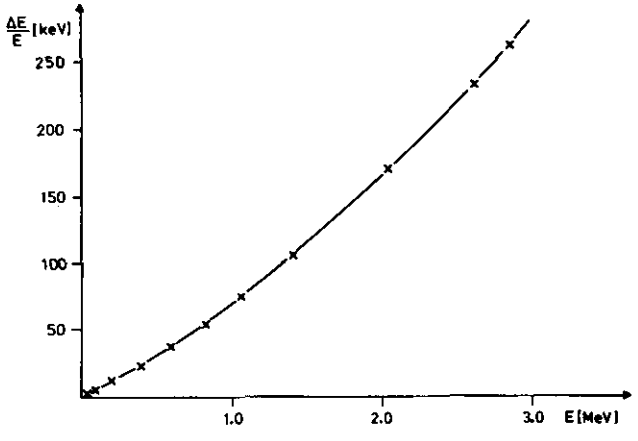

Fig. 1: The resolution of the spectrometer

The transformation of the time spectrum in an energy spectrum is performed using the relationship $N(E)\Delta E = N(t)\Delta t$. In order to extract the maximum information from the measured spectrum, the transformation is done in steps of a constant fraction from the energy resolution of the spectrometer at each energy.

Fig. 3 shows the energy spectrum obtained when the transformation was done in steps of 0.35 FWHM. The spectrum was corrected for the energy dependence of the efficiency. The energies of the peaks are listed in Table 1, together with the widths of the peaks and their relative intensities.

One salient feature of the spectrum is the presence of

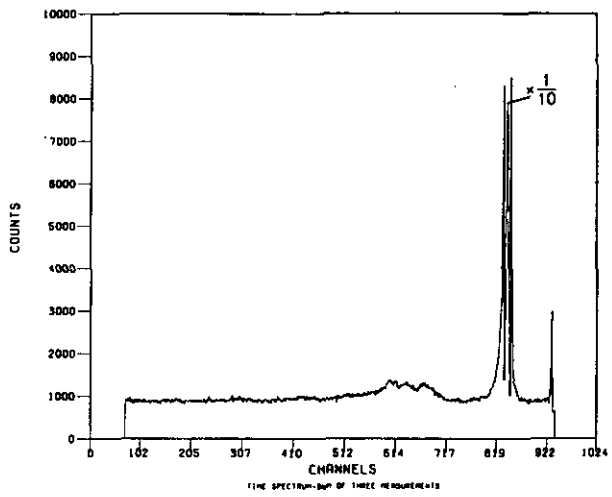

Fig. 2: The time spectrum-sum of 3 measurements

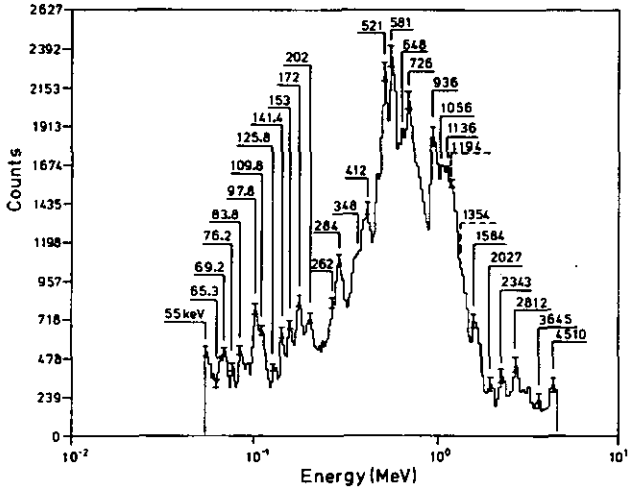

Fig. 3: The energy spectrum of the delayed neutrons from the decay of ^{85}As

peaked structure above 2 MeV, not seen in previous measurements with the ^{3}He spectrometers. This structure accounts for 10 % of the total neutron intensity contained in the peaks. Another interesting feature of the time-off-flight spectrum is the width of the different neutron lines, as compared with the ^{3}He spectrum. The width of the peak at 516 keV in the ^{3}He spectrum is about 42 keV, while in the TOF spectrum the width is equal to the resolution of the spectrometer, i. e. ∼33 keV. At lower energies the width of the lines decreases according to the resolution of the spectrometer. The

FWHM of the 172 keV line in the TOF spectrum is about 10.5 keV as compared with 20 keV in the ^{3}He spectrum. At lower energies there is even a splitting of lines, previously known as single peaks, in two or more peaks, like the 97 keV line. This leads to the conclusion that in order to define the natural width of the lines, the resolution of the spectrometers should be still improved. In this spectrum, 23 peaks have been resolved. The only line which fits in the list of required neutron lines (Table 3 from reference 2) and has not been seen before is the 141 keV line. Within the error range assigned to the peaks, it is possible to conclude that the lines at 2038, 2394, 2840 and 3553 keV have also been confirmed. But the approach adopted in this work[2] is not able to account for three peaks - 97, 110 and 172 keV - which contain about 25 % of the total neutron intensity in the peaks.

Table 1: The energies, relative intensities and widths of the peaks in the ^{85}As delayed neutrons spectrum. E/E is the resolution.

Energy (keV)	Rel. Intens.(%)	FWHM(keV)	ΔE/E (keV)
55.0± 1.0	32±12	3.8	3.20
65.3± 1.25	33±11	4.6	3.65
69.2± 1.35	44±10	4.4	3.67
76.2± 1.47	20±10	4.2	4.20
83.8± 1.63	41±11	4.9	4.60
97.8± 1.91	86±12	7.6	5.40
109.8± 2.15	84±11	11.0	6.20
125.8± 2.50	20±10	5.2	7.00
141.4± 2.80	53±10	7.6	7.85
152.9± 3.03	27± 9	7.8	8.20
172.1± 3.45	55± 9	10.6	10.10
201.6± 4.05	37± 9	14.0	11.60
283.9± 5.85	46± 9	22.8	17.00
412.0± 8.80	36± 9	35.0	25.40
520.9± 11.40	100± 7	36.0	33.50
580.9± 12.60	47± 9	37.0	35.60
726.0± 16.25	29± 8	42.0	42.00
936.7± 22.50	52± 8	72.0	64.00
1583.9± 42.80	16± 8	126.0	120.00
2027.4± 56.50	11± 7	148.0	152.00
2342.1± 68.00	20± 8	240.0	210.00
2811.6± 86.10	19± 8	235.0	240.00
4510.0±161.40	16± 7	457.0	457.00

References

1) J.C. Hardy, B. Jonson, P.G. Hansen, Nuclear Physics A305 (1978) 15

2) K.-L. Kratz et al., Nuclear Physics A317 (1979) 335

3) O.K. Gjotterud, P. Hoff, A.C. Pappas, Nuclear Physics A303 (1978) 281

4) M. Shaanan, G. Sadler, Annual Report 1974, Institut für Kernphysik, KFA Jülich

2.14. The Life-Times of the 0_3^+- and 0_4^+-Levels in ^{98}Zr

G. Battistuzzi, K. Kawade, H. Lawin, K. Sistemich,
F. Schussler[+], E. Monnand[+], J.A. Pinston[+],
B. Pfeiffer[++] and G. Jung[++]

The nucleus ^{98}Zr is of special interest since it is situated at the rapid transition of nuclear shapes between the doubly submagic ^{96}Zr and the probably asymmetrically deformed ^{100}Zr. The energies of the first excited positive parity states, fig. 1, show that the structure of this nucleus is neither vibrational nor rotational like. The proposed coexistence[1,2] of spherical and deformed nuclear shapes does also not show up in the presently available data[3].

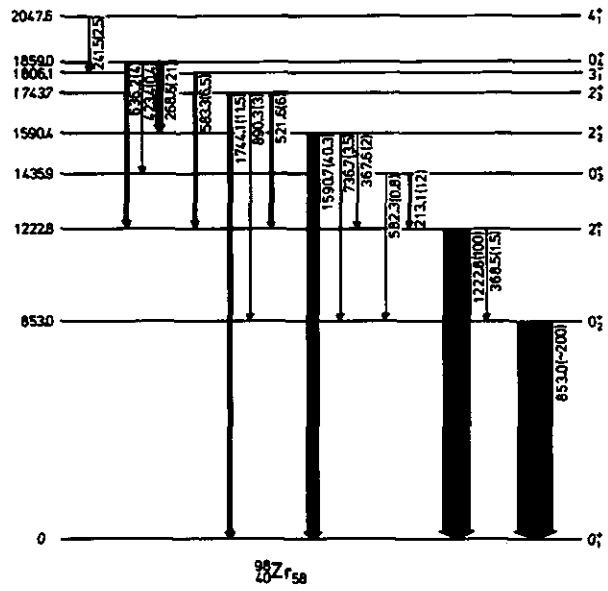

Fig. 1: Part of the level scheme of ^{98}Zr [3].

In order to get insight into the relative parentage of the levels of this nucleus, the life-times of the recently identified[4] 0_3^+- and 0_4^+-states have been determined at the fission product separator JOSEF. This was achieved through the measurement of the delayed coincidences between the β-particles from the β-decay of ^{98}Y and the γ-transitions of 213 keV and 269 keV, which depopulate the 0^+-levels. A thin scintillation detector (0.5 mm x 50 mm^2) and an intrinsic Ge-detector (16 mm x 1900 mm^2) were used for the observation of the β- and γ-radiation, respectively.

The time distribution between the β-particles and 269 keV γ-rays is shown in fig. 2a as an example of the experimental data. The life-times of the levels are deduced from the shifts of the centroids of the time distributions compared to the positions of the centroids of prompt β, γ - coincidences, which were simultaneously measured, cf fig.3.

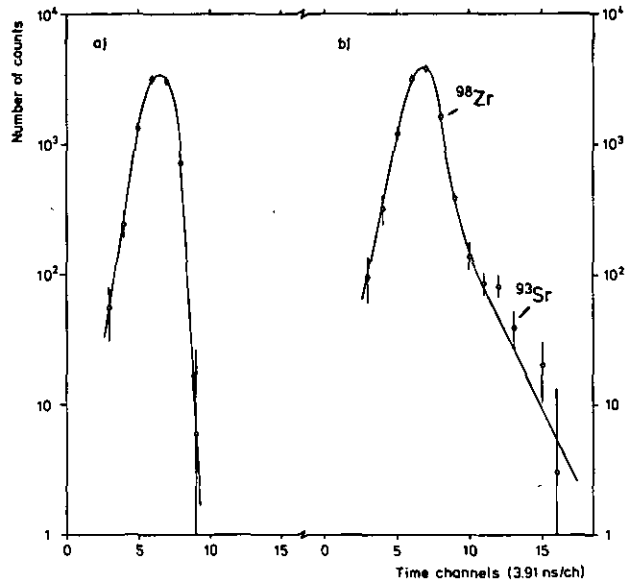

Fig. 2: Examples for the measured time distributions a) β,268.6 keV coincidence, b) β,213.1 keV coincidence, there the contribution from ^{93}Sr is clearly visible.

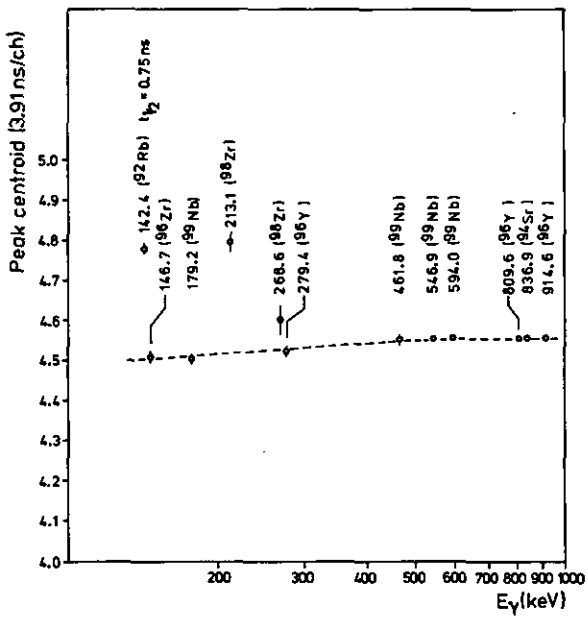

Fig. 3: The positions of the centroids of the β,213.1 keV and β,268.6 keV coincidences compared to those of some prompt distributions.

In the case of the 213 keV γ-ray contamination from the 213 keV transition in ^{93}Sr was present, as is shown in fig. 2b. In a separate run where the separator was optimized for the study of ^{93}Sr, the halflife of the 213.4 keV-level was determined to be 5±1 ns. The centroid position of the β, 213 keV-coincidence in fig. 3 has been obtained after subtraction of this contamination.

Two independent experimental runs were performed which yielded the following results:

	$t_{1/2}$ (0_3^+-level)	$t_{1/2}$ (0_4^+-level)
Run I	(0.74 ± 0.13)ns	(0.19 ± 0.12)ns
Run II	(0.64 ± 0.10)ns	(0.29 ± 0.12)ns
Average	(0.69 ± 0.08)ns	(0.24 ± 0.08)ns

The following reduced transition probabilities result from these half-lives and the relative intensities of the γ-transitions:

$B(E2:0_3^+ \rightarrow 2_1^+) = (1743 \pm 202)\ e^2fm^4 \rightarrow 65$ spu
$B(E2:0_4^+ \rightarrow 2_2^+) = (1639 \pm 546)\ e^2fm^4 \rightarrow 61$ spu
$B(E2:0_4^+ \rightarrow 2_1^+) = (22.7 \pm 7.6)\ e^2fm^4 \rightarrow 0.8$ spu

In these calculations the weak population of the 0_3^+-and 0_4^+-levels through E0 transitions[5] has not been taken into account. Their contribution would not change the B(E2) values beyond the given uncertainties.

It can be concluded that there are strongly collective transitions which connect the new 0^+-states of ^{98}Zr with selected 2^+-states. This indicates a close parentage between these levels.

References

1) R.K. Sheline, I. Ragnarsson, S.G. Nilsson, Phys. Lett. 41B (1972) 115

2) P. Federman, S. Pittel, Phys. Rev. C20 (1979) 820

3) K. Sistemich, G. Sadler, T.A. Khan, H. Lawin, W.-D. Lauppe, H.A. Selič, F. Schussler, J. Blachot, Z. Physik A281 (1977) 169

4) K. Kawade, G. Battistuzzi, H. Lawin, K. Sistemich, F. Schussler, KFA Jül-Spez-72 (1980) 62

5) J.A. Pinston, Proc. Workshop on Nuclear Spectroscopy of Fission Products, Grenoble, France, Mai 1979, Conference Series 51, The Institute of Physics, Bristol and London (1980) 258

+CEN Grenoble/France
++ ILL Grenoble/France

2.15. Half-life of the lowest $7/2^+$-level in ^{99}Mo

K. Sistemich, H. Lawin, G. Battistuzzi, K. Kawade and H.A. Selič

The half-life of the second excited state in ^{99}Mo with spin and parity $7/2^+$ has been determined through the measurement of delayed β,γ-coincidences at the fission product separator JOSEF. This level is fed with 100 % in the β-decay of the high spin isomer of ^{99}Nb [1] and is depopulated through a 137.6 keV γ-transition to the first excited state with $I^\pi = 5/2^+$ shown in fig. 1. The details of the experimental procedure are described elsewhere in this report[2].

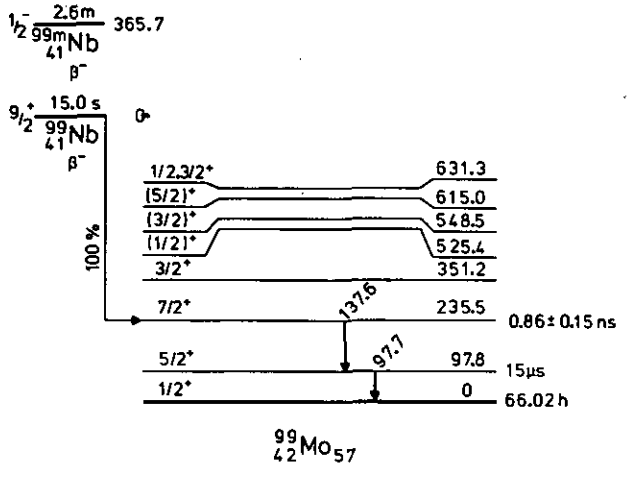

Fig. 1: β-decay of the $9/2^+$ ground state in ^{99}Nb to the $7/2^+$ in ^{99}Mo with the measured $t_{1/2}$ of 0.86 ± 0.15 ns.

Three different experimental runs have been performed. One of the timing distributions for the β,138 keV-coincidence is shown in Fig. 2 together with the distribution of the coincidences between the β-particles and the 142.4 keV transition in ^{92}Rb, which has been measured simultaneously. The 142 keV transition depopulates a level with a half-life of 0.75 ± 0.03 ns [1] and, hence, the β,142 keV distribution can serve as a reference. Compared to this reference distribution the centroid of the β,138 keV-distribution is drifted slightly to a larger time delay between β-particles and γ-rays. With the time calibration of 3.9 ns/time channel a half-life of $t_{1/2}$ = 0.91 ± 0.15 ns is deduced. The uncertainties contain statistical contributions from the evalution of the centroid shifts and a possible systematic uncertainty due to the different energies of the β-particles involved in the β,γ-coincidences[2].

The results of the two other measurements were

$$t_{1/2} = (0.93 \pm 0.20)\ \text{ns}$$

and

$$t_{1/2} = (0.80 \pm 0.17)\ \text{ns}.$$

Hence, a weighted average value of

$$t_{1/2} = (0.86 \pm 0.15)\ \text{ns}$$

is deduced for the 235 keV level in ^{99}Mo. Hence the transition probability of the 137.6 keV transition with main multipolarity M1 [3] is

$$T = 8.1 \cdot 10^8/\text{s}$$

which implies a hindrance factor of 100 compared to (Weißkopf) single particle units[1].

This relatively strong hindrance is to be expected since the transition takes place between two levels which contain a large contribution of the 1g7/2 and 2d5/2 single particle configurations of the 57th neutron[4]. The transition between these configuration is 1-forbidden, but it has been shown that the levels in ^{99}Mo are well explained through a coupling of the 57th neutron to the phonon states of the ^{100}Mo core[5]. Since N=56 does not represent a good shell closure for the Mo-isotopes the quasiparticle formalism has been applied. As has been shown for ^{93}Mo such a coupling can account for M1 transition strengths of about 1/100 spu[6]. To our knowledge no calculation of the probability of the $7/2^+ \rightarrow 5/2^+$ transition has been published for ^{99}Mo.

A comparison of such a calculation with the measured transition probability would provide a good test of the model.

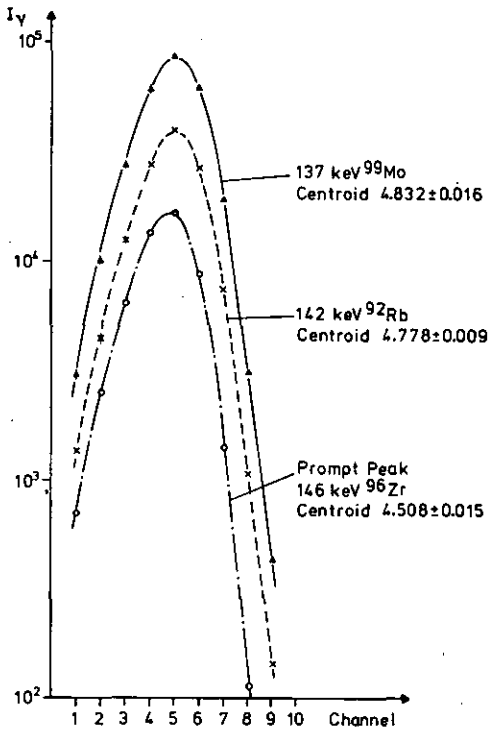

Fig. 2: γ-intensity vs. time distribution of β,138 and β,142 keV coincidences.

References

1) Lederer, Shirley: Table of Isotopes, Seventh Edition

2) IKP Annual Report 1980, contribution p.62

3) W. Dietrich, G.Ch. Hadneme, L. Westerberg, A. Bäcklin, Physica Scripta 12 (75) 271

4) R.C. Diehl, B.L. Cohen, R.A. Mayer, L.H. Goldman, Phys. Rev. C (70) 2132

5) B. Barman Ray, D. C. Chandhury, Phys. Rev. C12 (75) 323

6) D.C. Chandhury, J.T. Clemens, Nucl. Phys. A125 (69) 140

2.16. The Level Scheme of ^{131}Sb

F. Schussler[+], J.A. Pinston[+], J. Blachot[+], E. Monnand[+] and H. Lawin, K. Sistemich, K. Kaxade, G. Battistuzzi

The nuclei around doubly magic ^{132}Sn are of special interest since they allow valuable tests of the shell model[1,2]. For the odd-mass Sb nuclei having one proton outside the magic shell Z=50 the observed properties can be described by means of particle-core coupling or one-proton n-neutron-hole shell model calculations[3].

Up to now there exist only a small amount of data for the very neutron-rich Sb isotopes. They can most effectively be produced in fission. Systematic investigations are in progress at the recoil fission product separators LOHENGRIN and JOSEF for the odd masses $129 \leq A \leq 133$ [3,4,5].

The excited levels in ^{131}Sb were populated by two β-decaying isomers of ^{131}Sn with spin $3/2^+$ and $11/2^-$ having half-lives of 39 s and 50 s[4], respectively.

At LOHENGRIN γ-singles spectra for different kinetic energies of the mass-separated fission products were measured. Since the ratio of production of the isomers with low and high spin varies strongly with the kinetic energy these investigations allow the correlation of several γ-transitions in ^{131}Sb with the two β-decaying modes.

By measuring fission product, delayed γ-coincidences an isomeric level of (50 ± 8) μs half-life was confirmed at 1676 keV.

The analysis of the γ,γ-coincidences was carried out at the gas-filled separator JOSEF taking advantage of the high intensity achieved at this facility.

Fig. 1 shows a tentative level scheme for ^{131}Sb based on the results obtained so far. Fig. 2 gives the systematics of several levels in the odd-mass Sb isotopes. With neutron numbers increasing to 82 the low spin levels with positive parity are steadily increasing while the μs-level is decreasing.

Shell model calculations to describe the observed properties are in progress by K. Heyde et al.

References

1) K. Sistemich, Conference Series Number 51, The Institute of Physics, Bristol and London (1980), p. 208

2) K. Heyde, M. Waroquier, P. Van Isacker, J. Sau, Conference Series Number 51, The Institute of Physics, Bristol and London (1980), p. 177

3) K. Heyde, J. Sau, R. Chery, F. Schussler, J. Blachot, J.P. Bocquet, E. Monnand, K. Sistemich, Phys. Rev. C 16, 6 (1977) 2437

4) F. Schussler, J. Blachot, J.P. Bocquet, E. Monnand, Z. Phys. A281 (1977) 229

5) K. Sistemich, W.-D. Lauppe, T.A. Khan, H. Lawin, H.A. Selič, J.P. Bocquet, E. Monnand, F. Schussler, Z. Phys. A 285 (1978) 305

+ CEN Grenoble/France

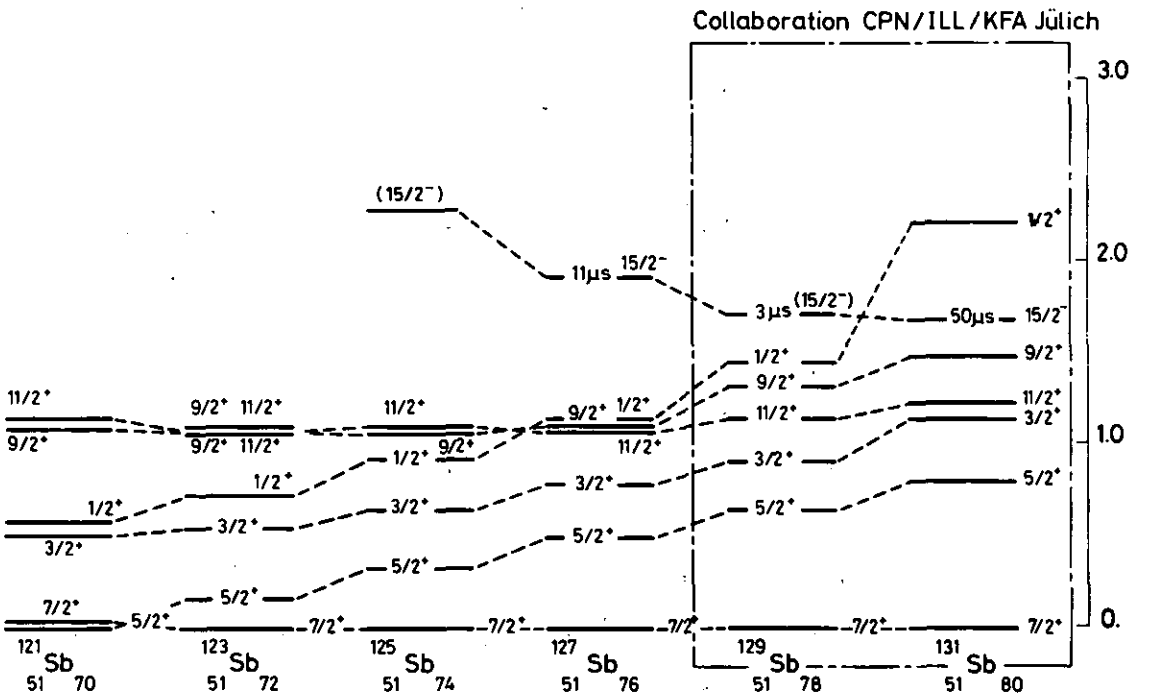

Fig. 2: Level systematics of odd-mass Sb isotopes

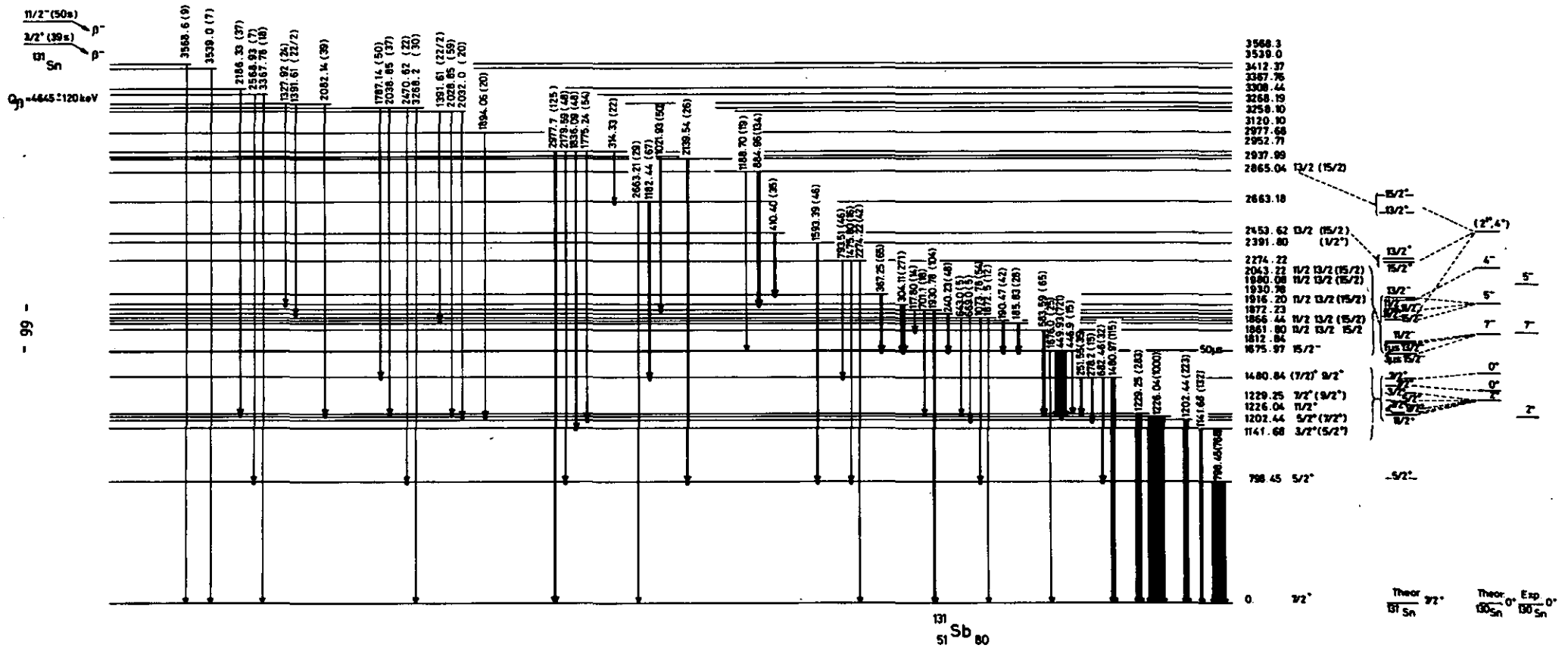

Fig. 1: Tentative level scheme of ^{131}Sb

2.17. A μs-Isomer in ^{135}Te

K. Kawade[+], *G. Battistuzzi, H. Lawin, K. Sistemich, and J. Blomqvist*[++]

It has been confirmed recently that strong shell closures exist at Z = 50, N = 82. Hence it is expected that the neighbours of ^{132}Sn are good shell model nuclei, the properties of which are determined through the few particles or holes beyond the core. Such a nucleus is ^{135}Te with two valence protons and one valence neutron.

No level scheme has been established yet for ^{135}Te. It has been known, however, for a long time[3,4] that a μs-isomer with a half-life of about 0.5 μs exists in this nucleus and that γ-transitions of 325 and 1181 keV are emitted in the depopulation of this isomer. In addition, intensive X-radiation[3] and a 50 keV γ-transition[5] were attributed to this nucleus. In order to obtain a first level scheme the isomeric radiation has been studied[6] in more detail at the fission product separator JOSEF.

Measurements of the X,γ- and γ,γ-coincidences confirm the assignment of the 50 keV transition to ^{135}Te and show, that it forms a stretched cascade with the 325 and 1181 keV-lines, fig. 1. The strong X-radiation is due to the conversion of the 50 keV transition. The conversion coefficients α_K and α_T of this line have been deduced from a comparison of the relative intensities, table 1. Hence, the 50 keV transition has mainly multipolarity E2. The half-life of the μs-isomer has been determined to be 0.51 ± 0.02 μs.

From the experimental data the level scheme shown in fig. 2 has been deduced. This cascade of transitions is very similar to the cascade of E2 transitions which depopulate the 6_1^+-level in the neighbouring nucleus ^{134}Te. This analogy suggests that the observed levels in ^{135}Te might be due to a coupling of the 83rd neutron to the proton states of ^{134}Te. Then the γ-transitions follow the pattern

$$[\pi(g_{7/2}^2)_{6^+}\ \nu f_{7/2}]_{19/2^-} \rightarrow [\pi(g_{7/2}^2)_{4^+}\ \nu f_{7/2}]_{15/2^-}$$

$$\rightarrow [\pi(g_{7/2}^2)_{2^+}\ \nu f_{7/2}]_{11/2^-} \rightarrow [\pi(g_{7/2}^2)_{0^+}\ \nu f_{7/2}]_{7/2^-}$$

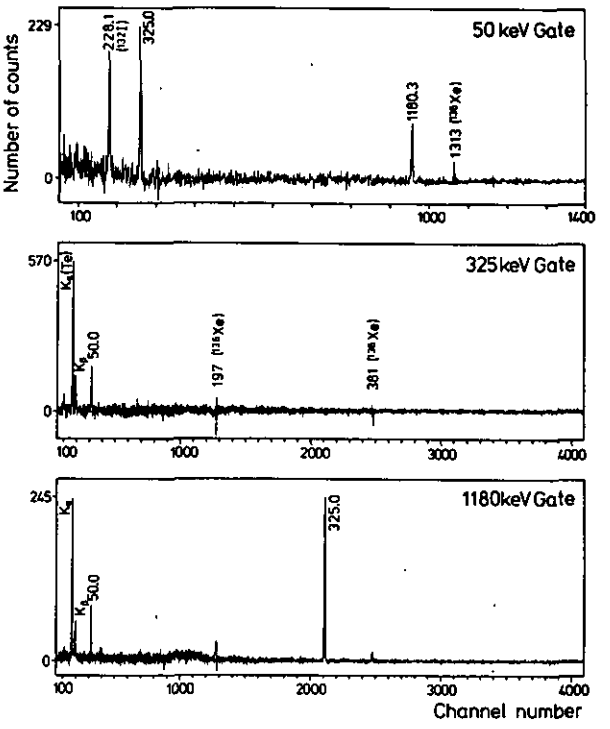

Fig. 1: γ,γ-coincidence spectra in ^{135}Te. The 50 keV gate was set on the intrinsic Ge-detector, the 325 and 1180 keV gates were set on the 61 cm^3 Ge(Li)-detector.

If this is true the reduced transition probabilities for the 50 keV transition in ^{135}Te and for the 115 keV line in ^{134}Te should be equal. This is approximately true:

$$B(E2;\ 50\ keV) = (161 \pm 7)\ e^2fm^4$$
$$B(E2;115\ keV) = (\ 70 \pm 3)\ e^2fm^4$$

The fact that the transition probability is about a factor of two larger in ^{135}Te is supposed[6] to be due to admixtures of configurations where the neutron is in other states, especially in the $3p_{3/2}$ state.

Hence, it can be concluded that the observed levels in ^{135}Te are most probably due to the coupling of the 83rd neutron to the 6_1^+, 4_1^+ and 2_1^+ proton states of ^{134}Te. The neutron is, however, not merely a spectator but takes an active part in the transitions between the levels.

Table 1: Results on the half-life of the μs-isomer in ^{135}Te

Present work			$t_{1/2}$ (μs)				
Radiation (keV)	Relative Intensity	$t_{1/2}$ (μs)	Ref. 3)	Ref. 4)	Ref. 5)	Ref. 6)	Ref. 7)
X-rays (K_α)	28.2 ± 2.9	0.52 ± 0.03	0.69 ± 0.15				
50.0 ± 0.1	4.7 ± 0.5	0.53 ± 0.11			0.30 ± 0.06		
325.0 ± 0.1	100 ± 5	0.51 ± 0.03	0.57 ± 0.05	0.57 ± 0.05	0.45 ± 0.03	0.47 ± 0.10	
1180.3 ± 0.3	100 ± 6	0.47 ± 0.05	0.59 ± 0.05	0.67 ± 0.09	0.58 ± 0.10		0.64 ± 0.06

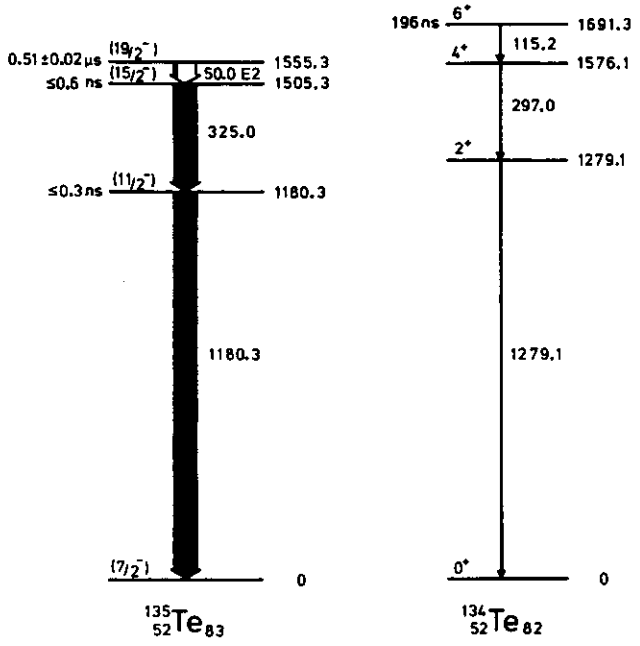

Fig. 2: Proposed level scheme of ^{135}Te in comparison with the partial level scheme of ^{134}Te.

References

1) W.-D. Lauppe, K. Sistemich, T.A. Khan, H. Lawin, G. Sadler, H.A. Selić, O.W.B. Schult: Journ. Phys. Soc. Jap. 44, 335 (1978)

2) T.Björnstad, L.-E. de Geer, G.T. Ewan, P.G. Hansen, B. Jonson, K. Kawade, A. Kerek, W.-D. Lauppe, H. Lawin, S. Mattsson, K. Sistemich: Phys. Lett. 91B, 35 (1980)

3) J.W. Grüter, K. Sistemich, P. Armbruster, J. Eidens, H. Lawin: Proc. Int. Conf. on Properties of Nuclei far from the Region of Beta-Stability, Leysin, CERN Rep. 70-30, p. 967

4) W. John, F.W. Guy, J.J. Wesolowski: Phys. Rev. C2, 1451 (1970)

5) R.G. Clark, L.E. Glendenin, W.L. Talbert Jr.: Physics and Chemistry of Fission 1973, IAEA Vienna, 1974, p. 221

6) K. Sellam, J.P. Bocquet, J. Blachot, E. Monnand, F. Schussler, J.W. Grüter, K. Sistemich: Annual Report 1976 of the Institut für Kernphysik der KFA Jülich, KFA-IKP 10/77, p. 50

7) H. Bartsch, W. Günther, K. Huber, U. Kneissl, H. Krieger, H.J. Maier: Nucl. Phys. A306, 29 (1978)

8) K. Kawade, G. Battistuzzi, H. Lawin, K. Sistemich, J. Blomqvist: Z. Phys., A298 (1980) 273

+ On leave from Nagoya University, Japan

++ Forskningsinstitutet för Atomfysik, Stockholm, Sweden

2.18. Studies of Primary Fission Products from ^{254}Cf

H.A. Selič, E. Cheifetz[+] and J.B. Wilhelmy[++]

An experiment on primary fission products[1,2] from the spontaneous fission of ^{254}Cf was carried out at the Weizmann Institute of Science in Rehovot, Israel. The measurement of γ-rays from $2_1^+ \rightarrow 0_1^+$ transitions in coincidence with fission fragment pulses proportional to their kinetic energy enables us to evaluate independent fission yields[3]. The identification of unknown γ-lines was performed from γ-ray intensities v.s. mass distribution plots (an example is shown in Fig. 1) obtained by converting the fission fragment pulse hight spectrum to the corresponding mass spectrum by means of the Schmitt[4]-calibration. The experimental arrangement[5] is shown in Fig. 2. Two SSD (F1 and F2) were used for detection of coincident light and heavy fission products. F_1 was placed at a fixed position. The source and F_2 were mounted so as to be movable by micrometers. A 2 cm^3 -Ge-Diode was used to measure the γ-rays. The experiment was carried out at distances of 0.04 cm, 0.08 cm, 0.16 cm, 0.28 cm, 0.6 cm, 1.15 cm and 3.1 cm between source and F_1 to evaluate $t_{1/2}$ of the observed γ-ray transitions. At each distance $\sim 10^7$ (F_1, F_2, TAC, γ)-events were recorded. The results for the even-even isotopes[5] are listed in table 1. The results of ref. 1,3 are given for comparison. The $\langle\beta_2\rangle$ values show the expected strong deformation for the $^{102,104}Zr$ isotopes (0.43±0.02 and ≈ 0.43, respectively), which is assumed to occur at the on-set of deformation[6] around A ≈ 100.

To the rudimentary energy level schemes of ^{105}Mo, $^{109,111}Ru$ and ^{146}La of Hopkins[7] are added the $t_{1/2}$ and relative intensities I_{rel} from our work.

These level schemes are shown in Fig. 3 - 5, respectively. An example for the intensity vs. time of flight is given in Fig. 6. In contradiction to the coincidence of the 246.5 keV line with 144.7, 138.2 and 94.9 keV lines of ref. 7. Kaffrell ref. 8 sees this line as a cross over to the g.s. This results in an additional level at 246.5 keV. The corresponding γ-rays with their $t_{1/2}$, independent yields, relative intensities and most probable mass $I(A)_{max}$ are given in table 2. Some unassigned short lived ($t_{1/2}$ < 10 ns) γ-rays are listed in table 3 and the longer lived γ-rays ($t_{1/2}$ > 10 ns) from the TAC-time slices are given in table 4 and compared with earlier works[9,10].

The fact that spontaneous fission of the Cf isotopes is accompanied by emission of approximately the same number of neutrons ν(250) = 3.49, ν(252) = 3.74 and ν(254) = 3.89[11] results on the average in more neutron rich fission fragments in ^{254}Cf than in any other readily available low-energy particle induced or spontaneous fission source. Table 5 gives a summary of the independent yield of all even-even isotopes observed in the ^{254}Cf experiment[12] (column 4 plotted in Fig. 7) and compares it with previous results from a ^{252}Cf source (column 3 [4]). The results clearly show the shift towards more neutron rich isotopes. If one compares the ΔA_p-values the shift anomaly between light and heavy fragments is obvious. Table 6 gives the mean values of ΔA_p of the light and heavy group which differ by about 0.5 mm.

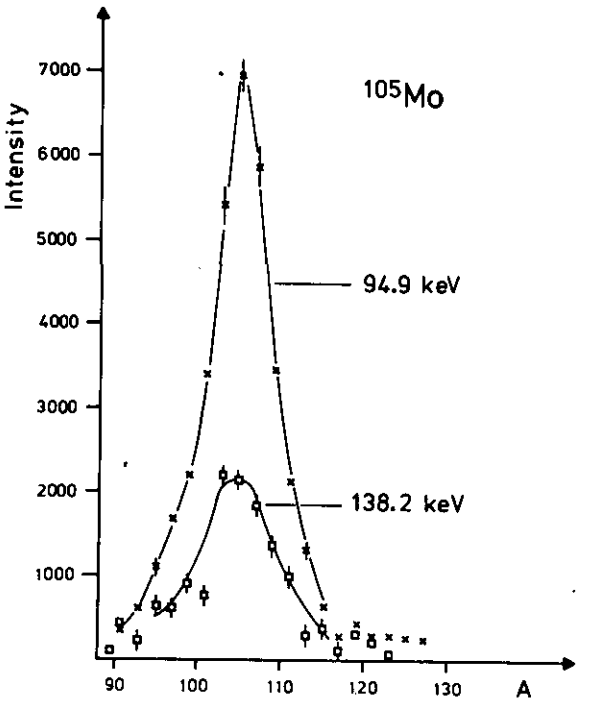

Fig. 1: Intensity $I_{\gamma_{YS}}$ mass A distributions of the 94.9 keV and 138.2 keV γ-ray transitions in ^{105}Mo

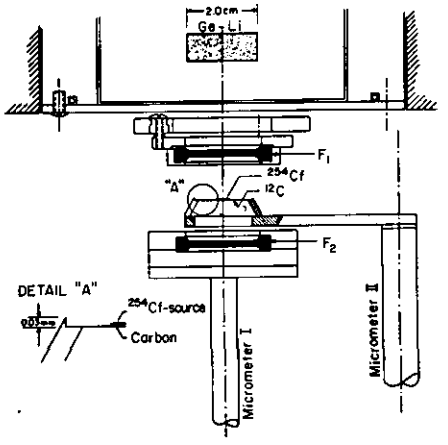

Fig. 2: The experimental arrangement for measuring independent yields and level life times in primary fission products by the time-of-flight method.

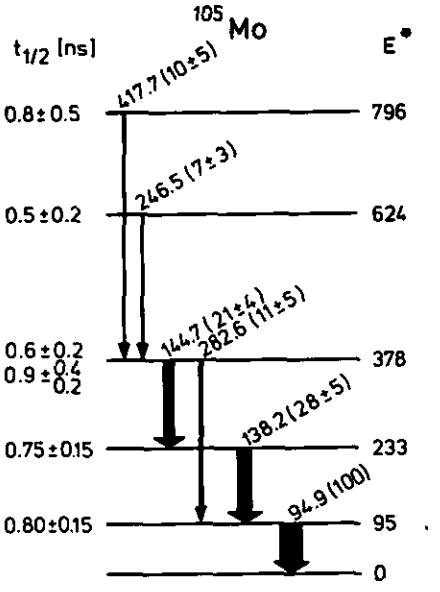

Fig. 3: The level scheme of ^{105}Mo from ref. 7. The level scheme of ref. 8, which is based on γ,γ-coincidences contains a level with an energy of 246.5 keV depopulating directly to the ground state. This is obviously the dashed 246.5 keV γ-ray transition depopulating the 624 keV level in ref. 7 with a $t_{1/2}$ = 0.5 0.2 ns we measured, therefore this level does not exist.

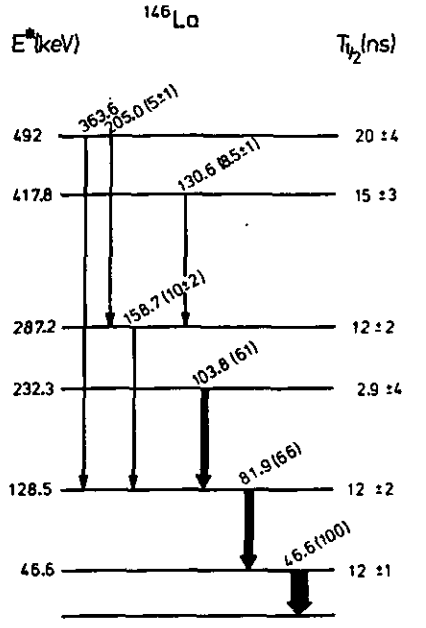

Fig. 5: The tentative level scheme of $^{146}_{57}La_{89}$ based on ref. 7 and lines seen in ref. 9.

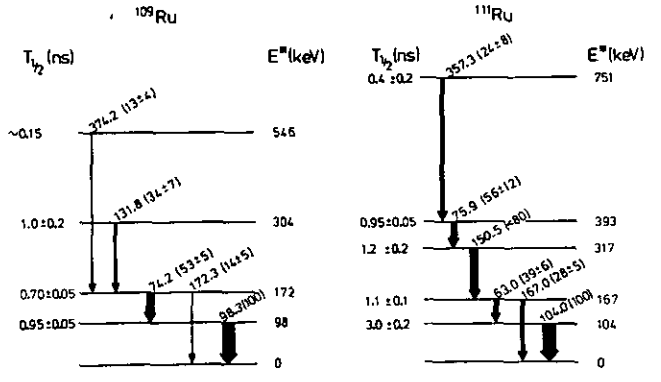

Fig. 4: The level scheme of ^{109,111}Ru from ref. 7.

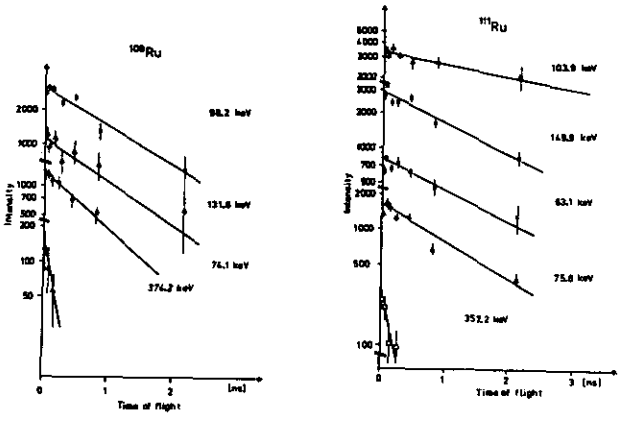

Fig. 6: An example of the half-life analysis of levels in ^{109,111}Ru.

Table 1: Properties of lowest $2^+ \rightarrow 0^+$ transitions in even-even fission fragments

Isotope	E (keV)	$T_{1/2}$ (ns) ^{252}Cf$_{exp.}$	Jared et al. (1973)	$\frac{B(E2)_{exp}}{B(E2)_{sp}}$	$<\beta_2>$
^{98}Sr	144.4	$4^{+3}_{-1.5}$	-	65^{+39}_{-28}	0.34 ± 0.09
^{100}Zr	212.5	0.62 ± 0.10	0.71 ± 0.03	64 ± 3	0.31 ± 0.01
^{102}Zr	151.6	1.71 ± 0.14	2.11 ± 0.25	120 ± 8	0.43 ± 0.02
(^{104}Zr)	140.1	≈ 2.5	-	≈ 112	≈ 0.43
^{104}Mo	192.0	0.88 ± 0.10	0.91 ± 0.03	77 ± 7	0.33 ± 0.02
^{106}Mo	171.4	1.34 ± 0.10	1.25 ± 0.03	82 ± 2	0.34 ± 0.01
(^{108}Mo)	172.1	$1.2^{+0.35}_{-0.2}$	-	88 ± 20	0.35 ± 0.04
^{108}Ru	242.0		0.34 ± 0.03		
^{110}Ru	240.5	0.30 ± 0.02	0.34 ± 0.04	70 ± 5	0.30 ± 0.01
^{112}Ru	236.4	0.48 ± 0.06	0.32 ± 0.03	48 ± 6	0.25 ± 0.01
^{140}Xe	376.4	0.113± 0.005	-	16 ± 1	0.11 ± 0.02
(^{142}Xe)	(205)	$0.34^{+0.12}_{-0.07}$	-	103 ± 28	0.30 ± 0.10
^{142}Ba	359.4	0.079± 0.006	0.07 ± 0.04	27 ± 2	0.15 ± 0.03
^{144}Ba	199.4	0.70 ± 0.07	0.70 ± 0.03	49 ± 4	0.20 ± 0.01
^{146}Ba	181.0	0.92 ± 0.12	0.85 ± 0.06	56 ± 7	0.21 ± 0.01
^{146}Ce	258.3	0.24 ± 0.03	0.26 ± 0.05	41 ± 5	0.18 ± 0.02
^{148}Ce	158.2	0.95 ± 0.08	1.06 ± 0.08	91 ± 5	0.26 ± 0.02
^{150}Ce	97.0	3.08 ± 0.54	3.6 ± 1.0	128 ± 20	0.31 ± 0.02

Table 2: Half-lives, fission yields and the maxima of γ-intensities vs. mass distribution for some known odd nuclei.

Isotope	Transition (keV)	$t_{1/2}$(ns)	Photons/f	Yield independ. if(E2)	Rel. Int. I_{rel}	$I_\gamma(A)_{max}$
^{103}Mo	102.8	1.7 ± 0.3	0.004(25)	1.3 ± 0.3	100	103.4 ± 0.5
	144.0		-			102.8 ∓ 0.6
	251.1	many comp.	-			-
^{105}Mo	94.9	0.80+0.15	0.0086 (9)	4.0 ± 0.3	100	104.95+ 0.10
	138.2	0.75+0.15	0.0031(0)	1.2 ∓ 0.4	28 ± 5	104.7 ∓ 0.3
	144.7	0.9 +0.4 -0.2	0.0028(50)	0.8 ± 0.2	21 ± 4	104.0 ± 0.8
	246.5	0.5 +0.2	0.0009(40)	0.24+ 0.10	7 ± 3	
	282.6	0.6 +0.2	0.0014(30)	0.36+ 0.15	11 ∓ 5	
	417.7	0.8 +0.5	0.0009(50)	0.35+ 0.15	10 ∓ 5	
^{107}Mo		< 10				
	65.4	220 ± 10	0.0007(25)	1.01+ 0.23	100	107.5 ± 0.4
^{109}Ru	74.2	0.70+0.05	0.0021(5)	1.8 ± 0.1	53 ± 5	
	98.3	0.95+0.05	0.0077(14)	3.6 ∓ 0.5	100	109.7 ± 0.6
	131.8	1.0 +0.2	0.0041(15)	1.2 ∓ 0.2	34 ± 7	108.9 ∓ 0.6
	172.3	0.70+0.05	0.003 (15)	1.0 ∓ 0.2	14 ∓ 5	
	374.2	~0.15	0.001 (20)	0.7 ∓ 0.2	13 ∓ 4	
^{111}Ru	63.0	1.1 +0.1	0.0013(17)	1.7 ± 0.3	39 ± 6	
	75.9	0.95+0.05	0.0028(17)	2.6 ∓ 0.6	56 ∓ 12	
	104.0	3.0 +0.2	0.0092(9)	3.8 ∓ 0.4	100	110.8 ± 0.3
	150.5	1.2 +0.2	0.0143(12)	3.7 ∓ 0.5	<80	110.7 ∓ 0.7
	167.0	1.1 +0.1	0.0050(18)	1.2 ∓ 0.2	28 ± 5	
	357.3	0.4 +0.2	0.0067(50)	1.3 ∓ 0.5	24 ∓ 8	
^{146}La	46.6	11 ± 2	0.001 (20)	3.3 ± 0.2	100	
	81.9	12 ∓ 2	0.0015(16)	2.2 ∓ 0.2	66 ± 6	146.1 ± 0.6
	103.8	2.9 ∓ 0.3	0.0040(5)	2.0 ∓ 0.1	61 ∓ 5	
	130.6	15 ∓ 2	0.0010(25)	0.28+ 0.09	9 ∓ 2	
	158.7	12 ∓ 2		0.34+ 0.04	10 ∓ 2	
	205.0	20 ∓ 4		0.17∓ 0.05	5 ∓ 1	
	363.6					

Table 3: Unassigned (assigned) γ-rays with most probable mass (isotope), energies, $t_{1/2}$ and intensities

$I_\gamma(A)_{max}$ Mass	E_γ(keV)	$T_{1/2}$(ns)	Intensities Photon/fiss.	Isotope
∿ 99.	53.2	2.4 ±0.5	0.0008(25)	^{99}Zr
∿101.	65.5	0.1 ±0.02	0.0006(25)	
107.6±0.4	65.9	2.1 ±0.4	0.0006(20)	^{107}Mo
113.7±0.5				
101.8±0.4	66.7	2.2 ±0.5	0.0007(25)	
		1.0 ±0.3		
109.5±0.5	67.1	1.1 ±0.2	0.012(25)	
99.6±0.5	68.8	2.2 ±0.2	0.0045(25)	
111.6±0.5				
107.4±0.3	69.3	0.9 ±0.1	0.0017(15)	
106.6±0.4	71.5	0.7 ±0.1	0.0020(20)	
101.7,	72.8	1.2 ±0.2	0.0034(15)	
107.2±0.4				
115.0±0.6				
98.9,	73.9	0.6 ±0.1	0.0022(20)	
107.5±0.5				
99.9±0.6	81.8	1.1 ±0.2	0.0008(25)	^{107}Tc
107.6±0.4				
105.4±0.6	84.2	2.7 ±0.2	0.0016(25)	
97.0±0.6	84.8	4.0 ±0.4	0.0028(25)	
105.7±0.5	85.3	> 6	0.0011(25)	^{105}Tc
107.7	87.2	1.2 ±0.1	0.0016(25)	
100.4±0.6	91.5	2.1 ±0.2	0.0020(25)	
98.2±0.5	94.6	0.78±0.05	0.0096(10)	
105.0±0.5		0.9 ±0.2		
110.5±1.6				
94.5±0.5	104.4	2.0 ±0.5	0.0073(11)	^{107}Tc
102.3±0.6				
106.6±0.4				
117.4±0.5				
100.4±0.5	105.9	2.5 ±0.4	0.0019	^{108}Tc
107.4±0.5				
102.4±0.5	109.7	1.4 ±0.2	0.0032(12)	
108.0±0.5				
116.8±0.6				
101.4±0.5	109.0	2.2 ±0.2	0.0016(15)	
106.8±0.6				
105.0±0.5	111.8	1.0 ±0.2		
111.0±0.5	112.8	0.8 ±0.1	0.0013(20)	
107.5±0.5	116.0	2.2 ±0.4	0.0008(25)	^{108}Tc
105.2±0.4	122.4	0.6 ±0.1	0.0009(27)	
109.7±0.5				
107.0±0.6	142.1	2.1 ±0.3	0.0029(20)	
108.6±0.5	146.6	0.1 ±0.05	0.0027(25)	
96.9±0.5	150.1	2.8 ±0.2	0.0118(10)	
104.2±0.5				
108.2±0.5	176.1	> 20	0.0044(12)	^{108}Tc
135.5±0.5	75.6	0.55±0.15	0.0054(10)	^{141}Cs
142.2±0.5				
147.6±0.6				
154.3±0.6				
141.4±0.5	76.9	1.8 ±0.3	0.0023(12)	^{141}Cs
151.4±0.6				
139.8±0.3	98.1	2.7 ±0.2	0.0022(12)	
147.0±0.5				
151.7±0.6				^{151}Pr
132.1±0.6	112.6	1.1 ±0.1	0.0073(11)	
138.6±0.6				
146.1±0.7				
136.8±0.3	117.4	3.5 ±0.5	0.0063(11)	^{143}Ba
143.7±0.5	117.9	4 ±0.5	0.0021(15)	^{137}I, ^{141}Cs

Table 4: Some long lived ($t_{1/2}$ > 20 ns) γ-rays evaluated from Time-to-Amplitude Converter-slices

$I_\gamma(A)_{max}$	E_γ(keV)	$T_{1/2}$(ns)	Intensities Photons/fiss.	Isotope
153.0±0.5	45.0	24± 4	0.0012(20)	
106.8±0.4	45.5	24± 4	0.0007(30)	^{107}Tc
	53.3	30± 5	0.0005(30)	^{109}Rh
111.8±0.6	60.3	45± 5	0.0013(25)	^{111}Rh
107.1±0.4	81.7	12± 4	0.00077(25)	^{107}Tc
108.8±0.6	86.1	130±20	0.00055(30)	^{108}Tc
	115.2	190±30	0.00012(25)	^{134}Te
99.2±0.4	121.8	10± 3	0.00011(40)	^{99}Zr
		∿300		
99.2±0.4	130.2	12± 2	0.00007	^{99}Zr
		∿300		
103.0±0.3	153.8	125±11	0.00077(25)	^{108}Tc
145.8±0.5				
100.6±0.5				
146.7±0.4	167.5	40± 5	0.00059(30)	^{147}La
	176.3	92± 5		^{108}Tc
95.5±0.4	204.0	26± 2	0.00017(30)	^{95}Sr

Table 5: Comparison of $2^+ \rightarrow 0^+$ fission yield of even-even isotopes obtained from spontaneous fission of ^{252}Cf and ^{254}Cf

Isotope	$2^+ \rightarrow 0^+$ E_γ(keV)	2^+ Yield (%) ^{252}Cf	^{254}Cf	A_p ^{252}Cf	A_p ^{254}Cf	Shift ΔA_p
$^{98}_{38}$Sr	144	-	∿ 0.36 ± 0.01			
$^{100}_{40}$Zr	212.5	1.8	1.41 ± 0.26			
^{102}Zr	151.6	1.43	1.98 ± 0.05	100.77	101.4	0.63 ± 0.032
^{104}Zr	140.1	-	0.8 ± 0.05			
$^{104}_{42}$Mo	192.0	3.37	3.1 ± 0.2			
^{106}Mo	171.4	3.37	4.96 ± 0.2	105.0	105.5	0.50 ± 0.047
^{108}Mo	172.1	-	0.9 ± 0.2			
$^{108}_{46}$Ru	242.0	1.94	1.47 ± 0.15			
^{110}Ru	240.5	3.49	4.1 ± 0.2	109.77	110.4	0.63 ± 0.055
^{112}Ru	236.4	0.97	2.96 ± 0.2			
$^{138}_{54}$Xe	589.5	2.3	2.0 ∓ 0.5			
^{140}Xe	376.4	1.5	4.27 ± 0.4	138.45	139.4	1.05 ± 0.14
^{142}Xe	205.0	-	1.5 ± 0.5			
$^{142}_{56}$Ba	359.4	2.9	1.45 ± 0.3			
^{144}Ba	199.1	3.6	5.54 ± 0.6			
^{146}Ba	181.0	1.01	3.31 ± 0.4	143.29	144.5	1.21 ± 0.12
^{148}Ba	142.5	-	0.636± 0.26			
$^{146}_{58}$Ce	258.3	1.04	0.98 ± 0.2			
^{148}Ce	158.2	2.31	2.19 ± 0.4	147.95	149.0	1.05 ± 0.18
^{150}Ce	97.0	0.98	> 2.01 ± 0.3			

Table 6: ΔA_p shift anomaly between light and heavy fission group for ^{252}Cf - ^{254}Cf

	ΔA_p experiment	Division according to neutron numbers
Change in the light group	0.59 ± 0.04	0.69
Change in the heavy group	1.10 ± 0.147	1.01
Total change	1.69 ± 0.152	1.70
Change of ^{254}Cf - ^{252}Cf - $\Delta\nu$ = 1.58		

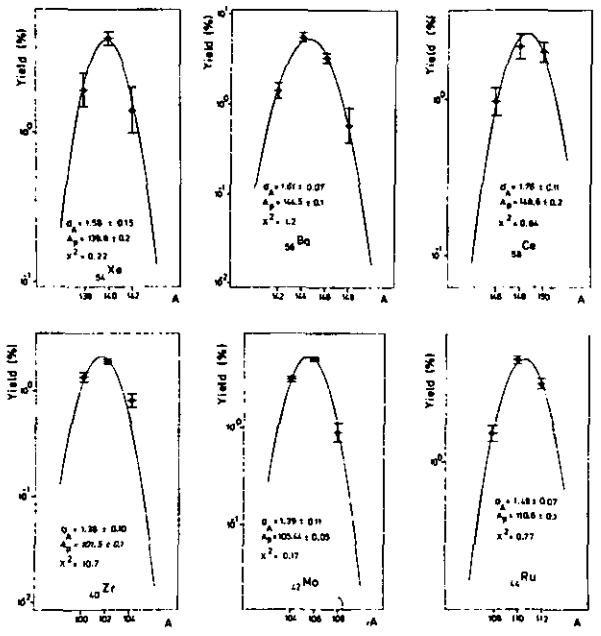

Fig. 7: Independent fission yields for the even-even isotopes. The solid lines show the χ^2 fit of the data based on the previously determined value of σ_A (data from ^{252}Cf experiment ref. 3).

References

1) R.C. Jared, H. Nifenecker and S.G. Thompson, Proc. 3rd IAEA Symp. Phys. Chem. Fission, Rochester (1973), Vienna: IAEA

2) H.A. Selič, E. Cheifetz and J.B. Wilhelmy in Scientific Activities (1979) The Weizmann Inst. of Science, p. 65

3) E. Cheifetz, J.B. Wilhelmy, C.R. Jared and S.G. Thompson, Phys. Rev. C4 (1971), p. 1913

4) H.W. Schmitt, J.H. Neiler and F.J. Walter, Phys. Rev. 141 (1966), p. 1146

5) E. Cheifetz, H.A. Selič, A. Wolf, R. Chechik and J.B. Wilhelmy, Inst. Phys. Conf. Ser. No. 51 chapter 4, p. 193 (1980)

6) T.A. Khan, W.D. Lauppe, G. Sadler, H.A. Selic, H. Lawin and K. Sistemich, Report-KFA-Jülich, KFA-IKP 10/77, p. 44
R.K. Sheline, I. Ragnarson and S.G. Nilsson Phys. Lett. 41B (1972) 115
K. Sistemich, W.D. Lauppe, H. Lawin, H. Seyfarth, B.D. Kern, Z.Phys 289 (1979) p. 225 - 226

7) F.F. Hopkins, J.R. White, C.F. Moore and P. Richard, Phys. Rev. C8 (1973), p. 380

8) N. Kaffrell, Univ. Mainz, private communication

9) R.G. Clark, L.E. Glendenin and W.L. Talbert, Proc. 3rd, IAEA Symp. Phys. Chem. Fission, Rochester (1973), Vienna: IAEA

10) J.W. Grüter, K. Sistemich, P. Armbruster, J. Eidens and H. Lawin, Phys. Lett. 33B (1970), No. 7, p. 474

11) C.D. Hoffmann, Symp. Phys. Chem. Fission, Jülich (1979) Vienna: IAEA (1980), Vol. II, p. 275

12) H.A. Selič, E. Cheifetz, A. Wolf and J.B. Wilhelmy, *Inst. Phys. Conf. Ser. No. 51 chapter 5, p. 316 (1980)*

+ Weizmann Inst. Rehovot, Israel

++ LASL, Los Alamos, NM, USA

2.19. High Energy Gamma-Rays from Fission Products Prompt and After β-decay

H.A. Selič and H. Seyfarth

An integral γ-ray spectrum from fission fragments in the range from 1.2 up to about 8 MeV was recorded by means of a pair-spectrometer with a resolution of 4.5 keV for the 7646 keV Fe γ-ray. A sample of 29 mg of ^{235}U (90 % enriched) was exposed to the n_{th}-beam of the reactor FRJ2-Dido with a flux of $n_{th} = 2.5 \cdot 10^8$ n/sec cm^2 Because of the thickness of the ^{235}U-source all fission-fragments were stopped immediately (< 3 ps flight time, stopping power of ^{235}U) which enabled us to see non doppler shifted transitions in this time range for primary fission products. Nevertheless the γ-ray transitions seen in the spectrum shown in Fig. 1 are fed via both: prompt population and deexcitation in fission process and β-decay of the corresponding mother nuclei. Thus the intensities are usually a mixture of the two decay-modes. This is shown[1] for example in Fig. 2 of mass A = 91 and 92 and the preliminary results are listed in table 1. The γ-ray pair spectrometer was calibrated for energy and efficiency by $Cl(n,\gamma)$[2], $C(n,\gamma)$[3] and $^{235}U(n,\gamma)$[4] transitions (see fig. 3). The intensities of the γ-lines have been normalized to the efficiency of the pair spectrometer and are given as relative intensities I_{rel} in table 1. Besides the known γ-ray energies the corresponding isotope[5], the β-decay chain yield[6] and the independent yield[1] of the isotope are given. For comparison the relative intensities from the level schemes[7] are given.

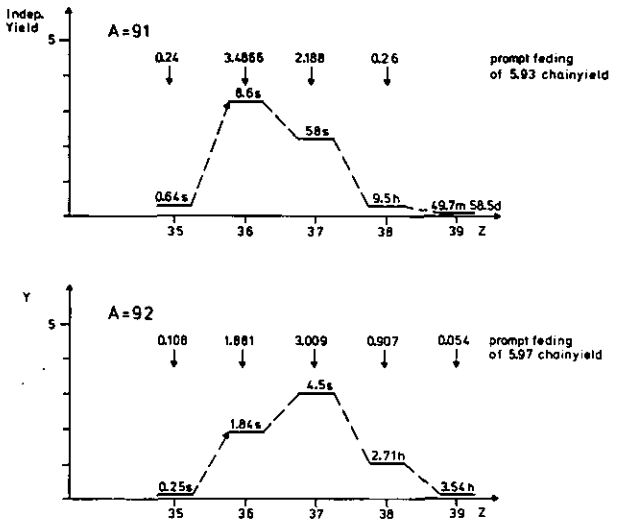

Fig. 2: An example of the feeding of γ-ray transitions via primary population in fission and β-decay.

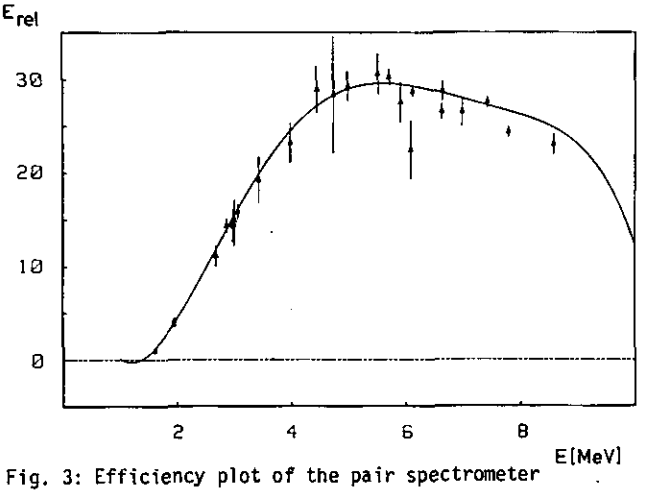

Fig. 3: Efficiency plot of the pair spectrometer

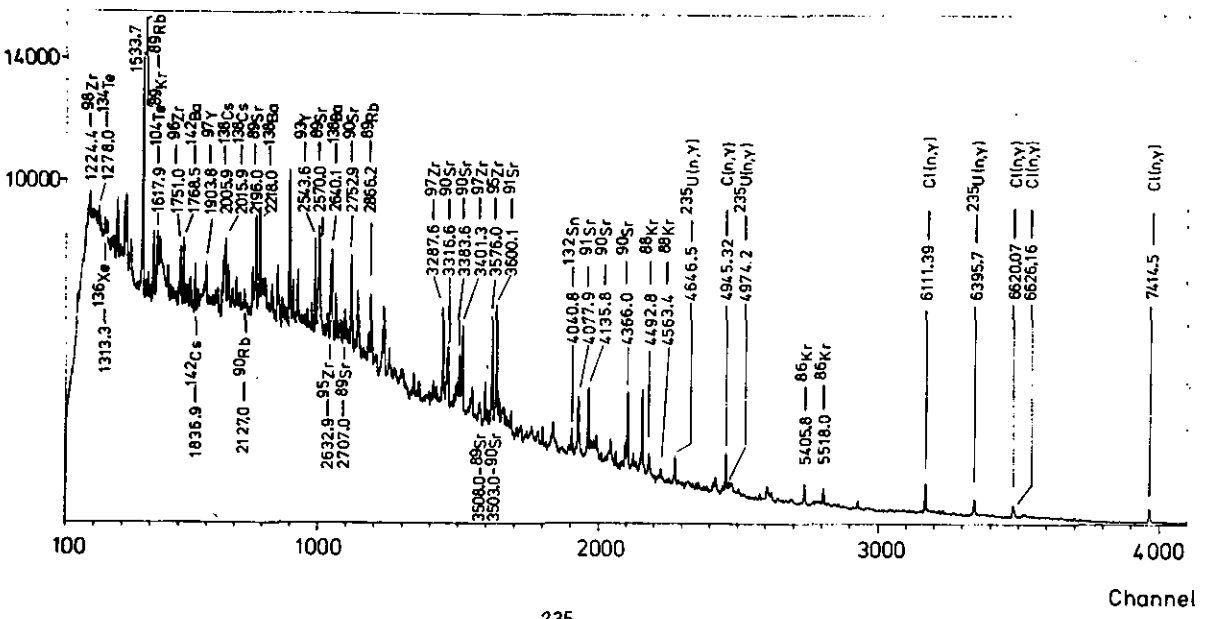

Fig. 1: Pair-spectrometer spectrum from $^{235}U(n_{th},f)$

Table 1: γ-rays from $^{235}U(n_{th},f)$ measured by a pair-spectrometer

E_γ	Isotope[7]	I_{rel} Pairspectr.	I_{rel}[7] Level-sch.	β^- decay chain yield[6]	indep. yield[1]
1217.35	^{130}Sn	76.70	100	1.70	
1272.02	^{133}Te	80.81	98	6.75	
1279.00	^{100}Mo, ^{134}Te	126.33	(85),(100)	7.65	
1313.39	^{136}Te	88.00		6.60	
1324.48	^{95}Zr	105.00	27.7	6.50	0.059
1384.89	^{142}Cs, ^{139}Cs ^{92}Sr	273.72	(14),(20)	5.87,5.97	0.92
1436.71	^{138}Ba	330.66	100	6.8	
1442.40	^{140}Ba	111.40	β^-,0.6	6.36	
1533.61	^{89}Rb	365.44	β^-,5.6	4.80	0.23
1742.9	^{93}Rb	11.10	β (0.7)	6.40	3.14
1750.89	^{96}Zr	29.22	β (100)	6.28	0.25
1768.49	^{138}Cs, ^{142}Ba	30.60	β (34),21	5.87	
1836.93	^{88}Sr, ^{144}Ba	18.55		3.62,5.39	
1850.98	^{91}Sr, ^{136}Cs	6.22	β (10)	6.80	
1855.51	^{88}Kr	7.00	β (0.7)	3.62	1.67
1903.76	^{89}Rb, ^{138}Ba	15.26	(5.6) (0.6)	4.80,6.80	0.23
1970.97	^{91}Sr	7.94	β (4,7)	5.93	0.26
1997.34	^{97}Zr, ^{137}Xe	10.21	β (2)	6.03,6.26	0.65
2005.88	^{90}Rb, ^{138}Cs	18.59	β (10)	5.89	0.73
2015.94	^{104}Tc, ^{138}Cs	17.79	β (34)	1.83,6.80	
2031.53	^{95}Y, ^{131}Sb	12.00	β (5)	6.50,2.82	0.88
2048.92	^{140}Ba	2.01	β (3)	6.36	
2078.78	^{142}Cs	6.55	(22)	5.87	
2087.22	^{93}Sr	2.70	(9)	6.40	2.38
2127.46	^{90}Rb	4.42	β^-(1.3)	5.89	0.73
2175.90	^{95}Zr	8.15	β^-(12)	6.50	0.06
2196.02	^{89}Sr	17.69	β (33)	4.80	0.03
2211.55	^{97}Y, ^{138}Ba	4.67	β^-(42)	6.03,6.80	3.17
2218.30	^{138}Ba	18.11	β^-(14)	6.80	
2322.55	^{138}Cs	8.65	β (3.2)	6.80	
2349.84	^{93}Rb	3.16	β^-(11.5)	6.40	3.14
2392.42	^{88}Rb, ^{144}Ba	18.62	51	5.39	0.08
2416.03	^{136}Xe	5.36	β (6.2)	6.18	
2442.92	^{90}Sr	6.49		5.89	0.04
2543.26	^{93}Y, (^{99}Mo)	10.98	42,16	6.40,6.13	0.18
2564.50	^{91}Sr	11.22	β (15)	5.93	0.26
2603.50	^{93}Rb	1.15	β (11.5)	6.40	3.14
2632.89	^{95}Zr	6.76	β (6)	6.50	0.06
2640.06	^{138}Ba	9.63	β (9.1)	6.80	
2705.84	^{93}Sr	2.70		6.40	2.38
2717.17	^{95}Y	3.60	β (5)	6.50	0.88
2744.55	^{97}Zr	1.59	β (6.5)	6.03	0.65
2752.98	^{91}Rb	9.97	17	5.93	2.19
2769.59	^{91}Rb	0.99	4.8	5.93	2.19
2791.64	^{139}Cs	5.87	β (0.4)	6.50	
2820.19	^{92}Sr	1.12	β (0.7)	5.97	0.91
2866.19	^{89}Rb	6.04	β (4)	4.80	0.23
2890.62	^{93}Sr	1.44	30	6.40	2.38
2925.98	^{91}Sr	1.56	β (2.7)	5.93	0.26
2933.15	^{95}Y	3.89	β (8.4)	6.50	0.88
2942.62	^{98}Zr	5.74	β^-(11)	5.79	2.61
3114.88	^{91}Rb	1.84	49	5.93	2.19
3287.72	^{97}Zr	6.33	β (27)	6.03	0.65
3316.60	^{90}Sr	4.00	91	6.36	
3400.73	^{97}Zr	6.30	β^-(15)	6.03	0.65
3534.18	^{90}Sr	2.88	31	5.89	0.04
3575.94	^{95}Zr	7.00	β^-(9)	6.50	0.06
3600.01	^{91}Sr	7.71	β^-(11)	5.93	0.26
4077.59	^{91}Sr	3.48	61(3.9)	5.93	0.26
4147.63	^{88}Kr	0.93	62(4 %)	3.62	1.67
4266.04	^{91}Sr	1.42	64(1.4 %)	5.93	0.26
4365.93	^{90}Sr	4.24	62	5.89	0.04
4492.84	^{88}Kr	1.27	11	3.62	1.67
4563.37	^{88}Kr	0.78	95	3.62	1.67
4637.40	^{92}Sr	0.20	β(0.4)64	5.97	0.91
4945.71	$^{12}C(n,\gamma)$	2.18			
4973.58	^{90}Sr	0.59	33	5.89	0.04
4982.51	^{140}Ba	0.52		6.36	
5020.39	^{88}Kr	0.41	27	3.62	1.67
5187.81	^{92}Sr	0.85	β (0.4)81	5.97	0.91
5213.88	^{88}Kr	0.58	7.3	3.62	1.67
5405.80	^{86}Kr	1.17	93	1.95	0.16
5518.00	$CL(n,\gamma)$	0.93			
6111.64	$CL(n,\gamma)$	1.72			
6620.78	$CL(n,\gamma)$	0.73			
6629,75	$CL(n,\gamma)$	0.29			
7414.38	$CL(n,\gamma)$	0.93			

References

1) H. Wollnik, G. Siegert, J. Greif and G. Fiedler, Proc. 3rd Int. Conf. on Nucl. far from Stab., Cargese, Corsica, May 1976, p. 517

2) A.M. Spitz and J. Kopecky, Nucl. Phys. A264 (1976) 63

3) A.H. Wapstra, Neutr. Cap. γ-Ray-Spectroscopy, 2nd Int. Symp. (1974) Petten, Netherland, p. 686

4) H. Ottmar, P. Mattussek and I. Piper, 2nd Int. Symp. on Neutr. Capt. γ-Ray Spectroscopy (1974) Petten, Netherland, p. 658

5) J. Blachot and C. Fiche, Nucl. Data Tabl. Vol. 20, No. 3, Sept. 1977

6) W. Seelmann-Eggebert, G. Pfennig and H. Münzel, Karlsruher Nuklidkarte

7) C.M. Lederer and V.S. Shirley, Tables of isotopes, seventh Edition (1978)

2.20. Determination of primary γ-rays after thermal neutron capture in ^{74}Se

Y. Tokunaga, H. Seyfarth, O. Schult, H.G. Börner[+], C. Hofmeyr[+]

Primary γ rays after neutron capture in ^{74}Se have been studied at the research reactor DIDO in Jülich and the High Flux Reactor at the ILL-Grenoble, respectively. In both cases pair spectrometers have been used. Whereas at the Grenoble spectrometer use has been made of an internal target geometry exploiting the very high neutron flux of 5.5×10^{14} n/cm^2· s at Jülich the external target geometry was utilized with a neutron flux of $\sim 10^8$ n/cm^2· s. Due to the different solid angles the sensitivities of both set-ups are comparable. Yet a fundamental difference in both experiments is, that double neutron capture occurs in the high flux of the Grenoble reactor, whereas at Jülich only single neutron capture is relevant. A comparison of spectra, taken at Jülich and Grenoble offers therefore a unique possibility to assign γ-rays which occur after double neutron capture, even if they are very weak. In the case of Selenium the assignment of ^{75}Se(n,γ)^{76}Se primary γ-rays was further facilitated by the fact that the n-binding energy of ^{75}Se is $\sim$ 3 MeV lower than that of ^{76}Se. In addition the background is extremely low in the high energy region of the Grenoble spectrometer resulting in a very high sensitivity (Fig. 1).

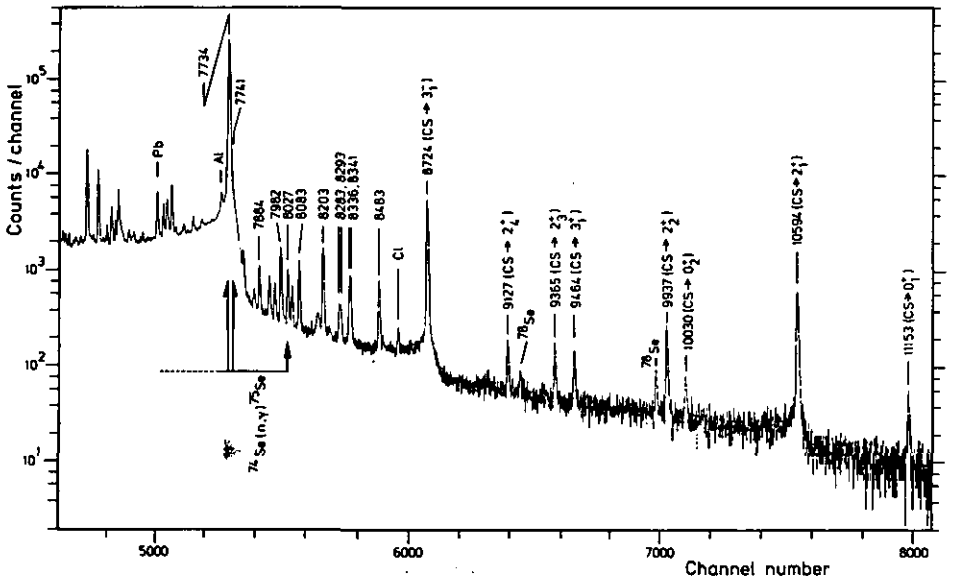

Fig. 1: Upper part of the γ-ray energy spectrum of the ^{74}Se(n,γ)^{75}Se and ^{75}Se(n,γ)^{76}Se reactions taken at Grenoble.

Fig. 2 shows a portion of the spectra obtained in Jülich. The preliminary value obtained for the n-binding energy is 8027.3 $\pm$ 0.3 keV in agreement with Wapstra and Bos [1]. The 7734 keV transition was found to be a doublet, supporting the close lying levels at 286.7 keV, $I^\pi = 3/2^-$, and 293.2 keV, $I^\pi = 1/2^-$, respectively, suggested by Agarwal et al.[2]. The final analysis which combines these data with the secondary γ-rays measured with the bent crystal spectrometers GAMS 1, 2/3 and the low energy conversion electrons taken with the β-spectrometer BILL at the ILL, is in progress.

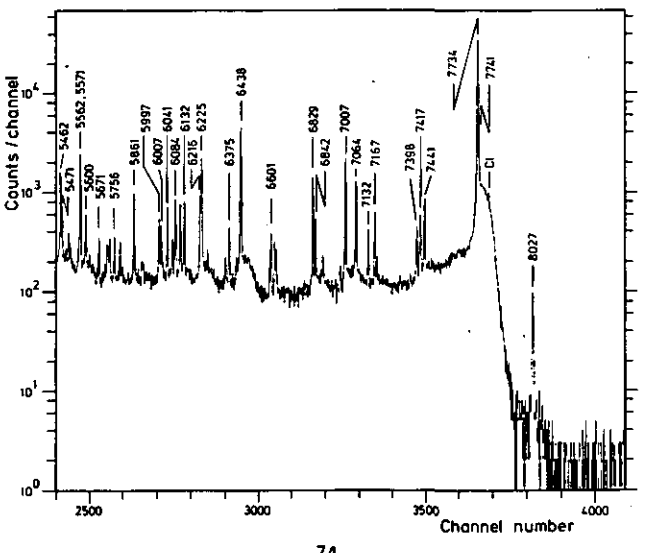

Fig. 2: Upper part of the ^{74}Se(n,γ) spectrum taken at Jülich.

Concerning double neutron capture into ^{76}Se the following preliminary results have been obtained so far:

1) The thermal neutron capture cross-section of the β^+-unstable isotope ^{75}Se - previously unknown - is $\sigma_{th} \sim 300$ barns.
2) The n-binding energy of ^{76}Se is 11154.0 $\pm$ 0.6 keV.
3) Primary transitions to the 0^+-groundstate ($2^+ \rightarrow 0^+$) and the 0_2^+ -level have been observed and additional levels above 2.8 MeV excitation energy were established.

[+] ILL, Grenoble/France

References

1) A.H. Wapstra and K. Bos, Atomic and Nuclear data tables, vol. 19, No. 3 (1977) p. 231
2) Y.K. Agarwal et al., Proc. of the international conference of Nuclear Physics, München 1973, p. 288 and Y.K. Agarwal et al., Pramana, vol.3, No. 4 (1974) p. 243

2.21. Low-lying states in doubly-odd ^{108}Ag and ^{110}Ag

M. Bogdanović[+], T.D. Mac Mahon[++], H. Seyfarth

Remaining open problems in the level schemes of ^{108}Ag and ^{110}Ag have been investigated by measurements of the primary thermal neutron capture γ-ray spectra with the pair spectrometer[1] at an external neutron beam of the FRJ-2 research reactor of KFA Jülich. These data for ^{108}Ag complete previous results from thermal[2-4] and resonance[5] neutron capture. Fig. 1 shows the preliminary low-energy level scheme up to ∿ 0.5 MeV excitation energy of ^{108}Ag. The final evaluation of the data for ^{110}Ag which shows a similar level sequence[6] is in progress.

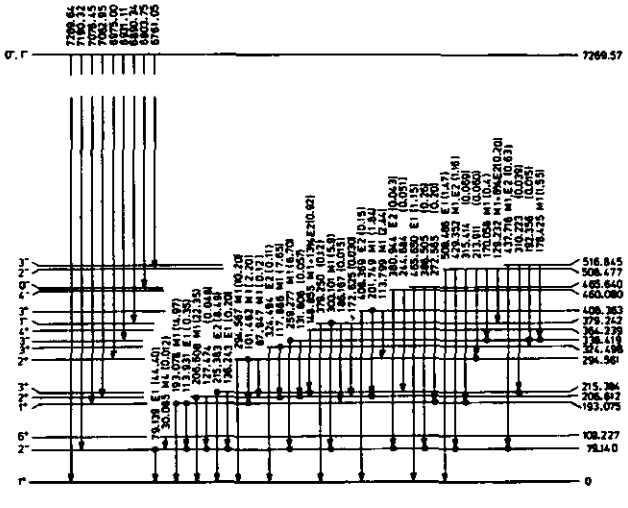

Fig. 1: Preliminary level scheme of ^{108}Ag for excitation energies below ∿ 0.5 MeV.

The low-lying states of both doubly-odd isotopes ^{108}Ag and ^{110}Ag can be classified as members of proton-neutron multiplets. With use of experimental information about the neighbouring odd-A nuclei it is possible to calculate in first approximation the energy of the multiplet members. The exchange of quadrupole and spin-vibrational 1^+ phonons between proton and neutron will split and mix the basic multiplet states and in lowest order will produce a parabolic structure of the multiplets[7]. In fig. 2 the preliminary results[8] of calculations for the even and odd parity multiplets in ^{110}Ag are depicted. Comparison with fig. 1 shows that e.g. it is possible to interprete the states at 0.0, 206.6, 324.4 and 109.2 keV as 1^+, 2^+, 3^+ and 6^+ members of the ($\pi 7/2^+$, $\nu 5/2^+$) multiplet. The detailed discussion of both ^{108}Ag and ^{110}Ag level schemes is in progress.

From the known energies of the low-lying states and those of the primary transitions the neutron binding energies in ^{108}Ag and ^{110}Ag have been calculated as (7269.57 ± 0.05) keV and (6809.19 ± 0.11) keV, respectively.

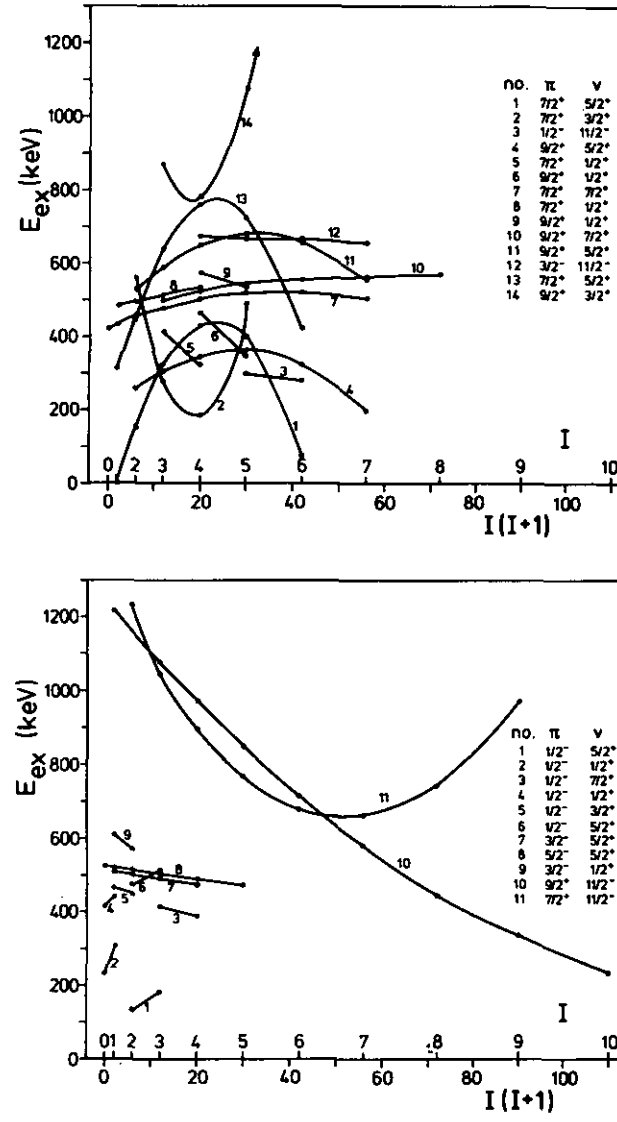

Fig. 2: Preliminary results (ref. 8) of calculations of even (upper part) and odd (lower part) parity multiplets in ^{110}Ag.

References

1) Annual Report IKP/KFA 1976, p. 127 and 1979, p. 71

2) D. Breitig, H.A. Baader, L. Wimmer, U. Heim, H.R. Koch, O.W.B. Schult, Neutron Capture Gamma-Ray Spectroscopy, ed. K. Abrahams, F. Stecher-Rasmussen, P. Van Assche (*Reactor Centrum Nederland, Petten, 1975*) p. 549

3) M. Thein, Ph.D. Thesis, University of London (1977)

4) G.R. Massoumi, K. Schreckenbach, T.D. Mac Mahon, Neutron Capture Gamma-Ray Spectroscopy, ed. R.E. Chrien, W.R. Kane (Plenum Press, New York, 1979) p. 684

5) G.B. Orr, W.R. Kane, G.J. Smith, ref. 4, p. 707 and private communication

6) *M. Bogdanović, S. Koički, J. Simić,* B. Lalović, D. Breitig, H.R. Koch, H.A. Baader, O.W.B. Schult, W.R. Kane, R.F. Casten, Fizika 11 (3) (1979) 157

7) V. Paar, Nucl. Phys. A331 (1979) 16

8) Z. Houšek, private communication

[+] Boris Kidrič Institute for Nuclear Sciences, Beograd, Jugoslavia

[++] University of London Reactor Centre, Ascot, Berkshire, England

II. THEORETICAL NUCLEAR PHYSICS

3. NUCLEAR STRUCTURE

3.1. Effect of the Core Polarization on the Transition Density in ^{207}Pb

T. Suzuki, S. Krewald, J. Speth

In a recent inelastic scattering experiment from ^{207}Pb [1] it has been observed that there is a systematic, multipolarity- and momentum-transfer-independent quenching $\sim$ 55 % in the transverse amplitude compared with single particle predictions. Hamamoto et al.[2] showed by using a perturbation calculation in r-space that the core polarization effects account for the quenching. Whereas in ref. 2 only the one-bubble polarization has been taken into account, it is important to include full correlations of the core such as of RPA-type.

The polarization effect can be renormalized into effective operators through the formalism of Feshbach[3]. Let us define the P-space as the one composed only of the 1-hole states $|i\rangle$ ($i,j,\ldots$ = $\nu 3p_{1/2}^{-1}$, $\nu 2f_{5/2}^{-1}$, etc.) and the Q-space the one of the 1-hole, 1-phonon states $|i,\mu\rangle$ (μ is the phonon of ^{208}Pb core). We omit the more complicated component of the wave function. Then the matrix element of the one-particle operator M is given by the one within the P-space as

$$\langle\Psi_j|M|\Psi_i\rangle = \langle P\Psi_j|\{P+PHQG(E_j)\}M\{P+G(E_i)QHP\}|P\Psi_i\rangle \qquad (1)$$

where E_i is the eigen-energy corresponding to the full wave function $|\Psi_i\rangle$ which has the main component $|i\rangle$:

$$H|\Psi_i\rangle = E_i|\Psi_i\rangle \qquad |\Psi_i\rangle = C_i|i\rangle + \ldots \quad (C_i \sim 1) \qquad (2)$$

(2)

G is the Q-space propagator: $G(E) = (E-QHQ)^{-1}$.

Neglecting the Pauli principle between the hole and the phonon, we obtain

$$\begin{aligned}\langle\Psi_j|M|\Psi_i\rangle/C_iC_j &= \langle j|M|i\rangle + \sum_\mu \{\langle j|V|i,\mu\rangle(E_j-\varepsilon_i-\omega_\mu)^{-1}\\ &\langle\mu|M|o\rangle + \langle o|M|\mu\rangle(E_i-\varepsilon_j+\omega_\mu)^{-1}\langle j,\mu|V|i\rangle\}\\ &+ \sum_{\mu\nu}\sum_{k\ell}\langle j|V|k,\mu\rangle\,(E_j-\varepsilon_k-\omega_\mu)^{-1}\langle k,\mu|M|\ell,\nu\rangle\\ &\times (E_i-\varepsilon_\ell-\omega_\nu)^{-1}\,\langle\ell,\nu|V|i\rangle\end{aligned} \qquad (3)$$

where ε_j, ω_μ are the single-particle and one-phonon energy, respectively. Each term of (3) is represented in fig. 1.

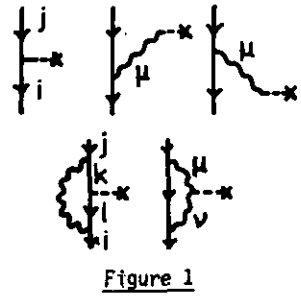

Figure 1

The amplitude C_i is given in this approximation by

$$C_i = \{1 + \sum_{k,\mu} |\langle i|V|k,\mu\rangle|^2/(E_i-\varepsilon_k-\omega_\mu)^2\}^{-1/2} \qquad (4)$$

In the actual calculation we have neglected the last term of (3) and also put $E_i = \varepsilon_i$ and $C_i = 1$. In this approximation, the effective operator coincides with the one derived from the Green's function method[4].

The RPA phonon in ^{208}Pb has been calculated using the Woods-Saxon single particle wave functions up to 4 $\hbar\omega$ excitations. For the interaction V we have used the delta+π+ρ force of ref. 5. The results are shown in fig. 2 where the magnetization current densities to the $5/2^-$ (0.571 MeV) state of ^{207}Pb are given. The solid line shows the calculation including all of the phonon excitation in ^{208}Pb. The broken line gives a corresponding single particle transition density. The quenching due to the polarization is about 15 % for M3 transition, whereas it is negligible in the inner part of E2 transitions although there is a sizable effect at the surface.

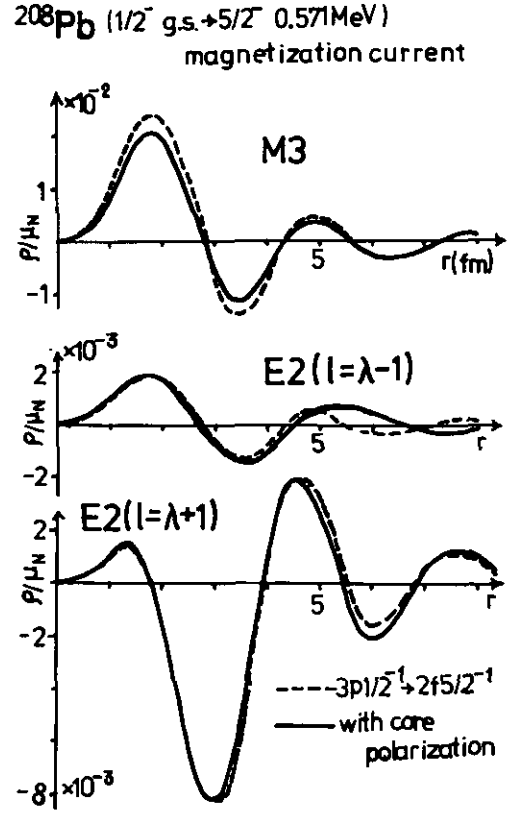

Figure 2

The calculation has been done also for the elastic (M1) scattering which measures the magnetization distribution of ^{207}Pb. Again the 15 % quenching was obtained which is much smaller than ref. 2.

One of the main differences from ref. 2 is the truncation of model space. (Within the 2$\hbar\omega$ calculation, the quenching was about 10 %.) It is desirable to repeat the calculation within a continuum RPA formulation. Also the reduction of C_i (see eq. (4)) should be included. On the other hand, the calculation of ref. 2 seems to overestimate the

polarization effect. This is seen in the second term of eq. (3): If the correlation is repulsive, the RPA value of $\langle\mu|M|o\rangle$ is reduced and also the energy denominator $E_j-\varepsilon_i-\omega_\mu$ becomes more negative than the one-bubble calculation. For the attractive correlation where V is negative, the RPA value of $\langle\mu|M|o\rangle$ is enhanced and acts against the quenching. The above discussion is dependent on the form of V in the q-space. Hamamoto et al.[2] used the delta interaction which has no momentum-transfer dependence. Within the present approximation of (3), however, the use of rather weakly-repulsive interaction ($g_0'\sim g_0 \sim 0.4$) without π and ρ gives only the same order of quenching ($\sim$ 15 %) for the transition densities.

References

1) C.N. Papanicolas, Ph.D. Thesis, MIT (1979); C.N. Papanicolas et al., Phys.Rev.Lett. 45 (1980) 106.

2) I. Hamamoto, J. Lichtenstadt and G.F. Bertsch, Phys. Lett. 96B (1980) 249; Phys.Lett. 93B (1980) 213.

3) H. Feshbach, Ann.Phys. 5 (1958) 357.

4) J. Speth, E. Werner and W. Wild, Phys.Rep. 33C (1977) 127.

5) J. Speth, V. Klemt, J. Wambach and G.E. Brown, Nucl. Phys. A343 (1980) 382.

3.2. Isoscalar Magnetic Dipole States in ^{208}Pb and the Spin Stability of the ph-Interaction

A.D. Jackson[+], *J. Wambach*[+*], *J. Speth*

In symmetric nuclear matter the Fermi liquid parameter of the ladder summation (G-matrix) of the Reid potential guarantees stability of the ground state with respect to spin excitations[1]. The Born approximation to the tensor parts of G based on the long range parts of the one-boson-exchange model[2]

$$V_T(\vec{k}) = -\frac{4\pi}{3}\left[\frac{f_\pi^2}{m_\pi^2}\frac{k^2}{k^2+m_\pi^2} - \frac{f_\rho^2}{m_\rho^2}\frac{k^2}{k^2+m_\rho^2}\right] S_{12}\,\vec{\tau}_1\vec{\tau}_2 \qquad (1)$$

gives almost the same Landau parameters as G itself (table 1). For Yukawa type interactions like V_T they are analytic expressions and easily calculated

$$H'_\ell = N_0(2\ell+1)\left[\frac{f_\pi^2}{m_\pi^2}Q_\ell(1+\frac{m_\pi^2}{2k_F^2}) - \frac{f_\rho^2}{m_\rho^2}Q_\ell(1+\frac{m_\rho^2}{2k_F^2})\right] \qquad (2a)$$

$$H_\ell = -3H'_\ell \qquad (2b)$$

The conclusion is that the model interaction (eq. (1)) is stable in the infinite system. For the 0^- T=0 state in ^{16}O and the low-lying 1^+ T=0 state in ^{208}Pb an instability develops as a function of the tensor force strength which in the above model is given by the value of the ρ-nucleon coupling constant f_ρ. This instability can be understood from the different propagation of spin-sound in infinite and finite systems due to shell structure. Consider ^{208}Pb for example. It is a non spin-saturated nucleus and consequently has a low energy spin-flip state from the ph-excitation of the spin-orbit partners. Via the tensor force this state mixes with $[\sigma Y_2]^{1^+}$-coherent $2\hbar\omega$ states (table 2) which are observed in calculations without tensor forces[3]. An RPA calculation including V_T shows strong sensitivity of the excitation energy of the lowest isoscalar state on the strength in the tensor channel, which in our picture transforms to the value of the ρ-nucleon coupling constant (Table 3). The enhancement of the $[\sigma Y_2]$-type amplitudes in the wave function of the lowest 1^+ state has interesting consequences for the response to external fields of both $\vec{\sigma}$ and $[\vec{\sigma}Y_2]^1$ character like the tensor component in an effective two-body potential for nucleon-nucleus scattering. In a DWBA-description of the scattering amplitude the response shows up in the knock-out exchange term with respect to V_T, which might cause sufficient interference between the L=0 and L=2 partial waves to be observed experimentally. Work to calculate the inelastic proton scattering cross section to the 1^+ T=0 final state as a function of the tensor force strength is in progress.

	H'_ℓ		H'_ℓ	
ℓ	Reid	model	Reid	model
0	.65	.63	-.26	-.21
1	.98	1.04	-.36	-.37
2	.83	.92	-.31	-.31
3	.62	.68	-.23	-.23
4	.43	.47	-.16	-.16

Table 1: Comparison of the tensor Landau parameters H_ℓ and H'_ℓ of a reaction matrix calculated from the Reid potential and the model interaction defined in eq. (1).

			G_o		$G_o + \hat{V}_\pi + \hat{V}_\rho$		$G_o + \hat{V}_\pi + \frac{1}{2}\hat{V}_\rho$		G_o	
ε_{ph}	$n\ell j$	$n'\ell'j'$	X_{mi}	Y_{mi}	X_{mi}	Y_{mi}	X_{mi}	Y_{mi}	X_{mi}	Y_{mi}
protons										
15.42	$2f\frac{5}{2}$	$2p\frac{3}{2}$	-.008	-.003	-.052	.037	-.166	.149	.076	-.018
16.01	$2g\frac{7}{2}$	$2d\frac{5}{2}$	.009	.003	.055	-.042	.182	-.166	.026	.003
16.40	$1h\frac{9}{2}$	$1j\frac{7}{2}$	-.032	-.012	-.108	.075	-.308	.277	.253	-.052
17.70	$1i\frac{11}{2}$	$1g\frac{9}{2}$	.030	.012	.107	-.083	.318	-.294	-.323	.056
21.08	$1j\frac{13}{2}$	$1h\frac{11}{2}$	-.023	-.011	-.082	.074	-.265	.254	.642	-.054
15.61	$2g\frac{9}{2}$	$1g\frac{7}{2}$	-.029	-.010	.063	-.033	.198	-.170	.023	-.005
5.57	$1h\frac{9}{2}$	$1h\frac{11}{2}$	-.916	.129	.765	-.216	.979	-.732	-.044	.028
neutrons										
11.35	$4p\frac{3}{2}$	$2f\frac{5}{2}$	.003	.001	-.069	.019	-.104	.073	-.003	.001
15.52	$3d\frac{5}{2}$	$1g\frac{7}{2}$	-.003	-.001	.054	-.021	.089	-.068	-.013	-.003
12.68	$3f\frac{5}{2}$	$3p\frac{3}{2}$	-.002	-.001	-.055	.025	-.139	.111	.013	-.004
14.09	$3f\frac{7}{2}$	$1h\frac{9}{2}$	.006	.002	-.069	.020	-.094	.04	-.022	.006
15.35	$2g\frac{7}{2}$	$2g\frac{5}{2}$	.005	.002	.061	-.039	.179	-.157	-.036	.008
15.12	$2h\frac{9}{2}$	$2f\frac{7}{2}$	-.004	-.001	-.059	.036	-.172	.149	-.010	-.001
17.84	$1i\frac{11}{2}$	$1g\frac{9}{2}$	.012	.005	.113	-.081	.306	-.280	-.141	.023
20.40	$1j\frac{13}{2}$	$1h\frac{11}{2}$	-.011	-.005	-.088	.068	-.253	.237	.233	-.023
22.41	$1k\frac{15}{2}$	$1i\frac{13}{2}$	.009	.005	.065	-.051	.199	-.188	-.416	.022
11.25	$3g\frac{7}{2}$	$2f\frac{5}{2}$	.004	.001	-.070	.035	-.217	.179	-.001	.001
13.96	$2g\frac{9}{2}$	$1g\frac{7}{2}$	.003	.001	.064	-.0046	.226	-.198	-.004	.001
14.09	$2h\frac{11}{2}$	$1h\frac{9}{2}$	.011	.003	-.085	.038	-.239	.194	-.001	.001
5.85	$1i\frac{11}{2}$	$1i\frac{13}{2}$	.417	-.049	-.651	.198	-.938	.716	.020	-.012
excitation energy			7.40 MeV		5.51 MeV		1.62 MeV		24.94 MeV	

Table 2: Largest components of the RPA wave functions of the lowest 1^+-state for different Fph. For a purely repulsive zero range force the wave function of the collective $2\hbar\omega$-state is also given.

f_ρ/f_ρ^3	E
1.0	5.5
.9	5.
.8	4.8
.7	4.2
.6	3.0
.5	1.4

Table 3: Excitation energy E of the low-lying isoscalar 1^+ state in ^{208}Pb as a function of the ρ-nucleon coupling strength. f_ρ^3 denotes the coupling constant of Höhler and Pietarinen[4] (strong-ρ).

References

1) S.O. Bäckman, O. Sjöberg, and A.D. Jackson, Nucl. Phys. A321 (1979) 10.

2) J. Speth, V. Klemt, J. Wambach, and G.E. Brown, Nucl. Phys. A343 (1980) 382.

3) J.P. Blaizot and L. Sips, Nucl. Phys. A337 (1980) 586.

4) G. Höhler and E. Pietarinen, Nucl. Phys. B95 (1975) 10.

+ SUNY at Stony Brook, Stony Brook, USA

* Supported in part by the Deutsche Forschungsgemeinschaft

3.3. Microscopic Structure of the Magnetic High Spin States in ^{208}Pb

S. Krewald, J. Speth

Recently, magnetic high spin states have been discovered in ^{208}Pb by inelastic electron scattering at backward angles[1]. These states are of considerable physical interest because as a consequence of the high multipolarity, the cross sections are peaked at a momentum transfer of approximately $qR \approx 2$ [fm^{-1}]. Therefore these states are an excellent test of the high momentum behaviour of our generalized spin- and isospin-dependent interaction. The number of 1p-1h configurations which can contribute to these states is severely restricted by the high multipolarity. Since the experimental excitation energies are close to the shell model ph-energies, the 12^- state at 6.43 MeV and the 14^- state at 6.74 MeV were tentatively interpreted as pure $\nu(1j_{15/2}, 1i_{13/2}^{-1})$ ph-excitations while the 12^- state at 7.06 MeV was assumed to be a pure $\pi(1i_{13/2}, 1h_{11/2}^{-1})$ configuration. This simple interpretation faces one problem, however, because the experimental cross section is only 50 % of the single ph-prediction[1]. In the following we will show that (i) the effects of the OPEP and ρ-exchange potential give rise to a very weak interaction in this momentum transfer region, and (ii) that the fragmentation of the single particle strength due to the phonon coupling is mainly responsible for the reduction of the cross section[2].

Model	E (MeV)	$\frac{B(M,L)}{B_1(M,L)}$	E (MeV)	$\frac{B(M,L)}{B_2(M,L)}$	E (MeV)	$\frac{B(M,L)}{B_3(M,L)}$
	$J^\pi = 12^-$		$J^\pi = 12^-$		$J^\pi = 14^-$	
1p-1h-*a*	6.49	1.00	7.18	1.00	6.49	1.00
1p-1h-*b*	6.77	0.44	7.86	0.91	7.14	0.82
1p-1h-*c*	6.60	1.18	7.52	0.94	6.68	0.96
2p-2h	6.55	0.60	7.37	0.54	6.65	0.45
expt	6.43		7.06		6.75	

Table 1: Excitation energies and B(M,L) values for the magnetic high spin states in ^{208}Pb obtained with the following models: 1p-1h-a = a single-particle, single-hole configuration; 1p-1h-b = random-phase approximation (RPA) with zero-range interaction; 1p-1h-c = RPA with finite-range interaction; 2p-2h = two-particle, two-hole calculation described in the text. The experimental data are from ref. 1. The B(M,L) values are divided by the shell model values (1p-1h-a)$B_1(M,L) = 0.57 \times 10^{23} \mu^2 \cdot fm^{22}$; $B_2(M,L) = 0.68 \times 10^{23} \mu^2 \cdot fm^{22}$; $B_3(M,L) = 1.33 \times 10^{27} \mu^2 \cdot fm^{26}$.

In table 1, the energies and B(M,L) values of the magnetic high spin states are shown. Using a zero-range force the B(M,L) values are reduced, but the excitation energies are pushed far above the shell model values. Only the one-pion and rho-exchange provide a mechanism to reduce the excitation energy.

It is well known that the coupling to the phonons may modify the single particle states appreciably. E.g., the $\nu j_{15/2}$ state comes at an excitation energy of 1.42 MeV relative to the ground state of ^{209}Pb which is only 1.2 MeV below the $(3^- \times \nu 2g_{9/2})_{15/2^-}$ configuration. Therefore a considerable mixing of these configurations has to be expected, which strongly reduces the single particle strength. This effect is especially large for the

so-called spin-orbit partners which are shifted into the next lower major shell and which possess therefore the "wrong" parity. All the dominant configurations of the high spin states are of that special type.

We evaluate the single particle strength by taking into account explicitly the coupling of phonons in ^{208}Pb to single particle states, thus obtaining quasiparticle states in the neighbouring nuclei. These quasiparticle and quasihole states are used to construct a core coupling random-phase wave function containing the most relevant 2p2h configurations. We mention, however, that we include in the present case also the interaction between the 2p2h configuration. Including as phonons only the 3^- state at 2.61 MeV and the 5^- state at 3.19 MeV, the single particle strength is reduced to Z=0.55 for the $\nu j_{15/2}\, i^{-1}_{13/2}$ configuration and to Z=0.55 for the $\pi i_{13/2}\, h^{-1}_{11/2}$ configuration. These single particle strengths were not further reduced when more phonons were taken into account. The results of the 2p2h calculations with a finite range interaction are given in table 1. The additional 2p2h components of the wave function strongly reduce the B(M,L) values and even produce a further decrease of the excitation energy. The mixing between the proton and neutron configurations in the case of the 12^- states is of the order of 0.03 (in the amplitudes).

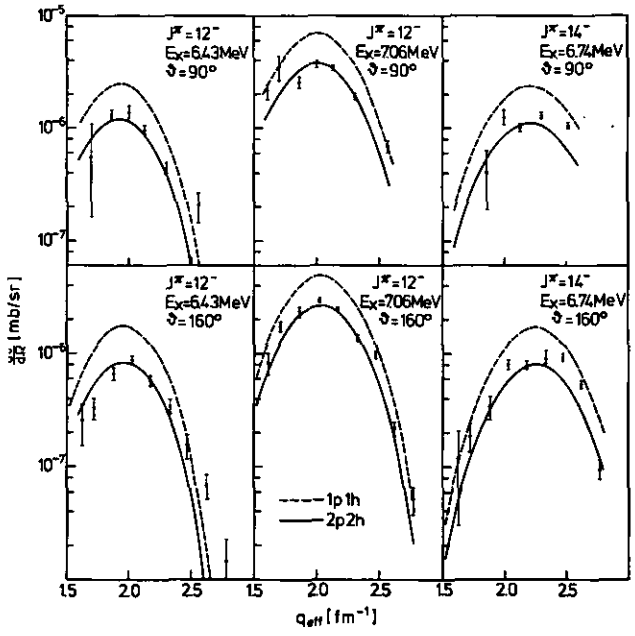

Fig. 1: The experimental cross sections for inelastic electron scattering of ref. 1 are compared with an RPA calculation (dashed line) and a 2p2h calculation described in the text (solid line). Both calculations were performed with a finite-range interaction including one-pion and ρ-meson exchange. The cross sections were obtained in DWBA.

In fig. 1, the inelastic electron scattering cross sections at $\theta = 90^0$ and $\theta = 160^0$ are shown for the three magnetic high spin states. The calculations were performed in Distorted Wave Born Approximation, using the code HEIMAG by J. Heisenberg. The inclusion of 2p2h configurations reduces the cross sections, as expected, so that both shapes and absolute magnitudes of the cross sections are in good agreement with the experimental data in the three cases considered. On a closer inspection, however, one finds that at high momentum transfer, the cross sections of the 12^- state at 6.43 MeV and the 14^- state at 6.75 MeV are underestimated. It is an open question, whether the cross sections are sensitive to exchange-current effects.

References

1) J. Lichtenstadt, J. Heisenberg, C.N. Papanicolas, C.P. Sarget, A.N. Courtemanche, and J.S. McCarthy, Phys. Rev. C20 (1979) 497, and Phys. Rev. Lett. 40 (1978) 1127.

2) S. Krewald and J. Speth, Phys. Rev. Lett. 45 (1980) 417.

3.4. On the Structure of the First $1/2^-$ State in ^{209}Bi

V. Klemt

In recent years much interest has been directed to the question of the single-particle strength of states in near magic even-odd nuclei. Even in the lead region, where one would expect fairly good quasi-particle states, often surprisingly high depletion is found, though almost never beyond 50 %. There is one exception however, the $1/2^-$ state in ^{209}Bi. A recent calculation by Li Chu-hsia and Klemt[1] shows a strength of 0.31 only for this state. Detailed inspection shows that almost all the strength is gone because of a coupling to a $1h_{9/2} \times 4^+$ state. One may distrust this result because of the perturbative treatment of the coupling to one phonon, but a theory worked out by Klemt[2] gives, in the limit of second order perturbation theory, the following formulas for the single-particle strengths and the perturbed energies (which is correct even if $Z_1 \ll 1$; see fig. 1):

$$1-Z_1 = \frac{Z_1}{2} \sum_{234} |V_{1234}|^2 \frac{n_2(1-n_3)(1-n_4)+(1-n_2)n_3n_4}{(E_1+E_2-E_3-E_4)^2}$$

$$E_1 = \varepsilon_1 + \frac{1}{2} \sum_{234} |V_{1234}|^2 \frac{n_2(1-n_3)(1-n_4)+(1-n_2)n_3n_4}{E_1+E_2-E_3-E_4}$$

Here the ε's are the Hartree-Fock energies and the n's are the quasi-particle occupation numbers (0 and 1). If we assume that in the unperturbed case we have $\varepsilon_1 = \varepsilon_3+\varepsilon_4-\varepsilon_2+\delta$ with δ small compared to all other energy differences and if we assume, for simplicity, that the states 2, 3 and 4 are shifted only negligibly (which will turn out to be justified later), then the formulas reduce, if one configuration is considered only and in obvious notation ($V = V_{1234}$, $Z = Z_1$):

$$1 - Z = \frac{Z}{2} \frac{V^2}{(\Delta+\delta)^2} \text{ and } \Delta = \frac{1}{2} \left(-\delta \pm \sqrt{\delta^2+2V^2}\right)$$

with $\Delta = E_1-\varepsilon_1$.

In the limiting case of $V \ll \delta$ this reduces to:

$$\Delta = \begin{cases} \frac{V^2}{2\delta} \ll 1 \\ -\delta - \frac{V^2}{2\delta} \approx -\delta \end{cases} \quad \text{and} \quad Z = \begin{cases} 1 - \frac{V^2}{2\delta^2} \approx 1 \\ \frac{V^2}{2\delta^2} \ll 1 \end{cases}$$

Since δ is the smallest occurring energy difference these expressions justify the above mentioned assumption (to proceed correctly one would have to solve four systems of equations simultaneously). One finds a big shift of about $-\delta$ (big compared to V) for one of the two solutions and a respective very small single particle strength. That means of course that the collective (two-particle one-hole state) is by an amount δ below the (almost) single particle state. In the work of ref. 1 the experimental single-particle energies were inserted in the denominator. As is shown here nothing is going wrong when it turns out finally that the "single-particle state" is in reality collective. The formulas in ref. 1 remain correct (at least for the single-particle strengths) even in the case of very small energy denominators.

The $1/2^-$ state in ^{209}Bi at 3.63 MeV is the only example in the lead region where a collective state lies below the single-particle one with the same quantum numbers. The single-particle $3p_{1/2}$ is found in a Woods-Saxon calculation using a harmonic oscillator basis at about 5 MeV, that means it is already in the continuum.

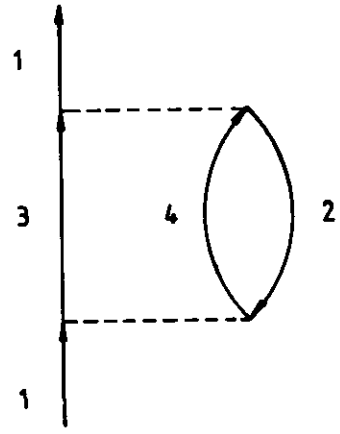

Figure 1

References

1) Li Chu-hsia, V. Klemt, to be published.
2) V. Klemt, to be published.

3.5. Continuum Fourier Bessel RPA

R. de Haro, Jr., S. Krewald, J. Speth

The Fourier Bessel RPA[1,2] is extended to embody the continuum in order to obtain the decay widths of giant resonant states.

Analogously to the discretized Fourier Bessel RPA[1], the basic idea is to express the RPA equations in terms of the transition densities $\rho(r)$ and $\sigma(r)$ and expand these in Fourier Bessel series

$$\rho(r) = \sum_{\mu} A_{\mu} j_J(q_{\mu} r)$$

and

$$\sigma(r) = \sum_{\nu} B_{\nu} j_J(q_{\nu} r)$$

making then use of the fast convergence properties of this series.

Setting the amplitudes in terms of the transition densities we can write down, using once more the definition of $\rho(r)$ and $\sigma(r)$, a dispersion relation for these quantities of the form:

$$\rho_{\tau}(r) = \int dt\, t^2 \sum_{\tau'} \left[G_{\tau}(r,t) h_{\tau\tau'}(t) \rho_{\tau'}(t) + H_{\tau}(r,t)\, h'_{\tau\tau'}(t) \sigma_{\tau'}(t) \right] + Q_{\tau}(r, \varepsilon_h + E)$$

and

$$\sigma_{\tau}(r) = \int dt\, t^2 \sum_{\tau'} \left[H_{\tau}(r,t) h_{\tau\tau'}(t) \rho_{\tau'}(t) + U_{\tau}(r,t) h'_{\tau\tau'}(t) \sigma_{\tau'}(t) \right] + W_{\tau}(r, \varepsilon_h + E)$$

where $h_{\tau\tau}$ and $h'_{\tau\tau}$, stand for linear combinations of the force parameters and G_{τ}, H_{τ} and U_{τ} are propagators connecting coordinate points r and t.

The indices τ and τ' run over proton and neutron and

$$Q_{\tau}(r, \varepsilon_h + E) = \sum_{ph} \frac{(-)^{k_p}}{\sqrt{4\pi}} \begin{pmatrix} J_p & J_n & J \\ \frac{1}{2} & -\frac{1}{2} & 0 \end{pmatrix} R_p(r, \varepsilon_h + E) R_n(r) D_{ph}(r, \varepsilon_h + E)$$

$$W_{\tau}(r, \varepsilon_h + E) = \sum_{ph} \frac{(-)^{\ell_p + 1 + k_p + k_n}}{\sqrt{4\pi}} \sqrt{k_p k_n} \begin{pmatrix} J_p & J_n & J \\ \frac{1}{2} & \frac{1}{2} & -1 \end{pmatrix} R_p(r, \varepsilon_h + E) R_n(r) D_{ph}(r, \varepsilon_h + E)$$

with $$k = j + \frac{1}{2}$$

Expanding r-dependent quantities we can set this system only in terms of the coefficients of the Fourier Bessel expansion, in the form:

$$A^{\tau}_{\mu} = \sum_{\nu\eta\tau'} \left[C^{\tau}_{\mu\nu} T^{\tau\tau'}_{\nu\eta} A^{\tau'}_{\eta} + H^{\tau}_{\mu\nu} S^{\tau\tau'}_{\nu\eta} B^{\tau'}_{\eta} \right] - Q^{\tau}_{\mu}$$

$$B^{\tau}_{\mu} = \sum_{\nu\eta\tau'} \left[H^{\tau}_{\mu\nu} T^{\tau\tau'}_{\nu\eta} A^{\tau'}_{\eta} + U^{\tau}_{\mu\nu} S^{\tau\tau'}_{\nu\eta} B^{\tau'}_{\eta} \right] - W^{\tau}_{\mu}$$

where

$$T^{\tau\tau'}_{\nu\eta} = \int r^2 h_{\tau\tau'} J_{\tau}(q_{\nu} r) J_{\tau}(q_{\eta} r)$$

and

$$S^{\tau\tau'}_{\nu\eta} = \int r^2 h'_{\tau\tau'} J_{\tau}(q_{\nu} r) J_{\tau}(q_{\eta} r)$$

The inhomogeneous system of equations above are our RPA-equations, expressed only in terms of the coefficients of the Fourier Bessel expansion of the transition densities which, in Born approximation, are the form factors.

That way we have a formulation for the RPA equations in terms of observables, numerically very fast to be solved because of the convergence properties of the Fourier Bessel expansion. A further advantage is that the dimension of the matrix that we must diagonalize is only proportional to the number of expansion terms taken in the Fourier Bessel expansion, avoiding the drawback of the usual methods of handling with huge matrices.

Using a force adjusted by Speth and Rinker[3] to the lead region, we were able to reproduce quite fairly the positions and transition rates of the low-lying states in ^{16}O and ^{208}Pb, as well as the transition densities for these bound levels.

Our main interest was directed to obtain the giant resonances, what we did for the nuclei quoted above.

In all the cases we got a good agreement of our results with the experimentally found values of peak energy and exhausted fraction of the energy weighted sum rules for the experimentally well known dipole and quadrupole electric giant resonances (cf. table).

For the high-lying (isovector) octupole electric giant resonance in ^{208}Pb we get a very wide peak in the 160 $A^{-1/3}$ MeV region showing that the strength is strongly dispersed.

The same trend is seen for the higher lying giant resonance states where no concentrated strength could be found (cf. figure), especially in the higher energy range where former predictions[4] expected a large amount of it corresponding to the 2 and 3 $\hbar\omega$-excitations giant resonances.

The most probable reason for this overestimation of former results compared to ours must be in the treatment of the continuum states which, in our case, are fully taken into account, permitting a fraction of formerly predicted strength to be carried to higher energy regions and bringing to the collective states the real decay widths of the single particle states, which are considerably large.

Remembering that, additionally to this fact comes that we are working in the frame of a one-particle one-hole RPA and when considering the effects of higher correlations, an additional (damping) width will be brought to our results by fragmentation of these states, it turns out that experimental observation of these higher states should not be possible.

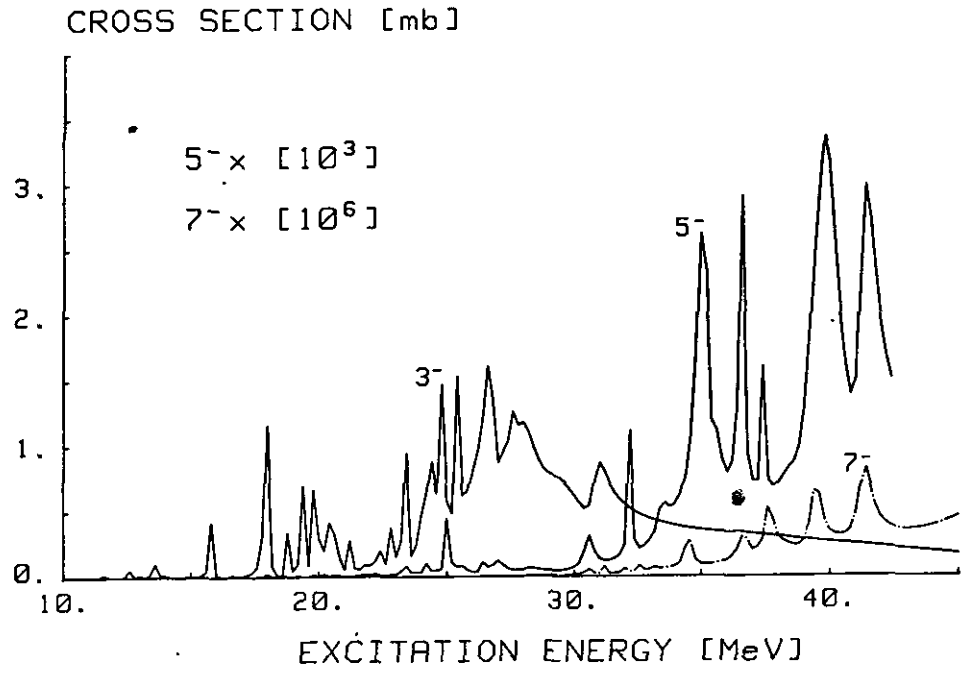

Figure 1

L^{π}	^{208}Pb-EWSR	^{16}O-EWSR
1^-	102.5	108.3
2^+	69.1	77.4
3^-	89.7	30.7
4^+	14.4	
5^-	62.8	
7^-	33.0	

Table 1: In all cases, the EWSR is given as percent ratio:directly calculated to model independent EWSR.

References

1) J. Heisenberg, S. Krewald, Jülich Report (1978).
2) R. de Haro, S. Krewald, J. Speth, Jülich Report (1979).
3) G.A. Rinker, J. Speth, Nucl. Phys. A306 (1978) 360.
4) R.A. Broglia et al., Phys. Lett. 89B (1979) 22.

3.6. A Proposal for the Approximate Treatment of the Continuum of a Single Particle Basis

V. Klemt

A very common problem in nuclear-structure calculations is the choice of the appropriate single-particle basis and, specifically, the question how to handle the continuum. In this note we assume that we have already found the best single-particle potential of, say, Woods-Saxon type. A widely used method is to diagonalize the potential within a basis of harmonic-oscillator wave functions. For bound states this is equivalent to an expansion of the eigenstate into oscillator functions:

$$\zeta^{WS}_{n\ell j}(r) = \sum_{m=1}^{M} a_m(n\ell j) R^{osc}_{m\ell}(r)$$

It turns out that with a proper choice of the oscillator constant the bound states in the lead region can be represented reasonably well by an expansion with

$$M = \frac{1}{2}(N-\ell+1) \text{ and } N = 15 ,$$

which means that the s-states have to be expanded into eight oscillators and the higher-ℓ states into correspondingly fewer. Furthermore, there is some indication that the first "unbound" states for each "partial wave" ℓj are in most cases fairly good approximations to the first resonant state.

But since its energy is not very well determined (it varies with M) one would like to have a simple and clear prescription how to describe the resonance. Now the total cross section for a certain partial wave ℓj (what means that only one partial wave contributes to the resonance) is given by

$$\sigma^{(\ell j)}_{tot} = \frac{4\pi}{k^2}(2\ell+1)\sin^2\delta_{\ell j}$$

and the phase shift $\delta_{\ell j}$ is given by the well-known integral formula

$$\sin\delta_{\ell j} = -\frac{2m}{\hbar^2}\int_0^\infty \hat{j}_\ell(kr)V(r)Y_{\ell j}(r)r^2dr ,$$

where $Y_{\ell j}(r)$ is the solution of the radial Schrödinger equation with the asymptotic form

$$Y_{\ell j}(r) \xrightarrow[r\to\infty]{} \frac{1}{r}\sin\left(kr - \frac{\pi\ell}{2} + \delta_{\ell j}\right)$$

If we assume that the resonance wave function can be expanded into our "unbound" radial eigensolutions

$$Y_{\ell j}(r) = \sum_{n=n_0}^{M} c_n(\ell j)\zeta_{n\ell j}(r)$$

then finding the wave function $Y_{\ell j}(r)$ that maximizes the cross section at a given energy is equivalent to solving the eigenvalue problem

$$\sum_{n'}\left[\int_0^\infty j_\ell(kr)V(r)\zeta_{n\ell j}(r)r^2dr \int_0^\infty j_\ell(kr)V(r)\zeta_{n'\ell j}(r)r^2dr - \omega\,\delta_{nn'}\right]c_{n'} = 0$$

This is a Hermitean eigenvalue problem with a matrix of the special type

$$A_{ij} = a_i a_j$$

One sees immediately that this is a matrix of rank one with one solution

$$c_i^{(1)} = a_i/\sqrt{\sum_i a_i^2} \text{ and eigenvalue } \omega^{(1)} = \sum_i a_i^2 ,$$

while all other eigenvalues vanish.

Varying the input energy or, correspondingly, the input momentum k one will find a maximum $\omega^{(1)}_{max}$ with a respective eigenvector $c_i^{(1,max)}$.

The latter may be interpreted as the first resonant state within the approximation of the oscillator space. The other eigenvectors are, by construction (Hermitean eigenvalue problem) orthogonal to all the bound ones and also to the resonance, and within this remaining space further resonances can be looked for with the same procedure.

3.7. RPA-Calculations for ^{132}Sn with Effective Forces Including Meson Exchange Potentials

C. Conci, V. Klemt

We have performed RPA-calculations for the doubly-magic nucleus $^{132}_{50}Sn_{82}$, using a generalized particle-hole interaction which includes in addition to the zero-range terms of the Landau-Migdal theory also explicitly the contributions of the one-pion and the one-rho exchange potentials[1].

In this way we have calculated excitation energies, transition probabilities from excited states to the ground state in the nucleus ^{132}Sn, and electric and magnetic moments and transitions in the neighbouring odd-mass nuclei $^{131,133}Sn$, ^{131}In and ^{133}Sb [2].

To perform our calculations the following values for Migdal's force parameters have been used:

$f_{in} = 0.2 \quad f'_{in} = 1.5 \quad g_{in} = 0.553 \quad g'_{in} = 0.697$
$f_{ex} = -2.45 \quad f'_{ex} = 1.5 \quad g_{ex} = 0.553 \quad g'_{ex} = 0.697$

The units used here are the same as in ref. 2. We could reproduce the experimental level scheme of ^{132}Sn [3] and the results of previous RPA-calculations performing using only a zero-range force[4]. To this purpose we have modified the values of the interpolation radii from $R_{nn} = 6.54$, $R_{pp} = 6.60$ to $R_{nn} = R_{pp} = 6.85$ (in fm). The increase in the values of R_{nn} and R_{pp} is justified by the fact that the one-pion and one-rho exchange potentials are attractive and therefore cause a lowering of the energy levels.

The results for the low-lying level scheme of ^{132}Sn are shown in fig. 1.

Taking into account the one-pion and one-rho exchange potential contributions, we can analyze their influence on the magnetic moments and transition probabilities, i.e. on the unnatural parity states, in the neighbouring odd-mass nuclei. As we can see in table 1, almost no effect of the attractive one-pion and one-rho exchange parts on the B(Mℓ)-values can be observed.

J^π	main config.	E_{ph}	δ		δ+π+ρ	
			E	B(Mℓ)	E	B(Mℓ)
1^+	$\pi g_{7/2}\text{-}\pi g_{9/2}^{-1}$	4.52	6.22	0.07	5.32	0.05
	$\nu h_{9/2}\text{-}\nu h_{11/2}^{-1}$	6.88	8.77	0.07	7.99	0.10
2^-	$\pi h_{11/2}\text{-}\pi g_{9/2}^{-1}$	7.05	7.46	29.6	6.74	11.0
	$\pi d_{5/2}\text{-}\pi p_{1/2}^{-1}$	7.29	7.70	11.8	7.68	27.4
3^+	$\pi h_{11/2}\text{-}\pi f_{7/2}^{-1}$	14.04	14.44	0.14	14.24	0.14
	$\pi i_{13/2}\text{-}\pi g_{9/2}^{-1}$	16.00	16.59	0.47	16.49	0.62
4^-	$\pi h_{11/2}\text{-}\pi g_{9/2}^{-1}$	7.05	7.42	0.16	7.33	0.18
	$\pi d_{5/2}\text{-}\pi p_{3/2}^{-1}$	8.44	9.23	0.05	9.00	0.04

Table 1: Some unnatural parity states in ^{132}Sn. (The energies are given in MeV and the B(Mℓ)-values in units of $(n\cdot m)^2$ $fm^{2(\ell-1)}$ multiplied by $10^{2\ell}$.)

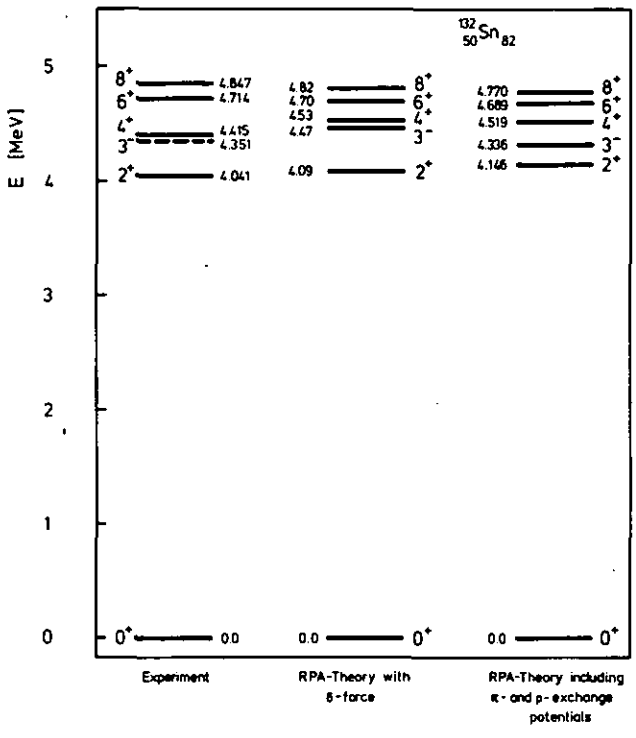

Fig. 1: Low-lying level scheme of ^{132}Sn.

References

1) J. Speth, V. Klemt, J. Wambach and G.E. Brown, Nucl. Phys. A343 (1980) 382.

2) P. Ring and J. Speth, Nucl. Phys. A235 (1974) 315.

3) T. Björnstad et al., Phys. Lett. 91B (1980) 35.

4) K. Kawade, G. Battistuzzi, H. Lawin, K. Sistemich and J. Speth, JÜl-Spez-72, p. 65.

3.8. Neutron and Proton Matrix Elements and Inelastic Hadron Scattering

V.R. Brown[+], *A.M. Bernstein*[++], *V.A. Madsen*[+++]

In the past several years measurements of neutron as well as proton transition densities and multipole matrix elements have received both renewed and increased attention. The neutron and proton multipole matrix elements are

$$M_{n(p)} = \int \rho_{fi}^{n(p)}(r)\, r^{\lambda+2}\, dr \,, \qquad (1)$$

where $\rho_{fi}^{n(p)}$ are the neutron or proton transition densities which depend on nuclear dynamics. In γ decay and in longitudinal electron scattering one obtains information about ρ_{fi}^{p}, whereas (h,h') reactions are sensitive to both the neutrons and the protons, particularly in the surface region. In principle one needs two experiments to determine both quantities.

In the usual collective model one assumes that neutrons and protons move in phase with the same amplitude so that $\rho_{fi}^{n}/\rho_{fi}^{p} = M_n/M_p = N/Z$. This implies that $(\beta R)_{h,h'} = (\beta R)_{EM}$, i.e. one should obtain the same value from the electromagnetic (EM) transition rate as from (h,h') for all hadrons. Empirically this is roughly true, and consequently it is often assumed to be a consistency check between the results of different (h,h') and EM experiments. However, one intuitively expects deviations from the collective model based on nuclear structure effects. Explicit model calculations[1] have predicted systematic differences between single-closed-shell (SCS) neutron and proton valence nuclei which have now been seen experimentally[2-4] (see fig. 1).

As the external field is varied by using different probes, the two matrix elements M_n and M_p can be determined experimentally. For example, from the EM transition rate one can obtain M_p directly. For a hadron probe one obtains some combination of M_n and M_p which depends on the isospin character of the probe. Combining the two, denoted here by h/EM, gives both M_n and M_p. As only two probes are required, additional measurements can be used as a consistency check.

In practice the collective model is often employed in analyzing the data and the parameter βR is obtained from fitting the magnitude of the cross section. The matrix elements $M \sim \beta R$ can then be obtained. This procedure appears model dependent; however, the differences between models show up primarily in the behaviour of $\rho_{fi}(r)$ for small values of r. In (h,h') reactions the hadron wave is attenuated, simulating the r^{λ} surface weighting (see eq. (1)) in EM transitions, so that these reactions are not generally sensitive to the interior. (This is particularly true for collective states, where the transition density is surface peaked.) Depending on the energy and the projectile the hadrons become more penetrating, and these assumptions[5] become less valid. On the other hand, the combination of two hadronically similar probes, which differ only in isospin, such as π^-/π^+ and p/n relaxes the need for such assumptions about surface weighting.

The results for M_n/M_p obtained from different external fields are presented in fig. 1. Within the limits of our assumptions M_n/M_p should be independent of external field, whereas the βR's used to obtain this ratio are external field dependent. Collective-model predictions (N/Z) are presented along with the results of our schematic model[1], which includes core polarization by virtual excitation of isoscalar and isovector giant-quadrupole resonances. It can be seen that for SCS neutron-valence nuclei $M_n/M_p > N/Z$ while for SCS proton-valence nuclei $M_n/M_p < N/Z$, as predicted. These effects are in the direction that one expects based on shell effects but are reduced almost back to the collective-model results because the valence particles mainly

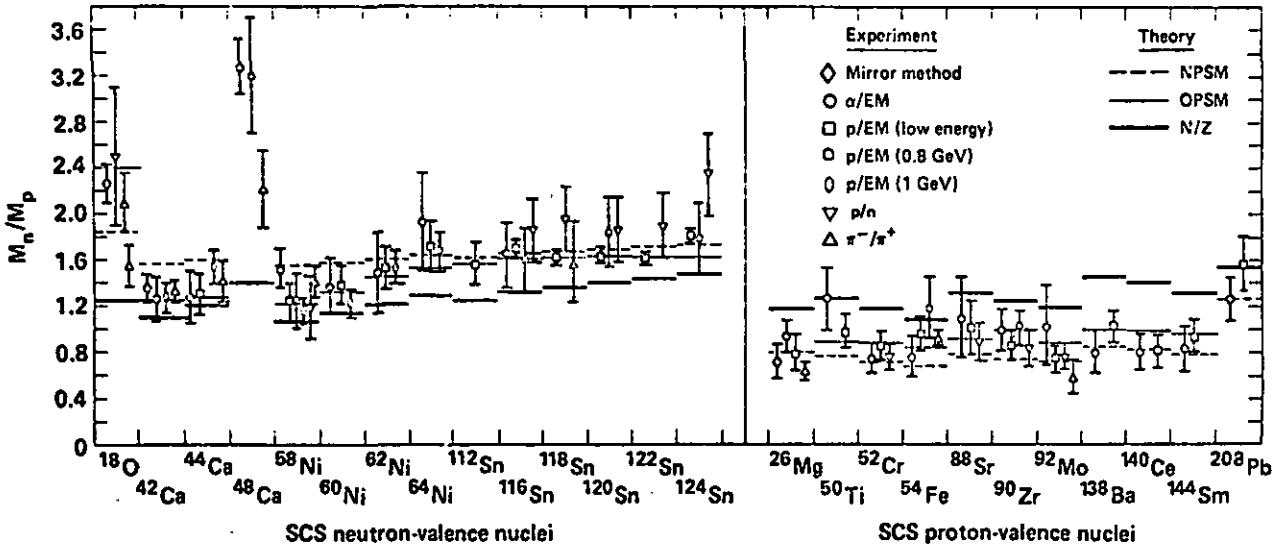

Fig. 1: M_n/M_p for single-closed-shell (SCS) nuclei, ^{26}Mg, ^{48}Ca and ^{208}Pb. The mirror EM transition rate data are from ref. 4. The α/EM data are primarily from ref. 3. The p/EM (low energy) data are primarily from ref. 2. The p/EM (0.8 GeV) data are from LAMPF. The p/EM (1 GeV) data are from Saclay. The p/n (low energy) data are from Ohio University. The π^-/π^+ data are from LAMPF + SIN. The heavy solid lines are N/Z which is the simple collective-model result. The results of the no-parameter schematic model (NPSM) are shown with dashed lines and the one-parameter schematic model (OPSM) with solid lines from ref. 1.

polarize core particles of the opposite type.

The question of the relative amount of neutron and proton strengths in transition densities is currently of considerable interest. The consistency of the M_n/M_p values presented here indicates that the combined model and experimental errors represented by this data set are of the order of 15 %; more accurate experimental determination of $\rho_{fi}^{n(p)}(r)$ is, of course, desirable.

References

1) V.R. Brown and V.A. Madsen, Phys. Rev. C11 (1975) 1298, and Phys. Rev. C17 (1978) 1943.

2) V.A. Madsen, V.R. Brown, and J.D. Anderson, Phys. Rev. C12 (1975) 1205.

3) A.M. Bernstein, V.R. Brown, and V.A. Madsen, Phys. Lett. 71B (1977) 48.

4) A.M. Bernstein, V.R. Brown, and V.A. Madsen, Phys. Rev. Lett. 42 (1979) 425.

5) F. Osterfeld, J. Wambach, H. Lenske, and J. Speth, Nucl. Phys. A318 (1979) 45.

+ Lawrence Livermore Lab., Livermore, USA

++ MIT, Cambridge, USA

+++ Univ. of Oregon, Corvallis, USA

3.9. On the Problem of Odd-Even Staggering of Nuclear Radii

D. Zawischa[+], *J. Speth*

When a neutron is added to an even-even nucleus, the change of the rms charge radius is generally less than half the change due to addition of two neutrons. This staggering phenomenon has been explained by Reehal and Sorensen[1] to be due to the blocking of RPA ground state correlations by the odd neutron. This is interpreted as a reduction of the amplitude of the zero-point quadrupole vibrations and a consequent reduction of the rms charge radius.

In the course of a microscopic investigation of vibrational states of deformed rare earth nuclei[2], isotope shifts of charge radii have been calculated using linear response theory[3] and a density dependent "Migdal type" interaction. The magnitude of the shifts is well reproduced, as well as the general trends that they decrease with increasing mass number, which holds for each group of isotopes and also for the whole region of deformed nuclei. The odd-even staggering, however, has not been obtained, even worse: the calculations yielded the inverted effect.

Variation of the force parameters within wide limits could not essentially change these results. It was suspected that the blocking of RPA-g.s. correlations might get lost in the course of the approximations of linear response theory, so we calculated this effect separately. This was done not along the lines of ref. 1, where incompressible flow is assumed in order to correlate $\delta\langle Q^2\rangle$ with $\delta\langle r^2\rangle$, instead $\delta\langle r^2\rangle$ was calculated directly from the changes of the Green functions.

The numerical results are quite disappointing; The order of magnitude of the RPA-blocking effect's contribution to $\delta\langle r^2\rangle$ is $10^{-3}fm^2$ in the rare earths, far too small to lift the discrepancy between theory and experiment.

It is fairly easy to understand how the reverse effect comes about in the calculations: On addition of a neutron, the shift in the Fermi energy just produces the average change of the charge radius. The blocking of one neutron level reduces the diffuseness of the neutron Fermi edge due to pairing. Thereby the population of the levels below the Fermi energy is increased for odd nuclei (relative to the average of their even neighbours). Proton states with the same quantum numbers are above the Fermi energy, and have large interaction matrix elements with the neutron states due to complete overlap of the wave functions. The short range attraction therefore favours an increased occupation also of these proton levels at the expense of lower ones with smaller rms charge radii, and thus the overall charge radius is increased.

In order to explain staggering, we must therefore look for physical effects which invalidate the above reasoning, which reduce the large interaction matrix elements between proton and neutron states with like quantum numbers. Presumably a simple density dependent residual interaction can never produce the desired effect; we may have to retain essential features of the nucleon-nucleon interaction, as the strong repulsion at short distances which leads to strong negative short range correlations.

Preliminary calculations with a schematic effective particle-hole force support the above arguments: We simulate the long range attraction by monopole and quadrupole forces, and the short range repulsion by a delta force. With this "multipole and delta" (MAD) interaction we obtain staggering with the right sign, but still too small: $2\delta\langle r^2\rangle_{N\to N+1}/\delta\langle r^2\rangle_{N\to N+2} = 0.95$ to 1.0 in the Gd region, depending on the force parameters. The correct magnitude could not be obtained, since the configuation space used[2] is too small, so that the wave functions are not flexible enough.

References

1) B.S. Reehal and R.A. Sorensen, Nucl. Phys. A161 (1971) 385.

2) D. Zawischa, J. Speth, and D. Pal, Nucl. Phys. A311 (1978) 445.

3) J. Meyer and J. Speth, Phys. Lett. 39B (1972) 330.

4) K. Heilig and A. Steudel, Atomic Data and Nuclear Data Tables 14 (1974) 613.

+ Inst. für Theor. Physik, Univ. Hannover

3.10. Higher Charge Exchange Resonances in Nuclei

H. Dermaxan, S. Krewald, F. Osterfeld, J. Speth

In the last year, new experimental information has been obtained on collective spin resonances in nuclei using high energetic protons in (p,n) reaction. The (p,n) reaction gives the possibility for studying the isovector resonances. At low energy (p,n) spectra the electric resonance like the well-known isobaric analog state (0^+ IAR), which is connected with the isospin operator $\vec{\tau}$ only, dominates the experimental cross sections. Above the 65 MeV the situation is changed, the spinflip transition like GTR, 1^+ will dominate then non-spinflip ones.

Both resonances can be described in the framework of the RPA theory as a superposition of proton-particle neutron hole states. In doubly closed shell nuclei such as ^{208}Pb the excitation energies and transition probabilities are obtained from the RPA equation. As we know from ref. 1, the spin-isospin dependent part of the p-h interaction is strongly repulsive for small momentum transfer, but as the momentum increases, the one-pion exchange cancels the repulsive components and above q = 1 fm^{-1} the interaction is weakly attractive. Therefore this p-h force can build collective magnetic states only, if the Fourier components of the wave functions are concentrated at low momentum transfer. We calculate the excitation energies and the ^{208}Pb(p,n) cross sections of the ΔL = 1 resonances (0^-,1^-,2^-), as has been observed in the experiment at the Indiana University[2]. With this calculation we can test the momentum dependence of the p-h force in the spin-isospin channel and want to know whether ΔL = 1 resonances exist with strengths comparable to the collective magnetic Gamow-Teller resonance 1^+.

In fig. 1 the momentum distributions (form factors) of 0^- (E_x = 26.61 MeV), 1^- (E_x = 26.35 MeV, spinflip transition) and 2^- (E_x = 22.63 MeV) in ^{208}Bi are shown. The excitation energies refer to the ground state of ^{208}Pb. The 0^- and 1^- resonances peak at a low momentum transfer (below 1 fm^{-1}), here the p-h force is strongly repulsive. Opposite to the 0^- and 1^- the form factor of the 2^- resonance peaks at a large momentum transfer (above 1 fm^{-1}), where the p-h force is very weak. The results in table 1 fulfil our expectation. The excitation energies of the 0^- and 1^- are strongly pushed up to higher energies, but the energies of the 2^- states are close to the unperturbed p-h energies.

The cross section at 5^0 from some resonances that may belong to experimentally observed peaks at (21.5±1.0) MeV[2] with E_p = 160 MeV is shown in the last column of table 1. The sum of the cross sections is 73.1 mb. Similar to the theoretical GTR (1^+) cross section in ^{208}Pb(p,n) the theoretical cross section of the ΔL = 1 resonance overestimates about a factor of two the experimental data. Oset and Rho suggest that the Lorenz-Lorentz effect might at least partially explain this reduction. Certainly more quantitative investigations in finite nuclei are desirable.

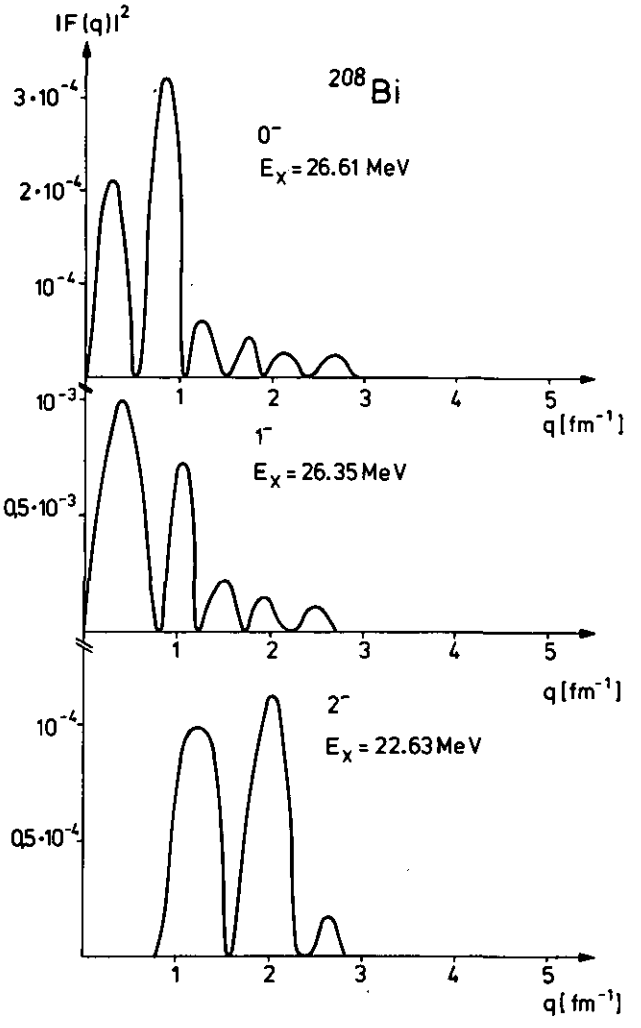

Figure 1

J^π	$E_{unperturbed}$ [MeV]	E_{RPA} [MeV]	ΔE [MeV]	$(d\sigma/d\Omega)\cdot(5^0)$ [mb/sr]
0^-	22.16	26.61	4.45	14.0
1^-	22.18	26.35	4.17	33.0
2^-	22.45	22.63	0.18	13.9
2^-	24.20	24.50	0.30	12.2
2^-	20.70	21.21	0.51	
2^-	28.04	28.76	0.72	

Table 1

References

1) J. Speth, V. Klemt, J. Wambach, G.E. Brown, Nucl. Phys. A343 (1980) 382.

2) D.J. Horen et al., Phys. Lett. 95B (1980) 27.

3.11. Nuclear Structure Effects Connected with Charge-Exchange Resonances

S. Krewald, F. Osterfeld, J. Speth, and G.E. Brown[+]

Using a highly energetic proton beam Goodman et al.[1] recently obtained detailed experimental results on the Gamow-Teller resonances (GTR) in many nuclei. We calulated the excitation energies and the (p,n) cross sections of the GTR as well as the isobaric analogue resonance (IAR) in ^{208}Pb using the generalized Landau-Migdal force of ref. 2. It turned out, however, that in a straightforward RPA calculation (using experimental single-particle energies) the energy of the GTR comes 2.7 MeV below the experimental value, whereas the IAS is nicely reproduced. As discussed in the following contribution we argue that one has to use the experimental single-particle energies only in the case of the IAR, whereas in the case of the GTR one should use a single-particle spectrum which corresponds to an effective mass of $m^*/m \sim 0.75$ (e.g. SK III).

Using the wave functions of the IAR and GTR we have calculated the (p,n) differential cross sections the results of which are shown in fig. 1. The effective

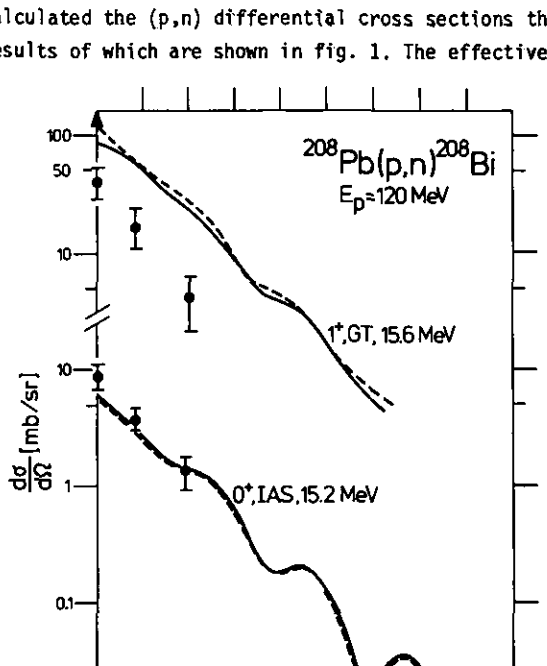

Fig. 1: Theoretical cross sections of the 0^+ (IAS) and 1^+ (GTR) of the ^{208}Pb(p,n)^{208}Bi reaction. The experimental results are taken from ref. 1. The dashed lines represent the results where the dynamical theory has been taken into account whereas the full lines follow from a conventional RPA calculation.

projectile target nucleon interaction and the optical model parameters are taken from ref. 3. Whereas the theoretical IAR cross section is in good agreement with the experimental one, our theoretical GTR cross section is about a factor of two too large. If we suppose that the coupling potentials $V_{\sigma\tau}$ and V_{τ} are known (which has to be checked independently) we find that similar to the results in electron scattering the theoretical spin-flip strength overestimates the experimental one appreciably.

References

1) C.D. Goodman et al., Phys. Rev. Lett. 44 (1980) 1755; D.E. Bainum et al., Phys. Rev. Lett. 44 (1980) 1751.

2) J. Speth, V. Klemt, J. Wambach, and G.E. Brown, Nucl. Phys. A343 (1980) 382.

3) W.G. Love, in "The (p,n) Reaction and the Nucleon-Nucleon Force", ed. C.D. Goodman et al. (Plenum, N.Y. 1980) p. 30;
F. Petrovich, ibid p. 135.

[+] Permanent address: SUNY at Stony Brook, USA, and Niels Bohr Institute, Copenhagen, Denmark

3.12. Influence of the "Dynamical Theory" on Gamow-Teller and Isobaric Analogue Resonances

S. Krewald, F. Osterfeld, J. Speth, and G.E. Brown[+]

In connection with the giant dipole resonances (GDR) it has been shown[1] that the single-particle energies which one uses in an RPA calculation depend on the excitation energy of the state one wants to calculate. This is connected with the coupling of the 2p2h states to the corresponding collective resonance. We shall show that this effect is very different for the Gamow-Teller (GTR) and the isobaric analogue resonances (IAR).

The coupling of the phonons to a given collective state with energy $\hbar\omega_\lambda$ can be expressed in terms of a selfenergy $\Sigma(\hbar\omega_\lambda)$ and the real part of it can be written as a principal value integral[2]:

$$\Sigma(\hbar\omega_\lambda) = P \int dE_i \, \frac{|M_\lambda(E_i)|\rho(E_i)}{\hbar\omega_\lambda - E_i} \qquad (1)$$

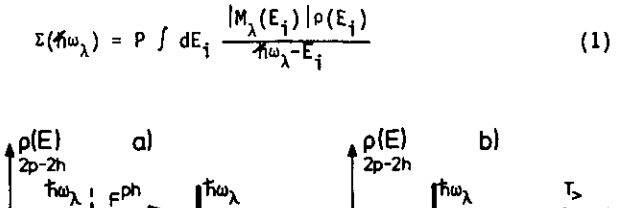

Fig. 1: Two limiting cases included in eq. (1).

In fig. 1 we show two limiting situations. In the GTR case (fig. 1a) the repulsive ph-interaction pushes this resonance right in between the corresponding 2p2h states. Since the GTR is the $T_<$ state it couples strongly to the 2p2h ($T_<$) states which are in the same energy region, i. e. the selfenergy (eq. (1)) is small. Therefore, the compression due to them in the empirical particle-hole energies must be removed[1]. Using the phenomenological formula of ref. 2 we obtain an effective mass of $m^*/m = 0.75$. We use in the actual calculation the Skyrme III spectrum which corresponds to $m^*/m = 0.76$.

The situation of the IAR is shown schematically in fig. 1b. Since the IAR is the $T_>$ state the corresponding 2p2h

($T_>$) states are much higher in energy. Therefore the principle value integral (1) is large which means that the phonon coupling is not removed and one has to use the experimental single-particle energies.

The results of our calculation are summarized in table 1.

	GDR (^{208}Pb)		IAR (^{208}Bi)		GTR (^{208}Bi)	
	Theory	Experiment	Theory	Experiment	Theory	Experiment[1,2]
E [MeV]	13.7	13.7	17.0	18.0	18.9	18.4±0.2
S.P. Spectrum	SK III		exp. energies		SK III	
Force Parameter	$f_0'^{in}$=0.60 $f_0'^{ex}$=1.8				g_0'=0.65	

Table 1: Comparison between theoretical and experimental energies of the electric dipole resonance (GDR), isobaric analogue resonance (IAR) and Gamow-Teller resonance, respectively. The energies refer to the ground state of ^{208}Pb.

References

1) G.E. Brown and J. Speth, in "Neutron Capture Gamma-Ray Spectroscopy" ed. R.E. Chrien and W.R. Kane (*Plenum Publishing Co., N.Y. 1979*).

2) G.E. Brown, J.S. Dehesa, and J. Speth, Nucl. Phys. A330 (1979) 290.

+ *Permanent address: SUNY at Stony Brook, USA, and* Niels Bohr Institute, Copenhagen, Denmark

3.13. On the Energy Dependence of the Coupling Potential in (p,n) Reactions

G.E. Brown+, *J. Speth, and J. Wambach*

In the recent highly energetic (p,n) experiments a strong energy dependence of the effective V_τ-coupling potential has been detected, whereas the $V_{\tau\sigma}$-potential remains essentially constant. We investigated the physical origin of the energy dependence of these potentials within a model which includes the one-pion and one-rho exchange potential as well as the second order effects of the tensor force. In addition we also take into account the effects of the other mesons (especially of the ω-meson) in a pair correlation function. The various contributions are shown in fig. 1.

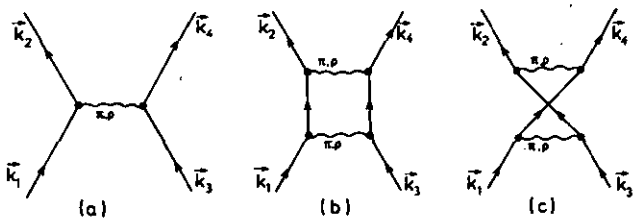

Fig. 1: First and second order contribution of the one-pion and one-rho exchange included in the present model.

We restrict the discussion to the momentum transfer q=0 (forward scattering). It is obvious that the direct term W_{dir} of the one-pion and one-rho exchange potential (fig. 1a) gives only a contribution in the $\sigma\tau$-channel and that for q=0 this term is energy independent. The corresponding exchange term W_{exch} is energy dependent (it decreases with increasing energy and it gives a contribution in the τ-channel, the magnitude of which, however, is too small. Therefore we include also the effects of the second order tensor contribution (fig. 1b). The direct term is of the form

$$U^T_{dir}(q) = 4\pi \int_0^\infty dz \, \frac{z^2 \cdot f(z)}{q^2 - 4z^2} \qquad (1)$$

The real part of this expression depends strongly on the energy of the incoming particle $q^2 = (\vec{k}_2 - \vec{k}_2)^2$ because eq. (1) is of the form of a principal value integral. Our effective coupling potential is given finally as:

$$V = W_{dir} + W_{exch} + U_{dir} + U_{exch} \qquad (2)$$

The final result is given in fig. 2 and table 1. In

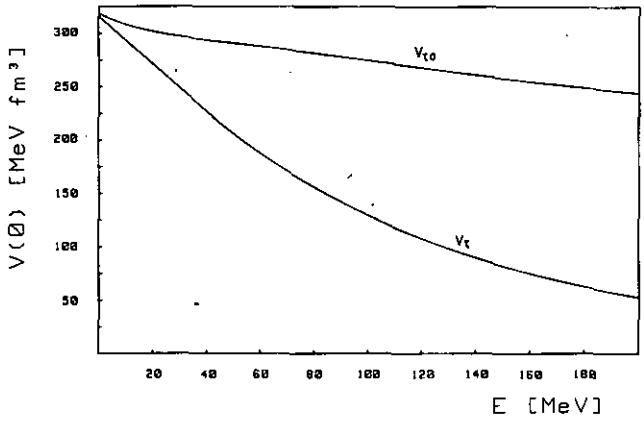

Fig. 2: Dependence of $V_\tau(q=0)$ and $V_{\tau\sigma}(q=0)$ on the energy of the incoming particle energy.

proton energy	V_τ	$V_{\tau\sigma}$	U_τ	$U_{\tau\sigma}$	W_τ	$W_{\tau\sigma}$
20	270	300	210	115	60	185
130	100	265	90	60	10	205

Table 1: The contributions U_τ and $U_{\tau\sigma}$ (second order tensor) and W_τ and $W_{\tau\sigma}$ (one-pion and one-rho exchange potential) to the isovector coupling potentials V_τ and $V_{\tau\sigma}$ in [MeV·fm³]. The calculation has been performed for two different proton energies (20 MeV and 130 MeV).

table 1 we give the various contributions to V_τ *and* $V_{\tau\sigma}$ for the proton energies E = 20 MeV and E = 130 MeV. At the lower energy about 3/4 of V_τ comes from the second *order effect and 1/4 from the exchange terms of fig.* 1a. The one-pion and one-rho exchange potential on the other hand give rise to 60 % of $V_{\tau\sigma}$ whereas 40 % are due to *the second order contribution. With increasing energy* not only the second order tensor contribution gets smaller because of the principal value integral, but *also the Pauli exchange terms decrease strongly. The* latter one is also responsible for the increase of $W_{\tau\sigma}$.

The theoretical results are in a good qualitative agreement with the experimental findings.

+ Permanent address: SUNY at Stony Brook, USA, and Niels Bohr Institute, Copenhagen, Denmark

3.14. Critical Analysis of a Precritical Phenomenon in Connection with Pion Condensation

T. Suzuki, F. Osterfeld, and J. Speth

From the analysis of experimental data follows that pion condensation does not exist in finite nuclei. However, the data do not exclude the possibility of being close to the point of pion condensation in real nuclei. In this case, one might expect results in some specific experiments which indicate the proximity of nuclei to the pion condensation threshold. It has been argued that the (e,e') form factor[1] of the 1^+ (T=1; 15.1 MeV) state in ^{12}C is a good candidate for such a precritical phenomenon since the second maximum of the theoretical (e,e') form factor derived from the Cohen-Kurath wave function[2] is a factor of five smaller than the experimental one. Since the corresponding momentum transfer is $q \sim 2$ [fm^{-1}], it is tempting to connect this deviation with a precritical phenomenon. On the other hand, high energetic proton experiments do not show any precritical behaviour[3]. The theoretical problem consists in describing the (e,e') and (p,p') cross sections simultaneously. The results shown in figs. 1 and 2 are derived from a 1p-1h RPA calculation using the generalized Landau-Migdal ph-interaction[4] which excludes precritical phenomena. We introduced a reduction factor R for the 1p-amplitude in order to correct this shortcoming. With R=0.5, we reproduce the experimental B(M1)-value. In fig. 1 we also demonstrate the dependence of the form factor on the form of the single-particle wave functions.

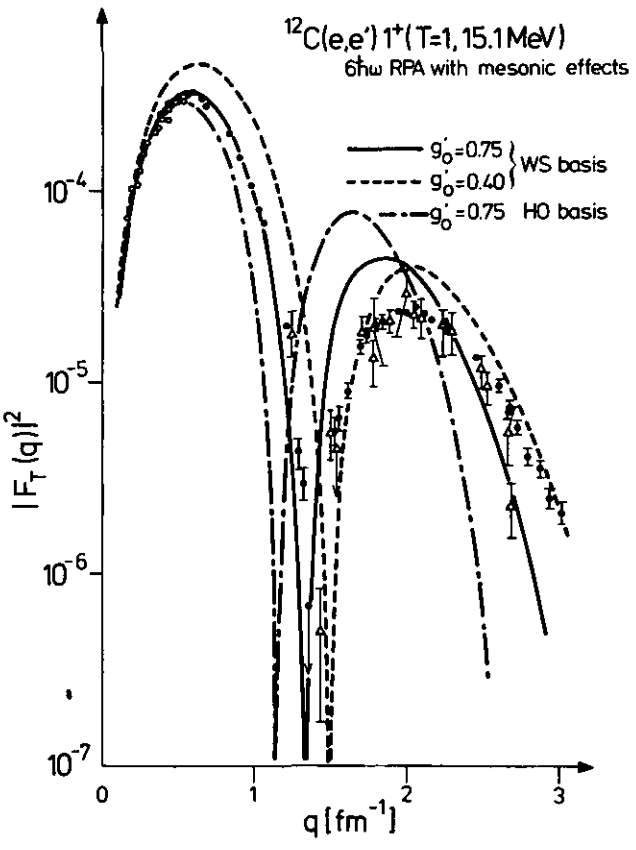

Fig. 1: Inelastic electron scattering form factors of the 1^+ state in ^{12}C calculated in the Born approximation including meson exchange effects.

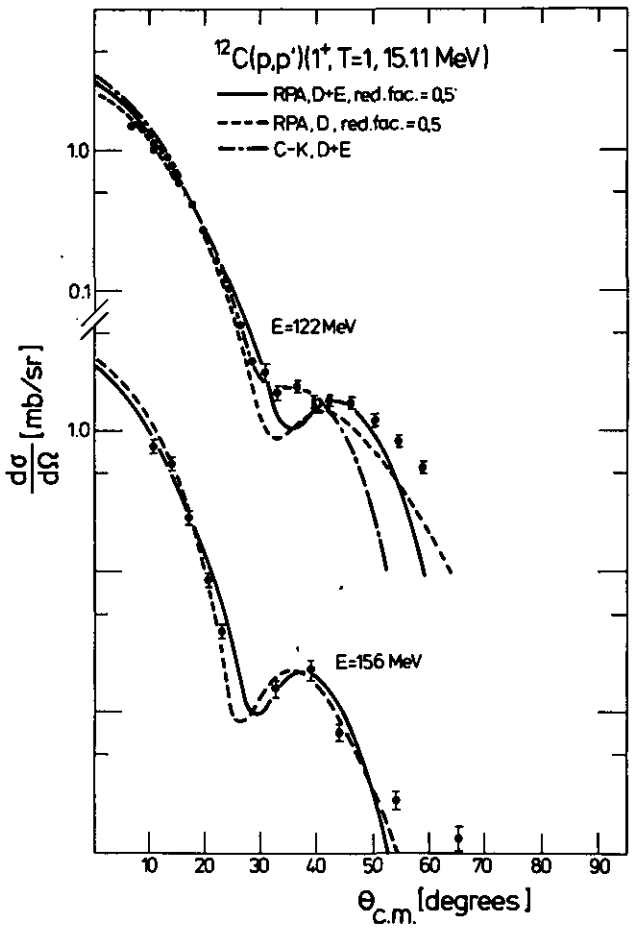

Fig. 2: (p,p') cross sections calculated in DWBA. Here D and D+E denote the results where direct and direct plus exchange amplitudes have been taken into account.

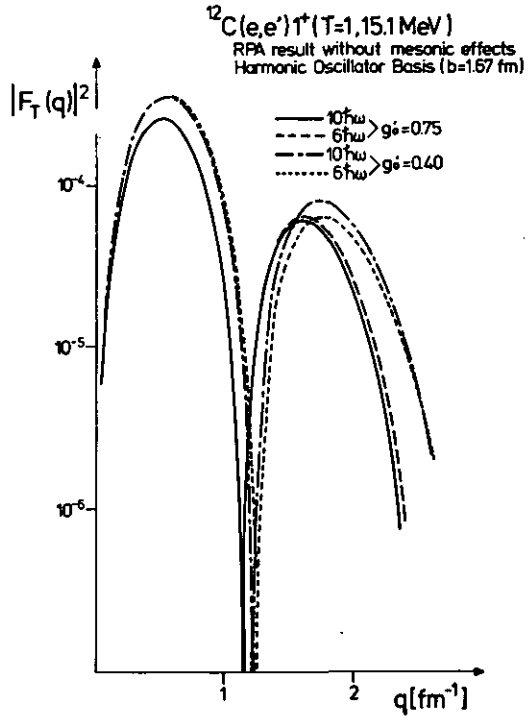

Fig. 3: Effect of the higher ph-configurations on the form factor.

The use of H.O. instead of W.S. functions not only shifts the position of the minimum and second maximum to lower q-values but also enhances the second maximum by nearly 70 %. In fig. 3 we investigate the conver-

gence of our results. If we increase our ph-configuration space from $6\hbar\omega$ to $10\hbar\omega$ in the case of H.O. functions, the form factor changes only little if we use our value of the Migdal parameter of $g_0' = 0.75$. Even in the case of the unrealistically small value of $g_0' = 0.4$ the changes are not large, but one notices the beginning of a "precritical" enhancement in the region $1.5 \leq q \leq 2.5$. If we use W.S. wave functions the changes are much smaller.

References

1) M. Ericson and J. Delorme, Phys. Lett. 76B (1978) 182.
2) S. Cohen and D. Kurath, Nucl. Phys. 73 (1965) 1.
3) J.R. Comfort and W.G. Love, Phys. Rev. Lett. 44 (1980) 1656;
   M. Haji-Saeid et al., Phys. Rev. Lett. 45 (1980) 880.
4) J. Speth, V. Klemt, J. Wambach, and G.E. Brown, Nucl. Phys. A343 (1980) 382.

3.15. No Evidence for Precritical Phenomena of Pion Condensation in Finite Nuclei

F. Osterfeld, T. Suzuki, J. Speth

Recently several authors[1] have discussed the possibility of observing precritical phenomena in finite nuclei related to the proximity of the pion condensation threshold. They suggested that the pion-like correlations could be enhanced at large momentum transfer ($q \sim 1$-2 fm^{-1}) which should lead to a corresponding enhancement in inelastic scattering cross sections to unnatural parity states. The occurrence of such an effect is known to depend sensitively on the repulsive correlations due to the spin-isospin dependent particle-hole interaction which are usually parametrized by the Landau-Migdal force parameter g_0'.

We have performed theoretical investigations on the electron and proton inelastic excitation of the 1^+ (10.24 MeV) state in ^{48}Ca nucleus[2] as all as on the charge exchange (p,n) reaction to the 1^+ (T=4, 16.8 MeV) ^{48}Sc state[3] which is the isobaric analogue of the former. The structure calculations have been performed within the RPA using a large model space up to 10 $\hbar\omega$ excitations. The single particle wave functions have been produced from a Woods-Saxon potential whose parameters have been adjusted to reproduce the single particle energies deduced from the averaging procedure on the experimental energies in neighbouring odd-A nuclei[4]. For the residual particle-hole interaction we adopted the generalized Landau-Migdal force of ref. 5 (m^*/m = 0.8) which includes the finite range π- and ρ-exchange potentials in addition to the δ-interaction.

The RPA calculations produce only one 1^+ state in the energy region around 10.24 MeV in ^{48}Ca, which has the $[\nu 1f_{5/2}\nu 1f_{7/2}^{-1}]_{1^+}$ configuration as the dominant component. The experimental excitation energy cannot be reproduced with small values of g_0' even when g_0 is large. The best fit is obtained with g_0' = 0.6 (= g_0) which is very unfavourable for precritical effects.

Using the RPA transition densities for the 1^+, 10.24 MeV state in ^{48}Ca we have calculated the inelastic electron scattering form factor (fig. 1). It can be seen that small values of g_0' ($\sim$ 0.2) produce an enhancement of the form factor at the second maxima, but these small values of g_0' cannot reproduce the experimental excitation energies. Similar calculations have also been performed for a 6 $\hbar\omega$ model space. From a comparison of both results we find that convergence of the calculations has already been achieved even for such small values of g_0' as 0.2.

In order to study the hadron scattering from A = 48 nuclei we have done the antisymmetrized DWIA-calculations using the G3Y-interaction[6] of Love for the effective projectile-target nucleon interaction. From the dependence of the ^{48}Ca(p,p')1^+, 10.24 MeV-differential cross sections on the parameter g_0' (E_p = 160), we observe a similar enhancement at high momentum transfer as in (e,e'), although the dependence is rather weak. The (p,n)-reaction to unnatural parity states is more selective than (e,e') and (p,p') because it always requires a spin-isospin flip. Therefore the (p,n)-reaction is a good probe for testing pion-like correlations. In fig. 2 we study the dependence of the ^{48}Ca(p,n)^{48}Sc(1^+, T=4, 16.8 MeV) reaction on the value of g_0'. The wave function of this 1^+ state in ^{48}Sc has been constructed by simply applying the isospin-lowering operator to the 1^+ state in ^{48}Ca as has been done in ref. 7. Then we have basically the form

$$|1^+,T{=}4,{}^{48}\mathrm{Sc}\rangle = \frac{1}{\sqrt{2T_0}}|1p1h\rangle + \sqrt{\frac{2T_0-1}{2T_0}}\,|2p2h\rangle$$

where T_0 = 4 is the isospin of the 1^+ state in the parent nucleus ^{48}Ca. Under the assumption of a direct process only the 1p-1h component of the wave function can be excited. In fig. 2 the calculated (p,n) cross sections are compared with the low momentum transfer data of ref. 3. The theoretical angular distributions agree with the data in shape although the absolute magnitude is overestimated by a factor of 4. As in the case of the (p,p') cross section, the dependence on the parameter g_0' is rather weak. It is seen that even for an unrealistically weak repulsive interaction (g_0' = 0.2) the enhancement in high-q region is very small.

From this analysis we conclude that the precritical phenomena are unlikely to occur in A=48 nuclei.

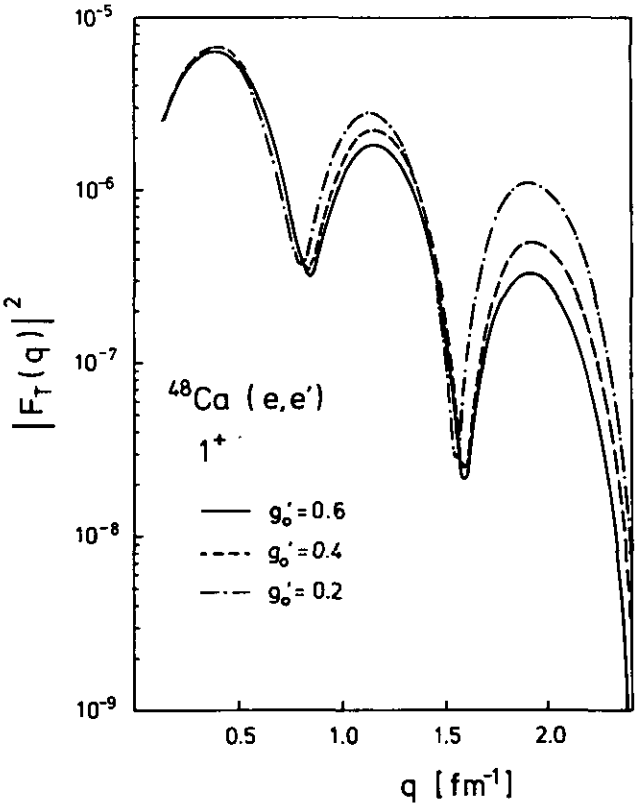

Fig. 1: Calculated DWBA form factors of the ^{48}Ca(e,e') 1^+, 10.24 MeV reaction (E_{in} = 250 MeV). The dependence on the force parameter g_0' is shown (g_0 = 0.6).

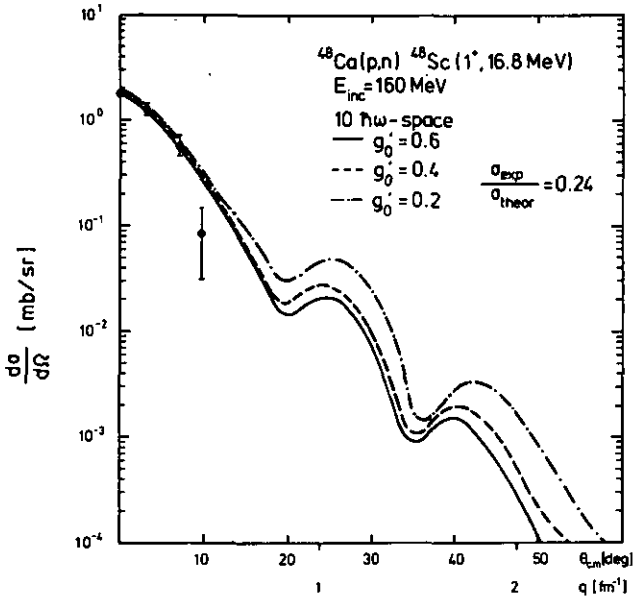

Fig. 2: Differential cross sections of the ^{48}Ca(p,n)^{48}Sc (1^+, 16.8 MeV) reaction at E_p = 160 MeV. The data are taken from ref. 3.

References

1) E.E. Saperstein, S.V. Tolokonnikov and S.A. Fayans, Sov. J. Nucl. Phys. 25 (1977) 510;
M. Ericson and J. Delorme, Phys. Lett. 76B (1978) 182;
H. Toki and W. Weise, Phys. Rev. Lett. 92B (1980) 265.

2) W. Steffen et al., Phys. Lett. 95B (1980) 23.

3) B.D. Anderson et al., Phys. Rev. Lett. 45 (1980) 699.

4) F. Malaguti, A. Uguzzoni, E. Verondini and P.E. Hodgson, Nuovo Cim. 49A (1979) 412.

5) J. Speth, J. Wambach, V. Klemt and G.E. Brown, Nucl. Phys. A343 (1980) 382.

6) W.G. Love, Proc. Conf. on the (p,n)-Reaction and the NN-Interaction, Telluride, Colorado, 1979, ed. by C.D. Goodman et al. (Plenum, New York, 1980) p. 23.

7) F. Krmpotić and F. Osterfeld, Phys. Lett. 93B (1980) 218.

3.16. Does Pion Condensation Prevent Pion Condensation?

W.H. Dickhoff[+], A. Faessler[++], J. Meyer-ter-Vehn[+++], H. Müther

During the last few years the question of the existence of pion condensation in nuclear matter of a certain density has extensively been studied. Nevertheless, the question under which conditions (critical density of nuclear matter ρ_c and critical momentum of the pionic state) such a phase transition to a pion condensation may happen, is still discussed quite controversially. It has been found[1] that, in order to clarify the critical point theoretically, it is essential to take into account the coupling of the pion to isobar ($\Delta(1236)$) excited states of nuclear matter and that the results depend quite strongly on the treatment of the residual nucleon-nucleon (NN) correlations. In schematic models these correlations or, to put it differently, the residual interaction of NN particle-hole states, which have the same quantum numbers as the pion, is represented by a constant γ. If this constant γ is more repulsive, one obtains a higher critical density for pion condensation. In the limit of pion momentum k=0, the constant γ can directly be related to the parameter g'_0 of the Landau-Migdal interaction. Calculations which determine the residual particle-hole interaction from a microscopically calculated Brueckner G-matrix indicate that it is a rather good approximation to replace the very complicated interaction by such a simple constant which hardly depends on the nuclear density considered[2,3]. Such calculations yield pion condensation at about $\rho_c = 2\rho_0$ (ρ_0 the normal density of nuclear matter).

The question is now: Is it sufficient to describe the particle-hole interaction in terms of the Brueckner G-matrix? The answer is: No, it is not. Let us consider a system which is fairly close to the critical point of pion condensation. This means that the pion strongly interacts with the excitation modes of nuclear matter, such that the propagator of the pion in the medium almost has a pole. In this case, however, one should take into account the coupling of the pion to the nuclear medium also in the One-Pion-Exchange part, which contributes to the residual interaction. This means that in nuclear matter the NN interaction is not constructed in terms of the exchange of bare mesons but of mesons which polarize the nuclear medium. This follows the concept of the induced interaction as discussed e. g. by Babu and Brown[4].

Calculations have been performed using the Brueckner G-matrix calculated for the Reid soft-core potential as a starting point. The dependence of this interaction on three momenta and the starting energy has been treated carefully. Beside the coupling to NN^{-1} particle-hole states also ΔN^{-1} states were considered. To characterize the resulting interaction the average interaction strength γ has been determined by considering the Landau limit for the particle-hole interaction. Results for the constant γ at normal densities are listed in table 1. One can see that already at normal densities the terms of the induced interaction yield a significant enhancement. The inclusion of isobar configurations is very important. At higher densities the contributions from the induced interaction will be more important, especially if one approaches the critical density ρ_c, and lead to a much more repulsive γ. This dynamic effect will push up the critical density for pion condensation to much higher values.

	G	$G+NN^{-1}$	$G+NN^{-1}+\Delta N^{-1}$
γ	0.48	0.6	0.66

Table 1: Results for the effective interaction strength γ for the bare G-matrix (G) and after inclusion of the induced interaction with NN^{-1} states ($G+NN^{-1}$) and also with isobar states ($G+NN^{-1}+\Delta N^{-1}$).

References

1) G.E. Brown, W. Weise, Phys. Rep. 27C (1976) 2.

2) S.O. Bäckman, W. Weise, Phys. Lett. 55B (1975) 1.

3) W.H. Dickhoff, A. Faessler, J. Meyer-ter-Vehn, H. Müther, Phys. Rev. C, in press.

4) S. Babu, G.E. Brown, Ann. Phys. 78 (1973) 1.

+ Vrije Universiteit Amsterdam, Netherlands

++ Institut für Theor. Physik, Univ. Tübingen

+++ Max-Planck-Gesellschaft Garching

3.17. Three-Body Forces from Intermediate $N^*(1470)$ States

K. Shimizu[+], *A. Polls*[+], *H. Müther*, *A. Faessler*[+]

The classical model for a microscopic description of ground state properties of a nuclear system is to consider nuclei as a system of inert nucleons, treated as elementary particles, which interact via a two-body nucleon-nucleon (NN) potential determined by adjusting it to fit the two-nucleon data. A possible extension of this conventional many-body theory for nuclear systems is to investigate effects due to internal excitation of single nucleons. Such investigations have been performed by several groups especially for the excitation to the $\Delta(1236)$ resonance. It was found that the explicit treatment of isobar excitations leads to a quenching of attractive parts of the effective NN interaction in the nuclear medium as compared to the NN interaction in the vacuum of the two-nucleon system[1-3]. This quenching is due to Pauli and dispersion effects and leads to a reduction of the calculated binding energy, which depends on the density of the nuclear system considered. Furthermore, the explicit treatment of excitations of the nucleons in a nuclear many-body theory also gives rise to three-body terms, which in a conventional theory have to be simulated by effective three-body forces. For the case of the intermediate $\Delta(1236)$ resonance the contribution from three-body terms with two interaction lines vanishes because of the spin-isospin quantum numbers of the Δ resonance[4]. Therefore the attractive contributions from these three-body terms are typically too weak to counterbalance the repulsion due to the quenching of the NN interaction[4,5].

In the case of the intermediate $N^*(1470)$ resonance, which has the same spin-isospin quantum numbers as the nucleon, already the lowest order terms contribute to the effective three-body force and therefore a significant contribution can be expected although the coupling to the N^* resonance is weaker than the $N\Delta$ coupling. The transition potentials ($NN \leftrightarrow NN^*$) describing the excitation of the N^* resonance are derived in the framework of the One-Boson-Exchange potential. The coupling constants $f(\alpha NN^*)$ (α stands for a meson) are assumed to be proportional to the corresponding $f(\alpha NN)$ coupling constant and the ratio $f^2(\pi NN^*)/f^2(\pi NN) = 0.125$ is determined from the experimentally observed width $\Gamma(N^* \to \pi N)$. Also the effects of two-body correlations on the effective transition potential G_{NN^*} are taken into account.

Using these transition potentials the effect of Pauli-quenching of the effective two-body interaction and the lowest-order three-body contributions on the binding energy of nuclear matter and ^{16}O are calculated. Results are presented in table 1. One can see that for intermediate N^* states the attractive contributions from the three-body terms are larger than the repulsive effects of the Pauli-quenching and an overall attraction remains. Beside the results for the whole transition potential $\hat{G}$ we also list the result if the transition potential is described by the bare one-π exchange term (V_π). The comparison shows that the one-π contribution is rather weak and that the main effect comes from exchange of heavier mesons and due to the consideration of two-body correlations. This indicates that the effects of intermediate N^* states cannot appropriately be described using dispersion relation[6], since then only the π-exchange contributions are taken into account.

		$\hat{G}$	V_π
^{16}O	W_P	0.11	0.01
	W_T	-0.41	-0.02
nuclear matter	W_P	0.30	0.02
	W_T	-1.26	-0.04

Table 1: Effects of Pauli-quenching (W_P) and three-body terms (W_T) with intermediate N^* states on the calculated binding energies per particle.

References

1) A.M. Green, Rep. Prog. Phys. 39 (1976) 1109.

2) B.D. Day, J. Coester, Phys. Rev. C13 (1976) 1720.

3) M.R. Anastasio, A. Faessler, H. Müther, K. Holinde, R. Machleidt, Phys. Rev. C18 (1978) 870.

4) A. Faessler, H. Müther, K. Shimizu, W. Wadia, Nucl. Phys. A333 (1980) 428.

5) T. Kouki, L.E.W. Samelter, A.M. Green, Nucl. Phys. A290 (1977) 381.

6) S.A. Coon, M.D. Scadron, P.C. McNamec, B.R. Barrett, D.W.E. Blatt, B.H.J. McKellar, Nucl. Phys. A317 (1979) 242.

[+] Institut für Theor. Physik, Univ. Tübingen

3.18. Non-Iterative Isobar Diagrams and their Effect in NN Scattering

K. Holinde[+], *R. Machleidt*[+], *A. Faessler*[++], *H. Müther*, *M.R. Anastasio*[+++]

The standard model for nuclear matter is to consider a collection of nucleons interacting through a two-body potential like e.g. the Reid soft-core potential. Considering such a static model for the NN interaction and employing e.g. Brueckner theory with inclusion of three-body correlations to solve the nuclear many-body problem, one typically obtains too much binding energy for systems of high density (nuclear matter)[1] and not enough energy for small densities (finite nuclei)[2]. This defect of the classical model for nuclear matter can at least partly be eliminated if a meson theoretical ansatz for the NN interaction is considered. In this framework a large fraction of the medium range attractive part of the NN interaction arises from irreducible 2π-exchange processes like e.g. the 2π cross-box terms or iterative 2π-exchange terms involving intermediate isobar excitations. Due to Pauli and dispersion effects these intermediate-range, attractive parts are suppressed in a nuclear medium especially at high densities. This means

that the effective NN interaction in the nuclear medium is less attractive than in the vacuum of NN scattering and therefore the overbinding of nuclear matter at high densities is prevented.

To investigate such modifications of the NN interaction in a nuclear medium, one has to calculate the irreducible 2π-exchange terms explicitly. This is done in the framework of non-covariant perturbation theory[3]. As an extension of earlier work we now also consider non-iterative 2π-exchange diagrams involving intermediate $N\Delta$ states ($M^X_{N\Delta}$). It has been argued[4] that these terms $M^X_{N\Delta}$ together with the iterative 2π-exchange contribution $M_{N\Delta}$, involving intermediate $N\Delta$ states, should give an isoscalar contribution to the NN interaction which could be approximated by an iterative 2π-exchange term neglecting retardation effect. Our investigations show that this approximation is reasonable for the $^1S_0$ channel of the NN interaction, but it grossly overestimates the isobar contribution in the $^3S_1$ channel (see fig. 1).

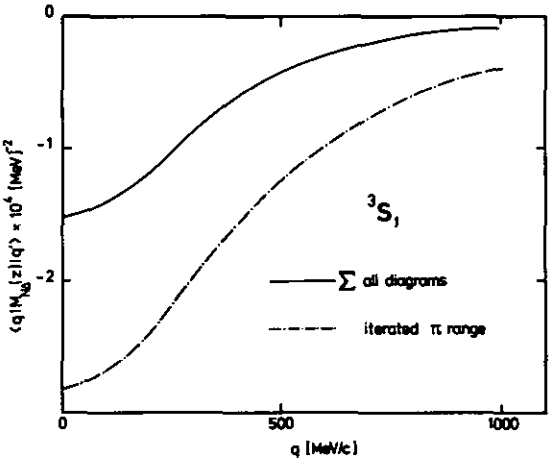

Fig. 1: Matrix elements $\langle q|M_{N\Delta}(Z)|q'\rangle$ in the $^3S_1$ channel for $q' = 100$ MeV/c and $Z = 2m$. While the solid curve shows the exact results treating all $N\Delta$ diagrams explicitly, the dashed-dotted curve represents the approximation by the isoscalar part of an iterated pion-range potential.

Our final ansatz for the NN interaction consists out of a One-Boson-Exchange part, iterative diagrams with $N\Delta$ and $\Delta\Delta$ intermediate states (the transition potentials contain π- and ρ-exchange)[2], and non-iterative 2π-exchange terms with intermediate NN[5] and $N\Delta$ states. The parameters of this ansatz (coupling constants and form factors) can be adjusted to obtain a reasonable fit of the NN data. The 2π exchange terms treated explicitly in our model replace about 50 % of the σ-exchange part in a pure One-Boson-Exchange potential. This is in reasonable agreement with the results of dispersion-theoretic models. In contrast to a dispersion-theoretical description, which only allows the calculation of the NN interaction in the vacuum, the present model for the NN interaction can also be used for calculations of nuclear many-body systems.

References

1) B.D. Day, Nucl. Phys. A328 (1979) 1.

2) M.R. Anastasio, A. Faessler, H. Müther, K. Holinde, R. Machleidt, Phys. Rev. C18 (1978) 870.

3) D. Schütte, Nucl. Phys. A221 (1974) 450.

4) J.W. Durso, M. Saarela, G.E. Brown, A.D. Jackson, Nucl. Phys. A278 (1977) 445.

5) H. Müther, A. Faessler, M.R. Anastasio, K. Holinde, R. Machleidt, Phys. Rev. C22 (1980) 744.

+ Inst. für Theor. Kernphysik, Univ. Bonn

++ Inst. für Theor. Physik, Univ. Tübingen

+++ CUNY, Brooklyn, N.Y., USA

3.19. Three-Body Forces and Three-Body Correlations

H. Müther, A. Faessler[+], J. Urbano[++]

During the last few years a lot of theoretical effort has been made to investigate the importance of isobar degrees of freedom, which means the inner excitations of single nucleons, for a microscopic description of ground state properties of nuclei. It has been found that especially an explicit treatment of the excitation to the $\Delta(1236)$ resonance yields significant, medium dependent effects for the effective NN interaction[1,2] and also non-negligible three-body terms with intermediate excitations which may be considered as effective three-body forces[3,4]. These three-body terms crucially depend on the correlations between the interacting nucleons[3]. The contribution to the binding energy[3] is comparable to the effects due to an explicit treatment of three-N correlations which are calculated by solving Bethe-Faddeev equations.

These two observations lead to the suggestion that it might be necessary to consider effects from three-body forces and three-body correlations simultaneously. This means, one should try to sum up all three-particle ladder diagrams containing intermediate NNN, $NN\Delta$ and if possible also $N\Delta\Delta$ and $\Delta\Delta\Delta$ states. Already the solution of the Bethe-Faddeev equations with only NNN intermediate states is very involved and there exist only very few calculations. With inclusion of isobar states, however, the numerical effort increases quite drastically and therefore certain approximations have to be made. First of all we consider wave functions of the harmonic oscillator for the single-particle wave functions. Then we allow only NNN and $NN\Delta$ intermediate states. Finally, we do not consider processes with "long-living" isobars, i.e. whenever a Δ resonance is excited, it will be de-excited by the next interaction. This "active isobar assumption" is supported by the results of lowest order calculations[3]. Using these approximations the extended Bethe-Faddeev equations may formally be written as

$$F_{NNN} = G\,\frac{XQ}{e}\,(G - F_{NNN}) + G^{+}_{N\Delta}\,\frac{XQ}{e}\,(G_{N\Delta} - F_{NN\Delta})$$

$$F_{NN\Delta} = G_{\Delta\Delta}\,\frac{XQ}{e}\,(G_{N\Delta} - F_{NN\Delta}) + G_{N\Delta}\,\frac{XQ}{e}\,(G - F_{NNN}) \qquad (1)$$

The quantities used in these equations are defined in analogy to ref. 5. $G_{N\Delta}$ and $G_{\Delta\Delta}$ are effective transition potentials describing $NN \to N\Delta$ and a transition like $N\Delta \to \Delta N$, respectively, with inclusion of 2-particle correlations. The permutation operator X may be defined by

$$X\ \Psi(k_1,k_2;k_3) = \Psi(k_2,k_3;k_1) + \Psi(k_3,k_1;k_2) \qquad (2)$$

where $\Psi(k_1,k_2;k_3)$ is a three-particle wave function which is antisymmetric with respect to an exchange of the "active" particles 1, 2 only. Q and e are the usual Pauli operator and energy denominator respectively. Using the solutions of eq. (1) the energy contribution can be calculated as the expectation value of

$$\Delta E = -\left(G\frac{Q}{e} \times F_{NNN} + G^{+}_{N\Delta}\frac{Q}{e} \times F_{NN\Delta}\right)(1 + X) \qquad (3)$$

Such extended Bethe-Faddeev equations have been solved for the nucleus ^{4}He. Preliminary results are given in table 1. The full calculation yields a result which is by 50 % larger than the contribution of the lowest order term (three interaction lines). It should be mentioned that it is very important to take into account the effects of the interaction in partial waves with $\ell>0$.

^{4}He	low order	full calc.
E/A [MeV/nucleon]	-1.03	-1.61

Table 1: Preliminary results from extended Bethe-Faddeev equations for He.

References

1) A.M. Green, Rep. Prog. Phys. 39 (1976) 1109.

2) H. Müther, Nucl. Phys. A328 (1979) 429.

3) A. Faessler, H. Müther, K. Shimizu, W. Wadia, Nucl. Phys. A333 (1980) 428.

4) T. Kouki, G.F.W. Smulter, A.M. Green, Nucl. Phys. A290 (1977) 381.

5) B.D. Day, F. Coester, G. Goodman, Phys. Rev. C6 (1972) 1942.

+ Inst. für Theor. Physik, Univ. Tübingen

++ Lab. de Fisica da Univ., Coimbra, Portugal

3.20. Magnetic Moments of Nucleons and Isobars in the Chiral Bag Model

J. Wambach[+*], *I. Hulthage*[++]

The chiral invariant bag model[1] introduces pions as Goldstone bosons outside a confined space-time region in which quarks and gluons couple perturbatively. The MIT-bag without pion cloud[2] predicts too small magnetic moments for nucleons and the Δ^+-N transition moment for bag radii less than $\sim$ 1.5 fm. In this model the moment is a linear function of the bag radius R

$$\langle B|\mu_q^z|B'\rangle = \frac{e}{6}\frac{4\Omega_0-3}{2(\Omega_0-1)\Omega_0}\cdot R\,\langle B|\sum_i \frac{1}{2}(\frac{1}{3}+\tau_i^z)\sigma_i^z|B'\rangle \qquad (1)$$

$\Omega_0 = 2.04$, $|B\rangle$ and $|B'\rangle$ denote the spin-isospin wave functions of the nonstrange baryons. Perturbative one gluon exchange corrections[3] are of the order of 10 %, which is no significant improvement. In the chiral invariant bag the pion field also carries electromagnetic current

$$\vec{J}_\mu^\pi = \frac{e}{2}\,(\vec{\pi}\times(\partial_\mu\vec{\pi}) - (\partial_\mu\vec{\pi})\times\vec{\pi}) \qquad (2)$$

(the arrow means vector in isospin space). Because of the static approximation to the chiral Lagrangian the time component of $\vec{J}_\mu^\pi$ vanishes. The 3-vector current $\vec{J}^\pi$, however, is non zero and contributes to the moment

$$\mu_\pi^z = \frac{1}{2}\int_{V^-}[\vec{r}\times\vec{j}]^z\,d\vec{r} \qquad (3)$$

The integration volume V^- in eq. (3) goes from the bag surface to infinity. In a perturbative expansion of the Euler-Lagrange equations of the chiral Lagrangian[4] the pion field is easily calculated from the Klein-Gordon equation outside the bag volume and the boundary conditions at the surface. To lowest order in the effective pion-quark coupling parameter $1/f_\pi$ (f_π: pion decay constant) we find the solution for the pion field

$$\vec{\pi} = -\frac{1}{8\pi}\frac{1}{16\pi}\frac{\Omega_0}{\Omega_0-1}\sum_i \sigma(i)\hat{r}\,\vec{\tau}(i) \qquad (4)$$

The operators act again on the spin-isospin wave functions of the baryons. After some simple algebra we get for the magnetic moment (eq. (3))

$$\mu_\pi^z = \frac{1}{f_\pi^2}\frac{1}{4\pi}\left(\frac{\Omega_0}{\Omega_0-1}\right)^2\frac{1}{24}\frac{1}{R}\sum_{i,j}\frac{1}{4}\left[\sigma(i)\times\sigma(j)\right]^z\left[\vec{\tau}(i)\times\vec{\tau}(j)\right]_z \qquad (5)$$

This expression contains genuine two-body terms ($i\neq j$) similar to the well known "Sachs-moment" from exchange currents and arises from effective quark-quark interactions where the two quarks are different. The "two-body" contributions to the nonstrange baryons are both large for the nucleon ($\mu^{2\text{-body}}/\mu^{1\text{-body}} = 6/5$) and the Δ^+-N transition ($\mu^{2\text{-body}}/\mu^{1\text{-body}} = 3/2$). For diagonal Δ-Δ terms they vanish, however, since the quarks are in an S = 3/2 T = 3/2 state. The total moments $\langle B|\mu_q^z+\mu_\pi^z|B'\rangle$ are rather independent of the bag radius for .6<R<1.5 fm (table 1), a feature, which is also observed in the "hogdohog"-moment[5].

Our treatment of the nonstrange baryon moments has two chief shortcomings:

(i) The pion cloud gives only contributions to the isovector part of the moments. To incorporate isoscalar terms three-pion effects have to be considered (the ω-meson in the vector dominance model would be a correlate state in this picture).

(ii) γ-ray coupling to the baryon via ρ-meson exchange is neglected; only the pion continuum is included.

Point (i) indicates a shortcoming of the chiral bag in its present form. The SU(4) ratio of -2/3 for neutron to proton moment given by the quark part of μ^z is not reproduced naturally by the model, since the cloud tends to decrease the ratio to -1 for small radii, i.e. strong pion fields. As known phenomenologically from the vector dominance model, however[6], the way the ω-meson contributes to the magnetic form factor of the nucleon, three pion effects will restore part of the empirical ratio. Point (ii) means that our results may not be quantitative yet. We think, however, that effects of long range in space are correctly handled in the model, since low mass effects in the ρ-channel are given by chiral theories, like the Weinberg description of the pion scattering length[7].

R (fm)	$\mu_N^{T=1}$	$\mu^{\Delta^+\text{-}N}$	μ^{Δ^+}	$\mu^{\Delta^{++}}$
0.5	3.45	4.46	1.71	4.18
0.6	3.20	4.06	1.78	4.19
0.7	3.05	3.77	1.88	4.30
0.8	3.02	3.68	2.01	4.48
0.9	3.01	3.61	2.15	4.71
1.0	3.01	3.59	2.30	4.97
1.1	3.02	3.61	2.46	5.25
1.2	3.10	3.65	2.62	5.55
1.3	3.18	3.75	2.79	5.86
1.4	3.26	3.80	2.96	6.18
1.5	3.40	3.91	3.13	6.51

Table 1: Magnetic moments of nonstrange baryons as the function of the bag radius R. All moments are in units of the nuclear magneton $\mu_0 = \frac{e\hbar}{2mc}$.

References

1) A. Chodos and B. Thorn, Phys. Rev. D12 (1974) 2733; G.E. Brown and M. Rho, Phys. Lett. 82B (1979) 177; R.L. Jaffe, Lectures at the Erice Summer School "Ettore Majorana", Erice, Sicily.

2) T. De Grand, R.L. Jaffe, K. Johnson, and J. Kiskis, Phys. Rev. D12 (1975) 2060.

3) A. Halprin and P. Sorba, Phys. Lett. 66B (1977) 177.

4) V. Vento, thesis, SUNY, Stony Brook (1980), unpublished.

5) J.F. Logeais, M. Rho, and V. Vento, unpublished; E. Nyman, private communication.

6) F. Iachello, A.D. Jackson, and A. Landé, Phys. Lett. 43B (1973) 191.

7) S. Weinberg, Phys. Lett. 17 (1966) 616.

+ SUNY at Stony Brook, Stony Brook, USA

* Supported in part by the Deutsche Forschungsgemeinschaft

++ NORDITA, Copenhagen, Denmark

3.21. The Mass Distribution Width of Heavy-Ion Induced Fission for Various Composite Systems

M.E. Faber[+]

Just recently Sahm et al.[1] determined the variations of the width of the mass distribution of fusion-fission events for various composite systems. They have discovered a correlation between the width and the height of the liquid drop fission barrier. In ref. 2 a microscopic calculation of the deformation energy in the fission valley has shown that the component of the driving force which tends to press an asymmetric composite system versus symmetry decreases with increasing angular momentum I. The calculation of ref. 2 tends to show that not only the fission barrier is responsible for the width but the whole fission valley influences the mass distribution. It seems that this fact has been underestimated in the earlier investigations. The recent measurements of Sahm et al.[2] support this idea. In fig. 1 a set of shapes along the liquid drop valley is shown. In fig. 2 the rotating liquid drop energy for the composite system ^{205}At at I = 60ħ is shown in the space of fig. 1. By a simple argument (see ref. 3) one can show that the equi-energy parabolae in the fission valley broaden with increasing Z^2/A. This effect can be seen in fig. 3. An asymmetric deformed nucleus ^{221}Pa has less tendency to reach symmetry than a ^{205}At nucleus with the same shape. Since the height of the fission barrier depends also on Z^2/A the broadening of the mass distribution is correlated with the decreasing height of the fission barrier.

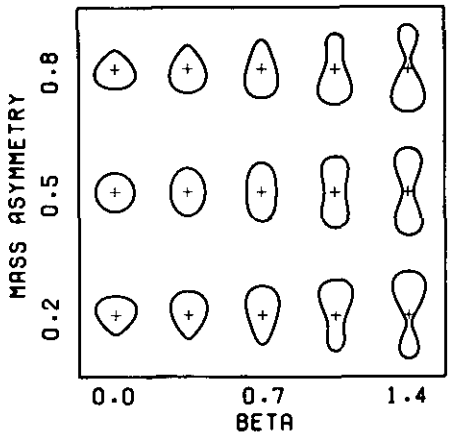

Fig. 1: A set of shapes along the liquid drop valley. The neck ratio r varies together with the elongation β according to r = 1.0 for β ≤ 0.6 and r = 1.6-β for β ≥ 0.6.

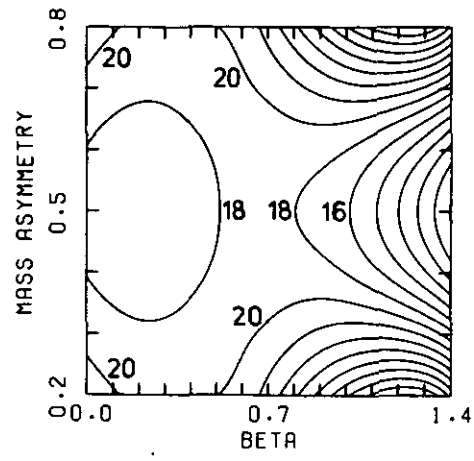

Fig. 2: Liquid drop energy of ^{205}At at I = 60ħ.

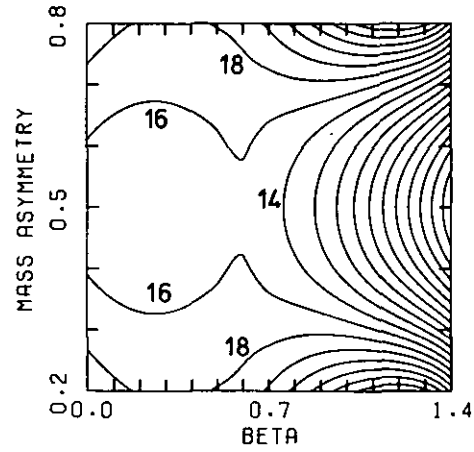

Fig. 3: Liquid drop energy of ^{221}Pa at I = 60ħ.

References

1) C.-C. Sahm et al., Z. Physik A297 (1980) 241.
2) M.E. Faber, submitted to Phys. Rev. C.
3) M.E. Faber, Z. Physik A297 (1980) 277.

[+] Atominstitut der österr. Universitäten, Wien, Austria

3.22. The Influence of Angular Momentum on the Mass Distribution of Heavy-Ion Induced Fission

M.E. Faber[+]

There exist two types of heavy-ion reactions: the complete fusion and the deep inelastic events. At "low" bombarding energies of about 200 MeV and sufficiently asymmetric systems like ^{40}Ar+^{165}Ho the two reaction types are well separated. The complete fusion events are centered around half the mass of the compound nucleus and show no dependence on the center of mass angle θ. Experiments[1] have shown that the width of the mass distribution of the fusion-fission events increases when the incoming angular momentum was increasing. With the help of a microscopic calculation of the driving force which tends to change the shape parameters of a rotating heated nucleus one can show that one should expect this

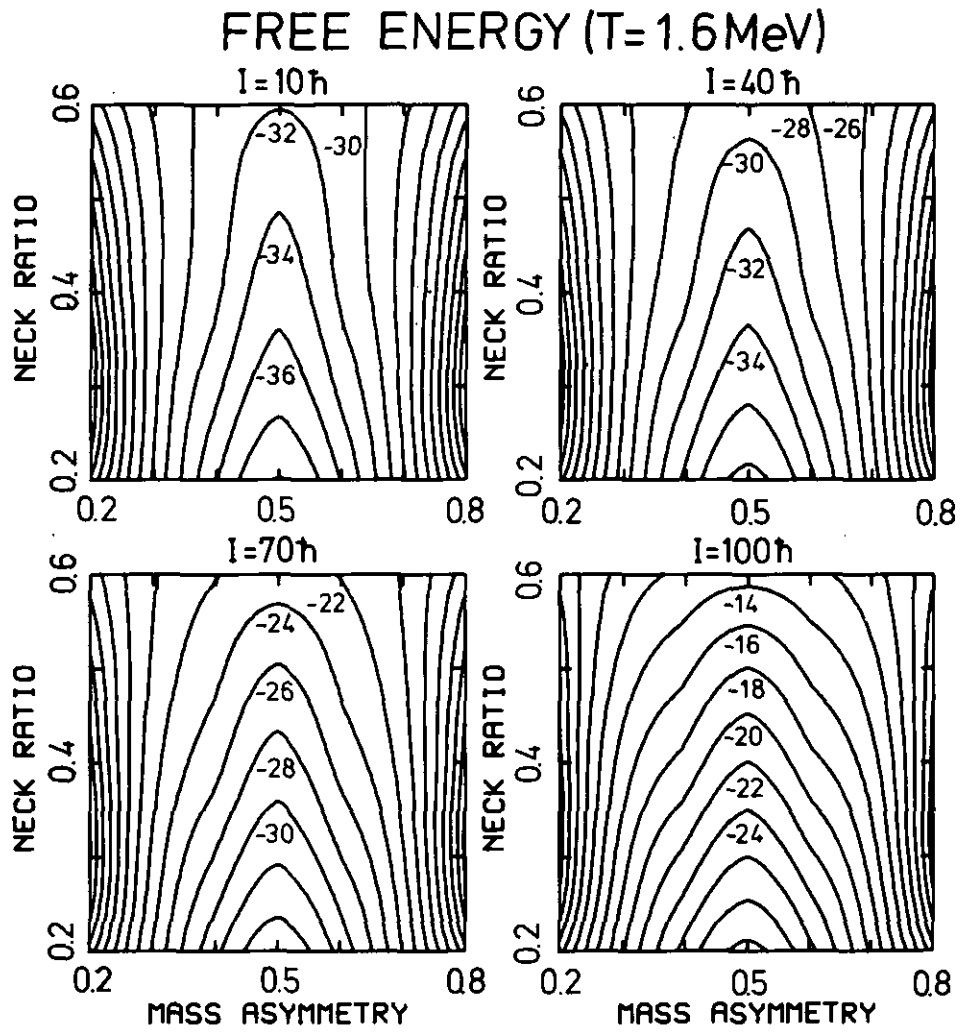

Fig. 1: Free energy surfaces of ^{205}At for mass asymmetric shapes along the fission valley at a temperature of 1.6 MeV. The elongation β varies together with the neck ratio r according to $\beta = 1.6-r$. The angular momenta I = 10, 40, 70, 100ħ are shown.

increase of the width of the mass distribution with increasing angular momentum. In fig. 1 equi-energy lines of the free energy are drawn along the fission valley for four angular momenta. The neck ratio[2] is plotted as ordinate and the mass asymmetry coordinate as abscissa. For low angular momenta the equi-energy lines are narrow parabolae. The driving force $\vec{p} = -\partial F/\partial \vec{q}|_T$ acting in the deformation parameter space $\vec{q}$ on a mass asymmetric compound nucleus has a strong component towards symmetry and a very small component along the fission valley. The width of the equi-energy parabolae increases slowly for low angular momenta and faster for high angular momenta I. Therefore, the component of the driving force towards symmetric fission decreases. Simultaneously the bottom of the valley descends steeper. The neck narrows faster, since the component of the driving force in the direction of the fission valley increases. An asymmetric compound nucleus at high angular momenta has less tendency and less time to develop towards symmetric fission[3].

References

1) C. Lebrun et al., Nucl. Phys. A321 (1979) 207.

2) M.E. Faber, M. Ploszajczak, A. Faessler, Nucl. Phys. A326 (1979) 129.

3) M.E. Faber, submitted to Phys. Rev. C.

+ Atominstitut der österr. Universitäten, Wien, Austria

3.23. Microscopic Calculation of Rotational Bands

F. Grümmer, K.W. Schmid+, A. Faessler+

A computer code has been developed which can be used for the description of rotational states within a given single particle basis giving an effective two-body Hamiltonian. The model uses angular momentum and particle number projection techniques applied to a basis of many-body wave functions consisting out of an HFB-reference wave function

$$|\phi_0\rangle = (\prod_\mu \beta_\mu)|\rangle \qquad (1)$$

and a set of two quasiparticle wave functions

$$|\phi_{\mu\nu}\rangle = \beta_\mu^+\beta_\nu^+|\phi_0\rangle \qquad (2)$$

Within this space a variation after projection is performed yielding wave functions for a given total angular momentum J of the type

$$|\Psi^J\rangle = \hat{P}_J\hat{Q}_N\hat{Q}_Z\left(C_0^J|\phi_0\rangle + \sum_{\mu\nu} C_{\mu\nu}^J|\phi_{\mu\nu}\rangle\right) \qquad (3)$$

where $\hat{P}_J$ is the angular momentum projection operator and $\hat{Q}_N$ and $\hat{Q}_Z$ are the particle number projection operators for neutron and proton numbers. The general formalism is described in more detail in refs. 1-2. Given a spherical single particle basis and an effective Hamiltonian the calculations are completely parameterfree and proceed in the following way:

1) A Hartree-Fock-Bogoliubov calculation is performed in order to obtain the reference wave function (1).
2) The effective Hamiltonian is transformed to the quasiparticle basis resulting from the HFB-calculation.
3) The projected overlap and energy matrices are built up for either the complete or a truncated basis of two quasiparticle states.
4) The resulting matrices are diagonalized giving energies and total wave functions of the form (3).
5) Finally the spectroscopic amplitudes

$$\langle\Psi^{J'}||[C_a^+C_b]^L||\Psi^J\rangle \qquad (4)$$

are calculated, which in turn may be used to calculate moments and transitions. They provide the complete information about the calculated wave functions.

It should be noted that the same effective Hamiltonian is used for the HFB-calculation and for the calculation of the energy matrices. This guarantees a fully self-consistent, parameterfree calculation. The program is planned to be applied to the description of low-lying rotational bands in heavy deformed nuclei in order to obtain more insight in the systematics of the backbending phenomenon, as well as to the description of the giant resonance region in light deformed N≠Z nuclei, which were up to now not accessible with the model of ref. 3.

References

1) F. Grümmer, K.W. Schmid, A. Faessler, IKP Annual Report 1979, Jül-Spez-72 (1979) 86.
2) F. Grümmer, K.W. Schmid, A. Faessler, preprint, Universität Tübingen.
3) K.W. Schmid, G. Do Dang, Phys. Rev. C15 (1977) 1515.

+ Inst. für Theor. Physik, Univ. Tübingen

3.24. g-Factors and Transition Probabilities in the $i_{13/2}$-Model

F. Grümmer, K.W. Schmid+, A. Faessler+

During the recent years simple models investigating the behaviour of particles in a single j-shell coupled to a rigid rotor have been quite helpful in understanding the mechanism and the systematic behaviour of the backbending phenomenon[1-3]. Thus it seems to be worth-while to calculate also moments and transitions with such a model in order to get some insight in the systematics of those quantities. We used a model proposed earlier[2] in order to calculate the variation of magnetic moments and B(E2)-values within the ground state rotational bands throughout the $i_{13/2}$-region. The wave functions of this model can be written as

$$|\Psi_{JMNi}\rangle = \sum_{\substack{R,N\\I,N_v,\alpha\\(N_c+N_v)=N}} C_{JMNi}^{R,N_c,I,N_v,\alpha}\left(|R,N_c\rangle|I,N_v,\alpha\rangle\right)_{JM} \qquad (1)$$

where R, I and J are the angular momenta of the core, the valence shell and the total angular momentum, N_c, N_v and N are the corresponding particle numbers and α and i are additional labels for the valence states and the total wave function. The coefficients c are obtained by diagonalizing a pairing + quadrupole Hamiltonian.

One can now easily calculate transitions and moments utilizing the wave functions (1). An extremely simple expression one obtains for the g-factors, namely

$$g_J = \frac{1}{2}(g_c+g_v) + \frac{1}{2}(g_c-g_v)\frac{\langle\Psi_{JMNi}|\tilde{R}^2-\tilde{I}^2|\Psi_{JMNi}\rangle}{J(J+1)} \qquad (2)$$

where the g-factors for the core and the valence-shell are chosen to be $g_c = 0.42$ and $g_v = -0.3$, which are appropriate for the rare-earth region and an $i_{13/2}$-neutron shell.

First we performed calculations with a fixed even number of particles in the valence shell coupled to a rotor. The resulting g-factors within the yrast band as function of the total angular momentum are plotted in fig. 1. One finds a strong angular momentum dependence for two neutrons in the $i_{13/2}$-shell, the g-factor becoming even negative at high spin values. With increasing valence-shell occupation the curves become smoother and for a

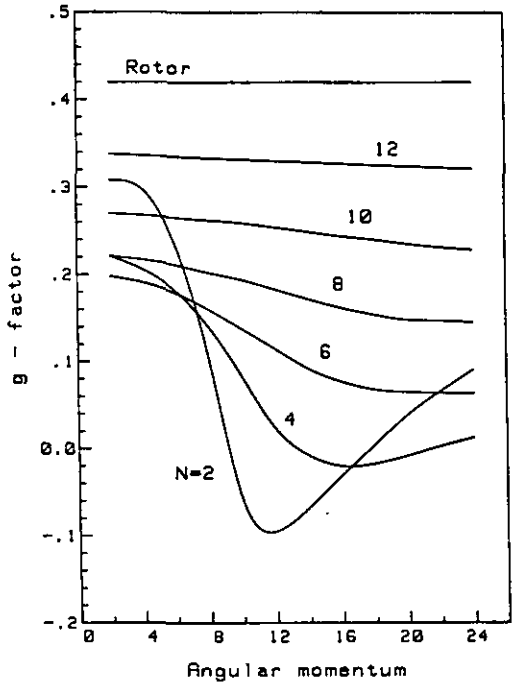

Figure 1

nearly filled valence-shell the g-factor stays approximately constant. This reflects that the g-factor as a function of the angular momentum depends strongly on the degree of rotational alignment.

If one includes the possibility of scattering pairs of particles between core and valence-shell the behaviour of the g-factors is not much affected. We do not observe any behaviour which is connected with the oscillations of the yrast-yrare interaction[1,3].

On the other hand, the behaviour of the B(E2)-values within the yrast band reflects those oscillations very sensitively. For values of the chemical potential where the yrast-yrare interaction is large, we obtain only a reduction of the B(E2)-values of 10 % at the critical angular momentum, whereas the reduction can be more than 50 % when the yrast-yrare interaction is roughly zero.

Summarizing we may say that the g-factors within the yrast band should decrease strongly for nuclei at the beginning of the rare-earth region and remain constant for the heavier nuclei, whereas the B(E2)-values should vary strongly for all nuclei which exhibit a sharp backbending behaviour.

References

1) R. Bengtsson, I. Hamamoto, B. Mottelson, Phys. Lett. 73B (1978) 259.

2) F. Grümmer, K.W. Schmid, A. Faessler, Nucl. Phys. A317 (1979) 287.

3) F. Grümmer, K.W. Schmid, A. Faessler, Nucl. Phys. A326 (1979) 1.

+ Inst. für Theor. Physik, Univ. Tübingen

4. NUCLEAR REACTIONS

4.1. Elastic and Inelastic Breakup Processes in Nucleus-Nucleus Collisions

G. Baur, F. Rösel[+], *R. Shyam*[++], *D. Trautmann*[+]

In peripheral nucleus-nucleus collisions the fragmentation of the projectile is a dominant reaction process. The quasifree interaction of a part of the projectile (nucleon, or cluster of nucleons), which can be elastic or inelastic, leads to strongly forward peaked energy spectra of the spectator particle. The peak energy is around the energy $E_b = \frac{m_b}{m_a} E_a$, where E_a is the energy of the incident projectile. With the help of unitarity and the peripheral nature of the process the sum over all inelastic channels can be performed, in order to calculate the inclusive spectra. We study (d,p), (^{3}He,d), (^{3}He,p), (α,^{3}He) and (α,t) inclusive spectra. ^{6}Li-induced breakup spectra of d, t, ^{3}He and α-particles at $E_{^6Li}$ = 156 MeV are studied in collaboration with B. Neumann and H. Rebel (Institut für Angewandte Kernphysik, Kernforschungszentrum Karlsruhe).

Simple gross properties are found for the breakup probabilities, like $A^{1/3}$-dependence and "factorization". For further details see ref. 1.

Reference

1) G. Baur, R. Shyam, F. Rösel, and D. Trautmann, Phys. Rev. C21 (1980) 2668, and submitted to Helv. Phys. Acta.

+ Institut für Theor. Physik, Univ. Basel, Switzerland

++ SRC Daresbury Laboratory, Warrington, England

4.2. Coulomb Dissociation of the Deuteron

B. Hoffmann, G. Baur

In general, deuteron breakup is well explained in terms of the post form DWBA[1,2,3], which is a good approximation as long as the final state interaction V_{np} can be neglected. Recently, experiments[4,5] with 15 MeV deuterons on ^{232}Th showed that the approach cited above underestimates the observed inclusive proton spectra for rather low energies, $E_p \lesssim 6$ MeV. It is shown that in this region of energy the dominant breakup mechanism is Coulomb excitation of the deuteron into a continuum state.

The Hamiltonian H describing scattering of deuterons from a heavy target nucleus A is:

$$H = H_o + V_{np} + V_{pA} + V_{nA} \qquad (1)$$

where H_o denotes the kinetic energy and V_{xy} the interaction between particles x and y. To discuss breakup as consequence of Coulomb excitation, we choose the same channel Hamiltonian for the entrance channel α and the exit channel β

$$H_\alpha = H_\beta = H_o + V_{np} \; ; \; V_\alpha = V_\beta = V_{nA} + V_{pA} \qquad (2)$$

where $V_{\alpha(\beta)}$ denotes the corresponding channel interactions. As distorting potential we choose

$$W = V_{dA} = Ze^2/R \; ; \; \vec{R} = 1/2\,(\vec{r}_p + \vec{r}_n) \qquad (3)$$

The transition amplitude for the process d+A→A+p+n is given by:

$$T_{\beta\alpha}^{-DWBA} = \langle \chi_\beta^- | V_\alpha - W | \chi_\alpha^+ \rangle = \langle \chi_\beta^- | V_\beta - W | \chi_\alpha^+ \rangle$$
$$= T_{\beta\alpha}^{+DWBA} = \langle \chi_\beta^- | V_{nA} + V_{pol} | \chi_\alpha^+ \rangle \qquad (4)$$

V_{pol} denotes the polarization potential

$$V_{pol} = Ze^2\,(1/r_p - 1/R) \qquad (5)$$

Actual calculations were done neglecting the nuclear part of the interaction and approximating V_{pol} by its dipole term

$$T_{\beta\alpha} = \frac{4\pi}{3} Ze^2 \langle \chi_{\vec{k}_f}^-(\vec{R}) \varphi_{\vec{k}}(\vec{r}) | \frac{r}{2} Y_{1m}(\hat{r}) | \varphi_o(\vec{r}) \chi_{\vec{k}_i}^+(\vec{R}) \rangle \qquad (6)$$

Here $\chi^\pm$ denote pure Coulomb scattering wave functions for the deuteron's c.m. motion. φ_o describes the deuteron ground state:

$$\varphi_o = \left(\frac{\alpha}{2\pi(1-r_o\alpha)}\right)^{1/2} \frac{e^{-\alpha r}}{r} \qquad \begin{matrix} \alpha = 0.2317\ \mathrm{fm}^{-1} \\ r_o = 1.79\ \mathrm{fm} \end{matrix} \qquad (7)$$

including corrections for finite range. The results given in fig. 1 show that the model of Coulomb dissociation gives the order of magnitude for the breakup cross section. The shape of the angular distribution cannot be reproduced so well, one reason being that inelastic processes (excitation of the target nucleus) are not taken into account. Both effects are included in the calculations according to refs. 2,3. We included nuclear effects using a strong absorption model (SAM, see e.g. ref. 6) in our calculations.

The conclusion, at least for the reaction[4,5] investigated here, is that breakup processes cannot be described over the whole region of energy by one step DWBA models. One has to include either higher order terms or one must solve integral equations of Faddeev type.

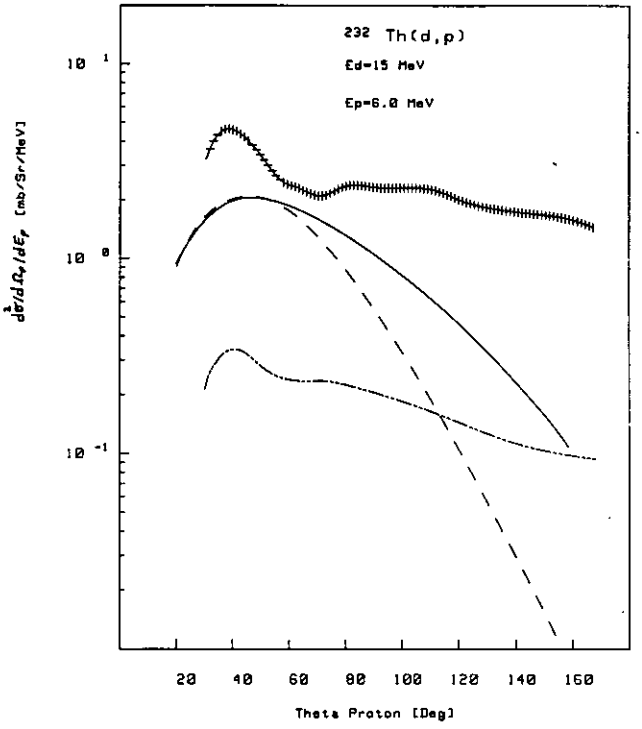

Fig. 1: Comparison of various theoretical approaches for breakup reactions with experiment.
+++++++ experiment (refs. 4, 5)
— -- — calculated according to refs. 2, 3
———— Coulomb dissociation
-------- Coulomb dissociation and SAM.

References

1) G. Baur, D. Trautmann, Phys. Rev. 25C (1976) 293.

2) J. Pampus, J. Bisplinghoff, J. Ernst, T. Mayer-Kuckuk, J. Rama Rao, G. Baur, F. Rösel, D. Trautmann, Nucl. Phys. A311 (1978) 141.

3) U. Bechstedt, H. Machner, G. Baur, R. Shyam, C. Alderliesten, A. Djaloeis, P. Jahn, C. Mayer-Böricke, F. Rösel, D. Trautmann, Nucl. Phys. A343 (1980) 221.

4) J. Bisplinghoff, J. Ernst, J. Kleinfeller, T. Mayer-Kuckuk, Proc. Int. Conf. Nucl. Phys., Aug. 24-30, 1980, Berkeley, California, USA, p. 905.

5) J. Kleinfeller, Diplomarbeit, unpublished.

6) K. Alder, D. Trautmann, Ann. Phys. 66 (1971) 884.

4.3. Theoretical Study of Line Shapes in $^{13}C(\alpha,\alpha')$ Inelastic Scattering to Resonant States

H. Lenske[+] and G. Baur

The line shape of the $J^{\pi} = 3/2^+$, $E_x = 7.677$ MeV resonance excited by inelastic scattering of α-particles shows an asymmetry with a dip on the high energy side. This is in contrast to the line shape of that resonance as seen in the $^{12}C(n,n)^{13}C$ elastic scattering and the corresponding $^{12}C(d,p)^{13}C$ reaction, where the dip is on the low-energy side. The asymmetric line shape in the inelastic α-scattering, which can be parametrized by a (complex) parameter q [1] is explained theoretically as the interference of a continuum transition and the excitation of a quasibound configuration, in close analogy to the analysis by Fano[2] of asymmetric line shapes in inelastic electron-atom scattering. The line shape parameter q is sensitive to nuclear models and thus is a new tool in the study of nuclear wave functions. For details see ref. 3.

References

1) G. Baur and H. Lenske, Nucl. Phys. A282 (1977) 201.
2) U. Fano, Phys. Rev. 124 (1961) 1866.
3) H. Fuchs, J.A. Nolen, G.J. Wagner, H. Lenske, and G. Baur, Nucl. Phys. A343 (1980) 133.

[+] Present address: Center for Nuclear Studies, University of Texas at Austin, USA

4.4. The Role of the Coulomb Interaction in Isospin-Violating Direct Nuclear Reactions[1]

H. Lenske[+] and G. Baur

Possible sources of isospin mixing in direct nuclear reactions are investigated. We find that there are mainly two effects which enter coherently into the direct reaction amplitude: "induced isospin mixing" caused by the Coulomb interaction between the target and the projectile, and "wave function effects" of the target nuclear states. These arise mainly through the difference of corresponding neutron and proton single-particle wave functions. These differences are especially noticeable just in the surface region where direct reactions take place. As illustrative examples we perform model calculations for the pickup reactions $^{13}C(d,^3H)^{12}C^*(1^+,15.11\ MeV)$ and $^{13}C(d,^3He)^{12}B_{g.s.}(1^+)$ and the inelastic scattering $^{12}C(d,d')^{12}C^*$ leading to the 1^+ states at 12.71 MeV and 15.11 MeV. These model calculations are compared with the corresponding experimental data.

Reference

1) H. Lenske and G. Baur, Nucl. Phys. A344 (1980) 151.

[+] Present address: Center for Nuclear Studies, University of Texas at Austin, USA

4.5. Theoretical Study of the Elastic and Inelastic Breakup of the ^{3}He Particle[1]

R. Shyam[+], G. Baur, F. Rösel[++], and D. Trautmann[++]

Within the framework of the post form distorted-wave Born approximation theory of breakup reactions[2] we study the elastic and inelastic breakup of the ^{3}He particle. With a standard set of parameters for the optical model potential we are able to understand coincidence and inclusive data for this process which were recently measured by Matsuoka et al.[3] at the incident ^{3}He energy of 90 MeV. The elastic breakup accounts only for about 20 % of the total inclusive (^{3}He,d) yield. With our theory we are able to understand quantitatively the breakup process of the ^{3}He particle; a dominant peripheral reaction mechanism. As an example we show in fig. 1, taken from ref. 1, a comparison of our theoretical calculations for inclusive (^{3}He,d) spectra with the experimental results of ref. 3.

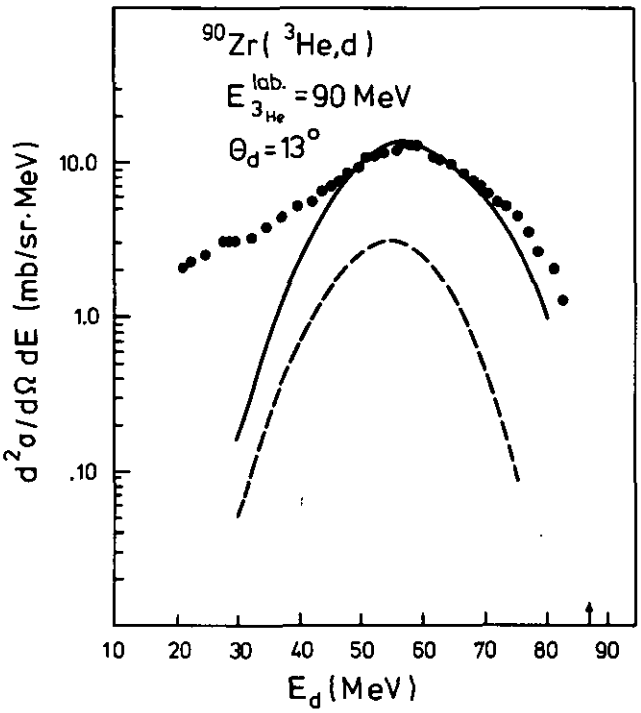

Fig. 1: Comparison of experimental $^{90}Zr(^3He,d)$ inclusive spectra[3]) with our theoretical calculations (continuous line) for inclusive breakup. The theoretically calculated contribution due to elastic breakup alone is shown separately in the dashed line.

References

1) R. Shyam, G. Baur, F. Rösel, and D. Trautmann, Phys. Rev. C22 (1980) 1401.
2) see G. Baur, F. Rösel, R. Shyam, and D. Trautmann, this annual report p. 104
3) N. Matsuoka, A. Shimizu, K. Hosono, T. Saito, M. Kondo, H. Sakaguchi, A. Goto, and F. Ohtani, Nucl. Phys. A337 (1980) 269;
N. Matsuoka, A. Shimizu, K. Hosono, T. Saito, M. Kondo, H. Sakaguchi, Y. Toba, A. Goto, F. Ohtani, and N. Nakanishi, Nucl. Phys. A311 (1978) 173.

[+] SRC Daresbury Laboratory, Warrington, England
[++] Institut für Theor. Physik, Univ. Basel, Switzerland

4.6. D-State Effects in (d,t) and (d,^{3}He)Reactions

A.A. Iaonnides[+], M.A. Nagarajan[+], and R. Shyam[+]

The measurements of the tensor analyzing power for (d,t) reactions have shown[1] that they are sensitive to the D-state components in the triton wave function. In the lowest approximation the components T_{2q} yield a value for the D_2 parameter of -0.24 fm^2 where D_2 is defined by

$$D_2 = \frac{1}{15}\frac{\int_0^\infty u_2(r)r^4dr}{\int_0^\infty u_0(r)r^2dr} \qquad (1)$$

where u_0 and u_2 are the S and D state components of the relative motion of neutron and deuteron in the triton, i.e.

$$R(\vec{r}) = \langle \chi^{\sigma_n}_{1/2}\varphi^{\sigma_d}_d(\vec{\rho})|\varphi^{\sigma_t}_t(\vec{r},\vec{\rho})\rangle$$

$$= \sum_{L=0,2}\sum_{\Lambda,\sigma} u_L(r)Y_{L\Lambda}(\hat{r})\langle L\Lambda S\sigma|1/2\sigma_\tau\rangle \qquad (2)$$

$$\times \langle 1\ \sigma_d\ 1/2\ \sigma_n|S\sigma\rangle$$

$$\psi(\vec{p},\vec{q}) = (p^2+\tfrac{3}{4}q^2+E_\tau)^{-1}\Big[u_s(\vec{p},\vec{q})\frac{1}{\sqrt{2}}\Big(\big|\chi_{1d}^{1/2}\eta_{1d}^{1/2-1/2}\big\rangle - \big|\chi_{1s}^{1/2}\eta_{1s}^{1/2-1/2}\big\rangle\Big) + v''(\vec{p},\vec{q})\frac{1}{\sqrt{2}}\Big(\big|\chi_{1s}^{1/2}\eta_{1s}^{1/2-1/2}\big\rangle - \big|\chi_{1d}^{1/2}\eta_{1d}^{1/2-1/2}\big\rangle\Big)$$

$$+ v'(\vec{p},\vec{q})\frac{1}{\sqrt{2}}\Big(\big|\chi_{1s}^{1/2}\eta_{1d}^{1/2-1/2}\big\rangle - \big|\chi_{1d}^{1/2}\eta_{1s}^{1/2-1/2}\big\rangle\Big) + \sqrt{4\pi}\sum_\mu \langle 2\ \mu\, 3/2 m_\tau-\mu|1/2 m_\tau\rangle\big|\chi_{1d}^{3/2 m_\tau-\mu}\big\rangle$$

$$\times\Big[W_{\mu'}(\vec{p},\vec{q})|\eta_{1s}^{1/2-1/2}\rangle - W_{\mu''}(\vec{p},\vec{q})|\eta_{1d}^{1/2-1/2}\rangle\Big]\Big] \qquad (3)$$

where the χ*'s and* η*'s are the spin and isospin* functions. u_s is the wave function for the totally symmetric S-state, v" and v' are two components of the mixed symmetric S' state and $W_{\mu'}$ and $W_{\mu''}$ are the two components of the D-state. The explicit form for this wave function may be found in ref. 2. We calculate the overlap function $R(\vec{r})$ from this wave function and extract the functions $u_0(r)$ and $u_2(r)$. The deuteron wave function used in this calculation is given by

$$\Phi_d(p) = (p^2+\epsilon_d)^{-1}\Big[g_{d_0}(p)\phi_{1M_d} + \sqrt{32\pi}\,p^2 g_{d_2}(p) \qquad (4)$$

$$\times \sum_\mu \langle 2\ \mu\ 1\ M_d-\mu|1\ M_d\rangle Y_{2\mu}(\hat{p})\phi_{1M_d-\mu}\Big]\chi_{T=M=0}$$

After having calculated $u_0(r)$ and $u_2(r)$ the D_2 parameter defined by eq. (1) is simple to calculate. The results[3] are shown in table 1. In this table we show the results of our calculation for D_0 (zero range normalization constant) and D_2 parameters with two sets of triton and deuteron wave functions corresponding to different D-state probabilities. It can be seen that our results for D_2 are in a good agreement with the value obtained by fitting the experimental results[1]. Also the S'-state of the triton has only a 10 % effect on D_2 parameter whereas it is quite substantial for D_0 parameter.

% D-state deuteron	% D-state triton(^{3}He)	Reaction type	D_0 (MeV·fm$^{3/2}$) with S'-state	D_0 (MeV·fm$^{3/2}$) without S'-state	D_2 (fm^2) with S'-state	D_2 (fm^2) without S'-state
4.0	5.09	(d,^{3}He)	-153.73	-137.87	-.221	-.238
		(d,t)	-163.22	-147.52	-.219	-.236
7.0	9.6	(d,^{3}He)	-151.26	-136.55	-.203	-.216
		(d,t)	-160.42	-146.03	-.202	-.215

Table 1

The calculation of D_2 from a number of variational triton wave functions yields values which are smaller than the empirically extracted value of -0.24 fm^2 by a factor of 2. The reason for this discrepancy may be due to the fact that the "best variational" triton wave functions optimize the binding energy and the charge radius of the triton and do not necessarily yield the correct asymptotic wave function. D_2, on the other hand, depends upon the 4th (2nd) moment of $u_2(r)(u_0(r))$, and hence is expected to be inaccurate when evaluated from a wave function which is not correct in the asymptotic region.

In the present study, we use the triton wave function given by Phillips[2]. This wave function has been obtained as an approximation to the solution of the Faddeev equation and consists of the S, S' and D states. It is designed to include the observed two and three nucleon properties in the manner in which the spectator wave function is parametrized, and it is correct in the asymptotic region. In momentum space it is given by

The exact finite range analysis of the (d,t) and (d,^{3}He) data using the wave functions $U_0(r)$ and $U_2(r)$ is in progress.

References

1) L.D. Knutson, B.P. Hichwa, A. Barroso, A.M. Eiro, P.D. Santos, and R.C. Johnson, Phys. Rev. Lett. 35 (1975) 1570.

2) A.C. Phillips and F. Roig, Nucl. Phys. A234 (1974) 378.

3) A.A. Iaonnides, M.A. Nagajaran, and R. Shyam, Nucl. Phys. A (to be published).

[+] SRC Daresbury Laboratory, Warrington, England

4.7. Nuclear Structure Approach to the Calculation of the Imaginary α-Nucleus Optical Potential

H. Dermawan, F. Osterfeld, V.A. Madsen[+]

A microscopic calculation of the second-order imaginary optical potential for $^{40}Ca(\alpha,\alpha)$ is made for incident energies of 31 and 100 MeV using RPA transition densities[1] for intermediate excited states. Since we treat the α-particle as elementary, no exchange effects are included explicitly. The α-nucleon interaction is normalized by fitting the inelastic cross section to the first 3^- collective state with a folded M3Y potential[2] at each energy. We use an optical Green's function for the intermediate α-particle propagator, which for α-scattering gives rather different results than a free-particle propagator or a pure-Coulomb propagator does.

In second order the generalized imaginary optical potential is given as

$$W(\vec{r},\vec{r}') = \mathrm{Im} \sum_N \langle \Psi_0|V|\Psi_N\rangle_{\vec{r}}\, G_N(\vec{r},\vec{r}')\langle \Psi_N|V|\Psi_0\rangle_{\vec{r}'}$$

where Ψ_N are the intermediate states of the target, $G_N(\vec{r},\vec{r}')$ is the intermediate projectile Green's function with kinetic energy $E-E_N$, and V is the α target-nucleon interaction. We find that the resulting imaginary potential is highly non-local and that the local approximation usually made for nucleons is doubtful. The local approximation was nevertheless used to calculate an "equivalent" local potential.

In figs. 1 and 2 the comparison of the local equivalent potentials W(r) with phenomenological potentials for E_α = 31 and 100 MeV is shown. Results of calculations with both RPA and pure particle-hole intermediate states are included. Collectivity of the RPA wave function still plays a role even at 100 MeV incident energy. The sum over intermediate RPA states gives a considerably larger cross section than the sum over the corresponding pure particle-hole states.

In contrast to the results for 30 MeV (n,n) scattering[3], the resulting imaginary optical potential is sensitive to the type of the intermediate Green's function used in its calculation. The imaginary potential of the microscopically calculated equivalent local potential has been used in the calculation of the elastic scattering cross section. Figs. 3 and 4 show comparisons of elastic scattering differential cross sections calculated with each of the potentials of figs. 1 and 2 with data[4,5]. At 31 MeV the RPA-theoretical potential gives 92 % of the reaction cross section of the phenomenological potential and agrees fairly well with the experimental data; the particle-hole theoretical potential gives 80 %. At 100 MeV the RPA-theoretical potential gives only 78 % of that of the phenomenological one, indicating too little absorption.

At 31 MeV incident energy, we would not expect large contribution from breakup processes, and the RPA-theoretical potential should account quite well for the absorptive strength. On the other hand, at 100 MeV the limitation of the RPA basis to 3 $\hbar\omega$ probably makes the RPA spectrum inadequate to describe the intermediate inelastic strength. Furthermore, at 100 MeV, breakup channels not included in our calculation will undoubtedly make a substantial contribution to absorption from the elastic channel. It is likely that breakup accounts for a large fraction of the absorption outside the nucleus and for the long range of the phenomenological imaginary potential[6]. We conclude that the nuclear structure approach including only inelastic channels as doorways to absorption gives a sensible description of the imaginary optical potential at lower energies. When E_α is much greater than the binding energy of the α-particle, breakup effects are expected to make important contributions to α-absorption. Serious questions remain concerning the adequacy of the local approximation[7] which we have used. The highly nonlocal form of this potential suggests that test using the calculation nonlocal $W(\vec{r},\vec{r}')$ in a fully nonlocal calculation would be valuable in assessing the validity of a local optical model for α and heavy-ion elastic scattering.

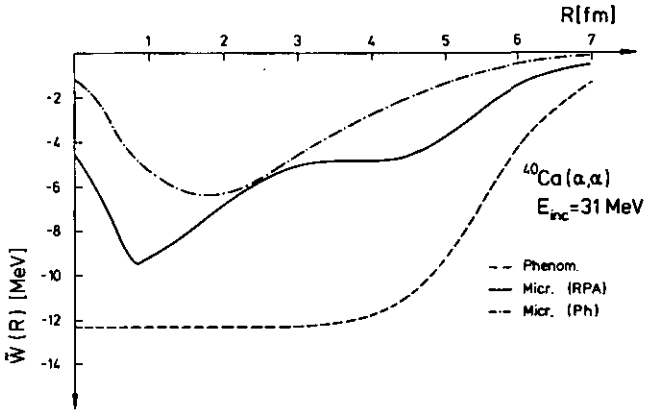

Figure 1

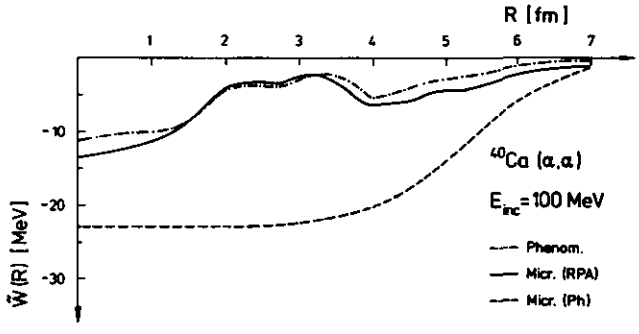

Figure 2

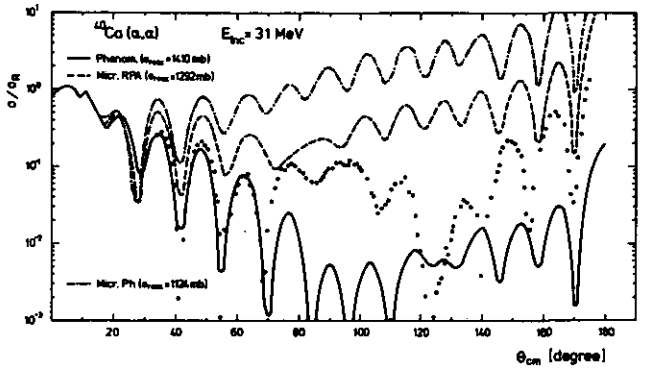

Figure 3

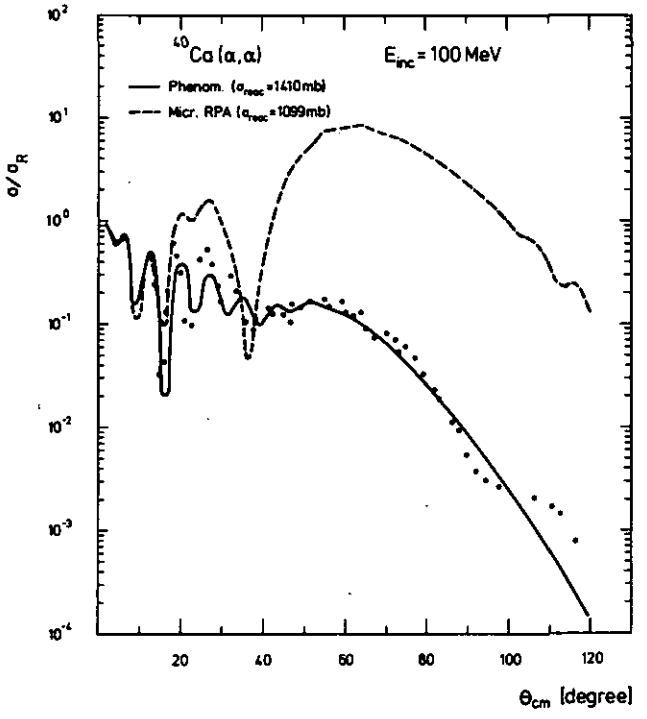

Figure 4

References

1) S. Krewald, J. Speth, Phys. Lett. 52B (1974) 295.

2) G. Bertsch, J. Borysowicz, H. McManus, W.G. Love, Nucl. Phys. A284 (1977) 399.

3) F. Osterfeld, J. Wambach, V.A. Madsen, submitted to Phys. Rev.

4) H.O. Meyer, Proc. 2nd Louvain-Cracow Seminar, Université de Louvain.

5) H. Eickhoff, W. Frekers, H. Löhner, K. Poppensieker, R. Santo, G. Gaul, C. Mayer-Böricke, P. Turek, Nucl. Phys. A252 (1975) 333.

6) G. Baur, R. Shyam, F. Rösel, D. Trautmann, Phys. Rev. C21 (1980) 2668.

7) F. Perey and W.S. Saxon, Phys. Rev. C1 (1970) 1377.

+ Univ. of Oregon, Corvallis, USA

4.8. General Properties of Energy Independent Nuclear Optical Model Potentials

S.Y. Lee[+], F. Osterfeld, K. Tam[+], T.T.S. Kuo[+]

In a recent paper[1] we formulated a new microscopic theory of the optical potential for elastic nucleon-nucleus scattering which, in contrast to the Green's function formalism[2] and also Feshbach's formalism[3], leads to a formally energy-independent optical potential. This energy-independent potential is complex and non local, and can be written in an exact diagrammatic perturbation expansion based on the Rayleigh-Schrödinger (folded diagram) type of perturbation theory. Here we investigate the specific properties of the energy independent potential in more detail, in particular we study its threshold effects and also derive a generalized dispersion relation for it. In order to do this we follow ref. 1 and transform the (A+1)-many body problem into a one body, model-space problem which, when antisymmetrization between the projectile nucleon and the nucleons in the target is neglected, is given by

$$(T_o+V_{opt})P|\Psi^{(+)}_{A+1}(E)\rangle = E\,P|\Psi^{(+)}_{A+1}(E)\rangle \ . \qquad (1)$$

In eq. (1) T_o is the kinetic energy operator of the incident nucleon, V_{opt} the optical potential operator, $\Psi^{(+)}_{A+1}(E)$ the full (A+1)-body wave function, and P the projection operator defined by

$$P = \int d\vec{k}\,|\vec{k},\Psi^o_A\rangle\langle\vec{k},\Psi^o_A|\,;\ \langle\vec{r}|\vec{k}\rangle = \frac{1}{(2\pi)^{3/2}}\,e^{i\vec{k}\cdot\vec{r}} \qquad (2)$$

with $|\Psi^o_A\rangle$ being the true ground state of the target nucleus.

In order to derive the energy independent potential we introduce the Möller wave operator Ω which is defined by the equation

$$|\Psi^{(+)}_{A+1}\rangle = \Omega\,P|\Psi^{(+)}_{A+1}\rangle \ . \qquad (3)$$

In Feshbach's theory[3] of the optical potential, the Möller wave operator, $\Omega^{(+)}_F$, is energy dependent, i.e.

$$\Omega^{(+)}_F = P + \frac{1}{E^+-QHQ}\,QVP\ ;\ P+Q=I \qquad (4)$$

One can, however, also construct an energy independent wave operator. Following Lee and Suzuki[4], we may write the operator Ω in the form

$$\Omega = P + Q\omega P \qquad (5)$$

where the second term on the right hand side (rhs) of eq. (5), QωP, is an operator which transforms the P-space wave function $P|\Psi^{(+)}_{A+1}\rangle$ into the Q-space wave function $Q|\Psi^{(+)}_{A+1}\rangle$. To obtain an equation for Ω, or QωP, we use eq. (5) in eq. (3) and the fact that $|\Psi^{(+)}_{A+1}\rangle$ fulfills the Schrödinger equation

$$H\Omega P|\Psi^{(+)}_{A+1}(E)\rangle = E\Omega P|\Psi^{(+)}_{A+1}(E)\rangle = \Omega PH\Omega P|\Psi^{(+)}_{A+1}(E)\rangle \qquad (6a)$$

The last equality sign in eq. (6) is obtained by replacing $EP|\Psi^{(+)}_{A+1}(E)\rangle$ in the first line of eq. (6) with $EP|\Psi^{(+)}_{A+1}(E)\rangle = P(H\Omega)P|\Psi^{(+)}_{A+1}(E)\rangle$. It is <u>this</u> step which eliminates the energy dependence from our equations and which leads to an energy independent, but nonlinear operator equation[4] for the Möller wave operator Ω

$$H\Omega P = \Omega PH\Omega P \qquad (6b)$$

By acting with the projection operators P and Q on eqs. (6) from the left we obtain the following two equations (hereafter, we use $|\phi^{(+)}_E\rangle = P|\Psi^{(+)}_{A+1}(E)\rangle$ for brevity)

$$(PH\Omega P)|\phi^{(+)}_E\rangle = E|\phi^{(+)}_E\rangle \qquad (7a)$$

$$Q\Omega PH\Omega = QH\Omega \qquad (7b)$$

The first equation, (7a), states the model state problem while eq. (7b) is a defining equation for the effective interaction to be used in solving eq. (7a). It is obvious that eq. (7b) is nonlinear in Ω, and that it is independent of the energy E. Using eq. (5) in eqs. (7) *we may rewrite eqs. (7) in the form*

$$\big|PT_oP + PVP + PV(Q\omega P)P\big|\,|\phi^{(+)}_E\rangle = E|\phi^{(+)}_E\rangle \qquad (8a)$$

$$QVP + QHQ(Q\omega P) = Q\omega P\big[PT_oP + PVP + PV(Q\omega P)P\big] \qquad (8b)$$

Eq. (8b) can be solved for QωP which, when inserted into eq. (8a), leads to the energy independent optical model equation. The energy independent optical potential is then given by

$$V_{opt} = PVP + PVQ\omega P \ . \qquad (9)$$

The operator QωP has a rather complicated structure. When QωP operates on an <u>eigenstate</u> of eq. (8a) we obtain formally

$$(Q\omega P)|\phi^{(+)}_E\rangle = \frac{1}{E^{(+)}-QHQ}\,QVP|\phi^{(+)}_E\rangle \qquad (10)$$

It is important to notice that the whole set of solutions $|\phi^{(+)}_E\rangle$ with variable E forms a complete basis of the P space. This fact allows us to write the operator QωP in its spectral representation

$$Q\omega P = \int dE'\,\frac{QV}{E'^{(+)}-QHQ}\,|\phi^{(+)}_{E'}\rangle\langle\tilde{\phi}^{(+)}_{E'}| \qquad (11)$$

where $\langle\tilde{\phi}^{(+)}_E\rangle$ is the biorthogonal vector to $|\phi^{(+)}_E\rangle$ normalized such that $\langle\tilde{\phi}^{(+)}_{E'}|\phi^{(+)}_E\rangle = \delta(E'-E)$. Insertion of the rhs of eq. (11) into eq. (9) gives us the energy independent optical potential

$$V_{opt} = PVP + \int dE'\ PV\,\frac{Q}{E'^{(+)}-QHQ}\,V|\phi^{(+)}_{E'}\rangle\langle\tilde{\phi}^{(+)}_{E'}| \qquad (12)$$

To discuss the general properties of V_{opt} we introduce a complete system of eigenfunctions of the Q-space Hamiltonian QHQ. Inserting this into eq. (12) we obtain

$$
\begin{aligned}
V_{opt} &= PVP + \sum_{\mu} \sum_{i} \frac{PV|q_i><q_i|V}{E'_{\mu}-\varepsilon_i} \; |\phi_{E'_{\mu}}> <\tilde{\phi}_{E'_{\mu}}| \\
&+ \int_0^{\infty} dE' \sum_{i} \frac{PV|q_i><q_i|V}{E'^{(+)}-\varepsilon_i} \; |\phi^{(+)}_{E'}><\tilde{\phi}^{(+)}_{E'}| \\
&+ \sum_{\mu} \int d\alpha \int_0^{\infty} d\varepsilon \frac{PV|\varepsilon,\alpha><\alpha,\varepsilon|V}{E'_{\mu}-\varepsilon} \; |\phi_{E'_{\mu}}> <\tilde{\phi}_{E'_{\mu}}| \\
&+ \int_0^{\infty} dE' \int d\alpha \int_0^{\infty} d\varepsilon \frac{PV|\varepsilon,\alpha><\alpha,\varepsilon|V}{E'^{(+)}-\varepsilon} \; |\phi^{(+)}_{E'}><\tilde{\phi}^{(+)}_{E'}|
\end{aligned}
\tag{13}
$$

Here, the sums over μ and i represent the sums over the bound state wave functions of the P-space and of the Q-space, respectively.

Several observations are now in order, which are also partly found for the energy dependent optical potentials[3]:

(1) The numerators in expansion (13) are positive definite, i.e. for an arbitrary wave function $|\chi>$ we have

$$
<\chi|PV|q_i><q_i|VP|\chi> = |<\chi|PV|q_i>|^2 \geq 0 \tag{14}
$$

(2) The first three terms in expansion (13) contribute only to the real part of the optical potential.

(3) The only term which contributes to real absorption in the sense that incident flux goes to energetically open inelastic channels is the fourth term on the rhs of eq. (13). The imaginary part of V_{opt} is given by the energy conserving contribution to this term

$$
\begin{aligned}
\mathrm{Im}\, V_{opt} &= -\pi \int\!\!\int dE' \, d\alpha \; PV|E',\alpha> \\
&<\alpha,E'|V|\phi^{(+)}_{E'}><\tilde{\phi}^{(+)}_{E'}|
\end{aligned}
\tag{15}
$$

(4) Projecting eq. (13) from left and right onto the elastic channel wave function $|\phi^{(+)}_E>$ we obtain the well known energy dependent optical potential

$$
\begin{aligned}
V_{opt}(E) &= P_E V P_E + \sum_{i} \frac{P_E V|q_i><q_i|VP_E}{E^{(+)}-\varepsilon_i} \\
&+ \int_0^{\infty} d\varepsilon \int d\alpha \frac{P_E V|\varepsilon,\alpha><\varepsilon,\alpha|VP_E}{E^{(+)}-\varepsilon}
\end{aligned}
\tag{16}
$$

where $P_E = |\phi^{(+)}_E><\tilde{\phi}^{(+)}_E|$. From eq. (16), it is clear that the scattering process of a nucleon with incident energy E is governed effectively by the same optical potential in the energy dependent and energy independent version of the optical model theory. Therefore the energy independent potential includes the same threshold effects as the energy dependent potentials do.

Finally we formulate a type of dispersion relation. From eq. (13) we find the real part of the optical potential as

$$
\begin{aligned}
\mathrm{Re}\, V_{opt} &= PVP + \mathcal{P}\!\!\!\!\!\!- \int dE \sum_{i} \frac{PV|q_i><q_i|V|\phi^{(+)}_E><\tilde{\phi}^{(+)}_E|}{E-\varepsilon_i} \\
&+ \mathcal{P} \int dE \int d\varepsilon \frac{\int d\alpha \; PV|\varepsilon,\alpha><\varepsilon,\alpha|V|\phi^{(+)}_E><\tilde{\phi}^{(+)}_E|}{E-\varepsilon}
\end{aligned}
\tag{17}
$$

with $\mathcal{P}$ meaning Cauchy principal value. The imaginary part Im V_{opt} has already been given in eq. (15). By comparison of eqs. (15) and (17) it is evident that Im V_{opt} involves a single integration over the energy E' while the last term of Re V_{opt} in eq. (17) involves a double integration over energies E and ε. Therefore a "simple" replacement of the kernel of the principal value integral by Im V_{opt} is not possible as it is in the energy dependent optical potentials[3]. However, one can add a zero term to eq. (17)

$$
\begin{aligned}
\mathrm{Re}\, V_{opt} &= PVP + \mathcal{P}\!\!\!\!\!\!- \int dE' \sum_{i} \frac{PV|q_i><q_i|V|\phi^{(+)}_E><\tilde{\phi}^{(+)}_E|}{E'-\varepsilon_i} \\
&+ \sum_{\mu} \int_0^{\infty} d\varepsilon \int d\alpha \frac{PV|\alpha,\varepsilon><\alpha,\varepsilon|V}{E_{\mu}-\varepsilon} \; |\phi_{E_{\mu}}><\tilde{\phi}_{E_{\mu}}| \\
&+ \int_0^{\infty} dE' \int d\varepsilon \frac{d\alpha \; PV||\alpha,\varepsilon><\alpha,\varepsilon|-|\alpha,E'><\alpha,E'||V|\phi^{(+)}_{E'}><\tilde{\phi}^{(+)}_{E'}|}{E'-\varepsilon}
\end{aligned}
\tag{18}
$$

It can be noticed that the subtractive term in the numerator of the last term of eq. (18) integrated over E' is just the imaginary part of eq. (15). This term actually does not contribute to the principal value double integral because it is a "zero term", but it has the nice feature that it makes the numerator vanish for $\varepsilon = E'$ so that the kernel in the double integral is smoothed and therefore well behaved. It is interesting to multiply eq. (18) from left and right with the projection operator $P_E = |\phi^{(+)}_E><\tilde{\phi}^{(+)}_E|$ since then we recover the dispersion relation for the energy dependent potentials

$$
\begin{aligned}
\mathrm{Re}(P_E V_{opt} P_E) &= P_E V P_E + \sum_{i} \frac{P_E V|a_i><q_i|VP_E}{E-\varepsilon_i} \\
&- \frac{1}{\pi} \mathcal{P} \int \frac{\mathrm{Im}(V_{opt}(\varepsilon))}{E-\varepsilon} \, d\varepsilon
\end{aligned}
\tag{19}
$$

Because of the fact that eq. (18) implicitly contains the dispersion relation in eq. (19) we may view eq. (18) as a generalized dispersion relation for the energy independent optical potential.

References

1) T.T.S. Kuo, F. Osterfeld, S.Y. Lee, Phys.Rev.Lett. 45 (1980) 786;
S.Y. Lee et al., Phys. Rev. to be published.

2) J.S. Bell and E.J. Squires, Phys.Rev.Lett. 3 (1959) 96;
J.S. Bell, Lectures on the Many-Body Problem, ed. by E.R. Caianello (Academic, New York, 1962).

3) H. Feshbach, Ann.Rev.Nucl.Sci. 8 (1958) 49;
H. Feshbach, Ann.Phys. 5 (1958) 357, and 19 (1962) 287.

4) S.Y. Lee and K. Suzuki, Phys.Lett. 91B (1980) 173.

+ SUNY at Stony Brook, Stony Brook, USA

4.9. Nuclear Structure Approach to the Coulomb Correction of the Imaginary Nucleon-Nucleus Optical Potential

F. Osterfeld, V.A. Madsen[+]

The difference in neutron and proton optical potentials due to the Lane symmetry potential V_1+iW_1 has been known for some time[1,2,3]. It is usually determined empirically by analyzing proton optical potentials for different nuclei as a function of the neutron excess N-Z or by comparing neutron and proton optical potentials of a fixed nucleus, for which the Lane term has opposite sign. Besides the Lane term, a Coulomb correction[2] is made in the real part of the proton optical potential accounting for the difference in kinetic energy of neutrons and protons in the region of the nucleus. This correction is necessary because the nuclear part of the optical potential is energy dependent, and the presence of a Coulomb potential means that a proton senses the nuclear potential at an energy reduced by the average Coulomb potential in the nucleus.

In this contribution[7] we calculate the Coulomb effect on the imaginary optical potential[4] for a finite nucleus using the so-called nuclear structure approach to the optical potential as basis for our calculations[5]. Differences between proton and neutron imaginary optical potentials are expected due to the following charge-dependent effects: Coulomb excitation, dependence of the intermediate projectile Green's function on the Coulomb potential, Coulomb shifts of the states of the intermediate nuclei excited by charge exchange, and isospin impurities in intermediate states of the target. We have calculated the various Coulomb effects using the microscopic, fully antisymmetric formulation of the imaginary optical potential of ref. 5 which uses an optical Green's function for describing the propagation of the intermediate particle. The optical Green's function includes, of course, the Coulomb potential in case of a propagating proton. The energetically open, intermediate target states are described by RPA doorway states, which have been obtained by using empirical single particle energies and a nuclear plus Coulomb potential for protons. Thus, Coulomb effects due to both target and projectile are taken into account properly.

Our method of calculating the optical potential for a finite nucleus seems ideally suited to study the Coulomb dependence of the potentials, since all the Coulomb effects are rather realistically included in the different phases of the calculations. In addition, we have the advantage that the spectrum of intermediate particle-hole strength is fairly realistically described by the RPA transition densities[6].

To eliminate other Coulomb effects and to study Coulomb excitation alone, we calculated the imaginary potential with a free-particle Green's function and used the same force for proton and neutron scattering. In our calculations Coulomg excitation was largest beyond the nuclear surface where it amounted to about a 3 % effect, which is negligible.

The isospin purity effect has been tested by using a free particle Green's function for the intermediate projectile propagator both for neutrons and protons and turning of the Coulomb excitation. Only inelastic intermediate states are included in the comparison, so the only difference which can appear between (n,n) and (p,p) optical potentials comes from the lack of isospin purity of the RPA transition densities. However the effect is found to be very small and can be neglected.

In nuclear matter many intermediate states are excluded due to the constant, repulsive, background Coulomb potential, which effectively lowers the energy of protons and closes out high lying states. For scattering from finite nuclei, however, no states are actually excluded asymptotically since the Coulomb potential goes to zero at $r = \infty$. At finite radii high lying intermediate states may be effectively closed for protons because of the Coulomb repulsion. To isolate this effect a comparison of neutron and proton nonlocal potentials has been made with no Coulomb excitation. The results were unexpected and were characteristic of essentially all our calculated potentials: the diagonal nonlocal potential W(r,r) was greater for neutrons than for protons only at small radii $r \leq 2$ fm but at higher values of r it was larger for protons. In retrospect these results are not so surprising: the small-radius behaviour is the expected exclusion effect and at the larger radii the proton wave function is typically larger than that of the neutron, reflecting the larger amount of time spent by the slower moving proton in the repulsive Coulomb field. (In the WKB approximation this property is expressed by way of a $k(x)^{-1/2}$ factor in the wave function.)

This effect is, in addition, accentuated upon calculation of the local-equivalent imaginary potential, for which smaller local wave numbers are favoured leading to a larger absorbing potential for protons. These two effects are so great that, if it were not for charge exchange, the absorption would always be greater for protons than for neutrons.

A nuclear projectile not only can excite the nucleus inelastically, it can also exchange in charge with a nucleon in the target before returning to the elastic channel. In a self-conjugate nucleus like ^{40}Ca, charge exchange for neutrons, (n,p), (p,n) is favoured over (p,n), (n,p) because the analogue states formed in charge exchange are lower by twice the Coulomb energy for the former compared to the latter. In fact, at the projectile energies considered in our calculations the (p,n), (n,p) contribution is entirely negligible while the (n,p), (p,n) makes an important effect.

In table 1 we present volume integrals of the various contributions to the imaginary optical potential at 17.7 and 25 MeV incident energies.

J_n/A					J_n/J_p	
E(MeV)	(n,n')(n',n)	(n,p)(p,n)	(n,n)[a]	(p,p)	calc.	emp.[b]
17.7	25.5	18.1	43.6	35.2	1.23	1.26±18
25	32.0	15.6	47.2	48.8	.98	1.18±17

Table 1: Volume integrals of W.
a = sum of columns 2 and 3.
b = ref. 4.

The volume integrals are about 35 % smaller than those for the empirical potentials which are consistent with ref. 5. The agreement of the calculated and empirical ratios is reasonably good. At 17.7 MeV the neutron absorptive strength is somewhat stronger, but at 25 MeV the strengths are about equal, the proton value slightly larger. Such a trend is also seen in ref. 4 but the near equality starts at about 30 MeV. Since the nearly equal strengths come about differently for neutrons and protons, there is no reason to believe that a trend toward equality at $E \geq 25$ MeV should be expected. At very high energies, where the Coulomb potential is negligible, one would, of course, expect a trend toward $W_n = W_p$.

In summary we have shown that the Coulomb correction is complicated, that there are several Coulomb effects, some favouring larger W for protons and others favouring larger W for neutrons. In view of these results, a simple Coulomb correction, as has been made in the past for the real nuclear potential on the basis of the kinetic energy difference is not expected to be valid for the imaginary potential.

References

1) A.M. Lane, Phys.Rev.Lett. 8 (1962) 171.
2) F. Becchetti and G.W. Greenlees, Phys.Rev. 182 (1969) 1190.
3) D.M. Patterson, R.R. Doering, A. Galonsky, Nucl.Phys. A263 (1976) 261.
4) J. Rapaport, Phys.Lett. 92B (1980) 233.
5) F. Osterfeld, J. Wambach, V.A. Madsen, Phys.Rev. C23 (1981) 179.
6) S. Krewald, J. Speth, Phys.Lett. 52B (1974) 295.

+ SUNY at Stony Brook, Stony Brook, USA

4.10. Ionization of Atomic Inner Shells in Asymmetric Systems

F. Rösel[+], *D. Trautmann*[+], *G. Baur*

We study the ionization of inner shells by Coulomb excitation with light projectiles (p,α, ...)

$$(Z_t + e)_{K,L,\ldots\text{shell}} + Z_p \rightarrow Z_t + e + Z_p \qquad (1)$$

Starting from a quantum mechanical description (DWBA) a semiclassical approximation can be derived[1]. This corresponds to a classical (Rutherford) trajectory of the projectile, where a time-dependent perturbation acts on the target system. The transition of the electron into the continuum is caused by the interaction

$$\Delta V(\vec{r},\vec{R}) = -\frac{Z_p e^2}{\left|\vec{R} - \frac{m_t}{m_e+m_t}\vec{r}\right|} + \frac{Z_p Z_t e^2}{\left|\vec{R} + \frac{m_e}{m_t+m_e}\vec{r}\right|} \qquad (2)$$

where the distance between target nucleus and projectile is denoted by $\vec{R}$, the distance between target nucleus and electron is given by $\vec{r}$. The second term in eq. (2) denotes the recoil term, it becomes very important for small impact parameters (large scattering angles). In our formulation we can handle this term just as the first term. Another method to treat recoil effects is the use of an accelerated frame of reference[2,3]. We discuss the relation between the two methods. Furthermore, our theory contains the results of Migdal[4] and Levinger[5] as special cases.

References

1) D. Trautmann and F. Rösel, Nucl. Instr. and Methods 169 (1980) 259, and further references contained there.
2) P.A. Amundsen, J. Phys. B11 (1978) 3197.
3) M. Kleber and K. Unterseer, Z. Physik A292 (1979) 311.
4) A. Migdal, J. Phys. (USSR) 4 (1941) 449.
5) J.S. Levinger, Phys. Rev. 90 (1953) 11.

+ Inst. für Theor. Physik, Univ. Basel, Switzerland

5. HEAVY ION REACTIONS

5.1. The Real Part of the Low Energy HI Optical Potential

K. Goeke, P.-G. Reinhard[+], J.N. Urbano[++]

Elastic HI scattering is mostly described by means of an optical potential $V(r) = V(r) + iW(r)$ to be inserted into the scattering equation

$$\left(-\frac{\hbar^2}{2\mu}\frac{d^2}{dr^2} + V+iW + \frac{\hbar^2}{2\mu}\ell(\ell+1)\right)\chi_\ell(r) = E_{CM}\chi_\ell(r) \qquad (1)$$

with r being the distance between the heavy ions. In recent years there has been an increasing activity towards a microscopic understanding of V(r). Approaches of this kind are based on choosing an appropriate set of many body wave functions $|\phi(r)>$, obtained e.g. from constrained Hartree-Fock or density functional approaches[1-3]. Then a quantization procedure has to be invoked which allows one to derive V(r) from $|\phi(r)>$. As has been shown[4-6] in the past by ATDHF the scattering equation to be solved is

$$\left(-\frac{d}{dr}\frac{\hbar^2}{2M(r)}\frac{d}{dr} + V(r) - Z(r) + iW(r) + \frac{\hbar^2}{2\Theta(r)}\ell(\ell+1) - E_{CM}\right)\chi_\ell = 0 \qquad (2)$$

Here $V(r) = <\phi(r)|H|\phi(r)>$ with H being a two body microscopic Hamiltonian. The $M(r)$ and $\Theta(r)$ are mass parameters and rotational moment of inertia taken e.g. from dynamic theories like ATDHF or, less fundamental, from the cranking model. The $Z(r)$ contains the corrections to $V(r)$ due to spurious zero point energies contained in $V(r)$. Those are

$$Z(r) = Z_k(r) + Z_p(r) + Z_{rot}(r) \qquad (3)$$

with
$$Z_k(r) = \lambda(r)/4M(r)$$
$$Z_p(r) = V''(r)/4\lambda(r)$$
$$Z_{rot}(r) = \hbar^2<J^2>/2\Theta(r)$$

where $\lambda(r)$ is given by $\lambda(r) = 2<\phi(r)|\frac{\overleftarrow{\partial}}{\partial r}\frac{\overrightarrow{\partial}}{\partial r}|\phi(r)>$. The Z_k and Z_p are associated to the spurious radial relative motion of the two ions and Z_{rot} to the spurious rotational relative motion of the two ions.

Although the above considerations are well known, in most practical calculations the following simplifications are used: $M(r) \to \mu$, $Z(r) \to 0$ and $\Theta(r) \to \mu r^2$. The justification for this in case of the $^{16}O+^{16}O$ reaction is investigated in the present paper by means of the liquid drop model including Strutinski corrections based on the two-centre-shell model and pairing corrections. The $M(r)$ is shown in fig. 1 together with $\lambda(r)$. Both quantities show a peak at $r \sim 4$ fm which originates from both the internal change of the single particle wave functions and quasi level crossings. Actually the $\Theta(r)$ is quite different from $M(r)r^2$ invalidating some results of ref. 3. Fig. 2 shows the three zero point energy corrections. Altogether they show a variation of about 5 MeV and an increasing tendency with increasing r. The corresponding potentials are given in fig. 3 where a constant is added to Z in order to make it vanishing with $r \to \infty$ such that both the uncorrected $V(r)$ and the corrected $V(r)-Z(r)$ have asymptotically a Coulomb tail. Apparently the effects of $M(r)$ and $Z(r)$ on the mass and the potential are rather large and one does not see off hand a justification to neglect them. The only possibility is perhaps the presence of the imaginary part W(r) of the optical potential. This will be investigated in a separate contribution.

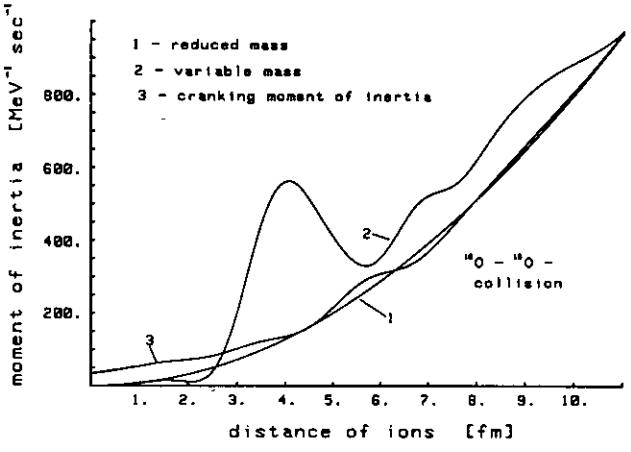

Figure 1

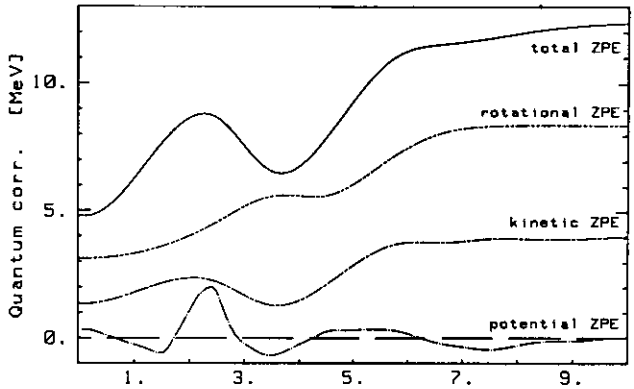

Figure 2

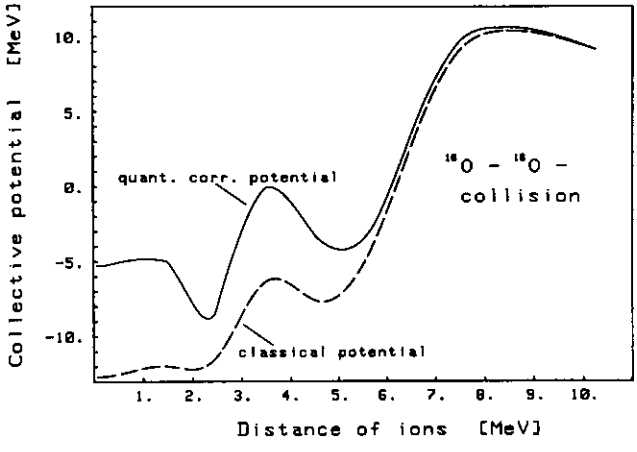

Figure 3

References

1) F. Stancu, D.M. Brink, Nucl. Phys. A270 (1976) 236.
2) J.F. Berger, D. Gogny, Nucl. Phys. A333 (1980) 302.
3) H. Flocard, P.H. Heenen, D. Vautherin, Nucl. Phys. A339 (1980) 336.
4) K. Goeke, P.-G. Reinhard, Ann. Phys. 112 (1978) 328.
5) P.-G. Reinhard, K. Goeke, J. Phys. G4 (1978) 245.
6) K. Goeke, P.-G. Reinhard, Ann. Phys. 124 (1980) 249.

+ Inst. für Kernphysik, Univ. Mainz
++ Lab. de Fisica da Univ., Coimbra, Portugal

5.2. Quantum Corrections to HI Elastic Scattering and Molecular Resonances in the ^{16}O-^{16}O-Reaction

K. Goeke, P.-G. Reinhard+, J.N. Urbano++

If one derives the real part of the optical potential from large amplitude collective theories like ATDHF[1-3] and adds ad hoc an imaginary part of the optical potential in order to take into account the nonelastic channels, one ends up with a scattering equation[1-3]

$$\left\{-\frac{d}{dr}\frac{\hbar^2}{2\,\theta(r)}\frac{d}{dr} + Y(r) - Z(r) + i\,W(r) + \frac{\hbar^2}{2\theta(r)}\,\ell(\ell+1) - E_{CM}\right\}\chi_\ell(r) = 0 \qquad (1)$$

Actually in practical calculations often the collective mass M(r) is replaced[4] by the reduced mass μ, the zero point corrections Z(r) are ignored and $\theta(r)$ is replaced by μr^2. The evaluation of these quantum corrections and their physical origin are described in a separate contribution. For low energy scattering the effect of these approximations is studied at the ^{16}O-^{16}O reaction. For the numerical solution the scattering equation is transformed by means of r↦R,

$$dR = \sqrt{\frac{M(r)}{\mu}}\,dr \qquad (2)$$

to a new one with $\tilde{M}(R) = \mu$ and with modified boundary conditions. The subsequent evaluation of the elastic scattering cross section is straightforward and can be seen at fig. 1 and fig. 2 for $E_{CM} = 20$ MeV using a volume- and a surface-absorbing imaginary part. In both cases the σ/σ_{Coul} is plotted resulting from the Schrödinger equation with and without quantum corrections. Apparently the corrections are quite remarkable for the surface-absorbing potential and less, but still noticeable, for the volume-absorbing one, which is taken from a phenomenological fit. For higher energies the effect becomes more pronounced, however, the adiabatic assumptions made in the derivation of the theory are less justified.

The effect of the quantum corrections can also be demonstrated at the width and position of the molecular resonances. Those can be identified by the minima of the reflection coefficient for a given partial wave L in dependence on the relative energy E_{CM}:

$$R_L(E_{CM}) = \left|e^{2i\delta_L(E_{CM})}\right| \qquad (3)$$

where $\delta_L(E_{CM})$ is the total phase shift of the elastic channel. Figs. 3 and 4 show various reflection coefficients for both kinds of absorbing potentials. For a surface absorbing one the resonances are clearly pronounced and are shifted in their position by about 2 MeV which is a change of 15-20 %. Also the slope of $R_L(E_{CM})$ is remarkably changed. For a volume absorbing potential the shifting is still there although the resonance as such is less pronounced since it is very broad and coincides with the overall fall off. In summary one must conclude that quantum corrections have to be taken into account in order to have a proper description of elastic HI properties.

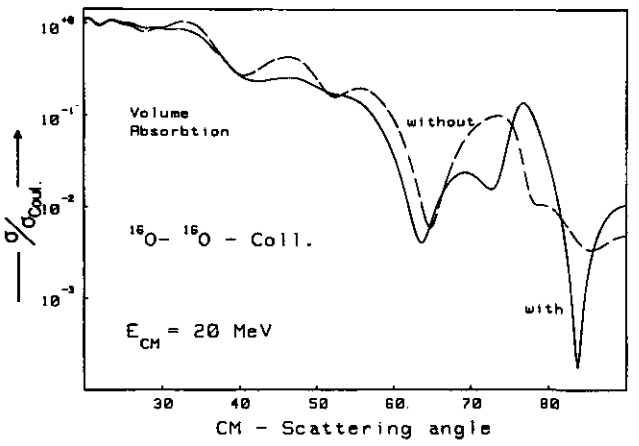

Figure 1

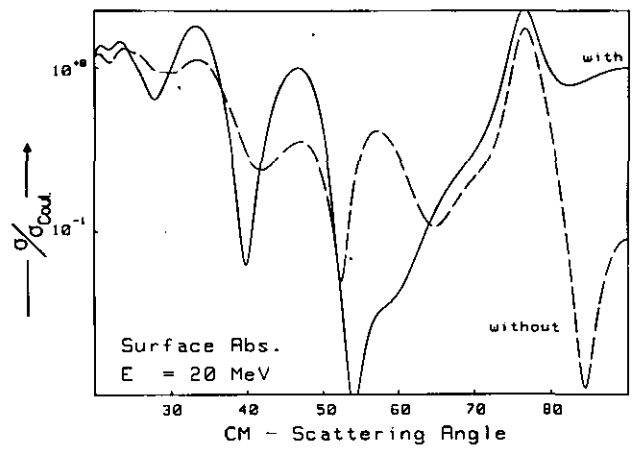

Figure 2

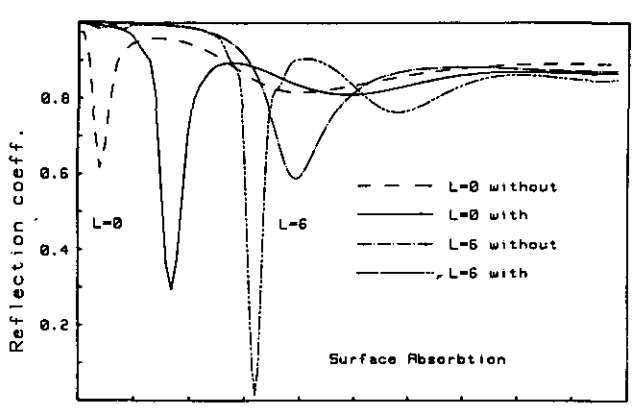

Figure 3

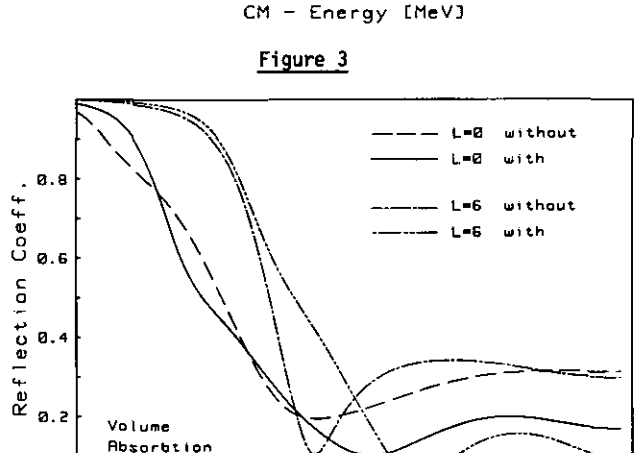

Figure 4

References

1) K. Goeke, P.-G. Reinhard, Ann. Phys. 112 (1978) 328.
2) P.-G. Reinhard, K. Goeke, J. Phys. G4 (1978) 245.
3) K. Goeke, P.-G. Reinhard, Ann. Phys. 124 (1980) 249.
4) F. Stancu, D.M. Brink, Nucl. Phys. A270 (1976) 236.

+ Inst. für Kernphysik, Univ. Mainz
++ Lab. de Fisica da Univ., Coimbra, Portugal

5.3. Calculation of Astrophysical S-Factors

K. Goeke, P.-G. Reinhard+, J.N. Urbano++

For the understanding of the abundance of elements in the universe and the various stages of the stellar evolution the knowledge of heavy ion fusion cross sections at energies of about 0.1-5 MeV is indispensible. Nevertheless, only little theoretical work has been done although even the experimental data are often very uncertain and need unjustified extrapolation to low energies[1]. Actually the situation is difficult since the fusion cross sections vary over several orders of magnitude over a change of E_{CM} of few hundred keV, since one faces a penetration process through the Coulomb barrier. This process can be described in the WKB approximation. There the total fusion cross section is given by

$$\sigma_{fus} = \pi\lambda^2 \sum_L (2L+1)\, T_L(E_{CM}) \qquad (1)$$

with

$$T_L(E_{CM}) = \exp\left(-2 \int_a^b I(r)dr\right) \qquad (2)$$

Here a and b are the classical turning points from inside and outside and the I(r) is given by

$$I(r) = \sqrt{2M(r)/\hbar^2}\ \sqrt{V(r)-Z(r)+L(L+1)\hbar^2/2\Theta(r)-E_{CM}} \qquad (3)$$

The $V(r)$ is the usual classical potential energy surface, which is in the present case obtained by liquid drop with Strutinski-corrections[2]. The M(r) is the Inglis mass calculated by two centre shell model, the $\Theta(r)$ is the rotational moment of inertia, the Z(r) are quantum corrections due to spurious relative and rotational motions in $V(r)$. As a matter of convenience one does not plot in general the $\sigma_{fus}(E_{CM})$ but rather the astrophysical S-factor being defined as

$$S(E_{CM}) = E_{CM}\, e^{2\pi\eta}\, \sigma_{fus})E_{CM}) \qquad (4)$$

with $\eta = Z_1 Z_2\, e^2/\hbar v$.

Fig. 1 shows the S-factor of the $^{16}O+^{16}O$ reaction. Beside the known experimental data the figure shows two theoretical curves. The lower one includes the quantum corrections whereas the upper one is obtained by assuming $M(r)\to\mu$, $\Theta(r)\to\mu r^2$ and $Z(r)\to 0$. Two conclusions can be drawn. First: The theoretical curve is about one order of magnitude smaller than the experimental data. This is probably due to the fact that the liquid drop plus Strutinski-procedure is not good enough for those light systems as $^{16}O+^{16}O$. One should expect an improvement if one uses a full ATDHF approach[3]. Second: The quantum corrections play an important role since they reduce the S-factor by an order of magnitude. This can be concluded although the absolute magnitude of S is wrong since the quantum corrections are a difference effect.

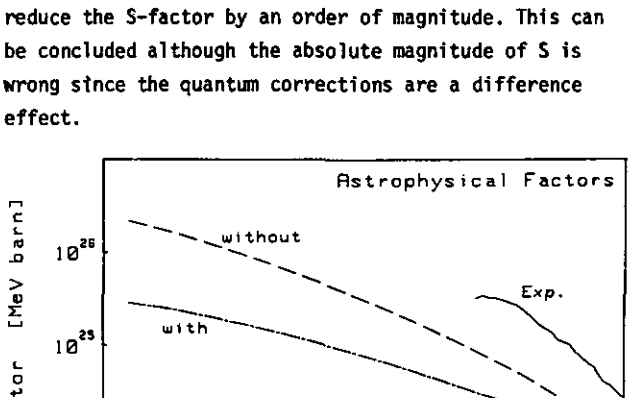

Figure 1

References

1) C. Rolfs, H.P. Trautvetter, Ann. Rev. Nucl. Part. Sci. 28 (1978) 115.

2) See this annual report.

3) P.-G. Reinhard, J. Maruhn, K. Goeke, Phys. Rev. Lett. 44 (1980) 1740.

+ Inst. für Kernphysik, Univ. Mainz

++ Lab. de Fisica da Univ., Coimbra, Portugal

5.4. TDHF Approaches to the Optimal Collective Path

K. Goeke, P.-G. Reinhard+, D.J. Rowe++

The present paper is concerned with a comparison of four adiabatic time dependent Hartree-Fock approaches for the description of large amplitude collective motion in terms of a collective path $|\phi(q)>$. The theories are formulated by Rowe and Bassermann and Marumori (RB), by Villars (VI), by Goeke and Reinhard (GR) and by Baranger and Veneroni (BV). Their common objective is to determine an optimal collective path $\{|\phi(q)>\}$ exclusively on the basis of an effective nucleon-nucleon interaction. The comparison is done in a two-dimensional potential landscape model and the results can be summarized as follows.

The Rowe-Bassermann-Marumori[1,2] approach defines the collective path by requiring the constraining operator to be the lowest solution of the local RPA equations. This path can be evaluated analytically in the potential landscape model. In general many body dynamics, however, it is less simple since it requires a double-iteration procedure at each point of the path. A graph is given in fig. 1 showing that it follows the bottom of the potential valley.

In the ATDHF approach of Villars[3] the collective path is defined by a coincidence of the constraining operator with the linear response to the collective momentum, the latter one being defined as the displacement operator along the path, i.e. $i\partial_q|\phi_q>$. This yields a coupled system of a constraint Hartree-Fock and a linear response equation which can be solved by double iteration procedure, according to a proposal of Villars. However the studies within the potential landscape model reveal an instability of this procedure, as can be seen at fig. 2. In addition the path is not uniquely defined.

The approach of Goeke and Reinhard[4-6] defines the collective path by a differential equation obtained by an adiabatic expansion of the TDHF equation. It provides in particular a criterion for adiabaticity which allows to select the collective initial conditions and to check the applicability of the theory to the considered phenomenon. The studies within the potential landscape model show that the collective path is the one which integrates the ATDHF differential equation from the saddle point to the potential minimum. This path optimizes the validity condition and it comes very close to the RB-path (see fig. 3). The latter feature means that the two approaches may be different in principle but in practice they seem to be interchangeable. However, the ATDHF differential equation of the GR-approach is preferable for reasons of numerical ease and computational speed. The similarity of the RB- and the GR-path allows a simple technique (the so-called "roll and kick" procedure) to approach rapidly the collective path.

The Baranger-Veneroni approach gives a trial-and-error procedure to find the collective path by superposing a bunch of classical trajectories with collective initial conditions and varying energies. The results in the potential landscape model do not show any remarkable bundling towards the collective path (see fig. 4). It is an open question whether some more selection criteria are needed to extract the collective path from a bunch of classical trajectories.

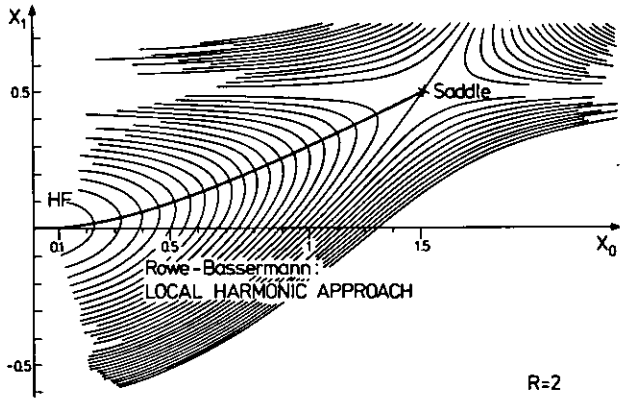

Figure 1

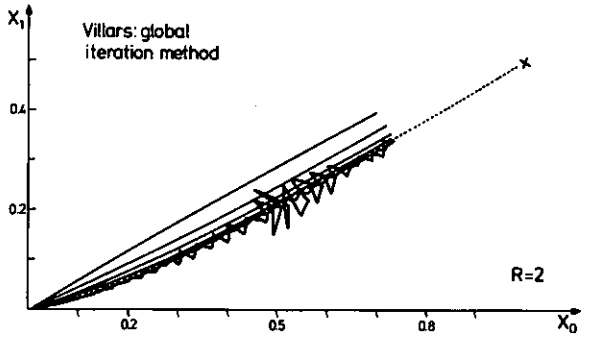

Figure 2

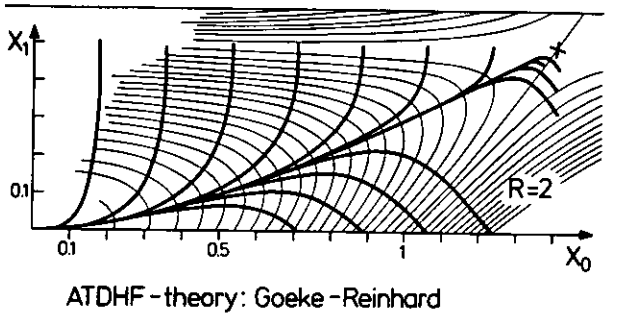

Figure 3

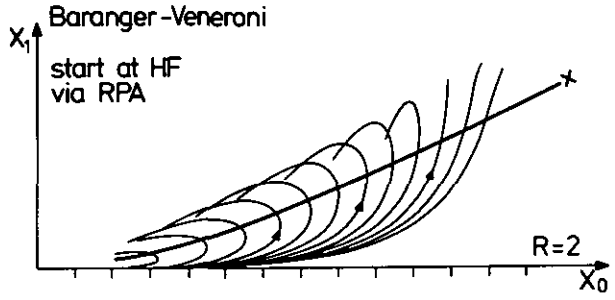

Figure 4

References

1) D.J. Rowe, R. Bassermann, Can. J. Phys. 54 (1976) 1941.

2) T. Marumori, Prog. Theor. Phys. 57 (1977) 112.

3) F. Villars, Nucl. Phys. A285 (1977) 269.

4) K. Goeke, P.-G. Reinhard, Ann. Phys. 112 (1978) 328.

5) P.-G. Reinhard, K. Goeke, Nucl. Phys. A312 (1978) 121, and Phys. Lett. B69 (1977) 17.

6) P.-G. Reinhard, K. Goeke, Phys. Rev. C20 (1979) 1546.

7) M. Baranger, M. Veneroni, Ann. Phys. 114 (1978) 123.

+ Inst. für Kernphysik, Univ. Mainz

++ Univ. of Toronto, Ontario, Canada

5.5. Time Dependent Ground State Correlations in an Extended TDHF Theory

R.Y. Cusson[+], *K. Goeke, P.-G. Reinhard*[++]

Time Dependent Hartree-Fock (TDHF) calculations for heavy ion reactions have gained great attention in the last years. In TDHF one approximates the time evolution of a many body system by a time dependent Slater determinant. This provides a reasonable description of one body properties, like multipole moments, fragment energies, fragment masses, mean scattering angles, etc. However, TDHF becomes inappropriate if one wants to describe properties which imply two body operators (or even higher ones), as e.g. spreading widths of one body operators. It is known by experience that TDHF applied to heavy ion scattering predicts far too small spreading width of particle number and internal excitation of the fragments and also a too small angular spread of the cross section.

Thus it is necessary to go beyond TDHF towards a theory which allows to describe two body correlations. Several attempts have been made in that direction; most of them try a statistical extension of TDHF, few of them aim at a quantum mechanical (coherent) description. We have concentrated on the second way and developed a theory of time dependent ground state correlations which is a dynamic extension of the RPA for stationary states[1]. In ref. 1 we have given a derivation using the equation-of-motion technique within the algebra of 1p-1h operators. In order to put the theory on a formally sound basis we have carried through an alternative derivation in the framework of a time dependent Generator-Coordinate-Method (GCM). This new derivation is explained shortly in the following and applied to some examples.

Usually GCM is a theory for stationary states, describing correlations by a continuous superposition

$$|\Psi\rangle = \int db\ |\Phi_b\rangle f(b)$$

of (collectively) deformed Slater determinants $|\Phi_b\rangle$. In the extension to a TD-GCM we describe time dependent ground state correlations by the superposition

$$|\Psi(t)\rangle = \int db |\Phi_b(t)\rangle f(b;t) \qquad (1)$$

where $|\Phi_b(t)\rangle$ is a TDHF trajectory for an initially deformed state $|\Phi_b(0)\rangle$; the type of deformations $|\Phi_b(0)\rangle$ determines the type of correlations described by the states (1). The interesting information about the size of the correlations is carried by the superposition function $f(b;t)$ whose time evolution is determined by the generalized Griffin-Hill-Wheeler equation

$$\int db'\{\langle\Phi_b(t)\hat{H}-i\partial_t|\Phi_{b'}(t)\rangle f(b';t) - \langle\Phi_b(t)|\Phi_{b'}(t)\rangle i\partial_t f(b';t)\} = 0 \qquad (2)$$

As in the stationary case we derive the RPA limit from the GCM by performing the Gaussian-Overlap-Approach up to second order in (b-b') for the kernels in eq. (2). This leads to a second order differential equation

$$(-\frac{1}{8}\left[\partial_b^2\mathcal{D}+2\partial_b\mathcal{D}\partial_b+\mathcal{D}\partial_b^2\right] - i\partial_t)\varphi(b;t) = 0 \qquad (3)$$

for the half-fold superposition function

$$\varphi(b;t) \sim \int db'\ \exp(-(b-b')^2/2\mu) f(b';t) \qquad (4)$$

with

$$\mathcal{D} = 2\mu^2\langle\Phi_b(t)|\hat{P}^2\hat{H}+\hat{H}\hat{P}^2|\Phi_b(t)\rangle \qquad (5)$$

$$\mu^{-1} = 2\langle\Phi_b(t)|\hat{P}^2|\Phi_b(t)\rangle \qquad (6)$$

where $H = H-\langle H\rangle$ and $\hat{P}|\Phi_b\rangle = i\partial_b|\Phi_b\rangle$. The parameter $\mathcal{D}$ can have both signs; a $\mathcal{D}>0$ broadens the distribution $|\varphi|^2$ whereas a $\mathcal{D}<0$ makes it sharper. It can be seen by eq. (5) that $\mathcal{D}$ "measures" exactly the 2p-2h part of $\hat{H}$ which, of course, is the driving force of 2p-2h correlations. A further step towards the RPA limit is to assume a Gaussian superposition

$$\varphi(b;t) \sim \exp(-b^2/2\alpha(t)) \qquad (7)$$

From eq. (3) we obtain for the width parameter $\alpha(t)$

$$\mathcal{R}e(\alpha(t)) = \alpha(0),\ \mathrm{Im}(\alpha(t)) = -\int_0^t dt'\,\mathcal{D}(0;t') \qquad (8)$$

Having all pieces to determine $|\Psi(t)\rangle$ we finally need to evaluate expectation values; in particular we are interested in the spreading width of a one body operator $\hat{A}$

$$\langle\Psi(t)|\Delta^2 A|\Psi(t)\rangle = \int dbdb' f^*(b,t)\langle\Phi_b(t)|\hat{A}^2_{ph}|\Phi_{b'}(t)\rangle f(b';t) \qquad (9)$$

We perform again a Gaussian-Overlap expansion of the kernel $\langle\Phi_b|\hat{A}^2_{ph}|\Phi_{b'}\rangle$, insert the Gaussian of eq. (7) and use the Quasi-Boson approach

$$\langle\Phi_b|[\hat{P},[\hat{A}^2_{ph},\hat{P}]]|\Phi_b\rangle = 2\,|\langle\Phi_b|[\hat{P},\hat{A}]|\Phi_b\rangle|^2$$

and

$$\langle\Phi_b|\{\hat{P},\{\hat{A}^2_{ph},\hat{P}\}\}|\Phi_b\rangle = 2|\langle\Phi_b|\{\hat{P},\hat{A}\}|\Phi_b\rangle|^2$$

This yields finally

$$\langle\Psi|\Delta^2\hat{A}|\Psi\rangle = \langle\Phi_o|\Delta^2\hat{A}|\Phi_o\rangle + \frac{1}{2}\left(\frac{\alpha^*\alpha}{\mathcal{R}e(\alpha)}-\mu\right)|\langle\Phi_o|[\hat{P},\hat{A}]|\Phi_o\rangle|^2$$
$$+ i\,\frac{\mathrm{Im}(\alpha)}{\mathcal{R}e(\alpha)}\,\mu\langle\Phi_o|\{\hat{P},\hat{A}\}|\Phi_o\rangle\langle\Phi_o||\hat{A},\hat{P}||\Phi_o\rangle \qquad (10)$$
$$+ \frac{1}{2}\left(\frac{1}{\mathcal{R}e(\alpha)}-\frac{1}{\mu}\right)|\mu\langle\Phi_o|\{\hat{P},\hat{A}\}|\Phi_o\rangle|^2$$

It is important to note that all quantities which we need, namely $\mu, \mathcal{D}$, $\langle[P,A]\rangle$ and $\langle\{P,A\}\rangle$, can be extracted from the knowledge of only two neighbouring TDHF trajectories $|\Phi_o(t)\rangle$ and $|\Phi_{\delta b}(t)\rangle$ by approaching $\partial_b|\Phi_b(t)\rangle|_{b=0} = (|\Phi_{\delta b}(t)\rangle - |\Phi_o(t)\rangle)|\delta b$. Thus the TD-GCM in the RPA limit can be easily implemented in existing TDHF codes.

For testing purposes, we have applied the above theory to heavy ion scattering in one dimension (SLAB-TDHF), using a two-body Yukawa force and a zero-range three-body force, a space grid representation for the single particle wave functions and the unitary time-step technique for solving the TDHF equations.

As a first test we have studied a case where the exact solution is known, viz. center-of-mass motion, exciting the deformation path by $|\phi_b(0)\rangle = (1-ib\hat{P}_{C.M.})|\phi_o(0)\rangle$. For the spreading width of $\hat{R}_{C.M.}$ one knows that $\Delta^2\hat{R}_{C.M.}(t) = \Delta^2 R_{C.M.}(0) + (\frac{t}{m})^2\Delta^2 P_{C.M.}$. This behaviour has been reproduced numerically with a precision of better than 1 % for a time interval of $5x10^{-22}$ sec, whereby Im(α) is the least precise quantity; the others (μ, $\langle[\hat{P},\hat{A}]\rangle$, $\langle\{P,A\}\rangle$) come much close to take exact value. This precision is also confirmed by other tests.

As a second test we have studied finite breathing oscillations. For these, the mean square diameter, Σx_i^2, is the collective operator. The $|\phi_o(t)\rangle$ is taken as a breathing TDHF vibration where $\langle \Sigma x_i^2\rangle$ oscillates in time; for the measuring operator we take the collective operator $\hat{A} = \Sigma\, x_i^2$ and the deformation path is initiated also by this $\hat{A}$, i.e. $|\phi_b(0)\rangle = (1-ib\hat{A})|\phi_o(0)\rangle$. The resulting time dependency of the spreading width $\Delta^2 A$ is given in the following figure.

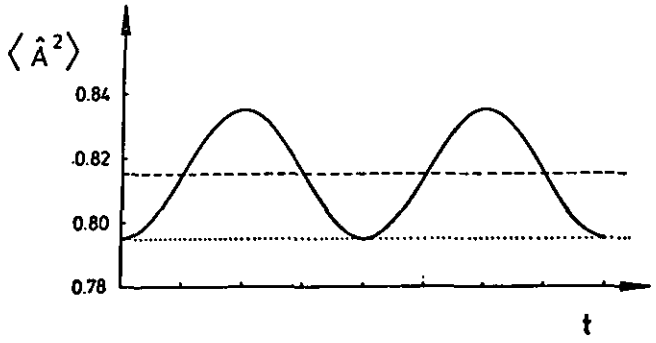

From pure TDHF we obtain the dotted line; this $\Delta^2 A$ is constant in time but too small, reflecting the fact that a determinantal condition enforces too small widths. The full line is obtained from a TD-GCM where we start with the pure TDHF state, $|\Psi(o)\rangle = |\phi_o(0)\rangle$, but allow correlations to develop in time; this exhibits nice oscillations due to the fact that we did not start with the proper spreading width. If we start $|\Psi(o)\rangle$ already correlated with the right $\Delta^2 A$, we obtain the dashed line which is constant in time (within 1 % precision) as .4 should be for a fairly harmonic motion. This picture shows clearly that the method is able to describe reliably (collective) correlations throughout all the many arithmetic operations involved in tracing two neighboured TDHF trajectories.

Finally we have studied the case of collision of two ions. As simplest example we took each ion to consist only in one "1s" state occupied with multiplicity 4, i.e. a "SLAB-α-particle". We have studied two different deformation paths, first relative center-of-mass excitation by $\hat{R}_{right}-\hat{R}_{lett}$ and second breathing excitation as above in each cluster separately. We have considered three measuring operators, the relative center-of-momentum $\hat{P}_{rel} = \hat{P}_{right}-\hat{P}_{left}$, the breathing in each cluster and the particle number shift $N_{right}-N_{left}$. We made following experience; For the $\Delta^2\hat{A}$ the dominating contribution comes always from that channel which also has been excited by $\hat{A}$, i.e. $a_b|\phi_o(0)\rangle \sim \hat{A}|\phi_o(0)\rangle$; all other channels give only small contributions (these many small contributions are best to be studied in a statistical theory). For the spreading width $\Delta^2\hat{P}_{rel}$ we obtain from TD-GCM a result which is 5-10 times larger than the TDHF result. That proves that coherent correlations can give a substantial increase of spreading widths in heavy ion reactions.

Reference

P.-G. Reinhard, K. Goeke, R.Y. Cusson, Z. Physik A295 (1980) 45.

+ Duke Univ., Durham, N.C., USA
++ Inst. für Kernphysik, Univ. Mainz

5.6. The Functional Approach and ATDHF

K. Goeke, F. Grümmer, H. Reinhardt[+], *P.-G. Reinhard*[++]

In the last years microscopic theories suitable for the description of large amplitude collective phenomena such as fission, soft vibrations, low energy HI scattering, subbarrier fusion, etc. have frequently been discussed. There appear to exist two distinct kinds of theories describing the same phenomena. One is the functional approach (FA) resulting in a sort of TDHF with periodic boundary conditions, the other is ATDHF. It is the objective of the present contribution to discuss the relationship between both approaches by performing an adiabatic approximation within the functional approach.

For a bound state with period T we have in the functional approach the periodic density matrix, i.e. $\rho(t+T) = \rho(t)$. If one extracts properly a phase one obtains also periodic single particle wave functions $|f_\nu(t+T)\rangle = |f_\nu(t)\rangle$ obeying the time dependent eigenvalue equation

$$(i\frac{\partial}{\partial t} - W)|f_\nu(t)\rangle = -\varepsilon_\nu|f_\nu(t)\rangle \qquad \nu = 1,\ldots,A \tag{1}$$

with W being the TDHF Hamiltonian, $W = T+Tr_v\rho$ and $\varepsilon_\nu = \varepsilon_\nu(T)$.

In ATDHF one starts from the assumption that for an adiabatic motion the intrinsic structure of the states involved should be independent of their classical velocity. Assuming the TDHF equation as equation of motion this yields the well known ATDHF equations for the Slater determinants constituting the collective path:

$$\frac{\partial}{\partial q}|\phi(q)\rangle = M(q)\,(\frac{\partial}{\partial q})^{-1}\,[H,W_{ph}]_{ph}|\phi(q)\rangle \tag{2}$$

where H is the total effective two-body Hamiltonian, the W is its HF part $W = T+Tr_v\rho$ and the suffix ph indicates the projection on the 1p-1h part.

An adiabatic expansion of the FA consists now in requiring $|f_\nu(t)\rangle = N(t)|\varphi_\nu(q(t),p(t))\rangle$ and inserting this into eq. (1). This gives $N = \exp(-iS)$ with $S = \int^t dt'\langle\varphi_\nu|W-\dot{q}P+\dot{p}Q-\varepsilon_\nu|\varphi_\nu\rangle$ and $P|\varphi_\nu\rangle = i\frac{\partial}{\partial q}|\varphi_\nu\rangle$ and $Q|\varphi_\nu\rangle = -i\frac{\partial}{p}|\varphi_\nu\rangle$. The equation corresponding to (1) is then

$$(W-\dot{q}P+\dot{p}Q)|\varphi_\nu\rangle = |\varphi_\nu\rangle\langle\varphi_\nu|Q-\dot{q}P+\dot{p}Q|\varphi_\nu\rangle \tag{3}$$

If one performs an expansion in powers of p, i.e. $|\varphi_\nu(q,p)\rangle = \varphi_\nu^0(q) + \ldots$ and considers each power separately one obtains

$$(W - \frac{\partial}{\partial q}Q)|\varphi_\nu^0(q)\rangle = |\varphi_\nu^0(q)\rangle\langle\varphi_\nu^0(q)|W - \frac{\partial V}{\partial q}Q|\varphi_\nu^0(q)\rangle \tag{4}$$

$$(|H,Q|_{ph} + \frac{i}{M}P)|\varphi_\nu^0(q)\rangle = |\varphi_\nu^0(q)\rangle\langle\varphi_\nu^0(q)||H,Q| + \frac{i}{M}P|\varphi_\nu^0(q)\rangle \tag{5}$$

Assuming furthermore Q to have only 1p-1h parts one can combine both equations to one equation for the 1p-1h part of P, which is sufficient to provide the ATDHF eq. (2). Thus the functional approach and ATDHF are closely related.

References

1) H. Reinhardt, Nucl. Phys. (1980).

2) K. Goeke, P.-G. Reinhard, Ann. Phys. 112 (1978) 328; Phys. Rev. C20 (1979) 1546.

[+] ZfK Rossendorf, Dresden, DDR

[++] Inst. f. Kernphysik, Univ. Mainz

5.7. Path Integral and Classical Dynamics of Many Fermion Systems

T. Suzuki

It is known that Feynman's path integral method is a very powerful approach for the investigation of the classical-quantum correspondence. The method has been extended to many fermion systems through the introduction of a set of Slater determinants as a basis of the quantum mechanical representation[1]. By applying a stationary phase condition to the path integral expression for the transition amplitude we can obtain the variational principle which leads to the time dependent Hartree-Fock equation. To define the path safely within a well defined state space we have utilized in ref. 1 the group theoretical information contained in the algebraic structure of the fermion pair operators. It is more convenient for a practical purpose, however, to express the quantities such as the invariant measure of the representation without asking for the group theory explicitly. For this aim we first pick up a set of path generators A_μ^+ ($\mu = 1,2,\ldots,M$) in such a way that they satisfy the following relations under a proper choice of the reference state $|0\rangle$:

$$\begin{aligned} &\text{a)}\ [[A,A^+],A^+] \sim \sum_\mu A_\mu^+ \\ &\text{b)}\ A|0\rangle = 0\ ,\ [A,A^+]|0\rangle \sim |0\rangle \end{aligned} \tag{1}$$

This allows us to define a set of states parametrized by complex numbers Z_μ ($\mu = 1,\ldots,M$) as

$$\{|Z\rangle = \mathcal{N}^{-1/2} \exp\Big(\sum_\mu Z_\mu A_\mu^+\Big)|0\rangle\} \tag{2}$$

where $\mathcal{N}$ is the normalization function dependent on Z_μ. From the relations (1) we can prove the relation

$$\begin{aligned} &\int |Z\rangle d\mu(Z)\langle Z| = 1 \\ &d\mu(Z) = \text{const} \cdot \det[g_{\mu\nu}] \cdot \prod_{\mu=1}^{M} dReZ_\mu dImZ_\mu \\ &g_{\mu\nu} = \partial_\mu^* \partial_\nu \log \mathcal{N} \end{aligned} \tag{3}$$

which holds within our space of states. Thus the set of states $\{|Z\rangle\}$ forms an overcomplete non-orthogonal family of basis states of a "continuous" representation[2]. Some examples from a nuclear many body problem are shown in the table, where we can check the validity of (3) from a group theoretical argument.

It is now straightforward to derive a path integral expression for the time evolution operator $U(T) = \exp(-iHT/\hbar)$ of the system. The transition amplitude between an arbitrary couple of initial and final states is given by

$$\begin{aligned} \langle\Psi_f|U(T)|\Psi_i\rangle = &\int d\mu(Z_i) d\mu(Z_f) \langle\Psi_f|Z_f\rangle\langle Z_i|\Psi_i\rangle \\ &\times \int \mathcal{D}\mu[Z] \exp(iS/\hbar) \end{aligned} \tag{4}$$

with the path integral measure and action functional given by

$$\begin{aligned} \mathcal{D}\mu[Z] &= \lim_{N\to\infty} \prod_{k=1}^{N} d\mu(Z_k) \\ S[Z(\cdot)] &= \int_0^T \langle Z(t)|\Big(i\hbar \frac{\partial}{\partial t} - H\Big)|Z(t)\rangle dt \end{aligned} \tag{5}$$

The boundary points of the path Z(t) are fixed by

$$Z(0) = Z_i\ ,\ Z(T) = Z_f \tag{6}$$

for each component of Z_μ ($\mu = 1,2,\ldots,M$). It is easily seen that the stationary phase condition on the path integral (4) gives a variational equation similar to TDHF. The resultant classical equations of motion have the form

$$i\hbar\, g_{\mu\nu} \frac{d}{dt} Z_\nu = \partial_\mu^* \mathcal{H},\ \mathcal{H} = \langle Z|H|Z\rangle \tag{7}$$

and define a path in a generalized phase space whose geometrical properties are represented by the Z-dependent metric $g_{\mu\nu}$. Special features of the solution of (7) are listed in the following:

a) The expectation value $\mathcal{H}$ of the Hamiltonian is conserved along the classical path. The corresponding classical action is given by

generators A_μ^+	spin raising operator $J_+ = J_x + iJ_y$	particle-hole pairs $a_i^+ b_k^+$ $\begin{cases} i=1,\ldots,m \\ k=1,\ldots,n \end{cases}$	quasiparticle pairs $a_\alpha^+ a_\beta^+$ $\alpha,\beta = 1,\ldots,n$
$\|0\rangle$	$\|J, J_z = -J\rangle$	p-h vacuum	BCS state
$\|Z\rangle$	spin (SU(2)) - coherent state	Slater determinant Z: m x n matrix	Slater determinant Z: n x n matrix ($Z_{\alpha\beta} = -Z_{\alpha\beta}$)
$\det[g_{\mu\nu}] \propto$	$\dfrac{1}{(1+Z^*Z)^2}$	$[\det(I+Z^+Z)]^{-(m+n)}$	$[\det(I+Z^+Z)]^{-(n-1)}$
classical equation of motion	motion on a sphere	time-dependent Hartree-Fock	time-dependent Hartree-Fock-Bogoliubov

Table 1

$$S_{cl} = \int_i^f \omega - \mathcal{H}T,\ \omega = \frac{i\hbar}{2}(dZ_\mu \cdot \partial_\mu - dZ_\mu^* \cdot \partial_\mu^*)\log\mathcal{N} \qquad (8)$$

where the first term gives the two-dimensional area of the phase space swept within the time interval T.

b) The equation (7) can be cast into a standard canonical form by a proper introduction of Poisson-type bracket. It is also possible to prove the extended Liouville theorem, the phase space density of which is given by $\det[g_{\mu\nu}]$ (see eq. (3)). These confirm the phase space nature of the description and also the consistency of the invariant measure (3).

c) Because of the boundary conditions (6) which are *twice as much as needed to solve (7), the solution* exists only for special couple of points (Z_i, Z_f). In a final expression for the transition amplitude (4), however, an infinited number of classical paths contributes because of the integration over Z_i and Z_f. To find the precise connection of the classical paths with the quantum mechanical amplitude (4) one has to take into account the fluctuation from the classical paths[3].

d) Although the equation (7) describes the path in a curved space it is possible to embed the description into a larger "flat" space using a method of Dirac[4]. This time, we regard Z_μ and Z_μ^* as 2M coordinates and introduce 2M new momenta which are redundant. This redundancy is removed by imposing a corresponding constraint. The Dirac bracket, which includes consistently the above constraint is shown to be equivalent with the bracket mentioned in b).

References

1) H. Kuratsuji and T. Suzuki, Phys. Lett. 92B (1980) 19.
2) J.R. Klauder, J. Math. Phys. 4 (1963) 1055.
3) T. Suzuki, following report.
4) P.A.M. Dirac, Can. J. Math. 2 (1950) 129.

5.8. Semiquantal Interference of Classical Paths in Phase Space

T. Suzuki

In ref. 1, we have investigated a classical dynamics of many body systems, the special case of which is the TDHF, starting with a path integral method based on a "continuous" representation. In order to find the direct relation between the classical paths and the quantum mechanical quantities such as transition amplitude, we must calculate the probability amplitude accompanied by each of the classical paths. This can be done by expanding the paths Z(t) in the path integral (P.I.) around the classical paths $\bar{Z}(t)$ with the same boundary condition, i.e.

$$Z(t) = \bar{Z}(t) + \zeta(t) \qquad (1)$$

and then by evaluating the Gaussian P.I. which is of the second order in the fluctuation $\zeta(t)$. For the standard P.I. defined in the coordinate space the result is well known[2]:

$$\langle x_f|U(t_f,t_i)|x_i\rangle_{S.C.} = \Sigma\ \Delta(x_f t_f, x_i t_i)\exp iS_{cl}/\hbar$$
$$\Delta(x_f t_f, x_i t_i) = [(\partial^2 S_{cl}/\partial x_i \partial x_f)/2\pi i\hbar]^{1/2} \times (\text{phase}) \qquad (2)$$

where $U(T) = \exp[-iH(t_f - t_i)/\hbar]$, x_i and x_f are the boundary points and the summation is taken over all the allowed classical paths. The pre-exponential factor Δ coincides with the square root of the "classical probability" calculated for the classical path which connects the boundary points. The phase factor is related to the number of times where the classical path touches the caustics. Thus the "semiclassical" formula (2) is expressed entirely with the classical quantities although the quantum mechanical superposition principle is fully incorporated[3].

For the path integral in continuous representation the situation is different because of its phase space nature and of boundary conditions. The classical probability which connects two points in phase space must be one or zero because of the Liouville's theorem. Since there is no caustics, the phase must be constant. Therefore we are led to the following formula for the semiclassical time evolution operator in continuous representation after taking into account properly the phase space density function $\rho(Z,Z^*)$:

$$\tilde{U}(t_f,t_i) = \mathcal{N}\int d\mu(Z_0)|\bar{Z}(t_f)\rangle\exp(i\bar{S}/\hbar)\langle\bar{Z}(t_i)| \qquad (3)$$

where $\bar{S}$ is the classical action corresponding to the classical path $\bar{Z}(t)$ and $Z_0 = \bar{Z}(t_0)$ is the point on the path at fixed time t_0 $(t_i \le t_0 \le t_f)$. We can choose the time t_0 arbitrarily because of the invariance of the phase space volume element $d\mu(Z) = \rho \cdot dReZ \cdot dImZ$ along the classical path. Physical pictures implied by (3) are illustrated in fig. 1.

In order to prove (3), we must calculate the pre-exponential factor similar to Δ in (2). By substituting the expansion (1) into the P.I. in continuous representation we obtain

$$\Delta(Z_f t_f, Z_i t_i) = \int \mathcal{D}\tilde{\mu}[\zeta]\exp i\tilde{S}/\hbar$$
$$\mathcal{D}\tilde{\mu}[\zeta] = \lim_{N\to\infty}\prod_{k=1}^{N}\rho(\bar{Z}_k,\bar{Z}_k^*)dRe\zeta_k \cdot dIm\zeta_k \qquad (4)$$

where $\tilde{S}$ is the fluctuation part of the action functional and is of the second order in ζ. The Gaussian P.I. of (4) can be calculated for a one (-complex)-parameter path case by modifying the technique developed by Dashen et al.[4]. The main steps of the proof are:
(i) Transform to real variables $(Z = (x+iy)/\sqrt{2}$, $\zeta = (\xi + i\eta)/\sqrt{2})$ and transform $\tilde{S}$ into a symmetric form through partial integration,

$$\tilde{S} = -\frac{1}{2}\int_{t_i}^{t_f} (\xi,\eta)\Lambda\begin{pmatrix}\xi\\ \eta\end{pmatrix} dt$$

$$\Lambda = -\hbar g \begin{pmatrix} 0 & \partial_t \\ \partial_t & 0 \end{pmatrix} + g^2 \begin{pmatrix} \mathcal{K}_{xx} & \mathcal{K}_{yx} \\ \mathcal{K}_{xy} & \mathcal{K}_{yy} \end{pmatrix} \qquad (5)$$

where $\mathcal{K}_{xy} = (g^{-1}\partial_x)(g^{-1}\partial_y)\langle H\rangle$, etc., and g is the metric function which is proportional to ρ. (ii) Introduce a set of arbitrary functions (F,G) of Z which satisfy $\Lambda\cdot{}^t(F,G) = 0$. For example, $(F,G) = (\dot{x},\dot{y})$ satisfy the requirement because of the time-translation invariance of the Hamiltonian. Using functions F,G we can introduce new variables p,q which diagonalize the matrix Λ, i.e.

$$\tilde{S} = \int\left[\frac{1}{2M}(\hbar G\dot{p})^2 - \frac{M}{2}(gq)^2\right]dt \qquad (6)$$

for $p = \eta/G$ and $q = \xi - \eta F/G + \hbar G\dot{p}/(gM)$ with $M \equiv \mathcal{K}_{xx}$. (iii) Perform the Gaussian path integration (4) by taking care of the boundary conditions $\zeta(t_i) = \zeta(t_f) = 0$. The result shows that Δ in (4) is constant (independent of $\bar{Z}$). This proves (3). The overall normalization constant $\mathcal{N}$ in (3) must be one at least for $t_f \to t_i$ (see below).

It is easily seen that the semiclassical fomrula (3) satisfies the following properties required by $U(t_f,t_i)$:

a) Trivial limit: $\hat{U}(t_i,t_i) = 1$.

b) Time reversal property: $\hat{U}(t_i,t_f) = \hat{U}(t_f,t_i)^*$

c) Gauge invariance. Expression (3) is invariant under the transformation of the basis, $|Z\rangle \to \exp\{i\alpha(Z,Z^*)\}|Z\rangle$ with an arbitrary function α of Z.

d) Composition rule: $\hat{U}(t_f,t_m)\hat{U}(t_m,t_i) = \hat{U}(t_f,t_i)$. Actually this is true only when we pick up the continuous paths which has already been assumed in the course of the stationary phase approximation.

e) Unitarity: $\hat{U}(t_f,t_i)^* = \hat{U}(t_f,t_i)^{-1}$ as a result of b) and d).

In addition, the substitution of (3) into the Schrödinger equation gives the relation

$$(i\hbar\partial_t - H)\hat{U}(t,t_i) \sim \int d\mu(Z_0)(1-|\bar{Z}(t)\rangle\langle\bar{Z}(t)|)$$
$$\times\left[(i\hbar\partial_t - H)|\bar{Z}(t)\rangle\right]\cdot\exp(i\tilde{S}/\hbar)\langle\bar{Z}(t_i)| \qquad (7)$$

where the r.h.s. must be equal to zero for the exact U. It is proven from (7) that $\hat{U}$ coincides with U for those systems where the Hamiltonian is a linear combination of the path generators. Apparently there is an infinite number of classical paths which contribute to the propagation kernel $\langle Z_f|\hat{U}|Z_i\rangle$. In some cases[5], the one-path approximation to the kernel gives already an exact result. In general, however, this does not satisfy many of the properties listed above. For a boson-pair creation Hamiltonian, for example, the one-path approximation is completely breakdown whereas the full expression (3) is almost exact.

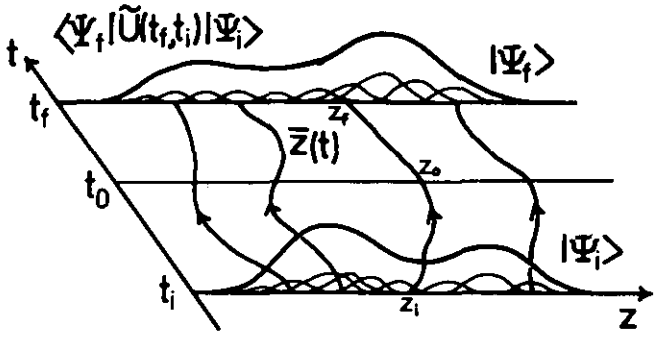

Fig. 1: Illustration of the semiclassical transition amplitude $\langle\Psi_f|\tilde{U}(t_f,t_i)|\Psi_i\rangle$: Initial wave function $|\Psi_i\rangle$ is decomposed into the mutually overlapping wave packets $|Z_i\rangle$, each of them propagates along classical paths and finally they are summed up to the final wave function $|\Psi_f\rangle$.

References

1) T. Suzuki, Jülich preprint 1980; the preceding report.

2) M.V. Berry and K.E. Mount, Rep. Prog. Phys. 35 (1972) 315.

3) W.H. Miller, Adv. Chem. Phys. 25 (1974) 69.

4) R.F. Dashen, B. Hasslacher and A. Neveu, Phys. Rev. C10 (1974) 4114;
R. Rajaraman, Phys. Rep. 21 (1975) 227.

5) T. Suzuki, Jülich Annual Report IKP (1979) p. 128.

5.9. Superposition of TDHF Paths in a Collision of Lipkin Nuclei

T. Suzuki

The time-dependent mean-field approximation (TDHF) is one of the most promising microscopic methods for the study of large amplitude motions such as heavy ion reaction and nuclear fission. One of the main problems of TDHF is its classical nature, i.e., it does not contain the wave function concept intrinsically. Therefore we cannot expect to obtain a good description for such a phenomenon where the interference of TDHF paths is important because of a lack of superposition principle. The recovery of this principle in TDHF has been done implicitly for a stationary problem[1,2] via path integral formalism. The concept of wave function is still hidden, however, since it was not easy to take into account the boundary conditions which is not periodic. In ref. 3 we have developed a path integral suitable for many nucleon systems by explicitly defining the representation basis. Stationary phase approximation gives the following "semiclassical" formula for the final state wave function $|\Psi(T)\rangle$ at time t=T evolved from the initial wave function $|\Psi_0\rangle$ at t=0[4]:

$$|\Psi(T)\rangle = \int d\mu(Z_0)\,|\bar{Z}(T)\rangle e^{i\bar{S}/\hbar}\langle\bar{Z}(0)|\Psi_0\rangle \qquad (1)$$

where $|Z\rangle$ is the overcomplete set of basis states, $\bar{Z}(t)$ is the classical (TDHF) path and $\bar{S}$ is the corresponding classical action. For simplicity we choose the integration measure $d\mu(Z^0)$ at t=0, i.e., $Z_0 = \bar{Z}(0)$.

To investigate the interference effect between TDHF paths we apply the formula (1) to the model of interacting schematic nuclei[5] which simulates a nucleus-nucleus collision. This analogy is not complete. But it is possible to compare with the exact result.

The model consists of two two-level (Lipkin) nuclei a and b, each of them is described by a quasi-spin J_k(k=a,b), and interacts within a limited time interval T:

$$H = H_a + H_b + V_{ab}$$

$$H_k = \epsilon_k J_{kz} - \frac{1}{2} V_k (J_{k+}J_{k+} + J_{k-}J_{k-}) \quad (k=a,b) \qquad (2)$$

$$V_{ab} = \begin{cases} -V(J_{a+}J_{b+} + J_{a-}J_{b-}) & 0\le t\le T \\ 0 & \text{otherwise} \end{cases}$$

The basis states are described by two complex parameters Z_a and Z_b,

$$|Z\rangle = \prod_{k=a}^{b} (1 + Z_k^* Z_k)^{-J_k} \exp(Z_k J_{k+})|0\rangle \qquad (3)$$

where $|0\rangle$ is the particle-hole vacuum, $|J_k J_{kz} = -J_k\rangle$. The invariant measure is the product of those for SU(2) coherent states.

The classical equation of motion is given by the two first-order differential equations in the complex variables Z_k,

$$2iJ_k\hbar\dot{Z}_k = (1 + Z_k^* Z_k)^2 \frac{\partial \mathcal{H}}{\partial Z_k^*}, \quad \mathcal{H} = \langle Z|H|Z\rangle \qquad (4)$$

Since it is practically impossible to perform the integration (1) over all the starting points $Z = (\bar{Z}_a(0), \bar{Z}_b(0))$, we have arbitrarily selected several points $Z_1,\ldots,Z_N$ so that the sum of the wave packets

$$|\Psi_0\rangle = n \cdot \sum_{i=1}^{N} \Delta\mu(Z_i)\,|Z_i\rangle\langle Z_i|\Psi_0\rangle \qquad (5)$$

simulates the initial wave function $|\Psi_0\rangle$ which is a product of the ground state of both nuclei. The simplest (N=1) of this N-path approximation corresponds to the ordinary TDHF apart from a phase $\exp i\bar{S}/\hbar$.

It turns out that for short reaction time T only the simulation (5) is important in obtaining good result. For longer reaction time it may be necessary to take the (quasi-) periodic path into consideration. Each nucleus is classified as spherical ($\alpha\le 1$) or deformed ($\alpha>1$) depending on the parameter $\alpha_k = (2J_k - 1)V_k/\epsilon_k$. We take $2J_1 = 2J_2 = 8$, $\epsilon_1 = \epsilon_2 = 1$ MeV.

Figure 1 shows the result for a spherical-spherical system ($V_a=V_b=V=0.1$ MeV). $P_N = |\langle N|\Psi(t)\rangle|^2$ denotes the wave function projected to the total number of excited particles N. The semiclassical results are produced in 8-path approximation. Because of the symmetry there is no N=odd component. It should be noted that there is no a priori favourable choice of the initial point for the ordinary (1-path) TDHF except for $|Z=0\rangle$ which, however, never develops in time. The semiclassical wave function simulates the exact one rather well, although the discrepancy becomes large at $T\sim 10$. After $T\ge 15$ it becomes smaller which may be due to the stability of the orbits. The observables such as $\langle J_z\rangle$ follow this trend. Fig. 2 shows the value of observables for a (weakly) deformed-deformed system ($V_a=V_b=V=0.2$ MeV). The 4-path approxima-

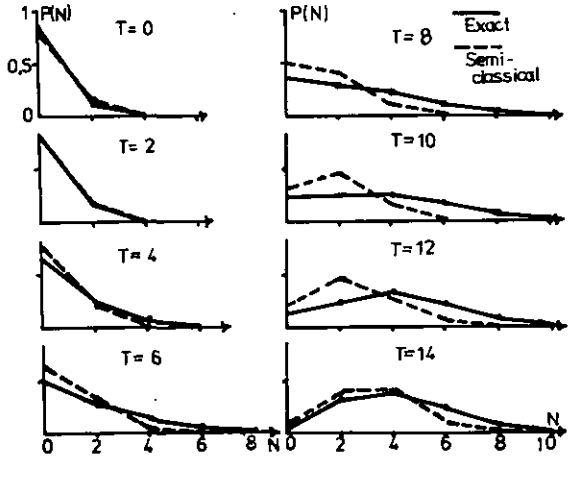

Fig. 1: Distribution of the final wave function over N at various reaction time (in units of 10^{-22} sec). Starting points of the semiclassical wave functions are: $(Z_a,Z_b) = (\pm 0.3, \pm 0.3)$, $(\pm 0.3, \mp 0.3)$, $(\pm 0.3, 0.0)$ and $(0.0, \pm 0.3)$.

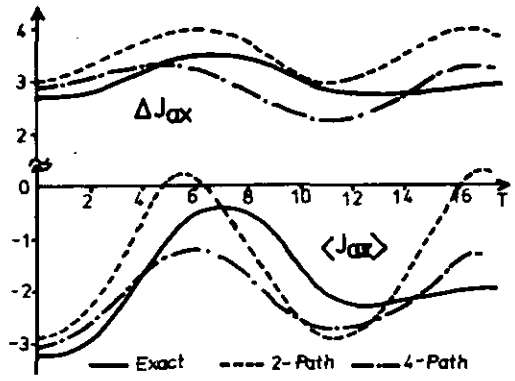

Fig. 2: Expectation value of J_{az} and the fluctuation ΔJ_{ax} for several values of T. The 2-path calculation starts with the points $(Z_a, Z_b) = (\pm 0.4, \pm 0.4)$, whereas in the 4-path approximation the points $(\pm 0.4, \mp 0.4)$ are added.

tion, starting with the HF-minima of both nuclei, corresponds to the fully projected TDHF. The 2-path approximation is the partially projected TDHF. Although the semiclassical calculations reproduce the trends of the exact results, the latter has a different time behaviour for $T \geq 10$ whereas the former is more or less periodic. This suggests the importance of other TDHF paths which have not been included in the present calculation. For strongly deformed nuclei, the 4-path approximation is expected to give a more satisfactory agreement.

References

1) H. Reinhardt, J. Phys. G5 (1979) L91; Nucl. Phys. A331 (1979) 353.

2) S. Levit, J.W. Negele and Z. Paltiel, Phys. Rev. C21 (1980) 1603.

3) H. Kuratsuji and T. Suzuki, Phys. Lett. 92B (1980) 19.

4) T. Suzuki, the preceding report.

5) P. Hoodbhoy and J.W. Negele, Phys. Rev. C18 (1978) 2380.

5.10. A Complex Effective Force for Heavy Ion Collisions

A. Faessler[+], *T. Izumoto*[++], *S. Krewald*, *R. Sartor*[+]

The optical potential model provides one of the most useful and general tools in the analysis of nuclear reactions. For the nucleus-nucleus scattering, a microscopic derivation is desirable, because the strong absorption only allows the tail region of the heavy ion optical to be studied phenomenologically. Doubly folding with an effective interaction seems to be one of the most promising methods to compute the optical potential[1]. So far, however, only real forces were used and thus nothing could be said about the imaginary part of the optical potential which had to be added subsequently "by hand"[1]. It might be tempting to use a complex interaction as derived by Brieva and Rook[5] for the case of nucleon-nucleus scattering in a folding calculation, however, it is clear[2] that the nature of the absorption in heavy ion reactions is fundamentally different of the one pertaining to nucleon-nucleus scattering. This fact makes necessary the construction of a complex effective force more directly related to heavy ion dynamics.

Here we obtain a complex G-matrix for a system of two interpenetrating Fermi gases which is more appropriate for heavy ion studies. Decomposed in partial waves, the G-matrix in momentum space is (using standard notation[2]):

$$G(\vec{K}\vec{W}|\vec{k},\vec{k}_o) = \frac{2}{\pi}\frac{\hbar^2}{m}\sum_{\substack{JST\\LL'M}} i^{L-L'} G^{JST}_{LL'}(\vec{K}\vec{W}\, kk_o) Y_{LSJ}(\hat{k}) Y_{L'SJ}(\hat{k}_o) P_T \qquad (1)$$

An effective interaction which reproduces the same binding energy in coordinate space is given by[3]:

$$V^{JST}_{LL}(r) = \frac{2}{\pi}\frac{\int_F d^3k_1 d^3k_2 j_L(k_{12}r)\int_0^\infty k^2 dk j_L(kr) G^{JST}_{LL}(K_{12}W_{12}|kk_{12}>}{\int_F d^3k_1 d^3k_2 j^2_L(k_{12}r)} \qquad (2)$$

For practical purposes, we use an averaged effective interaction

$$V^{ST}(r) = \frac{\sum_L V^{2T}_{LL}(2L+1)\int_F d^3k_1 d^3k_2 j^2_L(k_{12}r)}{\sum_L (2L+1)\int_F d^3k_1 d^3k_2 j^2_L(k_{12}r)} \qquad (3)$$

This interaction in the $^3S_1$ state for a non spherical Fermi sea is shown in fig. 1.

An analytical expression which parametrizes this interaction:

$$V^{ST}(r) = \frac{1}{x}(1-e^{-2x})^2 \sum_{m=1} Z^{ST}_m x^m \qquad (4)$$

with x = 0.7 r has been published in ref. 4.

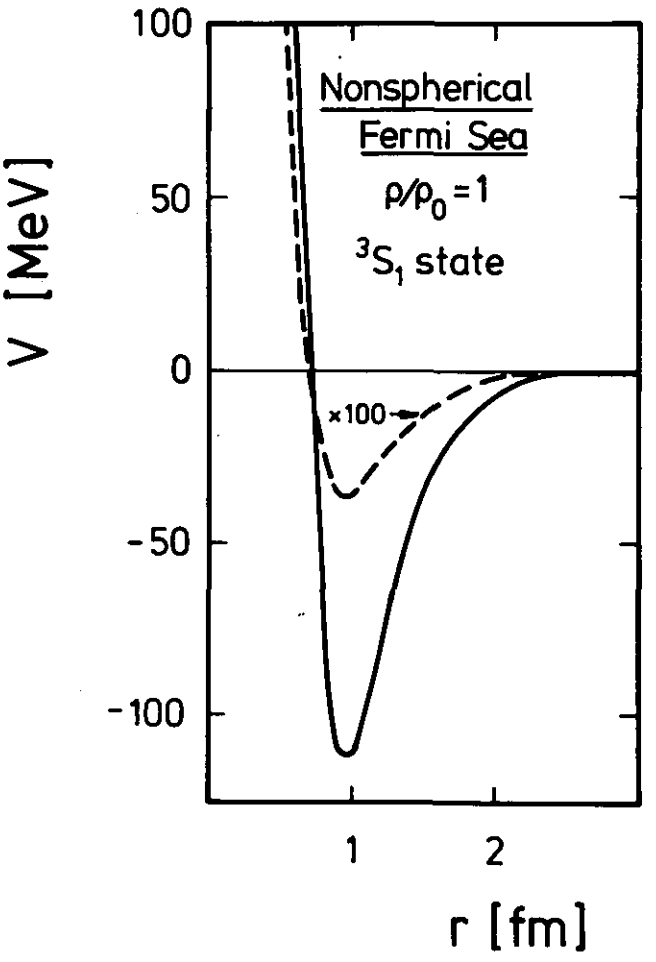

Fig. 1: Effective interaction in the $^3S_1$ state for a non spherical Fermi sea corresponding to a system of interpenetrating Fermi gases with a density of $\rho = 0.17$ fm^{-3} and an average relative momentum per particle of $K_r = 0.5$ fm^{-1}. Solid: real part; dashed: imaginary part x 100.

References

1) G.R. Satchler, W.G. Love, Phys. Rep. 55 (1979) 183.
2) M.I. Haftel, F. Tabakin, Nucl. Phys. A158 (1970) 1.
3) P.H. Siemens, Nucl. Phys. A141 (1970) 225.
4) A. Faessler, T. Izumoto, S. Krewald, to be published.
5) F.A. Brieva, J.R. Rook, Nucl. Phys. A297 (1978) 206.

[+] Institut für Theor. Physik, Univ. Tübingen
[++] Texas A&M University, College Station, Texas, USA

5.11. Folding Computation of the $^{16}O+^{16}O$ Optical Potential with a Complex Effective Force

R. Sartor[+], *A. Faessler*[+], *S.B. Khadkikar*[+], *S. Krewald*

One of the most successful approaches to a microscopic computation of the heavy ion optical potential is provided by the double folding method which defines the optical potential as follows:

$$V_{opt}(\vec{R}) = \int d^3r_1 d^3r_2 \rho_1(\vec{r}_1)\rho_2(\vec{r}_2) V_{eff}(\vec{R}+\vec{r}_2-\vec{r}_1) \qquad (1)$$

where ρ_i are the matter distributions of both projectile and target, and V_{eff} is the effective interaction[1]. In

general only phenomenological interactions (Skyrme, Gaussian) were used which cannot explain the energy dependence or the imaginary part.

Recently we have considered the possibility of defining a non-hermitian G-matrix directly related to the heavy ion collision dynamics. That G-matrix is obtained as the solution of a Bethe-Goldstone equation corresponding to two nuclear matter units streaming through each other. In contradistinction to the static nuclear matter case, two nucleons inside the Fermi sea can now suffer a real scattering which brings them into excited states above the Fermi surface. The energy denominator of the Bethe-Goldstone equation can thus vanish and this gives rise to the non-hermiticity of G. In ref. 2, the corresponding G-matrices were translated into a local, complex, relative momentum, density, and kinetic energy dependent effective force.

In this work we improve the folding model (i) by using this complex interaction of ref. 2 and (ii) by using a fully antisymmetrized cluster wave function which keeps the exchange terms dropped in eq. (1). Therefore our optical potential is:

$$V_{opt}(R) = \frac{\hbar^2}{2m} \int d^3r \Big(\sum_{ij} \varphi_i^*(-\nabla^2)\varphi_j B^{-1}_{ji} \Big) + \frac{1}{2} \sum_{ijkl} \sum_{ST} (2S+1)(2T+1) \Big[\langle ij|V^{ST}|kl\rangle - (-)^{S+T} \langle ij|v|kl\rangle \Big] B^{-1}_{ki} B^{-1}_{lj} \qquad (2)$$

with $B_{ij} = \langle i|j\rangle$ and φ_i are the single particle wave functions building up a Slater determinant which describes two colliding ions separated by a distance R.

In figs. 1 and 2 the depths of both real and imaginary parts of the potentials are shown to increase with increasing energy as expected from the decreasing role of Pauli principle effects. In fig. 3, we also compare our results with phenomenological Woods-Saxon potentials giving a "decent" fit to the experimental $^{16}O+^{16}O$ data. The agreement with the real part of the potential is particularly striking in the relevant tail region. On the other hand, the imaginary part has too short a range.

References

1) G.R. Satchler, W.G. Love, Phys. Rep. 55 (1979) 183.

2) A. Faessler, T. Izumoto, S. Krewald, R. Sartor, to be published.

3) J.V. Maher et al., Phys. Rev. 188 (1969) 665.

4) T. Izumoto, S. Krewald, A. Faessler, Nucl. Phys. A341 (1980) 319.

+ Institut für Theor. Physik, Univ. Tübingen

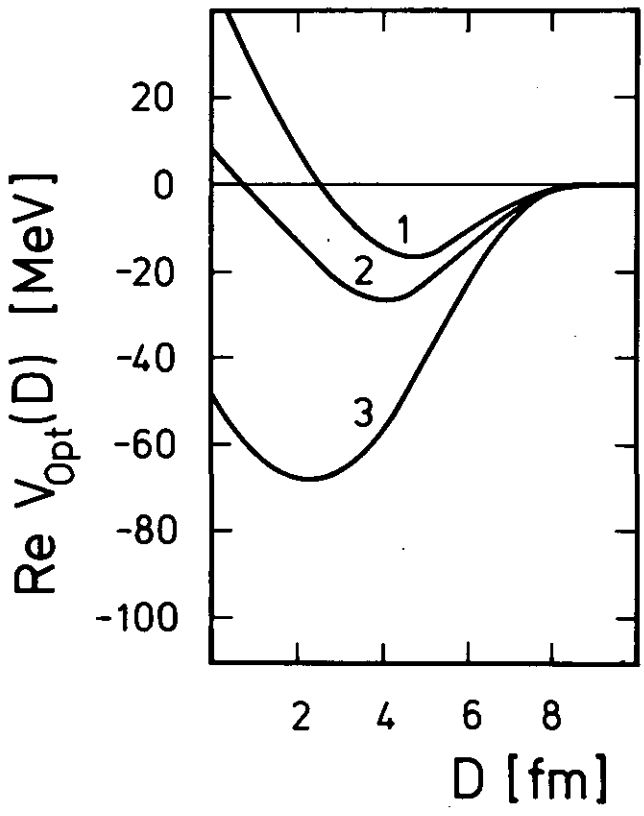

Fig. 1: Real part of the $^{16}O+^{16}O$ potential computed according to eq. (2). The curves marked 1,2,3 correspond to E_{LAB} = 0, 83 and 332 MeV.

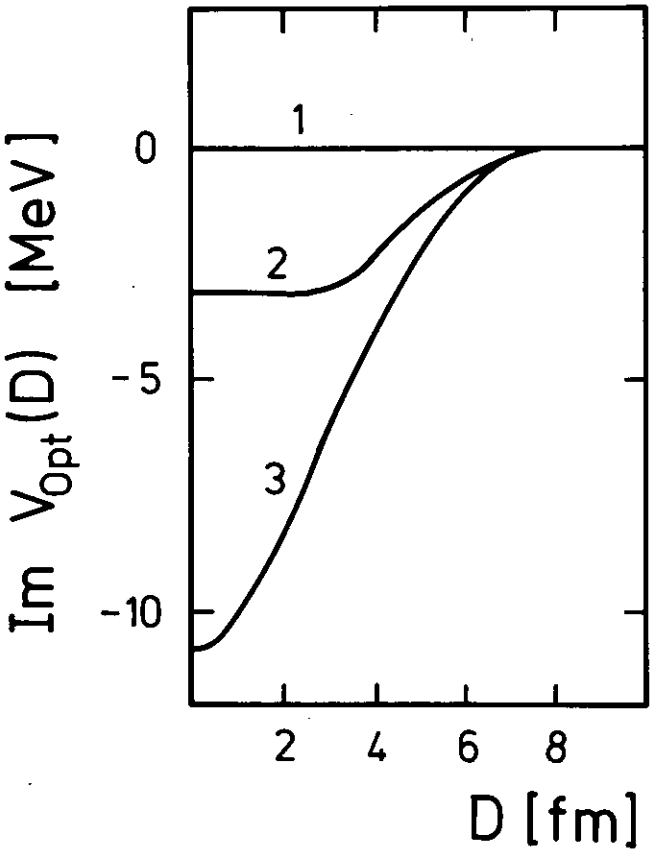

Fig. 2: Imaginary part of the $^{16}O+^{16}O$ potential described in fig. 1.

5.12. Nuclear Matter Approach to the Heavy Ion Optical Potential: Imaginary Part

T. Izumoto[+], *S. Krewald, A. Faessler*[++]

The imaginary part of the Heavy Ion Optical Potential is investigated in a nuclear matter approach. The Bethe-Goldstone equation is solved for a gas of two interpenetrating Fermi spheres (see fig. 1). Since two interacting nucleons can scatter into unoccupied states while conserving their energy, this system is not stable. This leads to a pole in the denominator of the Bethe-Goldstone equation:

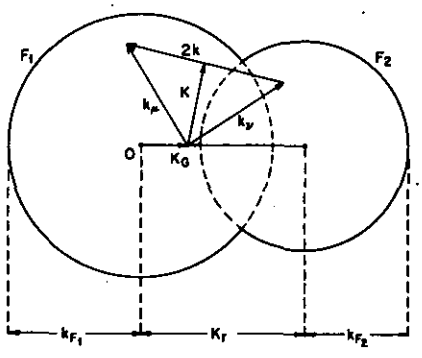

Fig. 1: Momentum space distribution of a gas of two interpenetrating Fermi gases, represented by two spheres with radii k_{F_1} and k_{F_2} which are separated by the average relative momentum per particle K_r. Two interacting nucleons k_μ and k_ν are shown.

$$G = V + V \frac{Q}{\omega - H_0 + i\varepsilon} G$$

which therefore acquires an imaginary part. In standard Brueckner-Hartree-Fock (BHF) calculations, however, the potential energy of the unoccupied states is assumed to be zero for computational convenience (fig. 2). Therefore a large gap between occupied and unoccupied levels occurs which artificially suppresses the decay process. Now Mahaux et al.[1] argue that even for unoccupied single particle states, the selfconsistent potential should be used, because this choice guarantees that the BHF approximation to the mass operator has the same analytic structure as the exact one. Fig. 2 shows the BHF single particle potentials both in the standard and in the "continuous" choice.

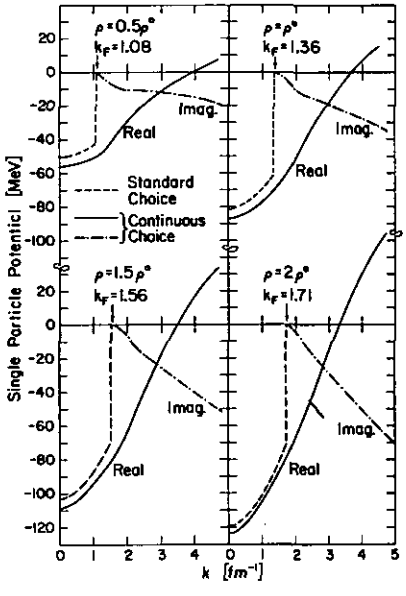

Fig. 2: Momentum dependence of the single particle potentials for spherical Fermi distributions; dashed: standard choice U(k) = 0 for k>k_F; solid and dash-dotted: real and imaginary part of the fully selfconsistently calculated single particle energies. The potentials are displayed for several nuclear matter densities.

The complex binding energy for two interpenetrating Fermi gases is computed using this continuous choice, using following numerical approximations: (i) An angle-averaged Pauli operator is employed. (ii) A spherical single particle potential was used for the unoccupied states.

In the spirit of the resonating group method, the optical potential is taken to be the interaction energy of the two ions at a given distance. The two ions are described by an antisymmetrized cluster function in coordinate space, so that both Pauli Principle and relative motion are carefully incorporated into the wave function. The results for a $^{40}Ca+^{40}Ca$ collision at E_{LAB} = *240 MeV are shown in fig. 3.*

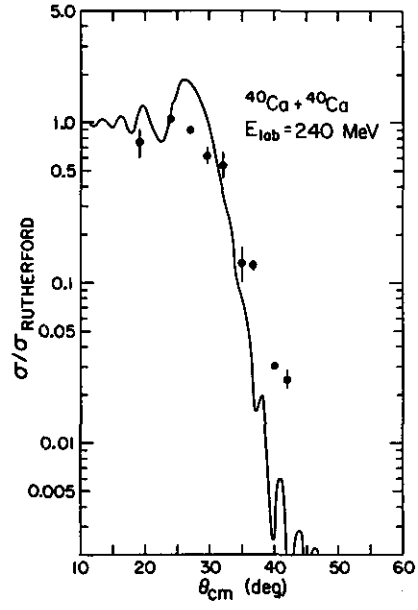

Fig. 3: Angular distribution of the $^{40}Ca+^{40}Ca$ elastic scattering at E_{LAB} = 240 MeV corresponding to K_r = 0.5 fm^{-1}. Note that the cross sections are normalized by the non-symmetrized Rutherford scattering.

The quality of the fit should not be compared with the one obtained from phenomenological fits, since this calculation is based on a microscopic derivation of the potential. The overall shape of the fit, however, is quite satisfactory. At larger angles, the processes other than two particles omission appear to dominate.

References:

1) J.P. Jeukenne, A. Lejeune, C. Mahaux, Phys. Rev. C16 (1977) 80.

2) T. Izumoto, S. Krewald, A. Faessler, Nucl. Phys. A341 (1980) 319.

+ Present address: Texas A&M University, Cyclotron Institute, College Station, Texas, USA

++ New address: Institut für Theor. Physik, Univ. Tübingen

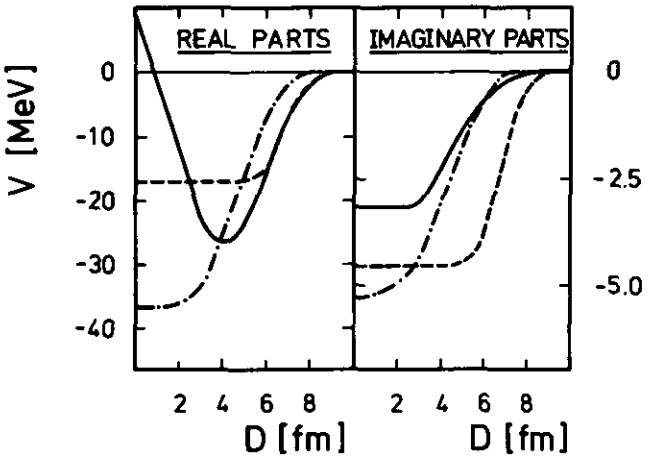

Fig. 3: Comparison of 83 MeV optical potential (solid) with phenomenological Woods-Saxon of ref. 3 (dashed) and local energy density results of ref. 4.

5.13. A Resonating Group Approach to the Heavy Ion Optical Potential

W. Bauhoff[+]

The Resonating Group Method (RGM) has been used extentively to describe the scattering of nuclei[1]. It is a rigorous approach leading to a nonlocal interaction between the two nuclei. By introducing suitable approximations it can be related to more intuitive expressions for the heavy ion optical potential as e.g. proposed by Fließbach[2]. The Hamiltonian kernel of the RGM can be related to the corresponding one of the Generator Coordinate Method (GCM) by the following transformation[3]:

$$H_{RGM}(\vec{R}',\vec{R}'') = \int d^3S'd^3S''\Gamma^*(\vec{S}',\vec{R}')H_{GCM}(\tfrac{i}{\alpha}\vec{S}',\tfrac{i}{\alpha}\vec{S}'')\Gamma(\vec{S}'',\vec{R}'')$$

with $$\Gamma(\vec{S}',\vec{R}') = e^{-\frac{N}{8\alpha}(\vec{S}'+i\alpha\vec{R}')^2} \qquad (1)$$

Here, N is the total number of nucleons in the scattering system, and α is the harmonic oscillator constant used for the internal wave functions of the nuclei. In the limit of large particle number the integrals in eq. (1) can be performed by using a stationary phase argument: Only the immediate neighbourhood of $\vec{S}' = -i\alpha\vec{R}'$ will contribute an appreciable amount to the integral. So the method of steepest descent leads to:

$$H_{RGM}(\vec{R}',\vec{R}'') = H_{GCM}(\vec{R}',\vec{R}'') \qquad (2)$$

Though the calculation of H_{GCM} is much simpler than that of H_{RGM} it is still a nonlocal interaction. A local approximation to it may be defined by:

$$V(\vec{R}) = \int d^3S\, e^{i\vec{K}(\vec{R})\vec{S}}\, H_{GCM}(\vec{R}+\tfrac{1}{2}\vec{S}, \vec{R}-\tfrac{1}{2}\vec{S}) \qquad (3)$$

Studies in the case of nucleon-nucleus scattering[4] have shown that $V(\vec{R})$ defined in this way is a reliable approximation to the nonlocal interaction in the sense of yielding the same phase shifts provided that $\vec{K}(\vec{R})$ is chosen selfconsistently as the local momentum, i.e.:

$$\vec{K}^2(\vec{R}) = \vec{K}_o^2 - \frac{2\mu}{\hbar^2}V(\vec{R}) \qquad (4)$$

($\vec{K}_o$ is the asymptotic momentum of the projectile.) The choice $\vec{K} = \vec{K}_o$, however, will lead to a potential which is much too deep.

So $V(\vec{R})$ calculated in this way can be considered as the heavy ion optical potential. If the definition H_{GCM} is written out fully, it will be seen immediately that it coincides with the expression given by Fließbach[2] and used recently in the calculation of the heavy-ion optical potential in a nuclear matter approach[5].

References

1) K. Wildermuth and Y.C. Tang, A Unified Theory of the Nucleus (Vieweg, Braunschweig, 1977).

2) T. Fließbach, Z. Physik 247 (1971) 117.

3) Y.C. Tang, M. Le Mere, and D.R. Thompson, Phys. Rep. 47 (1978) 167.

4) W. Bauhoff, H.V. Geramb, G. Pálla, to be published.

5) T. Izumoto, S. Krewald, A. Faessler, Nucl. Phys. A341 (1980) 319.

+ I. Inst. für Exp. Physik, Univ. Hamburg

5.14. Empirical Constraints on the $^{16}O+^{40}Ca$ Optical Potential

S. Krewald, A. Djaloeis, S. Gopal

In analogy to the light ion ($A_p \lesssim 3$) case, the description of the elastic scattering of heavy ion has been generally attempted in terms of optical model. Analyses performed so far have unfortunately given inconsistent pictures regarding how far the elastic scattering data could give information on the potential shape, in particular, in the interior region. For example, using the notch perturbation method, Cramer and De Vries[1] have found that neither light- nor heavy-ion scattering at any energy probes the interior of the nucleus. On the other hand, using a similar method, Delbar et al.[2] have shown that angular distributions for the α-particle elastic scattering on $^{40,44}Ca$ nuclei at E_α = 36.2 MeV are influenced not only by the tail region of the potential, but also by the very inner part around R = 2 fm. In fact, the details of the potential shape in the interior region was found to be responsible for the so-called "anomalous large angle scattering" (ALAS) observed in $^{40}Ca(\alpha,\alpha)$ elastic scattering[3-5]. It is worth mentioning that deep penetration of α-particles into the ^{40}Ca nucleus was also suggested by Friedman and Batty[6] from their model independent analysis of $\alpha+^{40}Ca$ elastic scattering at E_α = 140 MeV. Taking advantage of the transparency of ^{40}Ca to α-particles, Michel and Vanderpoorten[5] succeeded to obtain a consistent description of $\alpha-^{40}Ca$ elastic scattering over a wide range of incident energies using a "spline-parametrization" technique.

It is well known that the ALAS phenomenon has also been observed[7-9] in some heavy-ion elastic scatterings. Attempts to explain this phenomenon in terms of, e.g., quasi-molecular resonance, cluster exchange mechanism or simple ℓ-independent potential scattering have been summarized in ref. 10. While enhancement of the large-angle cross section can be obtained easily with a conventional ℓ-independent optical model potential having Woods-Saxon shape in both real and imaginary parts by simply reducing the strength of the imaginary potential[11], the details of the angular distribution cannot be reproduced correctly.

In this report, we present results of optical model analysis of $^{16}O+^{40}Ca$ elastic scattering angular distribution at $E_{c.m.}$ = 35.7 MeV, measured up to $\theta_{c.m.} = 180^o$ [9]. The objectives are:

1. to check whether a better description of the ALAS phenomenon can be obtained by giving more degrees of freedom to the real and/or imaginary part of the optical potential, and

2. to see whether the ^{40}Ca nucleus would also be transparent to ^{16}O projectile which is considered to consist of α-clusters; in particular, it is important to establish whether the elastic scattering cross section is also sensitive to the details of the optical potential in the interior region.

The experimental $^{16}O+^{40}Ca$ *elastic scattering angular* distribution[9] has been analyzed by means of the optical model code OPTY[12] which automatically searches the optimum values of the potential parameters by minimizing the χ^2 value. For both the real and imaginary parts, the standard Woods-Saxon (WS) and Spline-function (SPL)[13] parametrizations of the optical potential have been investigated. The starting spline parameters at the corresponding radii r_i are either read in or computed in the program from the best-fit WS potential. The values of r_i were chosen in view of the expected sensitivity of the cross section to the radial dependence of the potential in the surface region. Several sets of r_i were used to study the changes in the resulting best-fit potential with respect to the variation of the starting condition in the search-procedure. In addition the influence of changing the potential values in the deep interior region on the cross section was investigated.

In the angular region $\theta_{c.m.} \lesssim 112^o$, where the angular distribution exhibits practically no oscillatory structure, it is possible to obtain good fits using the standard WS-WS shapes for both the real and imaginary parts of the optical potential. However, no fit could be achieved when the complete data (i.e. $\theta_{c.m.} \leq 180^o$) is analyzed. No further improvement could be obtained by giving more degrees of freedom to the imaginary part using WS-SPL potential combinations. On the other hand, excellent fits to the complete angular distribution were obtained for either SPL-WS or SPL-SPL potential combinations. But SPL-SPL combinations did not produce significantly better fit quality compared to the SPL-WS ones. The success of spline parametrization of the real part in reproducing the data suggests in this case a direct dependence of the ALAS on the shape of the real potential *in the interior region. For the best-fit SPL-WS potentials,* the real part is found to exhibit significant wiggles in the interior region, similar to those observed by Barrette and Kahana[10] in their analysis of $^{16}O+^{28}Si$ elastic scattering angular distribution at $E_{c.m.}$ = 21.1 MeV. In addition, the imaginary part is found to have a radius $R_I \sim 1.60\ [A_p^{1/3}+A_T^{1/3}]$ fm, which is significantly larger than those extracted by Kubono et al.[9] and theoretically estimated by Izumoto et al.[14]. Further analysis is in progress.

References

1) J.G. Cramer and R.M. De Vries, Phys. Rev. C22 (1980) 91.

2) T. Delbar et al., Phys. Rev. C18 (1978) 1237.

3) D.M. Brink and N. Takigawa, Nucl. Phys. A279 (1977) 159.

4) H.P. Gubler et al., Phys. Lett. 74B (1978) 202.

5) F. Michel and R. Vanderpoorten, Phys. Lett. 82B (1979) 183.

6) E. Friedman and C.J. Batty, Phys. Rev. C17 (1978) 34.

7) C.K. Gelbke et al., Phys. Rev. Lett. 41 (1978) 1778.

8) P.B. Munzinger et al., Phys. Rev. Lett. 38 (1977) 944.

9) S. Kubono, P.D. Bond and C.E. Thorn, Phys. Lett. 81B (1979) 140.

10) J. Barrette and S. Kahana, Comments Nucl. Part. Phys. 9 (1980) 67.

11) G.R. Satchler, Nucl. Phys. A329 (1979) 233.

12) H. Dabrowski, R. Planeta and A. Djaloeis, Jül-Report-1637, IKP-KFA Jülich, 1980.

13) J. Borysowicz and J. Hetherington, Phys. Rev. C7 (1973) 2293.

14) T. Izumoto, S. Krewald, A. Faessler, Nucl. Phys. A341 (1980) 319.

6.2 Solar Collector Test Station in Brasil

J. Anhalt, H. J. Stein

Based on the bilateral agreement on scientific and technological co-operation between Brasil and the Federal Republic of Germany, the Instituto de Fisica of the University of Sao Paulo/Brasil and the Institut für Kernphysik of the KFA Jülich have started in 1977 a project for testing solar collectors in the temperature range above 100 °C. Three types of commercially fabricated collectors have been proposed and selected by the German side for that purpose:

- a double-glazed flat-plate collector with a selective aluminium rollbond absorber (temperatures up to 120°C),
- a tracking, low-concentrating collector (n≈3) consisting of a single-glazed, selective, flat-plate collector with booster mirrors (temperatures up to 160 °C),
- a tracking, linear-concentrating collector (n≈12) consisting of parabolic troughs in polar-axis orientation (temperatures up to 200 °C).

The overall scope of a two years testing programme should comprise:

- determination of efficiency curves following standard test procedures such as ASHRAE 93-77[1] or BSE, part A.[2],
- measurements of the daily, monthly, and yearly energy output of the different collector types,
- observation of deterioration of materials along the time.

Each collector type has been installed in a field having about 20 m^2 aperture area each, Fig. 1, and connected to separate high-temperature test loops. Since no commercial high-temperature test loops were available on the market we constructed our own loop, Fig. 2. It is a closed loop designed to match the following specifications:

- adjustable collector field inlet temperature: 30 to 100 °C, ± 0.3 K stability,
- maximum collector field outlet temperature: 250 °C,
- adjustable mass flow rate: 0.014 to 0.22 kg s^{-1}, ± 1 % stability,
- maximum pressure: 3 bar,
- working fluid: organic heat-transfer liquid.

Fig. 1: View of the collector test station in Atibaia, Sao Paulo/Brasil. A Radio Observatory operates in this place and gives all the necessary infrastructure.

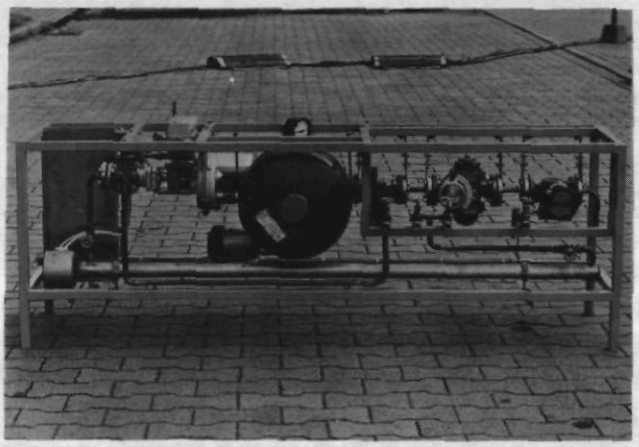

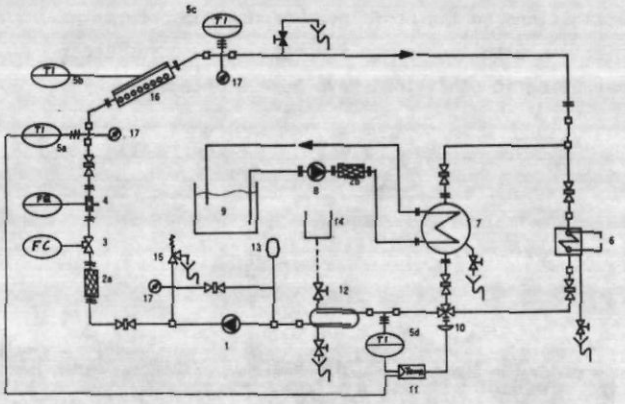

Fig. 2: Scheme of the high-temperature collector test loop. 1 circuit pump, 2 filter, 3 flow-controller, 4 flow-meter, 5 thermometer, 6 regulated heater, 7 heat-exchanger, 8 water pump, 9 lake, 10 three-way-valve, 11 temperature-controller, 12 mixing tank, 13 compensation tank, 14 hopper, 15 safety valve, 16 collector field. Most of the test loop components are integrated in a transportable frame, photograph above.

A small solar-meteorological data station has been additionally installed in order to correlate the long-term thermal performance test data to the meteorological conditions at the test site. The measured parameters are:

- the global solar irradiance in the horizontal plane (pyranometer),
- the direct solar irradiance (automatically tracked pyrheliometer),
- the dry and wet bulb temperature (psychrometer),
- the wind velocity and the wind direction (three cup anemometer and wind vane).

III. SOLAR ENERGY

6.1. Summary of Activities

J. Anhalt, W. Ebke, J. W. Grüter, H. R. Koch, K. Kruck, H. Labus, K. Maßmeyer, R. Posorski, H. Ringel, B. Sack, R. Schröer, O.W.B. Schult, H. J. Stein, H. D. Talarek, R. Wagner

The institute's solar energy group is engaged in the following three fields:

- Solar collector testing comprising development of thermal performance test procedures and long-term durability testing of a broad variety of collectors.
- Solar data acquisition in view of handling existing solar meteorological data and development of simple but precise instrumentation for the registration of solar and related weather data.
- Solar system testing with the aim of verifying theoretical simulation models and detecting design errors in commercially developed systems. Here, the institute's activity is restricted to a small number of representative installations. The responsibility for the observation and measurement programme for large scale hot water systems at military barracks has been transferred to a newly founded group at KFA, Zentralstelle für Solartechnik (STE-ZfS). As a new activity, investigations on the usefulness of heat absorbers in combination with heat pumps for heating purposes under German climatic conditions have been started.

The institute is participating in the solar energy programmes of both the International Energy Agency (IEA) and the Commission of the European Communities (CEC). H. D. Talarek is in charge of the Operating Agent for the IEA TASK III collector testing programme. J. W. Grüter[1)] acted as project leader for the CEC project F solar meteorological data project.

On a bilateral basis, there exist a number of cooperative efforts to promote solar energy in developing countries. The collector test station at Atibaia/Brasil has been in operation since spring 1980. Here, flat-plate and concentrating collectors are being tested for their applicability in the temperature range above 100 °C. A simple test loop for comparative testing of hot water collectors has been developed at KFA and partially put into operation at the site of several partner institutes as, e.g., Egyptian Electricity Authority, Cairo/Egypt, Universities of Joao Pessoa and Porto Alegre/Brasil, and University of Yogyakarta/Indonesia.

1) Since Oct. 1, 1980 with KFA-STE (Programmgruppe für Systemanalyse und Technologische Entwicklung)

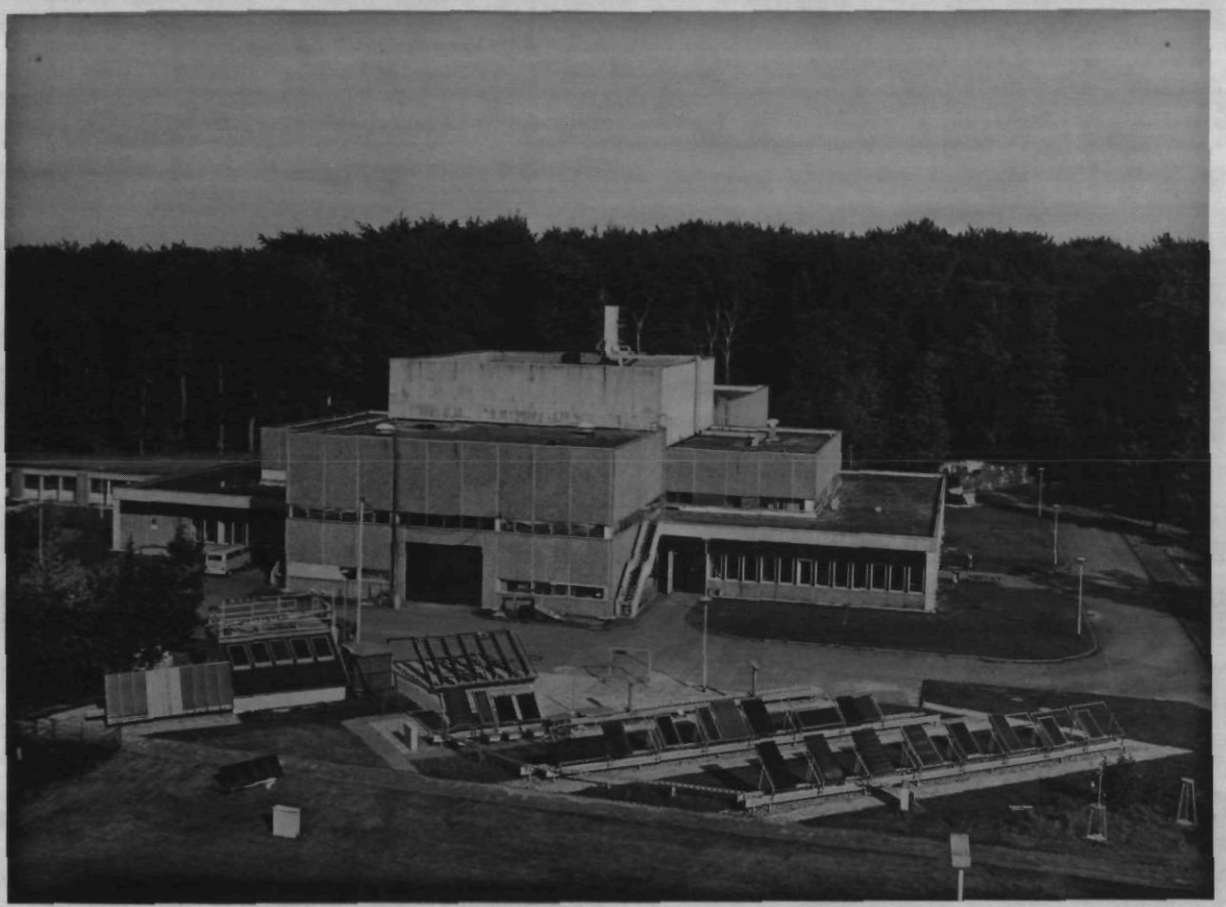

Fig. 1: View of the solar collector test field at KFA-IKP

For the registration of all data were installed two 12-channel strip-chart recorders and a 6-channel line recorder with appropriate transducing amplifiers.

The collector fields and the solar-meteorological station were mounted during 1979 and 1980. Full operation started in April 1980. Up to now there have been measured efficiency curves according to internationally used standards, Figs. 3 a), 3 b), 3 c).

It should be noted that the individual collector modules in a single field are interconnected in series. Neglecting a possible manufacturing scatter of the collector modules, the data points partially represent testing of the same collector type at different temperatures under identical weather conditions[3].

Whilst the parabolic-trough collector type up to now meets the expected performance, there have been difficulties with the flat-plate collectors and the booster-mirror collectors. In contrast to efficiency curves supplied by the manufacturer, the flat-plate collector has much higher thermal losses than expected. It is supposed that these high thermal losses are caused both by a poor back side insulation (soaked material) and deteriorated absorber surfaces. These conclusions are supported by BSE-type efficiency measurements of the same collector type at Jülich[4]. Similar disappointing observations were made with the booster-mirror collector. Therefore, the testing of these two collector types will be finished soon.

The future work will be aimed at detailed short-term and long-term testing of the parabolic-trough collector which is now functioning properly after having corrected the tracking system.

In addition to this main goal the collector test loops will be used by the Brasilian partner for his own purposes in order to develop collector test standards specifically applicable in Brasil. A forth loop has already been intensively used to test commercial flat-plate collectors from Brasilian companies.

We are grateful to José M. V. Martins and Christian Stegmann for the productive co-operation.

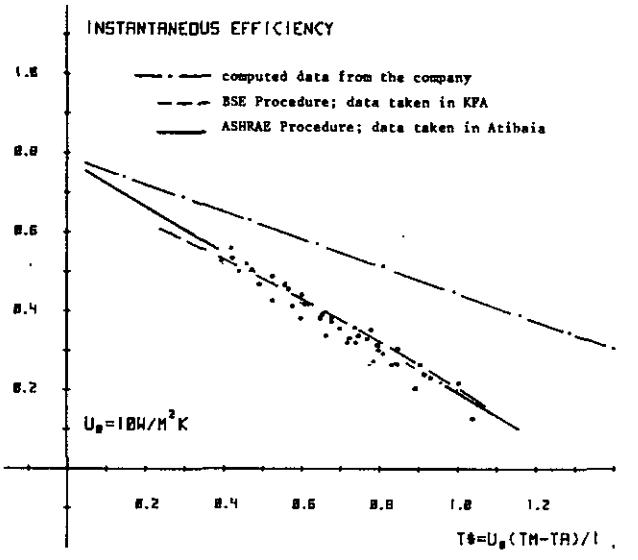

Fig. 3a): Instantaneous-efficiency data of the double-glass, selective-absorber, flat-plate collector type. The slight difference between the measured data in Atibaia and KFA could be explained by different test procedures (ASHRAE, BSE indoor), fluid (oil, water) and instruments.

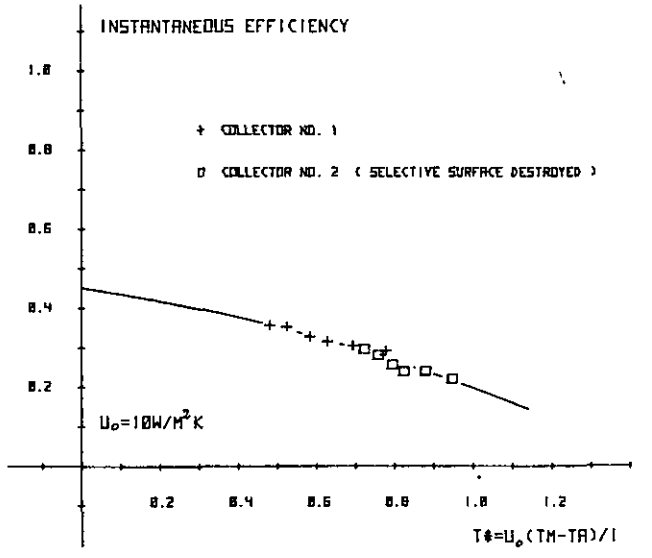

Fig. 3b): Instantaneous-efficiency data of the single-glass, selective-absorber, booster-mirror collector type. The efficiency is related to the global irradiance in the plane of the aperture area of the booster mirrors.

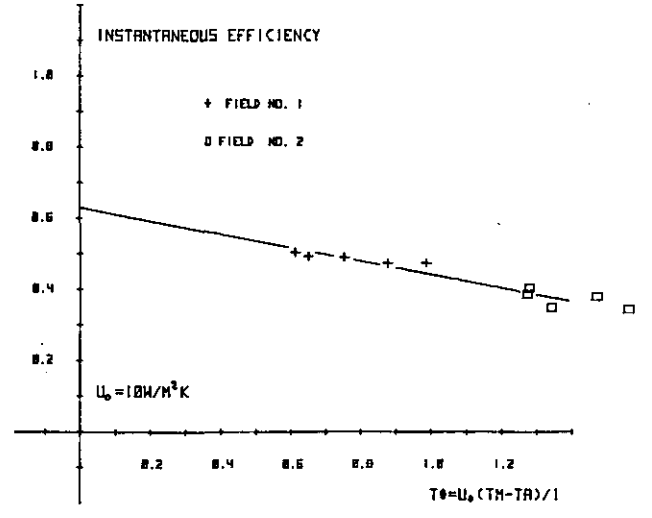

Fig. 3c): Instantaneous-efficiency data of the parabolic-trough collector type. Here, the efficiency is related to the direct component of the solar radiation.

References

1) ASHRAE Standard 93-77, ASHRAE, New York, 1977.

2) BSE Procedure, Part A. Efficiency Tests of Solar Collectors, Bundesverband Solarenergie e.V., Essen, 1979.

3) H. Tabor, Solar Energy, Vol. 20, p. 293-308, Pergamon Press, 1978.

4) R. Schröer, KFA-IKP, to be published.

6.3. IEA Round Robin Testing

H.D. Talarek

The International Energy Agency started a program to develop and test Solar Heating and Cooling Systems in early 1977.

A round robin testing of two liquid-heating flat-plate collectors was conducted. Thermal performance data according to standard test procedures from an international group of laboratories were intercompared and evaluated. While the first phase evaluation had already indicated that the uncertainty of measurements could explain most of the data scatter, it was considered worthwhile to reevaluate the data to quantify the measurement uncertainty and the meteorological impact. A flat-plate collector model[1] was applied to quantify different meteorological conditions during collector testing and the measurement uncertainty introduced by finite instrument accuracy.

The modelling was conducted under the assumption that the relevant meteorological parameters varied between extreme values allowed by the ASHRAE-standard 93-77 [2]. The requirements for the instrumentation implied an uncertainty of measurements.

Fig. 1 to Fig. 4 clearly demonstrate the inherent uncertainty of the testing procedures.
The scatter of data of the efficiency curves is in the "traditional" range obtained from round robin tests. 3, 4, 5)

The analysis has given an indication that systematic test uncertainties of the testing facilities are a key reason for the scatter of measured collector efficiencies.

Apart from the analysis conducted, Participants have expressed their concern about the uncertainty associated with the accuracy of the pyranometers. The Participants had difficulties to ascertain the nominal accuracy of ± 3 % for their pyranometers.

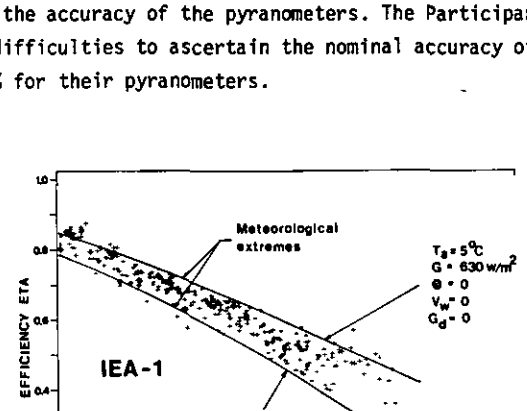

Figure 1: Data enclosed by extremes of collector performance (12 test facilities)

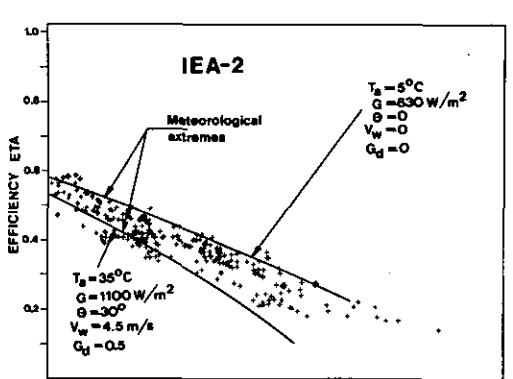

Figure 2: Data enclosed by extremes of collector performance (8 test facilities)

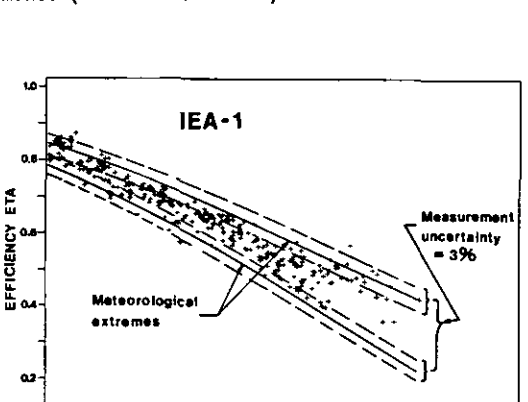

Figure 3: Data enclosed by the combined effect of meteorological extremes and measurement uncertainty (12 test facilities)

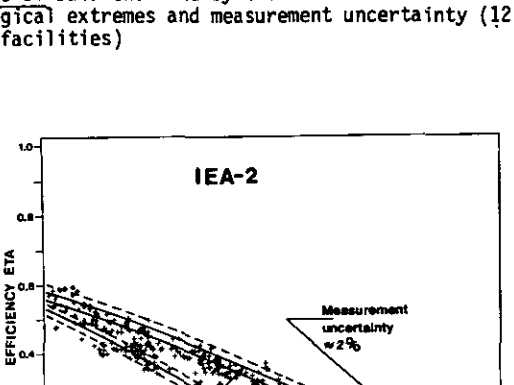

Figure 4: Data enclosed by the combined effect of meteorological extremes and measurement uncertainty (8 test facilities)

Nomenclature for all figures:

T_a = ambient temperature
T_m = mean fluid temperature
G = insolation
U = normalizing coefficient 10 $W/m^2.°K$

6.4. Investigations on all day collector performance

R. Posorski, H. D. Talarek

From June to November 1979 calorimetric measurements were made to determine the useful energy output of an one-cover flat-plate collector with non-selective coating. In addition to the test loop a second collector of the same model was run in no-flow condition to determine maximum stagnation temperature[1]. The meteorological data were recorded simultaneously. For data acquisition a MADAS-system[2] was used, which provides a data base of instantaneous measurements with a sampling rate of 25 seconds.

Figure 1: Test site
1) test-loop-collector
2) no-flow-collector

While the clear-day-performance was investigated in previous experiments with compatible results[3], emphasis was given to study collector-performance with respect to the influence of fluctuative solar radiation. A typical radiation pattern is shown in fig. 2.

In the vincinity of the conversion factor η_0 the collector performs as a linear converter of insolation to sensitive heat.

A significant impact on the efficiency during transient insolation was not observed if reflexion losses (diffuse fraction, angular modifier of the $(\tau\alpha)_e$ product for direct solar radiation) and thermal losses were taken into account. The model used for computing the collector efficiency from the meteorological data showed for all operating conditions an accuracy of ± 2 % compared with the measured results (fig. 2 and 3).

Prediction of all-day collector efficiency based on the instantaneous efficiency curve according to the BSE-procedure for an air velocity of 5 m/s showed deviations of 6 % from the measured results, which lead under low efficiency conditions to considerable differences between predicted and measured useful energy output (fig. 1 and 2). For meteorological conditions of the test site and neighbouring regions the accuracy of the estimations could be improved by using an efficiency curve for an average air velocity of 3 m/s if no specific wind speed data is available.

For predicting the useful energy output more accurately a higher resolution of the efficiency curves with respect to air velocity is necessary, alternatively a method to model the influence of air velocity is adequate. The results indicate that the usability of BSE-Test procedures in the climatic conditions of middle Europe could be largely enhanced, if transient conditions were accepted.

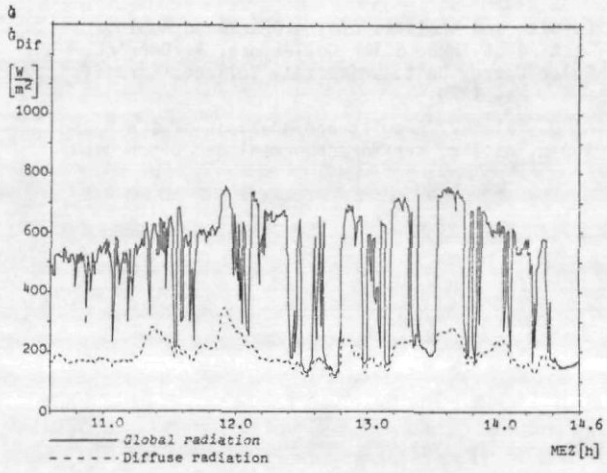

Figure 2: Typical radiation pattern (2.11.79)

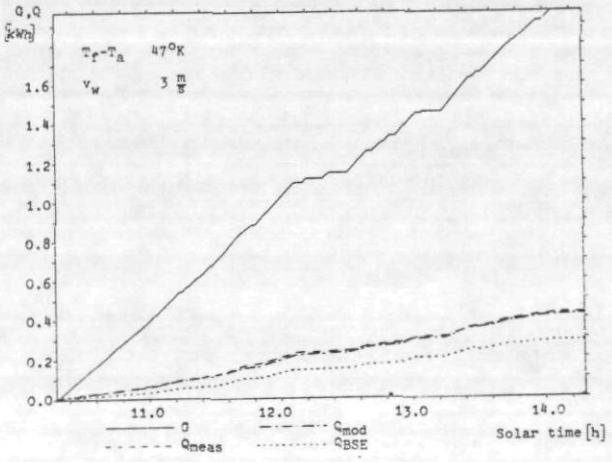

Figure 3: Accumulated values of insolation and useful energy output (2.11.79)

Nomenclature for all figures:

A	= aperture
v_W	= air velocity
G	= $A\int \dot{G}\, dt$
T_a	= ambient temperature
T_f	= mean fluid temperature
Δt	= integration time interval
Q_{MEAS}	= measured useful energy output (ueo)
Q_{BSE}	= predicted ueo by BSE efficiency curve
Q_{MOD}	= predicted ueo by the collector model

References

1) J.A. Duffie, W.A. Beckmann: Solar Energy Thermal Process, John Wiley and Sons, New York, 1974

2) Methods of Testing to Determine the Thermal Performance of Solar Collectors, ASHRAE Standard 93-77, ASHRAE, 345 Est 47th Street, New York, N.Y.10017, 1977

3) E.R. Streed, W.C. Thomas, K.G. Dawson, B.D. Woods, J.E. Hill: Result and Analysis of a Round Robin Test Programme for Liquid-Heating Flat-Plate Solar Collectors, NBS Technical Note 975, August 1978, Washington, D.C.

4) Results and Analysis of the CEC Round Robin Testing of Three Solar Collectors, A. Derrick, Solar Energy Unit, University College, Cardiff, U.K., May 1979

5) H. D. Talarek: Results and Analysis of IEA Round Robin Testing, Kernforschungsanlage JÜlich GmbH

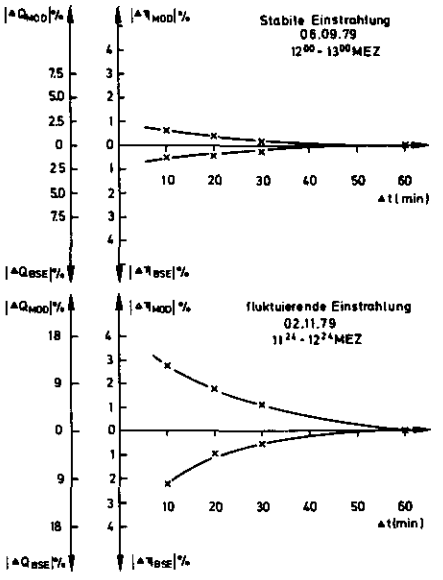

Figure 4: Measurement uncertainty dependent on integration intervals for clear-day and transient radiation conditions

Experimental determination of the collector efficiency is possible for fast transients of radiation if time intervals for data acquisition is properly extended. An integration interval Δt of 30 to 60 minutes is recommended (fig. 4). Additional efforts in equipment and instrumentation are required if this idea is adopted in standard test procedures.

References

1) K. Maßmeyer, Einflüsse meteorologischer Parameter auf die Stillstandstemperatur thermischer Flachkollektoren, University Cologne 1979

2) J.W. Grüter, K.P. Kruck, H. Labus, 1978, MADAS a microprocessor aided data acquisition system Jül Spez-15 issn 0343-7639 /3/

3) J.W. Zerlaut, R.F. Dokos, Heiskell, The use of ASHRAE standard 93-77 in predicting all-day performance of flat-plate collectors Desert Sunshine Exposure Tests, Arizona

6.5. Development of instrumentation

H. Labus

High resolution ΔT-amplifier

For solar measurement applications a low cost amplifier has been developed to detect a small temperature difference (< 20 K) between two platinum resistance thermometers with very high resolution ($<3\cdot10^{-4}$K noise) and long time stability ($<3\cdot10^{-3}$K from 10 to 40°C) and simultaneously the absolute temperature of one of the thermometers with moderate accuracy (< 1%), linearity (< 1%, depending on dynamic range) and response time (< 2 sec). For further cost reduction a very simple adjust procedure allows the use of not narrowly toleranced thermometers.

To achieve these unique features a special scanning process[1] is used as shown in the basic circuit and timing diagram of Fig. 1. A 100Ω reference resistor R0 and two platinum resistors R1 and R2 are fed through their supply lines LI and FET switches SI0, SI1 and SI2 during succesSsive time intervals T0, T1 and T2 by the same current I from a common current source Q. Within time intervals F0, F1 and F2 each beginning after and ending before T0, T1 or T2, the differential FET-switches SU0, SU1 and SU2 are closed and capacitors C0, C1 and C2 are charged via sense lines LS to the voltage drop across their assigned resistors R0, R1 or R2. During a time interval FD, following immediately after T2, the FET-switches SD0, SD1 and SD2 are closed simultaneously to transfer the voltage differences between C1 and C0 to capacitor C10 and between C2 and C1 to capacitor C21. The voltages across C10 and C21 are proportional to the resistor differences R1-R0 and R2-R1 and can easily be amplified as they are referred to ground with single ended amplifiers V10 and V21. All FET-switches are plastic dual-in-line packed COS/MOS analogue multiplexers CD 4053 from RCA. The layout of amp V21 is chosen to give at its output a sensitivity of 1.0 Volt/K within a range of ± 18 Volt for the temperature difference between R2 and R1. Amp V10 has a sensitivity of 0.1 Volt/K within ± 18 Volt for the temperature difference between R1 and R0, which is equal to the absolute temperature of R1 if R0 is a 100Ω reference resistor. Other values of R0, which is connected to the front panel in the same way as the platinum resistors, may be used to center the output of V10 to other points, e.g. 100°C if R0 is 140Ω. R0 may itself be a platinum resistor to measure a second temperature difference between R1 and R0. A dual instrument was first packed in a 2/12 NIM module. A single instrument is now designed to fit on a Single Europe Board.

Fixed current i1 and variable current i2 (i1, i2~0,01·I) from auxiliary current sources Q1 and Q2 allow to compensate slightly different platinum resistors. By adjusting i2 with a front panel trimmer to become zero volt at the output of amp V21 after both resistors R2 and R1 have been forced to any but an exactly equal temperature one can use extremely mismatching resistors for very high resolution difference measurements.

One reason for the good performance of this instrument arises from the pulsed currents through the platinum resistors which can be much higher (10 mA) than in standard dc-circuits without causing auto warm-up. Another reason is the capability of the scanning process to supress the high offsets of the platinum resistors right in the origin, to prevent different common mode levels between the parallel arranged resistors, and to compensate to a high degree drifts of parasitic capacitors of the switches.

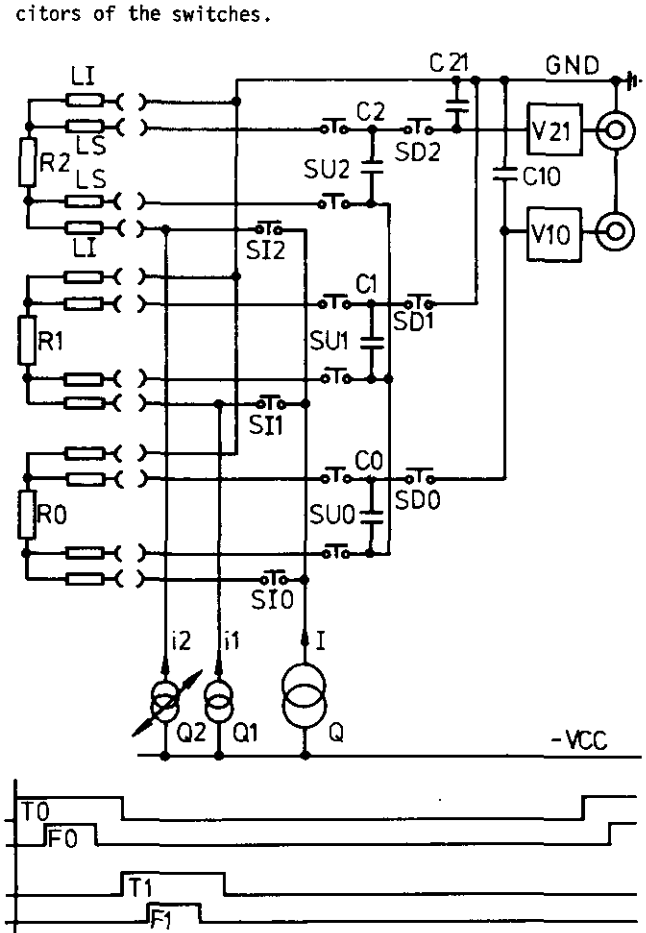

FIG 1: BASIC CIRCUIT AND TIMING DIAGRAM

Reference

1) H. Labus, Messgerät für die praktisch simultane ΔT,T-Messung, Deutsches Patentamt, Offenlegungsschrift P 29 10 608.

Integrating Solar Power Meter

A low cost integrating solar power meter has been developed with following specifications:

The true differential input accepts differential voltages of max. 100 mV. Common mode input voltage is max. ± 3.0 V; permanent overvoltage between any inputs may be ± 50 V.

Calibration voltages from pyranometers or pyrheliometers between 5.0 and 25.0 mV·m^2/KW may be normalized by a front panel trimmer to a sensitivity of 1000 c·m^2/KW.

Normalized radiation power N is displayed by a 4-digit LED-display with a resolution of 1 W in the range $0 < N < 4095$ W. Stability is 1 W from 10 °C to 40 °C, linearity is < 0.02 %. The display indicates negative input polarity and overvoltage. Nonvolatile integration of the solar power is accomplished by a mechanic counter with a sensitivity of 1 pulse/Wh.

The good overall performance of the instrument is achieved by a circuit as basically shown in Fig. 1, which consists of only 3 IC's: a dual-slope-integrator ICL-7109, a one chip microcomputer MCS-8748, and an intelligent LED-display DL-1416A. The use of monolithic dual-slope-integrators as input-pickup for this and related applications is patended[1]. Voltage to frequency converters, normally used as input device, cannot compete regarding linearity, zero-stability and even costs, as they need high performance preamplifiers.

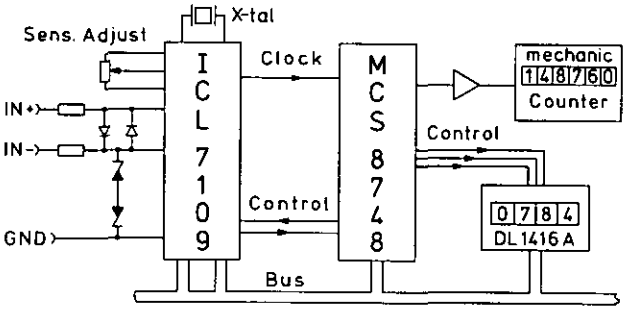

Fig1: Basic Circuit

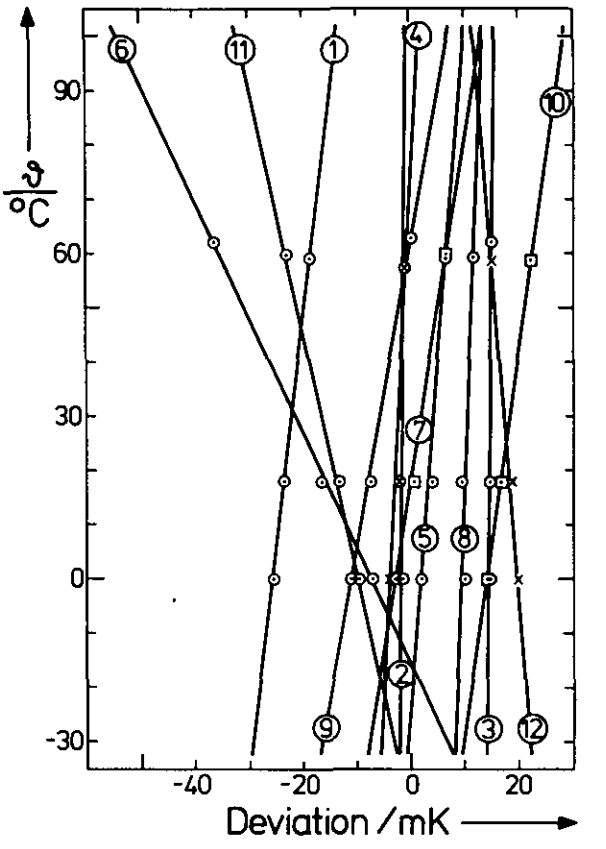

Figure 1: Deviations of measured temperature values obtained from twelve platinum resistance thermometers of high precision (1/10 DIN tolerance) as functions of the temperature ϑ. The diagram can be used to select matched pairs of P.R.T. sensors for very precise ΔT measurements, e.g. 2-4, 3-8, 5-7, 10-12, 6-11 and 1-9.

Reference

1) R. Nellen, H. Labus, Langzeitintegrator für eine Spannungsquelle kleiner Spannung, Deutsches Patentamt, P 2856 687

6.6. Use of ΔT Amplifier in Selecting Matched Pairs of Platinum Resistance Thermometers

H. Labus, R. Wagner

Though the ΔT amplifier described above was designed to allow precise ΔT measurements even with resistance thermometers not narrowly toleranced, its high resolution provides advantages in the handling of narrowly toleranced temperature sensors, too. As an example, the selection of matched pairs is described. The fulfilment of specifications ($^1/_{10}$ DIN tolerance) of a dozen platinum resistance thermometers (P.R.T.'s) had to be checked, and matched pairs were needed for a temperature range between -30 and +80 °C.

A thermally insulated temperature bath was used consisting of a small (2 l) Dewar vessel with a copper block for the twelve sensors, a polystyrene foam cover and an additional outer polystyrene foam insulation for the whole vessel.

As each plug-in unit of the pilot series contains two ΔT amplifiers, the P.R.T.'s No. 1 - No. 12 were divided into two groups of six, and in each group a reference sensor was chosen. At three temperatures of the bath (and the copper block), 18 °C, 0 °C, and 63 ... 58 °C (decreasing approximately 1 K/hour), the deviations between the P.R.T.'s and one of the reference P.R.T.'s, and also the deviation between the two reference sensors themselves were measured as virtual temperature differences. (The use of the second amplifier of the plug-in unit and, hence, of an auxiliary second reference P.R.T. is, of course, not essential, but in many cases time saving.)

For very precise absolute measurements of temperatures with the sensors thus examined, an absolute calibration of one, e.g. the reference sensor at two temperatures (e.g. the freezing and the boiling point of water) would have to be made. But for by far most of the possible applications the procedure described is sufficient.

In figure 1 the deviations of the twelve P.R.T.'s are recalculated relative to their mean value at the respective temperature and are thus independent of a certain reference sensor, but depend only on the ensemble as a whole. They are plotted versus the bath temperature.

6.7. Indoor measurements on the heat balance of an absorber plate

K. Maßmeyer, R. Posorski, H. J. Stein

With an appropriate set of parameters - measurable in principle by indoor experiments - it should be possible to characterize the heat transfer behaviour of an absorber element and to calculate the instantaneous heat gains of such an element under actual weather and operating conditions.

To minimize the influence of uncontrolled meteorological parameters, such as global irradiance, thermal radiation and wind speed, all experiments were performed by indoor testing under steady state conditions. Calorimetric measurements were carried out on two absorber plates mounted in series on a comparative test stand designed for solar flat plate collector testing. The plates were tilted under an angle of 45^{0} and their back sides were isolated.

In addition to the above mentioned meteorological data, ambient temperature (indoor air temperature $\sim 22\ ^{o}C$) and humidity were recorded together with the inlet/outlet temperature of the heat transfer fluid. The mass flow ($72\ l/(hm^2)$) was kept constant by a mass flow controller.

The inlet temperatures ranged from 4 to 76 ^{o}C though producing heat gains and losses of the absorber plate. The results for natural (a) and forced (b) convection are shown in Fig. 1. Plate temperatures below the dew point make the utilization of latent heat of the condensed water vapour possible. Only in the case of strongly forced convection - 6 m/s in the plane of the absorber - the dew formation was fertile enough to show a significant heat gain represented by a steeper gradient. The deficiency of such an additional heat gain for natural convection may be an indication that the accuracy of the measurements has to be improved. Recalibration of the sensors and detailed measurements concerning the heat transfer are currently carried out together with developing a reliable model to predict the energy output of an absorber plate under outdoor conditions.

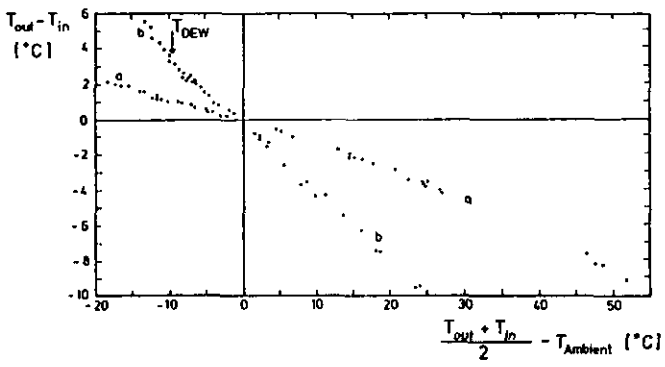

Figure 1: Measured temperature spread of the heat transfer medium in a two sheet type absorber plate (area = 1.1 m^2) monitored under different operational indoor conditions (a: natural convection, b: forced convection)

6.8. An outdoor test facility for heat absorbers

R. Wagner

For a reliable assessment of the heat absorber technology and its potential use for house heating, the validity and accuracy of computer simulations should be checked by experiments.

An outdoor studies facility was constructed for this purpose having the following features:

1. Four parallel fluid loops to study simultaneously
   a) different configurations and/or orientations of equal absorber elements or
   b) equal configurations (and orientations) of different absorber elements.

   At present, case (a) is realized for the outlined fundamental studies; switching to case (b) later for comparative tests of different types and products is no problem.
2. The inlet temperature of all loops is the same; it is controlled by a thermostat with a heating power of 3 kW, a cooling power of 4.5 kW at + 10 ^{o}C and 3 kW at -10 ^{o}C, and a lower temperature limit of -40 ^{o}C. The thermostat contains a buffer bath with a volume of nearly 20 liters.
3. At present, the thermostat allows two operational strategies:
   a) constant inlet temperature or
   b) a constant difference between the inlet temperature of the fluid and the ambient temperature.

   (If necessary or desirable, an optional accessory will allow to program a variety of temperature profiles, linear in time dependence, instead of the constant inlet temperature.)
4. Whilst the inlet temperature is the same for all four loops, the fluid flow can be set individually for each loop in the range 10-150 liters/hour or 30-350 liters/hour, is kept constant within about $\pm$ 2 percent by a mechanical flow controller, is indicated by a flow meter and measured by a volume flow counter with a pulse output (0.01 liters/pulse) and a mechanical counter.
5. Solar absorber panels (2.00 m x 0.55 m) of the two sheet type (originally designed for the construction of fully roof-integrated collector areas covered by glass tiles) are used as heat absorber elements for the first equipment of the facility. Three of the four loops are used for studying three different configurations of these absorber elements:
   a) Configuration I consists of four elements. Orientation: south; inclination: ca. 60^{o} from horizontal. The rear sides of the elements are thermally insulated with 5 mm of polyurethane foam plus 20 mm of polystyrene foam.
   b) Configuration II consists of three elements with the same orientation and inclination, but without thermal insulation: the ambient air has free access to the rear surface, too.

   Configurations I + II are mounted on a simulated wooden roof half 2.25 m x 5.75 m on a steel support which allows to change the inclination. The distance between the roof surface and the rear surface of configuration II is 13.5 cm.
   c) Configuration III consists of four elements (in two groups of two) mounted vertically at the north façade of the prefabricated steel cabin which houses the data acquisition systems of the solar group. The rear sides of the absorbers are not thermally insulated; their distance from the façade surface is 16.5 cm.
6. By using a combination of fix copper tubing and interchangeable rubber hosing and a sufficient number of valves, it is possible in each configuration to use the absorber elements in parallel or in series, or in any combination of parallel and series circuits. Besides, any of the absorber elements can be short-circuitted and excluded from the fluid flow for stagnation temperature measurements.
7. Ports for temperature sensors are provided at the inlet and outlet of each absorber element, and, if necessary, a second temperature sensor is applicable at the inlet or outlet of any absorber element without soldering (e.g. for analog registration of selected data in parallel to the automatic data acquisition of the facility).

Data acquisition and meteorological instrumentation will be described in a further communication.

6.9. Heat and radiation balance measurements at the solar energy test stand of KFA-IKP

K. Maßmeyer, J.W. Grüter

Efficiency, thermal losses and stagnation temperature of solar collectors are very sensitive to changes in meteorological parameters as solar insolation, air temperature or wind speed. The influence of these variables on the stagnation temperature of a flat plate solar collector is discussed by Maßmeyer[1]. Moreover the meteorological station[2] enables the calculation of the daily variation of the energy exchange at the surface of the ground. The governing equation for this physical process at the surface is

$$(1)\quad Q = H + V + B$$

where Q is the all wavelength radiation balance, B the soil heat flux. The turbulent fluxes of sensible heat H (not involving changes of state) and of latent heat V which is the contribution of latent heat of evaporation and evapotranspiration of plants were calculated according to the method of Sverdrup[3,4].

This relative rough model derived for horizontal homogeneous terrain yields also good results in the inhomogeneous surrounding of the collector test field. Figures 1 and 2 show the daily variation of the components of the radiation balance for clear sky conditions on August 19, 1978 and the rather cloudy sky of September 10, 1978. The radiation balance in the spectral region greater than 3 µm is negative all day long. This cooling of the earth's surface is balanced by the gain of energy in the spectral range between 0.3 µm and 3 µm due to the absorption of radiation. The size of the radiation balance is a function of cloudiness and cloud type. The vertical profile of water vapour, carbon dioxide and ozone describes the atmospheric counter radiation $E_L\downarrow$. Cloudiness raises the counter radiation in the "atmospheric window".

On August 19 the counter radiation sinks below 300 W/m^2 because of the absence of clouds. During the first hours of September 10 the cooling of the earth's surface is lowered by higher counter radiation (370 W/m^2). With increasing global radiation $E_G\downarrow$ the longwave radiative fluxes raises, too, due to the solar heating of the atmosphere and of the ground surface. A sharp increase of the counter radiation coupled with a decrease of solar insolation was found on September 10 at 8.30 MEZ.

The radiation balance must be known for the calculation of the fluxes of latent and sensible heat, whereas the soil heat flux can be computed from the soil temperature profiles alone. Sensible and latent heat fluxes were calculated with the Sverdrup method according to the profiles of dry and wet bulb temperatures, the radiation balance and the soil heat flux. The results are shown in fig. 3 and 4.

On August 19 the energy balance is characterized by the following features. The energy fluxes are nearly constant at night because of constant cloudiness, the variation during daytime is nearly sinusoidal and symmetric to local noon (12.34 MEZ). Because of the intensive increase in the radiation balance, high vertical energy transport develops. Soon after sunrise the soil heat flux decreases until the latent heat flux stagnates. The course of the energy transport is strongly coupled with a transfer coefficient which is dependent on wind speed and temperature profile of the atmosphere[5].

Future investigations will involve other models for determining the heat fluxes. In particular the influence of the inhomogeneity of the surrounding will be considered.

The study is being carried out in collaboration with the Institut für Geophysik und Meteorologie of the University of Köln.

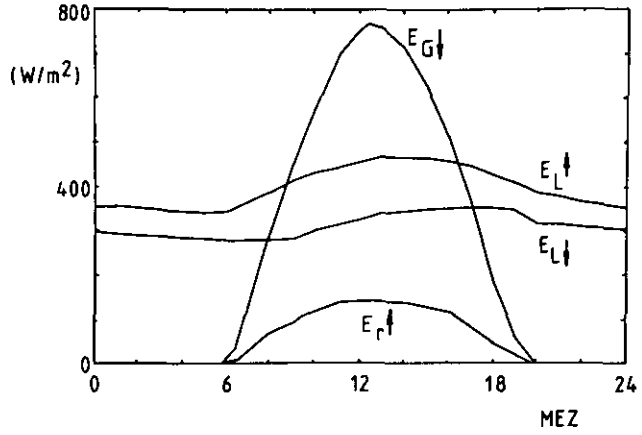

Figure 1: Daily cycle of the components of the radiation balance $Q = E_G\downarrow + E_L\downarrow - E_r\uparrow - E_L\uparrow$ from August 19, 1978

$E_G\downarrow$ global radiation
$E_L\downarrow$ atm. counter radiation
$E_r\uparrow$ global radiation reflected from the ground
$E_L\uparrow$ thermal radiation from the ground plus reflected counter radiation

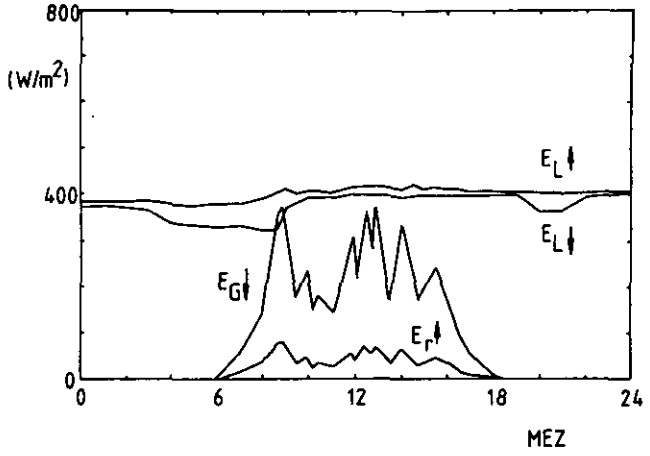

Figure 2: Daily cycle of the components of the radiation balance from September 10, 1978

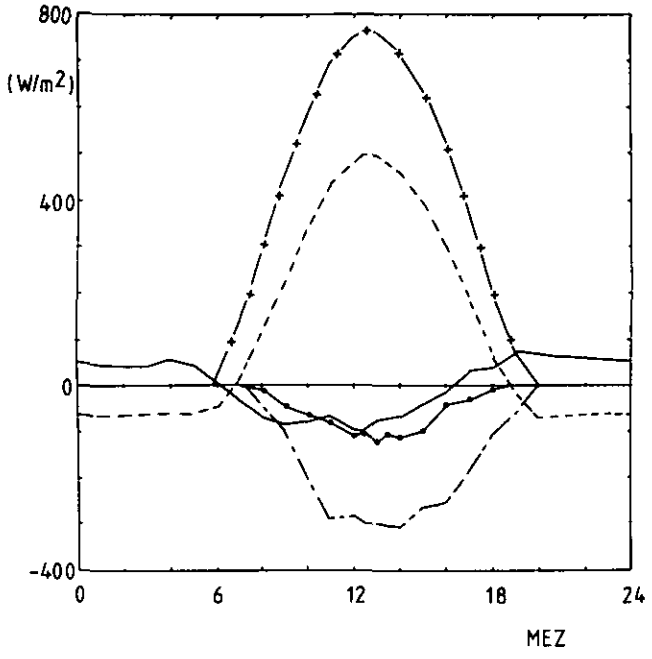

Figure 3: Daily variation of the vertical energy fluxes of August 19, 1978

- + — + — global radiation
---------- radiation balance
- — - — latent heat flux
—— soil heat flux
—o—o— sensible heat flux

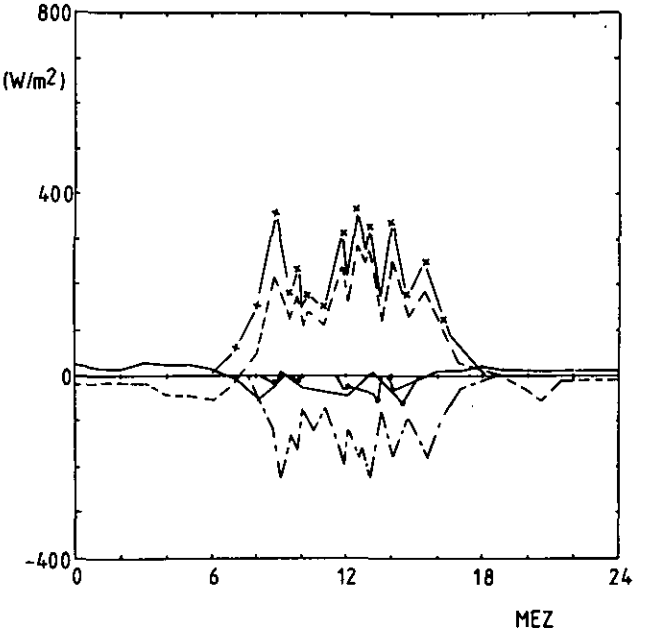

Figure 4: Daily variation of the vertical energy fluxes of September 10, 1978

References

1) K. Maßmeyer, Einflüsse meteorologischer Parameter auf die Stillstandtemperatur von thermischen Flachkollektoren, Diplomarbeit an der Universität Köln, 1979

2) K. Maßmeyer, J. W. Grüter, Instrumentation for energy exchange measurements in the Prandtl layer, JÜl-Spez-15, 9.5.1978

3) I.S. Bowen, The ratio of heat losses by conduction and by evaporation from any water surface, Phys. Review 27, 779-787, 1926

4) H.U. Sverdrup, The eddy conductivity over a smooth snow field, Geophys. Publikasjoner 11 (7), 1936

5) H. Häckel, K. Häckl, H. Kraus, Die Tagesgänge des Energiehaushaltes der Erdoberfläche auf der Alp Chukhung im Gebiet des Mount Everest, Universitätsverlag Wagner, Khumbu Himalaya 7, 71-134, 1970

6.10. Radiation temperature correlations for the computation of the heat production of collectors

H. R. Koch, K. Maßmeyer, W. Scheller

One of the necessities for the development of optimized solar systems is a reliable computation of the expected energy output of solar collectors on the basis of meteorological data. We have learned from collector test experiments that this energy is easily determined for short periods of steady state conditions with the help of an efficiency curve η which is a function of the reduced temperature $T^* = U_o(T_c - T_a)/G$.[1)]

U_o = 10 W/(K·m^2) (normalizing coefficient)
T_c = mean collector temperature
T_a = air temperature
G = incident radiation power (W/m^2)

In a more precise representation corrections should be applied for effects caused by wind speed and by variable angles of radiation incidence. Nevertheless, the determination of the short time energy output of a low temperature solar collector with the help of an efficiency curve may be regarded as sufficient in view of the considerable uncertainties in the estimation of the overall efficiency of a complete solar system.

For low temperature collectors the main contribution to energy losses arises from heat flow to the ambient air and it is obvious that the correlation between radiation and air temperature must be accounted for in energy output calculations. The seasonal and stochastic variations of our climate lead us to regard these correlations separately for every month. Relevant data sets should be derived from measurements during several years.

The complete information on weather conditions is only preserved in data sets containing time sequential measurements. An appropriate integration length for one data point is about 1 hour for flat plate collectors.[2)] The amount of data obtained in this way, is difficult to handle. Data reduction methods are needed in order to apply relatively simple procedures for useful energy computations.

Within our contribution to the action F 3.4 of the solar research programme of the European Community we have started to study a method of data reduction which preserves the radiation temperature correlation. The method is based on the work of P. Kesselring and his co-workers.[3)]

The heat output of a collector for short intervals Δt, distinguished by "i", can be written as

$$\Delta E_i = A \cdot \eta(T^*) \cdot G_i \cdot \Delta t \qquad (A = \text{collector area})$$

The energy contributions which are obtained during a longer period, for example 1 month, can be grouped according to the magnitude of T^*. The groups are distinguished by "j":

$$\Delta E_{ij} = A \cdot \eta_j \cdot G_{ij} \cdot \Delta t$$

The efficiency η depends only on T^* or the index j, leading to the following expression for the sum of the energy output:

$$E = \sum_{i=1}^{m} \Delta E_{ij} = A \cdot \sum_{j=1}^{n} \eta_j \cdot \sum_{i=1}^{m} G_{ij'} \cdot \delta_{jj'} \cdot \Delta t$$

m = number of measurements
n = number of T^*-groups
$\delta_{jj'}$=1 if j=j'
$\delta_{jj'}$=0 if j≠j'

We define a radiation energy distribution RED(T^*) which is represented by

$$RED_j = \sum_{i=1}^{m} G_{ij'} \cdot \delta_{jj'} \cdot \Delta t / \Delta T^*$$

ΔT^* = width of the T^*-groups

and we obtain

$$E = A \cdot \sum_{j=1}^{n} \eta_j \cdot RED_j \cdot \Delta T^*$$

or

$$E = A \cdot \int \eta(T^*) \cdot RED(T^*)\, dT^*$$

The above given equations correspond with the mathematical formalism described by Kesselring[3)]. We have replaced the integrals by sums, which can be directly used in the application of the method. We hope that in this way the procedure is understood more easily. The aim of this formalism is, to separate to a certain degree the collector dependent parameters from weather parameters. The function RED(T^*) is computed with the global radiation on the collector surface as a function of T^* which is given by a fixed average collector temperature and by the air temperature. The properties of the collector are given by its efficiency $\eta(T^*)$. The definition of our RED-function differs in the following way from Kesselring's MURD-function: we use the quantity T^* as ordering parameter instead of the x-parameter which contains as further collector specific characteristics incident angle modification and an assumption on the temperature variation of the thermal loss coefficient of the collector. Therefore, the RED function is more general and it can be computed more easily. On the other hand the MURD function eventually gives more precise results for the computed energy output. An example of the RED-function is shown in figure 1. The roughness of the curve is due to statistical fluctuations as only one month was considered. We have started to study the usefulness of reduced meteorological data sets of the discussed types within the CEC action 3.4 and we hope to achieve quantitative results which will have some influence on the measurement of meteorological data and suitable ways of data reduction.

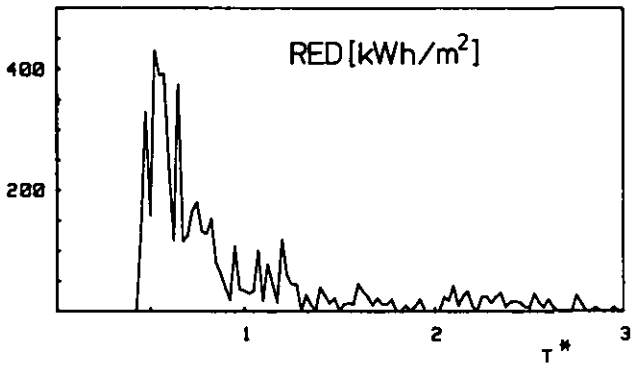

Figure 1: The RED-function (see text) for Jülich, May 1980. Collector temperature: 60 °C; collector tilt: 60° south; $\Delta T^* = 0.025$.

References

1) IEA-report: Results and Analysis of IEA Round Robin Testing Jülich, December 1979

2) H. R. Koch, W. Grüter: Report on the 1st Solar Research Programme of the CEC, action F 3.3, 1980

3) P. Kesselring, A. Duppenthaler: Contribution to the ISES 1979 International Congress on Solar Energy, May 28 - June 1, Atlanta/USA

6.11. Observation and measurement program for large solar hot water supply systems at military barracks

J. W. Grüter[+], *H. Riemer*[++] *and H. Ringel*[+++]

In the years 1978 to 1980 eight solar hot water supply systems (SHWS) were installed and brought into operation[1] in various military barracks in the F.R.G. Since summer 1980 all installations but one are formally accepted and operated by the staff of the military barracks. The SHWS are flat-plate collector systems, different in size and orientation. The collector areas range from 130 to 230 m^2. The tank sizes are from 6 to 12 m^3 covering 1 to 2 daily nominal loads of hot water. The solar systems are combined with the existing central hot water supply system in two ways:

1. a mixing of hot water from the central supply with hot water from the solar system,
2. the solar system is used as a preheating system and a secondary heat source boosters the temperature of the solar heated water to the nominal temperature.

The system's design was made by the manufacturers.

In June 1979 a first seminar was held in the KFA where the manufacturers gave reports about design and construction of the 8 systems. 55 invited participants from the federal and county financial and building administrations discussed very openly the different problems of solar energy systems. In autumn 1979 a commission of engineers from the financial governmental administration on behalf of the Ministry of Defense and a member of the KFA research group made a first inspection tour to all systems. A comprehensive German report on these two events combined with the first results of the observation and measurement program of the KFA has been published in summer 1980.[2]

Three major problems have been identified:

1. Bad quality of collectors. In one system the third generation of collectors has been installed.
2. Connection with the secondary supply system. Pressure problems are to be solved.
3. Low load demand. Most of the systems have too large dimensions compared with the real load in the buildings.

Regarding point 2: the mixing which suppresses the low temperature heat source "solar energy" will be omitted in the near future by reassembling the installations. In most cases modifications are possible which solve also topic 3: The SHWS output is transferred through the circulation tubes into the central supply. By this the SHWS is used as a preheating system. In summer, especially on weekends, the SHWS can cover the load demand of the whole camp with at least ten additional barracks of the same size, as observed in Kassel for example.

The measurements are performed regularly since spring 1980 in two ways. Three installations have been observed by "solarnet"[3], 5 installations are equipped with integration units so that staff personnel of the camps can read off the integrated heat fluxes in regular intervals. Several difficulties in the measurement equipment and data transfer system resulted in only preliminary data on the performance of the SHWS:

- hang up in the mass flow meters, not recognized by the operator (missing training),
- late data communication to the KFA, sometimes months after read off,
- inoperable data communication lines,
- a flash destroyed the data acquisition system at Unna in July 1980.

The winter 1980/81 will be used to remedy the different errors.

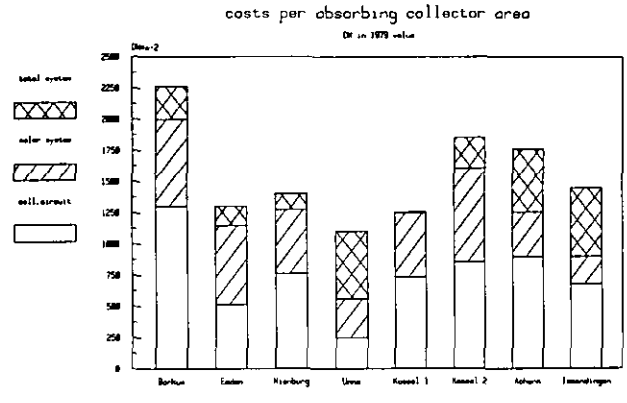

Figure 1

Regarding costs figure 1 shows the specific costs/m^2 installed. For the average system, installed for a nominal daily load of 195 kWh at 311 °K, one gets average installation costs of 295 TDM resulting in a specific price(costs/loadpower)of 36 DM/Watt installed.

For the whole project inclusive installation too few manpower was available. Recognizing this difficulty the project was transferred into the responsibility of the "Zentralstelle für Solartechnik" (ZfS), a working group founded at the STE in October 1980, stimulated partly by the experience in the described project. The ZfS is responsible for the observation and measurement of 35 HSWS installed in 1980/81 at military barracks and other projects sponsored by the BMFT.

+ now at Programmgruppe für Systemanalyse und technologische Entwicklung (STE)

++ STE

+++ left KFA July 1980

References

1) Annual report 1978, JÜL-SPEZ-36

2) Zwischenbericht Solaranlagen Bundeswehr 1980

3) Annual report 1980

6.12. Data acquisition from solar test facilities by telecommunication

H. Ringel[+], *J. W. Grüter*[++], *F. Rongen*[+++]

In 1979 MADAS[1] type data acquisition systems have been installed at three hot water supply systems in Unna, Achern and Borkum[2]. In addition a radiation station on the roof of the IKP building and the small energy balance station[1] at the IKP are monitored by MADAS. These five systems are connected as a network called "Solarnet", fig. 1.

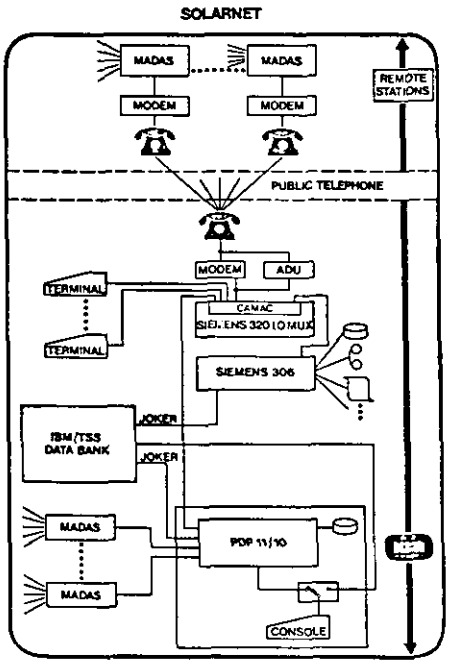

Figure 1

Four systems are connected via the public telephone network with MODEM to a Central Communication Prozessor (CCP1) in the ZEL[+++], 1 system is connected to the CCP2 (a PDP11/10).

The data acquisition network is run by the method of "distributed intelligence". MADAS is an autonomeous switch on system, based on the INTEL 8080 CPU with 24 K data buffer memory. The monitoring program resides on PROM starting immediately after power on. The program synchronized to a battery buffered real time clock dumps the data after the programmed averaging period into the buffer memory.

A data handling overhead structure based on methods developed in CERN[3] is superimposed in order to allow easy orientation in the data flow in case of disturbances during transfer. At fixed terms the CCP calls the stations and transfers the data onto the disk system of the CCP. The data transfer procedure is developed in cooperation with the ZEL simplifying standard procedures. On MADAS the transfer routines are identically programmable in BASIC, for the two CCP's, only the connection module differs occupying the same position in the crate. The according assembler routines are used by identical BASIC-calls using the same space in the EPROM's.

Automatically, the data are transferred from the CCP's via JOKER[4] into TSS[5] residing on the central IBM computer system of the KFA at ZAM. Data handling routines have been developed which strip the data transfer overhead and sort the data into the data bank system "Sonne". This data bank is easily accessible for scientific programmers familiar with FORTRAN. Simple procedures are available for printing and plotting of basic parameters of the stations. An extensive documentation is under preparation.

The experience with the system components is quite reasonable. The MADAS is functioning well; no malfunction was detected during the past 2 years. Difficulties had to be overcome for the data line via the PDP11. There are still hang ups of the system during transfer which occur every 1-2 weeks. A decision was taken to cancel this line of development. The data from the energy balance station until now transferred via the PDP11 will then be transmitted via telephone starting in February 1981.

The telecommunication via public telephone functioned quite well but no permanent connection to Borkum was possible because of malfunctions and damping in the lines. An improvement will be achieved in January 1981 as indicated by the Federal Post Office.

An analysis of the costs and system configuration for the ZfS[++++] which has to order additional data acquisition systems led to the following conclusions:

- for the non-experienced user the system components are too manyfold,
- the CAMAC overhead is too expensive, the advantages are applicable only if variability is mendatory,
- BASIC is well-adapted to the problem of data acquisition in solar energy.

These facts stimulated the decision to change the hardware configuration of MADAS. By now the ZfS will order a MADAS based on the personal computer APPLE II[6].

+ left KFA July 1980

++ now at Programmgruppe für Systemanalyse und technologische Entwicklung (STE)

+++ Zentrallabor für Elektronik (ZEL)

++++ Zentralstelle für Solartechnik

References

1) Annual report 78, JÜL-SPEZ-36

2) Zwischenbericht Solaranlagen Bundeswehr 1980

3) Per Scharff Hansen CERN, Experimental physics division, private communication
further details, CERN-DD/OC/79/1, internal report

4) JÜl/1004/MA/73

5) Time sharing Multiuser system of IBM

6) Apple Computer Inc., Cupertino, USA

IV. TECHNICAL DEVELOPMENT

7. ISOCHRONOUS CYCLOTRON

7.1. Cyclotron Operation and Improvement

L. Aldea, H.G. Böge, W. Brautigam, H. Borsch, R. Brings, R. Fiedler, I. Jannakos, C. Mayer-Böricke, J. Reich, A. Retz, U. Rindfleisch, G. Schlienkamp, H. Schwan, P. Wucherer

In 1980 the cyclotron was in 21 shifts per week operation during 45 weeks being available for experiments, beam development and testing new components for 84% of the scheduled operating time (see table 1). This result has been achieved in 167 different runs, for which energy and/or target station were changed.

CYCLOTRON OPERATION		
Cyclotron tuning and beam handling	546 h	7.3 %
Beam on target	5223 h	69.7 %
Beam time for experiments	5769 h	77.0 %
Beam development, testing new components	529 h	7.1 %
CYCLOTRON OPERATIONAL	6298 h	84.1 %
SCHEDULED MAINTENANCE	232 h	3.1 %
SYSTEM FAILURES	958 h	12.8 %
SCHEDULED OPERATING TIME	7488 h	100.0 %
BEAM TIME DISTRIBUTION		
Guest scientists (U.Bonn, TH Darmstadt, U. Hamburg, MPI Heidelberg, KfK Karlsruhe, U.Köln, U.Münster, IPN Orsay, U.Tübingen)	1323 h	22.9 %
Scientists of KFA exclusing IKP (ICH1-IME,-ARA)	569 h	9.9 %
Scientists of IKP	3877 h	67.2 %
Beam time for experiments	5769 h	100.0 %

Table 1: Cyclotron time distribution in 1980

In the following the improvements and developments at the cyclotron are shortly described. In first place they have been carried out to improve the performance of experiments with the spectrograph BIG KARL.

1. After the EVIDAL Aluminum cooling plates of the 3 RF-resonators had to be cured from corosion in 1979[1] the shorts between inner and outer conductor (being the parts with maximum RF-power dissipation) have been replaced by new cooling plates during the annual shut down. They have been manufactured from copper plated Aluminum sheets to which stainless steel tubes have been soldered. The interchange of cooling plates at the RF-resonators has to be carried on.
2. A new frequency control unit has been installed and tested during the annual shut down. The design details are given in chapter 8.2.
3. The focusing channel[2] leading the beam through the fringe field of the cyclotron has been modified for remote positionning (see also chapter 15) to improve the beam extraction. At the same time detailed field mapping within the focusing channel was done at three cyclotron magnet excitations. The analysis of the field data by means of a modified program SOTRM[3] was in progress by the end of the year. The program calculates the first and second order transfer matrices and searches for a reference trajectory giving minimum beam distortion. According to this evaluation 2 smaller graphite diaphragms shall be inserted in the focusing channel in spring 1981.
4. The adjustment of the beam line to the spectrograph BIG KARL has been revised to find the origin of steering effects in the region following the switching magnet SM3. A vertical offset of 1 mm in the optical axis before and after SM3 was the main origin.
5. To facilitate the steering procedures in the beam handling system two additional steering magnets have been installed (1 within the cyclotron vacuum chamber, 1 in the beam line to BIG KARL).
6. The first order focusing in the Jülich double monochromator[4] can now be monitored via an object plunger at the intermediate slit IS and a viewing screen at the outlet slit DS2. The slits AS1 and 2, which are the entrance and exit slits for achromatic mode operation and angular defining slits in dispersive mode operation have been made additionally movable in their center position and serve as beam diagnosis tools as well (see also chapter 13).
7. The components of the new microprocessor controlled emittance measuring device, which was designed last year[1], were delivered in May, assembled and successively tested. According to the specifications the manufacturer (NTG Gelnhausen) eliminated hard- and software bugs. The system was finally accepted in December. Since in the meantime the software, which handles the data transfer between microprocessor and PDP 11/34, has been written and debugged (see also chapter 12.2) the system is now working off line. It will be installed at the cyclotron in spring 1981.
8. A voltmeter and scanner system (Fluke) monitoring the actual values of parameters at the cyclotron and the beam handling system has been installed and interfaced via CAMAC to the PDP 11/34. For this a total of 70 shunts, which are independent from the individual power supply, has been calibrated and installed. Some of the necessary handling, display and cyclotron operator guiding software has been written. The parameter monitoring led to an improved reproducibility.

References

1) Annual Report 1979, Jül-Spez-72, March 1980, p. 141
2) H. Thimmel, P. Wucherer, IEEE Trans. N.S. 16, No. 3, June 1969, p. 474
3) E.R. Close, Nucl. Instr. and Meth. 89 (1970) 205
4) J. Reich, C. Mayer-Böricke, K.L. Brown, F.E. Johnson, AIP Conf. Proceedings 9 (1972) 407

7.2. A New Frequency Control Unit

*W. Bräutigam, K. Kennepohl**

As the RF-system of JULIC is of self oscillating type, the actual frequency in the range of 20-30 MHz is achieved by a mechanical tuning of the three dees. Coarse frequency setting is done with the aid of panels, while the closed loop control uses servo motor driven rotating loops in the space between dee and dummy dee. A brief description shows the disadvantages of the present situation: The instantaneous frequency is measured by a normal gated counter with a sampling rate of about 100 sec^{-1}. The digital output of the counter is compared with the preselected value in a simple computing circuit, which feeds the difference between actual and nominal value including the sign to a digital/analog converter. The DC output via servos then controls the angular position of the tuning loops in the cyclotron. This system establishes a good long term stability, dependant only on the quality of the gate time reference in the counter, but operates very slowly and cannot provide sufficient suppression of short term (>1Hz) instabilities. Other disadvantages are obvious too: The frequency resolution is principally restricted to 100 Hz minimum. There is only a limited continuous regulation, which forbids the future use of high speed tuning elements.

To overcome these limitations we decided to develop a new device with the following features: compatible with the present serve system, real time frequency information, resolution better than 1 Hz, adequate for a future more sophisticated fast frequency tuning system. The principle of real time frequency detection is well known from FM radio communication, but we had to built an instrument, which meets our special requirements. Comparing various high quality frequency discriminators we found, that quartz devices would be the best choice, because they are easily available in various types and offer exceptional good performance. An idea of the total system is given in Fig. 1.

A signal f_{cy} from the cyclotron is fed via a bandpass filter for the operating range (20-30 MHz) to the RF port of a double balanced mixer, where it is mixed with the local oscillator frequency generated by a synthesizer. It is programmed in such a way, that its output offsets the cyclotron frequency f_{cy} by the intermediate frequency f_{IF}. An impedance matching amplifier A1 couples the signal f_{IF} to a crystal filter with a bandwidth of B=5kHz. The subsequent limiting amplifier A2 provides a constant amplitude signal for the discriminator independant from the input level in the range of -30 - +20 dbm. The characteristics of the discriminator are the following: peak to peak distance $f_0 \pm \Delta f$ = 9 MHz ± 2,5 kHz, slope $\Delta U/\Delta f \geq 2$ mV/Hz for an input voltage of $5V_{rms}$, linearity ≤ 1 % for a bandwidth of 1 kHz, temperature stability of the zero crossing is ≤ 1 Hz/°C. So with the discriminator in a relative constant temperature enviroment it is easy to detect frequency deviations of less than 1 Hz with good sensitivity. - As the slope of the discriminator in the operating range changes sign at the peak points it is not well suited for regulation purposes. We had to add some logic to achieve the desired shape: The input frequency counted by a frequency counter, is available as a 6 digit BCD coded information, labeled A in the block diagram. Comparator 1 decides whether the actual frequency A is greater or smaller than the preselected value B. A subtractor computes the absolute value $|\Delta F|=|A-B|$, which is then compared in comparator 2 with a switch selected constant value K. The output $|\Delta F|<K$ is combined with A<B and A>B in a simple logic. Now if $|\Delta F|>K$ is true, then the output voltage of the discriminator is substituted by a constant voltage +U or -U when the logic controlled switches S_+ or S_- are actuated. If $|\Delta f|<K$ is true than S_0 is closed and the discriminator output is switched through. The characteristic at the output of 5 identical buffers A_4-A_8 is indicated in the circeled diagram. One of this outputs can be directly connected to servo motors without ambiguity in respect to the sense of rotation during closed loop operation.

We use this instrument with a new frequency tuning servo system with 3 low inertia disc rotor motors. They are electronically coupled for synchronous operation at the three dees of the cyclotron.

*Zentrallabor für Elektronik, KFA Jülich

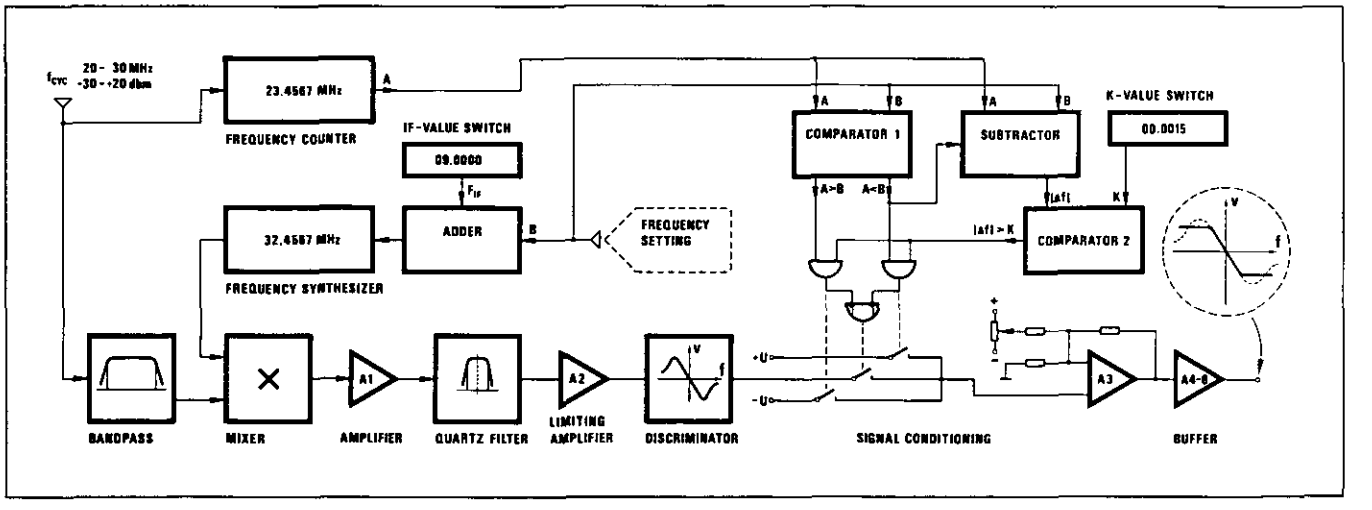

Figure 1: Block diagram of the frequency control unit.

7.3. Status of ISIS

H. Beuscher, C. Mayer-Böricke and J. Reich

For the acceleration of heavy ions up to Neon between 22.5 and 45 MeV/nucleon the project ISIS (Injektion schwerer Ionen nach EZR-Stripping: Injection of heavy ions after ECR-stripping) has been started at the beginning of 1980. This project comprises

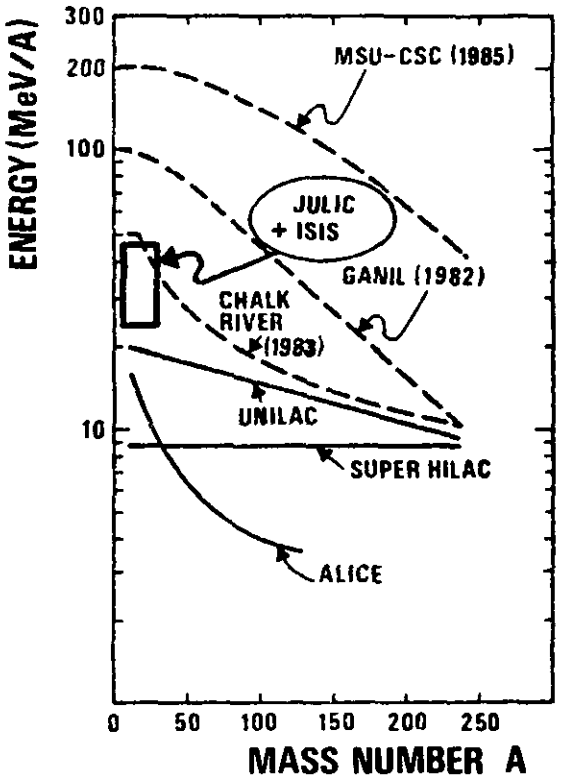

Figure 1: JULIC after realization of ISIS in comparison with other accelerator facilities. Accelerators under construction are represented by dotted lines.

the design and construction of an Electron-Cyclotron-Resonance (ECR)-ion source, a beam preparation, -guiding and injection system as well as a new RF-center region for JULIC. Last year in spring the funding of the project has been included in the budget of KFA.

In fall the design of ISIS was well advanced and specifications of the main components were sent out for first bids. These main components are a superconducting magnet structure and high power microwave generators for the ECR-source as well as magnets and power supplies for the beam guiding and injection system. By the end of the year a detailed report on the design of ISIS has been worked out together with a cost estimate. The following sections describe the design of the ECR-source, the injection system and the new RF-center region of the cyclotron.

7.4. Design of the Electron-Cyclotron-Resonance (ECR)-ion source

H. Beuscher, H.-G. Mathews and J. Reich

The first ECR-source which was able to produce highly charged heavy ions was the Super-Mafios B (SMB) built by Geller in Grenoble[1]. The proposed ECR-source for Jülich (in Fig. 1) is designed for higher beam intensities and higher charge states.

The source consists of two plasma stages: The injector- and the stripper-stage. In the injector stage with a small aperture and a gas pressure of 10^{-3} Torr a cold plasma is produced by ECR. The ECR is caused by microwave injection into a suitable axial magnetic field. The cold plasma consisting mainly of ions in the lowest charge state diffuses into the second plasma stage with a larger aperture and a very low pressure ($<10^{-7}$ Torr). This stripper stage is a magnetic bottle with a rising magnetic field in the axial and radial direction, a so-called B_{min}-structure. The B_{min}-structure is realised by super-position of a magnetic mirror field and a hexapole field. The B_{min}-structure of the magnetic field and the low gas pressure lead to a long confinement time of the electrons in the plasma. By injecting microwaves from a second powerful generator into this stage a plasma with a high density of fast electrons is produced (hot plasma), which is able to generate in a step by step process highly charged heavy ions.

The magnet system of the proposed Jülich source is designed to be completely superconducting. This choice was made because of the low power consumption at considerably high fields. The device consists of one short solenoid for the first plasma stage, two mirror coils, one additional weak solenoid to adjust the mirror ratio and a hexapole magnet for the second stage (see fig. 1). For the vacuum system of the source it is planned to use only refrigerator cryopumps (CP) and turbomolecular pumps (TP). The required high pressure gradient between the cold and hot plasma stage is achieved by differential pumping. Since the extracted heavy ions will be injected into the Jülich cyclotron with an energy up to 10 keV per charge the whole plasma chamber of the source has to be on a positive potential up to 10 kV relative to the extraction electrodes.

Fig. 2 shows the magnetic field along the source axis (z-axis) for about the maximum current in the coils. The maximum mirror field is about 1 Tesla (z=42 cm). The mirror ratio in this case is B(z=42)/B(z=0)=2.1, but can be adjusted within a wide range. The radial dependence of the magnetic field in the middle of the source (z=0) can be seen in fig. 3. The lower curve represents the field of the hexapole alone ($|B| \sim r^2$). The other one is the superposition of the hexapole and mirror field. At the inner diameter of the vacuum chamber (r=10 cm) the total field has about the same value as the maximum mirror field (≈1 Tesla). In this superimposed field of the hot plasma stage the points where ECR can occur form a closed surface. The projection into the drawing plane of this resonance surface for 18 GHz belonging to a magnetic field of 0.64 Tesla is included in fig. 1. The mirror and hexa-

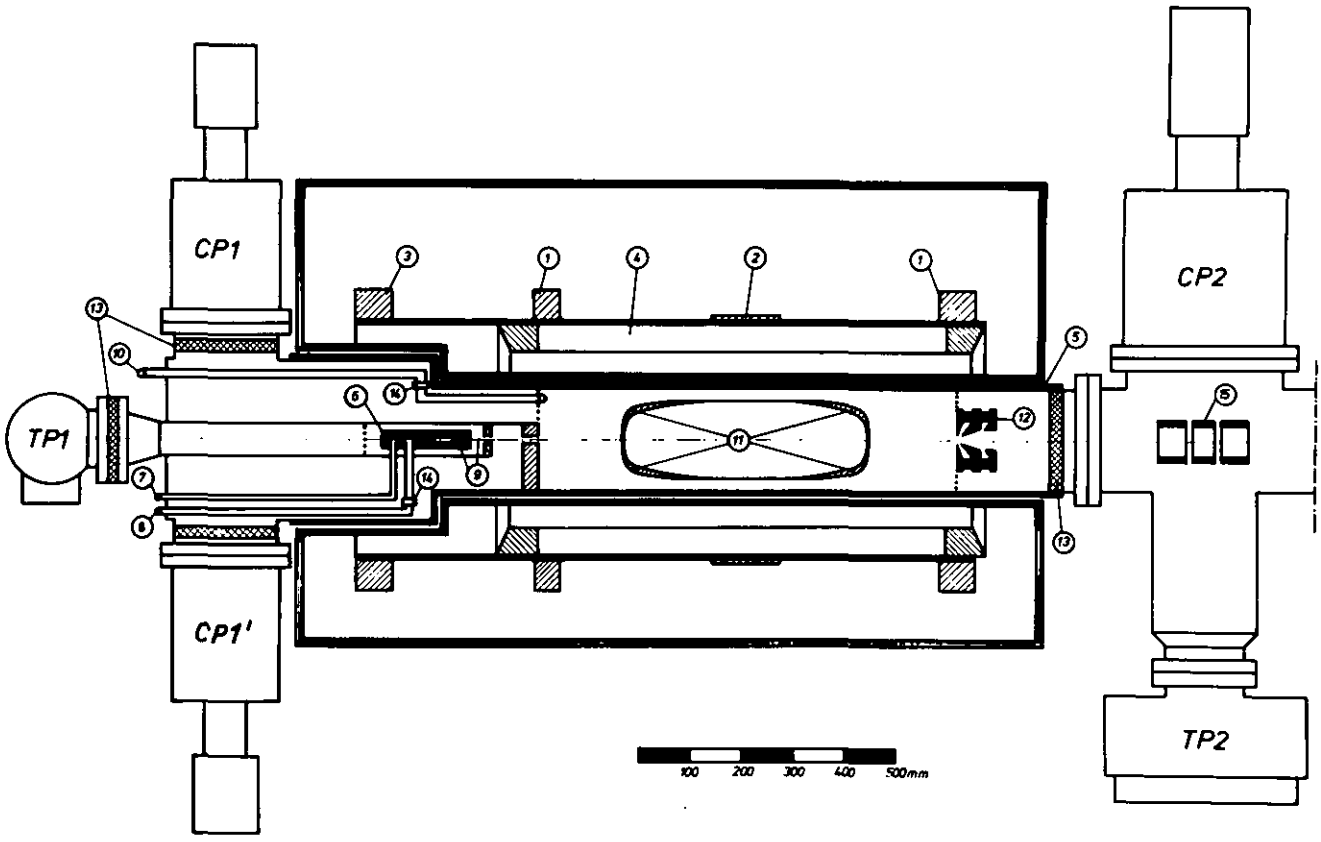

(1) mirror coils
(2) thin additional solenoid
(3) first stage solenoid
(4) hexapole magnet
(5) watercooled vacuum chamber
(6) watercooled 1. plasma stage
(7) gas inlet
(8) microwave injection to 1. stage
(9) resonance point and cold plasma of 1. stage
(10) microwave injection for 2. stage
(11) resonance zone of 2. stage for 18 GHz
(12) extraction electrodes
(13) high voltage insulation
(14) microwave window
(15) einzellens

Figure 1: Schematic view of the proposed ECR-source for the Jülich Cyclotron.

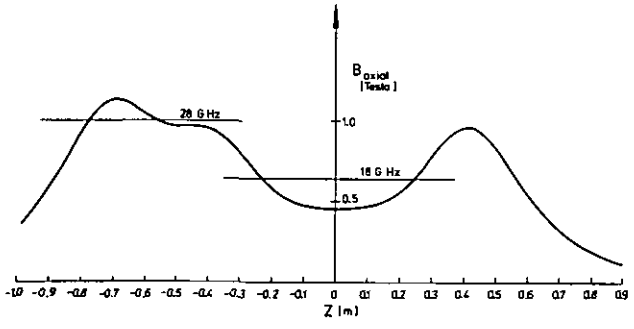

Figure 2: Magnetic field along the axis of the source.

pole fields have to be strong enough to keep this resonance zone fully within the vacuum chamber. In order to achieve a sufficient confinement time for the accelerated electrons the magnetic field has to increase strongly from the resonance zone towards the walls of the hot plasma stage. The chosen magnet configuration provides an increase in $|B|$ of at least 1.5, i.e. $|B| \geq 0.96$ Tesla at any point on the walls of the second stage.

The shown field shape in fig. 2 allows to use microwave frequencies of 28 and 18 GHz in the first and second stage respectively. These frequencies are considerably

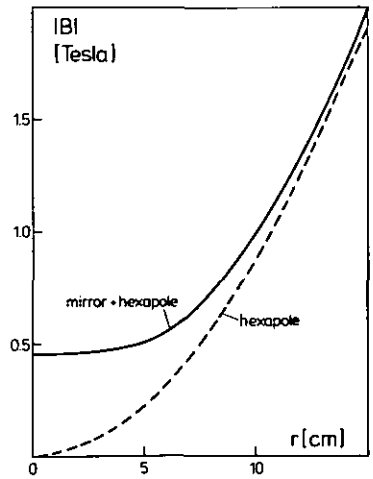

Figure 3: Radial dependence of the magnetic field at the mirror center (z=0).

higher than those used in existing ECR-sources (Grenoble[1]) or sources under development (Karlsruhe[2], Louvain-la-Neuve[3]). Since the attainable electron density n_e increases with *the square of the microwave frequency* an improvement in the production of highly stripped ions can be expected. Since the required microwave power is proportional to the electron density, powerful and expensive microwave generators of 1.5 kW at 28 GHz for the first plasma stage and 10 kW at 18 GHz for the second stage are needed for the Jülich ECR-source.

Fig. 4 gives an estimate for the increase in charge with rising electron density under the assumption, that the confinement time τ remains constant. The two $n_e\tau$-lines in

the picutre represent experimental values for SMB[1] and extrapolated values for the Jülich ECR-source. According to the different microwave frequencies for the two sources of 8 GHz (SMB) and 18 GHz for the Jülich source the $n_e\tau$-value

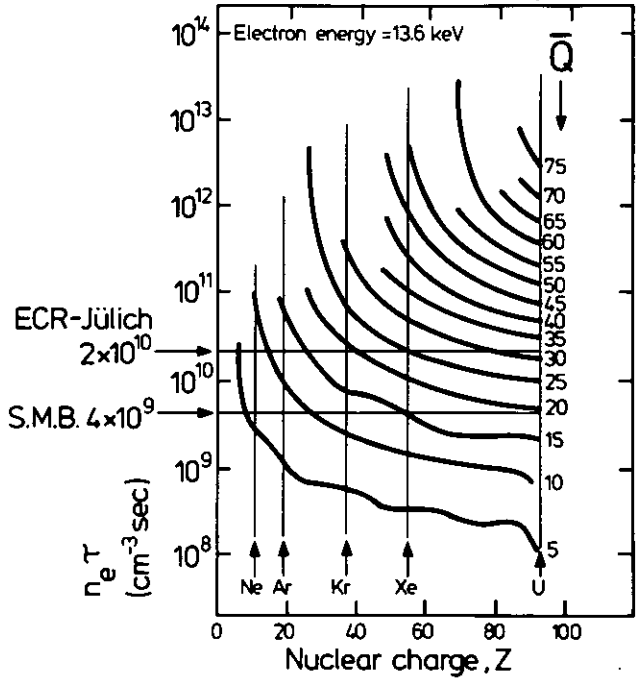

Figure 4: Average charge states, $\bar{Q}$, produced in a plasma for various $n_e\tau$ and ion species Z (ref. 4).

is expected to increase by a factor of 5. Applying this extrapolation one can expect the ion species given in table 1 to be accelerated in the Jülich cyclotron and to be available with currents larger than 10 particle-nA for experiments.

Ion	q/A	max. energy per nucleon (MeV)	max. particle energy (MeV)
$^{12}C^{4+}$	0.333	22.5	270
$^{12}C^{5+}$	0.417	31.3	375
$^{12}C^{6+}$	0.500	45.0	540
$^{14}N^{5+}$	0.357	22.9	321
$^{14}N^{6+}$	0.429	33.1	463
$^{14}N^{7+}$	0.500	45.0	630
$^{16}O^{6+}$	0.375	25.3	405
$^{16}O^{7+}$	0.438	34.5	552
$^{16}O^{8+}$	0.500	45.0	720
$^{20}Ne^{7+}$	0.350	22.5	450
$^{20}Ne^{8+}$	0.400	28.8	576
$^{20}Ne^{9+}$	0.450	36.5	730
$^{40}Ar^{14+}$	0.35	22.5	900
$^{40}Ar^{15+}$	0.375	25.3	1012

Table 1: Ion species and their maximal energy which can be expected with a current >10 particle-nA at the exit of the cyclotron.

References

1) R. Geller, IEEE Trans. NS 26, No. 2 (1979) 2120
2) V. Bechthold et al., IEEE Trans. NS 26, No. 3 (1979) 3680
3) Y. Jongen et al., IEEE Trans. NS 26, No. 2 (1979) 2160
4) J.D. Daugherty et al., Phys. Rev. Lett. 20, No. 8 (1968) 369

7.5. Design of the External Injection System for JULIC

R.K. Bhandari, J. Reich

An external injection system has been designed to transport heavy ions from the ECR source[1] and inject them axially into JULIC. The ECR source will be located in the radiation free south hall in the cyclotron building. It is expected to deliver ion beams with an emittance of about 160 π mm·mrad in each plane and a momentum spread of about ±0.5 %. The ions will travel nearly 25 meters from the source to the center of the cyclotron through the injection system which consists of various subsystems. These subsystems will do the charge and mass selection, beam transport, phase space matching, achromatic bending etc. in a simple way such that a) beam envelopes are small with a minimum no. of elements and parameters for simplicity during operation; b) the subsystems are telescopic as far as possible allowing easy and reliaoly diagnostics at various stages as well as maintaining the modular character; c) second order and chromatic aberrations are small; d) corrections for space charge blow-ups are possible without increasing the no. of parameters; e) magnetic elements are used as far as possible to take advantage of space charge neutralization.

A hyperboloid type inflector[2] will inflect the transported ions into the median plane of the cyclotron. During the evolution of the present design of the injection system various alternatives were studies[3]. Various subsystems were designed using the TRANSPORT code[4]. Calculations and optimization of space charge effects were carried out using the MIRKO code[5] which is based upon the Kapchinskij-Vladimirskij formalism[6]. Layout of the injection system envolved thus is shown in figure 1. The subsystems are briefly described below in the sequential order.

1. TELESCOPIC SYSTEM OF EINZEL LENSES: This system has a property of point to point and waist to waist imaging (telescopic). It consists of two einzel lenses and forms a magnified real image of the extraction aperture. In this way the divergence of the beam will be reduced for a given emittance and an extraction aperture of 1.5 cm Ø. Beam envelopes in the subsequent subsystems will consequently be reduced. The effect of the fringing field of the ECR source on the beam optics in this region has, however, not been taken into account in the calculations so far. The subsystem may hence be modified in the future.

2. 180° BENDING + CHARGE STATE ANALYSIS SYSTEM: This system bends the beam by 180° and translates it vertically down by 3.65 meters. The bending is doubly achromatic. It consists of four identical unit cells each made up of one dipole magnet 'MS' and two quadrupole magnets 'QS'. Two such cells in succession form a dispersive system with the spacial part of the transformation matrix being -I. So, the charge state selection of up to 1 in 30 will be done at the end of first two cells. However, the full transformation matrix of four cells in succession is +I. This system has no second order aberrations. Moreover, all the second order chromatic aberrations also vanish if proper radii of curvature are given to the faces of the dipole magnets. Such systems are known as second order

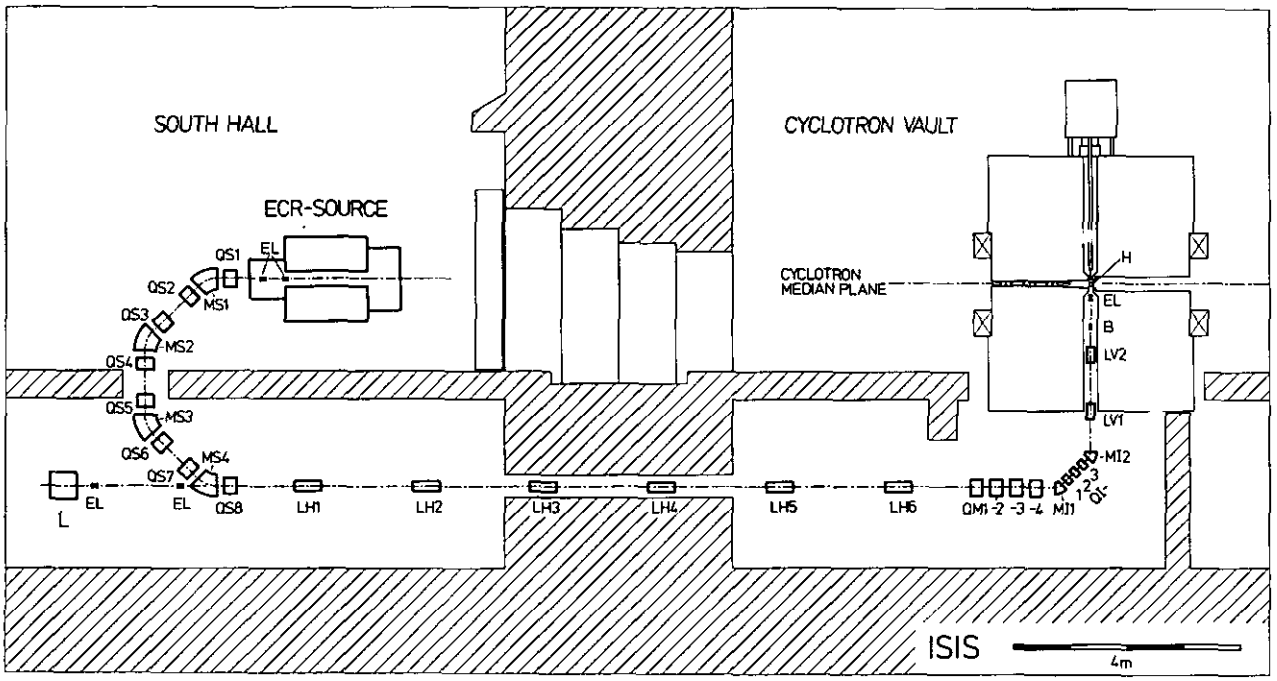

Figure 1: Layout of the external injection system for ISIS at JULIC. L source for light ions up to Helium, B buncher, H hyperboloid inflector.

achromats[7,8]. The total system is thus doubly telescopic. It has only two parameters - the strengths of the two quadupoles 'QS' of the unit cell.

3. BEAM GUIDING SYSTEM OF SOLENOIDS : It is about 12.5 meters long and consists of six identical solenoid 'LH' all operating at the same field level. The transformation matrix at the middle of the system is +I and so is at its end making it doubly telescopic.

4. PHASE SPACE MATCHING SYSTEM: This system is used for matching in transverse planes the emittance of the injection system at the exit of the inflector to the acceptance of the cyclotron central region depending on the ν_r and ν_z values, the latter of which will vary slighly with accelerating conditions. The system consists of four equispaced independent quadrupole magnets 'QM'. Four matching conditions in two planes can thus be satisfied. We have done the calculations for ν_r=1 and ν_z=0.5. The beam was traced back from the exit of the inflector up to the exit of this system. Having the beam conditions from the source side at the entry, the quadrupole strengths were calculated for matching.

5. DOUBLY ACHROMATIC 90° BENDING SYSTEM: This system below the cyclotron bends the beam up by 90° into the axial hole in the lower magnet yoke. It consists of two 45° dipole magnets 'MI' interspaced by three quadrupole magnets 'QI'. The system is symmetric. It operates with two parameters and has small second order aberrations.

6. TRANSPORT SYSTEM IN THE AXIAL HOLE: There are two identical solenoids 'LV' in the axial hole operating at the same field level but with opposite polarity. They form a 2 meters long telescopic system with -I transformation. At the end of the system an einzel lens converges the beam into the narrow opening of the inflector. An einzel lens was chosen because of its compactness.

7. HYPERBOLOID INFLECTOR AND HOLE LENS: We calculated the trajectories through this part analytically[2,9]. The matrix elements were calculated using the measured magnetic field. In analytical treatment this system consists of a solenoid without an exit edge (hole lens) and the hyperboloid inflector. The field strength of the solenoid is equal to the cyclotron median plane field. A coordinate

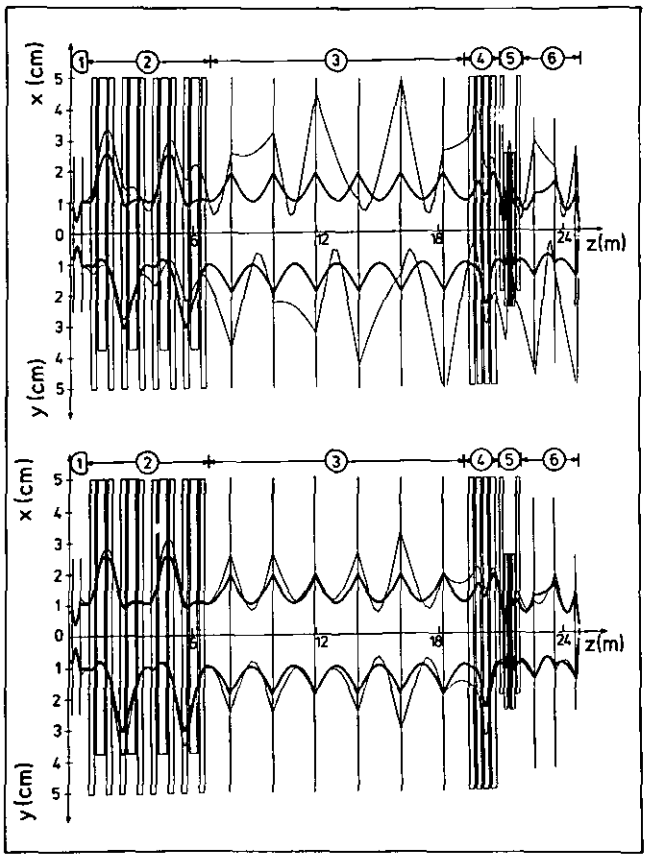

Figure 2: (Top): Beam envelopes through the total system for zero beam current (thick lines) and 100 μA beam current (thin lines). (Bottom): Beam envelopes optimized for 100 μA beam current (thin lines). Beam envelopes for zero beam current system (thick lines) for comparison. The numbers refer to the subsystems as given in the text.

rotation was applied to decouple the motions in the two planes at the exit of the inflector[2].

SPACE CHARGE EFFECTS were calculated and optimized for a 100 μA beam of 10 keV deuterons. In figure 2 (Top) beam envelopes are shown in the total system up to the entry of the hole lens-inflector system for the cases of zero and 100 μA beam current. Optimization of the system for a 100 μA beam was done in 3 steps. First, the parameters of subsystems 1 and 2 were varied to obtain beam conditions closest possible to the zero beam current case at the exit of subsystem 2. Then the subsystem 3 was optimized in the same way with the new beam conditions at its entry. Finally, the parameters of subsystems 4 and 6 were varied to obtain the conditions at the end corresponding to zero beam current. Fig. 2 (Bottom) shows the beam envelopes for 100 μA beam in the optimized system. The corresponding phase space ellipses are shown in figure 3. It should be mentioned that after the beam has passed the ∿ 8 cm hole lens and the inflector the corresponding phase ellipses are both upright. They then correspond to $\nu_r = 1$ and $\nu_z = 0.5$. The overall effective emittance increase due to second order effects is below 7 % in each plane which is a small number for a source-emittance $\epsilon_x = \epsilon_y = 160\ \pi$ mm·mrad.

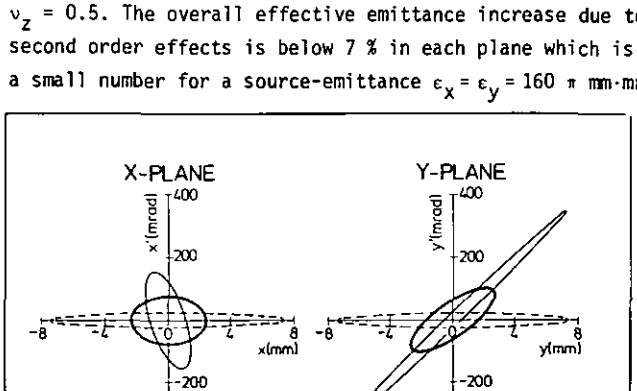

Figure 3: Phase space ellipses for the cases of figure 2: dotted lines: at the beginning of the system; thick lines: at the end of the system for zero beam current and for the optimized 100 μA beam current case; thin lines: at the end of the non-optimized system for 100 μA beam current.

References

1) H. Beuscher, H.G. Mathews, J. Reich, this annual report, previous chapter

2) R.W. Müller, Nucl. Instr. & Meth. 54 (1967) 29

3) L. Aldea, H. Beuscher, R.K. Bhandari, C. Mayer-Böricke, J. Reich, P. Wucherer, 17th European Cyclotron Progress Meeting, Karlsruhe, June 1980 and IKP-Annual Report 1979

4) K.L. Brown, D.C. Carey, Ch. Iselin, F. Rothacker, Report No. CERN 73-16, November 1973

5) B. Franczak, private communication

6) I.M. Kapchinskij and V.V. Vladimirskij, Proc. Int. Conf. on High Energy Accelerators, CERN, 1959

7) K.L. Brown, IEEE Trans. Nucl. Sc. NS-26 No. 3 (1979) and Report No. SLAC-PUB-2257, February 1979

8) K.L. Brown, private communication

9) N. Hazewindus, Nucl. Instr. & Meth. 76 (1969) 273

7.6. Design of a Center Region for External Beam Injection at JULIC

L. Aldea, P. Wucherer

The center region of JULIC had to be redesigned for the project ISIS[1] because of two reasons: 1) The inflector[2] needs more space than the internal ion source and 2) the energy at the starting point (ion source slit or exit of the inflector, resp.) has increased from zero to 2.2 - 4.5 keV/amu. The beam has well defined properties now at this point. Since for some ions the dc-current from the ECR-source[3] may be rather low, there is a strong demand to have a large acceptance of the cyclotron. At the same time an excellent beam quality is required by some experiments. It turned out that this goal cannot be achieved for a center region, which is designed as a compromise between internal and external ion source operations. Therefore, we decided to give preference to external injection and to couple an external light ion source to the injection system[4] in addition to the ECR-source.

The harmonic number h=3 will not be changed and the orbits will be scaled as before. For technical reasons the Dee structure should only be changed up to the 4th orbit, but it turned out that this was no restraint for the design procedure. For a good design a self optimizing computer code is needed. Therefore, in this stage, an analytic orbit calculation procedure[5] was used: The magnetic field and the electric field in the gaps are homogenous i.e. the electric field is constant in the gap but varies in time as a cosine function. Only the particle motion in the median plane was calculated. The emittance was assumed to be 160 π mm mrad[4]. For all the calculations we started with an upright phase ellipse with a radial spread of ± 1.6 mm and maximum divergence of ± 100 mrad (ν_r=1). This ellipse was represented by a center particle and 8 particles on its circumference. Another fixed parameter was the phase width of ± 20° RF at the exit of the inflector. We expect that a buncher in the beam line is able to focus the beam in this time interval. The phase width is represented by 3 particles with central phase ϕ_0, ϕ_0 + 20° and ϕ_0 - 20°. The total phase space is thus represented by 3 x 9 = 27 particles. The central phase ϕ_0 and the geometry of the puller region (coordinates of the inflector and the puller) are the most sensitive free parameters. The fit procedure minimizes the weighted sum of functions which take into account the following beam properties on the first 4 turns: 1) deviation of the center of gravity of the centers of curvature of the center particle orbits from machine center for $\phi = \phi_0$ (coherent amplitude, one particle); 2) spread of the orbit centers of the three center particles for ϕ_0, ϕ_0 ±20° (incoherent amplitude for zero emittance); 3) radial spread of all the particles relative to the center particle with $\phi = \phi_0$ ("radial bunching", 27 particles).

The axial focusing is guaranteed by the restriction to positive phases after the second gap. These phases are specified at the center of each gap. The fitting calculations were carried out in three steps. Various available

parameters were tried for fitting. In the first step the six free parameters were related to the first gap (inflector-puller gap). These are: 1-3) coordinates of the point and the angle at which the beam leaves the inflector 4) the distance between the inflector and the puller 5) the angle of the puller edge and 6) the central phase ϕ_0. In this step the geometry of the Dee-gaps was taken as the existing one and fixed. In the second step the Dee voltage and the injection energy were also set as free parameters. However, they did only change in a reasonable range during the fitting from their initial values of 40 kV and 5.3 keV/amu (maximum possible value). This fact is favourable because the higher the injection energy is the larger the inflector aperture and the lower the space charge effect are. Moreover, we wanted the optimum Dee voltage around 40 kV due to technical reasons as well as to keep a flexibility in tuning at higher energies. In the last step the geometries of the 2nd to the 7th gaps were also left variable but they did not tend to change much and neither the results changed significantly. The most important parameters are given in table 1 and the results of the above calculations are shown in figures 1 to 3.

Parameter	type	value
Horizontal emittance	fixed	$\pi \cdot 1.6$ mm·100 mrad
center phase at start, ϕ_0	free	- 105° RF
phase width at start	fixed	± 20° RF
injection energy	free	4.5 keV/amu
Deevoltage	free	41 kV
resonance frequency	fixed	29.3 MHz
magnetic field	fixed	1.28 Tesla

Table 1: The most important parameters in the fit procedure. For the free parameters the final results are given.

Figure 1 shows the spread of the centers of curvature in the median plane during the fourth revolution for the optimal phases and demonstrates the good centering of the beam. The distance between the machine center MC and the beam center BC corresponds to the fit function no 1 (coherent amplitude) and is less than 1 mm. The starting phase ϕ_0 is extremely negative and the particles leaving the inflector are first decelerated! The spread between the centers of curvature for the starting phases -85°, -105° and -125° (see fig. 1) corresponds to the fit function no 2 (incoherent amplitude) and is also less than 1 mm. Fig. 2 shows the first orbits in the median plane for all the 27 particles together with the fitted geometry of the accelerating gaps and the inflector. Small radial spread of the orbits is the result of the minimized fit function no 3. It shows further that the beam is sufficiently well matched to the starting phase space configuration corresponding to the radial oscillation number ν_r=1.

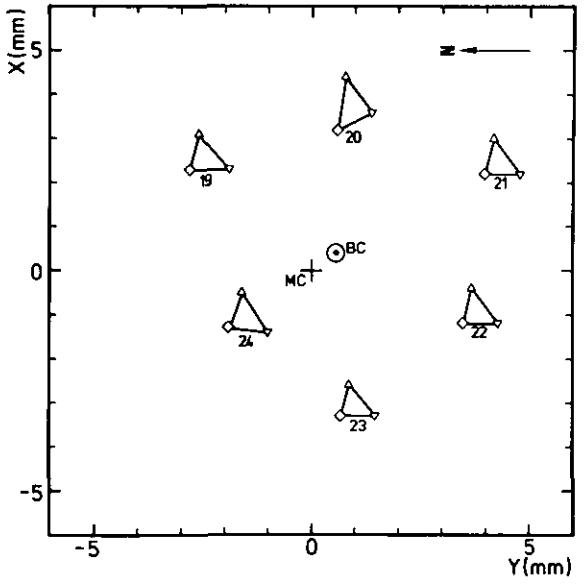

Figure 1: Centers of curvature before each gap on the fourth revolution for particles with different starting phase (Δ = -125°, ◇ = -105°, ▽ = -85°) but the same spatial starting coordinates (center particles) BC = Beam center; MC = Machine center.

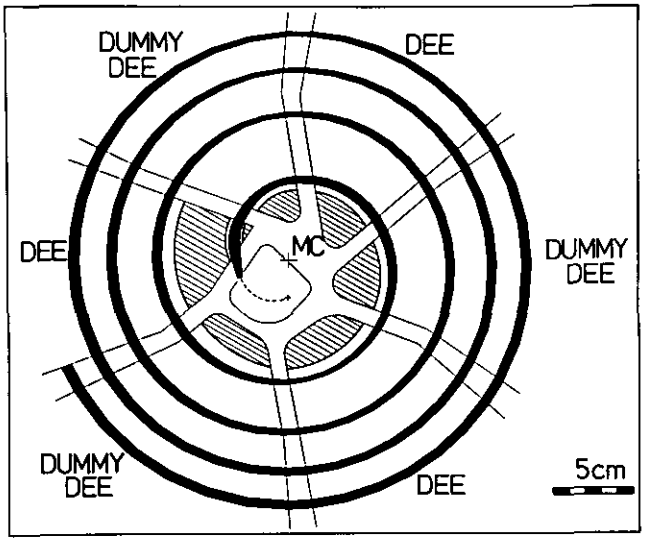

Figure 2: RF-structure of the center region together with the orbits of 27 particles (which effectively form a beam envelope) for starting phases of -(105±20)° and an emittance of 160 π mm mrad.

There are some other representations by which we have checked the quality of the design. Among them the phase plot vs. gap number in figure 3 seems to be an obvious

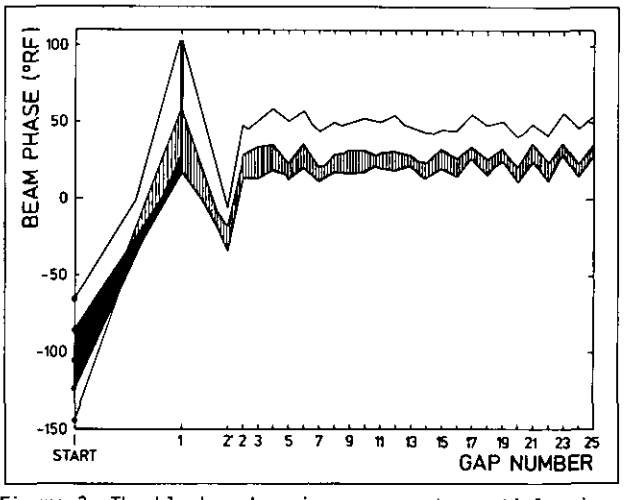

Figure 3: The blackened region represents particles in the first gap with starting phases of -(105±20)° RF but same spatial coordinates (zero emittance). The vertically hatched region shows the broadening caused by an emittance of 160 π mm mrad. The outmost lines are the envelopes for phases of -(105±40)° RF and the same emittance.

one. It shows clearly a very rapid motion of the particles in the time coordinate (phase) during the first two gap transitions. The particles with a starting phase from -85^{o} to -125^{o} RF and the identical spatial coordinates (center particles) are focussed in time within the first gap (blackened area). The first gap acts as an extremely strong buncher for these particles. The particles on the circumference of the phase ellipse (which represents an emittance of $\pi \cdot 160$ mm·mrad) are overfocused during the first gap crossing (blackened and vertically hatched area up to gap number 1) but get focussed again between the first and second gap (lable 2', vertically hatched area). This second focussing effect results from adequate path length variations in the section between first and second gap and corresponds to the broadening of the beam in this section which can clearly be seen in figure 2. Beyond the second gap the phase band remains practically constant with a width of about 10^{o} RF. The outmost lines show the envelopes for starting phases between -65^{o} and -145^{o} RF, i.e. a starting phase width of 80^{o} RF and the same emittance. Since all these particles are accepted by the cyclotron but have only a moderate beam quality the buncher in the beam line should focus them into the desired 40^{o}-phase width.

The realisation of the puller region satisfying the assumptions made in the calculations is a problem which now has to be worked out. We have to realize a sufficiently homogenous electric field in the first (and second) gap or find out a modified geometry which nearly gives the same good result. Three dimensional potential relaxation calculations and additionally magnetic analogue measurements are necessary. With the measured or calculated fields General Orbit Code integration has to be performed.

References

1) L. Aldea, H. Beuscher, R.K. Bhandari, C. Mayer-Böricke J. Reich, P. Wucherer, 17th European Cyclotron Progress Meeting, Karlsruhe, June 1980 and IKP-Annual Report 1979, Jül-Spez-72 (1980) 143

2) R.W. Müller, Nucl. Instr. & Meth. 54 (1967) 29

3) H. Beuscher, H.G. Mathews, J. Reich, this annual report, chapter 8.4.

4) R.K. Bhandari, J. Reich, this annual report, chapter 8.5.

5) M. Reiser, Nucl. Instr. & Meth. 13 (1961) 55

7.7. Correlation Measurements of the Energy Resolution of BIG KARL against the Cyclotron RF

I. Katayama and W. Bräutigam

At JULIC, the high resolution magnetic spectrograph BIG KARL has sometimes been found not to work well. This may come from the property of the cyclotron. Beams are extracted from several orbits with precessional beam density variation along radius in the extraction region[1]. The external beam quality, especially radial emittance and energy width, is therefore influenced by any type of RF fluctuations. Changes in beam quality may leave an impact on the overall resolution of the system cyclotron/spectrograph in case of second order and higher order aberrations.This will be furthermore pronounced in a case when magnets and quadrupoles in the system are not well set to meet the first order ion optical requirements. Therefore in principle correlations are expected between RF-amplitude and/or frequency deviation and the elastic line positions in the focal plane counter.

The RF amplitude is measured by a capacitive probe in the cyclotron. After rectification, the signal is amplified by a low pass amplifier and DC offset is subtracted. The frequency deviation signal is obtained as described in ref. 2. The system is able to demodulate signals with good phase linearity up to 10 kHz. The signals for the amplitude or the frequency deviation are sampled by a coincidence pulse from the MWPC and sent to ND 6600 multi-parameter data analyzer together with other counter signals. RF-instabilities of amplitude and frequency are observed as shown in fig. 1. As the RF-system of JULIC is of self-oscillating type, the residual frequency modulation of $1\text{-}2\cdot10^{-5}$ is due to mechanical vibration of the dee system and it will produce 2-3 turn fluctuations of 500 turns total. On the other hand, amplitude instabilities of $2\text{-}4\cdot10^{-3}$ are caused by a non sufficient ripple suppression in the RF system power supplies and it will produce 1-2 turn difference. One of the first results for the correlation between RF frequency instability and spectrograph resolution is shown in fig. 2. The elastic line was from $^{208}Pb(\alpha,\alpha)^{208}Pb$ at $\theta_{lab} = 8^{o}$ (E_{α} = 140 MeV) and BIG KARL dispersion was 19 cm/%. In this experiment no correlation for amplitude and frequency instabilities are found. Measurements will be further continued for various energies and different particles.

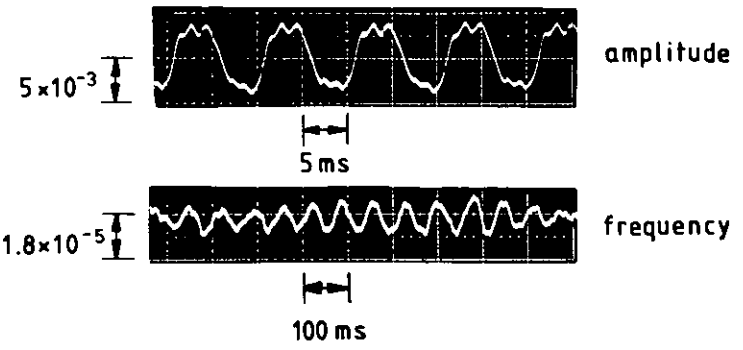

Fig. 1: Time structure of the RF amplitude and frequency instabilities.

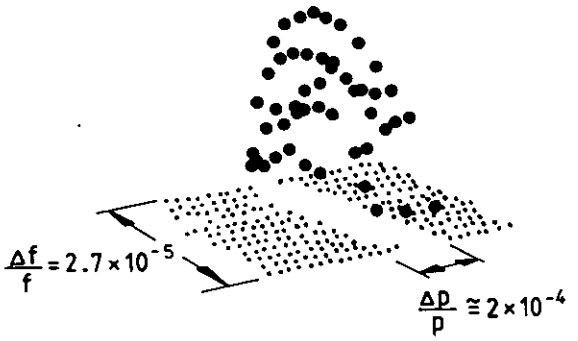

Fig. 2: One example to search a correlation between the RF frequency instability and elastic line position on the focal plane of BIG KARL.

References

1) H. Thimmel, P.Wucherer, Proc. 5th Int. Cycl. Conf. Oxford, 1969, p. 190.

2) W. Bräutigam, K. Kennepohl, IKP Annual Report 1980.

8.1. Study of a Storage Ring System with an Internal Target

S.A. Martin, W. Schott, C.A. Wiedner***

High resolution nuclear physics experiments e.g. with magnetic spectrographs require thin targets ($\leq 100 \frac{\mu g}{cm^2}$) and a high beam quality in order to obtain the desired resolution. Therefore the possibility of recycling the beam after the target has been investigated. This can be accomplished by a storage ring. The target is located in the ring. An image of the target spot is produced in a RF cavity after the beam has been bent by a 180 degree achromat. The cavity is able to cool down the phase space loss caused by energy and angular straggling in the target. The second 180 degree magnet system bends the beam back to the target. The feasibility of such a system has been studied.

* TU München

**MPI für Kernphysik Heidelberg

8.2. The Magnet Spectrometer BIG KARL

G.P.A. Berg, U. Hacker, A. Hardt, W. Hürlimann, I. Katayama, M. Köhler**, S.A. Martin, J. Meißburger, A. Retz, Th. Sagefka, O.W.B. Schult, B. Styczen*

Spectrometer development:
During the last year the spectrometer Big Karl has been used to perform different experiments***.

To improve the particle discrimination an ionization drift chamber with resistive wire position detectors has been built and is ready for a first test.

A second multi wire proportional chamber (MWPCII) has been built as back up system for the MWPC which is in use now. The active area of the MWPCII is 400 x 100 mm^2. It measures the two positions x and y using the delay line read out for two cathode planes on each side of the centered anode. Read-out electronics is already described[1].

A data acquisition system MEMPHIS[2] (MODULAR EXPERIMENT MULTIPARAMETER PULS HEIGHT INSTRUMENTATION-SYSTEM) has been built for use in connection with a VAX-11. First tests demonstrate a data rate of 20000 events/sec (128 bit/event).

Operating system:
a) Hardware: A new 64-channel multiplexer has been added to provide differential and floating voltage monitoring in a 1 μV to 5000 Volt range. This device is used to monitor shunt currents, scintillator voltages, MWPC voltages and gas pressures.

A separate set of 24 digital panel meters has been developed and replaces the old Ht correction current meters. True sign- and current values of all 24 Ht power supplies are now displayed with 4 digits accuracy and controlled by the operating system through an opto-coupled I/O-port.

b) Software: System: Most changes in software concern the handyness of the system to the experimental physicist. The whole operating system is now self-documenting at all levels. At startup, time and data are automatically set from a CAMAC real time clock and a self-test feature checks for CAMAC malfunction before installing the operating system. During operation automatic error logging keeps track of any device- or software malfunction in a fully user transparent way.

Operating support: In order to facilitate the bookkeeping of magnetic tape usage, CAMAC - and NIM status or any other experiment - related data Digital Equipments data base management system "Datatrieve" has been installed and made available with a set of supporting procedures. For easy program and data transfer tapes written in card image format can now directly be read and copied on disk in files-11 format. A sort program allows to sort data tapes written on our PDP 15 data acquisition machine directly under RSX and analyze the generated spectra.

Two independent kinematic programs "KINE" and "ELITE", the Osaka-RCNP kinematics program are available on the PDP 11 to support experimental setup. The cycling procedure for the main dipole magnets has been modified to provide fast rise while driving the magnets into saturation and an automatic wait/undershoot to compensate eddy current effects when approaching the final current value. This is important to save time during spectrometer optimisation where every change in correction current involves cycling of the main magnets.

References

1) M. Köhler, K.D. Müller, H. Stoff, M. Teske, G.P.A. Berg, A. Hardt, S. Martin, C. Mayer-Böricke, J. Meißburger, Nucl. Instr. and Meth. 175 (1980) 357

2) Proceedings Nucl. Sci. Symp. Orlando 1980 Florida

+ Permanent address: RCNP, Osaka University, Japan

++ Zentrallabor für Elektronik KFA

+++ see contributions

8.3. Interactive Graphics Monitor IGM

U. Hacker, J. Meißburger

In 1980 the "Big Karl" Interactive Graphics Monitor IGM[1] has further developed and now includes bar plots, collective histograms, two-dimensional scatter plots and a fast 3D plotting with labeling and hidden lines. As before high quality microfilm hardcopies can be made of either interactively or automatically created plots. Data input to the monitor is through an arbitrarily formatted data file on a line-by-line basis or directly from the keyboard in free format. The monitor has its own english-like command language and requires no programming to produce the desired graphical representation although for software people all commands are callable as Fortran subroutines too. For positioning text strings, defining windows or similar interactive tasks the keyboard or simply the graphics cursor may be used. To create standard plots or long series of plots with fixed legend layout the monitor runs in a batch mode requiring no interaction at all. At present the system runs on the KFA central IBM computer and supports all Tektronix 4010 compatible terminals. It will run on our forthcoming VAX-11 based data acquisition system since it intentionally was kept

fully portable to run on any virtual Fortran system.

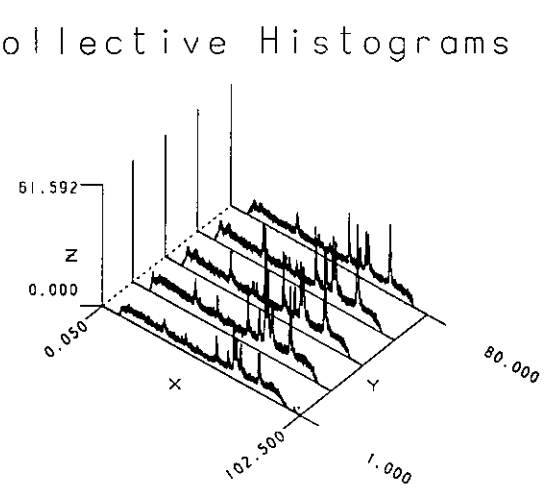

Reference
1) U. Hacker, Ingenieurarbeit Jülich 1979

8.4 8.4. Design of a Low Energy Pion Spectrometer

R.R. Johnson, S.A. Martin*

A series of measurements of π^- elastic scattering at the TRIUMF pion facilities is proposed[1] in the calcium region to measure nuclear radii. The experiments will involve ^{32}S, ^{36}S, ^{40}Ca and ^{48}Ca as target nuclei for pions in an energy region from 30 to 70 MeV. A QQD-spectrometer has been designed for these measurements. It is planned to use a magnet system which has been used for field measurement purpures during the design of Big Karl. The magnet system has a solid angle of about 8 msterad. Additional flux is obtained by installing a hodoscope in the dispersion plane of the pion channel.

*TRIUMF, University of British Columbia, Vancouver, Canada

9. A Bent Crystal Spectrometer for On-Line Measurements at the IKP Isochronous Cyclotron

J. Bojowald, G.L. Borchert, A. Ercan, O.W.B. Schult, B. Siefert, K.P. Wieder

The bent crystal spectrometer at the IKP[1] has been installed at the beam line G of the cyclotron. The performance of the instrument has been extended considerably by three major inprovements:

1. Computer control

A PDP11/10 computer has been incorporated in the electronical control system. It allows to run the spectrometer automatically under software control, thus providing a large flexibility with respect to measurement program. The data are stored on magnetic disquetts and can be transfered via the IKP computer link to a PDP11/34 for further analysis.

2. Intensity Normalization

To account for intensity fluctuations due to beam current variation or to a possible drift of the beam position on the target, a Ge(Li) detector has been installed close to the spectrometer. It monitors only the radiation from the target. A SCA is used in order to select out of the full spectrum one gamma or X ray transition, the intensity of which serves to normalize the count rate of the crystal spectrometer.

3. Fast electronics

To make use of the time structure of the cyclotron beam the data acquisition is now performed with an extended set-up of fast electronical devices. The anode signal of the NaI detector (risetime $\sim$ 2.5 ns) operates together with the RF signal of the cyclotron on a TAC. Its time spectra and the corresponding energy spectra are stored for each angular position of the crystal spectrometer after analog-to-digital conversion by the computer.

In the first on-line experiment with the crystal spectrometer we have studied the level scheme of ^{146}Eu populated through the ^{147}Sm(p,2n) reaction with a 22 MeV proton beam of about 3 μA.

To demonstrate the energy resolution of the spectrometer we measured the doublet of the 114.7 keV and 115.5 keV lines. It is shown in figure 1 and compared with the best GeLi data[2].

In the level scheme of ^{146}Eu a 275 keV transition is proposed to be a doublet with a spacing of the components of less than 200 eV[3]. Therefore we studied this transition in different orders of reflection.

As it is populated partly by the isomeric state we also measured the reflections in the prompt time peak, where we obtained a time resolution of 7 ns FWHM, and between the cyclotron bursts. The result is shown in figure 2 for the second order of reflection, where a line width of about 7 are sec has been obtained. The 275 keV reflection has also been recorded in the fifth order, where the doublet structure is clearly visible.

In the fifth order of reflection, which can be utilized for the spectroscopy of intense lines, the resolution (FWHM) of our spectrometer is $\Delta E_\gamma \gtrsim 2.8 \cdot 10^{-6} (E_\gamma/\mathrm{keV})^2$.

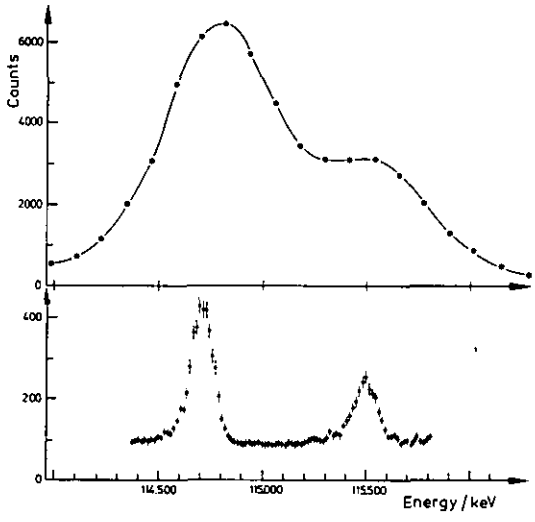

Fig. 1: Gamma-ray doublet in ^{146}Eu recorded with a 1 cm^3 Ge detector (upper part) and with the on-line curved crystal spectrometer (lower part). The FWHM is $\sim$ 120 eV for the 114.7 keV line. The measurement time was $\sim$ 40 sec per point.

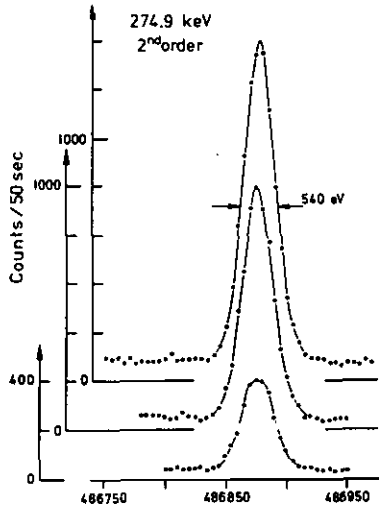

Fig. 2: Second order reflection of the 275 keV line. The upper line is obtained without a time window. The reflection in the middle was recorded with a time window of 18 nsec set on the burst. The lower peak was measured with a 28 nsec broad time window between the bursts (delayed component).

References

1) G.L. Borchert, W. Scheck, O.W.B. Schult, Nucl. Intr. Meth. 124 (1975) 107

2) A. Ercan, private communication

3) A. Ercan et al., Z. Physik A 295 (1980) 197

10. DETECTOR LABORATORY

10.1. Semiconductor Detectors

A. Hamacher, T. Künster, E. Lauin, H. Metz, K. Nicoll, D. Protić, G. Riepe

Similar to the last year a series of detector systems was kept available for charged particle spectroscopy and particle discrimination in nuclear reaction experiments (IKP and visiting groups): 7 large cryostats of different design (for a 100 cm scattering chamber) equipped with up to 4 side-entry Ge(Li) detectors or HPGe detectors with thin entrance contacts (areas between 80 mm^2 and 1000 mm^2), several cryostats with Ge(Li) detectors to be used as monitors, and 2 mounts with large area HPGe detectors (sensitive area 1400 mm^2) for the operation at 210 K. All these detectors were made by the detector laboratory, their parameters were checked before and after each experiment, and radiation damaged detectors were regenerated or replaced by new ones. More than 100 commercial Si ΔE detectors had to be checked routinely.

A problem of steady concern has been for quite some time the quality of ion-implanted n^+-contacts in HPGe. Many series of detector samples had been prepared, with various parameters of the technology being changed, until significant improvements were obtained. This refers mainly to the reproducibility and stability of the detector properties, and to the ability of the n^+p-junction to support high electrical fields (up to 10 kV/cm). The last feature is the crucial one for p-type HPGe, if high overvoltages are to be applied for creating a substantial electrical field at the rear contact, and thus reducing its dead layer.

A restriction in the choice of technology parameters resulted from the fact, that the ideal detector has to withstand heating up to 200° C - a treatment which practically elimimates also the effects of radiation damage caused by charged particles.

A general experience in detector preparation concerning critical procedures also applies to n^+-contacts: the chance to obtain a high field supporting detector is decreasing proportionally with its area.

More than 10 thin-contact HPGe transmission detectors with areas of up to 1450 mm^2 and thicknesses up to 15 mm were fabricated by the ion-implantation thechnology for a multi-detector telescope.

A stack arrangement consisting of 7 detectors of this type with a total thickness of 80 mm was used in a set-up for the investigation of the pre-equilibrium reaction-mechanism with 200 MeV protons at Orsay, France[1]. To eliminate the effects from slit scattering an active collimator was mounted at the first place of the stack. As shown in figure 1, it consists of a 2.3 mm thick HPGe detector with implanted contacts, one of which is divided into two circular areas by special etching techniques[2]. The diameter of the central area is 6 mm, the width of the grove around it is 0.2 mm.

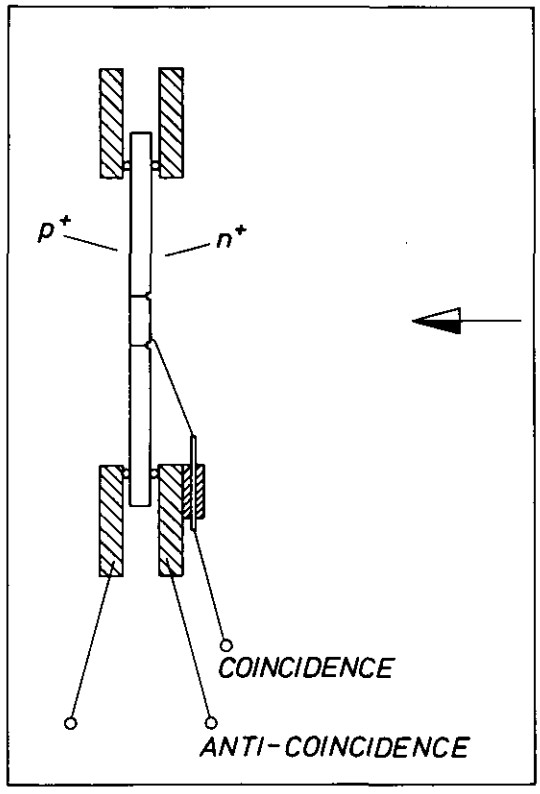

Fig. 1: Schematic view of the active collimator

A transmission type HPGe detector with a sensitive area of 20 cm^2 and a thickness of 1.1 cm was fabricated and two commercial HPGe detectors were regenerated for charged particle spectroscopy at SIN.

Several coaxial Ge detectors of commercial origin were regenerated or repaired.

References

1) See contribution 1.28. (Didelez et al.) in this report
2) A. Hamacher et al., IKP Annual Report 1979, Jül-Spez-72, März 1980, p. 147

11. Target Laboratory

J. Pfeiffer, G. Riepe

For the use in experiments (IKP and visiting groups) at the cyclotron, at the research reactor, and at university laboratories about 180 targets (with and without backing) were prepared from 25 different elements by the following techniques: vacuum deposition, rolling (mostly after reduction or melting), pressing and sedimentation. The thicknesses were ranging from 20 $\mu g/cm^2$ to 12 mg/cm^2, and the areas were between 30 and 530 mm^2.

Especially the preparation of large area targets to be used for a magnetic spectrometer (BIG KARL) was creating new problems.

12. COMPUTER DEVELOPMENT

12.1. New Hardware Components

J. Siefert, R. Nellen, B. Siefert

The following add-ons and modifications were installed for our ONLINE data acquisition systems:

- Six non-volatile fast BORER 1635/16 CMOS-CAMAC-memory modules (each containing 16 K 16-bits/word) were introduced as external data regions, accessible by any user task. A built-in buffer battery backup secures stored information (e.g. sorted gate spectra) during any power-down condition. For the support of about 3 times faster increments of memory locations for spectra generation during sorts or online data acquisition, the existing CAMAC function codes F and A of the BORER memory modules were altered and extended by hardware modifications. The former standard feature of auto-incrementation of the memory address pointer by both read and write functions is now optional available via FØAØ (read) and F16AØ (write) for fast memory area transfers, or may be suppressed via FØA4 (read) and F16A4 (write) in fast memory increment mode. Further, now FØA1 reads and F16A1 writes the memory address pointer. A set of FORTRAN callable subroutines were implemented for the support of the CAMAC memories, extending the logical data address space of a user task up to currently maximal 96 K. The new routines support considerably faster accesses to data structures built in the CAMAC memories than the excessive time-consuming address mapping procedures via virtual address windows of the RSX11-M executive. The PDP11 SORT system[1] was modified for the usage of the new CAMAC memories for fast gate spectra generation, reducing considerably the overall run-times of the sort tasks.

- A 4-colour-pen CALCOMP 1Ø12 drum plotter with an RS-232-C interface was installed at our PDO11/34 RSX11-M system, using a DZ11 V24 terminal channel with 96ØØ baud rate. The plotter will be used with an appropriate plot spooler task as common graphic output device for application programs, running under RSX-11M.

- Two low-cost SOROC IQ14ØG video display terminals were installed as additional user terminals for our PDP11/34 RSX11-M system[2]. Although cheaper than a DEC VT52 terminal, a SOROC IQ14ØG terminal is much more efficient, because of its functional capabilities and options. The SOROC terminals support either a RS232 or 2ØmA current loop interface as main port with transmission rates in the range 11Ø to 19ØØ baud. All options may be choosen easily by appropriate switch settings. This is especially useful for our applications, requiring either 2ØmA terminals as (TTØ:) system console or RS323 terminals as (TTn:) user terminals via DZ11 channels at different PDP11 systems. Moreover, an additional RS232 auxiliary printer port supports hardcopies of the screen on a printer. A low-cost IDS44Ø impact printer with graphics option was installed as either local hardcopy for a SOROC terminal or as additional RSX11-M line printer.

- A DEC KK11-A 1K fast cache memory was installed in our PDP11/34 RSX11-M system to decrease substantially the average access time to main memory. Thus e.g., every cache hit (85 to 9Ø percent) saves about 75Ø ns of an otherwise 1.2 µs MM11-DP memory read. Using the cache, system throughput is enhanced considerably (especially for our memory-bounded sort application tasks).

- A hardware correlation box for 4 parameter listmode γγ-coincidence experiments with high event rates was designed and built as a CAMAC module. The correlation module generates all additional external timing and control signals needed for 1ØØ% correlated ADC addresses of 4 parameter events[3]. The box is connected to four CAMAC BORER 13Ø2 ADC buffer modules. Each 13Ø2 ADC buffer is interfaced to a 8Ø6Ø CANBERRA ADC. The 13Ø2 CAMAC ADC buffers and the NIM 8Ø6Ø ADCs were modified to force the generation and acceptance of a zero address parameter for any possible ADC reject condition (e.g. overflow, invalid or no data, ...) as conversion result of an applied ADC event-gate signal. Special addtitional hardware modifications of the ADC 13Ø2 buffers support now under control of the correlation box a continuous fast ADC read-out via the two 256 16 bit/word memories with minimal dead times. First fast listmode experiments using the new setup were carried out with a higher degree of correlated events than check experiments, which were run concurrently with the ND666Ø multiparameter system.

- A special COMBUS-DMA interface for high-speed, half-duplex data-transfers from/to memory areas of our ND666Ø multiparameter system via a UNIBUS-DMA DA11-B interprocessor link to/from the PDP11/34 ONLINE system[2,3] was installed. The COMBUS-DMA interface consists of a general DMA board from NUCLEAR DATA and a special interfacing, simulating the bus interface of the companion computer of a DA11-B UNIBUS-link. The COMBUS interface operates similar as the DR11-B part of the DA11-B link in two different modes: either block transfers, using the DMA facilities of the COMBUS, or single-word transfers are supported with optional completion interrupt requests for both transfer modes. Data blocks up to 32 K words in length can be transmitted via the new link in a single operation with maximal transfer rate of about 5ØØ K words per second (about 2 µsec/word transfer in DMA mode). A special hardware echo mode, implemented in the COMBUS-DMA interface and by additional modifications of the UNIBUS DR11-B part, allows the optional, automatic re-transmission and data-checking during DMA block and single word transfers from the ND666Ø to the PDP11/34 ONLINE system by hardware. This option supports error detection without slowing down the transfer rates and simplifies the communication protocol to be used. The COMBUS-DMA interface was developed and implemented according our specifications by the MUNIC design engineer Mr. Stampka. All software tests and checks during the development and installation periods were carried out by members of our ONLINE DV group. The new ND666Ø-PDP11/34 high-speed DMA-link will be used in future for single spectra and listmode data transfers from the ND666Ø multiparameter system during ONLINE experiments to

the PDP11/34 ONLINE master for time-critical and more extensive ONLINE data analysis.

- The design and development for the interfacing of a CAMAC crate (as generalized I/O port for experiments) to the high-speed synchronous COMBUS of a ND6660 system was started. The interface consists of two parts: the interfacing to the COMBUS is performed with a general digital I/O board (GDB) from NUCLEAR DATA. The GDB is essentially a CLASS II COMBUS interface that converts signals of the synchronous COMBUS into a simpler, asynchronous I/O bus structure intended for user CLASS II non-DMA type peripherals. The GDB bus signals are interfaced via external cables to a new developed CAMAC module COMUNI. It converts the GDB I/O bus signals to a subset of standard DEC UNIBUS data, address and control signals and vice versa. The UNIBUS side of COMUNI is connected to a standard CAMAC BORER 1533A single crate controller, interfacing a CAMAC crate to any UNIBUS. The COMUNI module was built and first tests were carried out.

- An uninterruptaple power supply (UPS) DELTEC DSU 1510G with 1.5 KVA power was installed for only the system rack (without peripherals) of our ND6660 multiparameter system to secure the MOS memory contents against any power-down condition, spikes, surges, high- and low-frequency noise on the AC-lines. Bad experiences with too often system crashes, loss of stored spectral data, unexpected system halts, erratic system performance and unexplainable damage to electronic components were traced out prevailing to AC-line problems, using power line disturbance analyzer/recorders (e.g. DRANETZ serie 616). Further, they have shown the relative high sensitivity (in comparison with DEC systems) of the ND6660 system against any AC-line problems. First positive experiences with the UPS recommend to install a larger UPS to power also all peripheral devices.

- A microprocessor based DATA I/O system 19 PROM programmer with RS232 remote control and universal programming pak was introduced. The PROM programmer is used for PROM copies of control PROMs of our ND6660 multiparameter system[2,3], MACAMAC and other systems, as well as for the development of new control PROMs for the bit sliced microprocessors of the ND6660 system and other microprocessor based systems.

References

1) J. Siefert, B. Schmidt: PDP11 Software Development, IKP Annual Report 1979, Jül-Spez-72, März 1980, p. 150

2) J. Siefert, B. Schmidt, M. Karnadi: ONLINE Data Acquisition Network, IKP Annual Report 1978, Jül-Spez-76, April 1979, p. 170-171

3) J. Siefert, B. Schmid, R. Nellen: New Hardware Components, IKP Annual Report 1979, Jül-Spez-72, März 1980, p. 148

12.2. PDP11 Software Developments

J. Siefert, B. Siefert

- The program system ADCS for control and ONLINE data acquisition[2] of either 4 single spectra or up to 4 $\gamma\gamma$-coincidence listmode parameters for our PDP11/34 ONLINE system[1] was functionally extended and implemented with a new overlay structure under RT11/V3B. The ADCS software package for single and listmode acquisition consists currently of about 390 routines written in MACRO and 110 routines written in FORTRAN. According to the very critical real-time response of the implemented functions, most routines had to be implemented as MACRO routines. ADCS supports the high-speed data-taking of ADCs for single spectra (maximal 20 KHz/ADC) or a fast listmode for $\gamma\gamma$-coincidence experiments. A sum rate of maximal 12 - 14 KHz listmode data may be written onto a magtape, limited only by the speed of the used TE16 magtape drives. 3 K listmode records with data header informations are used now. All single or listmode events are converted by modified 8060 100 MHz ADCs and are derandomized by modified CAMAC BORER 1302 ADC buffer modules[3], using the two 256 word stacks of the ADC buffers. The single or listmode projection 4 K monitor spectra are generated in the high memory above 32 K of the PDP11/34 system, using new implemented high-speed memory access routines for the memory management of the PDP11/34 CPU. The user may specify for listmode experiment control by easy cursor inputs intensified gate regions for online gate sorting. Maximal ten 4 K gate spectra may be sorted online during data-taking without additional experiments dead-times. All gate spectra are also generated in the high PDP11 memory above 32 K. All single or listmode data may be written onto magtape either in 800 bpi NRZ or optionally 1600 bpi PE mode. The default density after ADCS start may be re-defined. The listmode output to tapes may be suppressed during experiment setup tests. ADCS supports optionally 1 or 2 magtape TE16 drives to be used for listmode output. Using 2 TE16 drives in a round-robin manner reduces substantially the experiment dead-times due to magtape rewind time after detection of physical end-of-tape and loading of a next tape. A new magtape driver package MTP with FORTRAN callable FUNCTIONs for all necessary magtape operations were introduced. The calibration of any monitor or related gate spectrum may be performed now during active data-taking. Moreover, any 4 K monitor or gate spectrum, or any part of it may be transmitted within maximal 1 second via a new supported fast DR11-C interprocessor data link of the IKPNETwork to the PDP11/34 RSX master system to be plotted either in a linear or logarithm scale on the new installed CALCOMP 1012 drum plotter[3]. Any gate or monitor spectrum may also be stored on a RK05 disk as sequential ASCII formatted file, pressing the FILOUT button of the user-oriented pushbutton console. The spectra stored on disk may later replayed into memory for display or further processing, pressing the FILIN pushbutton. 3 CAMAC JEA20 SCHLUMBERGER fast scalers are used for the dead-time measurements. They display the true experiment coincidence event rate, the reduced ADC gate rate after event pile-up

rejections via a new built CAMAC correlator module[3], and the number of accepted events by the ADCS control system. All scaler values are protocolled with additional information continuously in the data header of each written list-mode record. All calibration parameters, gate definitions, and common variables, flags and data values are stored automatically into a direct-access file on disk at definite checkpoints. This information may be restored by an optional RES(ART) procedure after a possible system crash due to e.g. power-down, or a new start of the ADCS task. A modified version of ADCS was developed for control and data acquisition of single spectra, using only one ADC with maximal 20 KHz conversion rate, but gating the ADC data after user-specified time intervals into different, maximal five 4 K memory regions (multi spectra mode). The time slices for one single spectrum accumulation may be defined in the range from 0.1 sec to hours. The switching times from the current to the next spectrum to be accumulated are less than 200 µsec. All defined multi-spectra are saved automatically onto tape by pressing the I/O pushbutton with the magtape selected as I/O device. All other ADCS online functions as energy calibration, integration, background or FWHM calculations, ... are also available. Another version of ADCS supports the event specified generation of maximal six 4 K spectra, using the same ADC. Each event signal must be accompanised by a user tag signal, which gates the converted address into the desired spectrum.

- A set of tasks were developed for the experiment control of a high resolution X-ray crystal diffraction spectrometer with a PDP11/10 system. The existing small PDP11/10 control system was extended by additional 16 K of memory, a RX11 floppy disk system with dual RX01 disk drives, a VT55 video terminal and a BORER 1533B single crate controller for interfacing of a CAMAC crate. RT11/V3B was introduced as operating system. All software developments for the crystal spectrometer were performed on our PDP11/34 ONLINE system[1], using an opto-coupled DL11-E data link between the PDP11/10 and PDP11/34 system to transfer the generated task files on the remote PDP11/10 system. The experiment supervisor overlay task CRY with about 20 implemented commands controls the ONLINE data acquisition and storage on a floppy data disk. CRY consists of about 40 FORTRAN and 10 MACRO written subroutines. A PAR(ARMETER) command defines (or optional lists) the number of spectrometer positions, the position values, the number of points, the step width between positions and the measurement time for each position to be used for a run. A spectrometer position is proportional to a number of stripes of an interference pattern. The up and down counting of interference stripes during any spectrometer positioning with a stepping motor is performed by a special PHOTO PICKUP NIM box with an internal fast scaler. CRY reads out the scaler, calculates all parameters and controls the stepping motor for a new spectrometer position. A TIME(E) command defines the present count for a JEA20 CAMAC scaler from SCHLUMBERGER used as timer during the data acquisition. The SAV(E) command saves all defined parameter values into a disk file. Parameters from that file may be restored for a later run by a RES(TORE) command. All accumulated data values during a run are stored in a direct-access file. A DIR(ECTORY) command generates a directory listing of the direct-access file with experiment-run specific informations. A ZER(O) command initializes the data file. During the measurement, the CRY task controls the exact positioning of the crystal spectrometer, using the stepping motor, as well as status information from a special PIEZO control box, which tries to compensate all mechanical jittering of the spectrometer, and the current scaler contents of the PHOTO PICKUP module. The task PLOT displays data points from the direct-access file for a specified position of a choosen experiment-run on the VT55 terminal as a graph with optional X- and Y-grid lines for scaling. A displayed spectrum may be send via the DL11-E data link to the PDP11/34 ONLINE system and plotted there on a local 1200 baud LS120 DECWRITTER III terminal. The task ADC supports the ONLINE data-taking of correlated 2-parameter events as monitor spectra (energy and time) via 100 MHz ADCS from NUCLEAR DATA and CAMAC ADC buffers for spectrometer checks and adjustements.

- The general SORT task/subtask system[2] for the PDP11/34 RSX11-M system was functionally extended by a new spectrum handling subtask system SPT (SORSPT, SPTARI). The spectrum processor subtask SORSPT may be invoked either at the SOR> levels of the SORT main task by a SPT command, or at the DIS> level of the display processor subtask SORDIS, or from the MCR command level by a RUN SPT command. The spectrum processor command input level is identified by a SPT> prompting. 9 spectrum handling commands are currently implemented at the SPT level. E.g., the ADD command adds two spectra SPEC1 and SPEC2 from disk files and stores the result in a COMMON main memory partition, referenced logically as ME for other SOR>, DIS> or SPT> commands. The ADD processor performs the function SPEC1 + F1/F2 * SPEC2 with optional normalization factors F1 and F2 (defaults are 1.0) for the second spectrum. The SUB(TRACT) command subtracts and the DIV(IDE) command divides spectra (SPECT1*F1/SPEC2). A COP(Y) command coppies either a sorted gate spectrum into the area of another gate spectrum of an direct-access library file with sorted gate spectra, or transfers a gate spectrum as single spectrum into a sequential ASCII formatted output file or vice versa, or a single spectrum file into another ASCII formatted output file. The DIS(PLAY) command issued at the SPT level exits the SPT subtask and enters the display processor subtask SORDIS, as well as the SOR(T) commands invokes the SOR> command level of the SORT main task. A TRA(NSFER) command at the SPT level copies the result spectrum, processed by a SPT command from the COMMON memory ME as single spectrum into a sequential ASCII formatted output file or prints all or specified spectral data from ME on the lineprinter. An INT(EGRATE) command at the SPT> level integrates all channels within a specified region and calculates the centroid of a peak. Further standardized spectrum arithmetic command will be implemented.

- A task/subtask-system EMA was developed for controlling a new cyclotron-beam emittance measurement device (EMA) (see contribution of the cyclotron group of this report

for further details). The RS232 I/O port of the EMA device was connected via a 9600 baud DL11-E interface to the cyclotron control PDP11/34 system. A high-priority, privileged subtask CYCEMA was written as interrupt driven front-end driver, controlling the data flow, command and status information between the micro-processor based EMA device and a COMMON partition in main memory. A set of commands with appropriate status and data printouts was implemented in the EMA main task as user interface. Simple commands as e.g. INI(T), PAR(AMETERS), STA(RT), TRA(NSFER), ... allow the complete control of the EMA device. The EMA task communicates via the COMMON memory partition and global event flags with the CYCEMA driver. Extensive test runs for checking all specifications of the EMA hardware system were carried out.

- An IKPNETwork task ONLLP was developed for the PDP11/34 system, running under RSX11-M/V3.1. ONLLP supports (together with a task MTONL under RT11/V3B on the PDP11/34 ONLINE system[1]) the transfer of ASCII files from an ANSII structured magtape, loaded on a local TE16 magtape drive, via the RH11 UNIBUS-A/UNIBUS-B DMA-link (1) into the memory, and as listings onto the local TELEPRINT 6720 linprinter of the PDP11/34 RSX system. ANSII magtape ASCII files with formats generated by utility programs of the operating systems RT11/V2C/V3B (e.g. PIP, MACRO, LINK, ...) and MIDAS+C of the ND6660 multiparameter system (e.g. EDIT, DKMT, ...) may be listed on the lineprinter. Two DR11-C interfaces are used as physical interprocessor link together with an appropriate communications protocol as logical command and status link between the PDP11 systems.

- A further IKPNETwork task system NETCYC was implemented for FILES-11 structured ASCII file transfers between our PDP11/34 RSX system and the cyclotron control PDP11/34 system, running also under RSX11-M/V3.1. A 9600 baud DZ11 RS232 terminal channel of each system is used as data link. ASCII files may be send by a simple TRA(NSFER) command from any UIC-area of the transmitter system to the login-UIC area of the receiver NETCYC task. Moreover, ASCII files from the cyclotron PDP11/34 system may be spooled on the lineprinter of the PDP11/34 RSX system.

References

1) J. Siefert, B. Schmid, R. Nellen: New Hardware Components, IKP Annual Report 1979, Jül-Spez-72, März 1980, p. 148-149

2) J. Siefert, B. Schmid: PDP11 Software development, IKP Annual Report 1979, Jül-Spez-72, März 1980 , p. 150

3) J. Siefert, R. Nellen, B. Siefert: New Hardware Components, contribution of this report

12.3. The New Desk-Top-Computer Configuration of the Theoretical Group in IKP

E. Brökel

Since a long time, it was desired to have a facility to digitize data from graphs and have them available under TSS. There was already a digitizer HP 9864 A connected to a desk-top-computer HP 9810 A from Hewlett Packard. But the installation of terminals from Hewlett Packard (HP 2648 A) for TSS by the Zentralinstitut für Angewandte Mathematik (ZAM) made it possible to realize this desire for the first time. To do it, our desk-top-computer HP 9810 A was replaced by a desk-top-computer HP 9835 A with 128 kbyte read access memory (RAM), fully programmable in BASIC and an integrated mini-card-ridge unit.

By interfacing, it is possible to connect the terminal HP 2648 A to the computer HP 9835 A. That is the way to transfer data from the desk-top-computer to the terminal but also from the terminal to the desk-top-computer.

This bi-directional processing made it desirable to have also a plotter connected to the desk-top-computer. So it became practicable to create graphs from data generated either by TSS or by MVS. It was decided to buy an HP 9872 A plotter and with it a large field of applications was opened for the use of HP 9835 A.

To document the programs for the HP 9835 A desk-top-computer, also to print the results of application programs, an HP 2631 G graphic printer was bought. The graphic facility of this printer should be used to make preliminary plots before one decides which set of data one would like to use for creating the final graph on the HP 9872 A plotter.

The configuration is shown in fig. 1.

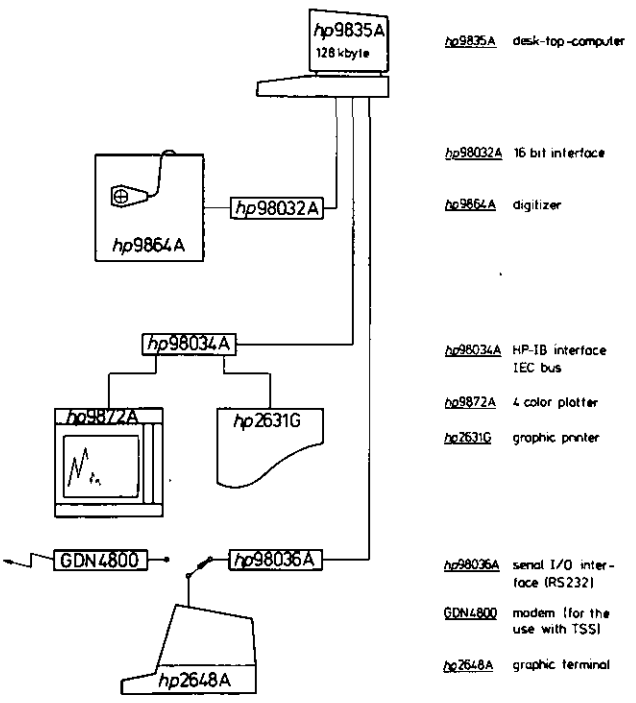

13. Electronic Division

H. Labus, J. Bojowald

The following devices, partly announced in the annual report 1979, have been set into operation:

1) A series of special NIM-modules to reduce costs and space of complex experiments to investigate nuclear reactions and scattering processes have been developed and produced:

1.1) An analog Sum-amplifier with 10 inputs each having its own attenuator and Pole-Zero-adjust.

1.2) An analog Fan-Out-amplifier with 14 outputs each having its own attenuator and on/off-switch.

1.3) A 14-fold 50 nsec delay for fast photomultiplier or Fast-NIM signals using packed RG-127/U coax cable.

1.4) An 8-fold frequency divider for TTL-signals each channel having switch selectable attenuation (1/10 to 1/10.000) and variable delay (0.2 to 2.0 µsec).

1.5) An 8-fold shaping and converting (TTL to Fast-NIM) module to adapt the Busy-signals of eight ADC's to special gating purposes.

1.6) A module to monitor the correct operation of the mag-tape of the ND-6660 Multi-Channel-Analyzer.

1.7) A plug on card to monitor the supply-voltages of WENZEL-NIM-Crates by LED displays.

1.8) An 8-fold high voltage distributor box, each output having its own attenuator and on/off-switch to adjust multi-photomultiplier-arrangements.

1.9) A coincidence control to gate a multi-purpose coincidence system.

(G. Lürken, K. Pelzer, K. Winkler)

2) The control units of the 24 current supplies of the BIG KARL H_t-windings have been equipped with five-digit LED-displays and read-out of the true current values. The current measurement is performed by Texas TL500/TL502 dual slope ADC with ±20.000 resolution, 0.001% linearity and high ripple suppression. Read-out is performed with a parallel bus, transferring the information as normally coded to drive multiplexed seven segment displays. This bus is connected via opto-isolators to a CAMAC I/O-module (BORER 1031A for further processing in a PDP11. To allow high common-mode-voltages of 50 volt between individual power supplies the analog circuit TL500 has a floating supply and is opto-isolated from the digital circuit TL502.

(K. Kruck, W. Ernst)

3) Difficult and time consuming maintenance and repair work caused by inappropriate components has been spent to the H_t-power-supplies. A lot of improvements were necessary to assure correct polarity inversion, current setting and on-off-switching.

(K. Kruck)

4) The following modifications and installations of devices within the cyclotron, the Beam Line and Big Karl have been performed:

4.1) The control electronic of the two axial phase slits has been adapted to redesigned mechanical devices.

4.2) The Beam Line slits AS1 and AS2 have been modified to allow independent width and offset displacements.

4.3) The slits SD1L and SD1R in the Big Karl have been equipped with remote control. For this purpose existing electronics has been modified to drive 24V-DC-motors instead of synchronous motors.

(N. Dolfus, K. Winkler)

5) The preregulation of the power amp of the external microscopic beam pulsing was accomplished within an engineering task[1] in cooperation with the Fachhochschule Aachen, Abt. Jülich.

(S. Matula, N. Dolfus, H. Labus)

6) The bent crystal spectrometer controlled by a PDP11/10 together with six NIM-modules has been up-graded to release the computer from counting the interferometer pulses. This was necessary to prevent skipping of position displacements due to mechanical disturbances, which could happen to be faster than the interrupt processing time of the computer. For this purpose two 24-bit comparators (SN74C85), two 24-bit latches (SN74C173), and one 24-bit multiplexer (SN74LS157) had to be inserted into the six NIM-modules together with various boards for logic interconnections.

(N. Dolfus, G. Lürken)

7) A modern concept[2] to control slow mechanical devices, as mounted in a large variety around the Beam Line of the cyclotron has been investigated using low cost personal computers with graphic capabilities to give quick image and comprehensive operating intructions to untrained users. To do this a lab-test model of an intrinsically safe scattering chamber with completely new layout of all features has been built to get improved reliability, easier maintenance, faster target motions and higher precision compared to the old models. This machine was then controlled by an APPLE-II-computer using a set of I/O-boards of the SMP-system (Siemens modular Micro-computer Board system) to act as a peripheral interface for the APPLE-II. The set of I/O-boards consisted of E211 (opto coupled parallel output), E212 (opto coupled parallel input), E230 (diff. analog input) and E240 (quad analog output). The interface between the SMP-Bus and the APPLE-II-BUS could be realized straightforward by buffering the data- and address-lines and by some simple interconnections between the clock- and control-lines of both systems. Software has been developed with support of the comfortable UCSD-operating system as implemented and extended by the APPLE computer inc. The main program has been written in Pascal, and the driving routines for the SMP-boards with the resident Macro-Assembler.

(H. Labus, H. Diesburg, K. Kruck, A. Retz, U. Rindfleisch, G. Brittner, K. Winkler)

8) About 160 repair- and maintenance-jobs of NIM- and CAMAC-modules, TV-cameras and monitors, power-supplies of all categories, electronically controlled scattering chambers and Beam slits and a great variety of special instruments from own or external production have been performed.

(H. Diesburg, G. Brittner, K. Winkler, W. Ernst)

Main activities are now concentrated to following subjects:

1) The crystal rotation of the bent crystal spectrometer now being controlled by eight 2/12-NIM-modules, which are connected to a PDP11/10 via DR11K Interfaces, is redesigned. It is intended to improve response times and reliability as well as space- and power-consumption by using Single Board Computers, e.g. Siemens SKC85. Within this task another attempt is made to suppress the crystal jitter caused by mechanic vibrations by a PID-controller acting onto the sandwitched piezo-ceramics. The latter has been equipped by an improved attachment giving less jitter than one band of the interferometer which is a pre-supposition for jitter compensation by electronic means.

(N. Dolfus, G. Lürken, H. Labus)

2) The control room of the nuclear experiments has disturbed line- and ground-potentials which prevent in some experiments high resolution spectroscopy at long distances between main amplifiers and ADC's. The reasons are manifold but ground-loops and wrong-wired line filters seem to be most important. Measurement techniques are developed to test line and ground potentials over a wide frequency range. Systematic trouble-shooting and removal of faults is done during measurement interruptions.

(J. Bojowald, K. Kruck, H. Labus)

References

1) S. Matula, Phasen- und amplitudenvariable Ansteuerung eines HF-Leistungsverstärkers, Fachhochschule Aachen, Abt. Jülich

2) H. Labus, Eine Prozeß-Steuerung mit dem Personal Computer APPLE-II, to be published

14. Radiation Protection

H.J. Probst

In 1980 the trend of the administrative authority to prescribe also details in the area of the radiation protection was continued steadily. The sum of all doses accumulated by the personnel working in the institute was 13 Rem. There were no large extremity irradiations. Nobody attained the dose limits even only approximately. For the radiation at an accelerator, measurement of the doses and dose rates near the surface of activated materials is very important. However, there are not dosimeter suitable for the purpose available commercially. Thus two measuring devices of Zentralabteilung Strahlenschutz, a surface barrier detector[1] and a "three times TL-dosimeter", were tested for practical use.

Some measured values at different places are compiled in the following table:

measuring point	dose rate (R/h)			
	Graetz X5E	surface barrier detector	"three times TLD"*	
internal beam probe	3.3	96	a) 93 b) 63 c) 42	100 67 51
near the degrader, outward the beam tube	2.6	3.4	a) 4.0 b) 3.6 c) 3.3	3.9 3.5 3.3
8 cm distance from the degrader box	4.0	4.5		
deflector flansch	0.60	0.60	a) 0.66 b) 0.58 c) 0.61	0.58 0.59 0.59
deflector-septum	1.3	7.2	a) 9.6 b) 4.8 c) 4.1	16.0 5.4 3.8
compensating channel, entrance slit	35	600	a) 1000 b) 570 c) 400	

*generally two "three times TLD" were used for a measuring point; the thicknesses of the 3 TLD in the stack were: a): 0.14 mm, b): 0.4 mm, c): 0.4 mm

The measurements show especially the following results:

1) The dose rate measurements using γ-dosimeter are sufficient, if the radioactive material is located inside the cyclotron or the beam line.

2) This measurement results totally incorrect values, if it is carried out near the surface of the activity, including also largely extented radioactive material.

3) The dose rate decreases very strongly at distances only a few millimeters away from the surface of the activity. A high fraction of low energy β-rays seems to be the reason for that.

References

1) W. Wahlen, H. Schüren, M. Heinzelmann, Laborbericht D 7/80 (1980) ZST der KFA

2) M. Keller, ZST-Bericht Nr. 0330 (1980)

15. Engineering Office and Mechanical Workshops

W. Briell, D. Groß, K.H. Ramacher, A. Retz, U. Rindfleisch, H. Schwan

In addition to the service and maintenance of the cyclotron and the experimental facilities there was an increase of activities for the solar group. During the annual maintenance several important components of cyclotron and beam line have been improved.

Cyclotron and beam line

- because of corrosion damages of the Dee-cooling platines new shorting plate were installed and tested.
- for the improvement of the extraction procedure a new remote controlled focussing channel and two steering magnets for correction in x and y direktion were installed (see fig. 1).

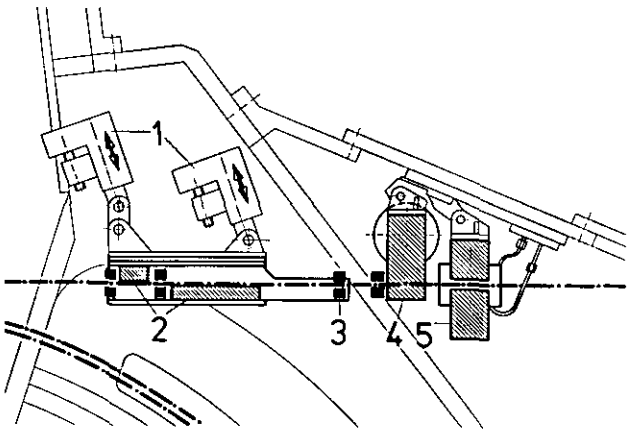

Fig. 1: 1 remote controlled motor drive
2 channel profile
3 slits
4 steering magnet for horizontal deflection
5 steering magnet for vertical deflection

- the phase slits were mechanically improved
- the beam line was equiped with additional movable slits, steering magnets and object diaphragms.

Magnetspectrometer BIG KARL

- additional slits in front of the first dipol and the detector plane are mounted for the reduction of back ground and the improvement of the optimization procedure.
- the large vacuum chamber with adjustable focal plane detectors inside was removed and the detectors are mounted as fixed stack. This became possible because it was found to be very easy to rotate and shift the focal plane electrically in the detector plane.
- a new gas supply system for the focal plane detectors with adjustable gas pressure has been installed.
- a second MWPC for 0^0- experiments was constructed.

Cristalspectrometer

- a new adjustable table for the optimization of the distance between cristal and source has mounted.
- a pneumatically coupled motor drive for the cristal rotation was installed.
- a variable source mount was constructed (see fig. 2). This arrangement allows the quasi-simultaneous measurements with two probes for the determation of energy shifts of $\Delta E \approx 10^{-7}$. As probes radioaktive and inactive sources can be used. With this adjustments it is possible to optimize the effective geometrical source width and the fluorescence yield.

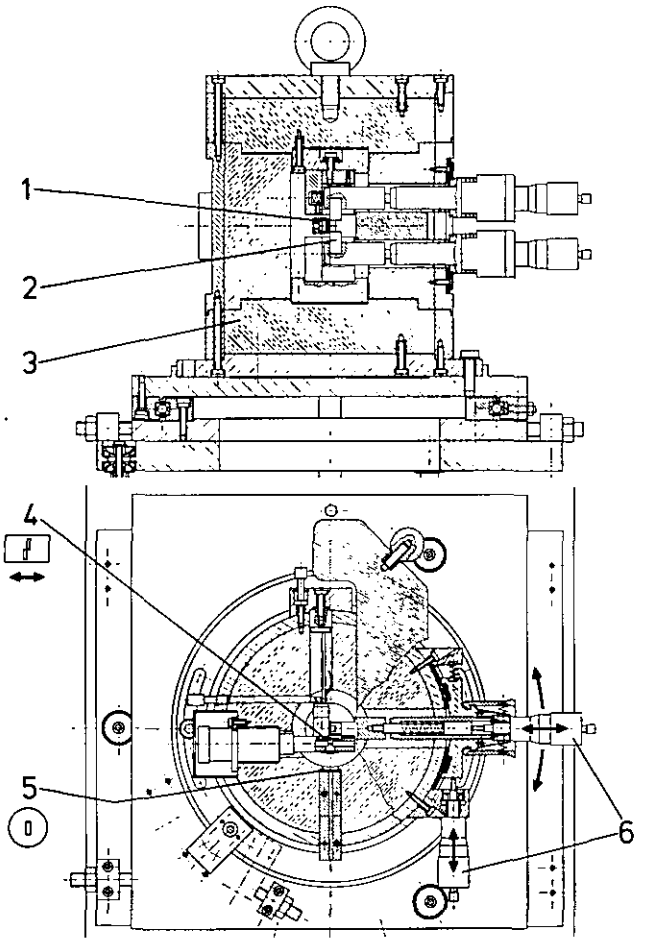

Fig. 2: 1 flourescence source
2 probe mount
3 lead shielding
4 chopper diaphragm
5 exit diaphragm
6 adjustment micrometers

V. SCIENTIFIC ADVISORY COUNCIL OF THE INSTITUTE OF NUCLEAR PHYSICS

Prof. Dr. K. Alder	University of Basel
Prof. Dr. R. Bock (Chairman)	GSI Darmstadt
Prof. Dr. P. von Brentano	University of Köln
Prof. Dr. W. Greiner	University of Frankfurt
Prof. Dr. P.G. Hansen	CERN, Genf, Switzerland
Prof. Dr. K.H. Lindenberger	Hahn Meitner-Institute, Berlin
Prof. Dr. H.-J. Mang	TU München
Prof. Dr. T. Mayer-Kuckuk	University of Bonn
Prof. Dr. P. Weinzierl	Research Center Seibersdorf, Austria
Prof. Dr. H. Wenzl	KFA Jülich

VI. EXTERNAL COMMITTEE FOR GUEST EXPERIMENTS

Prof. Dr. R. Bock	GSI Darmstadt
Prof. Dr. P. von Brentano	University of Köln

VII. PERSONNEL

Institute for Nuclear Physics:

Dr. C. Mayer-Böricke	Director of the Institute for Nuclear Physics (Experiment I) Professor of Physics at University of Bonn
Dr. O. Schult	Director of the Institute for Nuclear Physics (Experiment II) Managing director of the Institute for the year 1980 Professor of Physics at University of Köln
Dr. J. Speth	Acting Director of the Institute for Nuclear Physics (Theory) Professor of Physics at University of Bonn

Scientific Staff:

Dr. L. Aldea (Cy)

DP G. Battistuzzi (E2)
until Sep. 26, 1980

Dr. G. Baur (Th)

DP U. Bechstedt (E1)

Dr. G. Berg (E2)

Dr. H. Beuscher (E1)

R.K. Bhandari (Cy)
(BARC, Calcutta/India)

Dr. B. Bochev (E1)
(Bulgarian Academy
of Sciences, Sofia/
Bulgarien)

T. Bocheva (E1)
(Bulgarian Academy
of Sciences, Sofia,
Bulgarien)

DP J. Bojowald (Ec)

Dr. G. Borchert (E2)

DP O. Bousshid (E1)

DI.W. Bräutigam (Cy)

DP C. Conci (Th)

DP H. Dermawan (Th)

Dr. A. Djaloeis (E1)

Dipl. W. Ebke (E2)
since Sep. 1, 1980

DP A. Ercan (E2)

Dr. K. Göke (Th)
(Privat-Dozent at the
Univ. of Bonn)

Dr. S. Gopal (E1)
(Univ. of Mysore,
Mysore/Indien)

Dr. F. Grümmer (Th)

Dr. J.W. Grüter (E2)
until Oct. 1, 1980

Dr. D.R. Haenni (E1)
(Texas A&M Univ., College
Station, Texas/USA)

Dr. A. Hardt (Ms)
until March 9, 1980

DP R. de Haro (Th)

Prof. J. Hill (E2)
since Oct. 1, 1980
(Iowa State Univ., USA)

Dipl. B. Hoffmann (Th)

DM W. Hürlimann (E2)

Dr. P. Jahn (E1)

Dr. J. Katayama (E2)
since June 2, 1980
(Osaka Univ./Japan)

Dr. K. Kawade (E2)
until Aug. 9, 1980
(Nagoya Univ./Japan)

Dr. P. Kleinheinz (E2)

Dr. H.R. Koch (E2)

Dr. S. Krewald (Th)

Dr. H. Labus (Ec)

Dr. H. Lawin (E2)

Dr. R.M. Lieder (E1)
(Privat Dozent at the
Univ. of Bonn)

Dr. H. Machner (E1)

Dr. S. Martin (Ms)

DMT K. Maßmeyer (E2)

Dr. H.G. Mathews (E1)
since June 2, 1980

Dipl. H. Mattheß (E2)
since March 3, 1980

Prof. Dr. C. Mayer-Böricke (E1)
(Prof. at the Univ. of Bonn)

Dr. J. Meißburger (Ms)

Dr. T. Morek (E1)
until Feb. 15, 1980
(Warsaw Univ., Warsaw/Poland)

Dr. H.P. Morsch (E1)

Dr. M. Müller-Veggian (E1)

Dr. H. Müther (Th)
until Aug. 12, 1980

Dipl. C. Mund (E2)
until July 31, 1980

Dr. J. Nagai (E2)
until Apr. 30, 1980
(Osaka Univ./Japan)

Dr. A. Neskakis (E1)
since Oct. 15, 1980
(Univ. of Crete,
Iraklion/Greece)

Dr. W. Oelert (E1)

Dr. F. Osterfeld (Th)

Dr. M. Piiparinen (E2)
until July 31, 1980
Humboldt fellow
(Univ. of Jyväskylä)

Dipl. B. Poos (E2)
since Nov. 14, 1980

DI R. Posorski (E2)

DP H.J. Probst (Rp)

Prof. Dr. P. Prokofjev (E2)
since June 27, 1980
(Nucl. Research Center,
Riga/UdSSR)

DP D. Protič (Dt)

Prof. Dr. N.G. Puttaswamy (E1)
(Bangalore Univ., Bangalore/
Indien)

DP J. Reich (Cy)

Dr. G. Riepe (Dt)

Dr. M. Rogge (E1)

DI B. Sack (E2)

Prof. Dr. O. Schult (E2)
(Prof. at the Univ.
of Cologne)

Dr. H. Selič (E2)
since June 1, 1980

Dr. H. Seyfarth (E2)

Dr. M. Shaanan (E2)
since June 2, 1980
(Soreq Nucl. Res.
Center/Israel)

Dr. K. Shizuma (E2)
since Oct. 1, 1980
(Hiroshima Univ./Japan)

DP J. Siefert (Da)

Dr. K. Sistemich (E2)
(Privat Dozent at the
Univ. of Cologne)
from July 15, 1980 on
leave of absence to
Iowa State Univ./USA

Dipl. F. Soramel (E2)
since June 16, 1980

Prof. Dr. J. Speth (Th)
(Prof. at the Univ.
of Bonn)

Dr. H.J. Stein (E2)

Dr. B. Styczen (E2)
(Jagellonian Univ. Cracow/
Poland)

Dr. J. Styczen (E2)
(Institute of Nuclear Phys.
Cracow/Poland)

Dr. C. Sükösd (E1)
until Aug. 20, 1980
(Roland Eötvös Univ.,
Budapest/Hungary)

Dr. T. Suzuki (Th)

Dr. H. Talarek (E2)

DP Y. Tokunaga (E2)

Dr. P. Turek (E1)

Dr. R. Wagner (E2)

Dr. P. Wucherer (Cy)

Research visitors
(for one week to six
months):

Dipl. N. Abo Kirshien (Th)
from July 21 to Aug. 22, 1980
(Technion, Haifa/Israel)

Dr. W. Bauhoff (Th)
from July 1 to July 31, 1980
(Univ. of Hamburg)

Prof. Dr. J. Blomqvist (E2)
from June 1 to June 7, 1980
and from Dec. 16 to Dec. 20,1980
(Research Inst. for Physics,
Stockholm/Sweden)

Dr. R. Broda (E2)
from May 12 to June 7, 1980
and from Nov. 3 to Nov. 12, 1980
(Univ. of Cracow/Poland)

Prof. V.R. Brown (Th)
from Oct. 10 to Dec. 15, 1980
(Lawrence Livermore
Laboratory, Livermore/USA)

Prof. Dr. A. Budzanowski (E1)
from Apr. 24 to May 12, 1980
(Institute of Nuclear Physics,
Cracow/Poland)

Dr. T. Chakraborty (Th)
from Sep. 22 to Nov. 30, 1980
(Univ. of Köln)

Prof. R.Y. Cusson (Th)
from Feb. to March 1980
(Duke Univ., Durham/USA)

Prof. Dr. P.J. Daly (E2)
from May 30 to June 8, 1980
(Purdue Univ., W.Lafayette/USA)

Dr. P. Decowski (E1)
from Oct. 20 1979 to Jan. 19,1980
(Warschau Univ. Polen)

Prof. W.T. Donnelly (Th)
from Oct. 6 to Oct. 28, 1980
(MIT, Cambridge/USA)

Dr. S. Fantoni (Th)
from Aug. 28 to Oct. 31, 1980
(Univ. of Köln)

Research visitors
(for one week to six months):

Prof. Dr. H. Ikegami (E2)
from Sep. 12 to Nov. 11, 1980
(Osaka Univ./Japan)

Dr. C.H. Li (Th)
from May 15 to July 31, 1980
(SUNY at Stony Brook, Stony Brook/USA)

Prof. Dr. I. Lovas (E1)
from Apr. 18 to Apr. 24, 1980
(Central Research Institute of Physics, Budapest)

Dr. S. Lunardi (E2)
from Aug. 23 to Sep. 6, 1980
(INFN Padua/Italy)

Prof. V.A. Madsen (Th)
from June 10 to July 31, 1980
(Oregon State Univ., Corvallis/USA)

Prof. A.B. Migdal (Th)
from Aug. 30 to Sept. 23, 1980
(Landau Institute, Moscow/UdSSR)

Dipl. H. Nguyen-Quang (Th)
from May 19 to Aug. 31, 1980
(Univ. of Bonn)

Prof. J.V. de Passos (Th)
from Jan. 14 to Feb. 23, 1980
(Univ. of Sao Paulo, Sao Paulo/Brasil)

Dr. S. Pesič (E1)
from May 31 to June 6, 1980
(Boris Kidrič Institute, Belgrad)

Prof. Dr. J. Rama Rao (E1)
from Feb. 25 to March 7, 1980
(Banaras Univ. Indien)

B. Rubio (E1+E2)
until Oct. 16, 1980
(Univ. Madrid/Spain)

Dr. R. Shyam (Th)
from Apr. 21 to May 10, 1980
(Daresbury Lab., Warrington, England)

J. Tain (E1+E2)
until Oct. 16, 1980
(Univ. Madrid/Spain)

Dipl. K. Tam (Th)
from May 16 to Aug. 15, 1980
(SUNY at Stony Brook, Stony Brook/USA)

Prof. J.N. Urbano (Th)
from Jan. 1 to March 31, 1980
and from Sep. 20 to Oct. 4, 1980
(Univ. of Coimbra, Coimbra/Portugal)

Dr. J. Wambach (Th)
from Feb. 4 to Feb. 24, 1980
(SUNY at Stony Brook, Stony Brook/USA)

Dr. A. Wolf (E2)
from Sep. 22 to Oct. 1, 1980
(Nucl. Research Center Negev/Israel).

Dr. D. Zawischa (Th)
since Oct. 1, 1980
(Univ. of Hannover)

Technical and administrative staff:

J. Anhalt (E2)
K. Barth (Ec)
H.G. Böge (Cy)
W. Borgs (E2)
H. Borsch (Cy)
W. Briêll (Cd)
R. Brings (Cy)
G. Brittner (Ec)
E. Brökel (Th)
U. Burck (Ad)
since Nov. 3, 1980
J. But (Ws)
H. Diesburg (Ec)
A. Dohmen (Ad)
N. Dolfus (Ec)
F. Drees (Cy)
R. Enge (Ws)
P. Engels Cy)
W.R. Ermer (E2)
W. Ernst (Ec)
R. Fiedler (Cy)
N. Gad (Cy)
J. Geremeck (Cd)
G. Göbbels (Ws)
A. Golic (Ws)
E. Gollnick (E2)
D. Groß (Cd)
G. Groß (Ms)
from Sep. 24, 1979 to Feb. 22, 1980
U. Hacker (Ms)
H. Hadamek (Ws)
A. Hamacher (Dt)
M. Heese (Ad)
H. Heinrichs (Cy)
K. Hieble (Cy)
H. Hintzen (Rp)
W. Hoffmeister (Cy)
K. Hütten (Ws)
H.M. Jäger (E1)
I. Jannakos (Cy)
H.J. Jansen (Ws)
R. Janssen (Ad)
A. Jeglorz (E2)
E. Jutz (E2)
M. Karnadi (Da)
H. Klapperich (Ws)
K. Kraft (Rp)
R. Krewel (Ms)
K.P. Kruck (Ec)
T. Künster (Dt)
E. Lawin (Dt)
H. Lengerke (Ad)
G. Lürken (Ec)
S. Matula (Ec)
from Jan. 1 to Nov. 28, 1980
H. Mauel (Da)
H. Metz (Dt)
H. Meuser (Ws)
A. Müller (Cy)
G. Müller (E2)
R. Nellen (Da)
K. Nicoll (Dt)
P.K. Pelzer (Ec)
F.J. Pelzer (Ws)
from Jan. 31 to Juli 31, 1980
J. Pfeiffer (Dt)
J. Pitzen (Ms)
H.W. Pohl (E1)
K.H. Ramacher (Cd)
A. Retz (Cd)
U. Rindfleisch (Ws)
H. Ringel (E2)
until June 30, 1980
N. Rotert (Cy)
since July 1, 1980
T. Sagefka (Ms)
H. Sauer (Ad)
G. Schlienkamp (Cy)
P. Schmidt (E2)
Jos. Schmitz (Ws)
Jürg. Schmitz (Cy)
R. Schröer (E2)
F. Schultheiß (Ws)
H. Schwan (Ws)
R. Seidemann (E2)
B. Siefert (Da)
H. Sieling (Ad)
M.L. Stehr (Ad)
since Jan. 2, 1980
J. Strehl (Ws)
K.P. Wieder (E2)
W. Wilms (Cy)
K. Winkler (Ec)
J. Wolanski (Ws)

(E1) Institute for Experimental Nuclear Physics I
(E2) Institute for Experimental Nuclear Physics II
(Th) Institute for Theoretical Nuclear Physics

(Ad) Administration
(Cd) Construction and Design
(Cy) Cyclotron Laboratory
(Da) Data Acquisition Group
(Dt) Detector and Target Laboratory
(Ec) Electronics
(Ms) Magnetic Spectrograph 'Big Karl'
(Rp) Radiation Protection
(Ws) Mechanical Workshop

VIII. PUBLICATIONS (appeared before December 16, 1980)

IKP-100180
Aldea, L.; Seyfarth, H.
Analysis of the α-Particle Spectrum for $^{143}Nd(n_{th},\alpha)^{140}Ce$ and $^{143}Nd(n_{th},\gamma\alpha)^{140}Ce$.
Proc. 2nd Int. Symp. on Neutron Induced Reactions, Smolenice, CSSR, 25.-29.6.1979 (VEDA Publ. House of the Slovak Academy of Science, Bratislava, 1980) S. 95-102, Hrsg.: I. Ribansky, E. Betak.
2o.o6.o + 2o.3o.o

IKP-100280
Anhalt, J.; Schult, O.W.B.; Stein, H.J.
Teststation für Solarkollektoren in Brasilien - Stand Dezember 1979.
Statusbericht Sonnenenergie (VDI-Verlag GmbH, Düsseldorf, 1980) ISBN 3-18-419067-6, Bd. 1, S. 183-192.
2o.6o.1

IKP-100380
Ansari, A.; Civitarese, O.; Faessler, A.
The Pairing Correlations and Nuclear Shapes at Very High Angular Momenta.
Nucl. Phys. A334 (1980) S. 93-108.
2o.8o.o

IKP-100480
Arbeitsgemeinschaft "Mustersolarhäuser" - KFA-IKP, KFA-STE, VdZ/GFHK.
Vorphase des Projekts "Mustersolarhäuser", Arbeitsgemeinschaft Mustersolarhäuser - Stand Dezember 1979.
Statusbericht Sonnenenergie (VDI-Verlag GmbH, Düsseldorf, 1980) ISBN 3-18-419067-6, Bd. 1, S. 203-209.
2o.6o.1 + 64.2o.1

IKP-100580
Bäckman, S.-O.; Brown, G.E.; Klemt, V.; Speth, J.
Pauli Principle Sum Rule and Consistency Relations for Phenomenologically Adjusted Fermi Liquid Parameters.
Nucl. Phys. A345 (1980) S. 202-220.
2o.8o.o

IKP-100680
Battistuzzi, G.; Kawade, K.; Kern, B.D.; Khan, T.A.; Lauppe, W.-D.; Lawin, H.; Selič, H.A.; Sistemich, K.; Wolf, A.
Studies at the Fission Product Separator JOSEF.
IAEA Progress Report in Fission Product Nuclear Data, INDC (NDS) - 112U/G+P, June 1980, Vol. V, S. 35, Hrsg.: Qaim.
2o.65.o

IKP-100780
Baur, G.; Shyam, R.; Rösel, F.; Trautmann, D.
The Importance of the Break-Up Mechanism for Composite Particle Scattering.
Phys. Rev. C21 (1980) S. 2668-2671.
2o.8o.o

IKP-100880
Baur, G.; Shyam, R.; Rösel, F.; Trautmann, D.
The Importance of the Inelastic Break-Up Mechanism for Nucleus-Nucleus Scattering.
Proc. Int. Conf. Nuclear Physics, Berkeley, USA, 24.-30.8.1980, Report LBL-11118 (1980) S. 490.
2o.8o.o

IKP-100980
Baur, G.; Rösel, F.; Trautmann, D.; Shyam, R.
A Survey of Direct Reaction Mechanisms for Continuous Particle Spectra in Light Ion Induced Reactions.
Proc. Int. Symp. on Continuum Spectra of Heavy Ion Reactions, San Antonio, Texas, USA, 3.-5.12.1979 (Harwood Academic Publ., 1980) Vol. 2, S. 131-147, Hrsg.: T. Tamura, J.B. Natowitz, D.H. Youngblood.
2o.8o.o

IKP-101080
Baur, G; Rösel, F.; Trautmann, D.; Shyam, R.
The Contribution of Peripneral Fragmentation Processes to Continuous Particle Spectra in Nucleus-Nucleus Collisions.
Lecture Notes in Physics, Vol. 117 (Springer-Verlag, 1980) S. 268-280, Hrsg.: W. von Oertzen.
2o.8o.o

IKP-101180
Baur, G.
Inclusive Particle Spectra and Fragmentation in Nuclear Reactions.
Proc. 2nd. Conf. on Nuclear Reaction Mechanisms, Varenna, Italien, 18.-21.6.1979 (Cooperativa Libraria Universitaria Editrice Democratica, Milano, 1980) S. 247-266.
2o.8o.o

IKP-101280
Bechstedt, U.; Machner, H.; Baur, G.; Shyam, R.; Alderliesten, C.; Bousshid, O.; Djaloeis, A.; Jahn, P.; Mayer-Böricke, C.; Rösel, F.; Trautmann, D.
Experimental and Theoretical Study of Continuous Proton Spectra from High-Energy Deuteron Induced Reactions.
Nucl. Phys. A343 (1980) S. 221-233.
2o.6o.o + 2o.8o.o

IKP-101380
Bernas, M.; Pougheon, F.; Roy-Stephan, M.; Berg, G.P.A.; Berthier, B.; Le Fèvre, J.P.; Wildenthal, B.H.
$^{24}Mg(^{18}O,^{16}O)^{26}Mg$ Reaction at E_{18O} = 50 MeV Including Scattering in Entrance and Exit Channel.
Phys. Rev. C22 (1980) S. 1872-1884.
2o.o6.o

IKP-101480
Beyer; Birnbreier; Cordes; Falkenberg; Frühauf; Hußmann; Kehl; Kersten; Lüke; Mühle; Müller; Renner; Schubert; Stein, H.J.; Wallner.
Gebrauchstauglichkeit von Solarkollektoren, B. Langzeittest von Solarkollektoren.
Hrsg.: Bundesverband Solarenergie, Essen, Januar 1979, 6 Seiten.
2o.6o.1

IKP-101580
Björnstad, T.; Blomqvist, J.; Ewan, G.T.; Hansen, P.G.; Jonson, B.; Kawade, K.; Kerek, A.; Mattson, S.; Sistemich, K.
Neutron Particle-Hole States in ^{132}Sn.
Proc. Int. Conf. Nuclear Physics, Berkeley, USA, 24.-30.8.1980, Report LBL-11118 (1980) S. 169.
2o.65.o

IKP-101680
Björnstad, T.; DeGeer, L.-E.; Ewan, G.T.; Hansen, P.G.; Jonson, B.; Kawade, K.; Kerek, A.; Lauppe, W.-D.; Lawin, H.; Mattson, S.; Sistemich, K.
Structure of the Levels in the Doubly Magic Nucleus $^{132}_{50}Sn_{82}$.
Phys. Lett. 91B (1980) S. 35-38
2o.65.o

IKP-101780
Bochev, B.; Lieder, R.M.; Didelez, J.P., Kutsarova, T.; Beuscher, H.; Haenni, D.R.; Morek, T.; Müller-Veggian, M.; Neskakis, A.; Mayer-Böricke, C.
Measurement of Particle Spectra of α Induced Non-Equilibrium Reactions for $^{206-210}Po$.
Proc. Int. Conf. Nuclear Physics, Berkeley, USA, 24.-30.8.1980, Report LBL-11118 (1980) S. 452
2o.1o.o

IKP-101880
Bocquet, J.P.; Schussler, F.; Monnand, E.; Sistemich, K.
Dependence of Isomeric State Yields on the Kinetic Energy of Fission Fragments from ^{236}U.
Physics and Chemistry of Fission (IAEA Vienna, 1980) S. 179-191.
2o.65.o

IKP-101980
Bogdan, D.; Faessler, A.; Schmid, K.W.; Vertes, P.
Is Weak Magnetism Important for the Nuclear Beta Decay of ^{186}Re and ^{188}Re?
J. Phys. G6 (1980) S. 993-1016.
2o.8o.o

IKP-102080
Borchert, G.L.; Desclaux, J.P.; Hansen, P.G.; Jonson, B.; Ravn, H.L.
Comparison of the K X-Ray Energy Ratios of High Z and Low Z Elements with Relativistic SCF DF Calculations.
Proc. Int. Conf. on Atomic Masses and Fundamental Constants 6 (1980), East Lansing, USA, 17.-21.9.1979 (Plenum Publ. Corp., New York, 1980) S. 189-195, Hrsg.: Jerry A. Nolen, Jr., and Walter Benenson
2o.1o.o

IKP-102180
Borchert, G.L.; Hansen, P.G.; Jonson, B.; Ravn, H.L.; Schult, O.W.B.
Dynamic K X-Ray Energy Shifts.
Proc. XVII Int. Winter Meeting on Nuclear Physics, Bormio, Italien, 21.-26.1.1980, S. 579-584, Hrsg.: University of Milano, 1980.
2o.1o.o

IKP-102280
Bousshid, O.; Machner, H.; Alderliesten, C.; Bechstedt, U.; Djaloeis, A.; Jahn, P.; Mayer-Böricke, C.
Gross Structure in Triton Spectra from ^{3}He-Induced Reactions.
Phys. Rev. Lett. 45 (1980) S. 980-982.
2o.o6.o

IKP-102380
Cheifetz, E.; Selič, H.A.; Wolf, A.; Chechik, R.; Wilhelmy, J.B.
Even-Even Neutron-Rich Isotopes.
Inst. Phys. Conf. Ser. No. 51, Chapter 4 (1980) S. 193-207.
2o.65.o

IKP-102480
Daly, P.J.; Kleinheinz, P.; Broda, R.; Lunardi, S.; Backe, H.; Blomqvist, J.
Proton $h_{11/2}$ and Octupole Excitations in $^{149}_{66}Dy_{82}$ and $^{149}_{66}Dy_{83}$.
Z. Physik A298 (1980) S. 173-185.
2o.1o.o

IKP-102580
Daly, P.J.; Kleinheinz, P.; Broda, R.; Lunardi, S.; Backe, H.; Blomqvist, J.
How Particle-Octupole Exchange Coupling Affects the Yrast Lines of Dysprosium Nuclei.
Proc. Int. Conf. on Nuclear Behaviour at High Angular Momentum, Strasbourg, Frankreich, 22.-24.4.1980, Hrsg.; Centre de Recherches Nucléaires de Strasbourg, S. 61-62.
2o.1o.o

IKP-102680
Daly, P.J.; Kleinheinz, P.; Broda, R.; Lunardi, S.; Backe, H.; Blomqvist, J.
Twoparticle-Phonon Exchange Coupling in Yrast States of Dysprosium Nuclei.
Proc. Int. Conf. Nuclear Physics, Berkeley, USA, 24.-30.8.1980, Report LBL-11118 (1980) S. 361.
2o.1o.o

IKP-102780
Didelez, J.-P.; Lieder, R.M.; Beuscher, H.; Haenni, D. R.; Machner, H.; Müller-Veggian, M.; Mayer-Böricke, C.
Experimental Study of Excitation Functions and Isomer Ratios for ^{211,212}Po.
Nucl. Phys. A341 (1980) S. 421-439.
2o.o6.o + 2o.1o.o

IKP-102880
Djaloeis, A.; Gopal, S.
Elastic Scattering at E_τ = 130 MeV: A Model-Independent Analysis.
Proc. Int. Conf. Nuclear Physics, Berkeley, USA, 24.-30.8.1980, Report LBL-11118 (1980) S. 131.
2o.o6.o

IKP-102980
Djaloeis, A.; Alderliesten, C.; Bojowald, J.; Mayer-Böricke, C.; Oelert, W.; Turek, P.
Study of Some Selected Transitions in the ^{58}Ni$(\tau,\alpha)^{57}$Ni Reaction at E_α = 130 MeV.
Nucl. Phys. A342 (1980) S. 252-260.
2o.o6.o

IKP-103080
Ercan, A.; Broda, R.; Piiparinen, M.; Nagai, Y.; Pengo, R.; Kleinheinz, P.
The 235 µs 9^+ Isomer in $^{146}_{63}Eu_{83}$.
Z. Physik A295 (1980) S. 197-198.
2o.1o.o

IKP-103180
Faber, M.E.; Faessler, A.; Ploszajczak, M.
The Fission Barrier of Nuclei at Very High Angular Momenta.
Proc. Int. Symp. on Physics and Chemistry of Fission, Jülich, 14.-18.5.1979, Vol. I (IAEA Vienna, 1980) S. 361-371.
2o.8o.o

IKP-103280
Faessler, A.
Collective Description of Deformed and Transitional Nuclei.
Lecture Notes in Physics, Vol. 119 (Springer-Verlag, Berlin, 1980) S. 97-136, Hrsg.: G.F. Bertsch, D. Kurath.
2o.8o.o

IKP-103380
Faessler, A.
Description of Transitional Nuclei.
Inst. Phys. Conf. Ser. No. 51, Chapter 4 (The Institute of Physics, Bristol und London, 1980) S. 244-257, Hrsg.: Till von Egidy.
2o.8o.o

IKP-103480
Faessler, A.; Izumoto, T.; Krewald, S.; Sartor, R.
Brueckner Approximation to the Heavy Ion Optical Potential.
Proc. Int. Workshop VIII on Gross Properties of Nuclei and Nuclear Excitations, Hirschegg, 14.-19.1.1980 (TH Darmstadt, 1980) S. 80-83, Hrsg.: H. Feldmeier.
2o.8o.o

IKP-103580
Faessler, A.; Ploszajczak, M.; Schmid, K.W.
Description of High Spin States.
Prog. in Particle and Nuclear Physics 5 (1980) S. 79-142.
2o.8o.o

IKP-103680
Faessler, A.
Description of Multipole Resonances.
Anales de Física 76 (1980) S. 47-63.
2o.8o.o

IKP-103780
Faessler, A.; Ploszajczak, M.
Description of High-Spin Isomers in the N=82 Region.
Z. Physik A296 (1980) S. 237-250.
2o.8o.o

IKP-103880
Faessler, A.; Müther, H.; Shimizu, K.; Wadia, W.
$\Delta(3,3)$ Excitations and Effective Three-Nucleon Forces in Finite Nuclei.
Nucl. Phys. A333 (1980) S. 428-442.
2o.8o.o

IKP-103980
Faessler, A.; Kuo, T.T.S.; Müther, H.
Variational Definition of the Single-Particle Potential in the Brueckner-Hartree-Fock Approach.
Z. Physik A294 (1980) S. 95-100.
2o.8o.o

IKP-104080
Faessler, A.
Do we Understand the Spectra in Transitional Even Mass and Odd-Odd Mass Nuclei?
Future Directions in Studies of Nuclei Far From Stability (North-Holland Publ. Comp., 1980) S. 1-13, Hrsg.: J.H. Hamilton et al.
2o.8o.o

IKP-104180
Fuchs, H.; Nolen, J.A.; Wagner, G.J.; Lenske, H.; Baur, G.
Experimental and Theoretical Study of Line Shapes in ^{13}C(α,α') Inelastic Scattering to Resonant States.
Nucl. Phys. A343 (1980) S. 133-147.
2o.8o.o

IKP-104280
Goeke, K.; Reinhard, P.-G.; Cusson, R.Y.
Spreading Widths in Strongly Damped Heavy Ion Collisions.
Proc. Int. Workshop VIII on Gross Properties of Nuclei and Nuclear Excitations, Hirschegg, 14.-19.1.1980 (TH Darmstadt 1980) S. 84-86, Hrsg.: H. Feldmeier.
2o.8o.o

IKP-104380
Goeke, K.; Maruhn, J.A.; Reinhard, P.-G.
Adiabatic Time-Dependent Hartree-Fock Calculations for the Optimal Path, the Potential and the Mass Parameter for Large Amplitude Collective Motion.
Proc. Int. Conf. Nuclear Physics, Berkeley, USA, 25.-30.8.1980, Report LBL-11118 (1980) S. 344.
2o.8o.o

IKP-104480
Goeke, K.; Castel, B.; Reinhard, P.-G.
Isovector Giant Monopole Resonances: A Sum Rule Approach.
Proc. Int. Conf. Nuclear Physics, Berkeley, USA, 24.-30.8.1980, Report LBL-11118 (1980) S. 178.
2o.8o.o

IKP-104580
Goeke, K.; Reinhard, P.-G.
The Generator-Coordinate-Method with Conjugate Parameters and the Unification of Microscopic Theories for Large Amplitude Collective Motion.
Ann. Phys. 124 (1980) S. 249-289.
2o.8o.o

IKP-104680
Goeke, K.; Castel, B.; Reinhard, P.-G.
Isovector Giant Monopole Resonances: A Sum Rule Approach.
Nucl. Phys. A339 (1980) S. 377-389.
2o.8o.o

IKP-104780
Gopal, S.; Djaloeis, A.; Boussnid, O.; Bojowald, J.; Mayer-Böricke, C.; Oelert, W.; Puttaswamy, N.G.; Turek, P.
Observation of a Broad Structure in t-Spectra from (τ,t) Reaction at E_{inc} = 130 MeV.
Proc. Int. Conf. Nuclear Physics, Berkeley, USA, 24.-30.8.1980, Report LBL-11118 (1980) S. 253.
2o.o6.o

IKP-104880
Grüter, J.W.
The KFA Instrument Package.
Validation of the Guidelines for Portable Meteorological Instrument Packages, IEA Interim Technical Report Doc. No. USA DOE IER 0083 (U.S. Dept. of Energy, Washington, October 1980) S. 5-8.
2o.6o.1

IKP-104980
Harakeh, M.H.; Morsch, H.P.; v.d. Weg, K.; v.d. Woude, A.; Bertrand, F.E.
Isoscalar Giant Resonances in ^{232}Th.
Phys. Rev. C21 (1980) S. 768-771.
2o.o6.o

IKP-105080
de Haro, R.; Krewald, S.; Speth, J.
Giant Resonances in Heavy Nuclei with the Fourier-Bessel RPA.
Proc. Int. Conf. Nuclear Physics, Berkeley, USA, 24.-30.8.1980, Report LBL-11118 (1980) S. 189.
2o.8o.o

IKP-105180
Helmbold, M.; Allelein, H.J.; Koch, H.R.
The Combination of Laser Micro-Boring and High Resolution α-Spectroscopy for the Analysis of α-Emitting Isotopes in Irradiated High-Temperatur-Reactor Fuel.
Nucl. Instr. and Meth. 169 (1980) S. 235-238.
2o.1o.o

IKP-105280
Helmbold, M.; Allelein, H.J.; Koch, H.R.
Neue Methode zur Analyse von α-Strahlen im Brennstoff von Hochtemperatur-Gasreaktoren (Titel aus dem Russischen übersetzt).
Atomnaia Technika sa Rubejon 9 (1980) S. 32-35.
2o.1o.o

IKP-105380
Izumoto, T.; Krewald, S.; Faessler, A.
Microscopic Derivation of a Complex Heavy Ion Potential.
Phys. Lett. 95B (1980) S. 16-18.
2o.8o.o

IKP-105480
Izumoto, T.; Krewald, S.; Faessler, A.
Complex Heavy Ion Potential from Brueckner Theory.
Proc. Int. Conf. Nuclear Physics, Berkeley, USA, 24.-30.8.1980, Report LBL-11118 (1980) S. 502.
2o.8o.o

IKP-105580
Izumoto, T.; Krewald, S.; Faessler, A.
Nuclear Matter Approach to the Heavy-Ion Optical Potential.
Nucl. Phys. A341 (1980) S. 319-344.
2o.8o.o

IKP-105680
Izumoto, T.; Krewald, S.; Faessler, A.
Microscopic Derivation of a Complex Heavy Ion Potential.
Proc. Int. Workshop VIII on Gross Properties of Nuclei and Nuclear Excitations, Hirschegg, 14.-19.1.1980 (TH Darmstadt 1980) S. 192-193, Hrsg.: H. Feldmeier.
2o.8o.o

IKP-105780
Julin, R.; Kantele, K.; Luontama, M.; Passoja, A.; Kleinheinz, P.; Blomqvist, J.
Electromagnetic Decay of the 0_2^+ State in the Doubly Magic Nucleus $^{146}_{64}Gd_{82}$.
Proc. Int. Conf. Nuclear Physics, Berkeley, USA, 24.-30.8.1980, Report LBL-11118 (1980) S. 744.
2o.1o.o

IKP-105880
Julin, R.; Kantele, K.; Luontama, M.; Passoja, A.; Kleinheinz, P.; Blomqvist, J.
Electromagnetic Decay of the 0_2^+ State in the Doubly Magic Nucleus $^{146}_{64}Gd_{82}$.
Phys. Lett. 94B (1980) S. 123-126.
2o.1o.o

IKP-105980
Kleinrahm, A.; Günther, C.; Hübel, H.; Thirumala Rao, B. V.; Broda, R.
Magnetic Moments of the 10^- Isomeric States in ^{202}Bi and ^{204}Bi.
Nucl. Phys. A346 (1980) S. 324-328.
2o.1o.o

IKP-106080
Koch, H.R.; Kucheida, D.
Fission Products from the ^{197}Au(d,f) Reaction.
Z. Physik A295 (1980) S. 377-383.
2o.o6.o

IKP-106180
Koch, H.R.; Börner, H.G.; Pinston, J.A.; Davidson, W.F.; Faudou, J.; Roussille, R.; Schult, O.W.B.
The Curved Crystal Gamma Ray Spectrometers "GAMS 1, GAMS 2, GAMS 3" for High Resolution (n,γ) Measurements at the High Flux Reactor in Grenoble.
Nucl. Instr. and Meth. 175 (1980) S. 401-423.
2o.o6.o

IKP-106280
Koch, H.R.; Grüter, J.W.
Short Interval Meteorological Data for Computational Methods.
Final research report on the contributions to the actions 3.2 and 3.3 of project F, part of the Solar Energy Programme of the Commission of the European Communities 1975-1979, November 1980.
20.60.1

IKP-106380
Köhler, M.; Müller, K.D.; Stoff, H.; Teske, M.; Berg, G.P.A.; Hardt, A.; Martin, S.; Mayer-Böricke, C.; Meißburger, J.
A Two-Dimensional Position Sensitive Charged-Particle Detector for the Magnetic Spectrograph "BIG KARL" of the Jülich cyclotron "JULIC".
Nucl. Instr. and Meth. 175 (1980) S. 357-362.
20.o6.o + 52.95.o

IKP-106480
Krewald, S.; Speth, J.
Microscopic Structure of the Magnetic High Spin States in ^{208}Pb.
Phys. Rev. Lett. 45 (1980) S. 417-419.
2o.8o.o

IKP-106580
Krewald, S.; Negele, J.W.
On the Creation and Observation of a Pion Condensate in High Energy Heavy Ion Collisions.
Proc. Int. Workshop VIII on Gross Properties of Nuclei and Nuclear Excitations, Hirschegg, 14.-19.1.1980 (TH Darmstadt 1980) S. 33-35, Hrsg.: H. Feldmeier.
2o.8o.o

IKP-106680
Krewald, S.; Speth, J.
Magnetic High Spin States in ^{208}Pb.
Proc. Int. Conf. Nuclear Physics, Berkeley, USA, 24.-30. 8.1980, Report LBL-11118 (1980) S. 345.
2o.8o.o

IKP-106780
Krewald, S.; Osterfeld, F.; Speth, J.
Gamow-Teller Strength in ^{208}Bi.
Proc. Int. Conf. Nuclear Physics, Berkeley, USA, 24.-30. 8.1980, Report LBL-11118 (1980) S. 739.
2o.8o.o

IKP-106880
Krewald, S.; Negele, J.W.
Creation and Observation of a Pion Condensate in High-Energy Heavy-Ion Collisions.
Phys. Rev. C21 (1980) S. 2385-2397.
2o.8o.o

IKP-106980
Krmpotić, F.; Osterfeld, F.
A Comment on the Isovector Dipole and Gamow-Teller Transitions in ^{90}Zr.
Phys. Lett. 93B (1980) S. 218-222.
2o.8o.o

IKP-107080
Kuo, T.T.S.; Osterfeld, F.; Lee, S.Y.
A Theory of Energy-Dependent Nuclear Optical Model Potentials.
Phys. Rev. Lett. 45 (1980) S. 786-790.
2o.8o.o

IKP-107180
Kuratsuji, H.; Suzuki, T.
Path Integral in the Representation of SU(2) Coherent States and Classical Dynamics in a Generalized Phase Space.
J. Math. Phys. 21 (1980) S. 472-476.
2o.8o.o

IKP-107280
Kuratsuji, H.; Suzuki, T.
Path Integral Approach to Many-Nucleon Systems and Time-Dependent Hartree-Fock.
Phys. Lett. 92B (1980) S. 19-22.
2o.8o.o

IKP-107380
Lauppe, W.-D.; Sistemich, K.; Lawin, H.; Schult, O.W.B.
The Doubly Magic Nucleus ^{132}Sn.
Inst. Phys. Conf. Ser. No. 51 (1980) S. 282.
2o.65.o

IKP-107480
Lenske, H.; Baur, G.
The Role of the Coulomb Interaction in Isospin Violating Direct Nuclear Reactions.
Nucl. Phys. A344 (1980) S. 151-175.
2o.8o.o

IKP-107580
Lieder, R.M.
Band Structure in Strongly Deformed Nuclei.
Nucl. Phys. A347 (1980) S. 69-97.
2o.1o.o

IKP-107680
Lieder, R.M.; Sletten, G.; Bakander, O.; Bjørnholm, S.; Borggren, J.; Pedersen, J.
Study of Band Crossing in ^{182}Os.
Proc. Int. Conf. on Nuclear Behaviour at High Angular Momentum, Strasbourg, France, 22.-24.4.1980, Hrsg.: Centre de Recherches Nucléaires de Strasbourg, Vol. 1, S. 111.
2o.1o.o

IKP-107780
Lieder, R.M.; Didelez, J.P.; Beuscher, H.; Haenni, D.R.; Machner, H.; Müller-Veggian, M.; Mayer-Böricke, C.
Investigation of the Preequilibrium Reaction Mechanism Through the Study of Isomer Ratios in $^{211,212}Po$.
Proc. Int. Symp. on Continuum Spectra of Heavy Ion Reactions, San Antonio, Texas, USA, 3.-5.12.1979 (Harwood Academic Publ., 1980) Vol. 2, S. 21, Hrsg.: T. Tamura, J.B. Natowitz, D.H. Youngblood,
2o.o6.o + 2o.1o.o

IKP-107880
Li Chu-hsia; Klemt, V.
Dynamical Theory of Vibration.
Proc. Int. Conf. Nuclear Physics, Berkeley, USA, 24.-30. 8.1980, Report LBL-11118 (1980) S. 184.
2o.8o.o

IKP-107980
Lovhoiden, G.; Lien, J.R.; El-Kazzaz, S.; Rekstad, J.; Ellegaard, C.; Bjerregaard, J.H.; Knudsen, P.; Kleinheinz, P.
Studies of Single Neutron Holes in the Transitional Nuclei N = 83-89; The $^{150,148}Nd(d,t)$ and $^{150,148,146}Nd$ ($^{3}He,\alpha$) Pick-Up Reactions.
Nucl. Phys. A339 (1980) S. 477-502.
2o.o6.o

IKP-108080
Machner, H.
Testing the Exciton Model with Light Ions, Heavy Ions and Pions.
Proc. Int. Symp. on Continuum Spectra of Heavy Ion Reactions, San Antonio, Texas, USA, 3.-5.12.1979 (Harwood Academic Publ., 1980) Vol. 2, S. 20, Hrsg.: T. Tamura, J.B. Natowitz, D.H. Youngblood.
2o.o6.o

IKP-108180
Machner, H.
Composite Particle Emission from $^{65}Zn^{*}$.
Phys. Rev. C21 (1980) S. 2695-2698.
2o.o6.o

IKP-108280
Machner, H.; Bechstedt, U.; Djaloeis, A.; Jahn, P.; Mayer-Böricke, C.
Composite Particle Emission and Quantum Statistical Theories of Nuclear Reactions.
Proc. Int. Conf. Nuclear Physics, Berkeley, USA, 24.-30. 8.1980, Report LBL-11118 (1980) S. 403.
2o.o6.o

IKP-108380
Machner, H.
Investigations of ($\alpha,\alpha'x$) Reactions up to 40 MeV/A Bombarding Energy.
Proc. Int. Workshop VIII on Gross Properties of Nuclei and Nuclear Excitations, Hirschegg, 14.-19.1.1980 (TH Darmstadt 1980) S. 142, Hrsg.: H. Feldmeier).
2o.o6.o

IKP-108480
Madsen, V.A.; Osterfeld, F.; Wambach, J.
New Aspects of the DWBA for Giant Resonances.
Proc. Giant Multipole Resonance Topical Conf., Oak Ridge, Tenn., USA, 15.-17.10.1979 (Harwood Academic Publ., 1980) Vol. 1, S. 93-111, Hrsg.: F.E. Bertrand.
2o.8o.o

IKP-108580
Martin, S.; Berg, G.; Hardt, A.; Hürlimann, W.; Köhler, M.; Meißburger, J.; Sagefka, T.; Schult, O.W.B.
First Experience with the Magnet Spectrometer "BIG KARL".
Proc. Daresbury Study Weekend, 10.-11.3.1979 (Daresbury Laboratory, 1980) S. 38-41, Hrsg.: N.E. Sanderson.
2o.o6.o + 52.95.o

IKP-108680
Maßmeyer, K.
Einflüsse meteorologischer Parameter auf die Stillstandtemperatur von thermischen Flachkollektoren.
Berichte der Kernforschungsanlage Jülich, Jül-Spez 90, September 1980.
2o.6o.1

IKP-108780
Maßmeyer, K.; Talarek, H.D.; Grüter, J.W.
Determination and Variation of the Maximum Stagnation Temperature of a Flat-Plate Solar Collector.
Tagungsbericht des 3. Int. Sonnenforums (DGS-Sonnenenergie Verlags GmbH, München, 1980) S. 746.
2o.6o.1

IKP-108880
Morsch, H.P.; Rogge, M.; Turek, P.; Mayer-Böricke, C.
New Giant Resonances in 172 MeV α Scattering from ^{208}Pb.
Proc. Int. Conf. Nuclear Physics, Berkeley, USA, 24.-30. 8.1980, Report LBL-11118 (1980) S. 255.
2o.o6.o

IKP-108980
Morsch, H.P.
New Giant Resonances in Heavy Nuclei Excited in Higher Energy α and d Scattering.
Proc. 1980 RCNP Symp. on Highly Excited States in Nuclear Reactions, Osaka, Japan, 12.-16.5.1980 (Research Center for Nuclear Physics, Osaka, Japan) S. 168-183, Hrsg.: H. Ikegami und M. Muraoka.
2o.o6.o

IKP-109080
Morsch, H.P.; Sükösd, C.; Rogge, M.; Turek, P.; Machner, H.; Mayer-Böricke, C.
Giant Monopole and Quadrupole Resonances and Other Multipole Structures in ^{208}Pb Excited in 43 MeV/Nucleon α-Particle and Deuteron Scattering.
Phys. Rev. C22 (1980) S. 489-500.
2o.o6.o

IKP-109180
Morsch, H.P.; Rogge, M.; Turek, P.; Machner, H.; Sükösd, C.; Mayer-Böricke, C.
Experimental Investigation of the Giant Monopole Resonances in Heavy Nuclei.
Proc. Giant Multipole Resonance Topical Conf., Oak Ridge, USA, 15.-17.10.1979 (Harwood Academic Publishers, 1980) Vol. 1, S. 459, Hrsg.; F.E. Bertrand.
2o.o6.o

IKP-109280
Morsch, H.P.; Decowski, P.
Excitation of the Giant Dipole Resonance in the Scattering of Isoscalar Projectiles.
Phys. Lett. 95B (1980) S. 160-162.
2o.o6.o

IKP-109380
Morsch, H.P.; Rogge, M.; Turek, P.; Mayer-Böricke, C.
New Giant Resonances in 172-MeV α Scattering from ^{208}Pb.
Phys. Rev. Lett. 45 (1980) S. 337-340.
2o.o6.o

IKP-109480
Müller, G.; Berg, G.P.A.; Hardt, A.; Kelleter, H.J.; Martin, S.A.; Meißburger, J.; Retz, A.
Aufbau eines Plastikszintillationszählers für den Magnetspektrographen "BIG KARL" am Jülicher Zyklotron "JULIC".
Berichte der Kernforschungsanlage Jülich, Jül-Spez 84, Juli 1980.
2o.3o.o

IKP-109580
Müller-Veggian, M.; Beuscher, H.; Haenni, D.R.; Lieder, R.M.; Neskakis, A.; Mayer-Böricke, C.
Investigation of High-Spin States in ^{138,139}Nd.
Nucl. Phys. A344 (1980) S. 89-108.
2o.1o.o

IKP-109680
MUther, H.; Faessler, A.; Anastasio, M.R.; Holinde, K.; Machleidt, R.
Noniterative 2π-Exchange in the Nuclear Medium.
Phys. Rev. C22 (1980) S. 1744-1754.
2o.8o.o

IKP-109780
Müther, H.; Waghmare, Y.R.; Faessler, A.
Brueckner Random Phase Approximation, a Microscopic Description of Particle-Hole States.
Z. Physik A294 (1980) S. 87-94.
2o.8o.o

IKP-109880
Nagai, Y.; Styczen, J.; Piiparinen, M.; Kleinheinz, P.
The X- (or Δ-) Transition in ^{152}Dy.
Proc. Int. Conf. on Nuclear Behaviour at High Angular Momentum, Strasbourg, France, 22.-24.4.1980, Hrsg.: Centre de Recherches Nucléaires de Strasbourg, S. 71-72.
2o.1o.o

IKP-109980
Nagai, Y.; Styczen, J.; Piiparinen, M.; Kleinheinz, P.
The X- (or Δ-) Transition in ^{152}Dy.
Z. Physik A296 (1980) S. 91-92.
2o.1o.o

IKP-110080
Nagai, Y.; Styczen, J.; Piiparinen, M.; Kleinheinz, P.
Yrast Isomers in ^{152}Dy.
Proc. Int. Conf. Nuclear Physics, Berkeley, USA, 24.-30. 8.1980, Report LBL-11118 (1980) S. 304.
2o.1o.o

IKP-110180
Oelert, W.; Chung, W.; Djaloeis, A.; Mayer-Böricke, C.; Turek, P.
(d,^{6}Li) Reaction on ^{24}Mg and ^{26}Mg at E_d = 80 MeV.
Phys. Rev. C22 (1980) S. 408-421.
2o.o6.o

IKP-110280
Oelert, W.; Chung, W.; Djaloeis, A.; Mayer-Böricke, C.; Turek, P.
Few-Nucleon Transfer Reactions on Light Nuclei.
IOP Conference, Trends in Nuclear Structure Physics, Manchester, England, 16.-18.4.1980 (Schuster Laboratory, Manchester, 1980) S. 90, Hrsg.: A.R. Barnett und W. Gelletly.
2o.o6.o

IKP-110380
Oelert, W.; Chung, W.; Betigeri, M.; Djaloeis, A.; Mayer-Böricke, C.; Turek, P.
Investigation of Alpha-Transfer Reactions on Light Nuclei.
Proc. Int.Conf. on Nuclear Reaction Mechanisms, Varenna, Italy, 18.-21.6.1979 (Cooperativa Libraria Universitaria Editrice Democratica, Milano, 1980) S. 389-399.
2o.o6.o

IKP-110480
Oelert, W.; Chung, W.; Djaloeis, A.; Mayer-Böricke, C.; Turek, P.
Four-Nucleon Transfer Reactions on sd-Shell Nuclei.
Proc. Int. Conf. Nuclear Physics, Berkeley, USA, 24.-30. 8.1980, Report LBL-11118 (1980) S. 906.
2o.o6.o

IKP-110580
Osterfeld, F.
Microscopic Theory of Giant Multipole Resonances.
Proc. 1980 RCNP Int. Symp. on Highly Excited States in Nuclear Reactions, Osaka, Japan, 12.-16.5.1980 (Research Center for Nuclear Physics, Osaka, Japan) S. 320-343, Hrsg.: H. Ikegami und M. Muraoka.
2o.8o.o

IKP-110680
Osterfeld, F.; Wambach, J.; Lenske, H.; Speth, J.
The Hadronic Transition Operator for Inelastic Proton Scattering.
Proc. Giant Multipole Resonance Topical Conf., Oak Ridge, USA, 15.-17.10.79 (Harwood Academic Publ., 1980) Vol. 1, S. 460, Hrsg.: F.E. Bertrand.
2o.8o.o

IKP-110780
Osterfeld, F.; Wambach, J.; Madsen, V.A.
The Imaginary Part of the Nucleon-Nucleus Optical Potential.
Proc. Int. Conf. Nuclear Physics, Berkeley, USA, 24.-30. 8.1980, Report LBL-11118 (1980) S. 884.
2o.8o.o

IKP-110880
Paetz gen. Schieck, H.; Latzel, G.; Lenssen, W.; Berg, G.P.A.
Study of $T^{>}$ Fluctuations in $^{94,96}Zr(p,p')$ in the Energy Region from 11.2 to 13.4 MeV.
Z. Physik A293 (1979) S. 253-260.
2o.o6.o

IKP-110980
Paič, G.; Antolkovič, B.; Djaloeis, A.; Bojowald, J.; Mayer-Böricke, C.
Continuous Spectra of Protons and Deuterons from the α+α Interaction in the Incident Energy Interval 110-172 MeV.
Proc. 9th Int. Conf. on the Few Body Problem, Eugene,Oregon, USA, 1980, Vol. I, S. VI-21.
2o.o6.o

IKP-111080
Piiparinen, M.; Nagai, Y.; Styczen, J.; Kleinheinz, P.
High Spin Level Structure of ^{147}Sm.
Proc. Int. Conf. on Nuclear Behaviour at High Angular Momentum, Strasbourg, France, 22.-24.4.1980, Hrsg.: Centre de Recherches Nucléaires de Strasbourg, S. 53-54.
2o.1o.o

IKP-111180
Piiparinen, M.; Pengo, R.; Nagai, Y.; Kleinheinz, P.; Roy, N.; Carlen, L.; Ryde, H.; Lindblad, Th.; Johnson, A.; Hjorth, S.A.; Hammarén, E.
High Spin Shell Model Excitations in ^{149}Gd.
Proc. Int. Conf. on Nuclear Behaviour at High Angular Momentum, Strasbourg, France, 22.-24.4.1980, Hrsg.: Centre de Recherches Nucléaires de Strasbourg, S. 63-64.
2o.1o.o

IKP-111280
Piiparinen, M.; Kortelahti, M.; Pakkanen, A.; Komppa, T.; Komu, R.
Medium Spin States in the N = 80 Nuclei ^{139}Pr and ^{141}Pm.
Nucl. Phys. A342 (1980) S. 53-70.
2o.1o.o

IKP-111380
Płoszajczak, M.; Faber, M.E.
Competition between Fission and Neutron Emission of ^{210}Po at High Spins and Excitation Energies.
Proc. Int. Conf. on Nuclear Behaviour at High Angular Momentum, Strasbourg, France, 22.-24.4.1980, Hrsg.: Centre de Recherches Nucléaires de Strasbourg, S. 143-144.
2o.8o.o

IKP-111480
Posorski, R.
Vergleich zwischen berechneter und gemessener Nutzenergieabgabe eines Flachkollektors bei typischen Witterungen.
Berichte der Kernforschungsanlage Jülich, Jül-Spez 89, September 1980.
2o.6o.1

IKP-111580
Posorski, R.; Talarek, H.D.
Investigations on All-Day Collector Performance.
Tagungsbericht des 3. Int. Sonnenforums (DGS-Sonnenenergie Verlags GmbH, München, 1980) S. 744.
2o.6o.1

IKP-111680
Pushpalatha, B.R.; Puttaswamy, N.G.
A Function Generator Using Integrated Circuits for Mössbauer Effect Work.
Indian J. Pure & Appl. Phys. 18 (1980) S. 298-299.
2o.o6.o

IKP-111780
Reinhard, P.-G.; Maruhn, J.; Goeke, K.
Adiabatic Time-Dependent Hartree-Fock Calculations of the Optimal Path, the Potential, and the Mass Parameter for Large-Amplitude Collective Motion.
Phys. Rev. Lett. 44 (1980) S. 1740-1743.
2o.8o.o

IKP-111880
Reinhard, P.-G.; Goeke, K.
Quantum Corrections to Potential Energy Surfaces and their Influence on Barriers.
Physics and Chemistry of Fission, Vol. II (IAEA Wien, 1980) S. 399-410.
2o.8o.o

IKP-111980
Reinhard, P.-G.; Goeke, K.; Cusson, R.Y.
A Time Dependent RPA-Theory for Heavy Ion Reactions.
Z. Physik A295 (1980) S. 45-54.
2o.8o.o

IKP-112080
Rekstad, J.; Lovhoiden, G.; Lien, J.; El Kazzaz, S.; Ellegaard, C.; Bjerregaard, J.; Knudsen, P.; Kleinheinz, P.
Studies of Single Neutron Holes in the Transitional Nuclei N = 83-89: The $^{148,150,152}Sm(^{3}He,\alpha)$ Pick-Up Reactions.
Nucl. Phys. A348 (1980) S. 93-108.
2o.o6.o

IKP-112180
Ringel, H.; Grüter, J.W.; Rongen, F.
Data Acquisition at Remote Solar Systems via Telecommunication.
Tagungsbericht des 3. Int. Sonnenforums (DGS-Sonnenenergie Verlags GmbH, München, 1980) S. 292.
2o.6o.1 + 52.2o.o

IKP-112280
Rozanska, M.; Blum, W.; Dietl, H.; Grayer, G.; Lorenz, E.; Zütjens, G.; Männer, W.; Meißburger, J.; Richter, R.; Stierlin, U.; Chaband, V.; Hyams, B.; Rybicki, K.; Weilhammer, P.
A Partial Wave Analysis of the $\bar{p}p$-System Produced at Low Four-Momentum Transfer in the Reaction $\pi p \to \bar{p}pn$ at 18 GeV.
Nucl. Phys. B162 (1980) S. 505
2o.o6.o

IKP-112380
Sack, B.; Schröer, R.; Stein, H.J.
Ein Kollektorprüfstand zur vergleichenden Untersuchung von Sonnenkollektoren - Stand Februar 1980.
Statusbericht Sonnenenergie (VDI-Verlag GmbH, Düsseldorf, 1980) ISBN 3-18-419067-6, Bd. 1, S. 193-202.
2o.6o.1

IKP-112480
Selič, H.A.; Cheifetz, E.; Wolf, A.; Wilhelmy, J.B.
Neutron-Rich Fragments from Spontaneous Fission of ^{254}Cf.
Inst. Phys. Conf. Ser. No. 51, Chapter 5 (The Institute of Physics, Bristol und London 1980) S. 316-318, Hrsg.: Till von Egidy.
2o.65.o

IKP-112580
Shimizu, K.; Faessler, A.; Müther, H.
The Pionic Disintegration of the Deuteron and the Absorptive Pion-Nucleus Optical Potential.
Nucl. Phys. A343 (1980) S. 468-492.
2o.8o.o

IKP-112680
Shimizu, K.; Faessler, A.
The Absorptive Pion Nucleus Optical Potential.
Nucl. Phys. A333 (1980) S. 495-513.
2o.8o.o

IKP-112780
Shivaramu; Gopal, S.; Sanjeevaiah, B.
Incoherent Scattering of 279, 322, 662 and 1115 keV Gamma Rays in Cu, Sn and Pb.
J. Phys. B. Atom. Molec. Phys. 13 (1980) S. 273-282.
2o.o6.o

IKP-112880
Shyam, R.; Baur, G.; Rösel, F.; Trautmann, D.
Elastic and Inelastic Break-Up of the ^{3}He Particle.
Phys. Rev. C22 (1980) S. 1401-1405.
2o.8o.o

IKP-112980
Sistemich, K.
Magic and Doubly Magic Nuclei (and the A = 129, 131, 133 Chains).
Inst. Phys. Conf. Ser. No. 51 (The Institute of Physics, Bristol und London 1980) S. 208-217, Hrsg.: Till von Egidy.
2o.65.o

IKP-113080
Sistemich, K.; Khan, T.A.; Lauppe, W.-D.; Lawin, H.; Sadler, G.; Selič, H.A.; Seyfarth, H.; Kern, B.D.
The Onset of Deformation at A ∿ 100.
Inst. Phys. Conf. Ser. No. 51 (The Institute of Physics, Bristol und London 1980) S. 258-259, Hrsg.: Democritos Tandem Acc. Group.
2o.65.o

IKP-113180
Sommermann, M.; Müther, H.; Tam, K.C.; Kuo, T.T.S.; Faessler, A.
The Effect of Different N-N Interactions on the Convergence Properties of Core Polarization Diagrams.
Proc. Int. Conf. Nuclear Physics, Berkeley, USA, 24.-30. 8.1980, Report LBL-11118 (1980) S. 24.
2o.8o.o

IKP-113280
Speth, J.; Wambach, J.
Electric Giant Multipole Resonances.
Nucl. Phys. A347 (1980) S. 389-403.
2o.8o.o

IKP-113380
Speth, J.; Klemt, V.; Wambach, J.; Brown, G.E.
The Influence of the π- and ρ-Exchange Potential on Magnetic Properties of Nuclei.
Nucl. Phys. A343 (1980) S. 382-416.
2o.8o.o

IKP-113480
Speth, J.
The Microscopic Structure of Giant Resonances.
Proc. Giant Multipole Resonance Topical Conf., Oak Ridge, USA, 15.-17.10.1979 (Harwood Academic Publ., 1980) Vol. 1, S. 33-63, Hrsg.: F.E. Bertrand.
2o.8o.o

IKP-113580
Schmid, K.W.
Theoretical Description of the Giant Multipole Resonances in Light Deformed Nuclei.
Anales de Fisica 76 (1980) S. 63-88.
2o.8o.o

IKP-113680
Schröer, R.; Stein, H.J.; Talarek, H.D.
Use of Collector Test Data - Comparison of NBS-Type and BSE-Type Collector Efficiency Testing.
Proc. 1st Australian-German Workshop on Solar Energy System Design, Düsseldorf, 30.11.-1.12.1978, German Section of ISES, Düsseldorf, 1980, S. 189-203.
2o.6o.1

IKP-113780
Schröer, R.; Stein, H.J.; Talarek, H.D.
Thermal Efficiency Test of Flat-Plate Collectors According to the BSE Procedure.
Tagungsbericht des 3. Int. Sonnenforums (DGS-Sonnenenergie Verlags GmbH, München, 1980) S. 743.
2o.6o.1

IKP-113880
Stein, H.J.; Meliß, M.
Die Bedeutung der Sonnenenergie für die zukünftige Energieversorgung der Bundesrepublik Deutschland.
DIN-Mitt. 59, Nr. 8 (1980) S. 434-440.
2o.6o.1 + 64.2o.1

IKP-113980
Talarek, H.D.
Results and Analysis of IEA Round-Robin Testing.
IEA Technical Report, Document No. III.A.1, Dezember 1979, 121 Seiten.
2o.6o.1

IKP-114080
Talarek, H.D.; Stein, H.J.
Standardized Test Procedures for Solar Collectors - Evaluation, Status and Trends.
Tagungsbericht des 3. Int. Sonnenforums (DGS-Sonnenenergie Verlags GmbH, München, 1980) S. 711-721.
2o.6o.1

IKP-114180
Wambach, J.; Osterfeld, F.; Speth, J.
A Phenomenological Two-Body Interaction to Describe Nuclear Spectra and Inelastic Nucleon-Nucleus Scattering Simultaneously.
Proc. Giant Multipole Resonance Topical Conf., Oak Ridge, USA, 15.-17.10.1979 (Harwood Academic Publ., 1980) Vol. 1, S. 471, Hrsg.: F.E. Bertrand.
2o.8o.o

IKP-114280
Wambach, J.; Klemt, V.; Speth, J.
Magnetic Resonances and the Spin-Dependent Part of the p-h Interaction.
Proc. Giant Multipole Resonance Topical Conf., Oak Ridge, USA, 15.-17.10.1979 (Harwood Academic Publ., 1980) Vol. 1, S. 470, Hrsg.: F.E. Bertrand.
2o.8o.o

IKP-114380
Wambach, J.; Jackson, A.D.; Speth, J.
The Role of the Tensor Force for Isoscalar Collective Spin States.
Nucl. Phys. A348 (1980) S. 221-236.
2o.8o.o

IKP-114480
Wambach, J.; Speth, J.
Influence of a Dynamical Coupling between Single Particle and Collective States on the Density Distribution of the Breathing Mode.
Phys. Lett. 94B (1980) S. 458-462.
2o.8o.o

IKP-114580
Wolf, A.; Battistuzzi, G.; Kawade, K.; Lawin, H.; Sistemich, K.
Magnetic Moment of the First Excited 2^+-State in ^{100}Zr.
Proc. Int. Conf. Nuclear Physics, Berkeley, USA, 24.-30. 8.1980, Report LBL-11118 (1980) S. 89.
2o.65.o

IKP-114680
Yadav, H.L.; Faessler, A.; Toki, H.; Castel, B.
Electromagnetic Transitions in the Pt Nuclei.
Phys. Lett. 89B (1980) S. 307-312.
2o.8o.o

IX. CONFERENCE CONTRIBUTIONS, TALKS

IKP-200180
Aldea, L.; Bhandari, R.K.; Reich, J.; Wucherer, P.
First Design of the External Injection System at JULIC.
17th European Cyclotron Progress Meeting, Karlsruhe, 26.-27.6.1980.
2o.3o.o

IKP-200280
Aldea, L.; Beuscher, H.; Bhandari, R.K.; Mayer-Böricke, C.; Reich, J.; Wucherer, P.
The Project ISIS at JULIC.
17th European Cyclotron Progress Meeting, Karlsruhe, 26.-27.6.1980.
2o.3o.o

IKP-200380
Baur, G.
Breakup Effects in Nucleus-Nucleus Collisions.
University of Surrey, Guildford, England, 7.10.1980.
2o.8o.o

IKP-200480
Baur, G.
Fragmentation Processes in Nucleus-Nucleus Collisions.
IUCF Bloomington, Indiana, USA, 11.9.1980.
2o.8o.o

IKP-200580
Baur, G.
Fragmentation Processes in Nucleus-Nucleus Collisions.
KVI Groningen, Niederlande, 6.5.1980.
2o.8o.o

IKP-200680
Baur, G.
Elastic and Inelastic Breakup Reactions.
Universität Catania, Sizilien, 18.3.1980.
2o.8o.o

IKP-200780
Baur, G.; Shyam, R.; Rösel, P.; Trautmann, D.
The Importance of the Inelastic Breakup Mechanism for Nucleus-Nucleus Scattering.
Postervortrag auf der Int. Conf. Nuclear Physics, Berkeley, USA, 24.-30.8.1980.
2o.8o.o

IKP-200880
Baur, G.
Survey of Fragmentation Processes in Nucleus-Nucleus Collisions.
Daresbury Study Weekend on Topics of Heavy Ion Reactions, Daresbury, England, 4.-5.10.1980.
2o.8o.o

IKP-200980
Berg, G.
BIG KARL - Spectrometer and Experiments.
TRIUMF-Lab., Vancouver, Kanada, 2.9.1980.
2o.o6.o + 2o.3o.o

IKP-201080
Berg, G.
BIG KARL - Spectrometer and Experiments.
Nuclear Physics Lab., Univ. of Washington, Seattle, Wash., USA, 5.9.1980.
2o.o6.o + 2o.3o.o

IKP-201180
Beuscher, H.; Bochev, B.; Haenni, D.R.; Kutsarova, T.; Lieder, R.M.; Machner, H.; Mayer-Böricke, C.; Morek, T.; Müller-Veggian, M.; Neskakis, A.; Didelez, J.P.
Study of Reactions ^{209}Bi(α,charged particle xnγ) at E_α = 45 MeV and 75 MeV.
Frühjahrstagung der DPG, Sektion A: Kernphysik, München, 17.-21.3.1980.
2o.o6.o + 2o.1o.o

IKP-201280
Blomqvist, J.
Ground State Masses of Nuclei above ^{146}Gd Derived an Analysis of Yrast Levels.
Nobel Symposium, Örenäs, Schweden, 23.-27.6.1980.
2o.1o.o

IKP-201380
Borchert, G.L.; Hansen, P.G.; Jonson, B.; Ravn, H.L.; Schult, O.W.B.
Study of Higher Order Effects on the Energies of K X-Ray Transitions.
Int. Conf. on Hyperfine Interactions, Berlin, 21.-25.7.1980.
2o.1o.o

IKP-201480
Borchert, G.L.
Shifts in the K X-Ray Energies and the Role of Atomic and Nuclear Structure.
SCK/CEN, Mol, Belgien, 24.1.1980,
2o.1o.o

IKP-201580
Borchert, G.L.
Study of Higher Order Effects on the Energies of K X-Ray Transitions.
5th Int. Conf. on Hyperfine Interactions, Berlin, 20.-25.7.1980.
2o.1o.o

IKP-201680
Bojowald, J.; Mayer-Böricke, C.; Rogge, M.; Turek, P.
Elastische Deuteronenstreuung im Energiebereich 58-85 MeV.
Frühjahrstagung der DPG, Sektion A: Kernphysik, München, 17.-21.3.1980.
2o.o6.o

IKP-201780
Daly, P.J.; Broda, R.; Kleinheinz, P.; Backe, H.; Richter, L.; Blomqvist, J.
One- and Twoparticle-Phonon Exchange Coupling in Nuclei around ^{146}Gd.
Frühjahrstagung der DPG, Sektion A: Kernphysik, München, 17.-21.3.1980.
2o.1o.o

IKP-201880
Djaloeis, A.; Alderliesten, C.; Bojowald, J.; Mayer-Böricke, C.; Oelert, W.; Turek, P.
Study of Some Selected Transitions in the ^{58}Ni $(\tau,\alpha)^{57}$Ni Reaction at E_τ = 130 MeV.
Frühjahrstagung der DPG, Sektion A: Kernphysik, München, 17.-21.3.1980.
2o.o6.o

IKP-201980
Djaloeis, A.; Gopal, S.
Phenomenological ^{3}He-Optical Potential: Investigation of the Real Part.
Frühjahrstagung der DPG, Sektion A: Kernphysik, München, 17.-21.3.1980.
2o.o6.o

IKP-202080
Ercan, A.; Broda, R.; Piiparinen, M.; Nagai,Y.; Pengo, R.; Kleinheinz, P.
The 9^+ Isomer in $^{146}_{63}Eu_{83}$.
Frühjahrstagung der DPG, Sektion A: Kernphysik, München, 17.-21.3.1980.
2o.1o.o

IKP-202180
Fretwurst, E.; Lindström, G.; Palla, G.; v. Reden, K.F.; Riech, V.; v. Geramb, H.V.; Berg, G.; Hardt, A.; Martin, S.; Meißburger, J.; Oelert, W.; Hürlimann, W.
Protonenstreuung an Palladium-Isotopen mit hoher Energieauflösung.
Frühjahrstagung der DPG, Sektion A: Kernphysik, München, 17.-21.3.1980.
2o.o6.o

IKP-202280
Goeke, K.
Nuclear Large Amplitude Collective Motion.
Universität Coimbra, Portugal, 4.12.1980.
2o.8o.o

IKP-202380
Goeke, K.
Kernbewegungen mit großen Amplituden.
Universität Mainz, 13.2.1980.
2o.8o.o

IKP-202480
Goeke, K.
Isovector Monopole Excitations, a Sum Rule Approach.
Int. Conf. on High Precision Measurements, Bad Honnef, 9.-11.6.1980.
2o.8o.o

IKP-202580
Goeke, K.
The Adiabatic Time Dependent Hartree-Fock Theory.
Universität Trento, Italien, 29.5.1980.
2o.8o.o

IKP-202680
Goeke, K.
Das Schalenmodell des Atomkerns.
Universität Köln, 7.5.1980.
2o.8o.o

IKP-202780
Goeke, K.
Large Amplitude Collective Motion in Nuclei.
CNRS Strasbourg, Frankreich, 25.2.1980.
2o.8o.o

IKP-202880
Goeke, K.
Physikalische Methoden der Archäologie.
Volkshochschule Niederzier, 25.1.1980.
2o.8o.o

IKP-202980
Goeke, K.
Archäologie und Physik.
Volkshochschule Sinnersdorf, 28.1.1980.
2o.8o.o

IKP-203080
Goeke, K.
Kernphysik und Archäologie.
Volkshochschule Eschweiler, 8.5.1980.
2o.8o.o

IKP-203180
Goeke, K.
Kernphysik und Archäologie.
Volkshochschule Inden, 11.9.1980.
2o.8o.o

IKP-203280
Goeke, K.
Umbruch in der Archäologie.
Volkshochschule Düren, 25.11.1980.
2o.8o.o

IKP-203380
Goeke, K.
Archäologie im Wandel: Kernphysikalische Verfahren in der Archäologie.
Süddeutscher Rundfunk, Reihe Forum der Wissenschaft, Juli 1980.
2o.8o.o

IKP-203480
Goeke, K.
Archäologie im Umbruch: Physikalische Methoden in der Archäologie.
Rundfunksendung der Rätoromanischen Schweiz, Zürich, 14.7.1980.
2o.8o.o

IKP-203580
Goeke, K.
Spreading Widths in Strongly Dampes Heavy Ion Collisions.
Int. Workshop VIII on Gross Properties of Nuclei and Nuclear Excitations, Hirschegg, 14.-19.1.80.
2o.8o.o

IKP-203680
Goeke, K.
Theorien kollektiver Bewegungen großer Amplituden: Übersicht, Vergleich und Diskussion.
Frühjahrstagung der DPG, Sektion A: Kernphysik, München, 17.-21.3.1980.
2o.8o.o

IKP-203780
Goeke, K.
Realistische Anwendung von adiabatischem, zeitabhängigen Hartree-Fock auf das $^{8}Be \rightarrow \alpha+\alpha$ System.
Frühjahrstagung der DPG, Sektion A: Kernphysik, München, 17.-21.3.1980.
2o.8o.o

IKP-203880
Goeke, K.
Numerical Application of the Adiabatic Time Dependent Hartree-Fock Theory to the Calculation of the Optimal Collective Path of the $^{8}Be \rightarrow \alpha+\alpha$ Process.
Postervortrag auf der Int. Conf. Nuclear Physics, Berkeley, USA, 24.-30.8.1980.
2o.8o.o

IKP-203980
Goeke, K.
Isovektor-Monopol-Resonanzen: Ein Summenregel-Formalismus.
Frühjahrstagung der DPG, Sektion A: Kernphysik, München, 17.-21.3.1980.
2o.8o.o

IKP-204080
Grüter, J.W.
Data Acquisition at Remote Solar Systems.
Postervortrag auf dem 3. Int. Sonnenforum, Hamburg, 24.-27.6.1980.
2o.6o.1

IKP-204180
Grüter, J.W.
Solar Energy, a Possible Choice for Future Research Activities at Technical Faculties.
University of Heraklion, Kreta, Griechenland, 14.3.1980.
2o.6o.1

IKP-204280
Grüter, J.W.
Data Acquisition for Solar Hot Water Systems by Telecommunication.
IEA Task I Working Group on Data Acquisition and Measurement Systems in Solar Houses, Lausanne, Schweiz, 26.2.1980.
2o.6o.1

IKP-204380
de Haro, R.
Microscopic Description of Giant Resonances.
Universidade Federal do Rio de Janeiro, Brasilien, 17.9.1980.
2o.8o.o

IKP-204480
de Haro, R.
Decay Widths of Giant Resonances in Heavy Nuclei.
Universidade de Sao Paulo, Brasilien, 9.9.1980.
2o.8o.o

IKP-204580
de Haro, R.
The Decay Width of Giant Resonances.
1980 Int. Summer School on Nuclear Structure, Dronten, Niederlande, 12.-23.8.198o.
2o.8o.o

IKP-204680
de Haro, R.
Transition Densities in Very Large Model Spaces Obtained in Fourier-Bessel RPA.
Frühjahrstagung der DPG, Sektion A: Kernphysik, München, 17.-21.3.1980.
2o.8o.o

IKP-204780
de Haro, R.
The Decay Width of Giant Resonances in Heavy Nuclei.
Frühjahrstagung der DPG, Sektion A: Kernphysik, München, 17.-21.3.1980.
2o.8o.o

IKP-204880
Kawade, K.; Battistuzzi, G.; Lawin, H.; Sistemich, K.
Structure of ^{132}Sn and its Neighbours.
Frühjahrstagung der DPG, Sektion A: Kernphysik, München, 17.-21.3.1980.
2o.65.o

IKP-204980
Kern, B.D.; Sistemich, K.; Lauppe, W.-D.; Lawin, H.
Beta Decay of ^{104}Nb.
Minneapolis Meeting of the Division of Nuclear Physics, Minneapolis, USA, 9.-11.10.1980.
2o.65.o

IKP-205080
Kleinheinz, P.
High Spin Spectroscopy in Nuclei around ^{146}Gd and the Z=64 Shell Closure.
XVII Winter School on Nuclear Structure, Bielsko Biała, Polen, Februar 1980.
2o.1o.o

IKP-205180
Kleinheinz, P.
How Particle-Octupole Exchange Coupling Affects the Yrast Lines of Dysprosium Nuclei.
Int. Conf. on Nuclear Behaviour at High Angular Momentum, Strasbourg, Frankreich, 22.-24.4.1980.
2o.1o.o

IKP-205280
Kleinheinz, P.
Octupole Excitations and Particle-Phonon Interaction in Nuclei above ^{146}Gd.
Workshop on Nuclear Structure of Neutron-Deficient N=82 Nuclei, Padova, Italien, 12.-13.11.1980.
2o.1o.o

IKP-205380
Kleinheinz, P.
HighSpin Shell Model Spectroscopy and Yrast Isomers in the ^{146}Gd Region.
Workshop on Nuclear Structure of Neutron-Deficient N=82 Nuclei, Padova, Italien, 12.-13.11.1980.
2o.1o.o

IKP-205480
Kleinheinz, P.
Multiparticle and Phonon Yrast Excitations in Nuclei around ^{146}Gd.
Universität Grenoble, Frankreich, 6.6.1980.
2o.1o.o

IKP-205580
Kleinheinz, P.
Schalenmodellisomere im Gebiet von ^{146}Gd.
Universität Stuttgart, 19.5.1980.
2o.1o.o

IKP-205680
Kleinheinz, P.
High Spin Shell Model Spectroscopy and Particle Phonon Exchange Coupling in Nuclei around ^{146}Gd.
Lawrence Livermore Laboratory, Livermore, USA, 12.3.1980.
2o.1o.o

IKP-205780
Kleinheinz, P.
Particle Phonon Exchange Coupling in Tb and Dy Nuclei.
Nobel Symposium, Örenäs, Schweden, 23.-27.6.1980.
2o.1o.o

IKP-205880
Kleinheinz, P.
Octupole Excitations in the ^{146}Gd Region.
Universität Jyväskylä, Finnland, 3.10.1980.
2o.1o.o

IKP-205980
Kleinheinz, P.
High Spin Spectroscopy in the ^{146}Gd Region.
TU München, Garching, 25.7.1980
2o.1o.o

IKP-206080
Klemt, V.
On the Application of Landau's Fermi Liquid Theory to Finite Systems.
Rutgers University, Piscataway, USA, Januar 1980.
2o.8o.o

IKP-206180
Klemt, V.
Pauli Principle Sum Rule and Consistency Relations for Phenomenologically Adjusted Fermi Liquid Parameters.
Frühjahrstagung der DPG, Sektion A: Kernphysik, München, 17.-21.3.1980.
2o.8o.o

IKP-206280
Knöpfle, K.T.; Riedesel, H.; Schindler, K.; Wagner, G.J.; Mayer-Böricke, C.; Oelert, W.; Rogge, M.; Turek, P.
Existenz und Zerfallseigenschaften der isoskalaren Quadrupolriesenresonanz in ^{13}C.
Frühjahrstagung der DPG, Sektion A: Kernphysik, München, 17.-21.3.1980.
2o.o6.o

IKP-206380
Koch, H.R.
Radiation-Temperature Correlations for the Computation of the Energy Output of Collectors.
Tagung der Mitarbeiter am Solarprogramm der EG, Paris, Frankreich, 17.-19.12.1980.
2o.6o.1

IKP-206480
Krewald, S.
Der Imaginärteil des Schwerionenpotentials bei hohen Energien.
Universität Gießen, 6.11.1980.
2o.8o.o

IKP-206580
Krewald, S.
On the Creation and Observation of a Pion Condensate in High Energy Heavy Ion Collisions.
Int. Workshop VIII on Gross Properties of Nuclei and Nuclear Excitations, Hirschegg, 14.-19.1.1980.
2o.8o.o

IKP-206680
Krewald, S.
Magnetic Resonances and the Spin Dependence of the Particle-Hole Force.
Workshop on Nuclear Physics with Real and Virtual Photons from Collective States to Quarks in Nuclei, Bologna, Italien, 25.-28.11.1980.
2o.8o.o

IKP-206780
Krewald, S.
Magnetic Properties of Nuclei,
IKO Amsterdam, Niederlande, 23.10.1980.
2o.8o.o

IKP-206880
Krewald, S.
Microscopic Structure of the Magnetic High Spin States in ^{208}Pb.
Gordon Research Conference on Photonuclear Reactions, Tilton, USA, 18.-22.8.1980.
2o.8o.o

IKP-206980
Krewald, S.
Magnetic High Spin States.
University of Massachusetts, Amherst, USA, 13.8.1980.
2o.8o.o

IKP-207080
Krewald, S.
Heavy Ion Optical Potential Derived from Reid's Soft Core Interaction.
State University of New York, Stony Brook, USA, 11.8.1980.
2o.8o.o

IKP-207180
Krewald, S.
The Influence of One-Pion-Exchange on the Magnetic High Spin States.
Int. Symp. on High Precision Nuclear Physics, Bad Honnef, 9.-11.6.1980.
2o.8o.o

IKP-207280
Krewald, S.
Microscopic Derivation of Heavy Ion Optical Potentials.
ILL Grenoble, Frankreich, 23.4.1980.
2o.8o.o

IKP-207380
Krewald, S.
The Real and Imaginary Part of the Heavy Ion Optical Potential Derived from the Reid Soft Core Interaction.
Frühjahrstagung der DPG, Sektion A: Kernphysik, München, 17.-21.3.1980.
2o.8o.o

IKP-207480
Krewald, S.
Magnetic High Spin States in ^{208}Pb.
Frühjahrstagung der DPG, Sektion A: Kernphysik, München, 17.-21.3.1980.
2o.8o.o

IKP-207580
Krewald, S.
The Giant Gamow-Teller Resonance.
Frühjahrstagung der DPG, Sektion A: Kernphysik, München, 17.-21.3.1980.
2o.8o.o

IKP-207680
Lieder, R.M.
Study of α-Induced Non-Equilibrium Reactions Using Particle-γ Coincidence Techniques.
Universität Warschau, Polen, 31.10.1980.
2o.1o.o

IKP-207780
Lieder, R.M.
Band Structure in Strongly Deformed Nuclei.
Int. Conf. on Band Structure and Nuclear Dynamics, New Orleans, USA, 28.2.1980.
2o.1o.o

IKP-207880
Lieder, R.M.
Study of the Mechanism of the ^{209}Bi(α, charged particle xn) Reaction.
Cyclotron Institute der Texas A&M University, College Station, USA, 3.3.1980.
2o.1o.o

IKP-207980
Lieder, R.M.
Study of the Mechanism of the ^{209}Bi(α, particle xnγ) Reaction.
Oak Ridge National Laboratory, Oak Ridge, USA, 6.3.1980.
2o.1o.o

IKP-208080
Lieder, R.M.
Selective Population of Final Nuclei in Non-Equilibrium Reactions from Particle-Gamma Coincidence Studies.
Nobel Symposium on Nuclei at Very High Spin, Sven Gösta Nilsson in Memoriam, Örenäs, Schweden, 24.6.1980.
2o.1o.o

IKP-208180
Lunardi, S.
Yrast States in the N=84 Isotones ^{148}Gd, ^{149}Tb and ^{150}Dy.
XVII Winter School on Nuclear Structure, Bielsko Biala, Polen, Februar 1980.
2o.1o.o

IKP-208280
Machner, H.
Investigation of (α,α'x) Reactions up to 40 MeV/A Bombarding Energy.
Int. Workshop VIII on Gross Properties of Nuclei and Nuclear Excitations, Hirschegg, 18.1.1980.
2o.o6.o

IKP-208380
Machner, H.
Testing the Exciton Coalescence Model with Light and Heavy Ions and Pions.
MPI für Kernphysik, Heidelberg, 6.2.1980.
2o.o6.o

IKP-208480
Machner, H.
Präcompoundemission komplexer Teilchen.
Institut für Strahlen- und Kernphysik der Universität Bonn, 28.1.1980.
2o.o6.o

IKP-208580
Machner, H.
Particle Emission from Unbound States.
XVII Winter School on Nuclear Structure, Bielsko Biala, Polen, 11.-21.2.1980.
2o.o6.o

IKP-208680
Machner, H.
Kontinuierliche Spektren komplexer Teilchen.
Kernforschungszentrum Karlsruhe, 18.11.1980.
2o.o6.o

IKP-208780
Machner, H.; Bechstedt, U.; Djaloeis, A.; Jahn, P.; Mayer-Böricke, C.
Untersuchung der Reaktion ^{54}Fe(α,α'x) bei Einschußenergien im Bereich von 59 bis 160 MeV.
Frühjahrstagung der DPG, Sektion A: Kernphysik, München, 17.-21.3.1980.
2o.o6.o

IKP-208880
Madsen, V.A.
New Aspects of the DWBA for Giant Resonances.
Giant Multipole Resonance Topical Conf., Oak Ridge, USA, 15.-17.10.1979.
2o.8o.o

IKP-208980
Martin, S.A.
Der QQDDQ Magnetspektrograph am Jülicher Zyklotron.
Frühjahrstagung der DPG, Sektion A: Kernphysik, München, 17.-21.3.1980.
2o.3o.o

IKP-209080
Martin, S.
High Resolution Measurements Using the Magnet-spectrometer BIG KARL.
1980 RCNP-KIKUCHI Summer School, Osaka, Japan, 19.-23.5.1980.
2o.o6.o

IKP-209180
Maßmeyer, K.
Determination and Variation of the Maximum Stagnation Temperature of a Flat-Plate Solar Collector.
Postervortrag auf dem 3. Int. Sonnenforum, Hamburg, 24.-27.6.1980.
2o.6o.1

IKP-209280
Mayer-Böricke, C.
Recent Research and Development at JULIC.
Michigan State University, East Lansing, USA, 4.9.1980.
2o.o6.o

IKP-209380
Morek, T.
Study of the Nuclei in the Lantanum Region.
Warschau University, Polen, 18.4.1980.
2o.1o.o

IKP-209480
Morsch, H.P.
New Giant Resonances in Heavy Nuclei Excited in Higher Energy Alpha and Deuteron Scattering.
Int. Symp. on Highly Excited States in Nuclear Reactions, Osaka, Japan, 12.-16.5.1980.
2o.o6.o

IKP-209580
Morsch, H.P.
Compressional Modes of Nuclear Excitation.
Sendai, Japan, 20.5.1980.
2o.o6.o

IKP-209680
Morsch, H.P.
Monopole and Dipole Compressional Modes of Excitation.
University of Tokyo, Japan, 22.5.1980.
2o.o6.o

IKP-209780
Morsch, H.P.
Study of the Giant Monopole Resonance and Evidence for New Giant Resonances in Heavy Nuclei.
University of Grenoble, Frankreich, 10.10.1980.
2o.o6.o

IKP-209880
Morsch, H.P.
New Giant Resonances in Heavy Nuclei.
Int. Symp. on High Precision Nuclear Physics, Bad Honnef, 9.-11.6.1980.
2o.o6.o

IKP-209980
Morsch, H.P.
New Giant Resonances.
MPI Heidelberg, 4.6.1980.
2o.o6.o

IKP-210080
Morsch, H.P.
New Results on Giant Resonances from Jülich.
TIT, Tokio, Japan, 23.5.1980.
2o.o6.o

IKP-210180
Müther, H.
Different Concepts for a Fusion Reactor.
Vrije Universiteit Amsterdam, Niederlande, 21.4.1980.
2o.8o.o

IKP-210280
Müther, H.
Pion-Kondensation und realistische NN-Wechselwirkungen.
Expertentreffen für Kernphysik, Schleching, 27.2.-7.3.1980.
2o.8o.o

IKP-210380
Müther, H.
Pion-Kondensation mit realistischen NN und NΔ Wechselwirkungen.
Frühjahrstagung der DPG, Sektion A: Kernphysik, München, 17.-21.3.1980.
2o.8o.o

IKP-210480
Einfluß der induzierten Wechselwirkung auf die Landau-Migdal Parameter.
Frühjahrstagung der DPG, Sektion A: Kernphysik, München, 17.-21.3.1980.
2o.8o.o

IKP-210580
Müther, H.
Nichtiterative 2π-Austauschterme in der Nukleon-Nukleon-Wechselwirkung.
Frühjahrstagung der DPG, Sektion A: Kernphysik, München, 17.-21.3.1980.
2o.8o.o

IKP-210680
Nagai, Y.; Styczen, J.; Piiparinen,M.; Kleinheinz, P.
The X- (or Δ-) Transition in ^{152}Dy.
Frühjahrstagung der DPG, Sektion A: Kernphysik, München, 17.-21.3.1980.
2o.1o.o

IKP-210780
Oelert, W.; Chung, W.; Djaloeis, A.; Mayer-Böricke, C.; Turek, P.
Few-Nucleon Transfer Reactions on Light Nuclei.
IOP Conference on Trends in Nuclear Structure Physics, Manchester, England, 16.-18.4.1980.
2o.o6.o

IKP-210880
Oelert, W.
Diskussion von Alpha-Transfer-Experimenten in der sd-Schale.
Universität Tübingen, 5.12.1980.
2o.o6.o

IKP-210980
Oelert, W.; Djaloeis, A.; Mayer-Böricke, C.; Turek, P.
Alpha-Transfer an Kernen der sd-Schale.
Frühjahrstagung der DPG, Sektion A: Kernphysik, München, 17.-21.3.1980.
2o.o6.o

IKP-211080
Osterfeld, F.
Microscopic Analysis of Giant Resonance Experiments.
1980 RCNP-KIKUCHI Summer School, Osaka, Japan, 19.-23.5.1980.
2o.8o.o

IKP-211180
Osterfeld, F.
Microscopic Theory of Giant Multipole Resonances.
1980 RCNP Int. Symp. on Highly Excited States in Nuclear Reactions, Osaka, Japan, 12.-16.5.1980.
2o.8o.o

IKP-211280
Osterfeld, F.
Critical Analysis of Precritical Phenomena Related to Pion Condensation.
Rutgers University, Piscataway, USA, 3.11.1980.
2o.8o.o

IKP-211380
Osterfeld, F.
Microscopic Calculations of the Imaginary Part of the Optical Potential for Nucleus-Nucleus and Alpha-Nucleus Scattering.
University of Texas, Austin, USA, 13.10.1980.
2o.8o.o

IKP-211480
Osterfeld, F.
Microscopic Calculation of the Imaginary Optical Potential and Inelastic Form Factor.
Universität Mainz, 4.6.1980.
2o.8o.o

IKP-211580
Osterfeld, F.
Microscopic Calculation of the Imaginary Optical Potential and Inelastic Form Factor.
Universität Münster, 27.1.1980.
2o.8o.o

IKP-211680
Osterfeld, F.
Mikroskopische Berechnung des imaginären optischen Potentials für die Nukleon-Kernstreuung.
Frühjahrstagung der DPG, Sektion A: Kernphysik, München, 17.-21.3.1980.
2o.8o.o

IKP-211780
Osterfeld, F.
Theoretische Untersuchung von Isovektor-Dipol- und Gamow-Teller-Übergängen in ^{90}Zr.
Frühjahrstagung der DPG, Sektion A: Kernphysik, München, 17.-21.3.1980.
2o.8o.o

IKP-211880
Paić, G.; Antolković, B.; Djaloeis, A.; Bojowald, J.; Mayer-Böricke, C.
Continuous Spectra of Protons and Deuterons from the α+α Interaction at E_{inc} = 110-172 MeV.
Frühjahrstagung der DPG, Sektion A: Kernphysik, München, 17.-21.3.1980.
2o.o6.o

IKP-211980
Piiparinen, M.
The Structure of the Yrast States of the N=85 Isotones.
XVII Winter School on Nuclear Structure, Bielsko Biala, Polen, Februar 1980.
2o.1o.o

IKP-212080
Piiparinen, M.; Broda, R.; Nagai, Y.; Kleinheinz, P.
An $I^{\pi}= 9^{+}$ Isomer in $^{148}_{63}Eu_{85}$.
Frühjahrstagung der DPG, Sektion A: Kernphysik, München, 17.-21.3.1980.
2o.1o.o

IKP-212180
Piiparinen, M.; Pengo, R.; Broda, R.; Nagai, Y.; Kleinheinz, P.; Roy, N.; Carlen, L.; Ryde, H.; Lindblad, Th.; Johnson, A.; Hjorth, S.A.
High Spin Shell Model Excitations in N=85 Isotones.
Frühjahrstagung der DPG, Sektion A: Kernphysik, München, 17.-21.3.1980.
2o.1o.o

IKP-212280
Posorski, R.
Investigations on All-Day Collector Performance.
Postervortrag auf dem 3. Int. Sonnenforum, Hamburg, 24.-27.6.1980.
2o.6o.1

IKP-212380
Seyfarth, H., Berg, G.P.A., Demarteau, M., Hardt, A., Hürlimann, W., Köhler, M., Martin, S., Maier-Komar, P., Meissburger, J., Oelrich, I., Styczen,B.
^{102}Ru(d,p) ^{103}Ru reaction at 45 MeV incident energy
Frühjahrstagung der DPG, Sektion A: Kernphysik, München, 17.-21.3.1980
2o.o6.o

IKP-212480
Sistemich, K.
Microsecond Isomers near ^{132}Sn.
Oak Ridge National Laboratory, Oak Ridge, USA, 20.11.1980.
2o.65.o

IKP-212580
Sistemich, K.
Studium neutronenreicher Kerne mit dem Spaltproduktseparator JOSEF.
Universität Köln, 10.1.1980.
2o.65.o

IKP-212680
Sistemich, K.
The Doubly Magic ^{132}Sn.
Brookhaven National Laboratory, Upton, USA, 1.8.1980.
2o.65.o

IKP-212780
Sistemich, K.
The Onset of Nuclear Deformation at A = 100.
Iowa State University, Ames, USA, 30.9.1980.
2o.65.o

IKP-212880
Sistemich, K.
Study of Neutron Rich Nuclei with JOSEF.
State University of New York,Stony Brook, USA, 21.10.1980.
2o.65.o

IKP-212980
Sistemich, K.
Shell Structures in Medium Mass Nuclei.
Michigan State University, East Lansing, USA, 26.11.1980
2o.65.o

IKP-213080
Sistemich, K.
JOSEF and the Magic Nucleus ^{132}Sn.
Ames Laboratory USDOE, Ames, USA, 8.12.1980.
2o.65.o

IKP-213180
Speth, J.
Collective States in Nuclei.
ILL Grenoble, Frankreich, 8.1.1980.
2o.8o.o

IKP-213280
Speth, J.
Electric Giant Multipole Resonances.
Int. Conf. on Band Structure and Nuclear Dynamics, Tulane University, New Orleans, USA, 1.3.1980.
2o.8o.o

IKP-213380
Speth, J.
Influence of the π- and ρ-Exchange Potential on the Magnetic Properties of Nuclei.
Argonne National Laboratory, Argonne, USA, 25.2.1980.
2o.8o.o

IKP-213480
Speth, J.
Theoretical Description of Magnetic Properties of Atomic Nuclei.
APS-Meeting, Washington, USA. 28.4.1980.
2o.8o.o

IKP-213580
Speth, J.
Magnetic Properties of Nuclei.
University of Illinois, Urbana, USA, 23.4.1980.
2o.8o.o

IKP-213680
Speth, J.
Effective Mass in Single-Particle Energies in Finite Nuclei.
University of Illinois, Urbana, USA, 22.4.1980.
2o.8o.o

IKP-213780
Speth, J.
Giant Magnetic Resonances?
Indiana University, Bloomington, USA, 21.4.1980.
2o.8o.o

IKP-213880
Speth, J.
Giant Magnetic Resonances?
Texas A&M University, College Station, USA, 17.4.1980.
2o.8o.o

IKP-213980
Speth, J.
Magnetic Properties of Nuclei.
National Bureau of Standards, Washington, D.C., USA, 31.7.1980.
2o.8o.o

IKP-214080
Speth, J.
Critical Analysis of Critical Pion States.
Brookhaven National Laboratory, Upton, USA, 25.7.1980.
2o.8o.o

IKP-214180
Speth, J.
Microscopic Structure of the Gamow-Teller Resonances.
1980 Nuclear Structure Gordon Conference, Tilton, USA, 9.7.1980.
2o.8o.o

IKP-214280
Speth, J.
Magnetic Properties of Nuclei.
Brooklyn College of the City University of New York, Brooklyn, USA, 30.6.1980.
2o.8o.o

IKP-214380
Speth, J.
Critical Analysis of Precritical Phenomena.
State University of New York, Stony Brook, USA, 9.6.1980.
2o.8o.o

IKP-214480
Speth, J.
Spin-Isospin Modes and High Momentum Transfer Electron Scattering.
Symp. on Perspectives in Electro- and Photo-Nuclear Physics, Saclay, Frankreich, 29.9.1980.
2o.8o.o

IKP-214580
Speth, J.
Spin-Dependent Collective Nuclear Excitations.
Symp. on Spin-Dependent Vibrations in Nuclei, Kopenhagen, Dänemark, 5.11.1980.
2o.8o.o

IKP-214680
Sükösd, C.; Djaloeis, A.; Knöpfle, K.T.; Mayer-Böricke, C.; Riedesel, H.; Rogge, M.; Schindler, K.; Turek, P.; Wagner, G.J.
Charged Particle Decay of the Isoscalar Giant Resonances in ^{20}Ne.
Frühjahrstagung der DPG, Sektion A: Kernphysik, München, 17.-21.3.1980.
2o.o6.o

IKP-214780
Sükösd, C.; Martin, S.; Berg, G.; Hardt, A.; Hürlimann, W.; Mayer-Böricke, C.; Meißburger, J.; Morsch, H.P.; Rogge, M.; Turek, P.
High Resolution Study of ^{20}Ne-States Excited via 172.5 MeV inelastic α-Scattering.
Frühjahrstagung der DPG, Sektion A: Kernphysik, München, 17.-21.3.1980.
2o.o6.o

IKP-214880
Suzuki, T.
Test of the Critical Opalescence of Pion Condensation in A=12 and 48 Systems.
Int. School on Critical Phenomena in Heavy Ion Collisions, Poiana Brasov, Rumänien, 25.8.-10.9.1980.
2o.8o.o

IKP-214980
Suzuki, T.
Path Integral and Classical Dynamics of Many Body Systems.
Int. School on Critical Phenomena in Heavy Ion Collisions, Poiana Brasov, Rumänien, 25.8.-10.9.1980.
2o.8o.o

IKP-215080
Suzuki, T.
Path Integral Approach to Many-Nucleon Systems and TDHF.
ILL Grenoble, Frankreich, 13.3.1980.
2o.8o.o

IKP-215180
Suzuki, T.
Critical Analysis of the Precritical Phenomena of Pion Condensation in Finite Nuclei.
Frühjahrstagung der DPG, Sektion A: Kernphysik, München, 17.-21.3.1980.
2o.8o.o

IKP-215280
Suzuki, T.
Dynamical Interplay of Pairing and Quadrupole Modes in Collective Excited States of Transitional Nuclei.
Frühjahrstagung der DPG, Sektion A: Kernphysik, München, 17.-21.3.1980.
2o.8o.o

IKP-215380
Schröer, R.
Thermal Efficiency Test of Flat-Plate Collectors According to the BSE Procedure.
Postervortrag auf dem 3. Int. Sonnenforum, Hamburg, 24.-27.6.1980.
2o.6o.1

IKP-215480
Schult, O.
Nukleare und atomare Einflüsse auf die K-Röntgenenergien.
Universität Frankfurt, 3.1.1980.

IKP-215580
Schult, O.
Wie können wir solarthermische Energie nutzen?
Universität Gießen, 20.10.1980.
2o.6o.1

IKP-215680
Schult, O.
Studies of X-Ray Shifts.
XXVIII Winter Meeting on Nuclear Physics, Bormio, Italien, 25.1.1980.

IKP-215780
Schult, O.
Should we Deal with Solar Thermal Energy?
Kernforschungszentrum Krakau, Polen, 28.7.1980.
2o.6o.1

IKP-215880
Schussler, F.; Monnand, E.; Pinston, J.A.; Jung, G.; Koglin, E.; Pfeiffer, B.; Battistuzzi, G.; Kawade, K.; Lawin, H.; Sistemich, K.; Janzen, R.; van Klinken, J.
Excited 0^+ State around A=98.
Frühjahrstagung der DPG, Sektion A: Kernphysik, München, 17.-21.3.1980.
2o.65.o

IKP-21598O
Stein, H.J.
Praktische Erfahrungen mit Niedertemperatur-Solarkollektoren, Tests bei KFA und in Ispra.
Seminar über die praktische Nutzbarkeit von Sonnen- und Umgebungsenergie (Teil 1), Kernforschungszentrum Karlsruhe, 22.5.1980.
2o.6o.1

IKP-21608O
Stein, H.J.
Testen von Wasserkollektoren.
Jugoslawisch-Deutscher Workshop über Solarenergie, Belgrad, Jugoslawien, 7.-9.1.1980.
2o.6o.1

IKP-21618O
Styczen, J.
Proton Single Particle Energies above Z=64 from a Study of ^{147}Tb.
Workshop on Nuclear Structure of Neutron-Deficient N=82 Nuclei, Padua, Italien, 12.-13.11.1980.
2o.1o.o

IKP-21628O
Talarek, H.D.
Der Physiker in staatlichen Großforschungseinrichtungen,
Wochenendseminar der DPG, Gossenweilen/Stein, 15.11.1980.
2o.6o.1

IKP-21638O
Talarek, H.D.
Standard Testprozeduren für Sonnenkollektoren - Bewertung, Status und Trends.
3. Int. Sonnenforum, Hamburg, 24.-27.6.1980.
2o.6o.1

IKP-21648O
Wambach, J.
The Influence of the π- and ρ-Exchange Potential on Magnetic Properties of Nuclei.
Frühjahrstagung der DPG, Sektion A: Kernphysik, München, 17.-21.3.1980.
2o.8o.o

IKP-21658O
Wolf, A.; Battistuzzi, G.; Kawade, K.; Lawin, H.; Sistemich, K.
Determination of a g-Factor for ^{100}Zr.
Frühjahrstagung der DPG, Sektion A: Kernphysik, München, 17.-21.3.1980.
2o.65.o

IKP-21668O
Wolf, A.; Battistuzzi, G.; Kawade, K.; Lawin, H.; Sistemich, K.
g-Factor of the First Excited 2^+-State in ^{100}Zr.
Bull. of the Israel Phys. Soc. Vol. 26 (1980) S. 7.
2o.65.o

IKP-21678O
Wolf, A.
"g" Factor Measurements in ^{134}Te and the A=100 Region.
Iowa State University, Ames, USA, 3.9.1980.
2o.65.o

IKP-21688O

X. INTERNAL REPORTS

IKP-300180
Anhalt, J.
Meßdaten-Erfassungssystem HP 3052 - Aufbau und Programm-Beschreibung für universelle Meßwertaufnahme.
Interner Bericht IKP-IB-1/80

IKP-300280
Bundschuh, V.; Dittrich, A.+; Grüter, J.W.; Kleemann, M.; Meliß, M.; Pohlmann, D.+; Stein, H.J.; Wagner, H.J.
Mustersolarhäuser - Untersuchung der wissenschaftlichen Zielsetzung und Durchführbarkeit eines Forschungs- und Entwicklungsprojekts.
Studie der Arbeitsgemeinschaft Mustersolarhäuser, Interner Zwischenbericht KFA/BMFT Bd. 1 und Bd. 2, September 1989

IKP-300380
Ebke, H.; Grüter, J.W.
Ein relatives Eichverfahren für Pyranometer.
Interner Bericht IKP-IB-2/80

IKP-300480
Grüter, J.W.; Riemer, H.
Solaranlagen zur Brauchwassererwärmung in Liegenschaften der Bundeswehr.
Interner Zwischenbericht KFA/BMFT, Mai 1980

IKP-300580
Talarek, H.D.
Testing of Liquid-Heating Flat-Plate Collectors Based on Standard Procedures.
Interner Bericht IKP-IB-4/79

IKP-300680
Talarek, H.D. (Hrsg.)
Results of a Pyranometer Comparison, Task III, Performance Testing of Solar Collectors,
IEA Internal Report, Davos, Schweiz, März 1980

IKP-300780
Talarek, H.D.
Annual Progress Report Task III, Performance Testing of Solar Collectors.
IEA Internal Report, Januar 1980

XI. INDEX TO AUTHORS